CR-72548
REPORT DAC-68510A

FINAL REPORT

THE INTEGRATION OF QUIET ENGINES WITH SUBSONIC TRANSPORT AIRCRAFT

DOUGLAS AIRCRAFT COMPANY
MCDONNELL DOUGLAS CORPORATION

CR-72548
REPORT DAC-68510A

FINAL REPORT

THE INTEGRATION OF QUIET ENGINES WITH SUBSONIC TRANSPORT AIRCRAFT

prepared for
NATIONAL AERONAUTICS AND SPACE ADMINISTRATION

1 AUGUST 1969

CONTRACT NAS3-11151

Technical Management
NASA Lewis Research Center
Cleveland, Ohio
Propulsion Systems Acoustics Branch
Joseph F. McBride

Douglas Aircraft Company
McDonnell Douglas Corporation
Long Beach, California

FOREWORD

The work described herein was accomplished at the Douglas Aircraft Company, McDonnell Douglas Corporation, under NASA Contract NAS3-11151, with Mr. Joseph F. McBride, Propulsion Systems Acoustics Branch, NASA Lewis Research Center, as Project Manager.

ABSTRACT

This study was conducted to determine the feasibility of retrofitting an advanced technology, high bypass ratio engine, incorporating noise suppression design features, on a selected version of the DC-8 airplane. The DC-8-61 was selected. A new pylon would be required, but no other major structural changes would be necessary. The present wing is satisfactory. A powered elevator system would be required. The retrofit of the quiet engine would result in improved airplane takeoff and payload-range performance. However, direct operating costs would be increased by about 50 percent.

TABLE OF CONTENTS

TABLE OF CONTENTS (CONTINUED)

PAGE

INTRODUCTION

The simultaneous growth of air traffic and residential communities near airports has increased human exposure to aircraft flyover noise to objectionable levels. A number of methods of reducing this exposure are under study by both government and industry groups. One method is that of retrofitting quiet engines to existing large subsonic transport aircraft. This report is concerned with a study of the integration of a quiet engine into a DC-8 airplane. Objectives of the work are definition and evaluation of the nacelle-pylon designs and airframe changes required to retrofit a quiet engine and analysis of the technical and economic feasibility of retrofit.

This final report presents the results of the analyses and tests performed during the course of the contract. The work, covered in chronological order during six tasks, is as follows:

- Task I — Preliminary design studies for a selected DC-8 model (the DC-8-61 passenger airplane was selected).
- Task II — Airplane parametric performance studies to permit the identification of important quiet-engine characteristics.
- Task IV — Detailed design of a nacelle and pylon incorporating engine characteristics selected by the NASA technical manager of the program.
- Task III — Wind Tunnel Test program to determine the stability and control and drag characteristics of the nacelle-pylon design developed during Task IV.
- Task VI, Part 1 — Determination of the technical feasibility and cost of retrofitting the quiet engine to the DC-8-61.
- Task V — Determination of the aerodynamic performance and direct operating cost of the DC-8-61 with the quiet-engine design of Task IV and incorporating the wind-tunnel tests of Task III and the retrofit cost of Task VI.
- Task VI, Part 2 — Determination of the effect of the retrofit costs on the operators' return on investment. The retrofit costs were determined in Task VI, Part A, and the direct operating cost was determined in Task V.

The main body of this report is organized numerically by task number.

SUMMARY

This report presents the results of the analysis and tests conducted in accordance with the National Aeronautics and Space Administration's contract NAS3-11151. The purpose of work was to study the integration of an advanced-technology, high-bypass-ratio, quiet engine into a selected model DC-8 airplane. The engine and its nacelle incorporate design features intended to reduce airport-community flyover noise.

The DC-8-61 passenger airplane was selected for the study. Preliminary-design and parametric studies to determine performance and cost trade factors due to changes in engine characteristics were conducted. A detailed nacelle and pylon design for a specified engine configuration was then accomplished. Wind-tunnel aerodynamic and flutter tests were conducted to determine the stability and control, drag, and flutter characteristics of the DC-8-61 with the quiet engine. The technical feasibility and cost of retrofitting the quiet engine to the DC-8-61 was determined.

The performance of the DC-8-61 with the quiet engine is significantly better than that of the present DC-8-61. The range is improved by 650 nautical miles with a payload that is typical of domestic airline operation. The takeoff field length is reduced by 12 percent for a range of 847 nautical miles, which is the average range for DC-8 domestic flights. The height above the runway at 3 nautical miles from brake release is increased by about 250 feet (76 m), depending on gross weight.

No major structural modifications of the wing are required to retrofit the quiet engine to the DC-8-61. The strength and flutter characteristics of the present wing are adequate. A new pylon is required.

The longitudinal stability is significantly reduced because of the retrofit. A powered elevator system and a redundant yaw damper system are required to obtain acceptability and control characteristics.

The retrofit cost based on 300 airplanes is $6,982,000 per airplane (1975 dollars). The change in direct operating cost therefore strongly depends on the depreciation period selected for the modification. For a 5-year depreciation period, the increase in direct operating cost relative to the present DC-8-61 is 58.0 percent for the average (847-nautical-mile) DC-8 range.

CONCLUDING REMARKS

A conclusion to be drawn from this work is that it is not economically attractive to retrofit the DC-8-61 airplane with quiet engines. Although no other airplane models were studied, the fact that a DC-8-61 retrofit would require no unique modifications, except for the powered elevator, implies that retrofitting the quiet engine to other similar aircraft would not be significantly less expensive and might very well be more expensive. The operator's return on his investment would therefore suffer at least as much as has been estimated for the DC-8-61, whatever airplane was used.

It is interesting to find that the retrofit is not economically justified even though all aerodynamic performance parameters of the airplane are markedly improved by retrofitting with quiet engines. The improvements in specific fuel consumption more than compensate for the increase in operating weight empty, and even the payload-range capability of the airplane is improved.

TASK I
MODEL SELECTION
AND PRELIMINARY DESIGN STUDIES

LIST OF ILLUSTRATIONS

LIST OF TABLES

TASK I

MODEL SELECTION AND PRELIMINARY DESIGN STUDIES

MODEL SELECTION

The quiet engine definition provided at the beginning of Task I is presented in Table I-I. The engine weight, diameter, and length are all larger than the corresponding characteristics of the present JT3D engine. It was apparent that retrofit of the new engine would have an important effect on airplane flutter characteristics. Because the DC-8 family consists of a number of models differing widely in wing stiffness, the feasibility of retrofitting the quiet engine would vary widely. The study results would, therefore, be strongly conditioned by the selection of the DC-8 model for the study. Two important criteria were established for use in selecting a model.

1. The selected model must require intermediate airframe modification, rather than either the least or the most modification.

TABLE I-I
QUIET-ENGINE CHARACTERISTICS

	U.S.C. UNITS*	SI UNITS **
I. AT CRUISE (MACH 0.82 AT 35,000 FT [10,668 M])		
A. BYPASS RATIO	5.0:1	
B. FAN PRESSURE RATIO	1.60:1	
C. OVERALL CYCLE PRESSURE RATIO	25:1	
D. TURBINE INLET TEMPERATURE	1755°F	957°C
E. THRUST	4900 LB	21,796 N
F. THRUST SPECIFIC FUEL CONSUMPTION	0.61 LB/HR-LB	0.062 KG/HR-N
G. TOTAL ENGINE AIRFLOW: ACTUAL	347 LB/SEC	157 KG/SEC
CORRECTED	881 LB/SEC	400 KG/SEC
II. AT STANDARD SEA-LEVEL CONDITIONS, STATIC		
A. TURBINE INLET TEMPERATURE	1950°F	1066°C
B. THRUST	23,350 LB ***	103,865 N
C. THRUST SPECIFIC FUEL CONSUMPTION	0.33 LB/HR-LB	0.034 KG/HR-N
D. TOTAL ENGINE AIRFLOW	797 LB/SEC	362 KG/SEC
E. BYPASS RATIO	4.8:1	
F. FAN PRESSURE RATIO	1.54:1	
III. ENGINE SIZE		
A. FAN TIP DIAMETER AT INLET	70.0 IN.	1.78 M
B. FAN INLET HUB-TO-TIP DIAMETER RATIO	0.40	
C. FAN-EXIT-DUCT OUTER WALL DIAMETER	63.0 IN.	1.60 M
D. FAN DISCHARGE NOZZLE AREA	10.4 SQ FT	97 SQ CM
E. ENGINE DISCHARGE NOZZLE AREA	4.0 SQ FT	37 SQ CM
F. TURBINE EXIT AREA	802 SQ FT	74.5 SQ M
G. TURBINE EXIT TIP DIAMETER	40.0 IN.	1.0 M
H. ENGINE LENGTH: FAN ENTRANCE FLANGE TO ENGINE NOZZLE EXIT FLANGE	134 IN.	3.4 M
I. BASIC ENGINE DRY WEIGHT, INCLUDING STANDARD EQUIPMENT	5100 LB	2313 KG

* UNITED STATES CUSTOMARY UNITS
** STANDARD INTERNATIONAL UNITS
***A THRUST RATING OF 22,750 LB (101,197 N) WAS USED FOR PERFORMANCE CALCULATIONS

2. All factors being equal, the wing structure of the selected model must be in large supply within the total fleet.

An inventory of wing-structure configurations used in the various DC-8 models is presented in Table I-II. The 11 wing skin configurations are identified by the dash numbers at the head of each column (−1, −501, etc.). The table shows that the most common configuration (101 airplanes) is that used on models DC-8-55 and -61. Both the stiffness and the strength of this wing are intermediate between those of the wings introduced into production in earlier and later models. A forecast of the DC-8 fleet indicated that the DC-8-61 will be in wide use in 1972, more so than the DC-8-55. On the basis of these considerations, the DC-8-61 appeared the most suitable model for the study.

Other factors were considered to determine whether reasons might exist for selecting another model. A review of the relative flyover noise level indicated that the levels of the DC-8-61 are approximately the same as those of other long-range turbofan-powered transports in wide service with similar "short" fan exhaust ducts. The DC-8-61 model is thus representative in terms of airport-community noise.

TABLE I-II
DC-8 FLEET SURVEY

	DC-8 WING SKIN CONFIGURATIONS: 5640688										
DC-8 MODEL	−1	−501	−503	−505	−507	−509	−511	−513	−515	−517	−519
−11	21										
−12	4										
−21	18		14								
−31		4									
−32				43							
−33		2		3		3					
−41		4									
−42				7		1					
−43					2	16					
−51	25		4								
−52		6			13	3					
−53					9	17					
−54F					27						
−55							32				
−61							69				
−61F											10
−62								24	12		
−62F									8	2	
−63									26	CUTBACK PYLON	
−63F										32	
TOTAL	68	16	18	53	51	40	101	24	46	34	10
GROSS WEIGHT (1000 LB − 454 KG)	265/276	300	276	310	300/315	300/315	325	335	335/350	350	325

Additional thrust for the engines of the DC-8 family has not become an important requirement. It appears that the increased thrust of the quiet engine will not place any one model in a distinctly more favorable position than another.

On the basis of the preceding considerations, the DC-8-61 is confirmed as the most suitable single model for study purposes.

PRELIMINARY NACELLE DESIGN

Figure I-1 shows the nacelle design used for the work conducted during Tasks I and II. The design is based on the work described in this section. Figure I-2 shows the pylon structure.

ENGINE DEFINITION

The engine characteristics defined by the contract work statement are tabulated in Model Selection paragraph (Table I-I). Additional data, received later, are shown below.

		U.S.C. UNITS*	SI UNITS**
FAN-EXIT-DUCT INNER WALL DIAMETER		37 IN.	94 CM
NUMBER OF FAN BLADES		56	
FAN ROTOR SPEED	(AT TAKEOFF)	3350 RPM	56 Hz
	(AT 5000-LB (22,241 N) THRUST)	2234 RPM	37 Hz
FAN-CASE LENGTH		33 IN.	84 CM
NO INLET GUIDE VANES			

* UNITED STATES CUSTOMARY UNITS
**STANDARD INTERNATIONAL UNITS

A comparison of the engine with a JT3D-3B is shown in Table I-III. Preliminary engine-performance estimates were based on the performance of the Pratt and Whitney QB-3 (Reference I-1).

Engine gearbox and accessories used (generator, starter, etc.), were identical to those used with the present JT3D-3B-engine-powered DC-8-61.

TABLE I-III

COMPARISON OF THE BASELINE QUIET ENGINE AND THE JT3D-3B

	QUIET ENGINE		JT3D-3B	
	U.S.C. UNITS*	SI UNITS**	U.S.C. UNITS*	SI UNITS**
DIMENSIONAL DATA				
FAN TIP DIAMETER	70 IN.	1.78 M	50 IN.	1.27 M
NACELLE LENGTH	245 IN.	6.22 M	227 IN.	5.76 M
MAX NACELLE DIAMETER	84.3 IN.	2.14 M	70.0 IN.	1.77 M
INLET LENGTH	80 IN.	2.03 M	45 IN.	1.14 M
BARE ENGINE WEIGHT	5100 LB	2313 KG	4289 LB	1945 KG
PERFORMANCE DATA				
PERFORMANCE DOCUMENT	QB-3 TDM-2128		SPEC 1827	
TAKEOFF RATING, S.L.S., 59°F (15°C)	22,740 LB	101,152 N	18,000 LB	80,068 N
TAKEOFF LAPSE RATE TO M = 0.2	0.803		0.864	
MAX CRUISE RATING 35K M 0.82				
NET THRUST	4902 LB	21,805 N	4450 LB	19,794 N
SPECIFIC FUEL CONSUMPTION	0.613 LB	21,278 KG	0.80 LB	0.36 KG
BYPASS RATIO	4.96		1.31	

* UNITED STATES CUSTOMARY UNITS
**STANDARD INTERNATIONAL UNITS

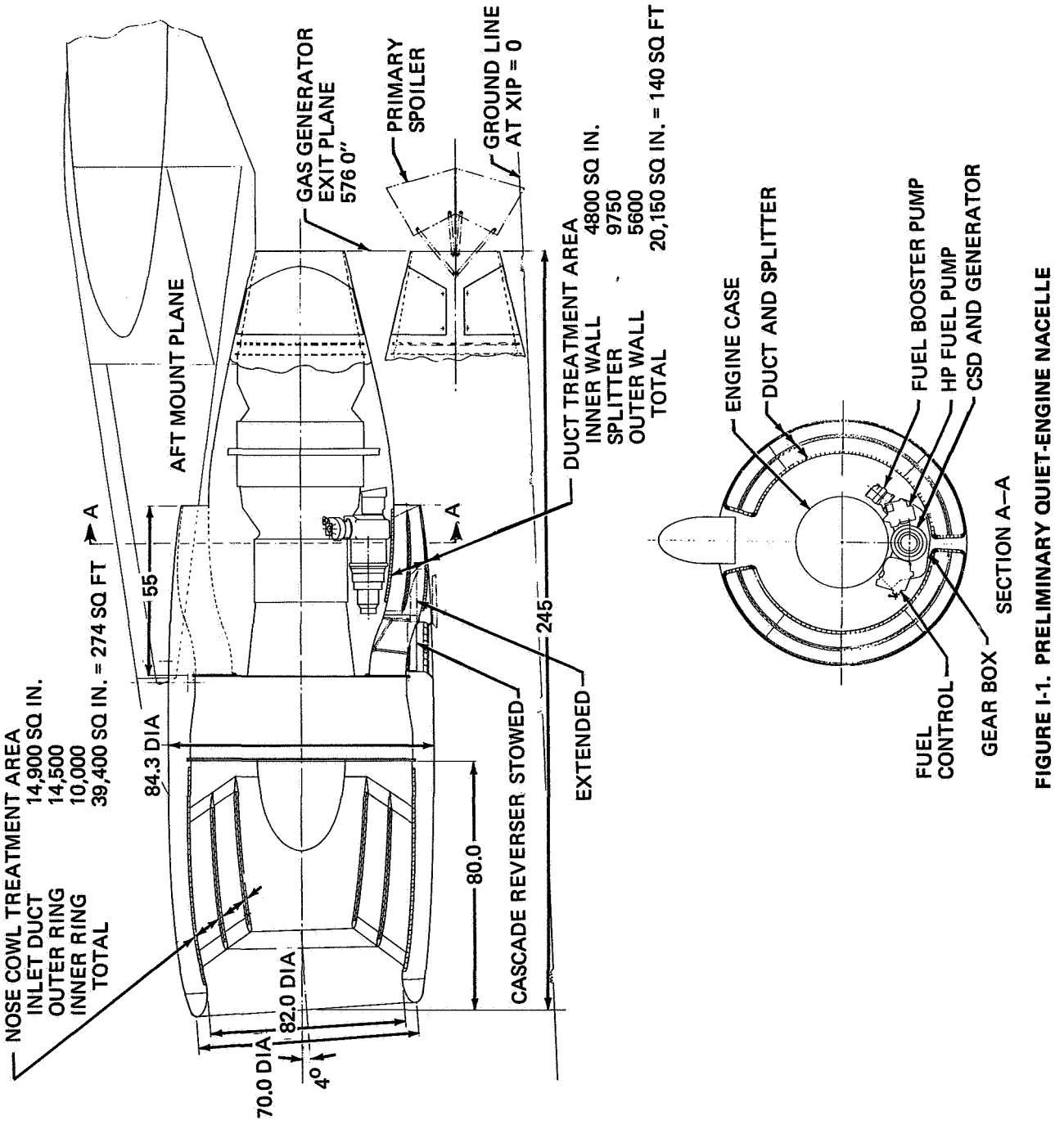

FIGURE I-1. PRELIMINARY QUIET-ENGINE NACELLE

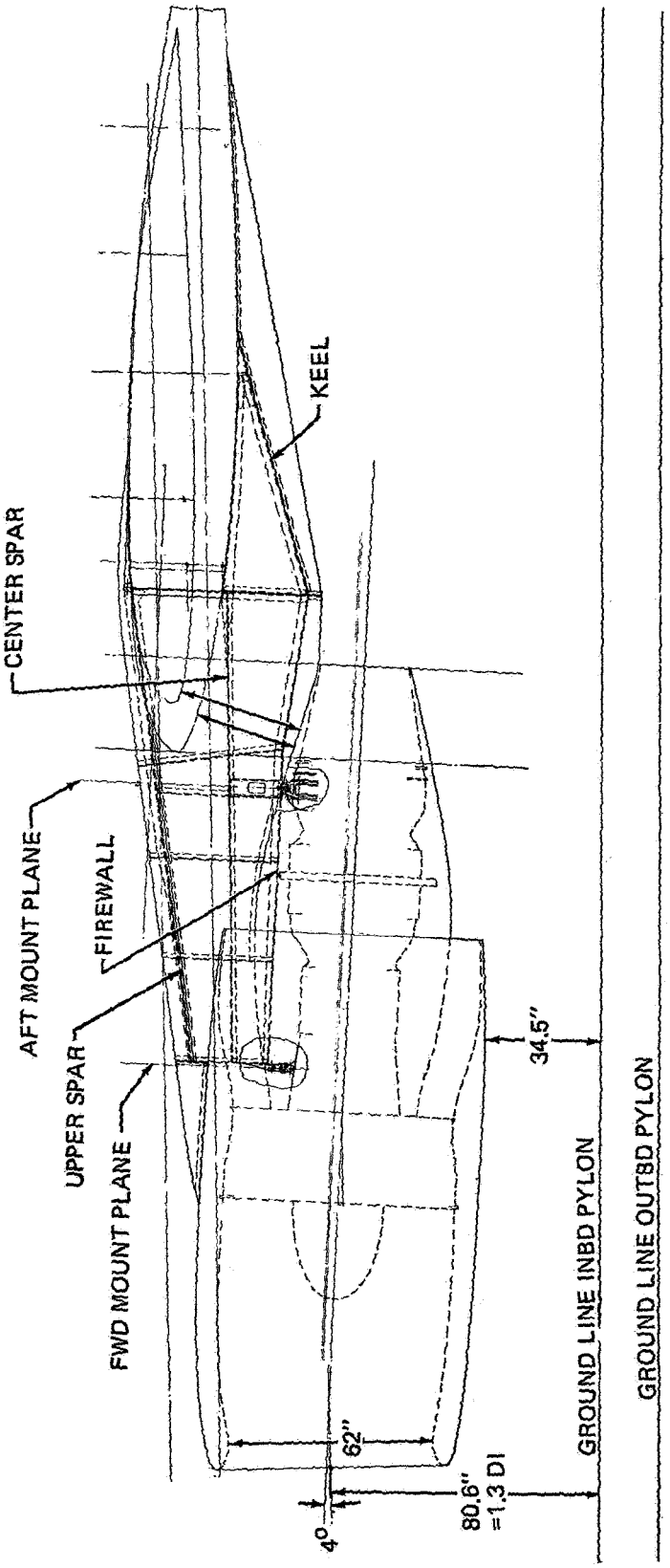

FIGURE I-2 PYLON STRUCTURE

NACELLE LOCATION

Ground Clearance and Inlet-Height Criteria

For adequate ground clearance, the following two basic considerations must be evaluated: (1) prevention of nacelle contact with the ground during both normal landing and takeoff operations and during ground operations with equipment failure (flat tires) and (2) prevention of nacelle contact with airport above-ground obstructions (e.g., runway and taxiway lights). The first consideration must ensure that the outboard nacelle does not make ground contact at landing touchdown with the aircraft at maximum rotation and a roll angle as high as 9.5 degrees (0.165 rad). In addition, there must be adequate clearance for both nacelles in case of a landing-gear flat tire with the landing-gear strut fully depressed. The second consideration must ensure that the inboard nacelle does not make contact with airport above-ground obstructions during taxiing, with adequate allowance for deflection resulting from wing flexibility.

Erosive damage resulting from aspiration of solid particles from the ground into the engine inlet during aircraft ground operation limits the vertical position of the nacelle. The ratio of inlet-centerline height to inlet diameter is used to describe the nacelle height; for a fan design having no inlet guide vanes, a ratio of 1.3 is satisfactory. That is, if the ratio is not less than 1.3, the aspiration of excessively large particles will be prevented.

Flutter and Divergence Considerations

The flutter characteristics of the DC-8-61 aircraft are affected by the following design parameters:

1. Wing bending and torsion stiffness.

2. Nacelle center-of-gravity location and moment of inertia.

3. Pylon stiffness.

4. Aileron Balance.

Changes in these parameters require careful study to ensure that proper flutter margins are maintained.

The proposed quiet engine is heavier than the present JT3D-3B engine used on the DC-8-61 airplane. Table I-IV shows weight and inertia comparisons between the JT3D-3B and the proposed quiet engine. The inertias in the table are about the wing elastic axis.

TABLE I-IV
WEIGHT AND INERTIA COMPARISONS

	JT3D-3B INSTALLED ON THE DC-8-61		QUIET ENGINE INSTALLED ON THE DC-8-61	
		SI UNITS *		SI UNITS *
NACELLE WEIGHT	6,930 LB	3143 KG	8,403 LB	3812 KG
PYLON WEIGHT	690 LB	313 KG	900 LB	408 KG
TOTAL PITCH INERTIA	2.082×10^8 LB-SQ IN.	0.0006×10^8 KG-SQ M	3.305×10^8 LB-SQ IN.	0.0009×10^8 KG-SQ M

* STANDARD INTERNATIONAL UNITS

Retrofitting the DC-8-61 with the heavier engine may require modifications of the airplane to maintain the present safety margins. Estimates were made, based on flutter-model tests and dimensional analysis, to determine the extent of the modifications. To maintain the existing design speeds, two possibilities were considered:

1. Relocating the engine 31 inches (79 cm) aft of the present layout position. Adding 330 pounds (150 kg) of aileron balance.

2. Locating the engine at the present layout position. Adding 330 pounds (150 kg) of aileron balance. Adding 4000 pounds (1814 kg) of wing skin to the wing structure inboard of the outboard pylon.

The numbers mentioned are estimates and were used only for evaluations of trends and orders of magnitude. A check of these estimates and an investigation of other possibilities, such as changing the pylon stiffness, was conducted for Task VI.

Nacelle-divergence studies were completed. The results show that the present DC-8-61 pylon stiffness is adequate to prevent divergence of the quiet engine.

Drag Considerations

The location of the nacelle relative to the wing was selected on the basis of considerations of interference drag, pylon weight and drag, foreign-object ingestion during aircraft ground operation, flap impingement, and the influence of acoustic loads. The nacelle exit is located at the 10-percent point of the local wing chord. This far forward location is necessary to minimize interference drag. Although wind-tunnel results show relatively small penalties resulting from moving the nacelle farther aft, flight experience has shown that these penalties are much greater at full-scale Reynolds numbers. The nacelle vertical location is set primarily by the amount of foreign-object ingestion that can be tolerated. The nacelle must, therefore, be close to the wing. However, with the nacelle located as far forward as it is, there is no interference problem. Wind-tunnel tests have shown that vertical location is of second-order importance relative to fore-and-aft location in determining interference drag.

Stability Considerations

This section summarizes the results of the Task I preliminary analysis of the effects of the quiet-engine installation on stability and control.

For the purposes of this analysis, the characteristics of the DC-8-61 were used. The effects of the larger nacelles and shorter pylons on static longitudinal and directional stability were assumed to be small enough to neglect, pending the availability of definitive data from the wind-tunnel tests of Task III.

Paragraph 4b.131 of the Civil Aeronautics Regulations (CAR) requires that at 1.4 V_{STALL}, with flaps and gear fully extended, thrust at zero, and airplane at maximum landing weight, the application of takeoff power be controllable with a column force of no more than 50 pounds (222 N). The DC-8-61 with the quiet engine will comply with this regulation.

The FAA-required minimum static-longitudinal-stability force gradient of 1 pound (4.45 N) of pulling force on the control column per 6 knots is critical during enroute climb at the most aft

center-of-gravity (c.g.) position on all DC-8 series. Because of the increased thrust pitching moment and increased thrust lapse rate, the larger quiet engines will degrade the stability under these conditions. At a 34-percent-mean-aerodynamic-chord (MAC) aft c.g. location, the force gradient with the quiet engine is 252 pounds (1121 N) of pushing force per 6 knots. It is estimated that meeting the FAA regulations will require holding the aft c.g. limit to 28-percent MAC, from 34-percent MAC on the basic DC-8-61. To keep the present c.g. range would require major modifications of the aircraft, such as a new horizontal tail or a powered elevator system. The power elevator also would improve controllability during the go-around maneuver. However, such a modification would require considerable analysis and design work.

The quiet engines are not relocated in the spanwise direction relative to the present JT3D-3B engines. Therefore, the minimum control speeds as functions of thrust will not be affected and need only be extrapolated to the higher thrusts available.

The final estimates of the effects of the engine change on stability and control characteristics are shown in Task III.

Accessories

The accessory gear box (Figure I-1) is the same Pratt and Whitney unit now in service on all JT3D-3 engines. Also, it is located and mounted in the same position as the present JT3D-3 because the engine case used for this task is basically a JT3D-3 case. The accessories used are standard DC-8 Series 50 units that will be interchangeable with the treated installation. The fan-air exit duct passes under the gear box and engine accessories and will have to be hinged to provide accessibility to the gear box and engine case.

ENGINE MOUNTING

The engine-mounting arrangement for Task I was designed with the following considerations:

1. The front mount will attach to the gas-generator case instead of to the fan case. This allows the pylon to become a much better torque box at the front mount point and also makes provisions for the pneumatic heat exchanger and Engine Service Lines Interface.

2. Only the left aft-engine mounts take forward thrust, except if the left mount fails. Then the right side shall be capable of taking maximum engine thrust.

3. Torque loads are taken by the aft mount.

4. All mounting points take vertical loads at the engine and the pylon.

5. Side loads are taken by the left aft-engine mount and forward engine mount at the engine. All engine mounting points take side load at the pylon.

DESIGN OF THE INLET, FAN EXHAUST DUCT, AND NACELLE

The inlet-and-nacelle design for the quiet engine is based on the results of wind-tunnel tests of the DC-8, DC-9, C-5A, and DC-10 models, as well as general investigations that include inlet, cowl, afterbody, and isolated-nacelle tests. Results of the flight-test program to develop the design for the DC-8-62 and -63 nacelle and pylon also were used. The aerodynamic design of the acoustically treated surfaces was based on potential-flow calculations that used Douglas IBM Program 50D.

Inlet Internal-Lip Thickness

The thickness of the inlet internal lip has been made large enough to maintain unseparated flow at high mass-flow ratios and large angles of attack and with crosswind. The thickness required to accomplish this has been well documented by Douglas model and full-scale tests. A lip thickness of 11 percent (relative to the radius of the inlet throat) has been shown necessary to prevent flow separation at inlet Mach numbers near 0.6. With an 11-percent lip, operation in crosswinds in excess of 40 mph (35 knots) has been demonstrated by the DC-8 and DC-9 with no inlet-distortion problems.

Inlet Internal Geometry

Tests conducted under contract NASI-7130 have shown that potential-flow techniques can be used to design inlet internal cowl and ring vanes that have satisfactory pressure distributions. The internal cowling pressure distributions measured during full-scale tests agree well with the distributions predicted for potential flow.

Mechanical Design of the Inlet

The mechanical design of the inlet duct is based on satisfaction of two criteria: assurance of adequate structural integrity and provision for the required acoustic treatment. The latter criterion must ensure not only that adequate treated area is provided, but also that the acoustical material is distributed – to the greatest extent practical – in accordance with the appropriate value of the ratio of channel height to wave length. This ratio is discussed in the Suppressor Design Section. These criteria dictate a design having a fully treated cowl and two concentric ring vanes (treated on both faces). Because the engine has a rotating centerbody, treatment was not used in this area.

External Cowl Design

The function of the cowl in a subsonic jet-engine installation is to provide a surface upon which a suction force may act to cancel the additive drag, which is the integral of the pressures on the entering streamtube.

If the additive drag is not opposed by a suction force on the cowl, an additional external drag is incurred (spillage drag). At cruise conditions, the additive drag is of the order of 10 to 20 percent of the total airplane drag. Therefore, the external cowl was designed with a diameter small enough to reduce the cowl skin-friction drag and weight but large enough to prevent shock waves and separations. An excessively large cowl diameter can cause large fan-cowl boattail angles or, conversely, large fan-nozzle offset, both of which are penalizing.

An external cowl shape (the Douglas 3-Series) has been developed that has a high drag-divergence Mach number and a small maximum diameter, but that still allows the use of the thick internal inlet lip for good low-speed performance. This cowl shape was used for the preliminary nacelle design.

Nacelle Design

The fan cowl has a 10 degree (0.17 rad) boattail angle, which allows the use of a low-offset annular fan nozzle. The gas-generator nacelle is tightly wrapped, to reduce wetted area, and terminates with a 15 degree (0.26 rad) boattail angle and a short conical exhaust nozzle.

Mechanical Design of the Exhaust Duct

Essentially the same mechanical criteria apply to the design of the fan exhaust ducting as to the inlet duct. However, trade studies such as those shown in Figure I-3 have shown that short ducting

can provide significant advantages over full-length fan exhaust ducting for high-bypass-ratio applications. As the figure shows, weight is always a disadvantage for the longer duct configuration. The short duct is therefore especially desirable in a retrofit program, where added nacelle weight requires additional wing stiffness. For these reasons, the exhaust duct was made as short as is consistent with the provision of the required acoustical material on the internal duct surfaces and on both faces of a circumferential splitter. In the interests of simplicity, the longitudinal struts that support the circumferential splitter are not treated.

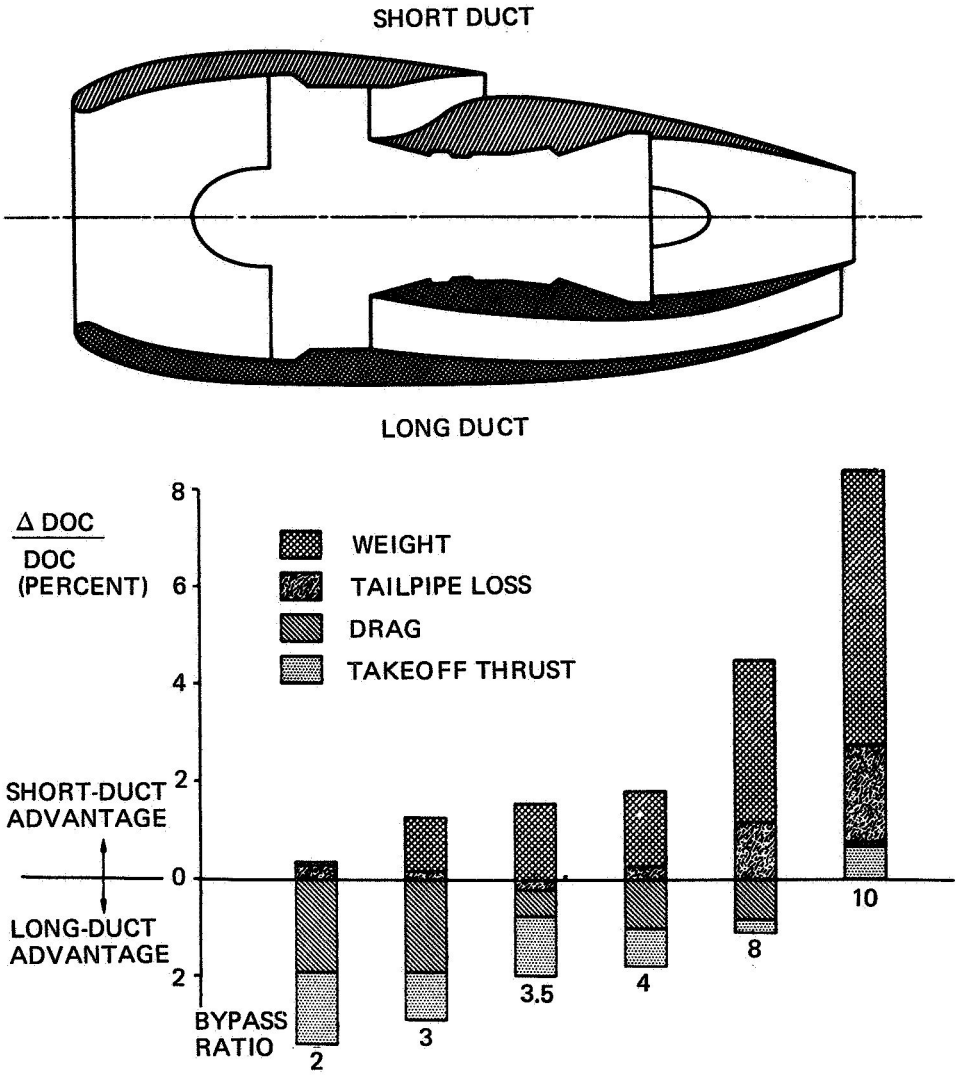

FIGURE I-3. LONG DUCT, SHORT DUCT PERFORMANCE COMPARISON

Thrust Reverser

Although current engines have reversers on the exhaust streams of both the fan and the gas generator, studies such as Reference I-2 suggest that the increasing bypass ratios of advanced engines may change this. For a total reverser effectiveness of the order of 35 to 45 percent (the effectiveness of reversers in current service), it may be possible to eliminate the gas-generator reverser in engines with bypass ratios as high as 8. This is indicated in Figure I-4 ($\eta_{GG} = -1.0$). Figure I-4 shows that an inordinately high fan-reverser effectiveness would be required if the gas-generator exhaust of a bypass-ratio-5 engine were not changed. However, it is apparent that

NOTES:

1) $\eta_{GG} = \frac{F_{R_{GG}}}{F_{G_{GG}}}$ 2) $\eta F = \frac{F_{R_F}}{F_{G_F}}$ 3) $\eta T = \frac{F_{R_{GG}} + F_{R_F}}{F_{G_{GG}} + F_{G_F}}$

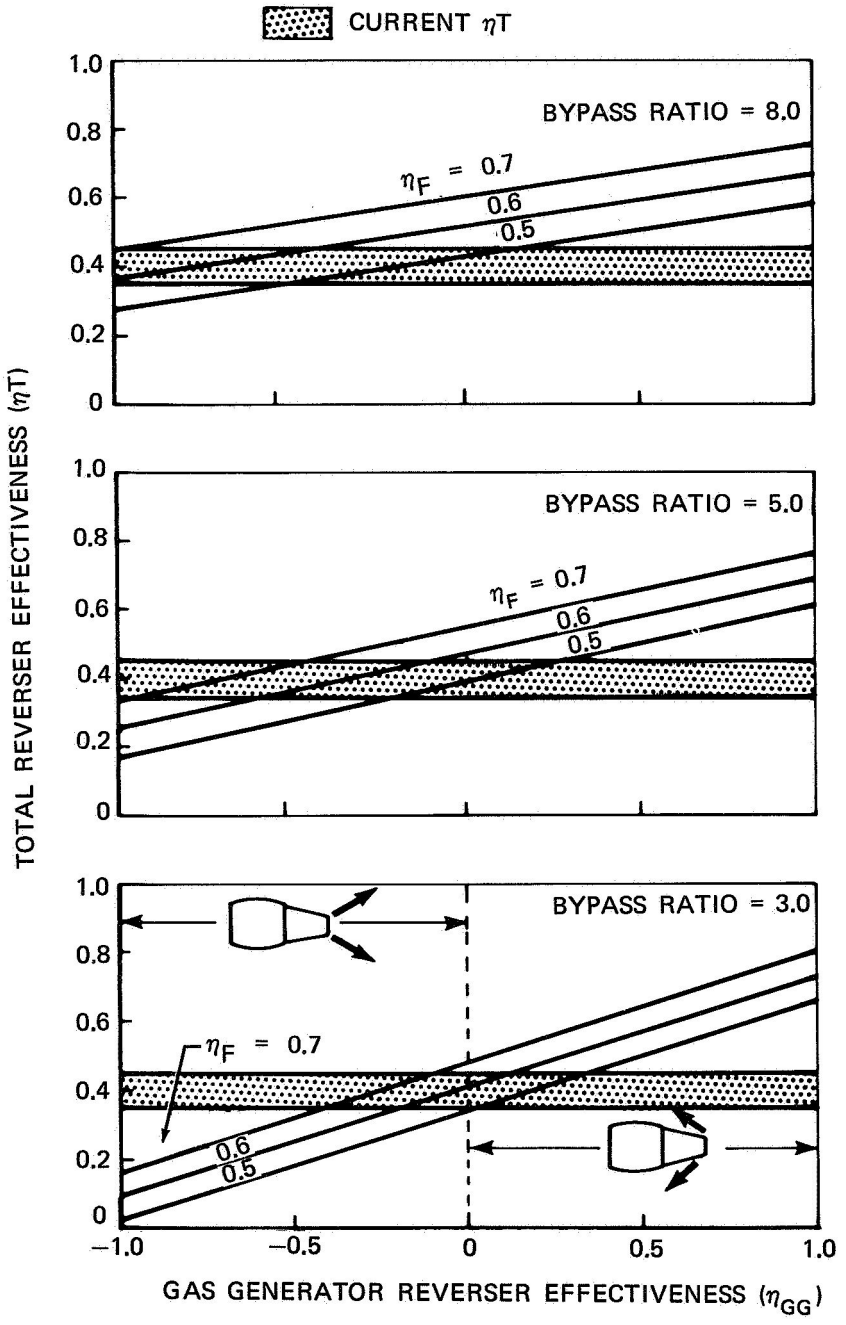

FIGURE 1-4. THRUST-REVERSER EFFECTIVENESS

reasonable levels of total effectiveness may be achieved by simply spoiling the gas-generator exhaust thrust (i.e., $\eta_{GG} = 0$) while providing realistic levels of fan-reverser effectiveness. In fact, increasing the effectiveness of the gas-generator exhaust reverser may not significantly improve the total 4-engine effectiveness, because the more forward projection of the hot gases will result in their ingestion by the outboard engines at a higher speed during the landing roll. It may then be necessary to retard the outboard engines to idle power to prevent their entry into surge. The resultant loss of outboard-engine reverse thrust may neutralize the increased reverser thrust obtained by the more effective gas-generator reversers on the inboard engines.

A spoiler of the simple target-type may be used to deflect the gas-generator exhaust 90 degrees (1.6 rad). However, examination of a target-type reverser for the fan exhaust suggested that obtaining an effectiveness greater than 35 percent would be difficult because of the geometric problems caused by the large diameter. Although mechanically more difficult, a cascade reverser was chosen, to take advantage of its greater effectiveness. A blocker-door arrangement channeling fan-duct flow through a cascade mounted at the duct entrance, in conjunction with a target-type gas-generator spoiler, was chosen. For simplicity, no acoustic treatment was used on the fan-exhaust thrust reverser (Figure I-1).

SUPPRESSOR DESIGN

In order that realistic quiet-engine nacelle weights and dimensions would be used in this integration study, fan inlet and fan exhaust noise suppressors were designed for the quiet engine installation.

Techniques for designing noise-suppression systems to achieve a specified reduction in flyover noise are not well established for existing engines. Design techniques for a noise suppressor for a study engine are even less well established. The criterion specified in the contract was to design a suppressor that would, by means of acoustical treatment of the inlet and fan-exhaust ducts, produce a reduction in perceived noise level (PNL) of 10 PNdB below that produced by a quiet engine fan during the landing approach.

In developing the suppressor design, key parameters were established and some critical assumptions were made. This section explains these design considerations and summarizes the decisions that were made.

DESIGN CONSIDERATIONS

Following are the key parameters considered in the design of the suppressor:

1. The area of the noise source, A_{ns}.

2. The number of rotor blades, B, and the rotational speed, N, of the rotor shaft at a landing-approach power setting.

3. The wave length, λ, of the fundamental blade-passage frequency (BPF).

4. The height, H, of the channel between two treated surfaces.

The noise-reduction goal was specified as 10 PNdB (perceived noise measured in decibels).

The first three parameters were fixed by the design of the engine. The principal item that had to be specified before the design could proceed was the amount of treated area needed to achieve the desired degree of suppression. The total treated area, A_t, that is required depends on the area of the noise source, the principal frequency of the discrete tone that is to be absorbed, and the noise-reduction goal. The design objective of having minimum penalties in weight and aerodynamic performance established the height H and the area A_t.

ASSUMPTIONS

In developing the design, the primary assumption was that the acoustical design charts presented in References I-3 and I-4 would be applicable. These charts were developed from the contractor's experience with lined ducts installed on a low-bypass-ratio turbofan engine (Pratt and Whitney JT3D) and on the results of duct-model transmission-loss tests. The original chart is presented in Figure I-5 in terms of nondimensional channel height, H/λ, as a function of the ratio of "effective" acoustically treated area to the noise-source area, $A_{t_{eff}}/A_{ns}$, for various amounts of noise reduction, PNL. The alternate chart, presented in Figure I-6, rearranged these parameters to simplify the method of estimating the potential noise reduction of various geometrical arrangements. The actual treated area, A_t must be made larger than the "effective" treated area $A_{t_{eff}}$ by a factor that allows for local losses of treated area resulting from manufacturing requirements, proximity of pipes, ducts, accessory equipment, etc.

The applicability of the present design charts to the quiet-engine installation is somewhat uncertain at this time. The spectrum of the noise generated by the quiet-engine fan is expected to be substantially different from that generated by the fan of the JT3D. It is likely that the effectiveness of duct linings will be different, but at present so little is known about the behavior of acoustical linings that it cannot be said whether or not the difference will be important. Another uncertainty in the present assumption concerns the effects of the wakes and thickened boundary layers shed into the inlet guide-vaneless-fan from the acoustically absorptive surfaces placed in the inlet duct. The noise from the fan may be increased by these wakes and boundary layers and thus create a requirement for additional treated area.

NOTES:

1. CHANNEL HEIGHT H MEASURED APPROXIMATELY NORMAL TO SURFACE OF TREATMENT
2. WAVELENGTH λ DETERMINED FROM SPEED OF SOUND c AND FREQUENCY f, $\lambda = c/f$. FOR JT3D ON DC-8, USE c = 1160 FT/SEC (100° F) AND f = 2000 Hz, λ = 1160/2000 = 0.58 FT = 7 IN.
3. "EFFECTIVE" ACOUSTICALLY TREATED AREA DEFINED IN TEXT.
4. NOISE SOURCE AREA: FOR FAN-EXHAUST DUCTS, USE AREA AT INLET TO FAN DUCTS. A_{ns} = 830 SQ IN. = 5.76 SQ FT FOR JT3D. FOR INLET DUCT. USE AREA AT IGV STATION $A_{ns} = \frac{\pi}{4}(51^2 - 17.5^2)$ = 1800 SQ IN. = 12.5 SQ FT FOR JT3D.

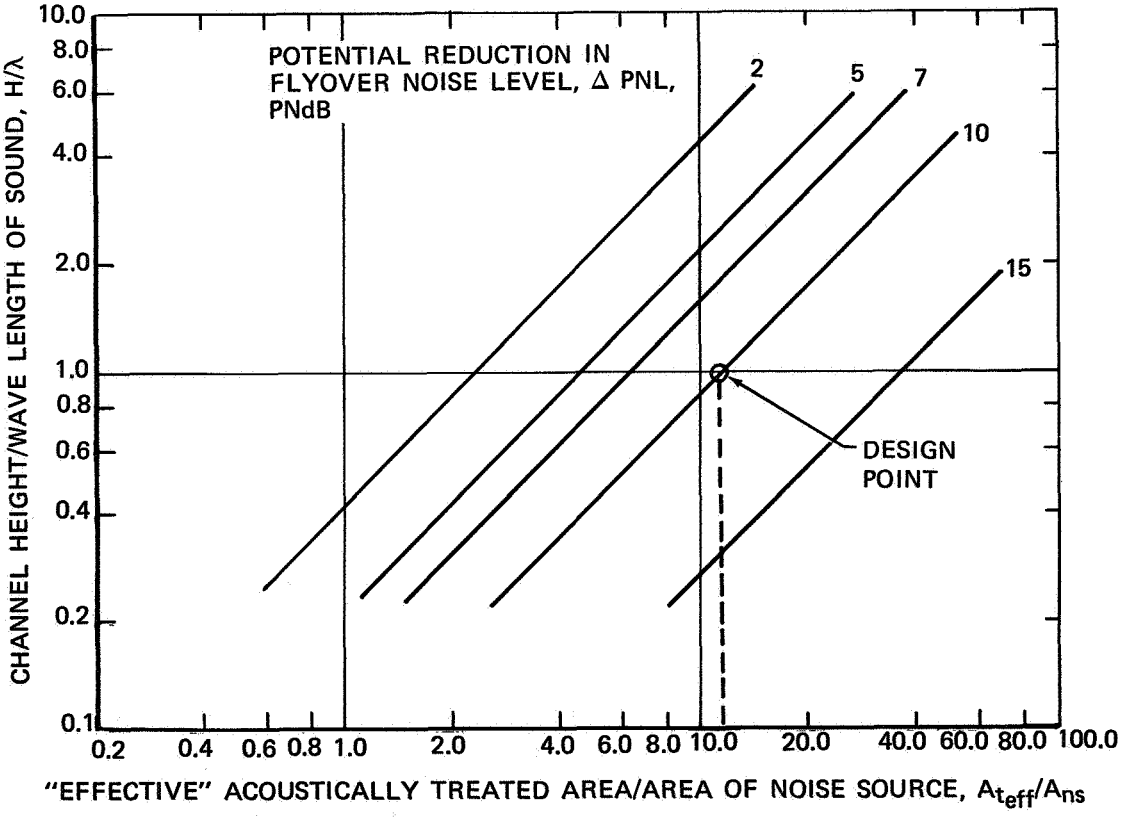

FIGURE I-5. ACOUSTIC DESIGN CHART

The noise-reduction goal was assumed to be in terms of PNL measured outdoors for an aircraft passing directly over a given point on the ground at a relatively low altitude (e.g., 200 to 500 ft – 61 to 152 m) during the landing approach. It was further assumed that the thrust required during landing would be approximately the same with the quiet engine as with the JT3D-3B engines, that is, 5000-pounds-per-engine (122,241 N) net thrust for a typical landing weight for DC-8 Series 50 or DC-8-61 airplanes.

Other critical assumptions were (1) that the flyover PNL for the condition described would be dominated by discrete-frequency noise at the fundamental BPF and harmonics of the fundamental and (2) that the intensity of the BPF noise would be distributed uniformly across the inlet and the fan-exhaust ducts. The first of these assumptions seemed reasonable in light of some preliminary information on the noise output of the Pratt and Whitney JT9D and of the General Electric TF-39, both of which are large high-bypass-ratio turbofan engines somewhat similar to the quiet engine. The assumption of a uniform distribution of BPF noise in the ducts also seemed reasonable because of the great variety of radial, circumferential, and other types of modes that can be excited and because the sound field in the JT3D inlet and fan-exhaust ducts seems to be almost uniform across the ducts at landing power settings.

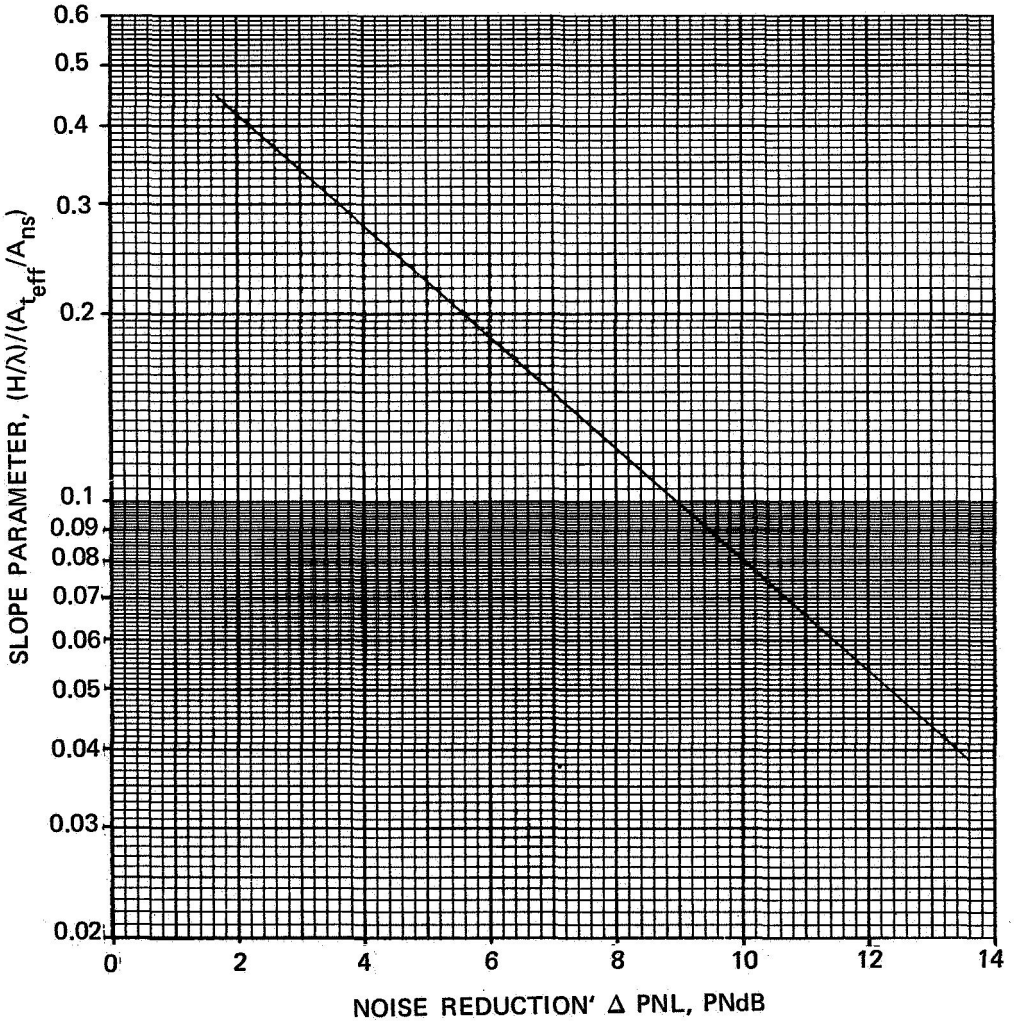

FIGURE I-6. GENERALIZED ACOUSTIC DESIGN CHART

Implicit in the assumption that BPF noise would predominate in the flyover PNL is the further assumption that "combination-tone" noise (i.e., discrete multiple pure tones at integral harmonics of rotor-shaft speed) and broad-band jet-exhaust noise would be 10 PNdB or more below the BPF noise. Combination-tone noise should be eliminated from the landing flyover-noise spectrum of the quiet engine, because the tip Mach number of the fan stage should be subsonic at the assumed landing power setting. Exhaust noise from the hot primary jet would definitely be less than the BPF noise. Other low-frequency broadband noise components from the fan blades were also assumed to be 10 PNdB or more below the BPF noise.

Another assumption, that had great influence on the design approach, was that the contribution of BPF noise radiated from the engine inlet was equal to the BPF noise radiated from the fan-exhaust ducts. This assumption, which was used in determining the peak PNL during a flyover, agrees well with the noise characteristics of the JT9D turbofan engine, as well as those of the advanced-technology engines proposed for the new medium-range three-engine transports.

The assumption of a uniform distribution of noise in the ducts and equal contributions of inlet and fan-exhaust noise requires that both inlet- and fan-exhaust-radiated noise must be reduced by 10 PNdB. To achieve this noise reduction most expeditiously, the duct passageways must be reduced in height, and each of the resultant channels must be designed to produce 10 PNdB, or more, noise reduction. For design purposes, the H/λ value of each channel preferably should be set at values not greater than 1.0. The treated area required in each channel was then selected (Figures I-5 or I-6), with ΔPNL kept constant at 10 PNdB. Increasing the design value of H/λ reduces the aerodynamic design problems of getting air through the channels with minimum losses, but increases the weight and structural problems, because of the larger treated area required. Decreasing the design value of H/λ increases the aerodynamic losses, but reduces the weight and structural problems. A value of approximately 1.0 for H/λ therefore appears to be a reasonable compromise.

DESIGN CHOICES

On the basis of consideration of the preceding parameters and assumptions, an acoustically treated circumferential flow splitter was placed in the fan-exhaust duct, and the inner and outer walls of the duct were acoustically treated. Treated circumferential ring vanes were placed in the inlet, and the cowl wall was treated. No acoustical material was placed on the rotating bullet on the fan in the inlet due to the small amount of surface area available for treatment and potential problems associated with an acoustically treated spinning surface.

The acoustical treatment chosen was a single layer of porous material supported by honeycomb. The single-layer design, with a porous surface material having distributed acoustic resistance and acoustic mass and with acoustic flow resistance that remains almost constant with airflow velocity through the porous surface, was considered adequate.

This type of single-layer acoustical treatment can produce large attenuations over a wide bandwidth, with maximum attenuation occurring at a frequency related to the depth of the cavity behind the porous surface, provided that the honeycomb cells are neither too small nor too large. A broad absorption bandwidth is desirable for the lining to be effective over the range of engine power settings used during landing and to achieve significant reductions in the BPF noise at harmonics of the fundamental BPF. The weight penalty for the treatment was based on an allowance for this type of design and the amount of treated area.

The following values of the parameters were used for the design:

1. A referred speed of the rotor shaft of 2234 rpm (37.23 Hz) during landing approach at 5000-pounds-per-engine (22,241 N) referred net thrust.

2. Fifty-six blades on the single-stage fan.

3. A fundamental BPF of 2090 Hz.

4. A wavelength of the fundamental BPF of 0.55 foot (16.76 cm) for a speed of sound of 1160 feet per second (354 m/sec) in both the inlet and fan-exhaust ducts.

5. An area of 22.4 square feet (2.08 m^2) of noise source at the annular opening ahead of the fan blades and 14.15 square feet (1.31 m^2) at the entrance to the fan-exhaust duct.

6. An area ratio, $A_{t_{eff}}/A_{n_s}$, of 12.3 for $H/\lambda = 1.0$ and $\Delta PNL = 10$ PNdB.

7. A cavity depth of 0.75 inch (1.90 cm) behind the porous surface on the cowl wall and on the inner and outer fan-duct walls.

8. A total thickness of the circumferential flow splitter and ring vanes of 1.1 inches (2.8 cm), consisting of two 0.5-inch-deep (1.27 cm) cavities on either side of a 0.02-inch (0.5 mm) impermeable septum.

9. A nominal honeycomb-cell size of approximately 0.75 inch (1.90 cm).

10. A nominal flow resistance (determined at an airflow velocity of 10 cm/sec) of about 10 rayls uniformly distributed over the treated surface.

The choice of a 10-rayl nominal flow resistance was based on the assumption that the sound-pressure levels of the tones incident on the absorptive surfaces and the Mach numbers of the flow over the surfaces would be comparable to those in the treated inlet and fan-exhaust ducts tested on the JT3D engine (Reference I-4).

Placing the treated circumferential flow splitter in the fan duct resulted in a nominal average H/λ ratio in the fan duct of approximately 0.89, with a treated surface area of 140 square feet (13.00 m^2). With the two treated ring vanes in the inlet, the H/λ ratio in the two channels between the rings was approximately 1.06 and the effective treated area was 275 square feet (25.54 m^2).

STRUCTURAL DESIGN

The diameter of the baseline-quiet-engine nacelle is 84.3 inches (2.14 m), compared with 70.0 inches (1.78 m) for the JT3D-3B nacelle. To avoid high interference drag, the nacelle must be located with the gas-generator-exhaust exit plane forward of the exit-plane location in the present JT3D-3B installation. This position requires a new pylon, which, because of strength requirements, must be an over-the-wing pylon rather than the more aerodynamically efficient cutback pylon.

FLUTTER

The more forward location of the baseline-quiet-engine nacelle results in a much higher value of nacelle-pylon moment of inertia about the wing elastic axis. Consequently, wing flutter considerations may limit the placard speed severely if no wing structural modifications are made. Figure I-7 shows the placard speed that would be required for dive- and cruise-type operation, as well as the typical altitude-speed profile for the DC-8-61. It was concluded that operating the airplane with the restrictions shown would be unacceptable to the operator. Of particular significance was the restriction below 30,000 feet (9144 m) that results when the maximum allowable cruising speed becomes progressively less than 0.82 Mach number as the altitude decreases. Other considerations included a large reduction in allowable descent speed.

On the basis of the foregoing structural considerations, it was concluded that additional wing stiffness might be required and, therefore, should be studied. Local reskinning of the top and bottom of the wing as shown in Figure I-8 appears to be a reasonable method of achieving the additional stiffness. An increase in torsoinal stiffness of approximately 37 percent is achieved with an increase of 0.22 inch (5.58 mm) in the local average skin thickness.

Figure I-9 shows how the wing skins could be spliced. The aerodynamic effects, if any, are not known at this time, but it is not believed that they would present a problem.

Reskinning Considerations

Consideration might be given to crease-forming the new skins to eliminate the skin splice at the aerodynamic break, which is located inboard of the outboard pylon, at the streamwise line callout "original joint retained" in Figure I-8. Consideration also could be given to complete disassembly of the wing at the aerodynamic-break station to permit reskinning of the outer panel in an on-edge position and to provide an additional holding point for the inner wing at the aerodynamic-break bulkhead. The latter requires rejoining of the panels after reskinning and before installing the pylons. There must then be a fill-and-drain operation and subsequent leak test of the wing.

Reskinning of the wing involves a major facility where all of the following operations can be performed:

1. The flaps, ailerons, and pylons can be removed.

2. The wing can be supported in the zero-g position by supporting the fuselage and holding the flap, aileron, and pylon support points.

3. Sixty percent of the wing-box area can be removed from both upper and lower surfaces by cutting the skins at the locations shown on the wing reskinning diagram (Figure I-8).

4. All sealant can be removed from the surfaces where fasteners will be replaced, both spanwise and chordwise.

5. The remnant skins can be tailored at the cut edges to receive the new tapered splice plates.

6. The new skin can be installed, back-drilled from inside the box, and riveted spanwise on both surfaces simultaneously with oversize fasteners.

7. The new pylons can be installed by using assembly fixtures.

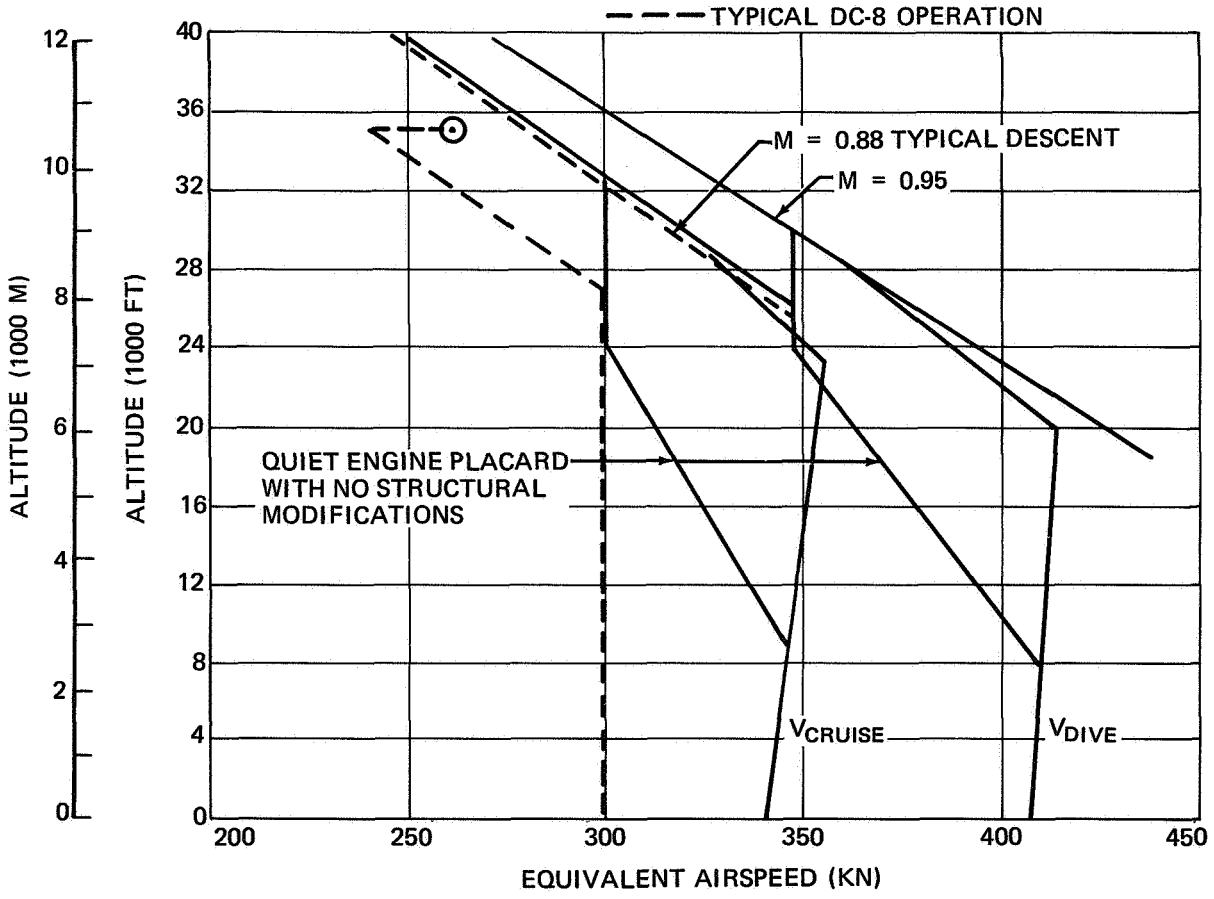

FIGURE I-7. PLACARD SPEEDS – MODEL DC-8-61

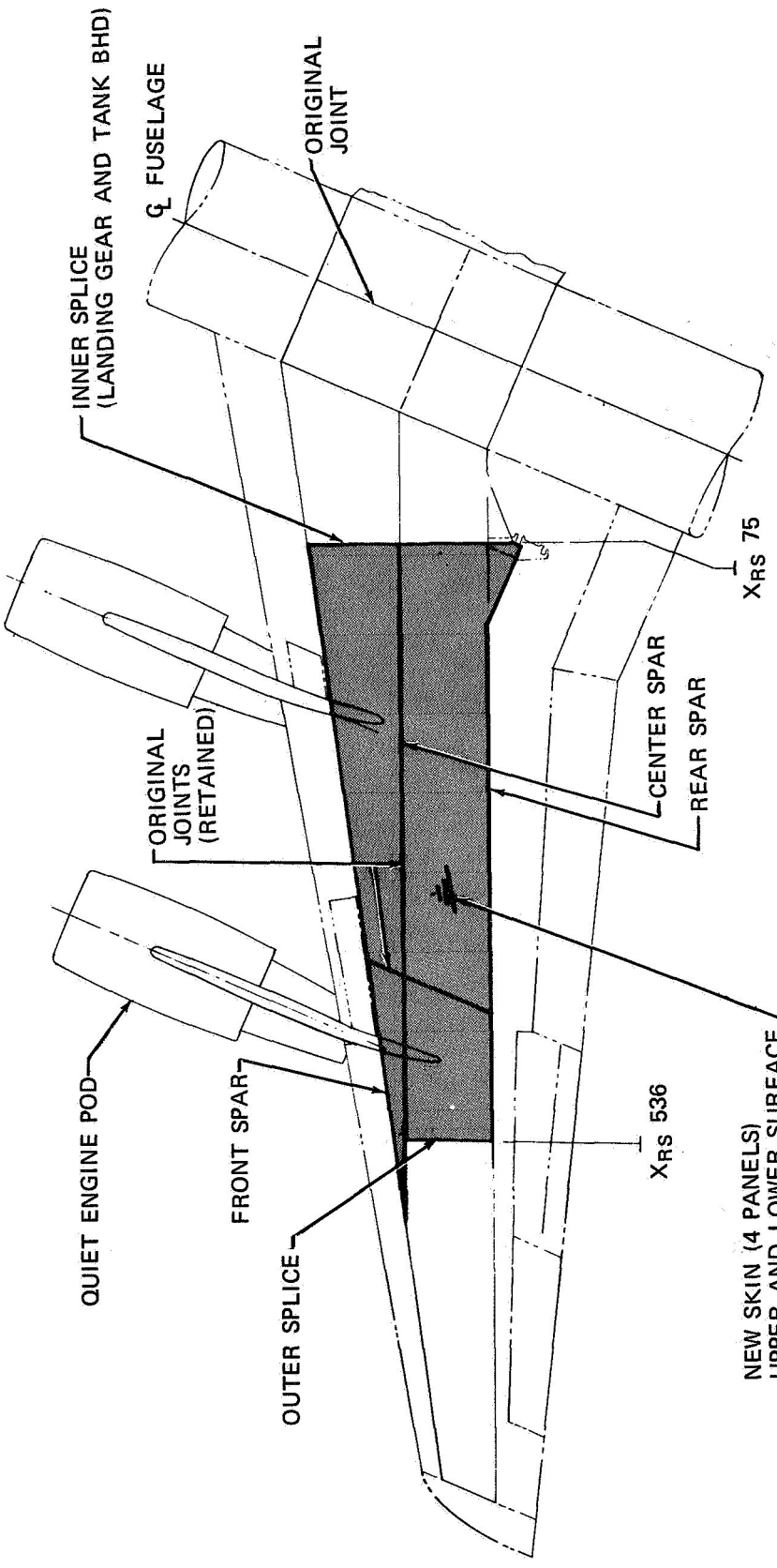

FIGURE I-8. POSSIBLE RESKINNING REQUIREMENT

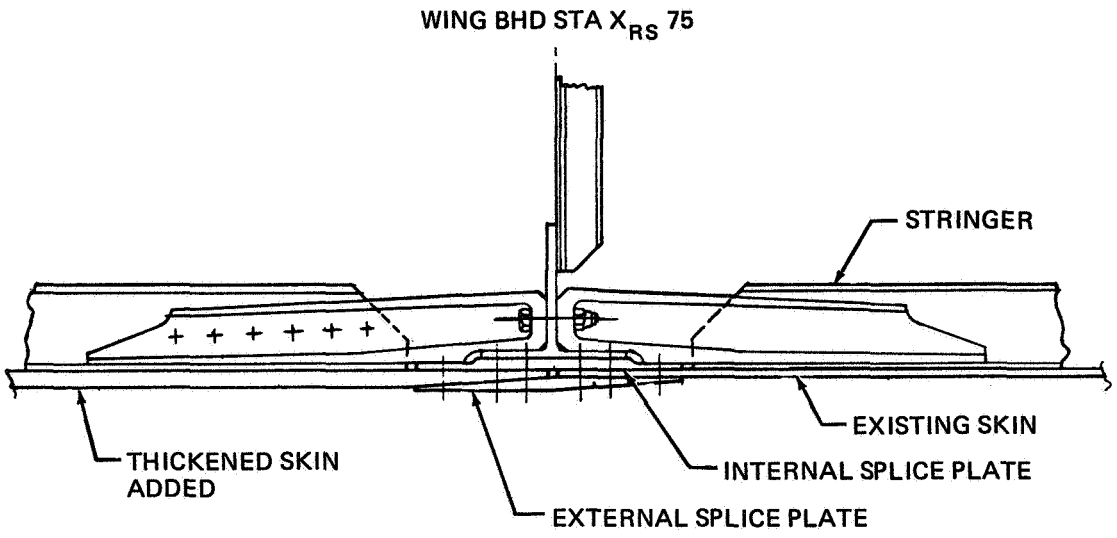

FIGURE I-9. WING RE-SKINNING SPLICE

Pylon

The quiet-engine pylon (Figure I-2) is a three-spar box beam with one spar terminating at the wing upper surface, one at the wing lower surface (both at the wing front spar), and the third spar terminating, via a keel along the pylon trailing edge, at a point midway between the wing front and rear spars. The lower spar, a titanium firewall, acts as a system interface for engine removal. The pylon side skins, which are stiffened fore and aft for lateral stability, penetrate the wing leading edge without attachment. There is an aerodynamic seal at this junction. The pylon leading edge is hinged for system access. The pylon skins within the wing have lightening holes for systems traverse.

The pylon apron (that portion of the nacelle affixed to the pylon) supports the thrust reverser and aft-cowl door hinges. The engine mounting system preferred is the JT3 link system with the load mounting points reversed on the engine; that is, the forward flanges take only vertical and side load and accommodate engine expansion, and the aft flanges take vertical, side, torque, and thrust loads.

If, for wing-pylon dynamic considerations, it becomes necessary to provide increased pylon flexibility during normal cruise operation, a slip joint or other lost-motion device will be used in the intermediate pylon structure to reduce the vertical bending stiffness.

REFERENCES

I-1. Pratt & Whitney Aircraft, *Preliminary Performance Estimates of the QB-3 Turbofan Study Engine,* TDM-2128, dated December 18, 1967.

I-2. Thompson, J.D., *Thrust Effectiveness on High Bypass Ratio Fan Powerplant Installations,* Douglas Paper 4059, October 1966.

I-3. Anon., *Study and Development of Turbofan Nacelle Modifications to Minimize Fan-Compressor Noise,* Quarterly Progress Report No. 1, Douglas Report DAD-61535, August 1967.

I-4. Pendley, R. E., *Design Concepts*, Conference on Progress of NASA Research Relating to Noise Alleviation of Large Subsonic Jet Aircraft, NASA SP-189, 1968.

TASK II

PARAMETRIC PERFORMANCE STUDY

LIST OF ILLUSTRATIONS

LIST OF ILLUSTRATIONS (Continued)

LIST OF TABLES

TASK II

PARAMETRIC PERFORMANCE STUDY

The primary purpose of Task II was to determine the performance of the selected DC-8 model powered by the baseline quiet engine and to compare it with that of the DC-8-61 powered by the JT3D-3B. In addition, Task II required the development of trade factors that show how parametric changes in quiet-engine characteristics affect aircraft performance.

DC-8-61 PERFORMANCE WITH THE JT3D-3B ENGINE

Table II-1 is a weight statement for the DC-8 model selected for this study. The maximum design takeoff weight, zero fuel weight, and landing weights are FAA limiting weights. The operational empty weight (OEW or OWE) includes the items the operator requires.

PAYLOAD

The selected DC-8 model is a passenger airplane and as such does not operate with a weight-limited payload. (A weight-limited payload is typical only of all-cargo operation.) The maximum payload considered for passenger service is space-limited and includes a full, mixed-class passenger load (193 passengers) with the entire cargo space beneath the floor filled with cargo having a density of 10 pounds per cubic foot (159 kg/m^3).

A survey showed that a more typical payload, hereafter referred to as the normal payload, consists of 193 passengers with baggage and a nominal cargo load. Each passenger is assumed to weigh 165 pounds (75 kg), and his baggage is assumed to weigh 35 pounds (16 kg). The cargo volume is based on using 25 percent of the space available after subtracting a 25-percent stacking loss (625 cubic feet – 18 m^3) and baggage space equal to 4.5 cubic feet (0.127 m^3) per passenger (868 cubic feet – 25 m^3). A cargo density of 10 pounds (5 kg) per cubic foot is assumed. On this basis, the passengers and baggage weigh 38,600 pounds (17,509 kg) and the cargo weighs 2516 pounds (1141 kg), for a total payload of 41,116 pounds (18,650 kg).

The normal payload is used as a basis for the Task II study, although some space-limited performance is also shown.

TABLE II-I
JT3D-3B ENGINES DC-8-61 WEIGHT STATEMENT

	WEIGHT			
	LB	KG	LB	KG
MAX DESIGN TAKEOFF WEIGHT			325,000	147,420
MAX DESIGN ZERO FUEL WEIGHT			224,000	101,606
MAX DESIGN LANDING WEIGHT			240,000	108,864
OPERATIONAL EMPTY WEIGHT			156,803	71,126
MANUFACTURER'S EMPTY WEIGHT	149,339	67,740		
OPERATIONAL ITEMS	7,464	3,386		
SPACE-LIMITED PAYLOAD			56,845	25,785
PASSENGERS (193 AT 165 LB – 75 KG)	31,845	14,445		
BAGGAGE AND CARGO	25,000	11,340		
NORMAL PAYLOAD			41,116	18,650
PASSENGERS (193 AT 165 LB – 75 KG)	31,845	14,445		
BAGGAGE (35 LB – 16 KG/PASSENGER)	6,755	3,064		
CARGO (251.6 CU FT AT 10 LB/CU FT – 7.36 CU M^3 AT 159 KG/M^3	2,516	1,141		

PERFORMANCE SOURCE

The airplane performance shown is based on flight-test results. The engine performance is based on test-stand and flight-test results for engines with the Douglas production inlet hardware and exhaust-system hardware installed. The performance shown is the same as that presented in the FAA-approved flight manual and in the Douglas performance report for the DC-8-61 airplane. Engine installation losses are shown in a later section.

AIRPLANE PERFORMANCE

Figures II-1 through II-8 include the airplane performance, as required in Task II, for the present DC-8-61. The resulting direct operating cost (DOC) data are covered in a later section.

Payload-Range

Figure II-1 shows the payload-range curve. For ranges less than those corresponding to Maximum Design Takeoff Gross Weight (Max TOGW), the payload is constant. The airplane is operated at 0.82 Mach number for these ranges, because the operators prefer to fly fast and pay the resulting penalty in specific range. For ranges corresponding to Max TOGW, the operators prefer to fly at the speed for nearly optimum specific range to reduce the fuel load and increase the payload. They therefore must fly slower. Figure II-2 shows the specific-range curve for the airplane at 35,000 feet (10,668 m) and illustrates the magnitude of specific-range penalties for nonoptimum operation. Figure II-3 shows the variation in TOGW and initial cruise weight (ICW) with range.

Takeoff Field Length

Figure II-4 shows the variation in FAA takeoff field length with airplane gross weight for two values of flap setting. FAA field length is based on four-engine operation and is defined as 1.15 times the distance measured from the start of roll to the point where the airplane is 35 feet (11 m) above the runway.

Initial Cruise Altitude

The highest altitude at which the airplane can safely cruise at 0.82 Mach number is shown as a function of gross weight in Figure II-5. The curve includes a margin for maneuvering before buffet onset.

Takeoff Flight Path

The takeoff flight path is an important parameter, since it directly affects the flyover noise level. Figures II-6 and II-7 show how flyover height is affected by airplane gross weight and distance during takeoff. Two flap angles are shown.

APPROACH NET THRUST AND AIRSPEED

The approach airspeed and corresponding net thrust required during approach are shown in Figure II-8 as functions of gross weight.

As is noted on the curve, the data are shown for sea-level altitude and at 1.3 times stall airspeed with full flaps. These data are important because the intensity of the approach noise depends on the thrust required and because the duration of the noise depends on the airspeed.

NOTE:
1. OWE = 156,803 LB (71,126 KG)
2. FAR 121.645 RESERVES
   200 N MI TO ALTERNATE
3. 193 PASSENGERS PLUS
   9271 BAGGAGE AND CARGO
4. STEP ALTITUDE CRUISE AT 0.82
   MACH NUMBER FOR RANGES
   SHORTER THAN INDICATED BY○.
5. STEP ALTITUDE CRUISE AT 99%
   MAXIMUM NAUTICAL MILES PER
   POUND FOR RANGES LONGER
   THAN INDICATED BY□.

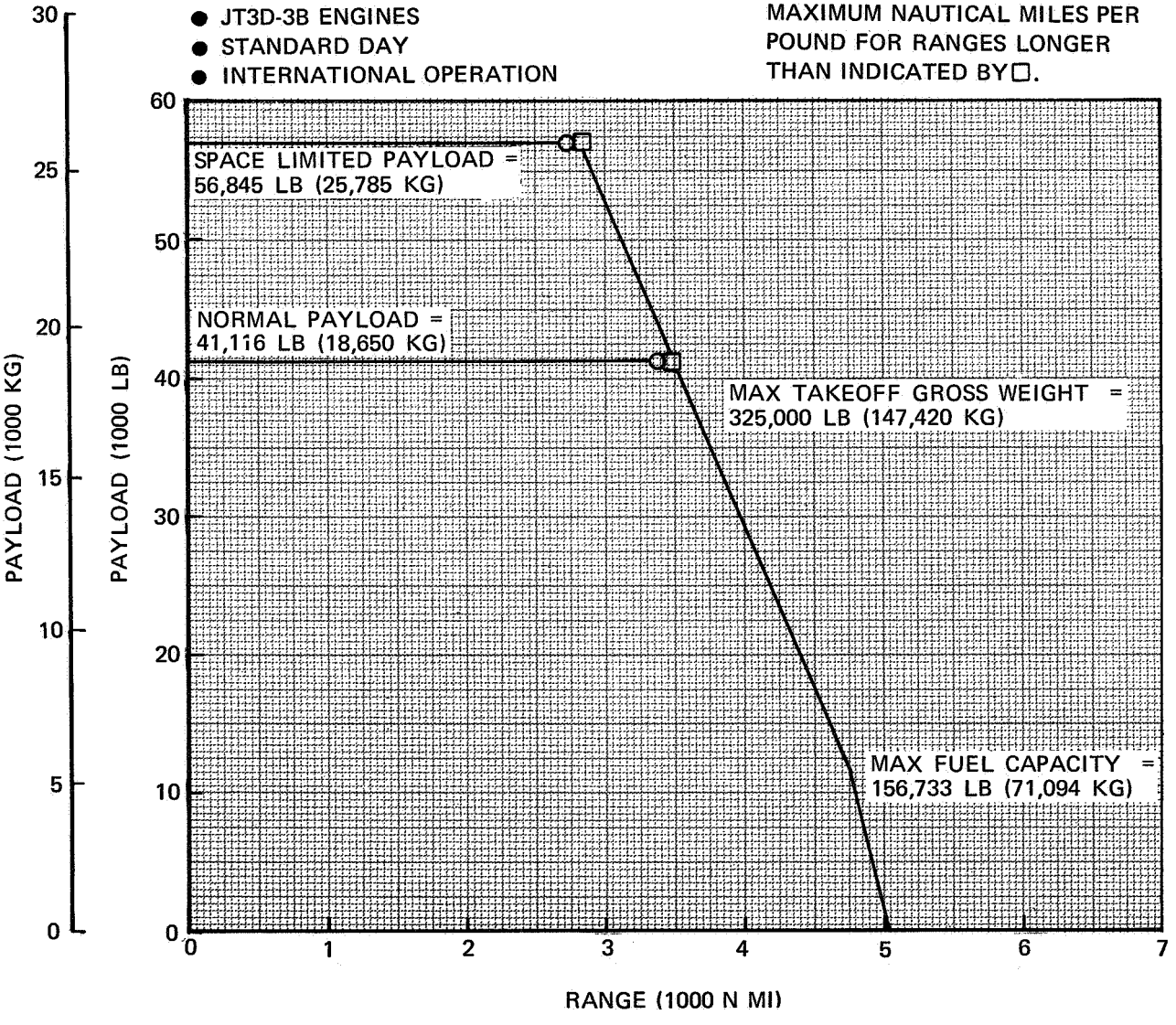

FIGURE II-1. PAYLOAD-RANGE CAPABILITIES – MODEL DC-8-61

- JT3D-3B ENGINES
- PRESSURE ALTITUDE = 35,000 FT (10,668 M)
- STANDARD TEMPERATURE = −54.3°C
- 4% LEADING EDGE EXTENSION
- FOUR-ENGINE OPERATION

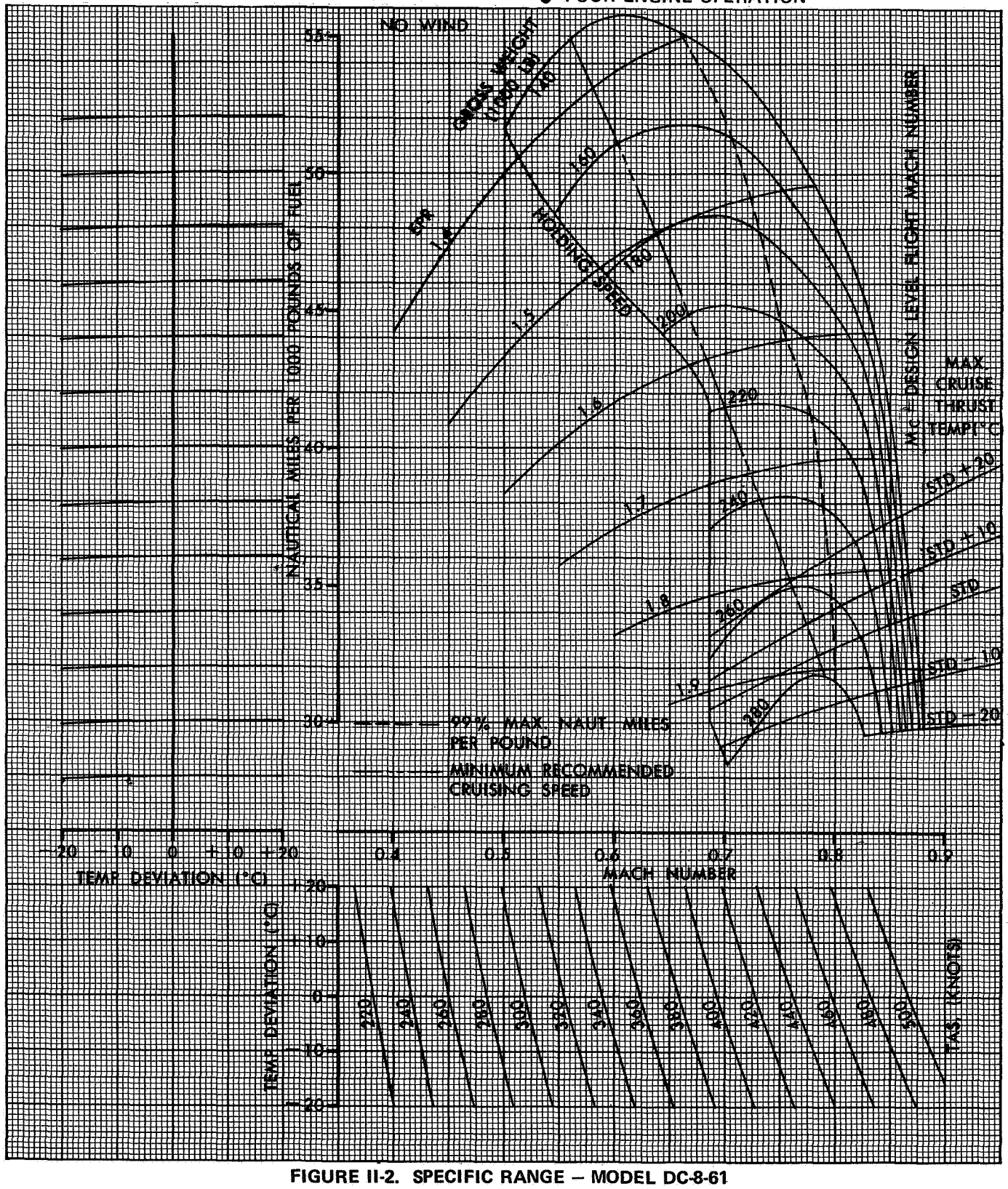

FIGURE II-2. SPECIFIC RANGE – MODEL DC-8-61

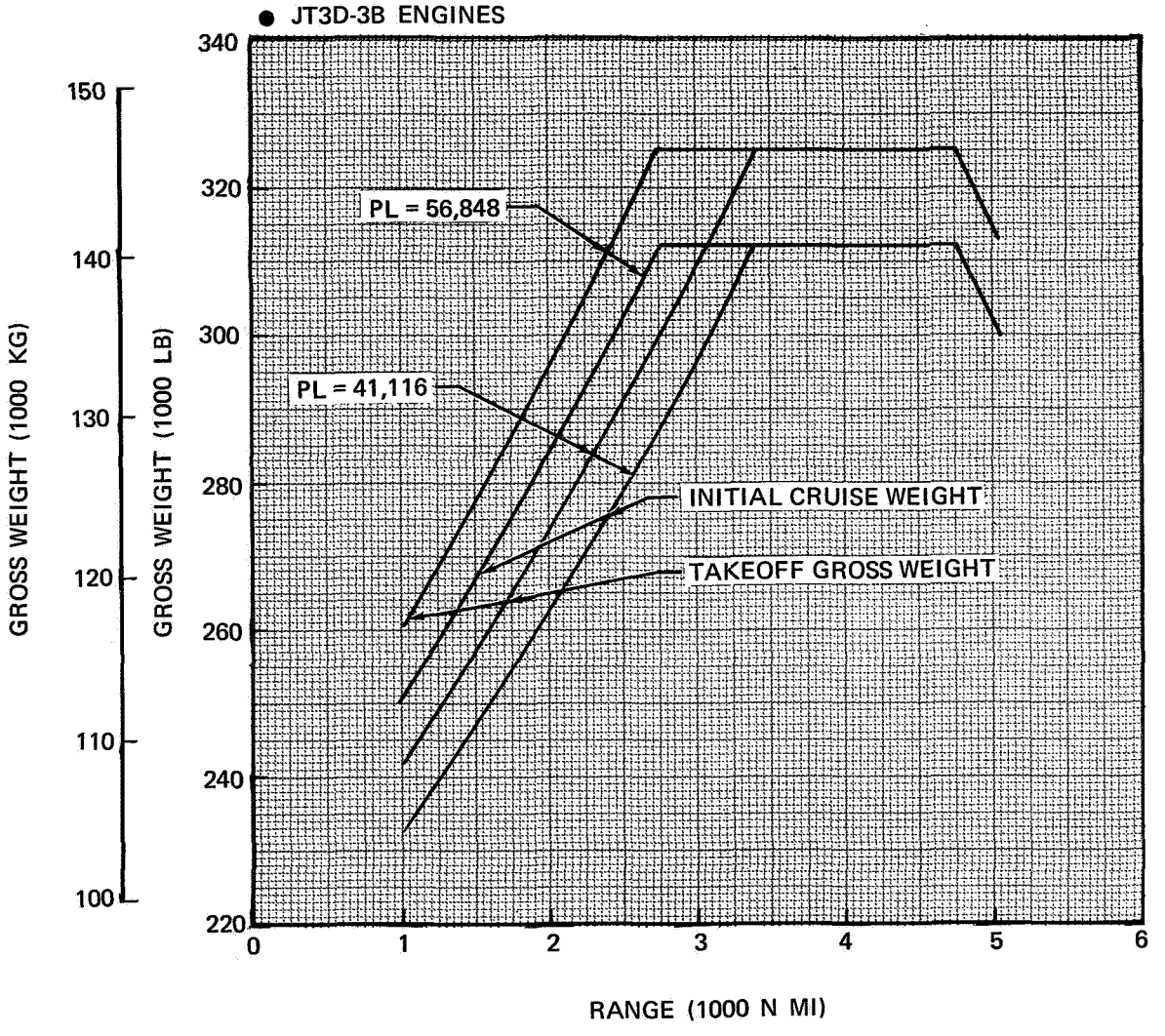

FIGURE II-3. AIRPLANE WEIGHT – MODEL DC-8-61

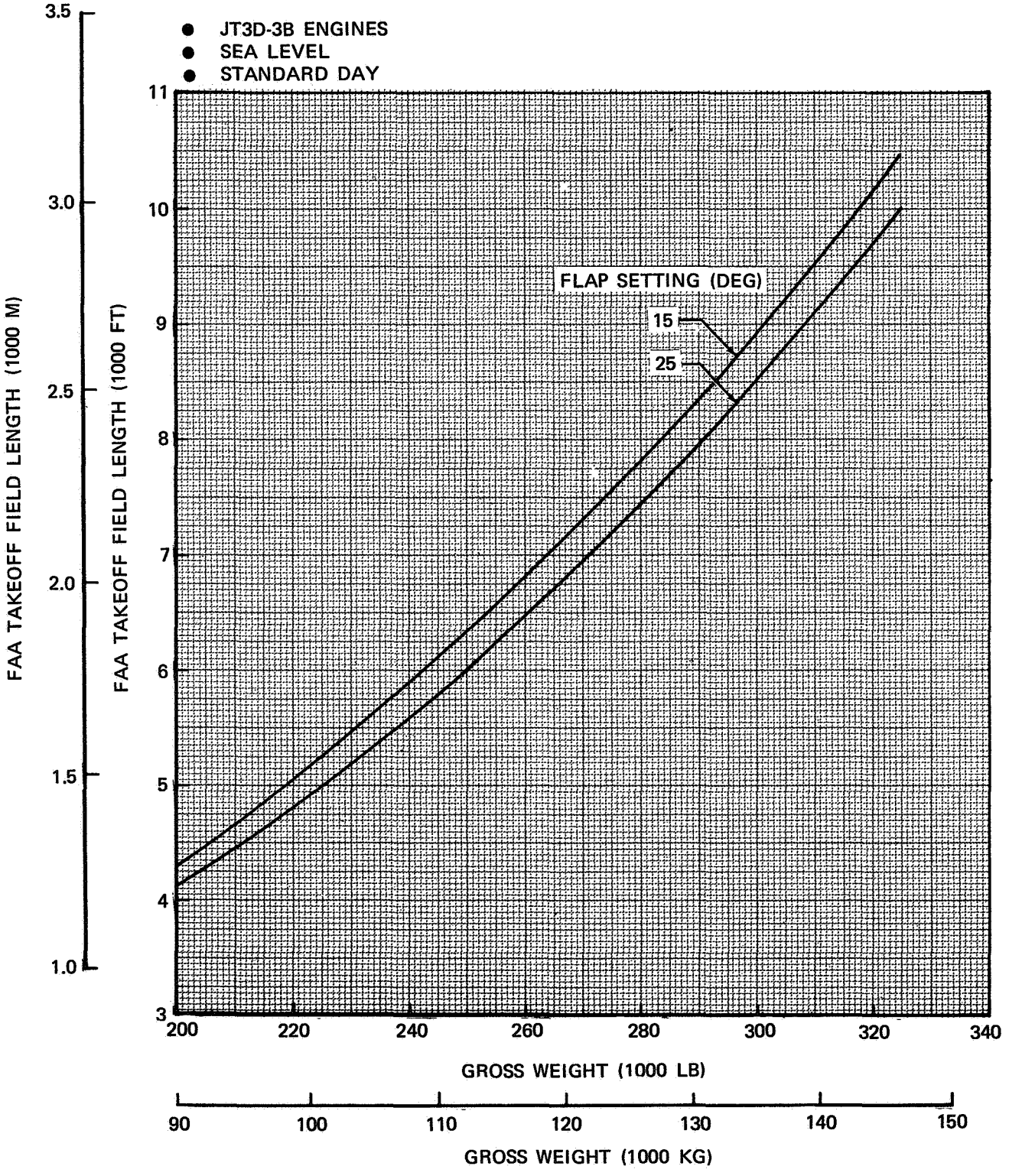

FIGURE II-4. FAA TAKEOFF FIELD LENGTH – MODEL DC-8-61

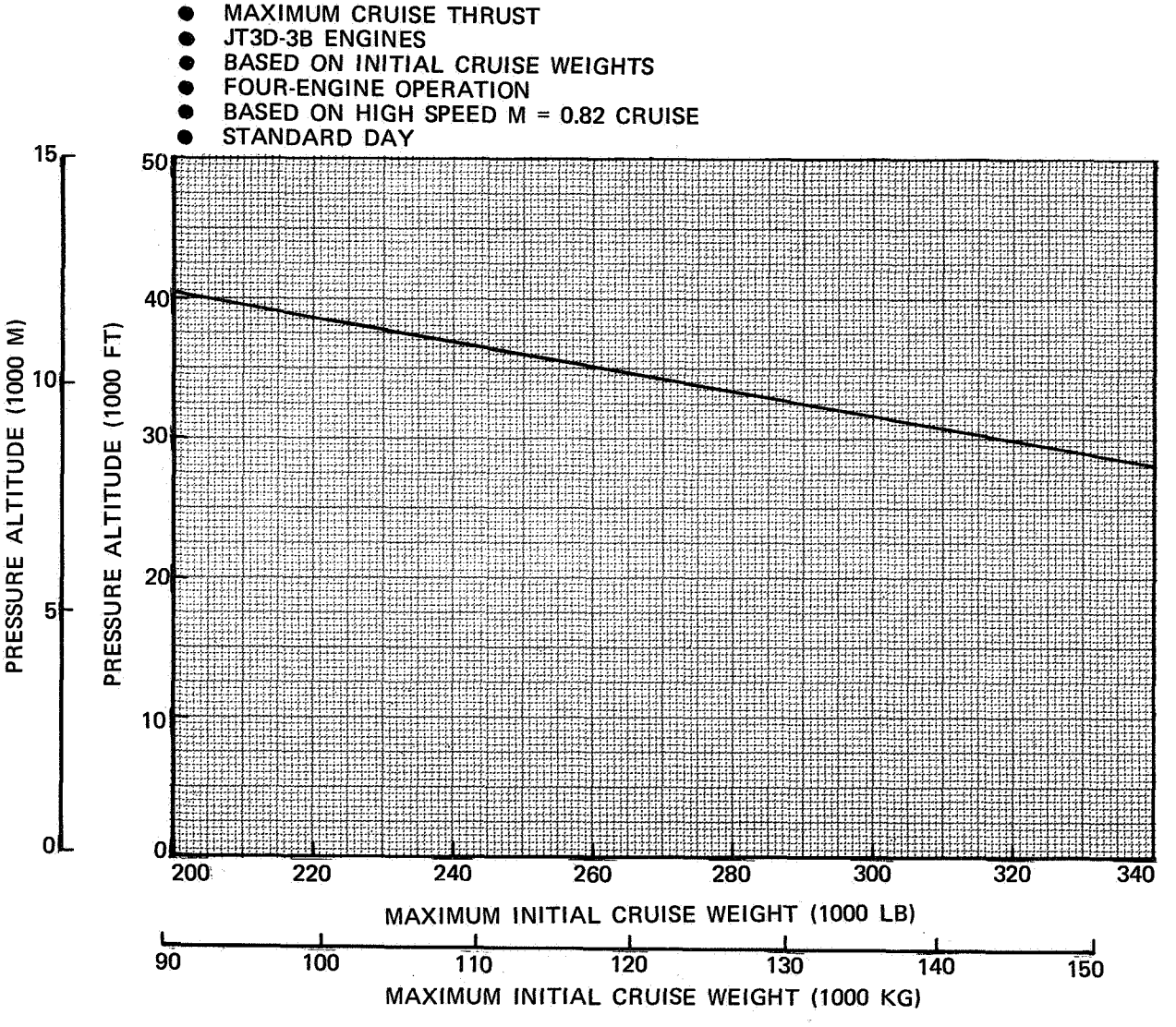

FIGURE II-5. MAXIMUM RECOMMENDED INITIAL CRUISE ALTITUDE – MODEL DC-8-61

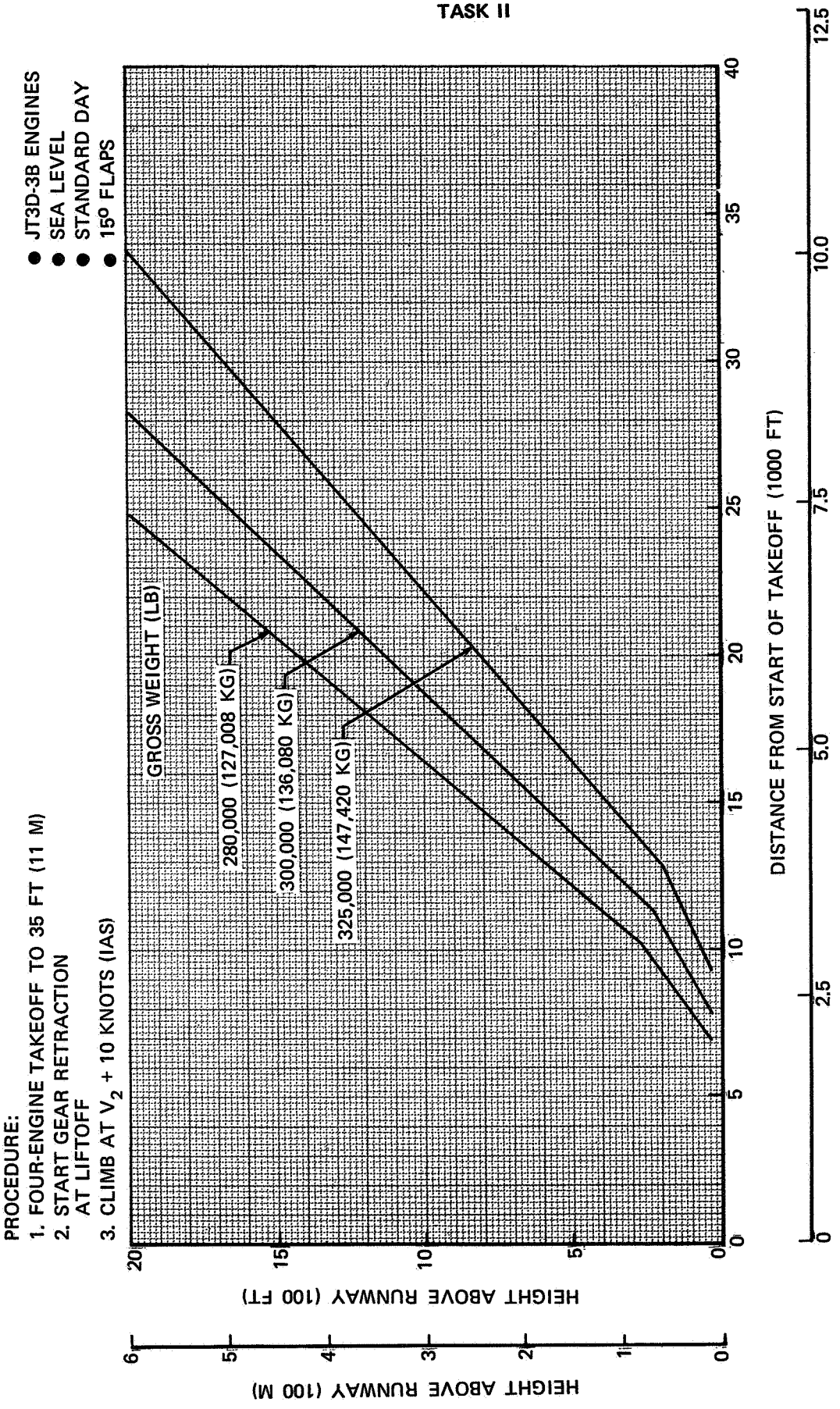

FIGURE II-6. FOUR-ENGINE FLIGHT PATH, 15° FLAPS – MODEL DC-8-61

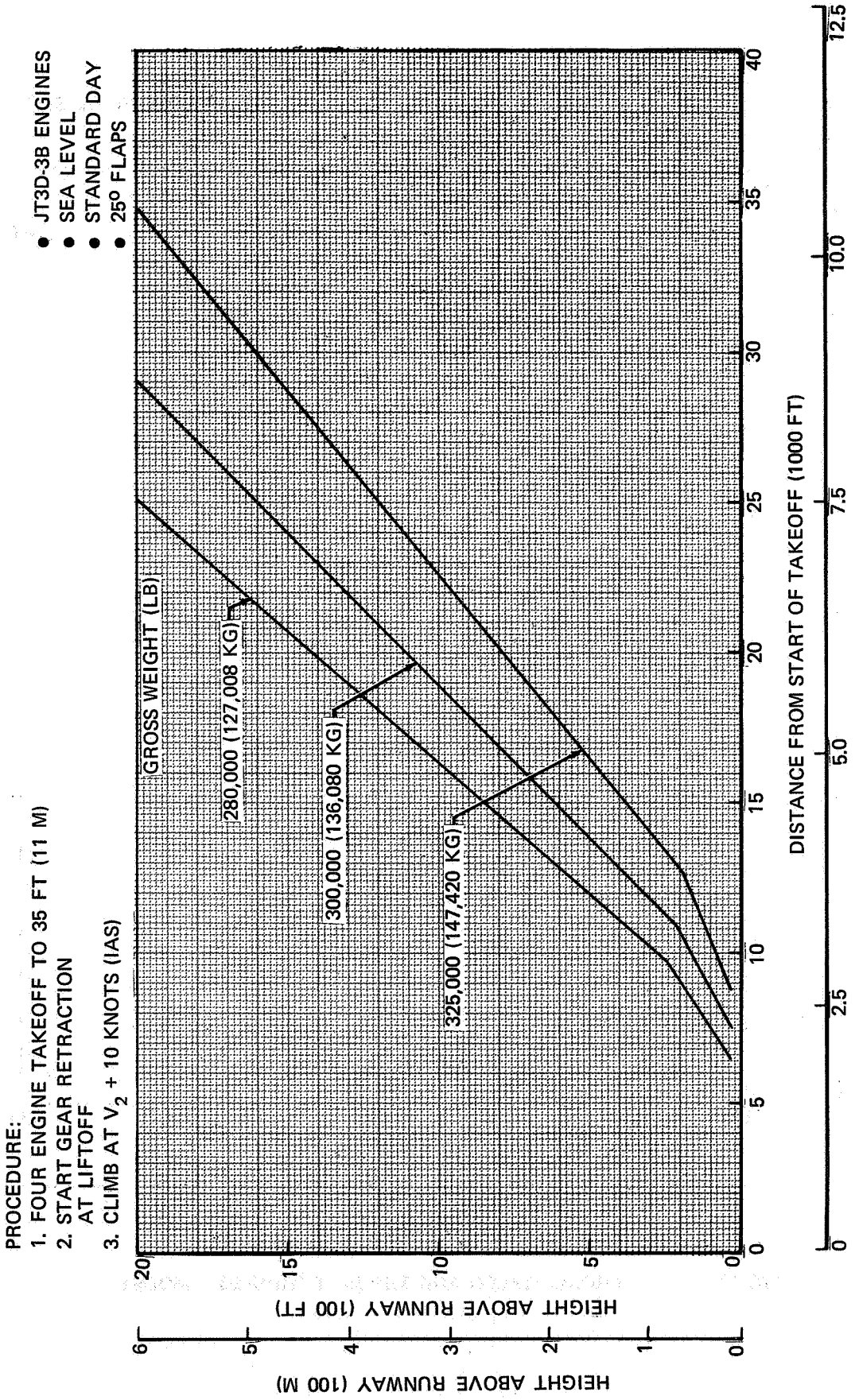

FIGURE II-7. FOUR-ENGINE FLIGHT PATH, 25°FLAPS – MODEL DC-8-61

- JT3D-3B ENGINES
- SEA LEVEL
- STANDARD DAY
- FLAPS FULL DOWN
- 1.3 V_{STALL}
- 2.75 DEGREE GLIDE SLOPE

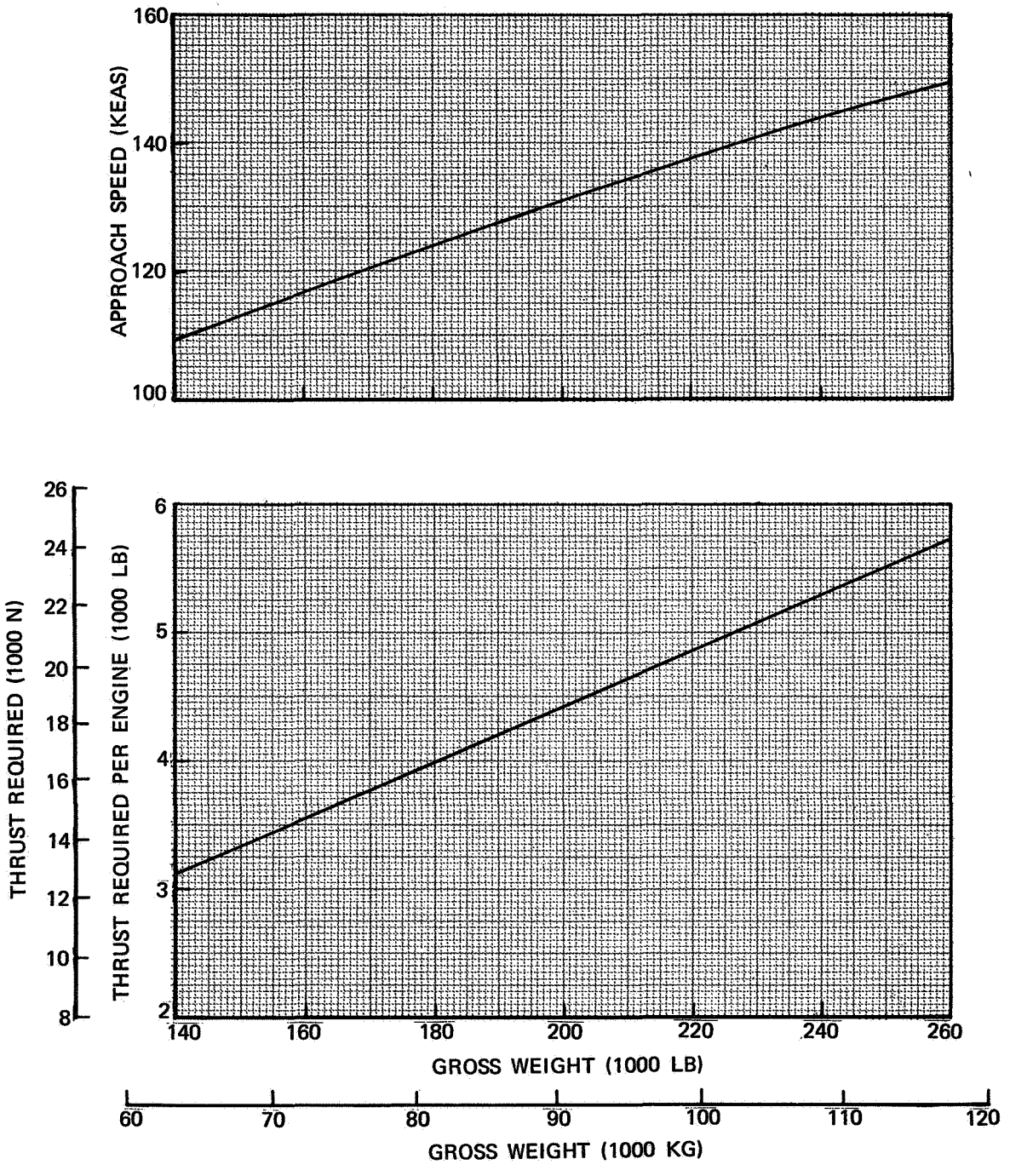

FIGURE II-8. APPROACH SPEED AND THRUST REQUIRED – MODEL DC-8-61

DC-8-61 PERFORMANCE WITH THE BASELINE QUIET ENGINE

This section presents the performance of the DC-8-61 with the baseline quiet engine. The model is designated DC-8-61-Q1.

PERFORMANCE CALCULATION METHOD

The performance of the DC-8-61-Q1 was obtained by calculating (by consistent methods) the differences between the installed performance of the quiet engine and that of the JT3D-3B and by then applying these differences to the performance of the JT3D-3B equipped DC-8-61. The effects of changed nacelle-pylon drag were included. Changes in OWE resulting from the addition of the quiet engine were also accounted for. Baseline quiet-engine performance was obtained from Pratt and Whitney data for the QB-3 study engine, which resulted from the NASA Quiet Engine Definition Programs. Installation correction factors were based on JT9D-1 data.

INSTALLED-ENGINE PERFORMANCE CALCULATION

The nacelle-pylon drag was calculated for both the present JT3D-3B and the quiet-engine installations by Douglas IBM program G3VA. The drag values were then subtracted from the QB-3 specification values of thrust and from the JT3D-3B flight-test values of thrust. Installation losses were also calculated for the quiet-engine installation for the inlet and exhaust systems, airbleed, shaft-power extraction, nacelle cooling, and leakage through the cascade reverser. These losses were not applied to the JT3D-3B performance, because the installation effects are already included in the flight-test engine performance.

INSTALLATION LOSSES

Table II-II shows a comparison of the installation losses for the JT3D-3B and for the baseline quiet engine. The JT3D-3B values shown were calculated with the engine-specification data and installation-handbook correction factors.

1. Inlet and Exhaust System

   The total-pressure losses resulting from acoustic treatment in the inlet and exhaust ducts were determined analytically by calculating the drag of the internal surfaces and then equating that drag to an equivalent total-pressure change. Wind-tunnel tests at Douglas show that typical acoustically treated surfaces are approximately 40 percent rougher than smooth aluminum. The resulting friction factor of 0.0039 was the value used for these calculations.

2. Airbleed and Shaft-Power Extraction

   DC-8-61 values of airbleed and shaft-power extraction were used. JT9D-1 low-pressure bleed-correction factors were used.

3. Nacelle Cooling

   Fan bleed was assumed for cooling the accessories and engine compartment. No thrust recovery is assumed for exhausting the flow overboard.

4. Thrust-Reverser Leakage

Analysis shows that the leakage that can be expected through the reverser cascade causes a loss of 0.135 percent of fan gross thrust. This value has been used to account for thrust-reverser leakage.

5. Nacelle-Pylon Drag

Table II-II shows that the fractional loss in net thrust due to drag is higher for the JT3D-3B than for the baseline-quiet-engine installation. Table II-III shows the drag breakdowns for the two installations. The large inlet cowl for the quiet-engine installation is the cause of a sizable drag increase relative to the JT3D-3B installation: 0.8356 square feet (0.0776 m^2) compared with 0.6481 square feet (0.0602 m^2). This is in part compensated for by the higher fan-exhaust scrubbing drag of the JT3D-3B installation: 0.6884 square feet (0.0639 m^2) compared with 0.5931 square feet (0.0550 m^2). The wetted surface area for the JT3D-3B is higher because the length of the gas-generator nacelle is greater and because the fan exhaust is ducted through a channel having a large wetted area. Although the absolute value of drag, D/q_o, is greater for the quiet-engine installation, that installation is more efficient and has a lower value of drag relative to thrust. This is also shown in Table II-III.

Until the wind-tunnel tests required in Task III were run, it was not possible to know whether or not the quiet-engine installation had any interference drag. For that reason, drag calculations in Task II do not include interference.

TABLE II-II
COMPARISON OF INSTALLATION LOSSES,
MAX CRUISE POWER (35,000 FT – 10,668 M; M = 0.82)

	BASELINE QUIET ENGINE		JT3D-3B*	
	$\Delta F_n/F_n$	$\Delta W_F/W_F$	$\Delta F_n/F_n$	$\Delta W_F/W_F$
INLET	0.0262	0.0109	0	0
FAN EXHAUST	0.0038	0	0	0
AIRBLEED	0.0320	0.0164	0.0238	0.0175
SHAFT POWER	0.0041	0.0010	0.0030	0.0010
NACELLE COOLING	0.0080	0	NEGLIGIBLE	0
THRUST-REVERSER LEAKAGE	0.0028	0	0.0013	0
TOTAL DRAG	0.0953	0	0.0975	0
FAN COWL	0.0612	0	0.0593	0
SCRUBBING	0.0341	0	0.0382	0
TOTAL LOSSES	0.1722	0.0283	0.1256	0.0185

*ASSUMES THE SAME CALCULATION METHOD AS FOR THE BASELINE QUIET ENGINE.

TABLE II-III
NACELLE AND PYLON DRAG COMPARISON

	FREE STREAM		FAN JET		CORE JET	
	COWL	PYLON	NACELLE	PYLON	NACELLE	PYLON
WETTED AREA-SQ FT						
JT3D-3B	198	68	87	0	0	0
Q/E	278	59	78	12	0	0
COMPONENT DRAG D/q_o						
SKIN FRICTION						
JT3D-3B	0.5154	0.1637	0.4731	0	0	0
Q/E	0.6576	0.1376	0.3995	0.670	0	0
ROUGHNESS						
JT3D-3B	0.0392	0.0127	0.0806	0	0	0
Q/E	0.0508	0.0106	0.0679	0.0151	0	0
PRESSURE						
JT3D-3B	0.0935	0.3029*	0.0859	0	0	0
Q/E	0.1232	0.3026*	0.0748	0.0013	0	0
BASE						
JT3D-3B	0	0	0.0488	0	0.0375	0
Q/E	0	0	0.0491	0	0.0388	0
TOTAL						
JT3D-3B	0.6481	0.4783	0.6884	0	0.0375	0
Q/E	0.8356	0.4508	0.5931	0.0834	0.0388	0

*INCLUDES 0.3 SQ FT FOR OVER-THE-WING-PYLON PENALTY

MAX CRUISE POWER
35,000 FT (10,668 M)
0.82 M_o

TOTAL CRUISE DRAG		
	JT3D-3B	Q/E
TOTAL D/q_o	1.853	1.996
D/F_n	0.0976	0.0953

WEIGHT STATEMENT

Table II-IV shows how the airplane OWE would be changed by installing the quiet engine.

Table II-V shows the weight statements for the DC-8-61-Q1 and DC-8-61 airplanes. The DC-8-61-Q1 Max Design Zero-Fuel Weight corresponding to space-limited payload exceeds the present FAA-certified value of 224,000 pounds (101,606 kg) by 812 pounds (368 kg). Analysis has not been conducted to determine whether the wing is strong enough to accept this increase with no modification. However, it is expected that such an analysis would show that the airplane can be certified with the additional zero-fuel weight.

AIRPLANE PERFORMANCE

Figures II-9 through II-14 show the aerodynamic performance of the DC-8-61-Q1. The direct operating cost for the airplane is shown in a later section. Except for the approach airspeed and thrust required, the data shown are for the same performance parameters presented earlier for the DC-8-61 with the JT3D-3B engine. The approach airspeed is the same for the DC-8-61-Q1 and the DC-8-61. The installed thrust required also will be the same, because the nacelle-pylon drag is included in the installation losses.

TABLE II-IV
WEIGHT-CHANGE SUMMARY

	WEIGHT REMOVED		WEIGHT ADDED		Δ WEIGHT	
	LB	KG	LB	KG	LB	KG
ENGINE AND NACELLE INBD	6893	3127	8509	3860	+1616	+733
ENGINE AND NACELLE INBD	6893	3127	8509	3860	+1616	+733
ENGINE AND NACELLE OUTBD	6837	3101	8453	3834	+1616	+733
ENGINE AND NACELLE OUTBD	6837	3101	8453	3834	+1616	+733
PYLON INBD	798	362	893	405	+95	+43
PYLON INBD	798	362	893	405	+95	+43
PYLON OUTBD	808	367	898	407	+90	+41
PYLON OUTBD	808	367	898	407	+90	+41
AILERON INBD	650	295	690	313	+40	+18
AILERON INBD	650	295	690	313	+40	+18
AILERON OUTBD	477	216	602	273	+125	+57
AILERON OUTBD	477	216	602	273	+125	+57
WING						
LOWER SURFACE	2032	922	4032	1829	+2000	+907
UPPER SURFACE	1900	862	3900	1769	+2000	+907
TOTAL PER AIRPLANE					+11,164	+5064

TABLE II-V
WEIGHT STATEMENT

	DC-8-61 (JT3D-3B)				DC-8-61-Q1 QUIET ENGINE			
	LB	KG	LB	KG	LB	KG	LB	KG
MAXIMUM DESIGN TAKEOFF WEIGHT			325,000	147,420			325,000	147,420
MAXIMUM DESIGN ZERO FUEL WEIGHT			224,000	101,606			224,812	101,975
MAXIMUM DESIGN LANDING WEIGHT			240,000	108,864			240,000	108,864
OPERATIONAL EMPTY WEIGHT			156,803	71,126			167,967	76,190
MANUFACTURER'S EMPTY WEIGHT	149,339	67,740			160,503	72,804		
OPERATIONAL ITEMS	7,464	3,386			7,464	3,386		
SPACE-LIMITED PAYLOAD			56,845	25,785			56,845	25,785
PASSENGERS (193 AT 165 LB – 75 KG)	31,845	14,445			31,845	14,445		
BAGGAGE AND CARGO	25,000	11,340			25,000	11,340		
NORMAL PAYLOAD			41,116	18,650			41,116	18,650
PASSENGERS (193 AT 165 LB – 75 KG)	31,845	14,445			31,845	14,445		
BAGGAGE (35 LB/PASSENGER)	6,755	3,064			6,755	3,064		
CARGO (250 CU FT AT 10 LB/CU FT – 7 CU M AT 160 KG/CU M)	2,516	1,141			2,516	1,141		

NOTE:

1. OWE = 167,967 LB (76,190 KG)
2. FAR 121.645 RESERVES
   200 N MI TO ALTERNATE
3. 193 PASSENGERS PLUS
   9271 LB (4,205 KG) BAGGAGE AND CARGO
4. STEP ALTITUDE CRUISE AT 0.82 MACH NO.
   FOR RANGES SHORTER THAN INDICATED BY
5. STEP ALTITUDE CRUISE AT 99% MAXIMUM
   NAUTICAL MILES PER POUND FOR RANGES
   LONGER THAN INDICATED BY

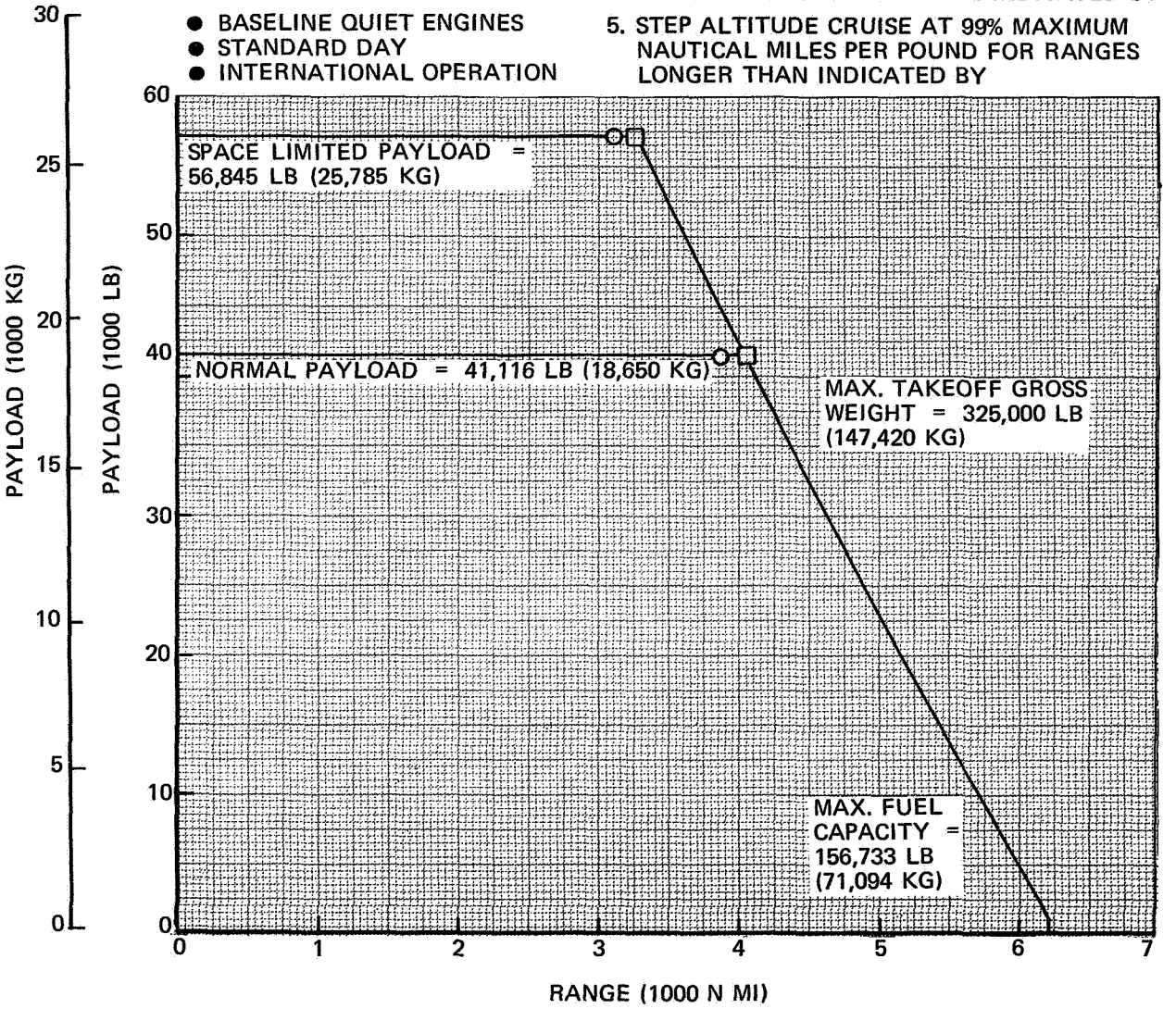

FIGURE II-9. PAYLOAD-RANGE CAPABILITIES – MODEL DC-8-61-Q1

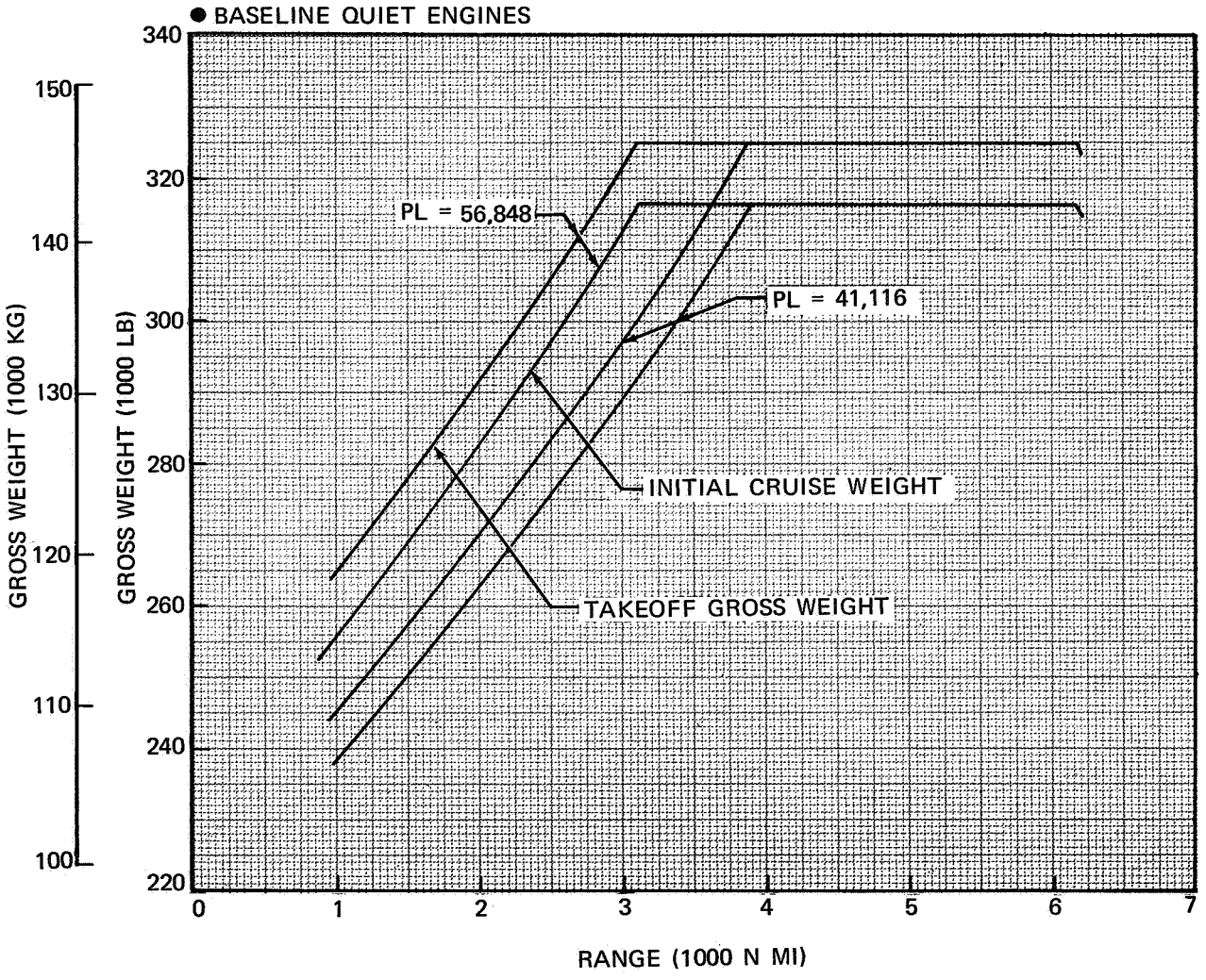

FIGURE II-10. AIRPLANE WEIGHT – MODEL DC-8-61-Q1

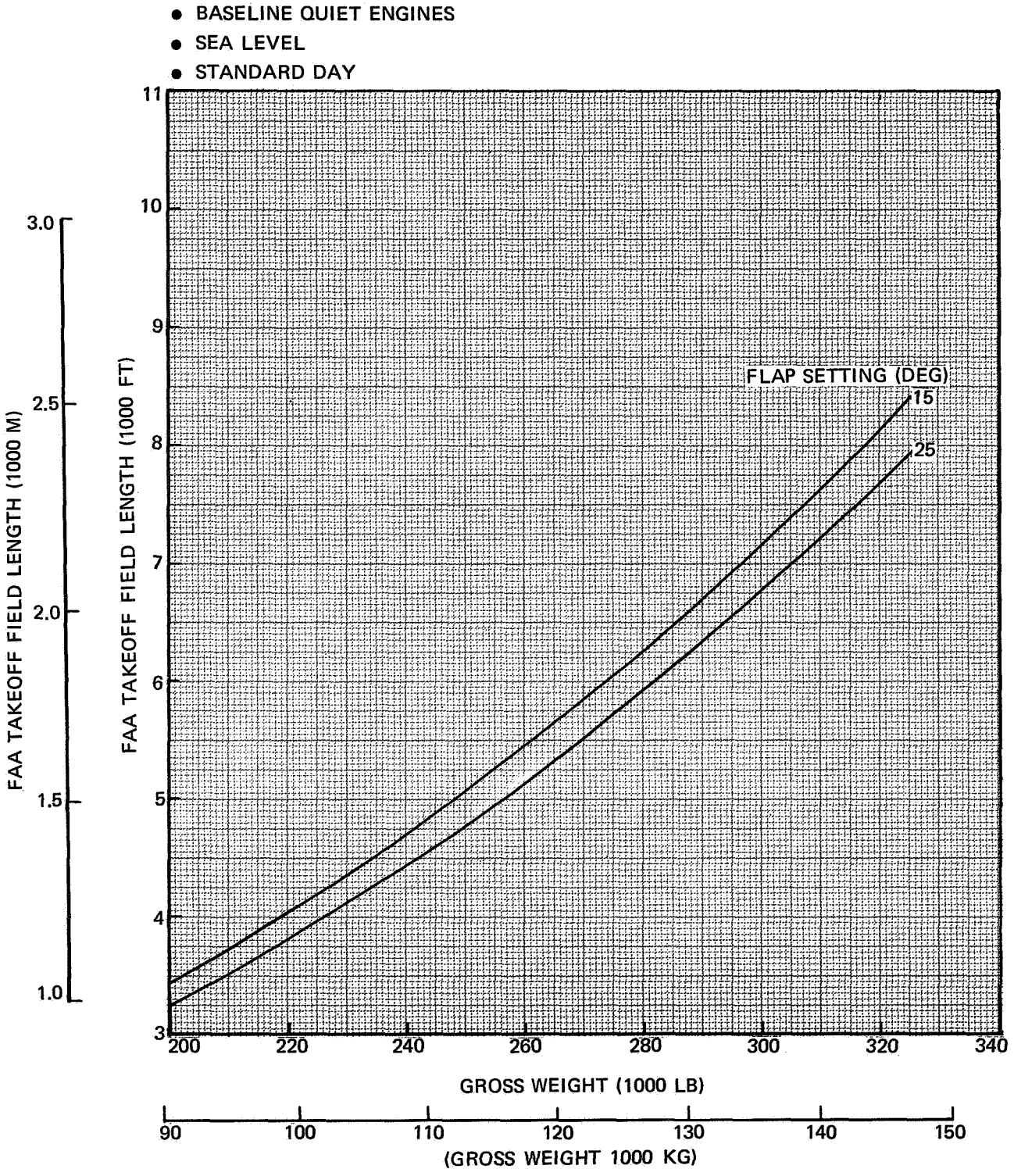

FIGURE II-11. FAA TAKEOFF FIELD LENGTH – MODEL DC-8-61-Q1

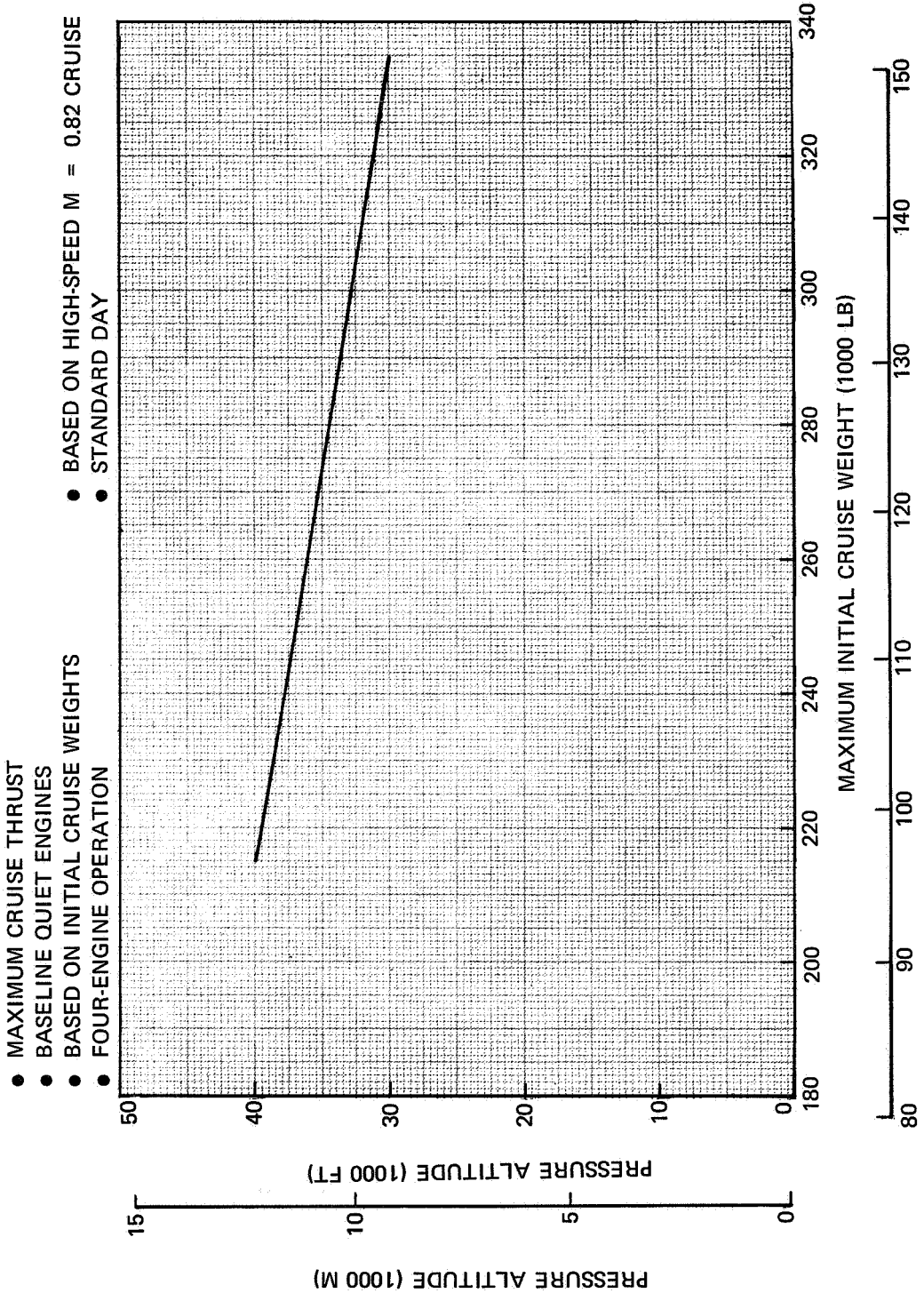

FIGURE II-12. MAXIMUM RECOMMENDED INITIAL CRUISE ALTITUDE – MODEL DC-8-61-Q1

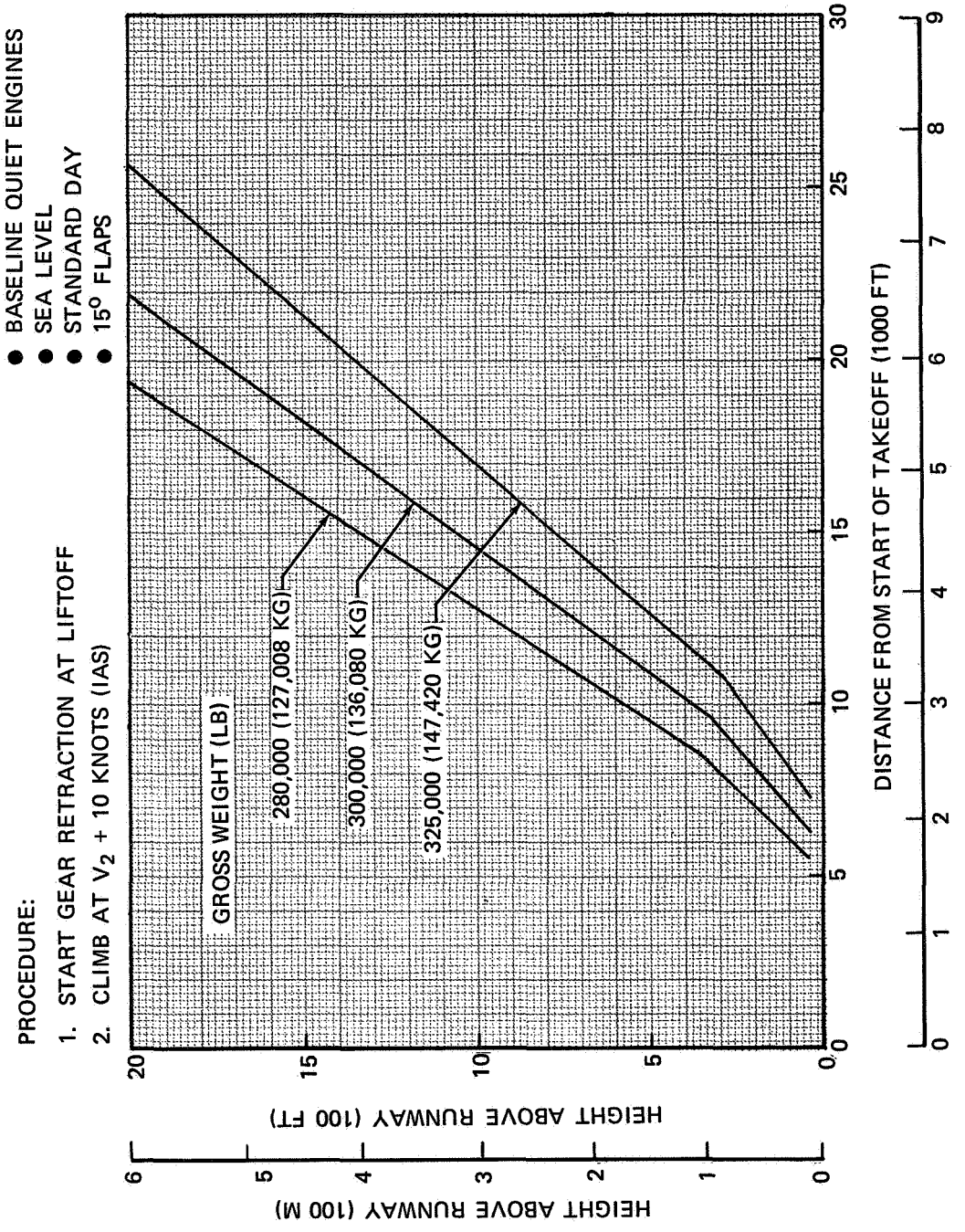

FIGURE II-13. FOUR-ENGINE FLIGHT PATH, 15° FLAPS – MODEL DC-8-61-Q1

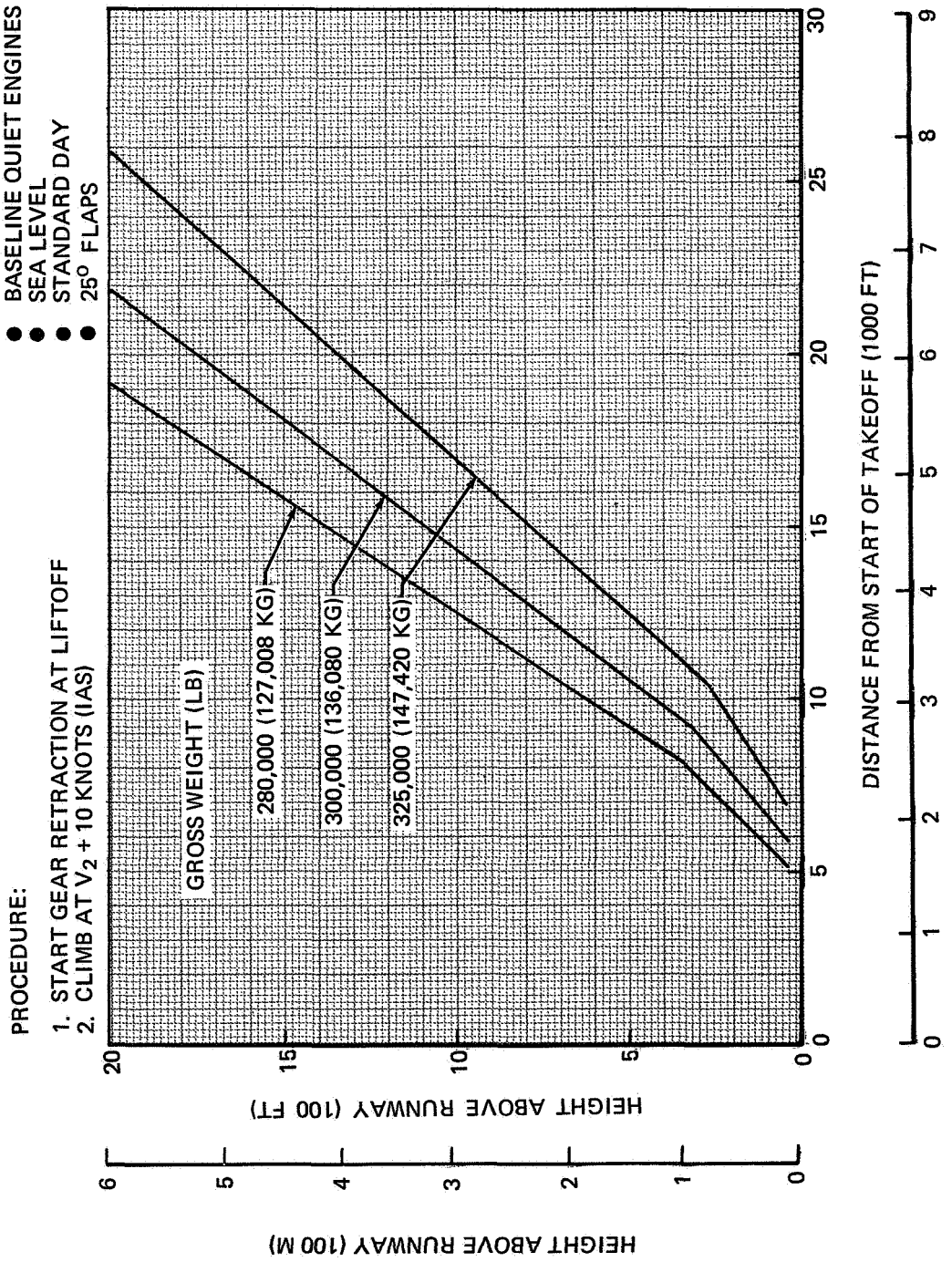

FIGURE II-14. FOUR-ENGINE FLIGHT PATH, 25° FLAPS – MODEL DC-8-61-Q1

PERFORMANCE COMPARISONS

The data presented in this section show how the installation of the quiet engine in the DC-8-61 airplane affects the airplane's performance. Also shown in the presentation is the performance corresponding to the range resulting from Max TOGW operation and two other performances corresponding to arbitrarily selected shorter ranges. The three ranges are for the quiet-engine-powered airplane with normal payload. The short ranges are important because they are typical of domestic operation. Also, it can be expected that by 1972 the number of shorter flights will have increased – and will continue to increase – when such aircraft as the DC-8 and Boeing 707 are replaced on the prime routes by the DC-10, Lockheed L-1011, and Boeing 747 aircraft.

TAKEOFF THRUST

A comparison of installed takeoff thrust is shown in Figure II-15. The increase in quiet-engine thrust results from sizing the engine for a high cruise thrust and also because of the higher natural thrust lapse rate with altitude for high-bypass-ratio engines.

The effect of the higher takeoff thrust on takeoff field length is shown in Figure II-16 for operation with 15 degree flaps. The improvement depends on TOGW and is of the order of 20 percent. Note the large increase in gross weight that is possible for operation from a given field length. The ranges indicated are for the DC-8-61-Q1 airplane.

Figure II-17 shows the increase in height above the runway at 3 nautical miles from start of roll that results from the higher takeoff thrust. The increase is approximately 500 feet (152 m), although it varies somewhat with gross weight.

CLIMB THRUST

The available net thrust for climb is shown in Figure II-18 for a typical climb profile. The curves show that the quiet-engine-powered airplane can get to cruising altitude faster but must climb at a slightly steeper angle. The small increase in angle would not be objectionable to the passengers.

MAX CRUISE THRUST

The comparison of initial cruise altitude is shown in Figure II-19. The three ranges previously mentioned are indicated. The advantage in initial cruise altitude for the Max TOGW case is shown. Note that the quiet-engine-powered airplane is approximately 5000 pounds (2268 kg) heavier at start of cruise. This tends to compensate for the advantage in initial cruise altitude it enjoys because of its higher cruise thrust.

CRUISE EFFICIENCY

A comparison of part-power installed specific fuel consumption (SFC) is shown in Figure II-20. The reduction in SFC is characteristic of the improvements provided by the new advanced-technology, high-bypass-ratio engines like the JT9D, CF6, and RB211.

PAYLOAD-RANGE

As previously noted, the OWE of the quiet-engine-powered airplane is 11,164 pounds (5064 kg) greater than the OWE of the present airplane. This means that for a given payload the fuel load must be less for operation at Max TOGW. Figure II-21 compares the payload-range curves for the two airplanes. Note that in spite of the heavier OWE the airplane has a 530-nautical-mile longer range with the quiet-engine. This is the direct result of the improved SFC (Figure II-20) which more than compensates for the increase in OWE.

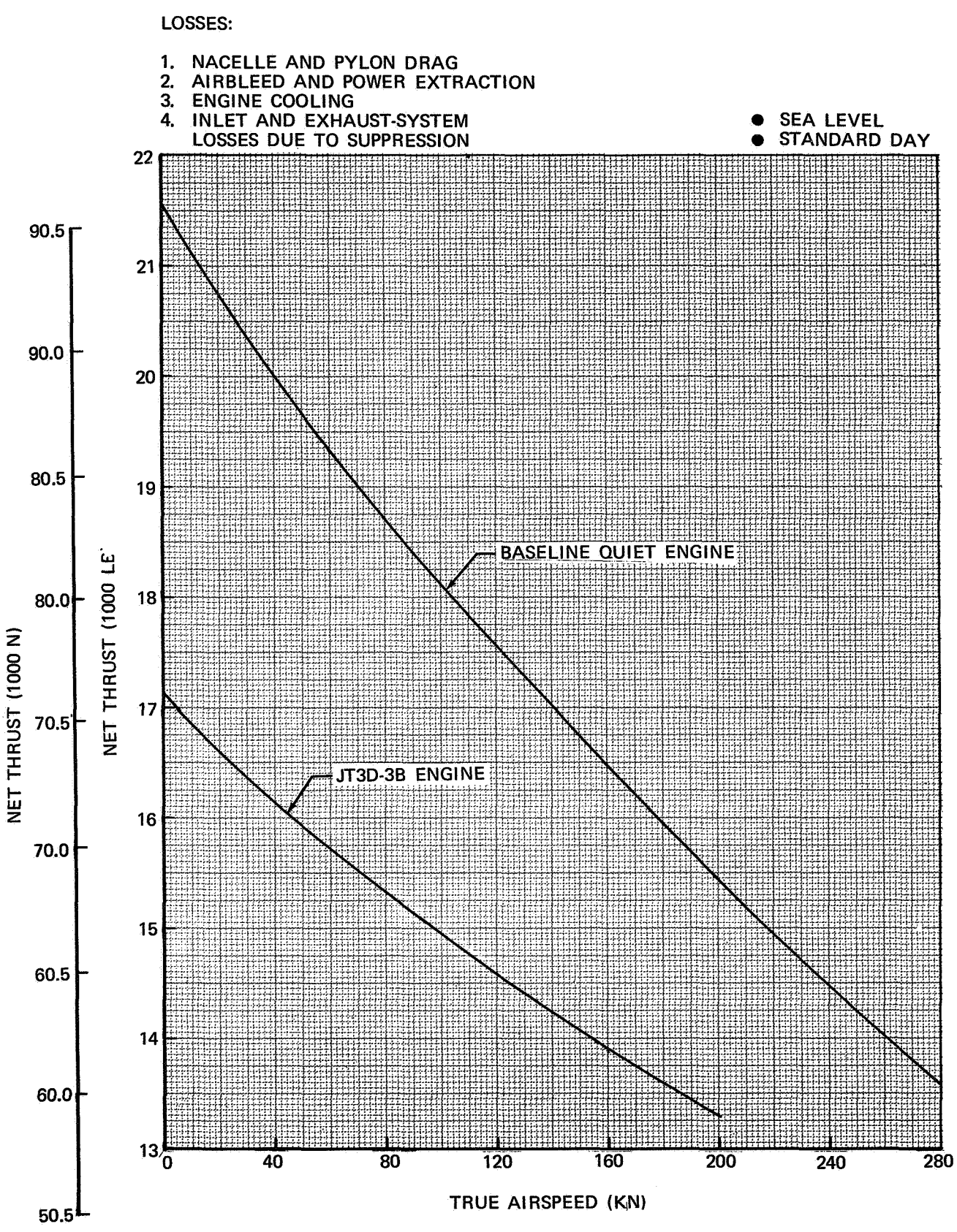

FIGURE II-15. TAKEOFF THRUST COMPARISON – MODEL DC-8-61

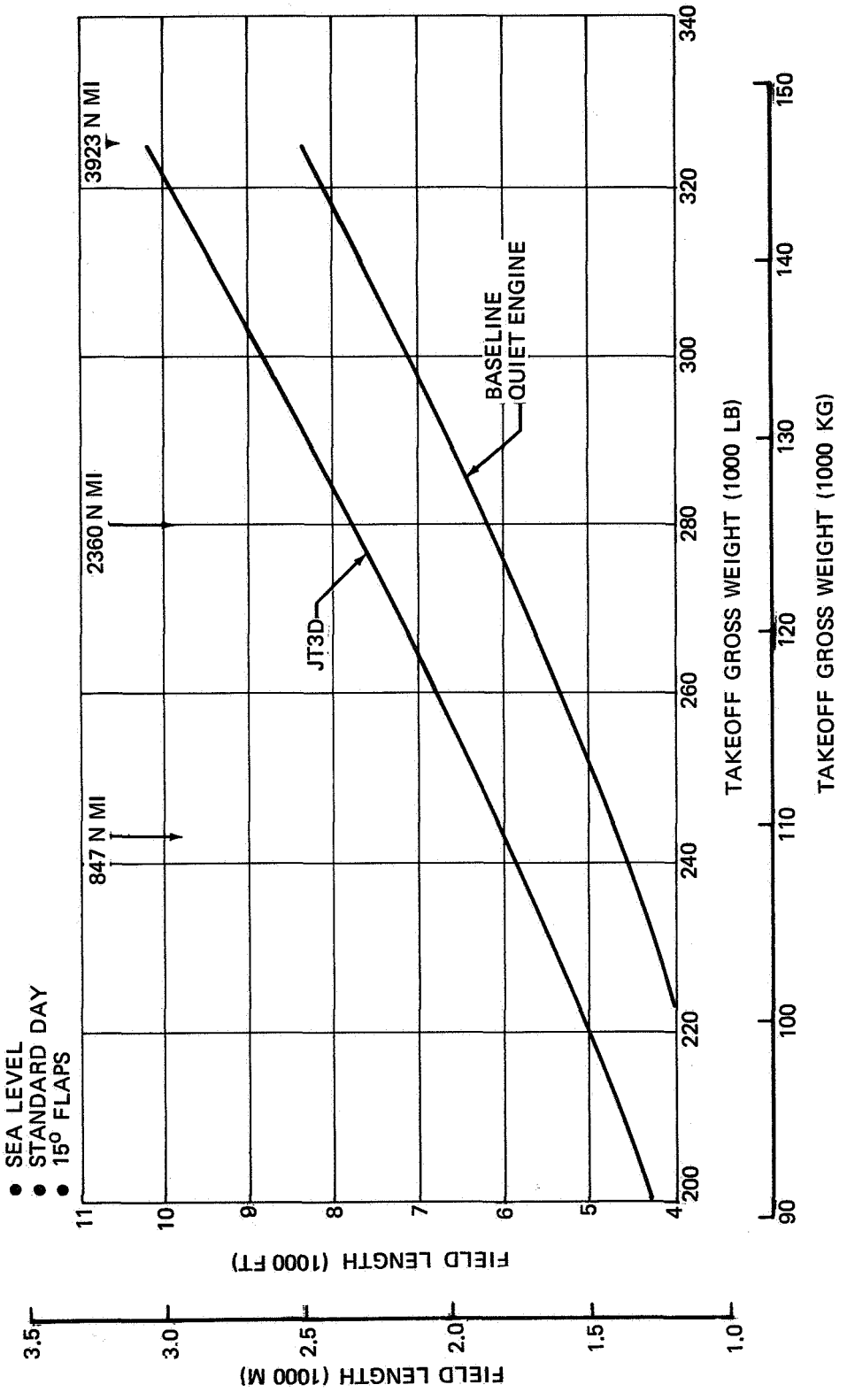

FIGURE II-16. TAKEOFF FIELD LENGTH COMPARISON – MODEL DC-8-61

It is to be expected then that the advantage gained from SFC improvement will be less and less as ranges get shorter. Figure II-22 shows that for ranges less than approximately 1400 nautical miles the OWE increase is the dominant factor and that the takeoff weight of the present airplane is less for a given range.

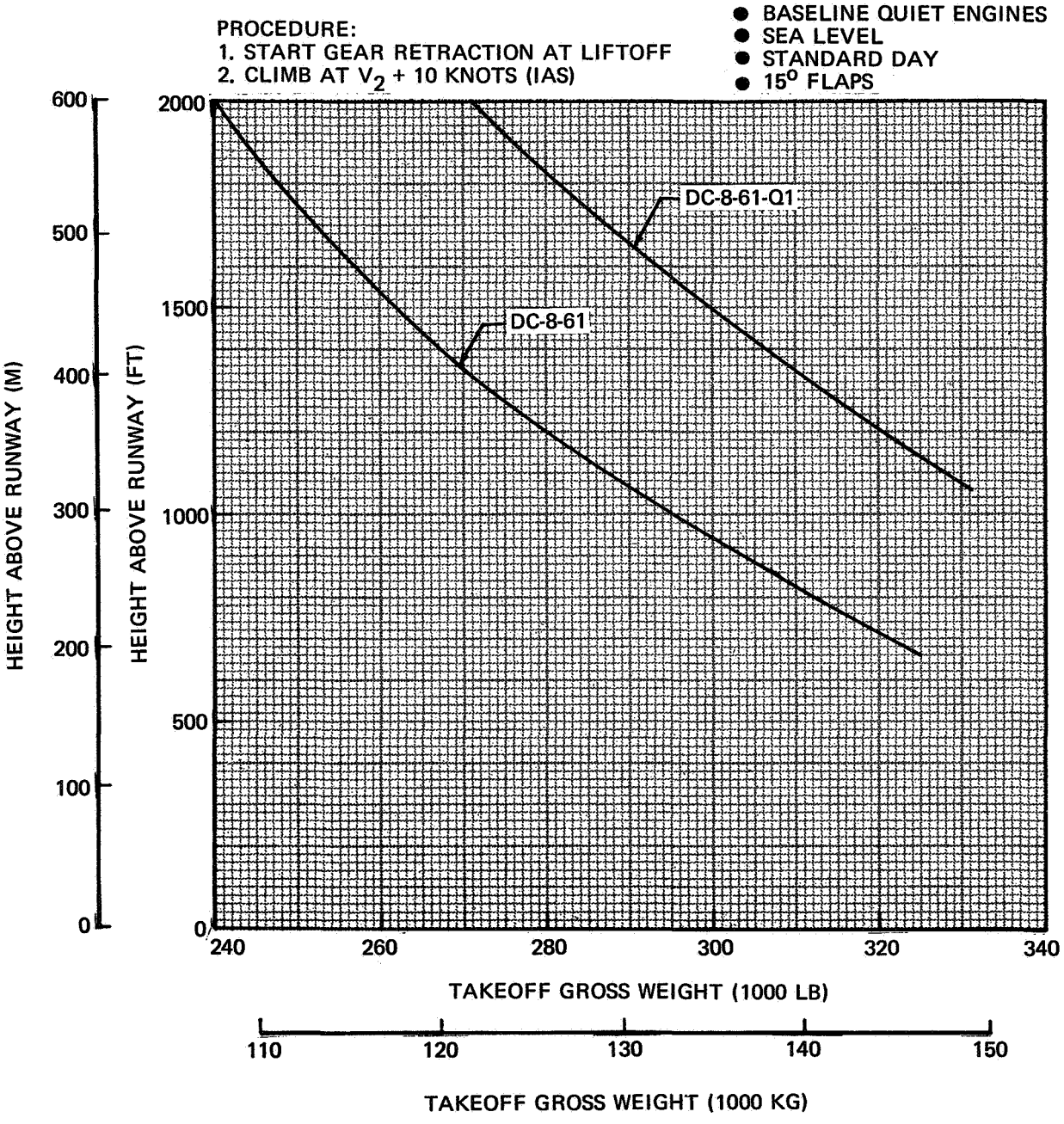

FIGURE II-17. HEIGHT ABOVE RUNWAY AT 3 N MI – MODEL DC-8-61

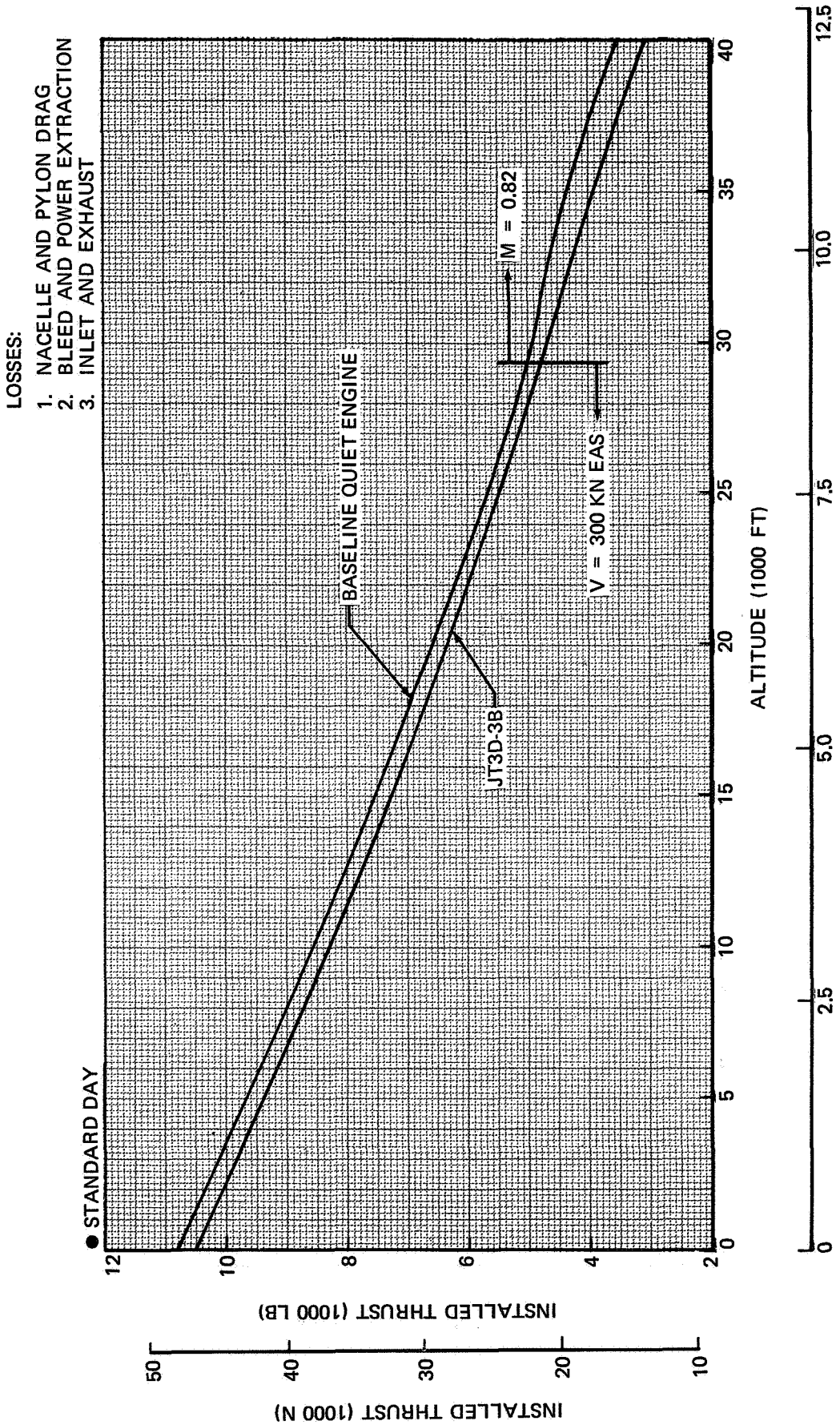

FIGURE II-18. CLIMB THRUST COMPARISON – MODEL DC-8-61

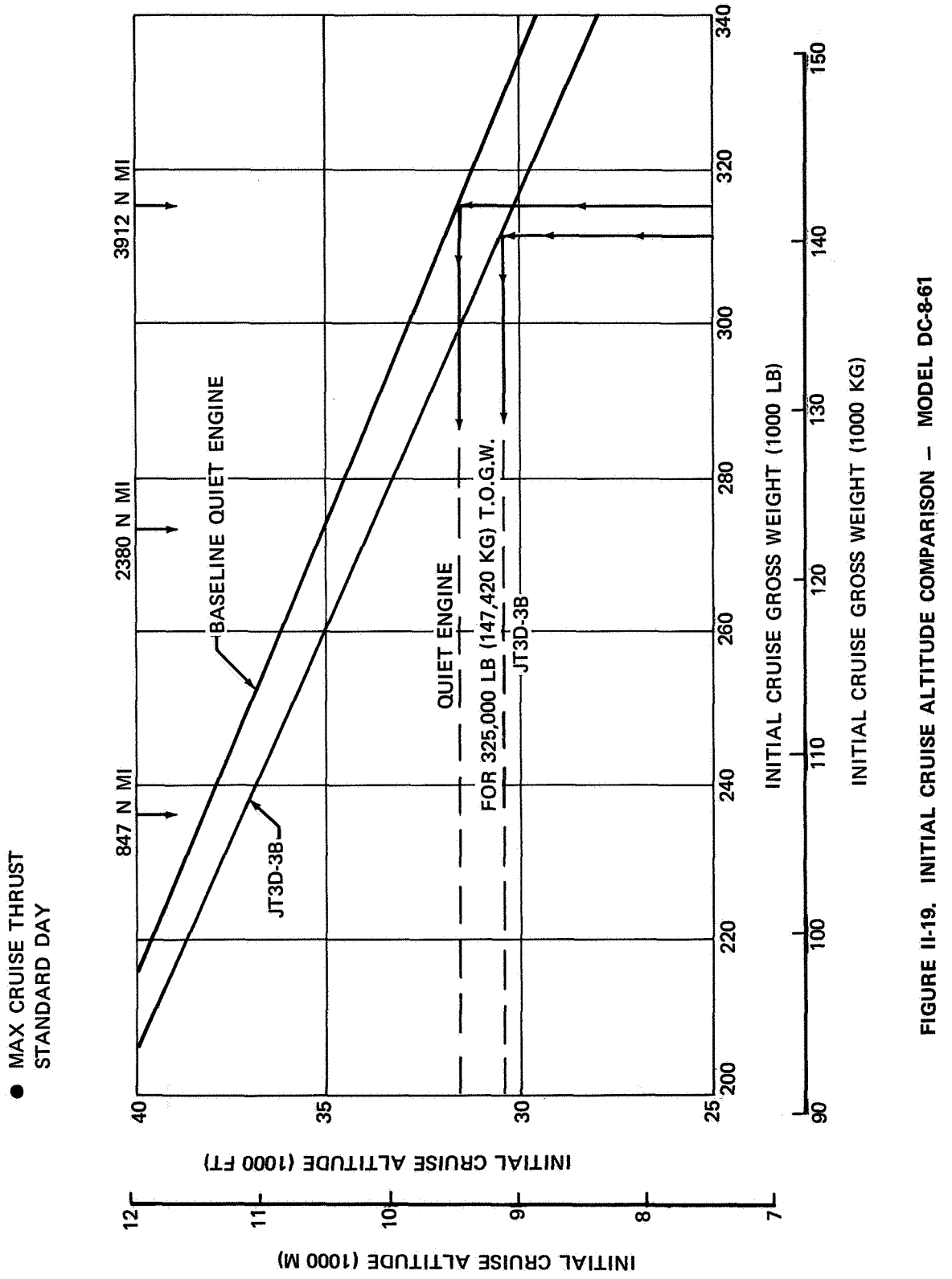

FIGURE II-19. INITIAL CRUISE ALTITUDE COMPARISON – MODEL DC-8-61

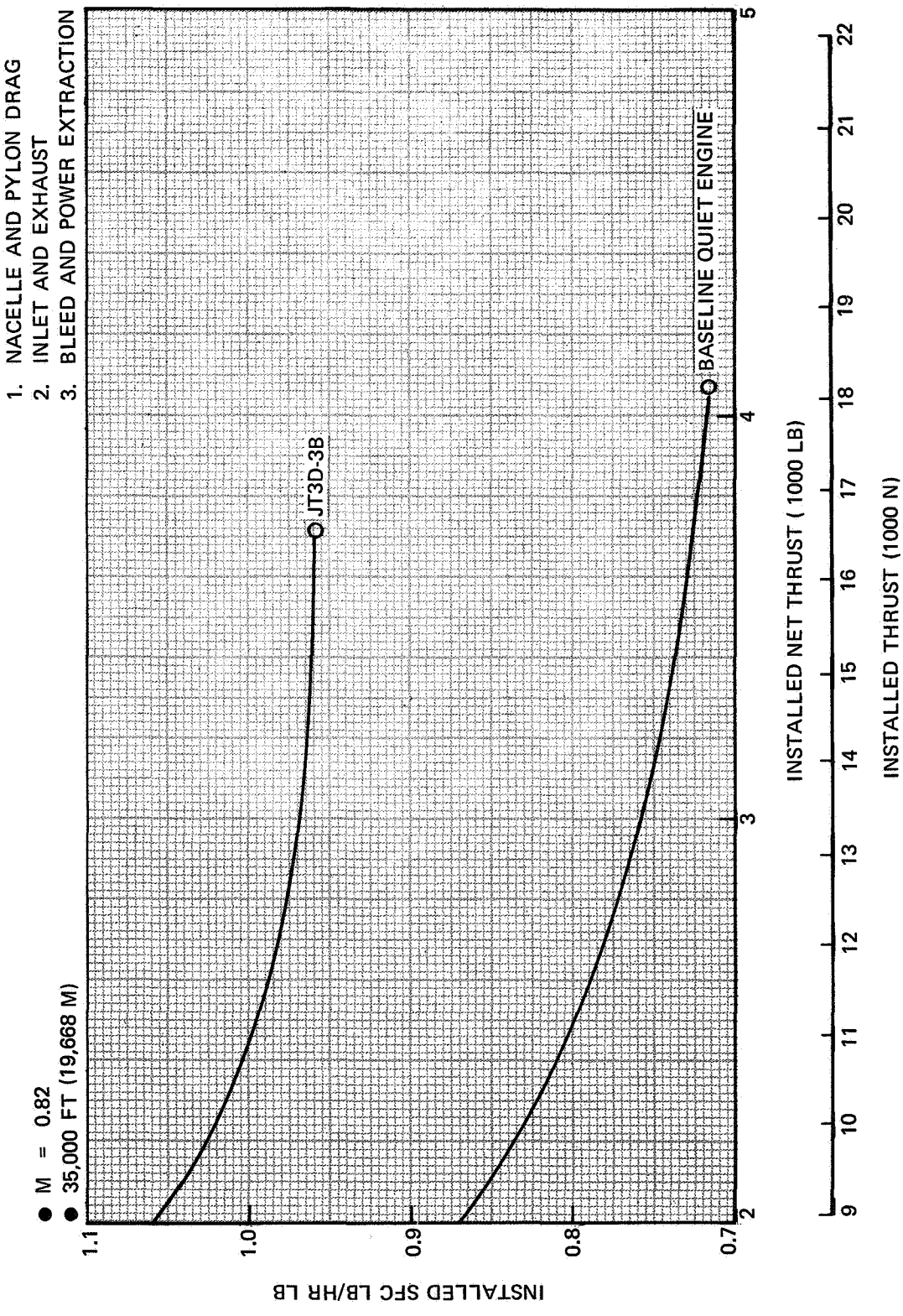

FIGURE II-20. CRUISE EFFICIENCY COMPARISON

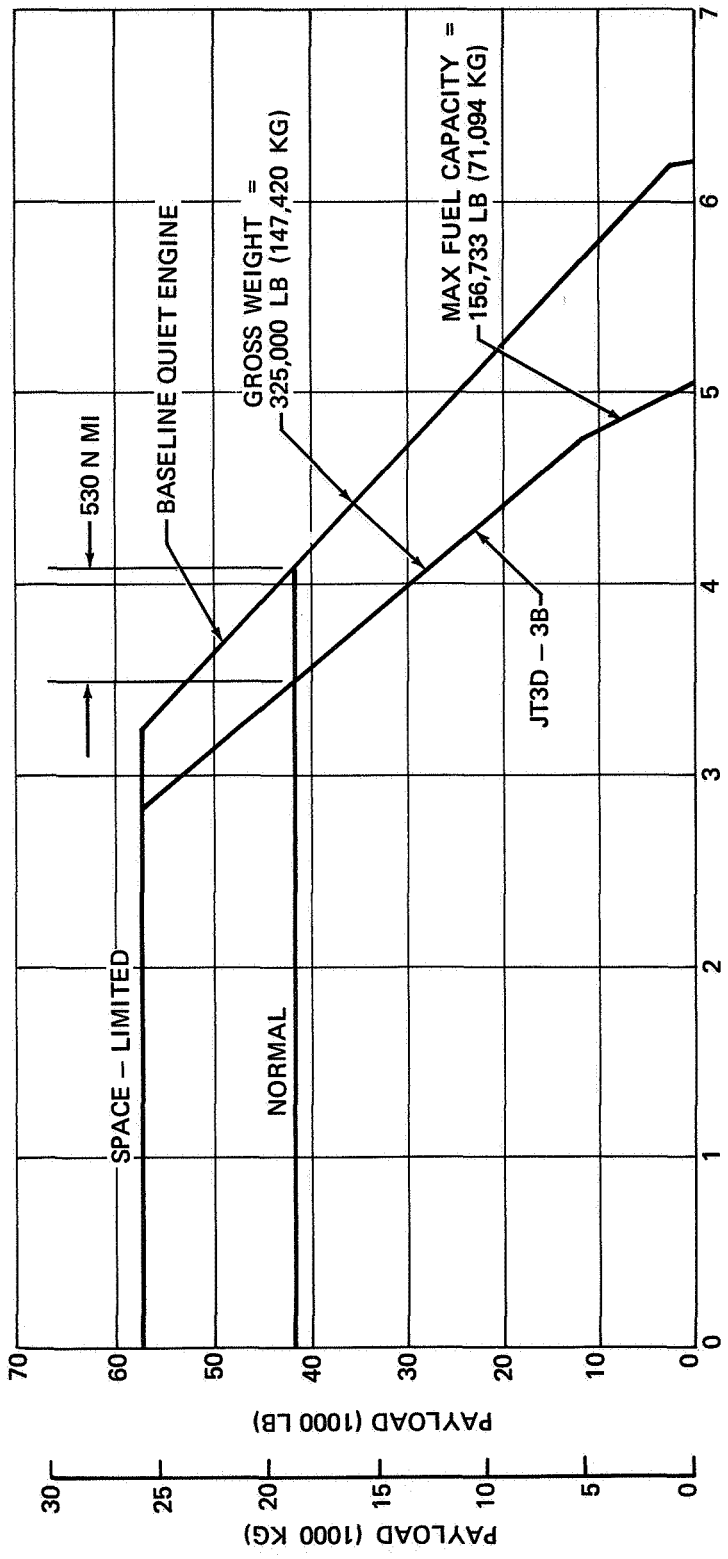

FIGURE 11-21. PAYLOAD-RANGE COMPARISON – MODEL DC-8-61

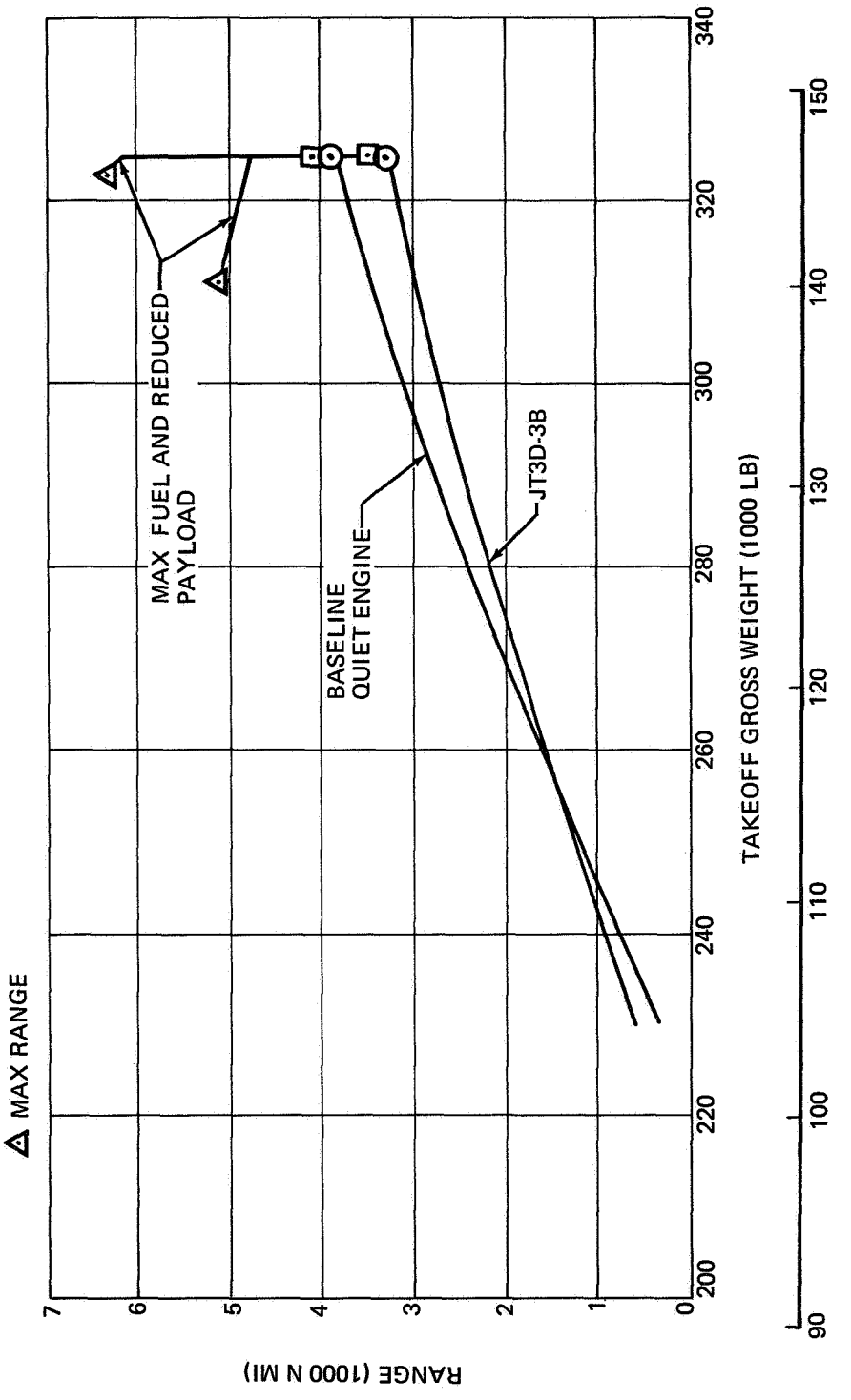

FIGURE II-22. RANGE COMPARISON – MODEL DC-8-61

COST ANALYSIS AND RESULTS

The total incremental cost of retrofitting quiet engines to a DC-8 fleet and operating them would be composed of a number of items, such as incremental increases in DOC and additional costs associated with new maintenance equipment and facilities, training, flight manuals, maintenance manuals, and loss of revenue because of retrofit downtime. The present study requires only an analysis of DOC effects. A more comprehensive study of total economic impact will be described later in Task VI. It is the purpose of this section to present and discuss the DOC calculations performed as part of Task II. The 1967 method of DOC calculations proposed by the Air Transport Association was the basis of the calculations made.

DIRECT-OPERATING-COST CALCULATIONS

The calculations of DOC for the quiet engine DC-8 is carried out in two stages. First, the DOC is calculated for the present DC-8-61 with the selected payloads. Then increments of cost elements that are specifically affected by the retrofit of a quiet engine and an acoustically treated nacelle are calculated. The two phases of the calculations are discussed separately in the following paragraphs.

Present DC-8-61 Airplane

For calculations relative to the base-case airplane, the proposed standard ATA Method is used (Reference II-1). In this, the cost elements are grouped into three categories comprising (1) flying operations (including insurance), (2) maintenance labor and material (both hourly and cyclic), and (3) depreciation charges for the airplane and the required spares.

A listing of the main cost elements and their functional dependencies is given in Table II-VI. The calculation procedure is shown sequentially in the sample worksheet, Table II-VII, which also tabulates values of the input parameters used for calculating the costs for the present airplane and the airplane retrofitted with the quiet engine.

The cumulative costs evaluated by the ATA formulas summarized in Table II-VIII (also given in Table II-IX for computational convenience), together with the pertinent parameters of payload-range, fuel burned, block speed, and block time, determined in separate performance calculations, are used to determine DOC in dollars per mile, or cents per seat-mile, as functions of range. Results of DOC-versus-range calculations for the DC-8-61 (standard day and International Fuel Reserves) using representative 1968 prices (for the aircraft, for maintenance labor rate, and for maintenance material costs) are displayed in Figure II-23 for the specified flight conditions.

Calculations of Incremental Direct Operating Costs

The elements of operating costs affected by retrofit of a quiet engine are as follows:

1. Flying operation
    a. Fuel consumption
    b. Insurance
2. Maintenance
    a. Airframe maintenance labor

b. Airframe maintenance material

c. Maintenance labor for quiet engine

d. Maintenance material for quiet engine

3. Depreciation

a. For cost of retrofit-kit acquisition

b. For cost of retrofit-kit installation

The incremental changes in these elements can be evaluated by the formulas of the 1967 ATA Method directly as functions of one or more of the airframe or engine parameters (Table II-VI). The incremental formulas are summarized in Table II-X. Some pertinent points to be noted relative to these formulas are considered under separate headings in the following paragraphs.

TABLE II-VI
OPERATING COST ELEMENTS

PROPOSED 1967 ATA METHOD MODEL DC-8-61 JT3D-3B ENGINES	
FLYING OPERATIONS	
CREW	f_1 (NUMBER IN CREW)
INSURANCE	f_2 (AIRCRAFT INVESTMENT)
OIL	f_3 (NUMBER OF ENGINES)
FUEL	f_4 (FUEL BURNED)
MAINTENANCE	
AIRFRAME LABOR	f_5 (AIRFRAME WEIGHT)
ENGINE LABOR	f_6 (ENGINE THRUST)
AIRFRAME MATERIAL	f_7 (COST OF AIRFRAME)
ENGINE MATERIAL	f_8 (COST OF ENGINES)
DEPRECIATION	
COMPLETE AIRCRAFT	f_9 (AIRCRAFT INVESTMENT AND DEPRECIATION PERIOD)

TABLE II-VII
1967 ATA DIRECT OPERATING COST, SUBSONIC JET AIRCRAFT, 1968 PRICES

AIRCRAFT TYPE		DC-8-61	DC-8-61-Q1
ENGINE TYPE		JT3D-3B	QB-3
$TOGW_{MAX}$ (MAX CERTIFIED TAKEOFF GROSS WT)	(LB)	325,000	325,000
MWE (MANUFACTURER'S WEIGHT EMPTY)	(LB)	149,339	160,503
W_e (DRY WEIGHT OF ENGINE)	(LB)	4,260	5,100
N_e (NUMBER OF ENGINES)		4	4
$W_3 = [MWE - (N_e \ W_w)]$	(LB)	132,299	140,103
NUMBER IN CREW		3	3
T (MAX STATIC TAKEOFF THRUST/ENGINE)	(LB)	18,000	22,750
U (ANNUAL UTILIZATION)	(HR/YR)	3,800	3,800
C_t (TOTAL AIRCRAFT PRICE)	($)	9,200,000	*
C_e (ENGINE PRICE)	($)	302,000	523,000
$C_a = [C_t - (N_e \ C_e)]$	($)	7,992,000	*
D_a (DEPRECIATION PERIOD)	(YR)	12	VARIABLE
R (RESIDUAL VALUE)	($)	0	0
IR_a (ANNUAL INSURANCE RATE)		0.02	0.02
t_{gm} (GROUND MANEUVER TIME)	(HR)	0.25	0.25
$K = (0.05 W_a/1000) + 6 - \left(\frac{630}{120 + W_a/1000}\right)$		10.12	11.673
FLYING OPERATIONS (LESS FUEL)			
CREW — 2-MAN CREW	$0.05 (TOGW_{MAX}/1000) + 100.0$		
CREW — 3-MAN CREW	$0.05 (TOGW_{MAX}/1000) + 135.0$		
ADD 20.0 FOR INTERNATIONAL OPERATION			
ADDITIONAL CREW MEMBER	35.0		
OIL	$0.125 N_e$		
HULL INSURANCE	$IR_a \cdot C_1/U$		
(A) TOTAL	($/BLK HR)		
DEPRECIATION FLIGHT EQUIPMENT			
COMPLETE AIRCRAFT	$(C_t - R) (D_a \cdot U)$		
AIRFRAME SPARES	$(0.1) C_a/(D_a \cdot U)$		
ENGINE SPARES	$(0.4) N_e \cdot C_e/(D_a \cdot U)$		
(B) TOTAL	($/BLK HR)		
HOURLY MAINTENANCE, FLIGHT EQUIPMENT			
LABOR, AIRFRAME	2.36 K		
LABOR, ENGINES	$(2.4 + 0.108 T/1000) N_e$		
MATERIAL, AIRFRAME	$3.08 C_a/10^6$		
MATERIAL, ENGINES	$2.5 N_e \cdot C_e/10^5$		
BURDEN	1.8 (TOTAL LABOR)		
(C) TOTAL	($/FLT HR)		
CYCLIC MAINTENANCE, FLIGHT EQUIPMENT			
LABOR, AIRFRAME	4.0 K		
LABOR, ENGINES	$(1.2 + 0.12 T/1000) N_e$		
MATERIAL, AIRFRAMES	$6.24 C_a/10^6$		
MATERIAL, ENGINES	$2.0 N_e \cdot C_e/10^5$		
BURDEN	1.8 (TOTAL LABOR)		
(D)	($/FLT CYCLE)		
FOR COMPUTATION			
(A) + (B) + (C)	($/BLK HR)		
(D) − (t_{gm} · (C))	($/FLT CYCLE)		

*FOR THE INCREMENTAL VALUES OF C_t AND C_a REQUIRED TO CALCULATE THE INCREMENTAL COST ELEMENTS, REFER TO TABLES II-IX AND II-X.

TABLE II-VIII
INCREMENTAL OPERATING COSTS FOR DC-8-61 WITH RETROFITTED QUIET ENGINE AND NACELLE

	$/BLOCK HOUR
Δ CREW PAY – DOMESTIC	0
Δ CREW PAY – INTERNATIONAL	0
Δ OIL	0
Δ INSURANCE	$0.02 (C_K + N_e C_{e_1} - N_e C_e) \div U$
Δ FUEL	Δ (FUEL BURNED LB/BLK HR) x (FUEL COST $/LB)
Δ DEPRECIATION – AIRFRAME	$1.1\, C_K \div (D_K U)$
Δ DEPRECIATION – ENGINES	$1.4\, N_e C_{e_1} \div (D_K U)$

MAINTENANCE	$/FLIGHT HOUR	$/FLIGHT CYCLE
Δ LABOR – AIRFRAME	$2.36(K_1 - K) + 0.3$*	$4(K_1 - K)$
Δ LABOR – ENGINE	$1.08 \times 10^{-4} \Delta T\, N_e$	$1.2 \times 10^{-4} \Delta T\, N_e$
Δ BURDEN	1.8 (TOTAL LABOR)	1.8 (TOTAL LABOR)
Δ MATERIAL – AIRFRAME	$3.08 \times 10^{-6} \Delta C_a$	$6.24 \times 10^{-6} \Delta C_a$
Δ MATERIAL – ENGINES	$25 \times 10^{-6} N_e (C_{e_1} - C_e)$	$20 \times 10^{-6} N_e (C_{e_1} - C_e)$
Δ TOTAL $/BLK HR = (Δ $/FLT HR) ÷ (BLK HR/FLT HR) + (Δ $/FLT CY) ÷ (BLK HR)		

C_K = COST OF AIRFRAME KIT INCLUDING INSTALLATION

C_{e_1} = COST OF QUIET ENGINE

D_K = RETROFIT-KIT USE PERIOD EXPRESSED IN YEARS

ΔT = THRUST INCREMENT FOR QUIET ENGINE

$$K_1 = 5 \times 10^{-5} W_{a_1} + 6 - \left(\frac{630}{120 + 10^{-3} W_{a_1}} \right)$$

W_{e_1} = WEIGHT OF QUIET ENGINE

MEW_1 = MANUFACTURER'S EMPTY WEIGHT FOR RETROFITTED AIRPLANE

$W_{a_1} = MEW_1 - W_{e_1} N_e$

$\Delta C_a = C_K - 57 \Delta W_a$ = NET INCREASE IN COST OF RETROFITTED AIRPLANE FOR MAINTENANCE-MATERIAL CALCULATION

ΔW_a = DECREASE IN TOTAL WEIGHT OF WING, NACELLE, AND PYLON PARTS DUE TO RETROFIT (APPROX 14,000 LB). THIS IS PRICED AT $57/LB FOR CALCULATION OF ΔC_a.

*DOUGLAS ESTIMATES FOR MAINTENANCE OF ACOUSTICAL LININGS.

TABLE II-IX
BASE-CASE DOC – SUMMARY OF THE 1967 ATA FORMULAS

	$/BLOCK HOUR
CREW PAY – DOMESTIC:	5×10^{-5} (MAX TOGW) + 100 2-MAN CREW
	5×10^{-5} (MAX TOGW) + 135 3-MAN CREW
CREW PAY – INTERNATIONAL:	ADD $20.00
OIL	$0.125\ N_e = 0.5$ N_e = NUMBER OF ENGINES = 4
INSURANCE	$0.02\ C_t \div U$
FUEL	(FUEL BURNED LB/BLK HR) x (FUEL COST $/LB)
DEPRECIATION – AIRFRAME: (12-YEAR PERIOD)	$1.1\ C_a \div 12U$
DEPRECIATION – ENGINES:	$1.4\ N_e C_e \div 12U$

MAINTENANCE	$/FLIGHT HOUR	$/FLIGHT CYCLE
LABOR – AIRFRAME	2.36K	4.0K
LABOR – ENGINES	$(2.4 + 1.08 \times 10^{-4}T)N_e$	$1.2(1 + 10^{-4}T)N_e$
BURDEN	1.8 x TOTAL LABOR	1.8 x TOTAL LABOR
MATERIAL – AIRFRAME	$3.08 \times 10^{-6}\ C_a$	$6.24 \times 10^{-6}\ C_a$
MATERIAL – ENGINES	$25 \times 10^{-6}\ N_e C_e$	$20 \times 10^{-6}\ N_e C_e$
TOTAL $/BLK HR = ($/FLT HR) ÷ (BLK HR/FLT HR) + ($/FLT CY) ÷ (BLK HR)		

NOTATION

C_t = TOTAL AIRPLANE PRICE

C_e = ENGINE PRICE

N_e = NUMBER OF ENGINES

$C_a = C_t - C_e N_e$

$$K = 5 \times 10^{-5} W_a + 6 - \left(\frac{630}{120 + 10^{-3} W_a}\right)$$

TOGW = TAKEOFF GROSS WEIGHT

W_e = ENGINE WEIGHT

MEW = MANUFACTURER'S EMPTY WEIGHT

W_a = MEW – $W_e N_e$

U = UTILIZATION. ASSUMED 3800 HR/YR

T = ENGINE TAKEOFF THRUST

BASE LABOR RATE = $4.0/HR

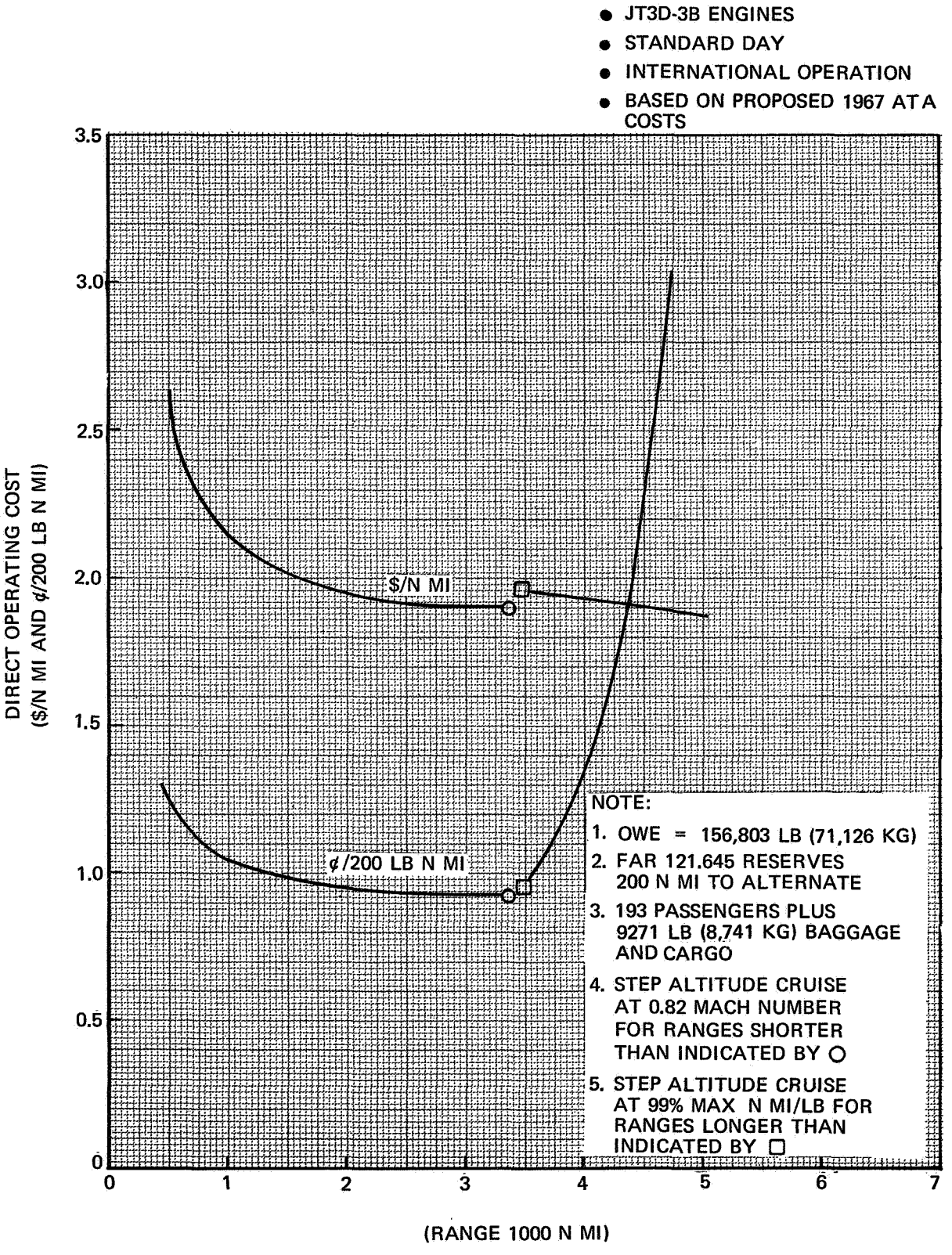

FIGURE II-23. DIRECT OPERATING COST vs RANGE – MODEL DC-8-61-Q1

TABLE II-X
RETROFIT COSTS IN 1968 DOLLARS

NO. OF AIRPLANE KITS PRODUCED	100	200	300
ESTIMATED AIRFRAME KIT PRICE	3,719,000	2,568,500	2,239,667
INSTALLATION COST	930,000	820,000	740,000
ESTIMATED PRICE OF 4 ENGINES	2,092,000	2,092,000	2,092,000
SPARES: 10% AIRFRAME + 40% ENGINE	1,208,700	1,093,650	1,060,767
TOTAL COST PER AIRPLANE	7,949,700	6,574,150	6,132,434

Definition of Retrofitted-Airplane Price for Insurance Calculations

The total airplane price, C_{t_1}, used in insurance calculations for the retrofitted airplane is taken as the sum of the original airframe cost, C_a, the airframe retrofit kit cost, C_K, and the cost of the kit of four quiet engines, $N_e C_{e_1}$, as follows:

$$C_{t_1} = C_a + C_K + N_e C_{e_1} = (C_t - N_e C_e) + C_K + N_e C_{e_1}$$

or

$$\Delta C_t = C_{t_1} - C_t = C_K + N_e C_{e_1} - N_e C_e$$

The preceding definition of ΔC_t, which deducts the cost of the replaced JT3D-3B engines, is used to calculate the increment in insurance costs.

Depreciation

The DOC increment for kit acquisition, which is by far the largest cost increment in this study, requires definition of the following:

1. The total number of airplanes to be retrofitted (to evaluate unit kit cost).

2. The retrofitted airplanes' effective operating period for depreciation.

Calculations were made for fleets of 150 and 300 aircraft. The mean operating period would vary according to each airline's fleet retrofit schedule and retrofitted airplanes' retirement dates. The airline industry does not appear to have established retirement plans for the present subsonic turbofan-powered transport fleets. To resolve this difficulty, a parametric approach has been adopted in which kit depreciation charges are presented for a series of assumed operating periods ranging from one to six years. With these data, each operator can assess the magnitude of the cost according to his individual projections on retirement dates. In the event that greater operating periods are considered, the corresponding depreciation increment can be calculated by prorating the data for six-year intervals.

Cost of Downtime for Retrofit

One fairly significant element of cost associated with the retrofit is the loss of revenue incurred by an airline for the downtime required to effect the quiet-nacelle retrofit. This element could reasonably be translated into an airplane lease cost of approximately $10,000 per day and charged

to operating cost. However, for the present phase of the study it was decided to consider downtime as a separate item.

ESTIMATED RETROFIT COSTS

A costing study was carried out relative to the Task II quiet-engine and nacelle configurations as shown on drawings supplied by the NASA Project Manager. Necessary definition activity prior to the costing study included preparation of:

1. Design-change work statement.

2. Weight-change summary.

3. Plans for laboratory tests, test-stand tests, wind-tunnel tests, ground tests, and flight tests.

4. Estimates of man-hours for necessary design engineering, laboratory work, flight test, and other support required for FAA certification of the nacelle-pylon modifications and wing reskinning.

With these inputs, budgetary price estimates were developed for the new nacelle-and-pylon retrofit kit as well as for the associated wing reskinning work.

The component costs, consisting of the recurring and amortized fixed costs, were determined for a series of assumed production runs at 1968 rates for material and labor (Table II-X).

The aircraft downtime for reskinning and other installation work was estimated at 46 days.

ASSUMED PROGRAM SCHEDULE

A tentative program schedule for the introduction of the quiet engine and nacelle is shown in Table II-XI. Basically, this schedule covers a 45-month time span from ATP to PFRT for the quiet engine. A design-to-certification cycle for the airframe integration part would take about the same time. Assuming an ATP date of October 1968 for the engine, the quiet engine would begin to enter airline service sometime in 1974.

A total number of retrofitted aircraft and the end point in time for completion of retrofit would be determined by equalizing two time-dependent populations, as follows:

1. Cumulative number (growth with time) of quiet engines and nacelle kits.

2. Cumulative number (decrement with time) of total DC-8 fleet (according to the airlines' retirement schedules).

Rough estimates of production potentials for the quiet engine and associated airframe parts indicate that it would be well into 1977 before a DC-8 quiet engine retrofit program could be completed.

EFFECT OF QUIET-ENGINE RETROFIT ON DOC

The increase in the DOC per mile resulting from retrofit of the quiet engine is shown in Figure II-24. Data are shown for two different fleet sizes for which retrofit was assumed. The two lowest curves show the increase in operating cost arising from all sources other than depreciation. The

increments shown thus account for the effects of changes in weight, drag, installed-engine performance, insurance, and maintenance costs.

As the no-depreciation curves indicate, the quiet engine causes little or no increase in DOC (less depreciation) over a large part of the DC-8-61 range. This means that the improved fuel economy of the quiet engine approximately compensates for increases in all items except depreciation.

The other curves (Figure II-24) include the increment in depreciation resulting from retrofit and thus show the total increase in DOC. Curves are presented for several depreciation periods, because of the previously discussed uncertainty about the length of the depreciation period.

Effects of the retrofit on DOC per passenger mile are shown in Figure II-25. Because the range of the DC-8-61 is extended by the quiet engine, the seat-mile costs are improved at ranges beyond that at which, for the DC-8-61, passengers must be off-loaded in favor of fuel. This advantage is not likely to be important, however, because it represents an improvement in a relatively unprofitable operation that is normally avoided.

TABLE II-XI
ASSUMED PROGRAM SCHEDULE

QUIET-ENGINE INTEGRATION STUDY

	JAN 68	JAN 69	JAN 70	JAN 71	JAN 72	JAN 73	JAN 74	JAN 75
ATP "Q" ENGINE	▽							
ATP "Q" NACELLE DESIGN		▽						
METAL MOCKUP ENGINE TO DOUGLAS			▽					
"Q" ENGINE FOR GROUND TESTS				▽				
ORDER LONG-LEAD-TIME MATERIAL BEGIN TOOLING OF "Q" NACELLE				▽				
PFRT "Q" ENGINE AND FLIGHT TEST "Q" ENGINES TO DOUGLAS					▽			
TEST AIRPLANE MODIFICATION COMPLETE						▽		
FLIGHT TESTS COMPLETE							▽	
FAA CERTIFICATION OF "Q" ENGINE AND DELIVERY OF 40 ENGINES							▽	
FAA CERTIFICATION OF "Q" NACELLE AND 40 PRODUCTION "Q" NACELLES COMPLETE								▽
DELIVERY OF 200 ENGINES COMPLETE								▽

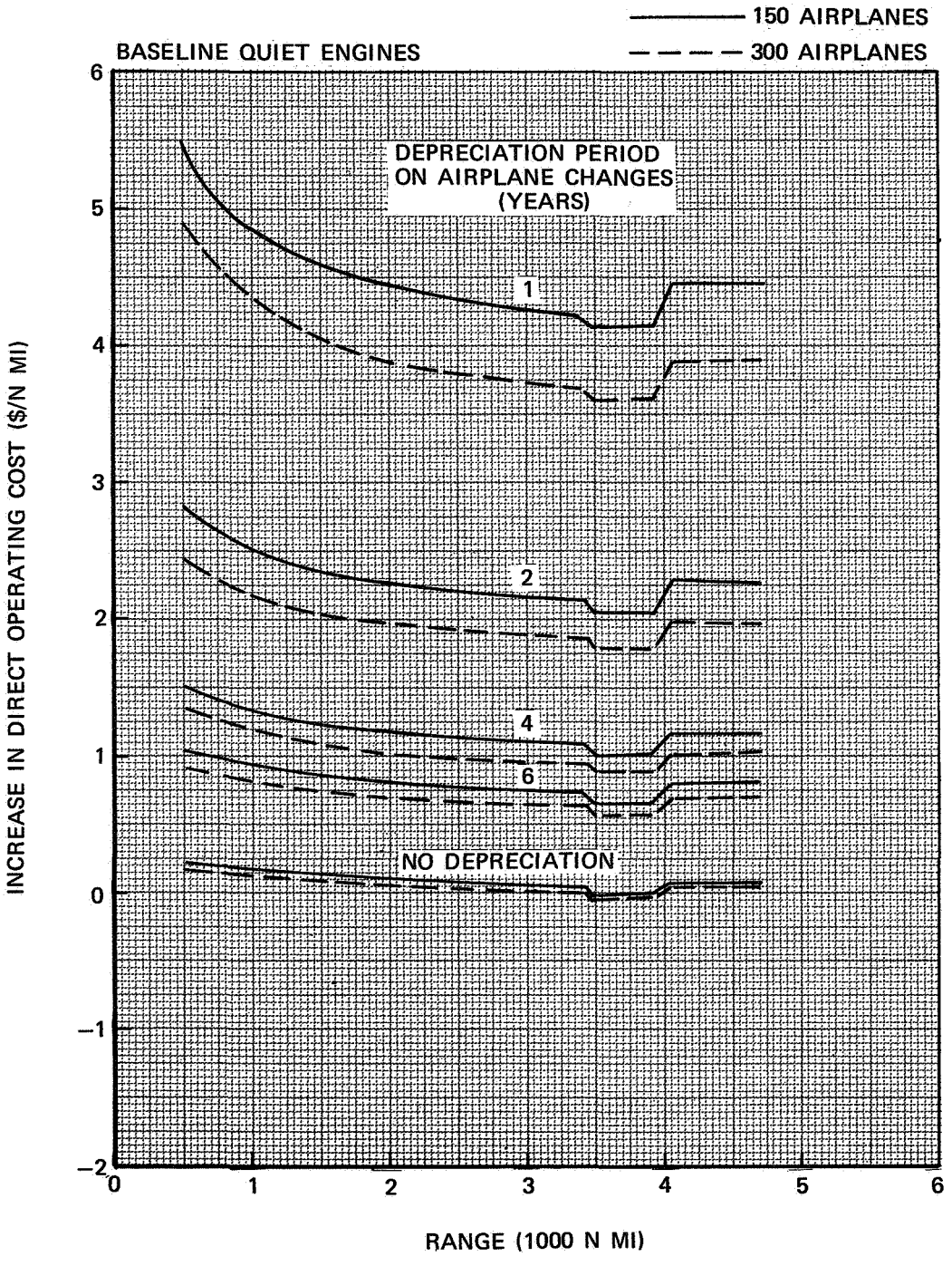

FIGURE II-24. INCREASE IN DIRECT OPERATING COST, Δ$/N MI — MODEL DC-8-61-Q1

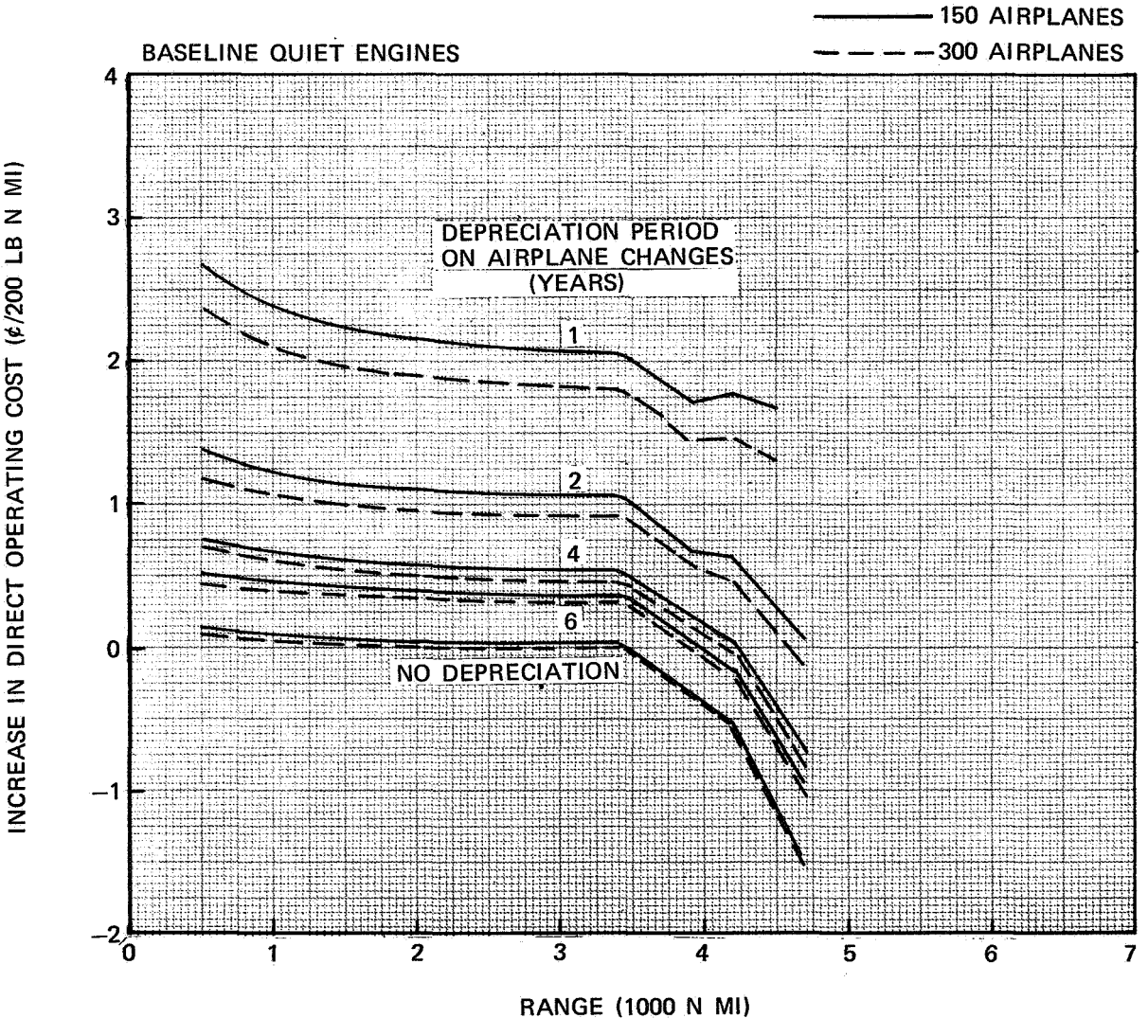

FIGURE II-25. INCREASE IN DIRECT OPERATING COST, Δ¢/200 LB N MI – MODEL DC-8-61-Q1

PARAMETRIC STUDY

A parametric study was conducted to generate trade-factor data that will be useful in analyzing the effects that changes in engine characteristics have on airplane performance. The study consists of two parts. Part 1 considers how independent changes in bare-engine weight, center of gravity, airflow, and dimensions affect installed nacelle drag, airplane empty weight, and inlet and tailpipe total-pressure losses. Part 2 considers the effects of nacelle drag, airplane empty weight, engine SFC, takeoff thrust, and maximum cruise thrust on the performance of the DC-8-61-Q1 airplane.

PART 1: BARE-ENGINE CHANGES

Changes in engine weight, center of gravity, length, diameter, and airflow were considered independently. The incremental changes in these parameters were selected to represent real design changes that could conceivably be made in the baseline quiet engine defined in Task IV. Care was taken to ensure that the nacelle configurations and locations that would result from making the selected bare-engine changes were reasonable. Figure II-26 shows the baseline DC-8-61-Q1 nacelle and its location relative to the wing and to the ground. Also shown are corresponding sketches for the variations considered for bare-engine diameter. The sketches for changes in bare-engine length are shown in Figure II-27. Table II-XII shows the characteristics of the nacelles and pylons that resulted from the bare-engine variations considered. In all cases, the clearance between nacelle and wing was the same as it was in the DC-8-61-Q1. This was accomplished by moving the nacelle longitudinally and by maintaining a ground clearance of at least 34.5 inches (87.6 cm), the ground clearance of the DC-8-61-Q1. Table II-XIII shows the results of the study for specific cases (Figures II-26 and II-27).

Weight Changes

Three variations in engine weight were considered. Table II-XII shows the nacelle and pylon weight changes that resulted from these variations. It was assumed that the engine center of gravity did not vary with engine weight. Because engine weight is changed independently of engine dimensions, there is no change in nacelle configuration, cowling weight, and nacelle drag. Nor is there a change in the total-pressure loss for the inlet and exhaust ducting.

Figure II-28 shows the variation of installed nacelle-pylon weight for the cases considered. Also shown in Figure II-28 are the data for the variations considered in the second part of the parametric study, which will be discussed later. The slopes of the lines drawn through the two sets of data are different because of differences in the methods of analysis. The bare-engine weight changes were considered to have no effect on dimensions, and hence the cowling weight was not affected. The variations used in the second part of the parametric study were analyzed as total differentials; that is, weight changes resulting from dimension and center of gravity changes were considered simultaneously with bare-engine weight changes.

A change in engine center of gravity within the limitations of the parametric variations set for this study would not affect nacelle weight, but would affect pylon weight, as is shown in Figure II-29 and in Table II-XII. The resulting increase in pylon weight would affect the combined nacelle-pylon moment of inertia as shown in the table.

Effect on Wing Reskinning

As previously mentioned, wing flutter considerations include the moment of inertia of the nacelle and pylon about the wing elastic axis. Therefore a change in either nacelle or pylon weight or in center of gravity would affect the wing skin thickness.

TABLE II-XII
EFFECT OF BARE ENGINE CHANGES ON NACELLE CHARACTERISTICS

	NACELLE-PYLON WEIGHT				NACELLE LENGTH		MAXIMUM NACELLE DIAMETER		NACELLE-PYLON MOMENT OF INERTIA**	
	NACELLE*		PYLON							
	LB	KG	LB	KG	IN.	M	IN.	M	(LB-SQ IN. x 10^{-6})	(KG-SQ M) x 10^{-6}
ENGINE WEIGHT (LB)										
5700 (2586 KG)	3409	1546	954	519	245	6.2	84.3	2.1	347.4	0.1008
5100 (BASE CASE) (2313 KG)	3409	1546	900	408	245	6.2	84.3	2.1	330.5	0.0959
4080 (1851 KG)	3409	1546	810	367	245	6.2	84.3	2.1	294.5	0.0854
ENGINE LENGTH (IN.)										
145 (3.7 M)	5439	2467	941	427	256	6.5	84.3	2.1	355.9	0.1033
134 (BASE CASE) (3.4 M)	3409	1546	900	408	245	6.2	84.3	2.1	330.5	0.0959
120 (3.0 M)	3372	1530	856	388	231	5.8	84.3	2.1	309.7	0.095
ENGINE FAN-TIP DIAMETER (IN.)										
76 (1.9 M)	3514	1594	951	431	245	6.2	90.0	2.3	367.4	0.0899
70 (BASE CASE) (1.8 M)	3409	1546	900	408	245	6.2	84.3	2.1	330.5	0.1033
68 (1.7 M)	3363	1525	895	406	245	6.2	82.0	2.0	332.2	0.0964
ENGINE CENTER OF GRAVITY CHANGE Δ (IN.)										
+10 + 25.4 CM	3409	1546	963	437	245	6.2	84.3	2.1	366.4	0.0897
0 (BASE CASE)	3409	1546	900	408	245	6.2	84.3	2.1	330.5	0.1033
–10 –25.4 CM	3409	1546	847	384	245	6.2	84.3	2.1	302.8	0.8790

*DOES NOT INCLUDE ENGINE WEIGHT.
**ABOUT THE WING ELASTIC AXIS

TABLE II-XIII
EFFECT OF BARE ENGINE CHANGES

	NACELLE AND PYLON WEIGHT		NACELLE AND PYLON DRAG D/q_o SQ FT			TOTAL PRESSURE LOSSES $\Delta P_T/P_T$		
	LB	KG	LB	KG	SQ M	INLET	FAN	PRIMARY
BARE ENGINE WEIGHT (LB)								
5700 (2586 KG)	9957	4516	1.996	8.878	0.1854	0.00738	0.00475	0.000115
5100 (BASE CASE) (2313 KG)	9303	4220	1.996	8.878	0.1854	0.00738	0.00475	0.000115
4080 (1851 KG)	8293	3762	1.996	8.878	0.1854	0.00738	0.00475	0.000115
BARE ENGINE LENGTH (IN.)								
145 (3.7 M)	9374	4252	2.054	9.136	0.1908	0.00738	0.00475	0.000115
134 (BASE CASE) (3.4 M)	9303	4220	1.996	8.878	0.1854	0.00738	0.00475	0.000115
120 (3.0 M)	9222	4183	1.924	8.558	0.1787	0.00738	0.00475	0.000115
BARE ENGINE FAN TIP DIAMETER (IN.)								
76 (1.9 M)	9465	4293	2.079	9.247	0.1931	0.00512	0.00252	0.000115
70 (BASE CASE) (1.8 M)	9303	4220	1.996	8.878	0.1854	0.00738	0.00479	0.000115
68 (1.7 M)	9252	4197	1.942	8.878	0.1787	0.00839	0.00658	0.000115
BARE ENGINE AIRFLOW (LB/SEC) (KG/SEC)								
360 (163 KG)	9303	4220	1.996	8.878	0.1854	0.00802	0.00512	0.000125
347 (BASE CASE) (157 KG)	9303	4220	1.996	8.878	0.1854	0.00738	0.00475	0.000115
340 (154 KG)	9303	4220	1.996	8.878	0.1854	0.00704	0.00453	0.000110
BARE ENGINE CENTER OF GRAVITY CHANGE (Δ IN.)								
+10 +25.4 CM	9366	4248	1.996	8.878	0.1854	0.00738	0.00475	0.000115
0 (BASE CASE)	9303	4220	1.996	8.878	0.1854	0.00738	0.00475	0.000115
−10 −25.4 CM	9250	4196	1.996	8.878	0.1854	0.00738	0.00475	0.000115

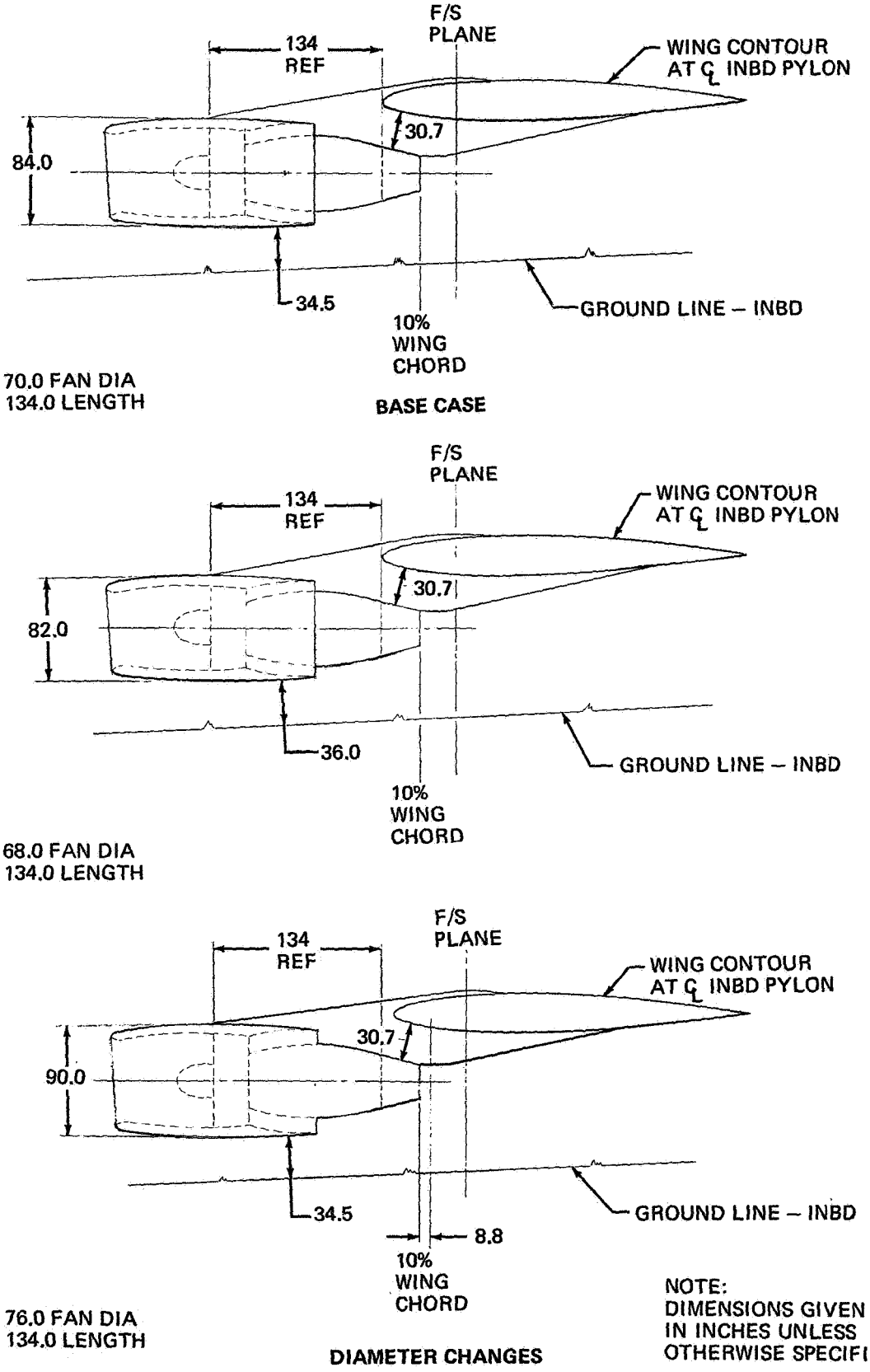

FIGURE II-26. DIAMETER VARIATIONS

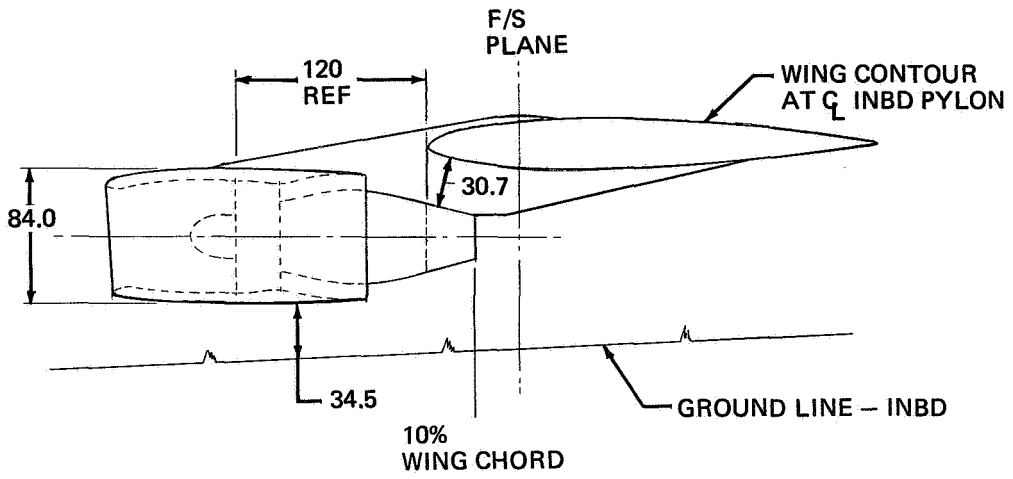

70.0 FAN DIA
120.0 LENGTH

BARE ENGINE VARIATIONS

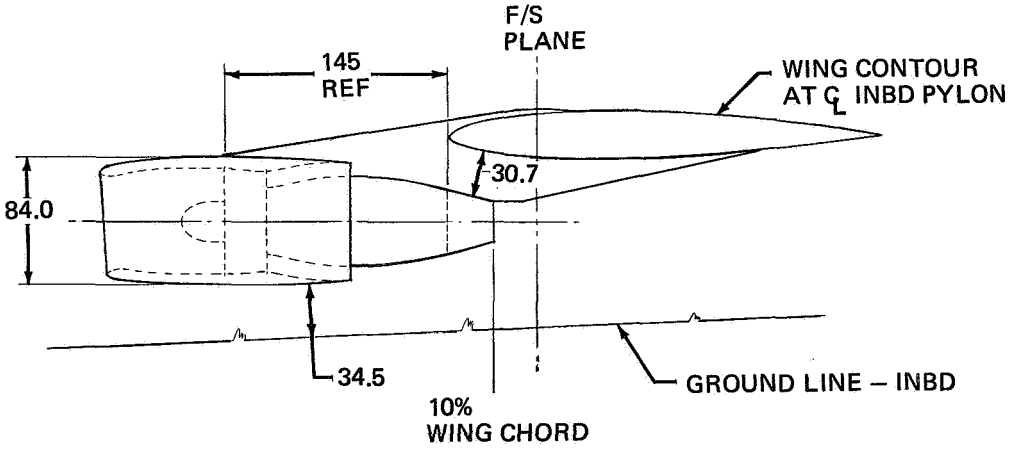

70.0 FAN DIA
145.0 LENGTH

LENGTH CHANGES

NOTE:
DIMENSIONS GIVEN ARE
IN INCHES UNLESS
OTHERWISE SPECIFIED

FIGURE II-27. LENGTH VARIATIONS

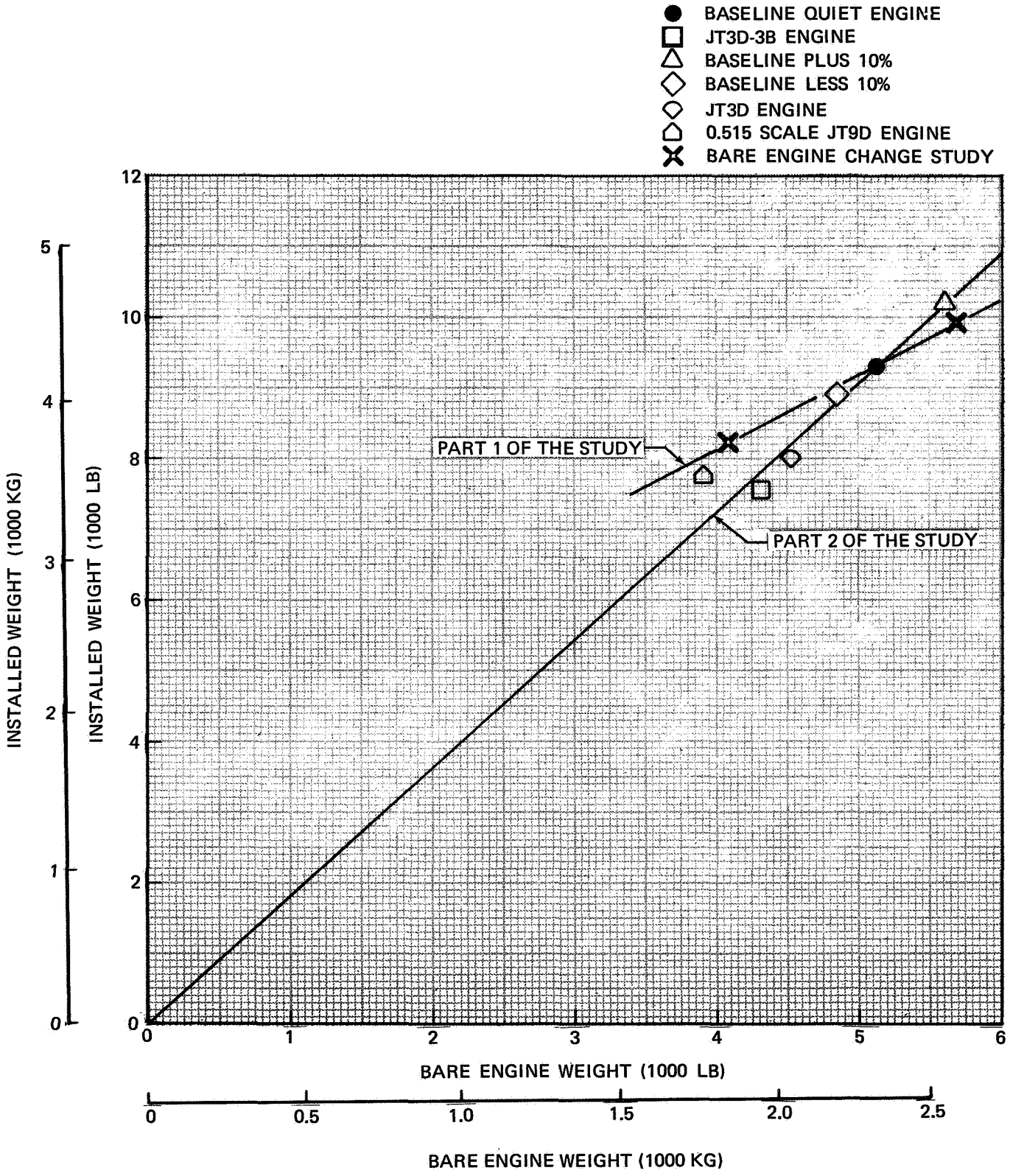

FIGURE II-28. EFFECT OF BARE ENGINE WEIGHT ON INSTALLED NACELLE AND PYLON WEIGHT – MODEL DC-8-61

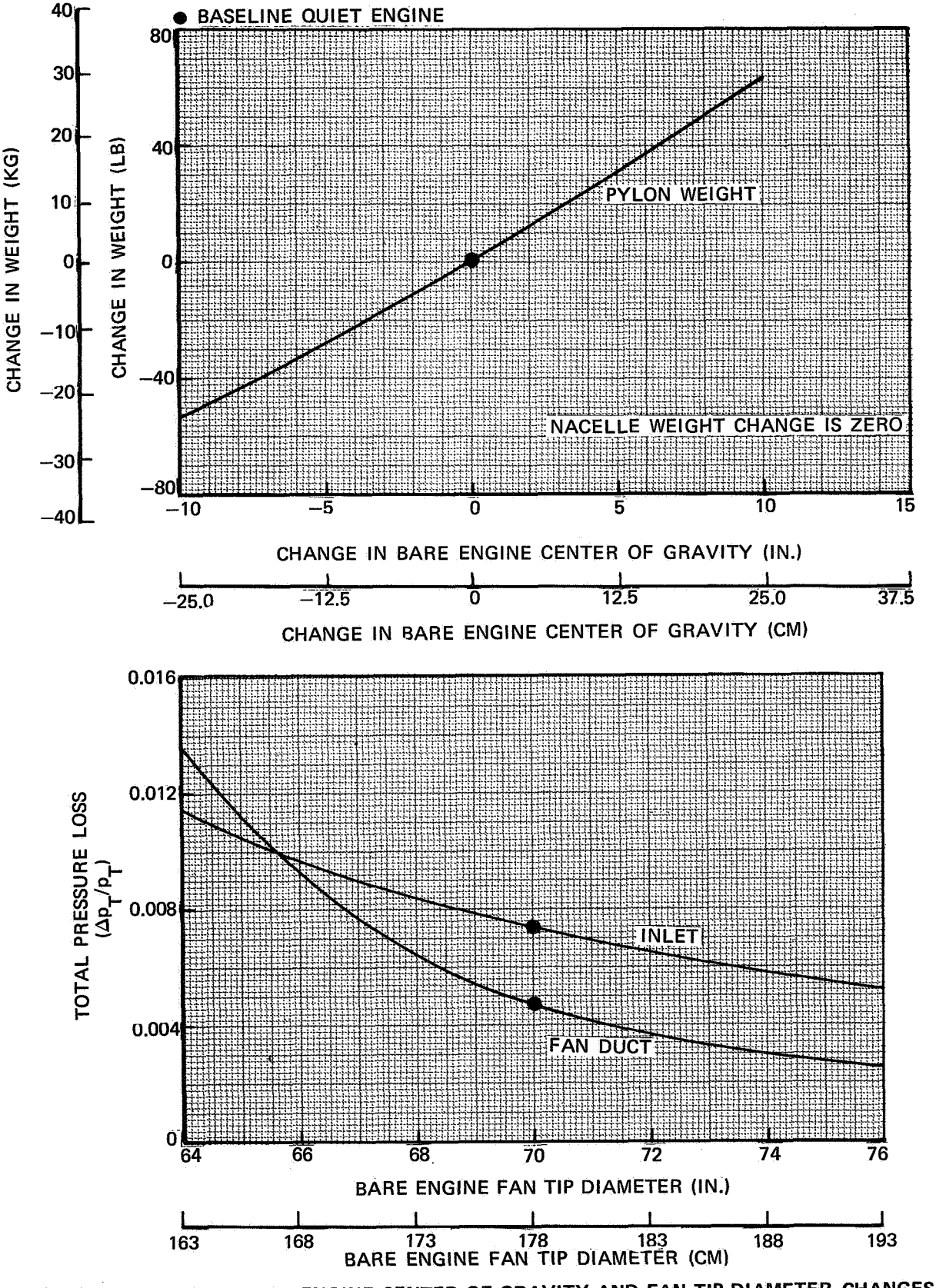

FIGURE II-29. EFFECT OF BARE ENGINE CENTER OF GRAVITY AND FAN TIP DIAMETER CHANGES – MODEL DC-8-61-Q1

Figure II-30 presents an estimate of the required wing weight changes resulting from change in nacelle-pylon moment of inertia about the wing elastic axis. The curve was used in the parametric study to indicate how the wing weight would change with changes in engine weight or location. Figure II-30 can be used with Figure II-28 to correlate wing-weight changes and OWE changes with bare-engine weight changes.

Dimensional Changes

Changes in engine length and diameter were considered independently of changes in engine weight and airflow.

Diameter Changes: The following rules were used to determine the effects of changes in engine maximum diameter on nacelle location (Figure II-26).

a. The engine turbine diameter was changed appropriately with changes in fan-tip diameter.

b. For increased fan-tip diameters, the ground clearance was maintained, and the nacelle was moved forward as required to prevent additional interference drag.

c. For decreased fan-tip diameters, the exit station of the nacelle primary exhaust was maintained, and the nacelle was raised as much as it could be without increasing interference drag.

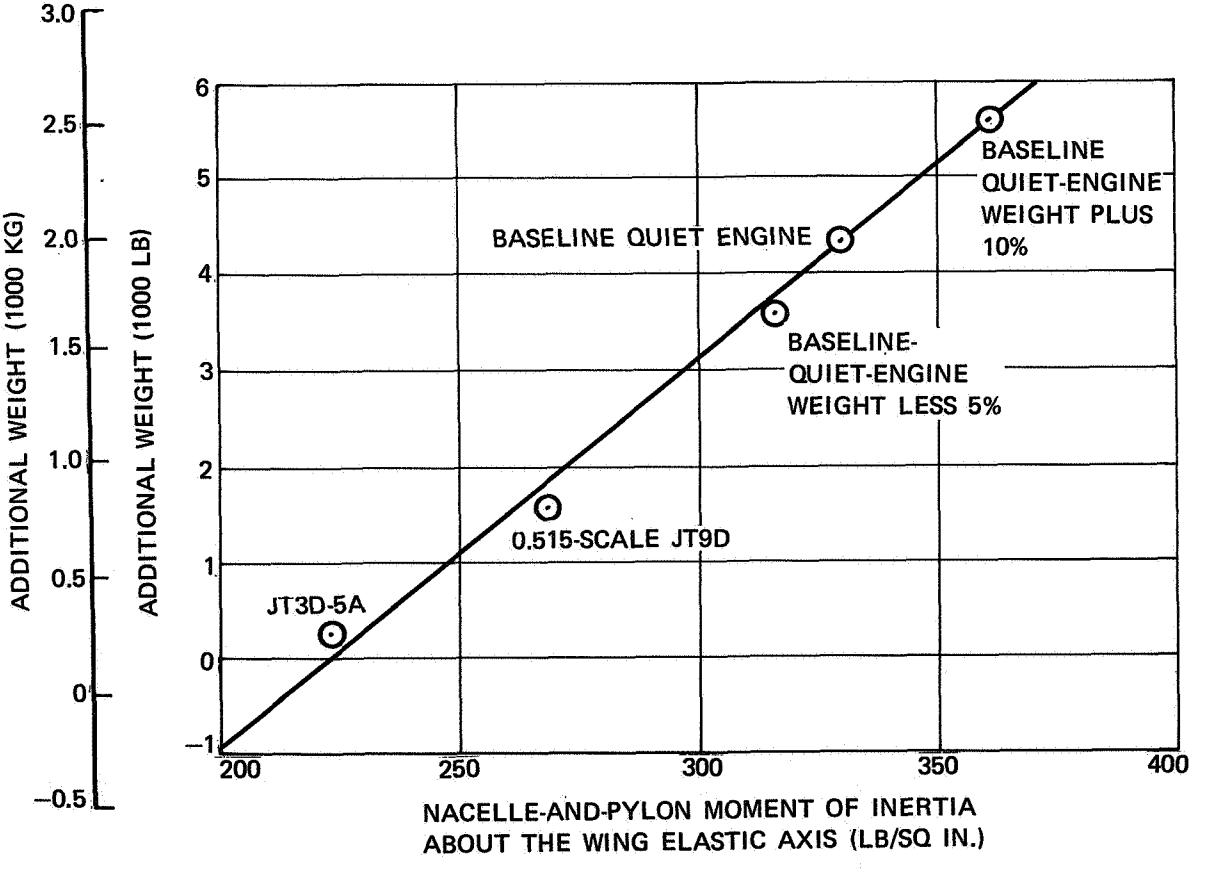

FIGURE II-30. REQUIRED ADDITIONAL WEIGHT FOR WING RESKINNING AND AILERON BALANCE – MODEL DC-8-61

Resulting changes in nacelle and pylon weight can be found in Table II-XII. Changes in nacelle-pylon moment of inertia about the wing elastic axis also are shown in the table.

Because engine airflow is unchanged, the inlet and exhaust total-pressure losses vary inversely with diameter changes.

Figures II-29 and II-31 show how nacelle drag, weight, and ducting total-pressure losses vary with changes in diameter.

Length Changes: Figure II-27 shows the engine length changes. The location of the nacelle primary exhaust nozzle relative to the wing was not changed. The engine center of gravity was assumed to shift half the distance of the length change. This results in a small change in pylon weight (Table II-XII). The moments of inertia about the wing axis are also shown in the table, and the corresponding change in wing weight can be found from Figure II-27. It was assumed that the fan-case length did not change. Therefore, the fan cowling, and hence fan-cowling drag, did not change.

The inlet and fan exhaust duct sound-suppressor configurations that produce the required noise reductions were assumed to be unaffected by changes in engine length. Therefore, there is no change in the inlet and tailpipe total-pressure losses.

Figure II-32 shows how nacelle-pylon drag and weight vary for the cases considered.

Airflow Changes

The effects of engine airflow changes were considered independently of changes in engine weight and dimensions. Engine specific airflow therefore changes, and nacelle drag and weight are not affected. It was assumed that the required sound suppression is not affected by changes in engine airflow. Figure II-33 shows how the inlet and exhaust system total-pressure losses are affected by changes in engine airflow.

PART 2: PARAMETRIC VARIATIONS

A study was conducted to determine the effects of parametric variations in nacelle drag, airplane empty weight, engine SFC, takeoff thrust, and maximum cruise thrust on DC-8-61-Q1 airplane performance. The airplane performance parameters considered were direct operating cost, payload-range, takeoff field length, takeoff flight path, initial cruise altitude, approach speed, and approach thrust required.

Table II-XIV shows the incremental changes that were selected for each of the related engine parameters noted. An attempt was made to associate the selected variations with possible real changes. One such real case is a scaled version of the JT9D engine. The engine was scaled to match the uninstalled maximum cruise thrust of the baseline quiet engine at 35,000 feet (10,668 m) and 0.82 Mach number. Other engines that were used included the JT3D-5A and study engines from the NASA Quiet Engine Definition Program (QA-1 and QC-3).

Nacelle Drag

The variations in nacelle drag include those that correspond to a scaled JT9D with and without external sound suppressing treatment. Also included are drag increments that correspond to two

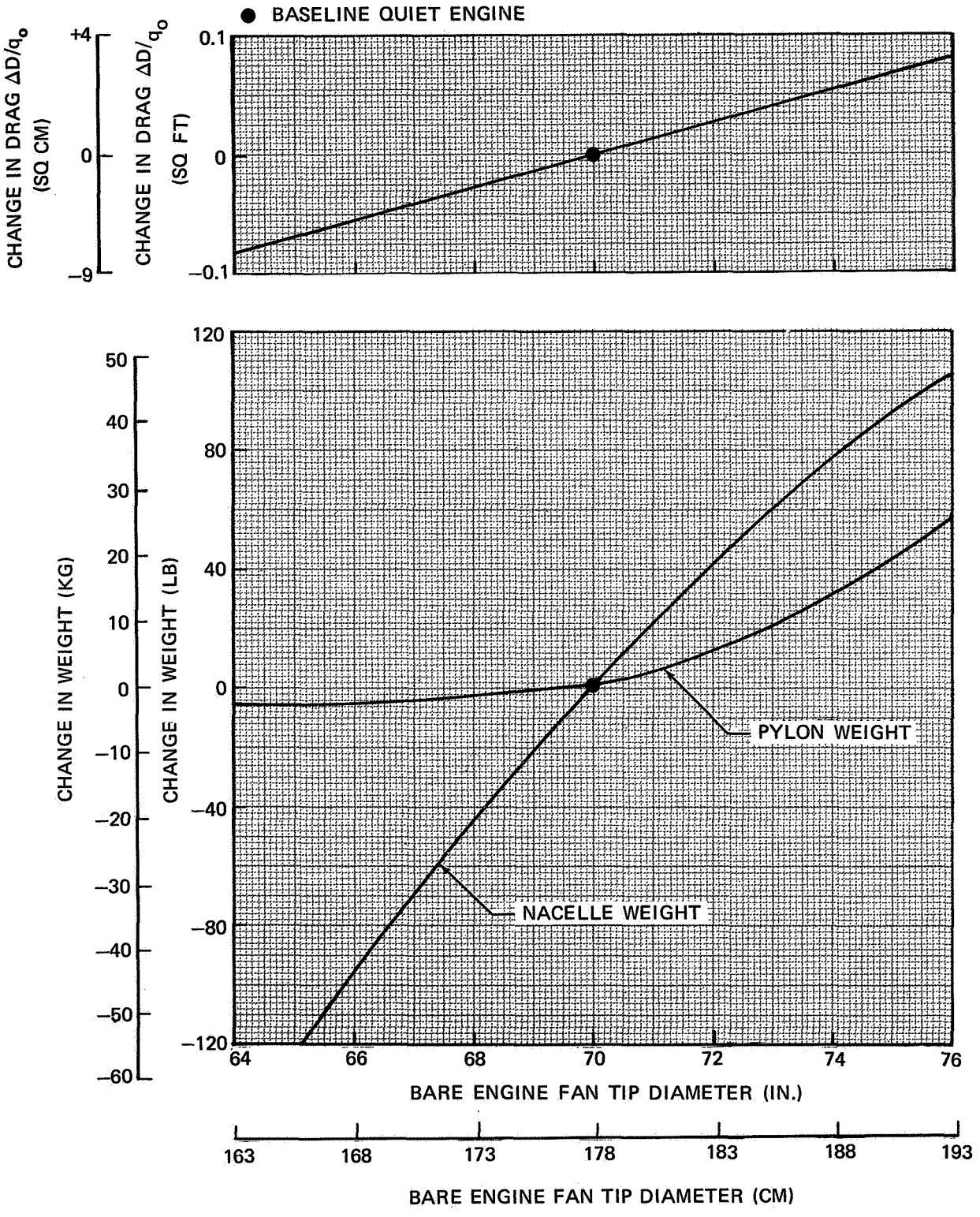

FIGURE II-31. EFFECT OF BARE ENGINE FAN TIP DIAMETER CHANGES ON NACELLE AND PYLON WEIGHT AND ON NACELLE-PYLON DRAG – MODEL DC-8-61-Q1

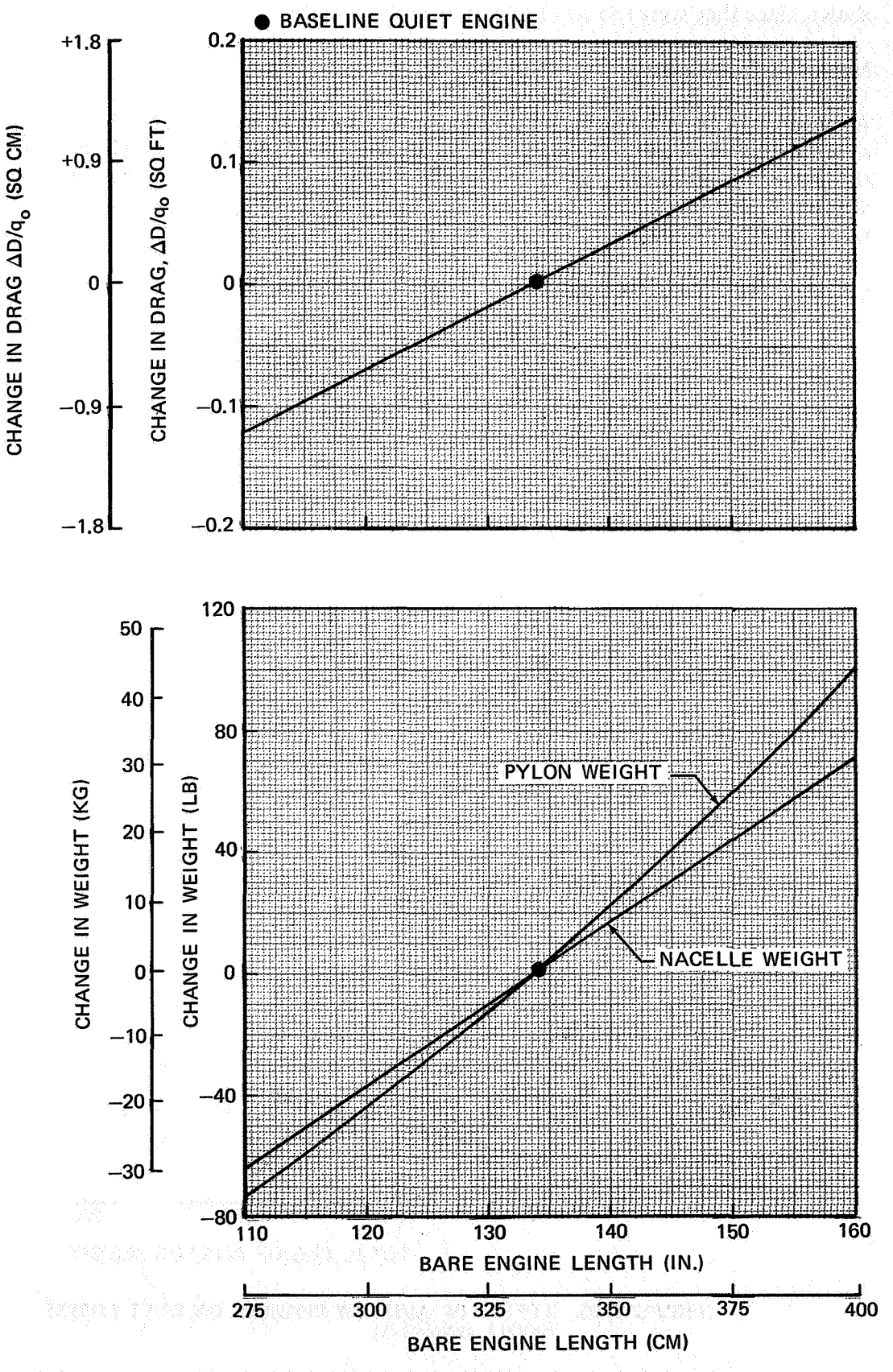

FIGURE II-32. EFFECT OF BARE ENGINE LENGTH CHANGES ON NACELLE-PYLON DRAG AND ON NACELLE AND PYLON WEIGHT – MODEL DC-8-61-Q1

different longitudinal locations of the baseline quiet engine. Figure II-34 shows the nacelles for the baseline quiet engine and for the scaled JT9D. The two changes in the longitudinal location are not shown, since they were too small to be seen in the picture.

Maximum Cruise Thrust

Analysis of DC-8-61 performance revealed that the maximum value of uninstalled cruise thrust the airplane can safely use before the onset of buffet is about 5100 pounds (22,686 N).Consequently, this value was selected as the upper limit for the parametric study. The lowest value selected is almost the same as that of the uninstalled thrust of the JT3D-3B. Also selected was a value that would produce the same installed thrust as that of the JT3D-3B.

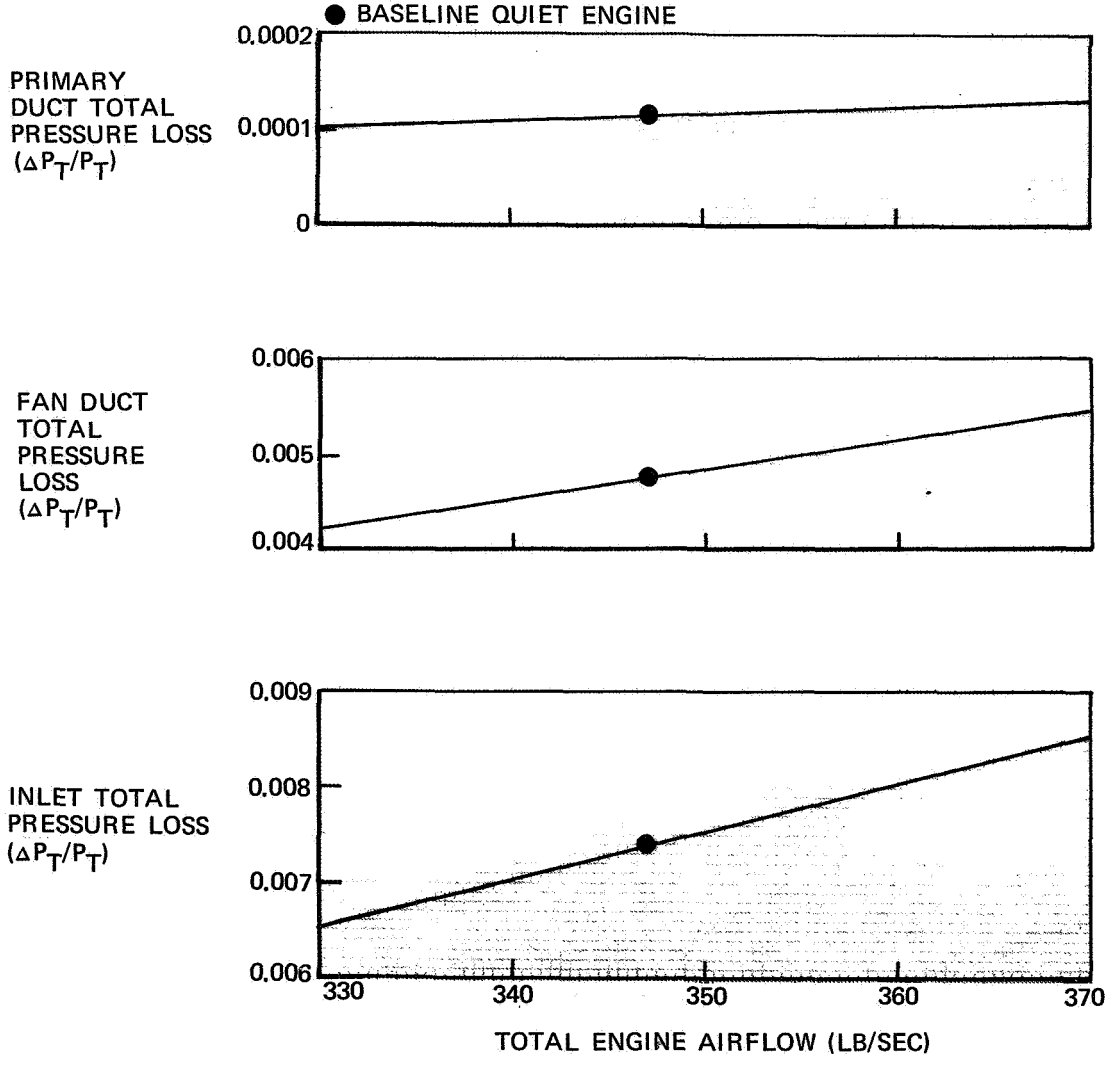

FIGURE II-33. EFFECT OF AIRFLOW CHANGES ON DUCT LOSSES – MODEL DC-8-61-Q1

TABLE II-XIV
INCREMENTS FOR PARAMETRIC STUDY

NACELLE DRAG

1.	UNSUPPRESSED JT9D-1 ENGINE SCALED TO 4900 LB (21,796 N) OF MAX CRUISE THRUST AT 35,000 FT (10,668 M) AND M = 0.82 SCALE FACTOR = 0.515	−16.8%
2.	ITEM 1 ABOVE WITH 10 PNdB NACELLE NOISE SUPPRESSION	−13.8%
3.	NACELLE LOCATION 5 IN. (12.7 CM) AFT OF BASE DESIGN	+6%
4.	NACELLE LOCATION 8 IN. (20.3 CM) AFT OF BASE DESIGN	+15%

MAX CRUISE THRUST
35,000 FT (10,668 M), M = 0.82

1.	BASE LESS 10% (F_n = 4400 LB − 19,573 N)	−10%
2.	BASE LESS 6% (F_n = 4600 LB − 20,462 N)	− 6%
3.	VALUE THAT PRODUCES THE SAME WING THRUST AS THE JT3D-3B, QE LOSSES, F_n = 4750 LB (21,129 N)	− 3%
4.	1.35-g LIMIT, QE LOSSES, F_n = 5100 LB (22,686 N)	+ 4%

TAKEOFF THRUST @ 100 KTS

1.	JT3D-3B	−16%
2.	QA-1 (BYPASS RATIO = 3.0)	− 7%
3.	0.515-SCALE JT9D-1	− 4%
4.	QC-3 (BYPASS RATIO = 8.0)	+ 8%

ENGINE WEIGHT

1.	WEIGHT OF 0.515-SCALE UNSUPPRESSED JT9D-1	−20%
2.	WEIGHT OF JT3D-5A (4540 LB − 2059 KG)	−11%
3.	QE WEIGHT LESS 5%	− 5%
4.	QC-3 WEIGHT (5610 LB − 2545 KG)	+10%

ENGINE SFC
MAX CRUISE, 35,000 FT (10,668 M), M = 0.82

1.	BASE CASE LESS 5%	− 5.0%
2.	QC-3 (BYPASS RATIO = 8.0)	− 1.3%
3.	QA-1 (BYPASS RATIO = 3.0)	+ 4.9%
4.	BASE CASE PLUS 10%	+10%

Engine Weight

The weight of the scaled JT9D was included as one weight increment. Two others were the weights of the JT3D-5A and the QC-3. The fourth was an arbitrary weight increment 5 percent less than the weight of the baseline quiet engine. Table II-XV shows the changes in airplane weight, including any necessary structure modifications, that result from the selected engine-weight increments. Also shown for reference are the weights for the DC-8-61 and DC-8-61-Q1 airplanes. Notice that the Maximum Design Zero-Fuel Weight for the 10-percent-weight-increment case is 4254 pounds (1930 kg) heavier than the present 224,000-pound (101,606 kg) limit for the space-limited payload. Analysis would be required to ascertain what structural modifications, if any, would be required to certify this weight. The normal payload considered in this study results in a maximum zero-fuel weight considerably less than 224,000 pounds (101,606 kg).

Takeoff Thrust at 100 Knots

The thrust values selected for the parametric study include those for the scaled JT9D, the JT3D-3B, the QA-1, and the QC-3 engines. Engines with a sea-level static-thrust rating higher than approximately 23,000 pounds (102,309 N) will produce a pitch-up moment that cannot be counteracted with the present DC-8-61 control system. Therefore, engines having ratings higher than 23,000 pounds (102,309 N) would have to be operated at less than takeoff power unless extensive modifications of the airplane control system were made.

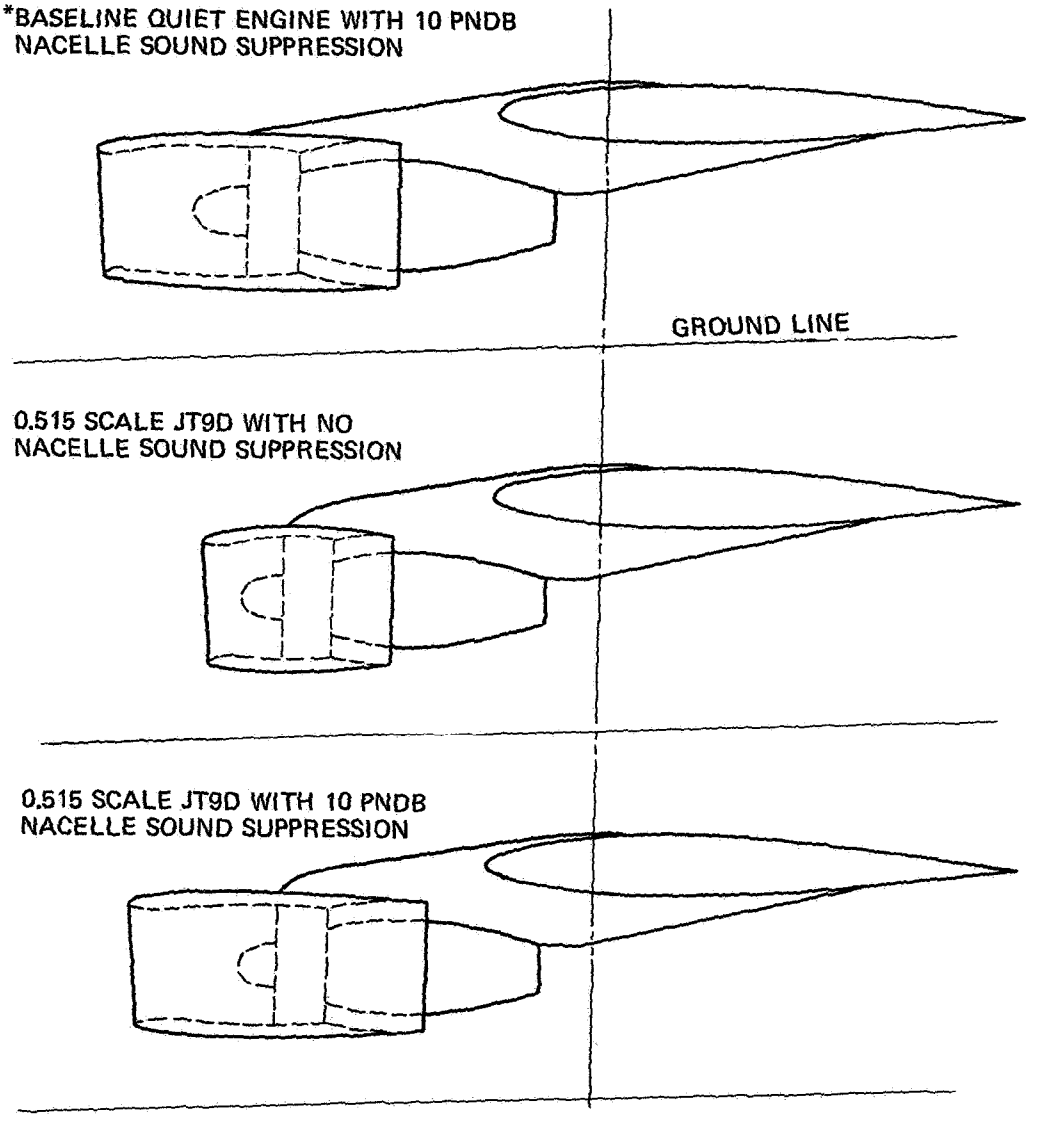

*THE TWO OTHER DRAG VARIATIONS USED WERE BASED ON THIS ARRANGEMENT LOCATED 5 IN. (12.7 CM) AND 8 IN. (20.3 CM) AFT RESPECTIVELY.

FIGURE II-34. ENGINE ARRANGEMENTS USED FOR NACELLE DRAG VARIATIONS

TABLE II-XV
PARAMETRIC WEIGHT VARIATIONS

	BASELINE EAL DC-8-61		BASELINE QUIET ENG DC-8-61-Q1		QUIET ENG (10%)		QUIET ENG (–5%)		SCALED JT9D		JT3D-5A	
	LB	KG	LB	KG	LB	KG	LB	KG	LB	KG	LB	KG
MAX TAKEOFF WEIGHT	325,000	147,420	325,000	147,420	325,000	147,420	325,000	147,420	325,000	147,420	325,000	147,420
MAX LANDING WEIGHT	240,000	108,864	240,000	108,864	240,000	108,864	240,000	108,864	240,000	108,864	240,000	108,864
MANUFACTURER'S WEIGHT EMPTY	149,339	67,740	160,503	72,804	164,945	74,819	157,945	71,644	151,557	68,746	151,293	68,627
OPERATOR'S WEIGHT EMPTY	156,803	71,126	167,967	76,190	172,409	78,205	165,409	75,030	159,021	72,132	158,757	72,012
MAX DESIGN ZERO-FUEL WEIGHT	224,000	101,606	224,812*	102,428	229,254*	103,990	224,000	101,606	224,000	101,606	224,000	101,606
SPACE-LIMITED PAYLOAD	56,845	25,785	56,845	25,785	56,845	25,785	56,845	25,785	56,845	25,785	56,845	25,785

*ZERO-FUEL WEIGHT (WITH SPACE-LIMITED PAYLOAD)

Engine SFC

Two of the SFC variations used in this part of the study are for the QA-1 and QC-3 engines, and two are arbitrary increments. These variations were applied over the entire flight profile.

Interpretation of Results

Table II-XVI shows the change factors that resulted from this study. All of the changes are essentially linear within the range of variations shown (Table II-XVI). The table may, therefore, be used with confidence for changes within these ranges. The effect on airplane performance is shown for three ranges: the range corresponding to Max TOGW, a medium range, and a short range. Note that the change factors shown apply to airplane performance, whereas the incremental changes apply to a single nacelle. The change DOC is shown as a percent. The reference value of DOC is the one that does not include depreciation.

Changes in two values of DOC are shown. The cost per mile is the total trip cost divided by the range. The cost per unit payload per mile, or seat-mile cost, has the effect of distributing the cost-per-mile value throughout the payload. The payload unit of 200 pounds (91 kg) corresponds to one passenger and his baggage. The values in the table represent the changes in the performance parameters due to the changes per nacelle at the tops of the columns. For example, a 200-pound (91 kg) increase (50 pound – 23 kg – per nacelle) in OWE will reduce the initial cruise altitude by 24 feet (7 m) for a 2360-nautical-mile mission. For the same increase in nacelle weight, the change in direct operating cost is negligible (zero for both cost parameters).

The first column (Table II-XVI) is the change factor for changes in OWE. This is a more flexible variable than engine or nacelle weight (which can be converted to a change in OWE by consideration of the data in Figures II-28 and/or II-30. Figures II-35 through II-52 show the effect of the change-factor study on the performance curves shown earlier for the DC-8-61-Q1. These effects are shown only for those cases where the change increments had a noticeable effect.

The change in seat-mile cost could be plotted only for the largest selected increment in nacelle drag and SFC.

The changes have no effect on approach airspeed. The approach thrust required changes by an amount equal to the nacelle-drag change and is too small to be plotted.

TABLE II-XVI
CHANGE-FACTOR SUMMARY FOR QUIET-ENGINE INSTALLATIONS – MODEL DC-8-61-Q1

PERFORMANCE-PARAMETER CHANGES	UNITS	4-ENGINE OPERATION: AIRPLANE EMPTY WEIGHT, OWE Δ = 200 LB Δ = 90.7 KG	CHANGE PER NACELLE: NACELLE DRAG $\Delta D/q_0$ = 0.25 SQ FT $\Delta D/q_0$ = 23 SQ CM	CHANGE PER NACELLE: ENGINE SFC Δ = 1%	CHANGE PER NACELLE: TAKEOFF THRUST AT 100 KTS Δ = 1000 LB Δ = 4448.2 N	CHANGE PER NACELLE: MAX CRUISE THRUST Δ = 100 LB Δ = 444.82 N
DOC AT CONSTANT RANGE ¢/200 LB/N MI						
LONG RANGE	Δ%	0.53	3.78	3.00	0	0
MEDIUM RANGE		0.021	0.647	0.171	0	0
SHORT RANGE		0.018	0.948	0.134	0	0
DOC AT CONSTANT RANGE $/N MI						
LONG RANGE	Δ%	0	0.750	0.231	0	0
MEDIUM RANGE		0.021	0.647	0.171	0	0
SHORT RANGE		0.018	0.948	0.134	0	0
PAYLOAD AT CONSTANT RANGE						
LONG RANGE	ΔLB	–200	–1170	–950	0	0
MEDIUM RANGE		0	0	0	0	0
SHORT RANGE		0	0	0	0	0
TAKEOFF FIELD LENGTH AT CONSTANT RANGE, 15° FLAPS						
LONG RANGE	ΔFT	0	0	0	–436	0
MEDIUM RANGE		13	75	49	–327	0
SHORT RANGE		8	13	9	–262	0
INITIAL CRUISE ALTITUDE						
LONG RANGE	ΔFT	0	–1450	0	0	1000
MEDIUM RANGE		–24	–600	–72	0	831
SHORT RANGE		–19	–300	–21	0	714
HEIGHT AT 3 N MI FROM START OF TAKEOFF ROLL, 15° FLAPS						
LONG RANGE	ΔFT	0	0	0	150	0
MEDIUM RANGE		–5	–19	–13	190	0
SHORT RANGE		–4	–7	6	210	0

LONG RANGE: 3912 N MI AND TOGW = 325,000 LB
MEDIUM RANGE: 2360 N MI AND TOGW = 280,000 LB
SHORT RANGE: 847 N MI AND TOGW = 242,000 LB

EXAMPLE

THE –24 IN THE COLUMN AIRPLANE OWE MEANS THAT AN OWE INCREASE OF 200 LB PER AIRPLANE WILL CAUSE A 24-FOOT DECREASE IN THE INITIAL CRUISE ALTITUDE FOR THE MEDIUM RANGE CASE.

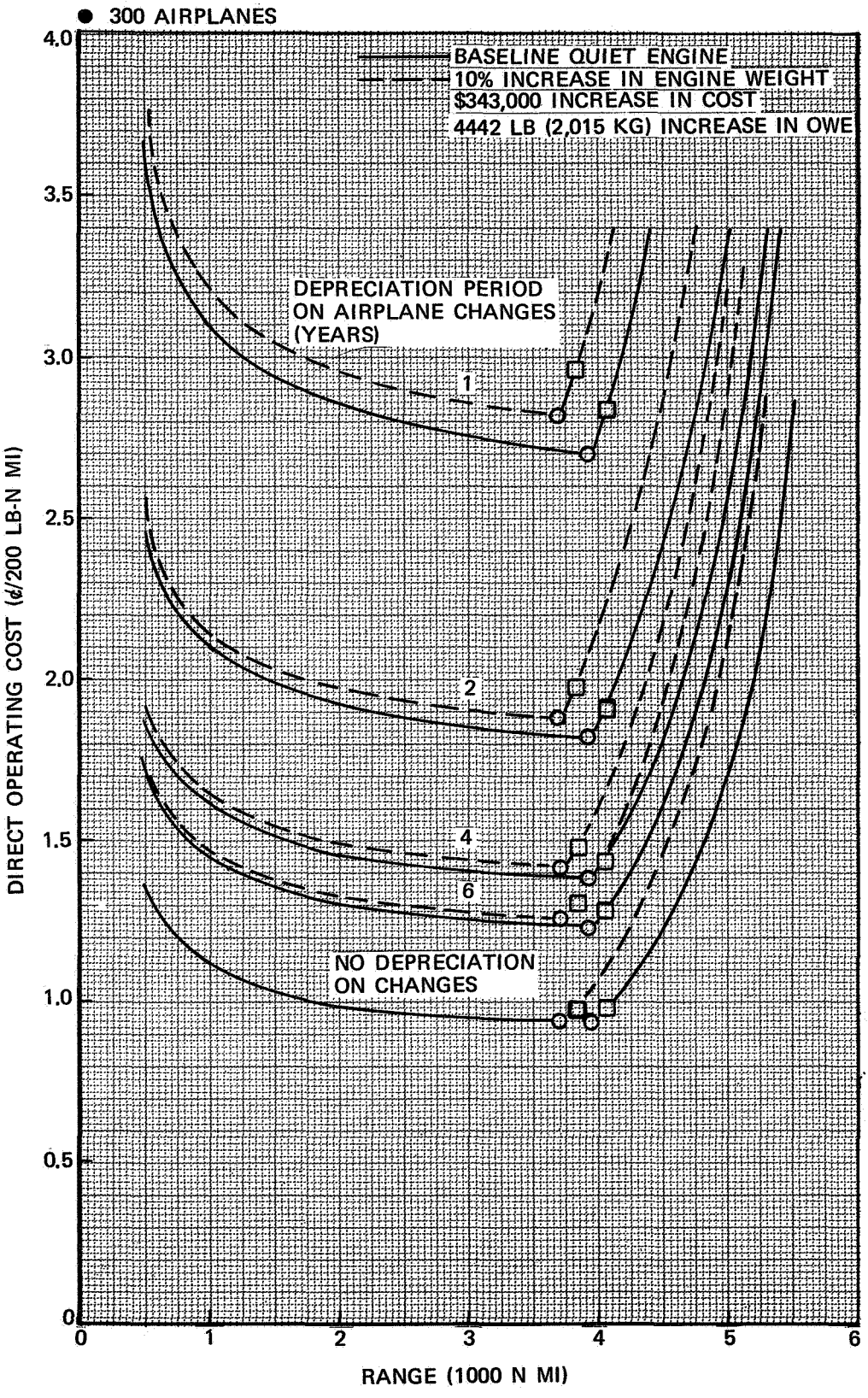

FIGURE II-35. EFFECT OF OWE INCREASE ON DOC (CENTS PER MILE) — MODEL DC-8-61-Q1

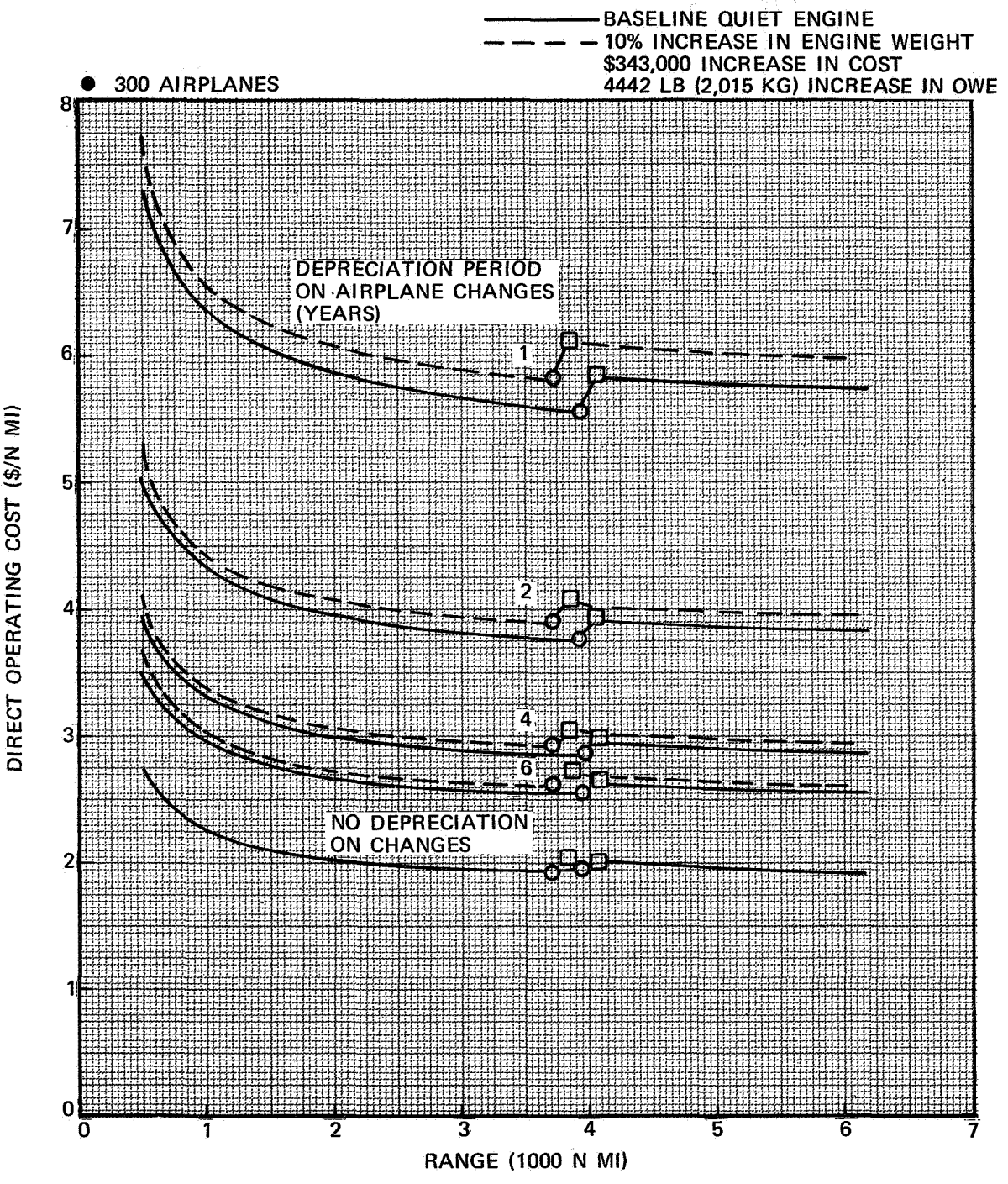

FIGURE II-36. EFFECT OF OWE INCREASE ON DOC (DOLLARS PER NAUTICAL MILE) – MODEL DC-8-61-Q1

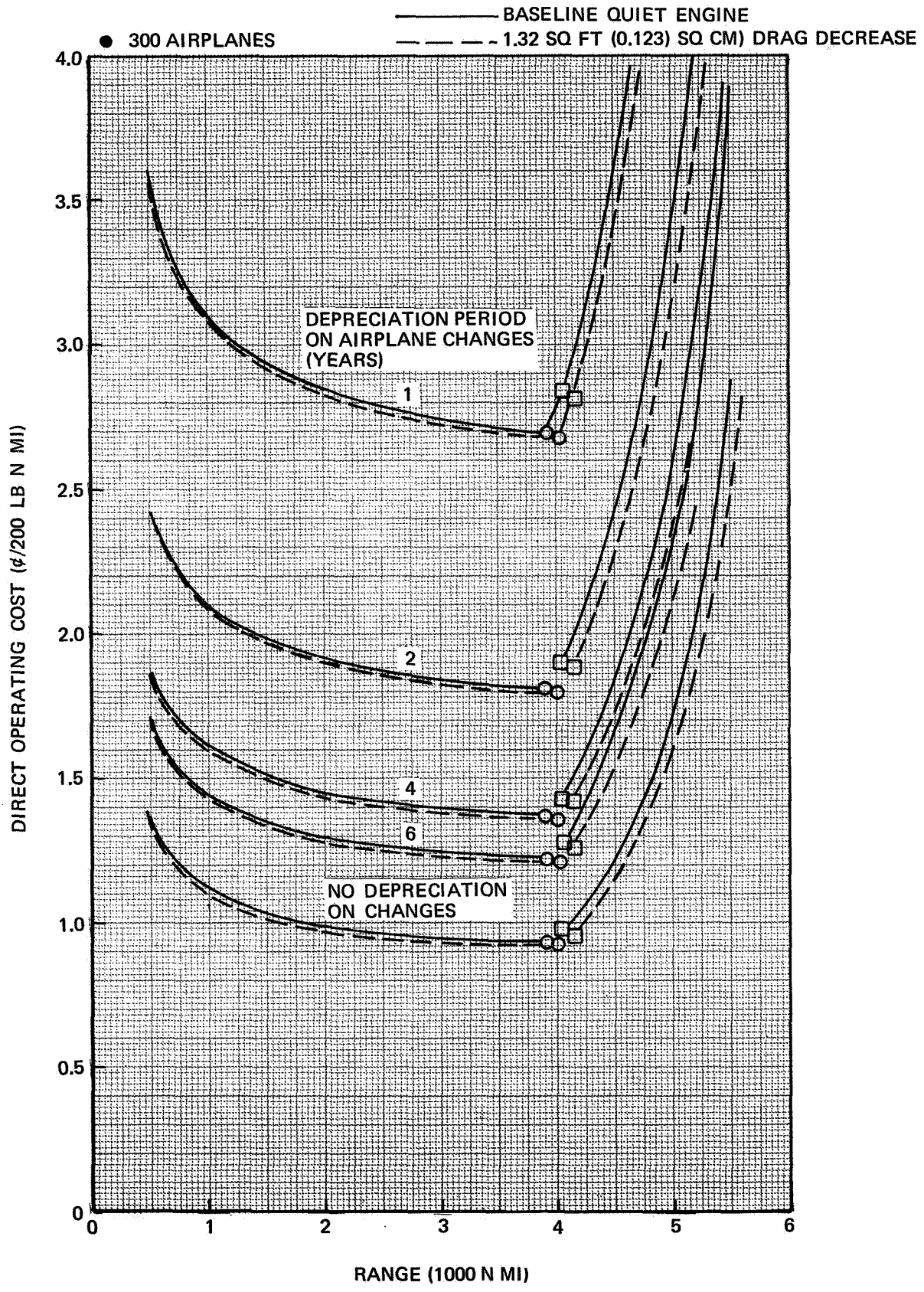

FIGURE II-37. EFFECT OF DRAG DECREASE ON DOC (CENTS PER MILE) – MODEL DC-8-61-Q1

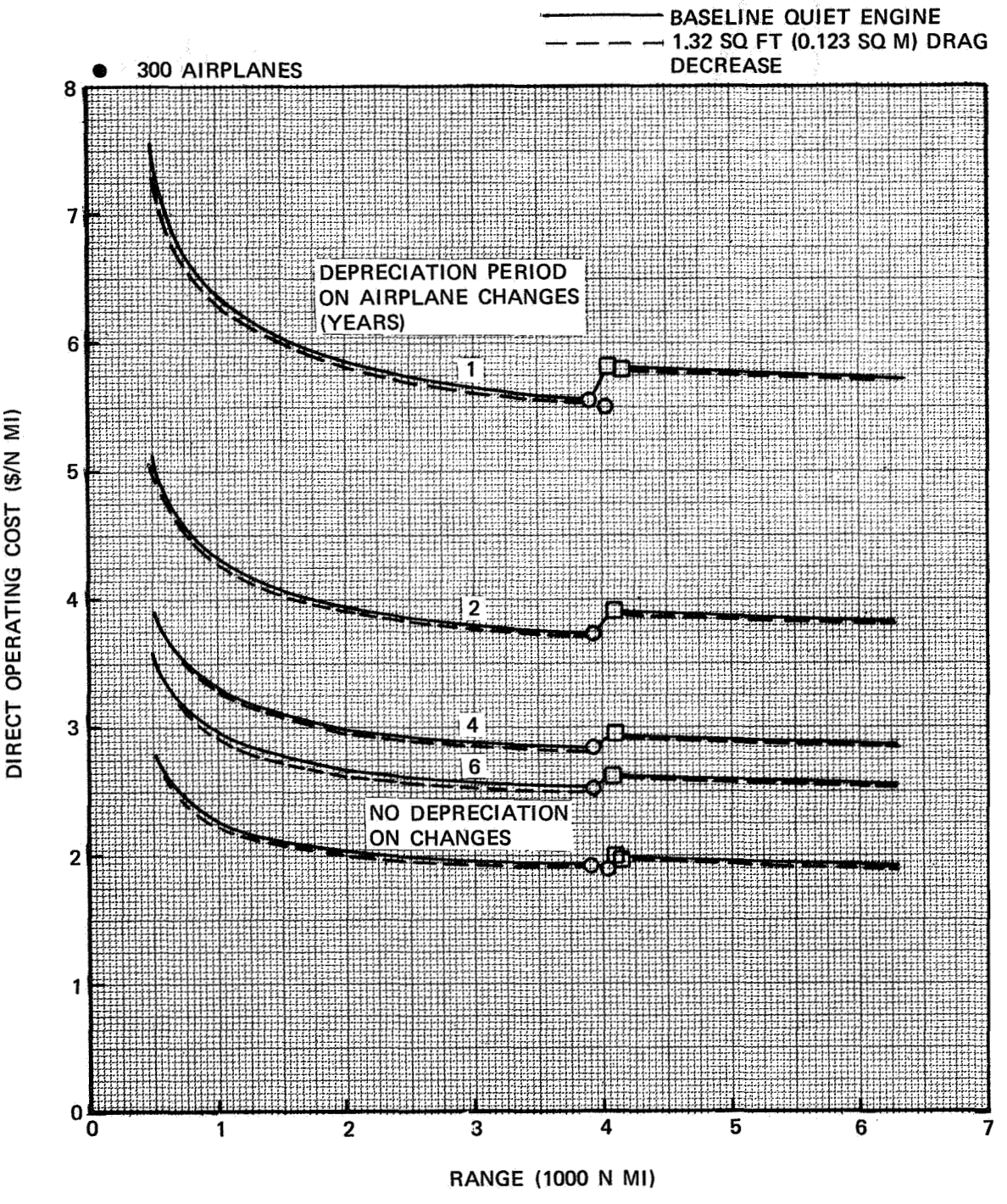

FIGURE II-38. EFFECT OF DRAG DECREASE ON DOC (DOLLARS PER NAUTICAL MILE) – MODEL DC-8-61-Q1

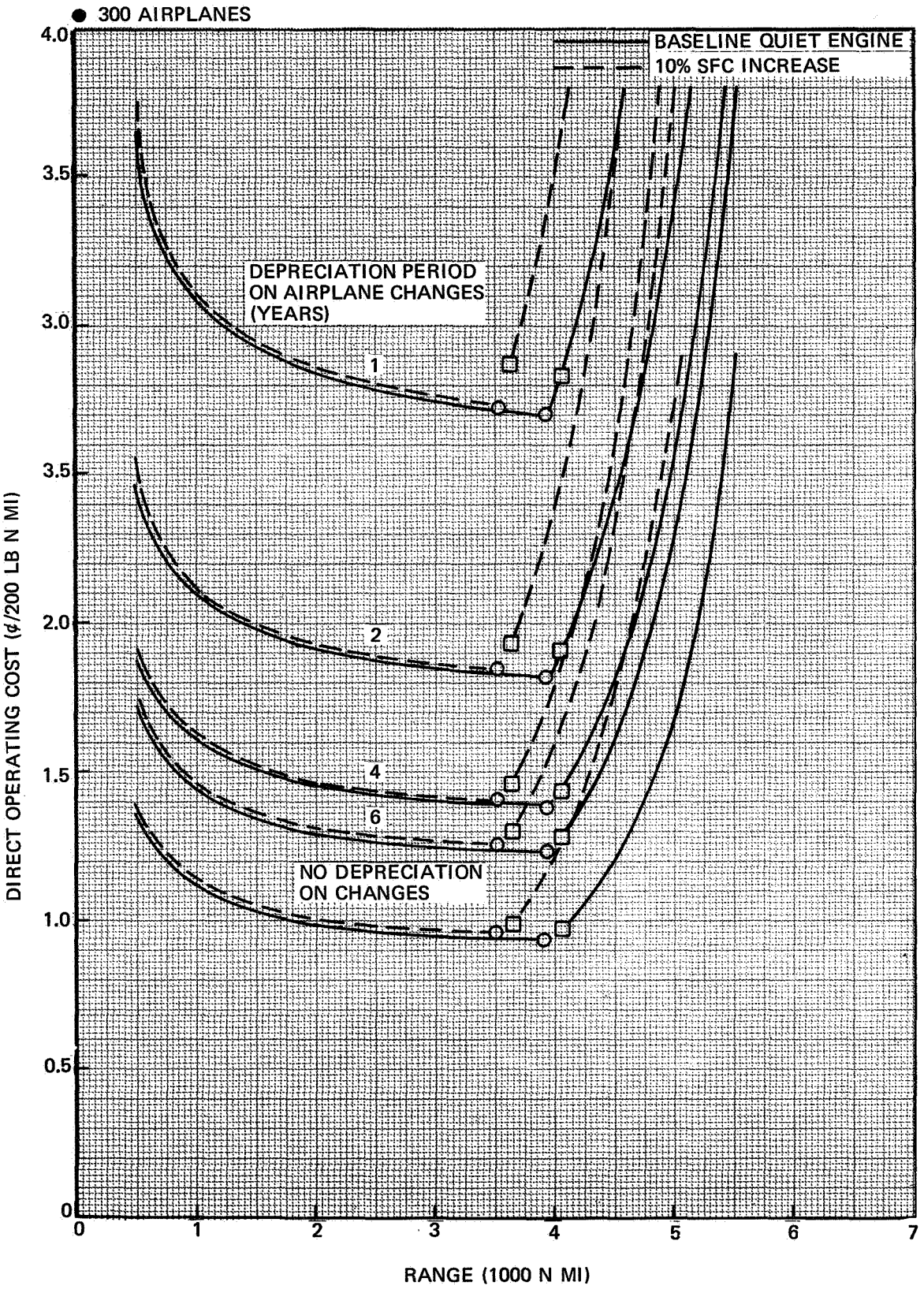

FIGURE II-39. EFFECT OF SFC INCREASE ON DOC (CENTS PER MILE) – MODEL DC-8-61-Q1

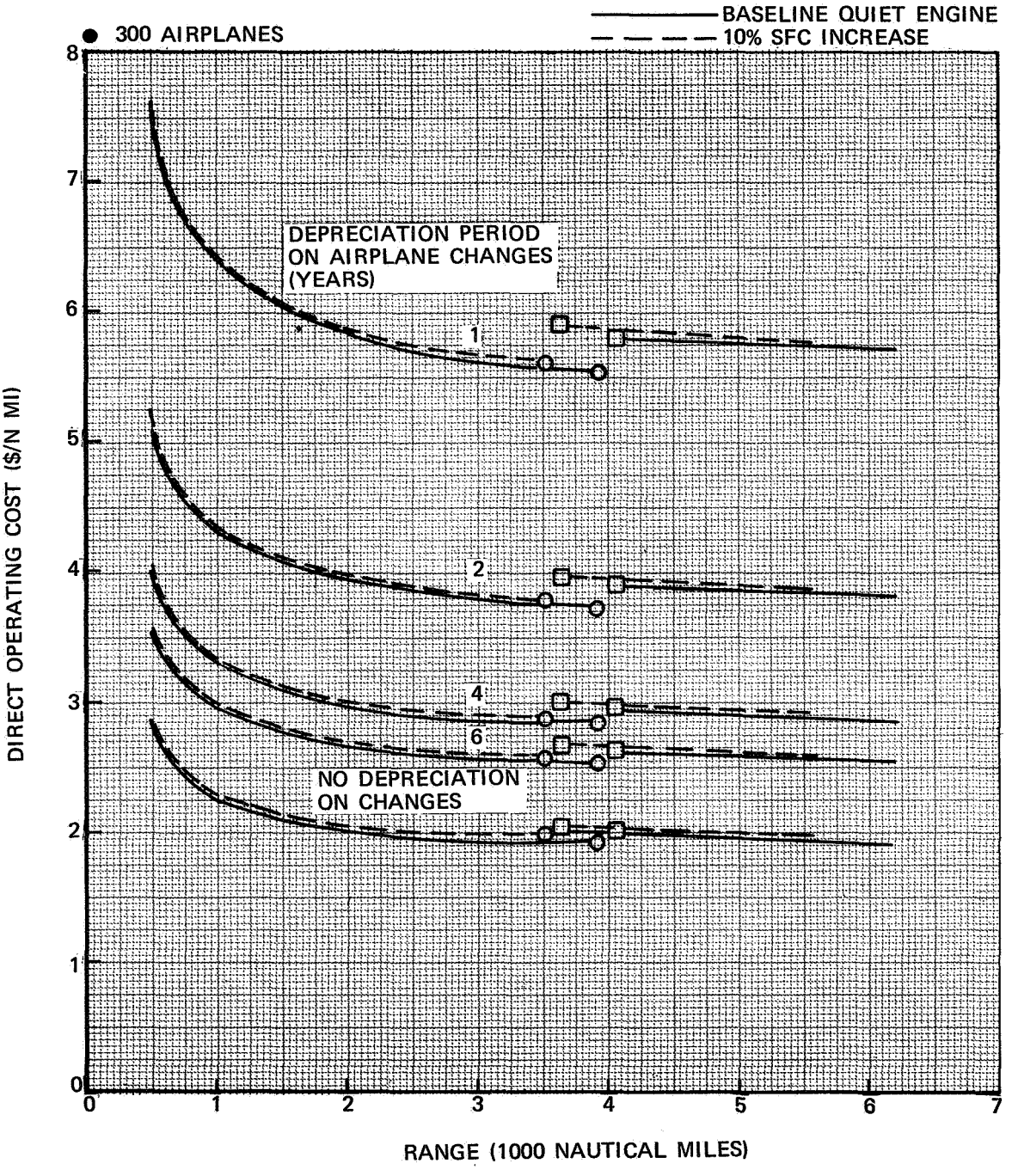

FIGURE II-40. EFFECT OF SFC INCREASE ON DOC (DOLLARS PER NAUTICAL MILE) – MODEL DC-8-61-Q1

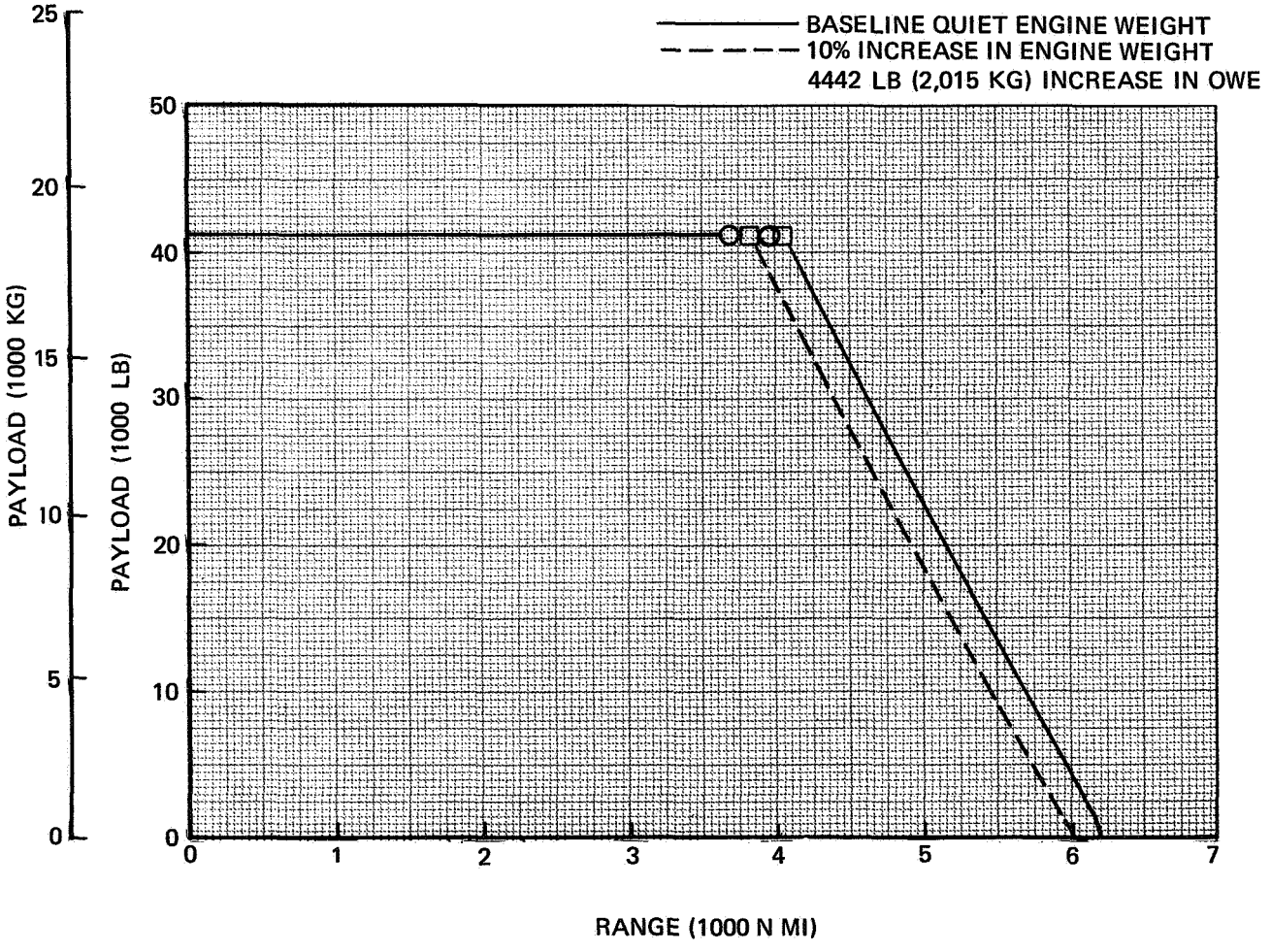

FIGURE II-41. PAYLOAD-RANGE CAPABILITY WITH WEIGHT CHANGES – MODEL DC-8-61

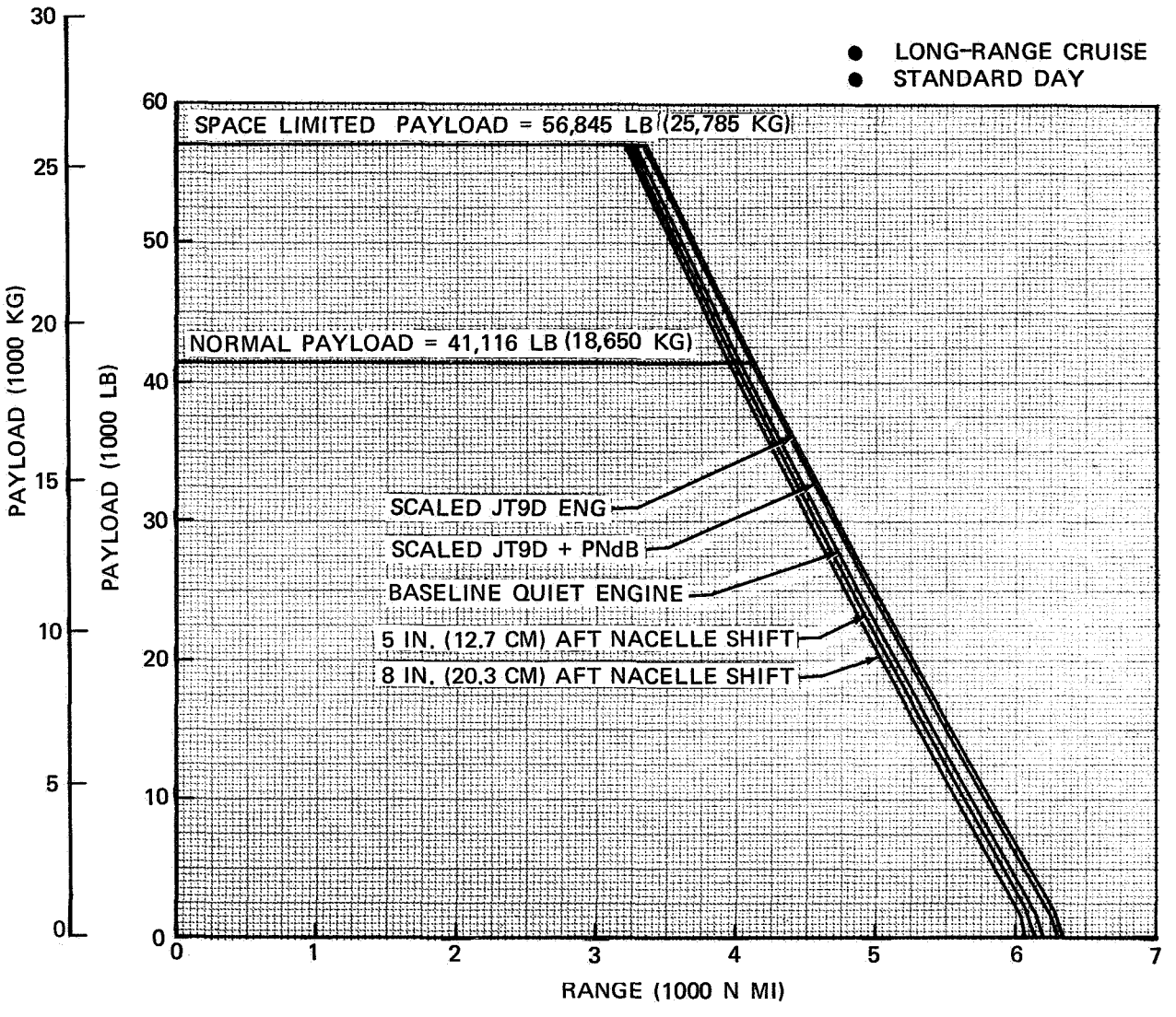

FIGURE II-42. PAYLOAD-RANGE WITH NACELLE DRAG CHANGES – MODEL DC-8-61

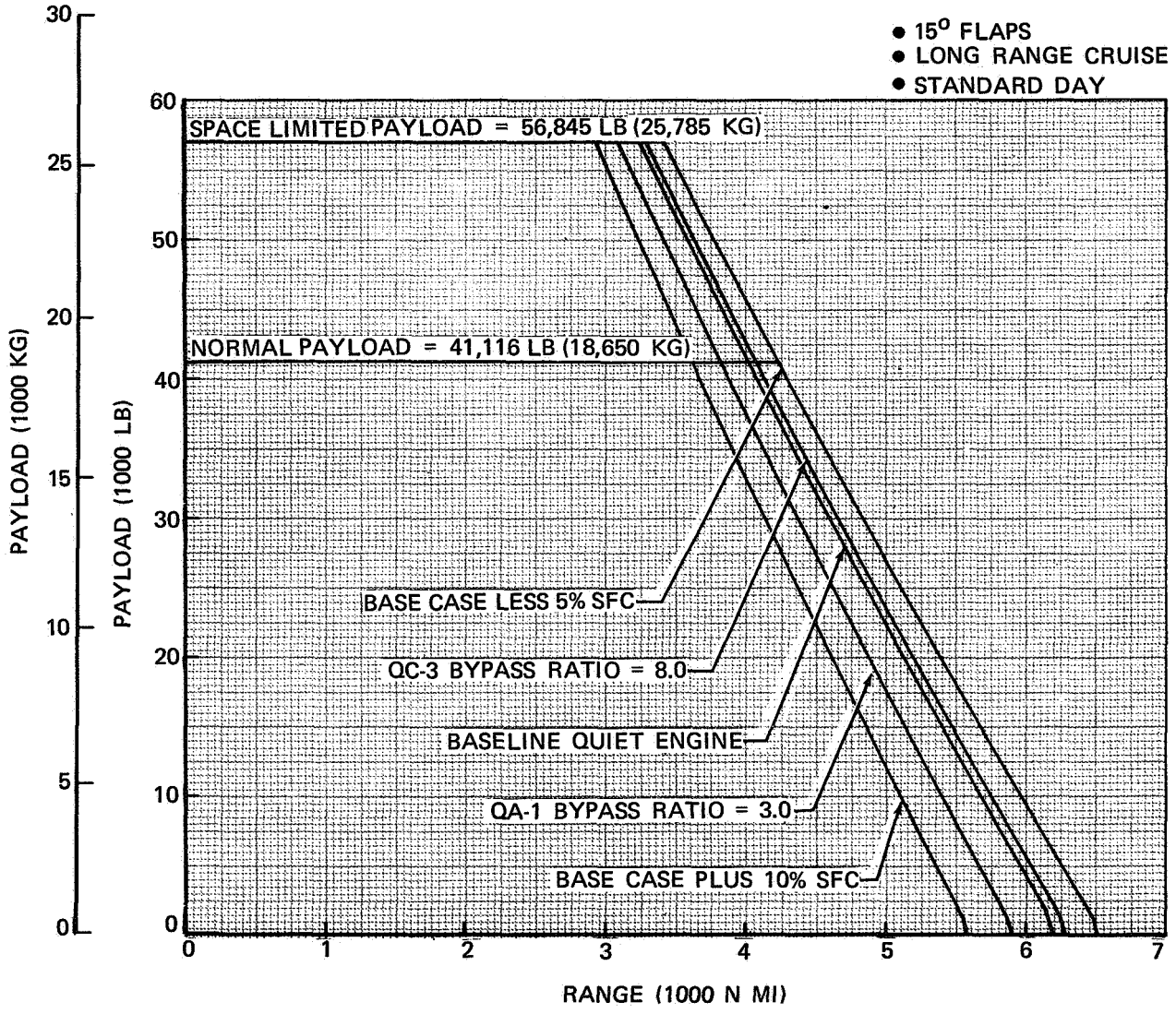

FIGURE II-43. PAYLOAD-RANGE WITH ENGINE SFC CHANGES – MODEL DC-8-61

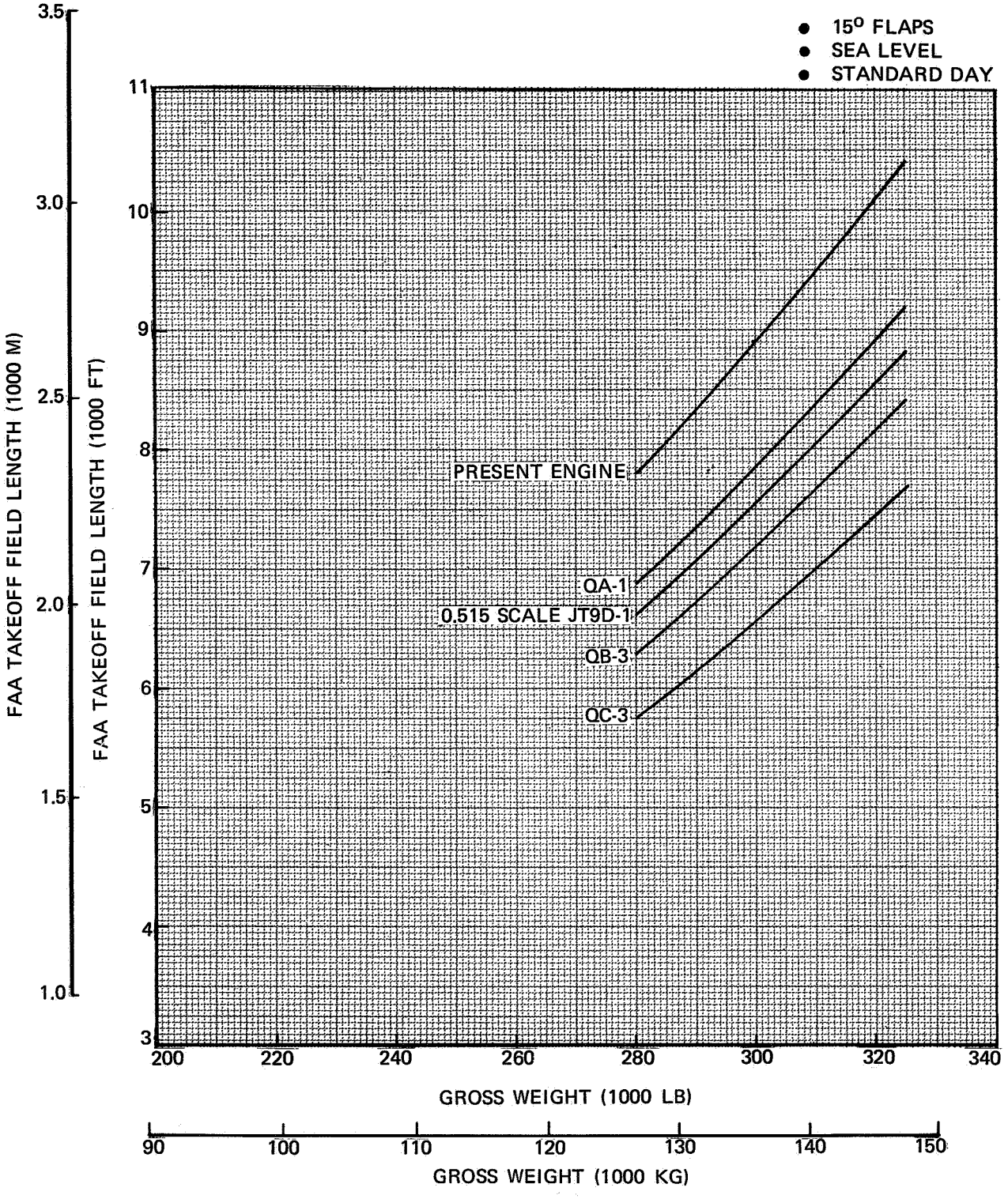

FIGURE II-44. FAA TAKEOFF FIELD LENGTH, 15° FLAPS – MODEL DC-8-61

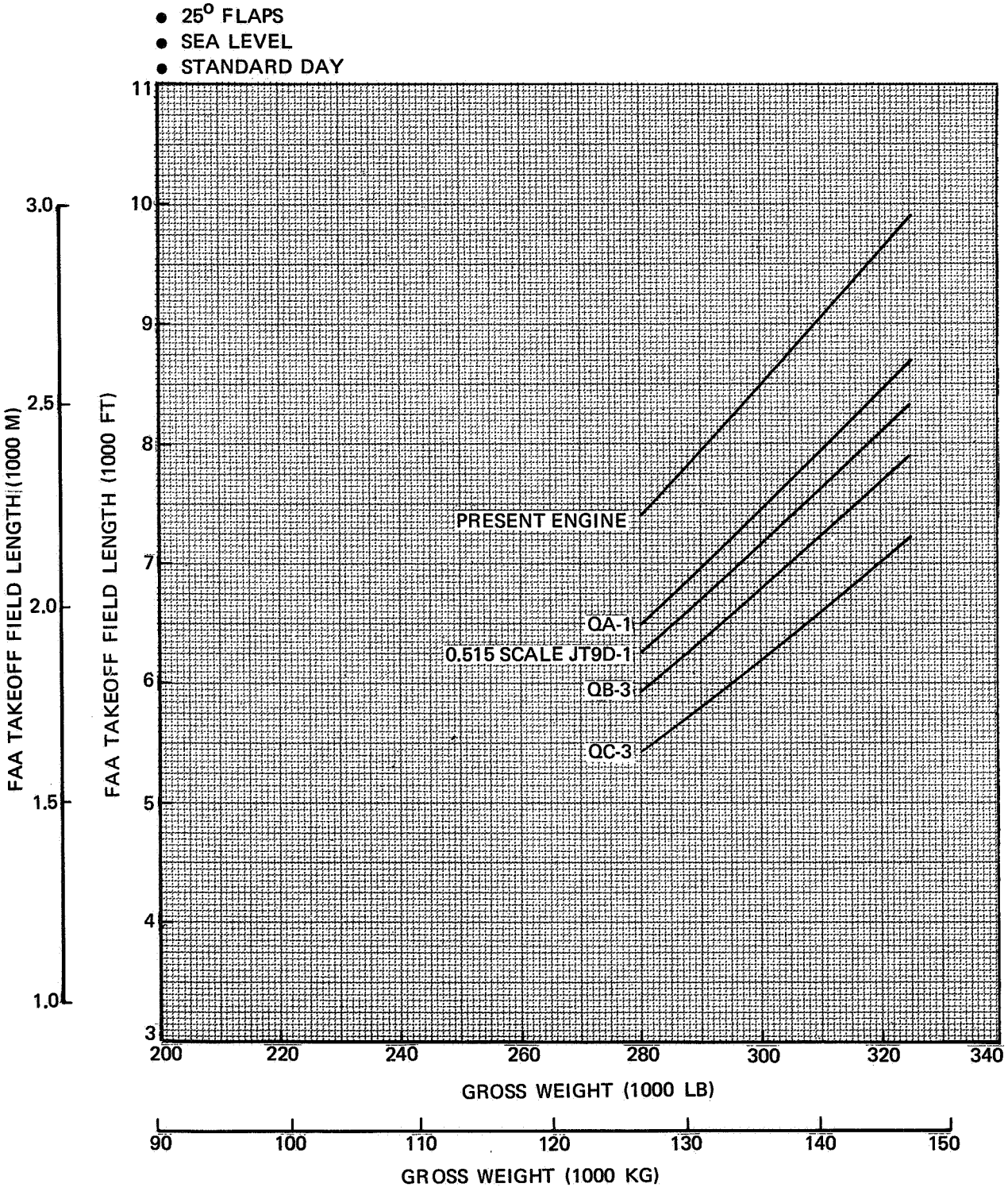

FIGURE II-45. FAA TAKEOFF FIELD LENGTH, 25° FLAPS – MODEL DC-8-61

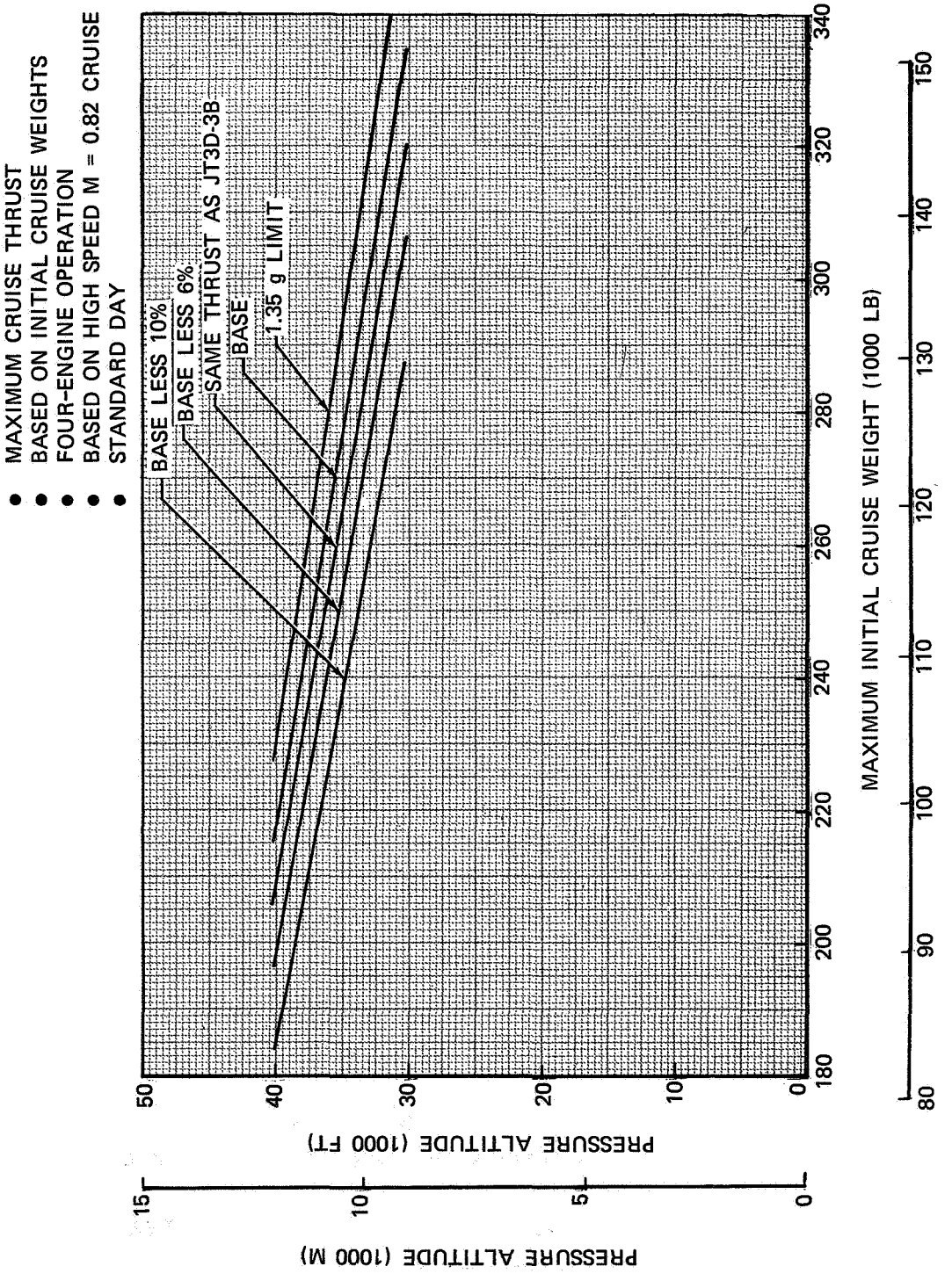

FIGURE II-46. MAXIMUM RECOMMENDED INITIAL CRUISE ALTITUDE – MODEL DC-8-61-Q1

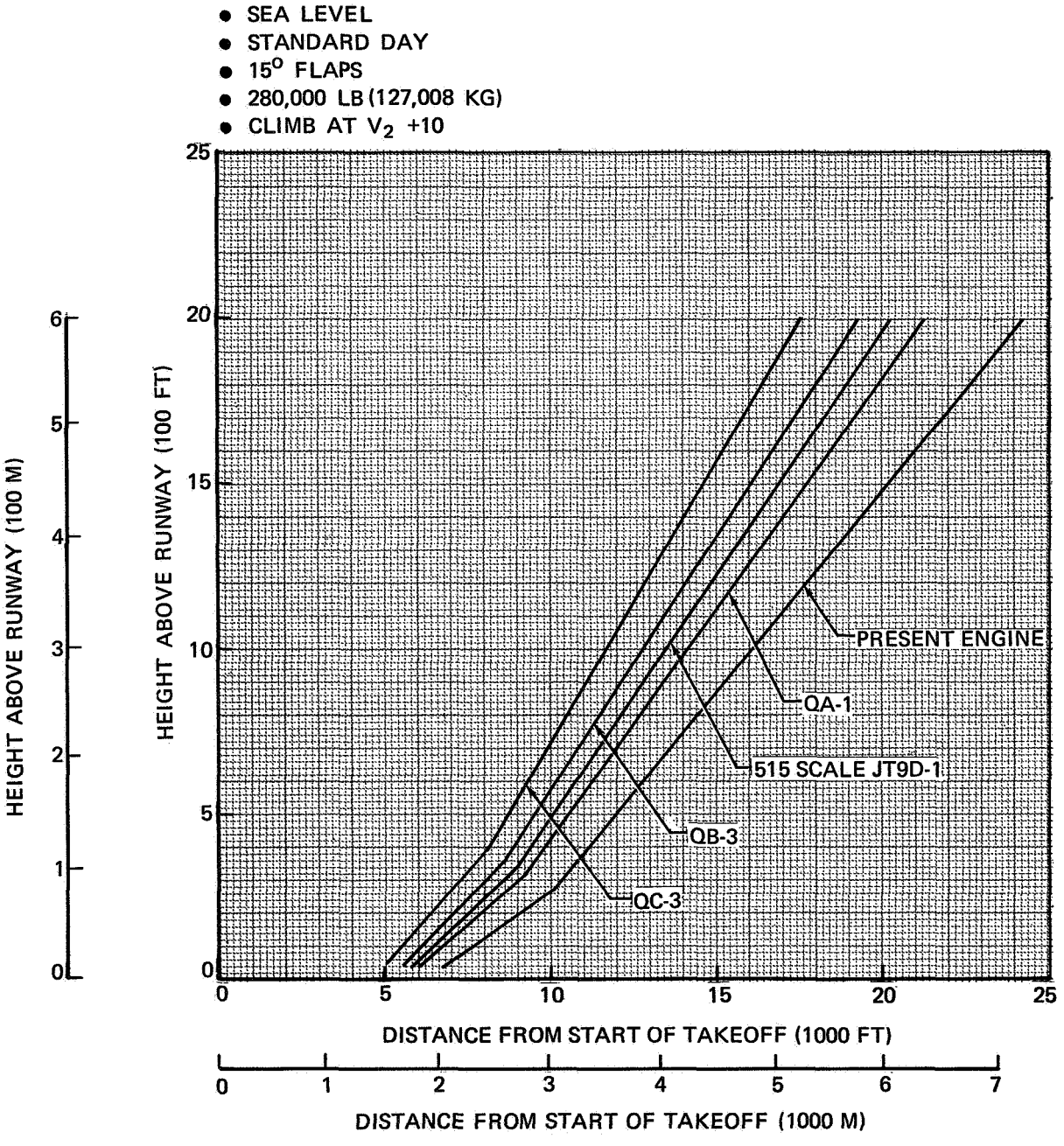

FIGURE II-47. FOUR-ENGINE FLIGHT PATH (280,000 LB – 127,008 KG – GROSS WEIGHT, 15° FLAPS) – MODEL DC-8-61

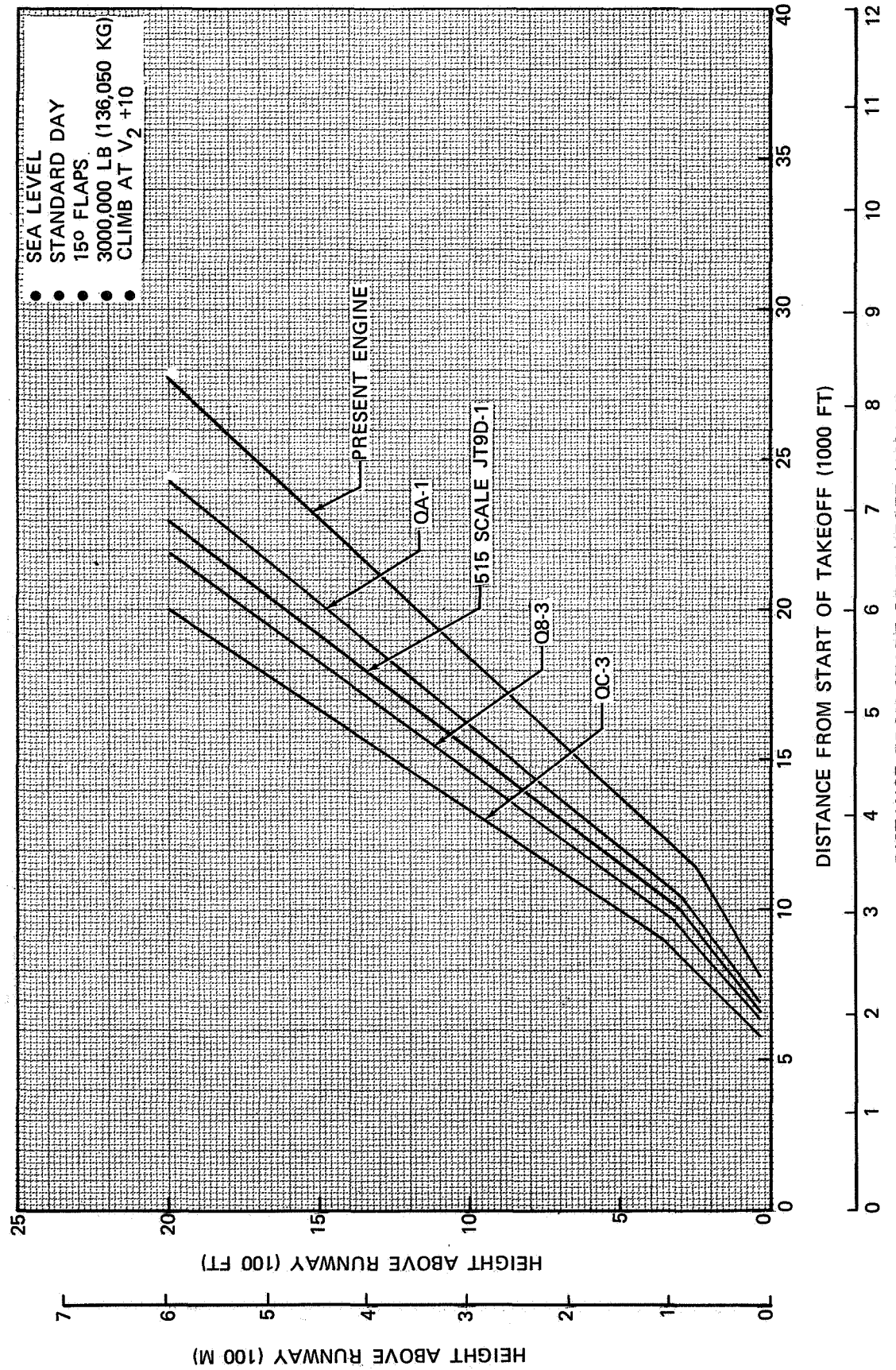

FIGURE 11-48. FOUR-ENGINE FLIGHT PATH (300,000 LB – 136,050 KG – GROSS WEIGHT, 15° FLAPS) – MODEL DC-8-61

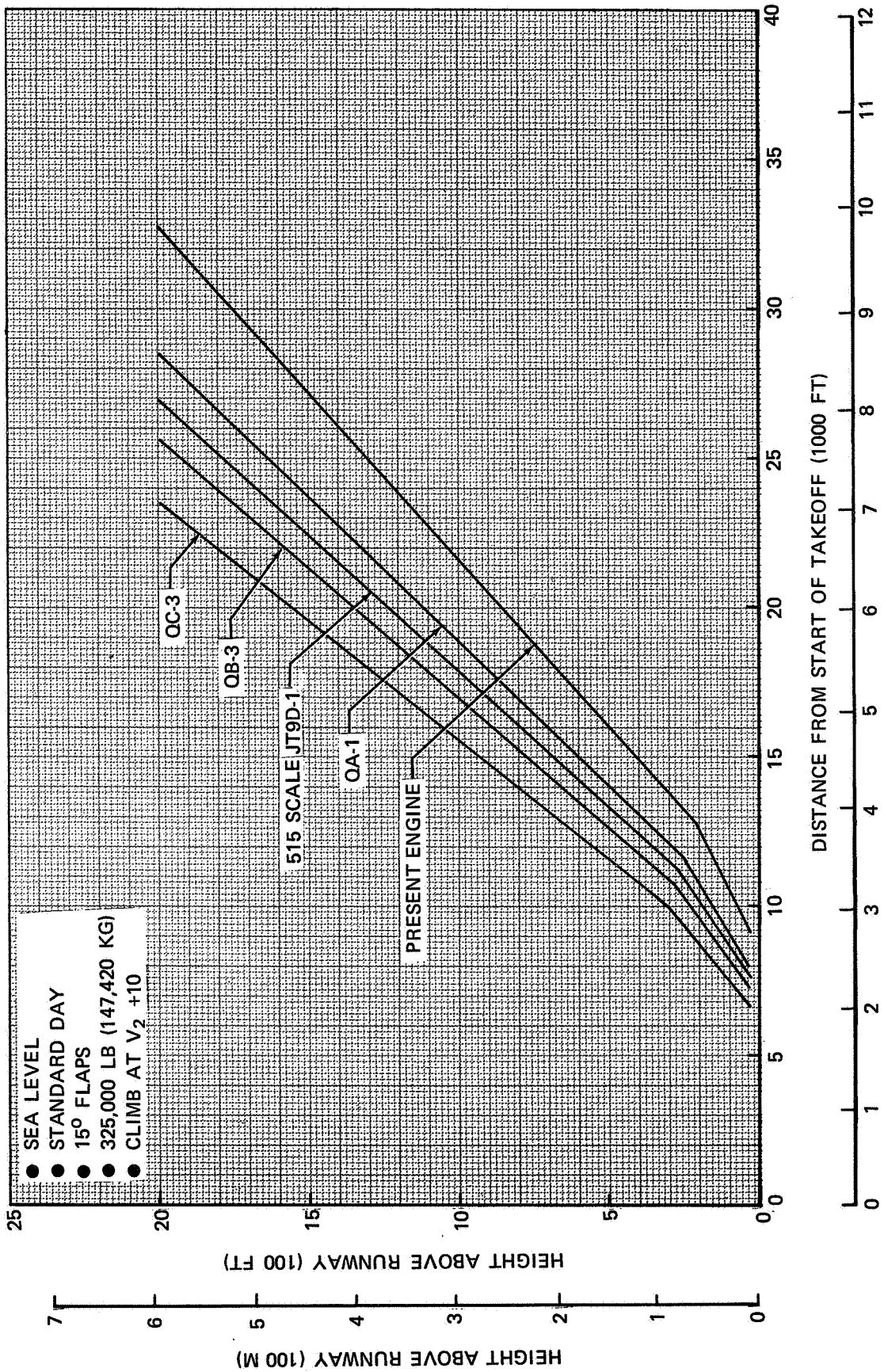

FIGURE II-49. FOUR-ENGINE FLIGHT PATH (325,000 LB – 147,420 KG – GROSS WEIGHT, 15° FLAPS) – MODEL DC-8-61-Q1

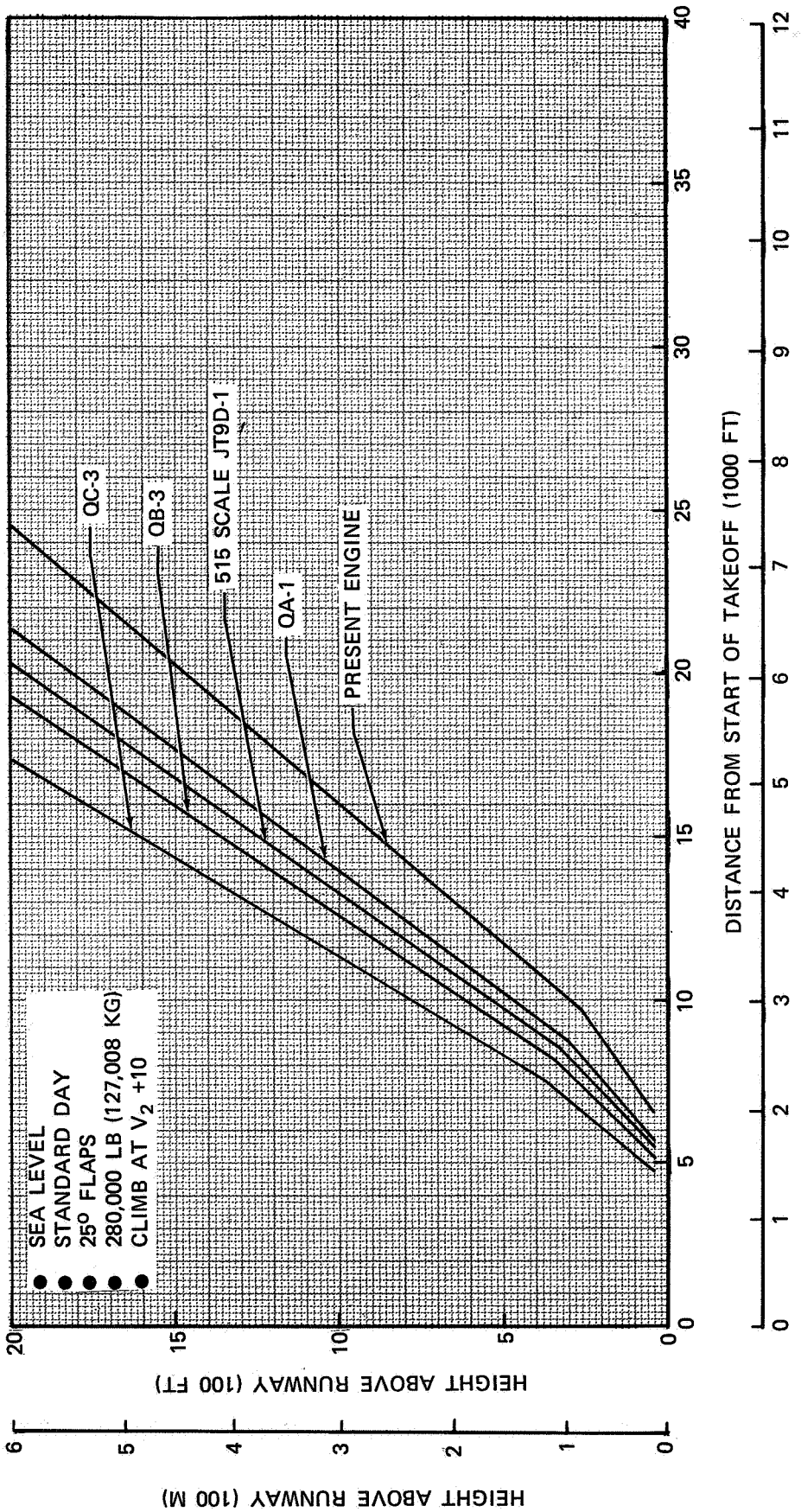

FIGURE II-50. FOUR-ENGINE FLIGHT PATH (280,000 LB – 127,008 KG – GROSS WEIGHT, 25° FLAPS) – MODEL DC-8-61-Q1

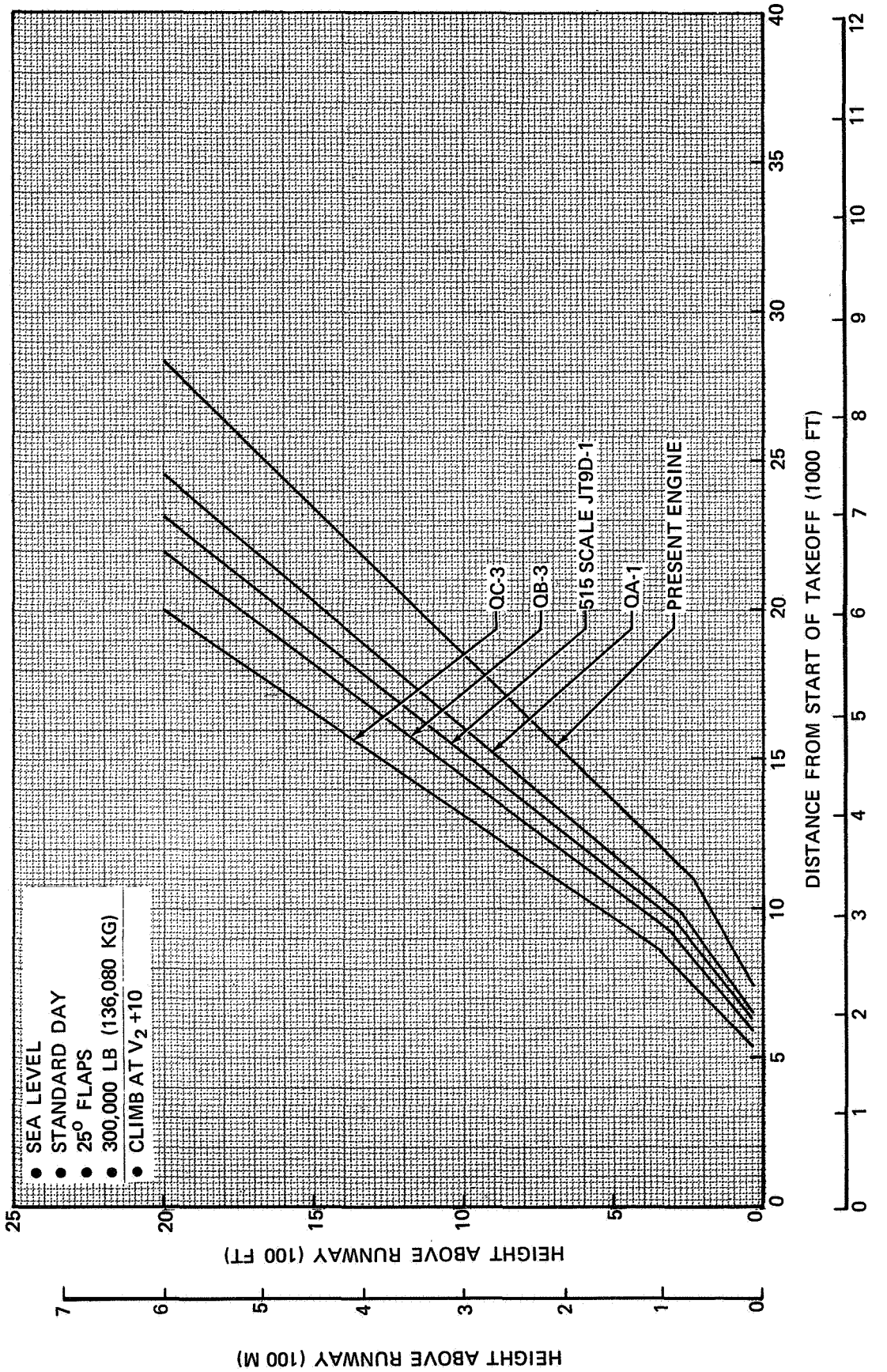

FIGURE II-51. FOUR-ENGINE FLIGHT PATH (300,000 LB – 136,080 KG – GROSS WEIGHT, 25° FLAPS) – MODEL DC-8-61-Q1

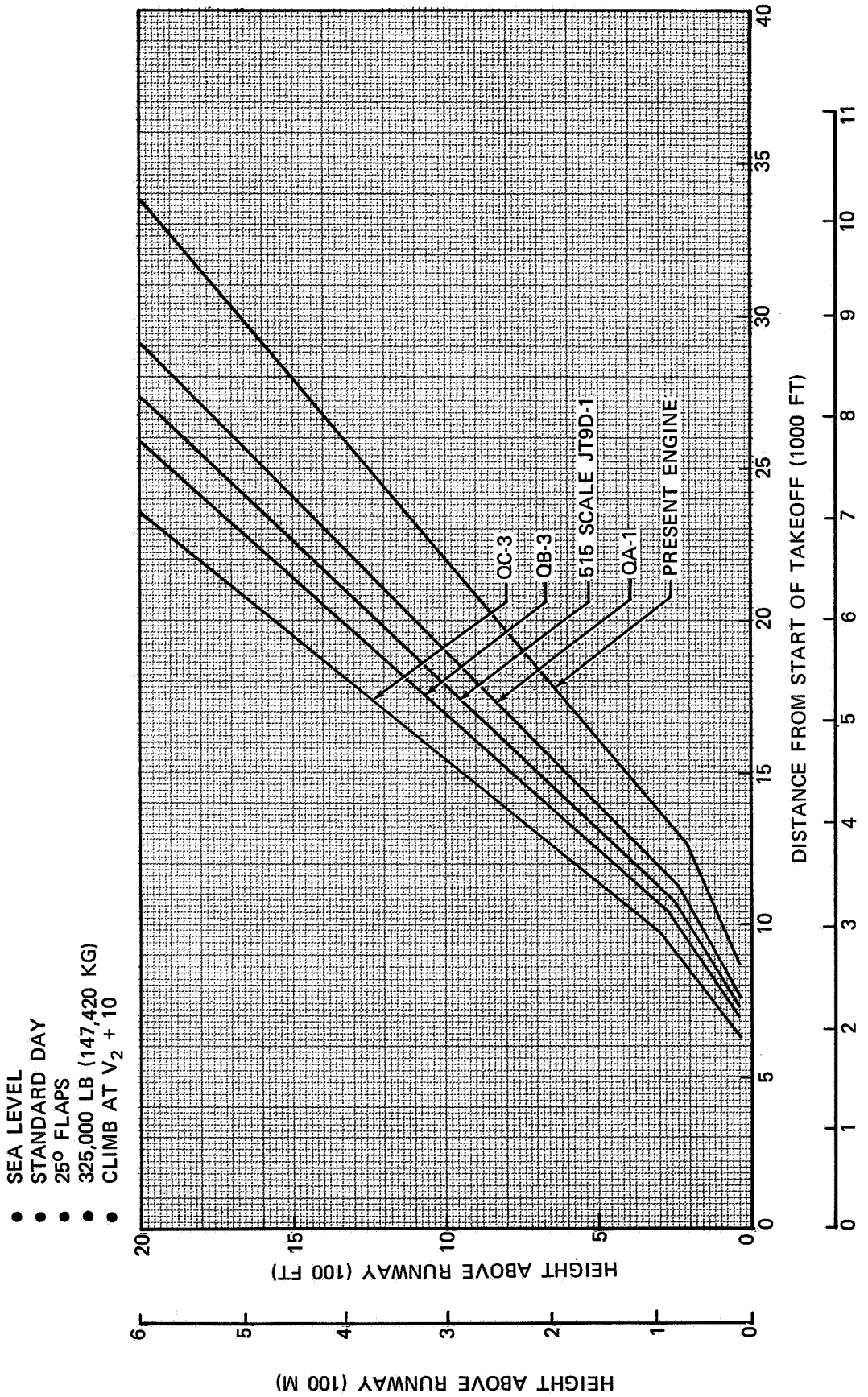

FIGURE II-52. FOUR-ENGINE FLIGHT PATH (325,000 LB – 147,420 KG – GROSS WEIGHT, 25° FLAPS) – MODEL DC-8-61-Q1

CONCLUSIONS

1. On the basis of the work performed in Tasks I and II retrofit of the DC-8-61 with quiet engines appears to be technically feasible.

2. The cost of retrofitting a 300-airplane fleet was estimated to be approximately $5 million per airplane, not including spares.

3. The DOC, not including depreciation, was essentially the same as that of the current DC-8 type aircraft. The increment in DOC due to depreciation would vary widely depending upon the time period over which the retrofitted airplanes would be operating.

4. Payload-range performance would be improved by retrofitting the airplane with quiet engines.

5. Takeoff field length and climb path would be improved by the quiet engine because of greater thrust.

6. A large increase in initial cruise altitude could not be realized by additional cruise thrust for the quiet engine because of airplane aerodynamic limits.

REFERENCES

II-1. Anon., *Standard Method of Estimating Comparative Direct Operating Costs of Turbine Powered Transport Airplanes.* Air Transport Association, December 1967.

TASK III

AERODYNAMIC MODEL TESTS

LIST OF ILLUSTRATIONS

LIST OF ILLUSTRATION (Continued)

LIST OF ILLUSTRATIONS (Continued)

LIST OF ILLUSTRATIONS (Continued)

LIST OF ILLUSTRATIONS (Continued)

Figure Page

DRAG RESULTS

TASK III

AERODYNAMIC MODEL TESTS

This section describes the wind tunnel program conducted to determine how the installation of the quiet engine on the DC-8-61 affects the aerodynamic characteristics of the aircraft.

Three separate tests were conducted. The first was a test of a 6-percent-scale model in the NASA Ames 12-foot low-speed pressure tunnel, in which stability and control characteristics were determined. The second test was a high-speed test in the Ames 11-foot transonic wind tunnel. The third test was a high-speed isolated nacelle-and-pylon test in the Douglas Aerophysics Laboratory 4-foot trisonic tunnel. The purpose of the high-speed tests was to determine the change in cruise drag and high-speed stability due to the installation of the quiet engine.

The wind-tunnel nacelle models were based on the nacelle loft lines developed in Task IV, which is presented in succeeding sections.

The complete definition of the models and test instrumentation is given in References III-1, III-2, and III-3.

Definition of symbols used in this task are shown in Appendix A.

MODEL DESCRIPTION AND TEST PROGRAM

LOW-SPEED TEST, NASA AMES TEST 12-361

The model used in this test is a 6-percent-scale model designated LB-161L, configured to simulate the DC-8-61. The wing was modified from the loft lines to simulate the twisting and bending resulting from flight loading. The tail surfaces were removable so that the effect of the tail could be evaluated. The movable elevator and rudder were not exercised. Interchangeable nacelles and pylons were provided to obtain data on the quiet-engine installation and also on the JT3D-3B installation so that the results could be compared and the effects of the quiet engine evaluated.

The reference JT3D-3B nacelle and pylon models are designated N_{13} and P_{24}, respectively. The quiet-engine nacelle is designated N_{17}. Inboard and outboard pylons are differentiated by superscripts, for example, $P^{I}{}_{24}$ and $P^{O}{}_{24}$. The pylons for location of the nacelle in forward and aft positions on the wing are designated P_{39} and P_{38}, respectively.

The comparison on the following page shows the two positions of the quiet-engine nacelle. At the forward location, the trailing edge of the quiet-engine nacelle was at the location of the trailing edge of the DC-8-63 nacelle.

The aft location for the quiet-engine nacelle, which was relatively heavy, was such that the existing wing skins were predicted to be sufficiently thick to prevent a flutter problem. This location was estimated to be 31 inches (79 cm), full scale, aft of the forward location. Over-the-wing pylons were used for both nacelle locations. Symmetrical (uncambered) pylons were used for the forward location. For the nacelle at the aft location, some wing-nacelle interference problems were expected, because of the possibility of the existence of supersonic flows and shock waves in the channel between the wing and nacelle. Slightly cambered pylons were used for the aft location, in the hope of reducing the wing-nacelle interference during high-speed operation.

The model was mounted on a three-strut support system through an internal force balance. The proper angle of attack was set by reference to a bubble pack mounted internally in the model.

The tunnel used for this test was the NASA Ames 12-foot high-pressure, continuous-flow tunnel. The Reynolds number was held constant at approximately 6 million per foot at a Mach number of 0.2.

HIGH-SPEED TEST, NASA AMES TEST 11-353

The high-speed model consisted of 3.429-percent-scale components of the DC-8-63. The model is designated LB-184L. The model representing the DC-8-63 airplane was used for the high-speed drag test, because of difficulties in simulating the DC-8-61 bifurcated-short-duct nacelle for the wind-tunnel model. Such a model would be difficult to build and the resulting test data would be difficult to analyze because the model bypass ratio and scrubbing drag could only be estimated. The model representing the DC-8-61 was used for the stability and control tests. The fuselage nose, nacelles, pylons, and empennage were removable to allow testing of individual components. The wing was modified from the loft lines to simulate the twisting and bending resulting from the wing loading for a typical flight condition. The same nacelle locations used for the low-speed test were used for the high-speed test.

The DC-8-63 nacelles and pylons designated N_{12} and P_{35} respectively, were used for the reference configuration. Flight-test data were used to account for drag differences between the DC-8-63 and

NASA AMES TEST 11-353

NOTE: 1. DC-8-63 CONFIGURATION: CUT-BACK PYLON AND SLIM LONG DUCT NACELLE

2. NACELLE LOCATION:

   INBOARD NACELLE T.E. AT 10 PERCENT POINT OF LOCAL WING CHORD
   OUTBOARD NACELLE T.E. AT 6.8 PERCENT POINT OF LOCAL WING CHORD

3. NACELLE-PYLON CHANGES: (A) OVER-THE-WING PYLON
   (B) BASELINE QUIET-ENGINE NACELLE
   (C) NACELLES MOVED 31 INCHES AFT

INBOARD NACELLE STATION

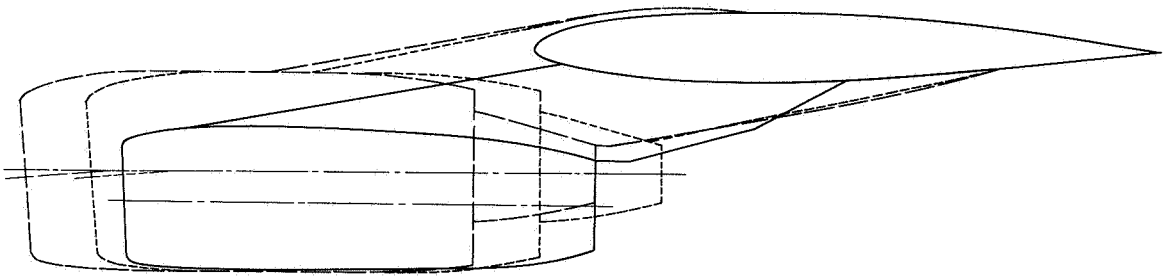

OUTBOARD NACELLE STATION

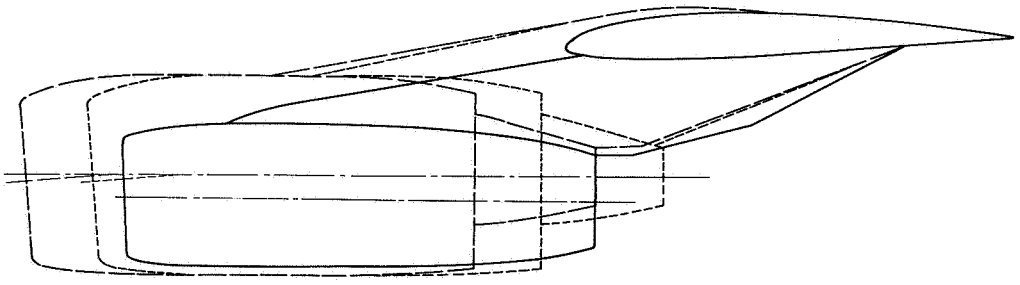

——— DC-8-63
— — FORWARD LOCATION } QUIET ENGINE NACELLE
— — — — AFT LOCATION

COMPARISON OF QUIET-ENGINE NACELLE-PYLON CONFIGURATION WITH DC-8-63 CONFIGURATION

the DC-8-61 airplanes. The DC-8-63 pylons are cut back to the 5-percent point of the local wing chord; over-the-wing pylons were used for the quiet-engine nacelle installation.

The external geometry of the DC-8-63 nacelle was geometrically similar to that of the full-scale nacelle. It was not necessary to modify the nacelle to simulate the cruise inlet mass-flow in flight, because, with a low-diameter-ratio cowling, a slight reduction in inlet-mass flow ratio does not measurably affect the drag. The nacelle duct was formed by a straight cylindrical bore.

The quiet-engine nacelle, designated N_{17A} is a short-duct, high-bypass-ratio, flow-through model. For the flow-through model, the exit area of the full-scale nacelle is not large enough to simulate the cruise inlet mass-flow ratio. The resulting low inlet mass-flow ratio has a measurable effect on the drag of the nacelle because of its high-diameter-ratio cowling. It was therefore necessary to increase the exit area to simulate the cruise inlet mass-flow ratio. The top half of the nacelle was scaled down to simulate exactly wing-flow-field interference effects, but the bottom half of the fan cowl was warped to increase the fan exit area. The distortion of the fan-cowl lower lines and fan exit introduced much more camber into the nacelle than would exist on the airplane nacelle.

The model was equipped with transition strips to establish turbulent boundary layer flow on the fuselage nose, wings, and pylons and on both the external and internal surfaces of the fan cowl and gas generator. Transition strips 0.003 inch (0.07 mm) high were used on the fuselage, and transition strips 0.0020 inch (0.05 mm) high were used on the pylons and on the nacelles. Triangular-shaped tape was used for these transition strips. Glass bends 0.0026 inch (0.06 mm) high were used for wing transition where various bead sizes were tested on the same model. Transition-fixing devices were not used in the stability and control tests, because previous experience indicates that accuracy of measurements of stability derivatives is impaired by such devices.

The instrumentation for the model consisted of a six-component internal strain-gage balance and an electronic bubble-pack for indicating true angle of attack. These were installed in the fuselage. Static orifices were located in the fuselage cavity. Rows of static-pressure tubes were located on a line 12 inches (30 cm), full scale, inboard of the pylon centerline on the wing upper and lower surfaces and on a line 12 inches (30 cm) outboard of the pylon centerline on the wing lower surface at both the inboard and outboard nacelle locations. A unit containing size 48S scanivalves was mounted in the nose of the model and used for measuring the pressures.

The test was run in the NASA Ames 11-foot transonic tunnel. The model was mounted on a single sting, which entered the aft fuselage through the lower surface. The lift, drag, and pitching moments for the DC-8-63 and for the quiet-engine configurations were measured at Mach numbers in the range from 0.70 to 0.84 for the drag study and in the range from 0.50 to 0.95 for the stability and control study. Reynolds numbers up to 8 million per foot are available; but it was not practical to test at the highest values, where the pitch (or yaw) range is limited by the risk of overstressing the sting. Static-pressure distributions were measured on the wing surfaces during the drag test. For the drag study, all the configurations were tested with both horizontal and vertical tails off.

ISOLATED NACELLE-PYLON TESTS, DAL TEST S-152

Quiet-engine nacelle model N_{17A}, which was tested during NASA Ames Test 11-353, was tested alone at the Douglas 4-foot tunnel to obtain the basic drag level. The nacelle was tested with all four forward-location pylons, P_{39}. It was also tested with the left-side inboard aft-location pylon, P_{38}. The model, designated LB-265B, was mounted on an ogive body of revolution. The lift, drag, and pitching moments were measured in the Mach number range from 0.70 to 0.84 of nearly constant Reynolds number, 6.2 million based on the DC-8-63 wing mean aerodynamic chord (MAC).

DATA REDUCTION

Reduction of the data was the responsibility of the NASA Ames Research Center and of the Douglas Aerophysics Laboratory. Details of the data-reduction equations are in the test Operating Reports, References III-1, III-2, and III-3. The force data are presented in the stability-axis system, with the moment center located in the plane of symmetry at the station of the quarter-chord point of the wing mean aerodynamic chord and on or slightly below the fuselage reference plane.

The high-speed moment data used in analyses of stability characteristics do not contain corrections for sting-cavity pressures. The magnitude of this correction is small, and correlation with flight-test data has been good without it.

STABILITY AND CONTROL TESTS

LONGITUDINAL CHARACTERISTICS

It was expected that the larger quiet-engine nacelles would be destabilizing in both pitch and sideslip, in comparison with the standard DC-8-61 nacelles. It was not known, however, whether the larger nacelles would have an adverse effect on lift characteristics at high angles of attack.

The low-speed lift data with the tail off, presented in Figures III-1 through III-5 for several flap angles, show small changes in lift-curve slope and angle of zero lift, but no change in maximum lift coefficient. The lift-curve slope is increased by 0.002, or about 2.5 percent, and the angle of zero lift is reduced slightly, which increases the lift coefficient at zero angle of attack by approximately 0.02. Although the maximum lift capability is unaffected, the stall occurs at a slightly lower angle of attack than with the basic JT3D nacelles.

These same effects, which are essentially independent of Mach number, are shown in the high-speed data presented in Figure III-6.

Additional lift curves for the complete model (tail on) are presented in Figures III-7 through III-20 at M = 0.2 and in Figure III-21 at higher Mach numbers.

The tail-off pitching-moment data are presented in Figures III-22 through III-26 and in Figure III-27 for low speed and high speed, respectively. These data show reductions in stability equivalent to forward shift of the tail-off aerodynamic center. That amounts to approximately 4 percent MAC for the quiet-engine nacelle in the forward position and 3-percent MAC for the nacelles in the aft position at low Mach numbers, increasing to 6- to 7-percent MAC at high Mach numbers. Pitching characteristics through the stall are not affected.

The tail-on pitching-moment data, presented in Figures III-28 through III-43, show the same destabilizing effect of the quiet-engine nacelles. The tail contribution and wing downwash are therefore unaffected. The values of downwash at the tail, ϵ have been obtained from the data by the formula

$$\epsilon = \alpha_F + i_H - \left[\frac{C_{M_A} - C_{M_{TO}}}{C_{M_{\alpha H}}} \right]$$

The calculated values are plotted in Figures III-44 and III-45 for low Mach numbers and in Figures III-46 through III-48 for high Mach numbers. The quiet-engine nacelles alter the variation of downwash at zero angle of attack, producing a variation with Mach number that is stabilizing below M = 0.7 and destabilizing at higher Mach numbers.

LATERAL-DIRECTIONAL CHARACTERISTICS

The quiet-engine nacelles were expected to be destabilizing in sideslip as well as in pitch and were expected to increase the side forces on the aircraft.

The tail-off yawing moment coefficients, presented in Figures III-49 through III-60, show a reduction in static directional stability of $\Delta C_{n_c} = -0.0002$ to -0.0003 due to the new nacelles. This represents an increase of 20 to 30 percent in the tail-off instability level. As with the pitching-moment data, the effect is largest at high Mach numbers.

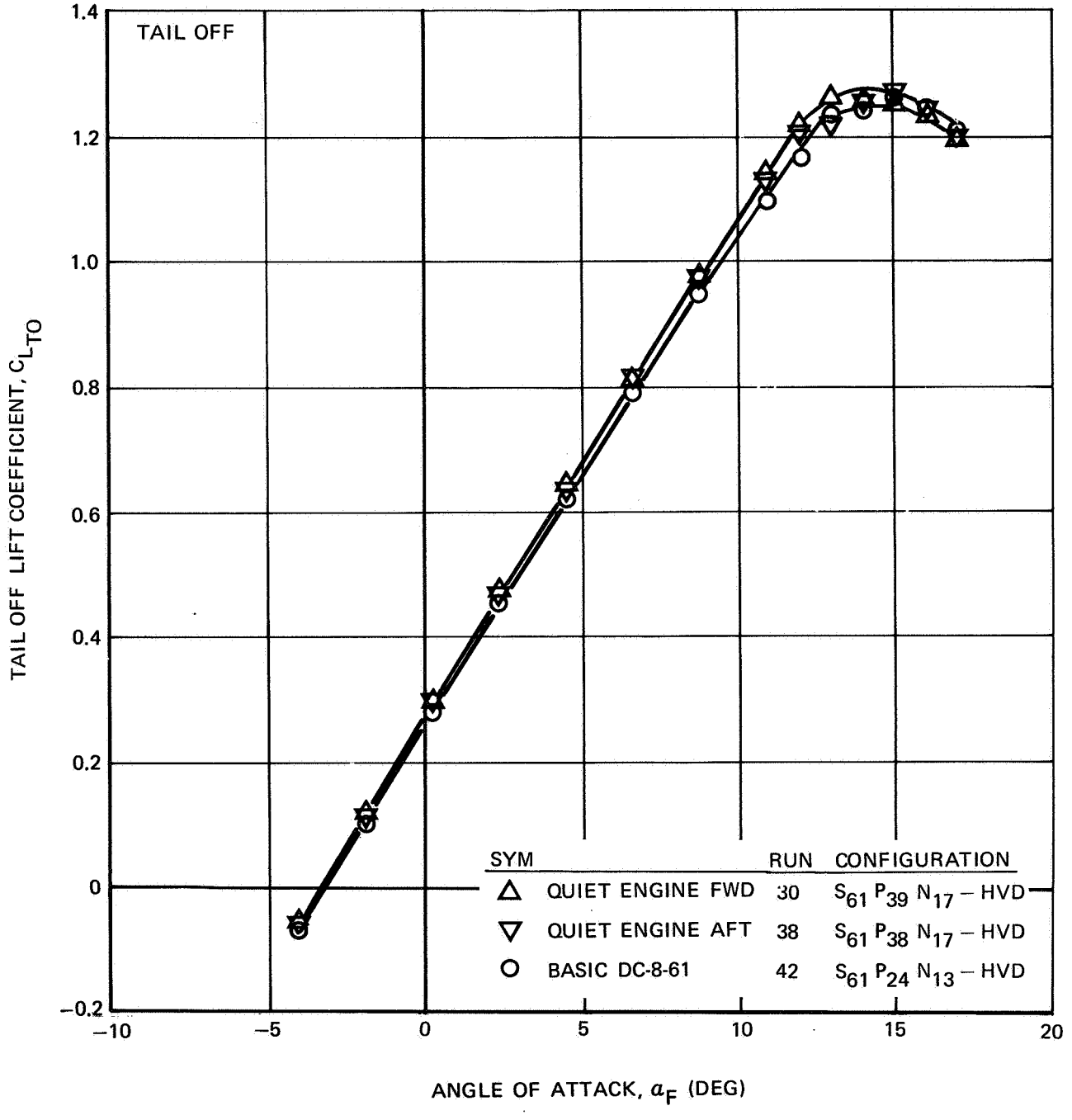

FIGURE III-1. EFFECT OF PYLONS AND NACELLES ON LIFT COEFFICIENT – $\delta_f = 0^o$

NASA AMES TEST 12-361

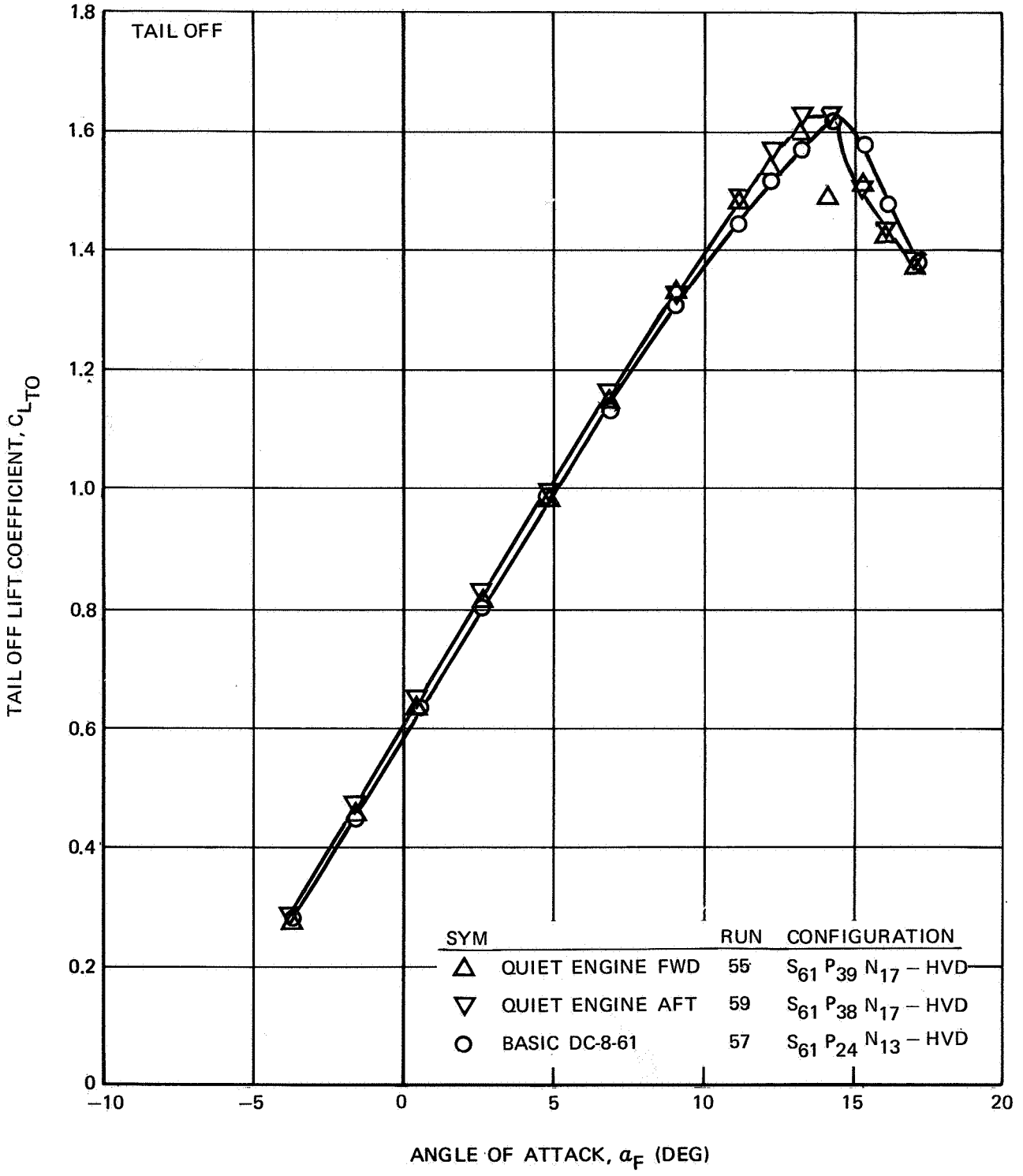

FIGURE III-2. EFFECT OF PYLONS AND NACELLES ON LIFT COEFFICIENT – $\delta_f = 15^o$

NASA AMES TEST 12-361

SYM		RUN	CONFIGURATION
○	BASIC DC-8-61	61	$S_{61}\,P_{24}\,N_{13}$ – HVD
▽	QUIET ENGINE AFT	65	$S_{61}\,P_{38}\,N_{17}$ – HVD
△	QUIET ENGINE FWD	69	$S_{61}\,P_{39}\,N_{17}$ – HVD
○	BASIC DC-8-61	135	$S_{61}\,P_{24}\,N_{13}$ – HVD
▽	QUIET ENGINE AFT	137	$S_{61}\,P_{38}\,N_{17}$ – HVD
△	QUIET ENGINE FWD	134	$S_{61}\,P_{39}\,N_{17}$ – HVD

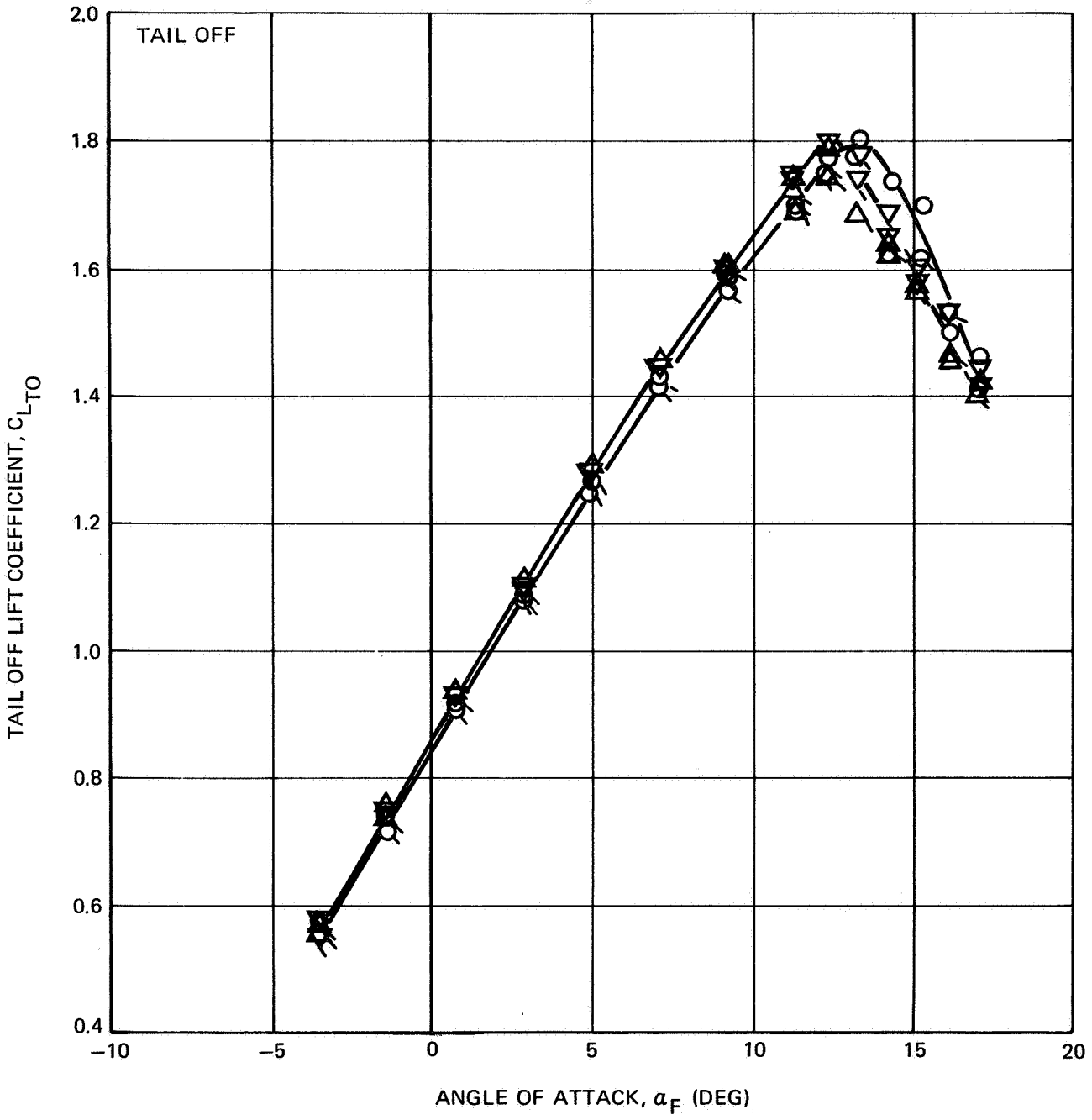

FIGURE III-3. EFFECT OF PYLONS AND NACELLES ON LIFT COEFFICIENT – $\delta_f = 25^o$

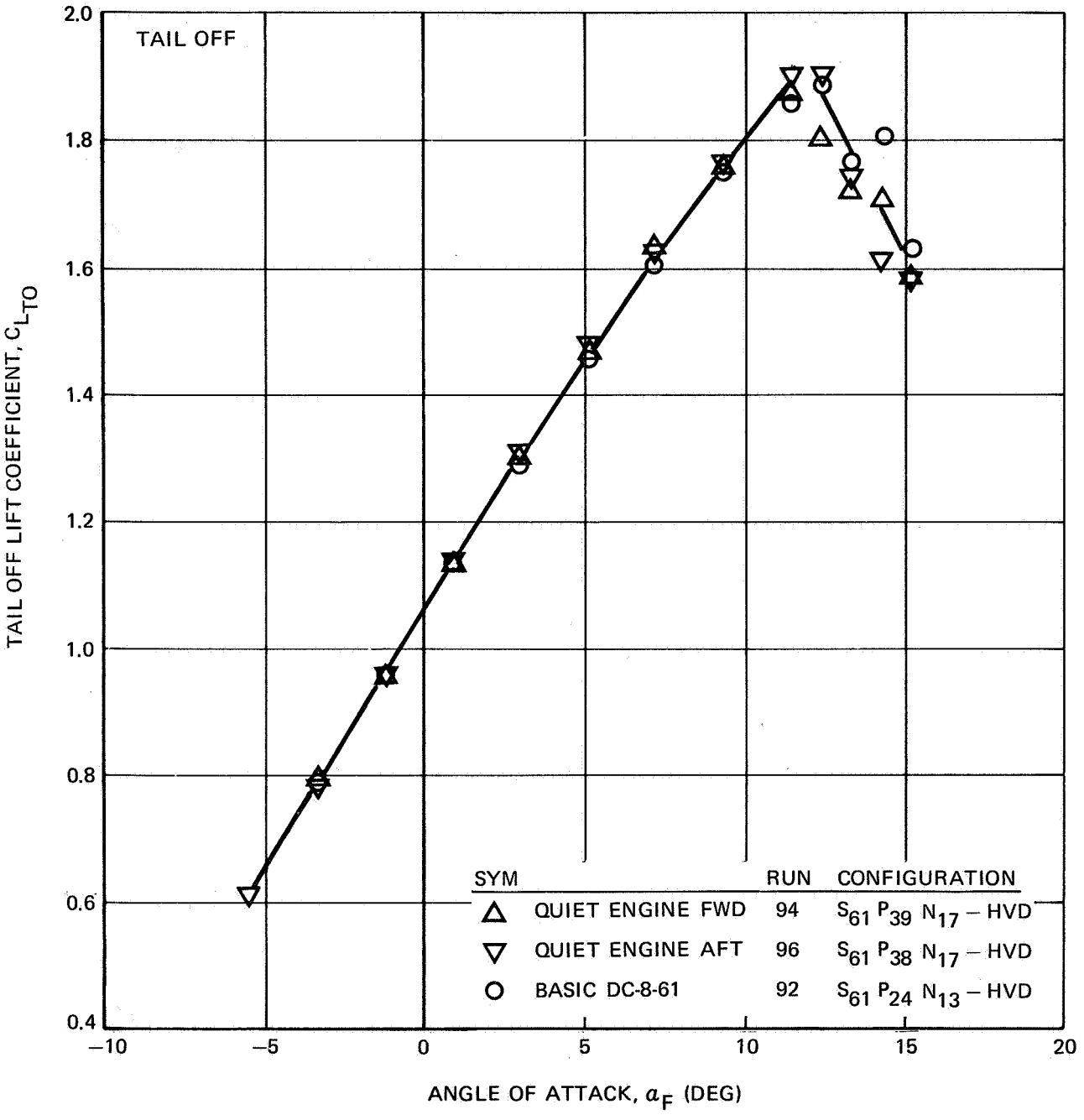

FIGURE III-4. EFFECT OF PYLONS AND NACELLES ON LIFT COEFFICIENT – $\delta_f = 35^o$

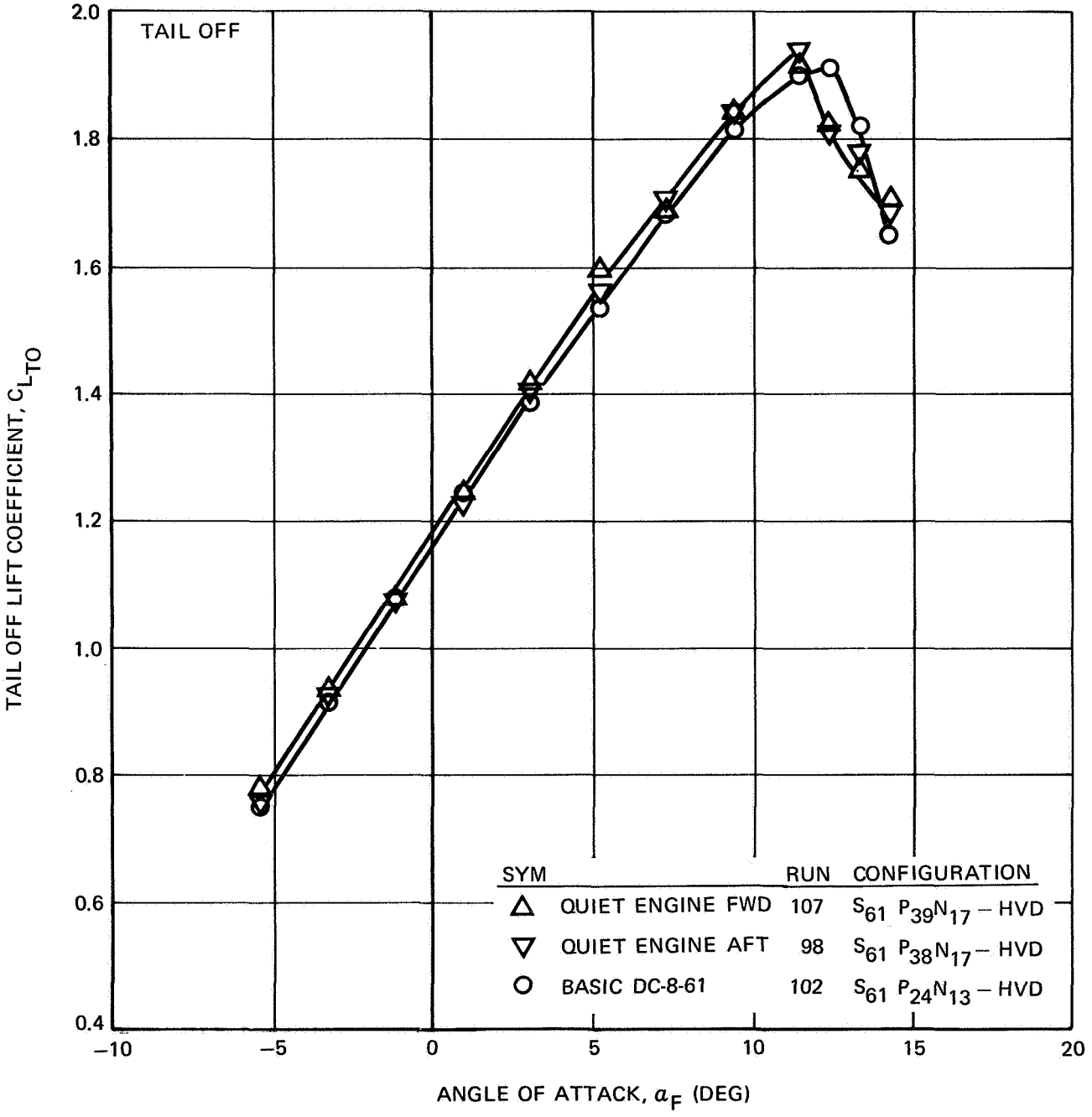

FIGURE III-5. EFFECT OF PYLONS AND NACELLES ON LIFT COEFFICIENT – $\delta_f = 50^o$

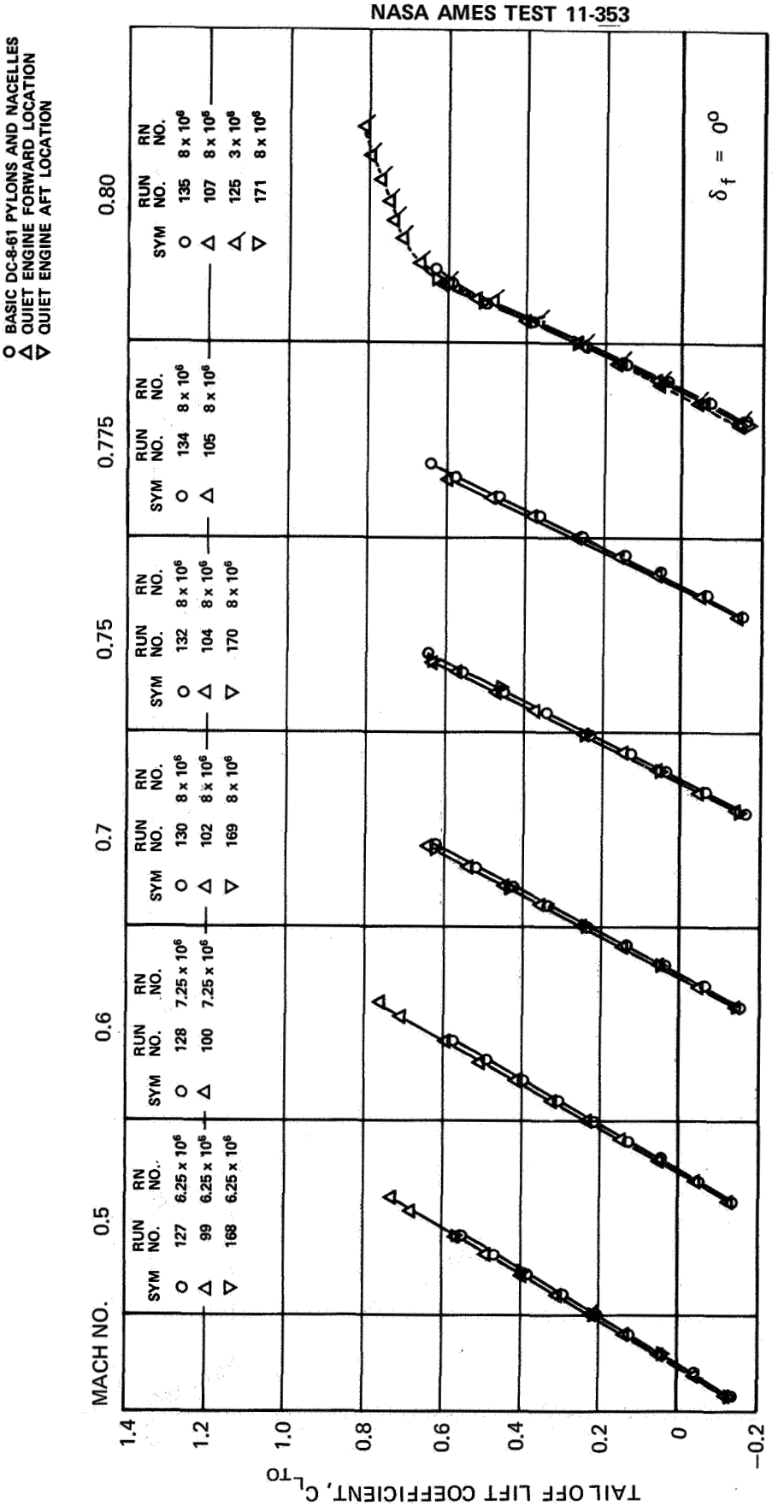

FIGURE III-6. EFFECT OF NACELLES AND PYLONS ON TAIL-OFF LIFT COEFFICIENT AT HIGH MACH NUMBER (SHEET 1 OF 2)

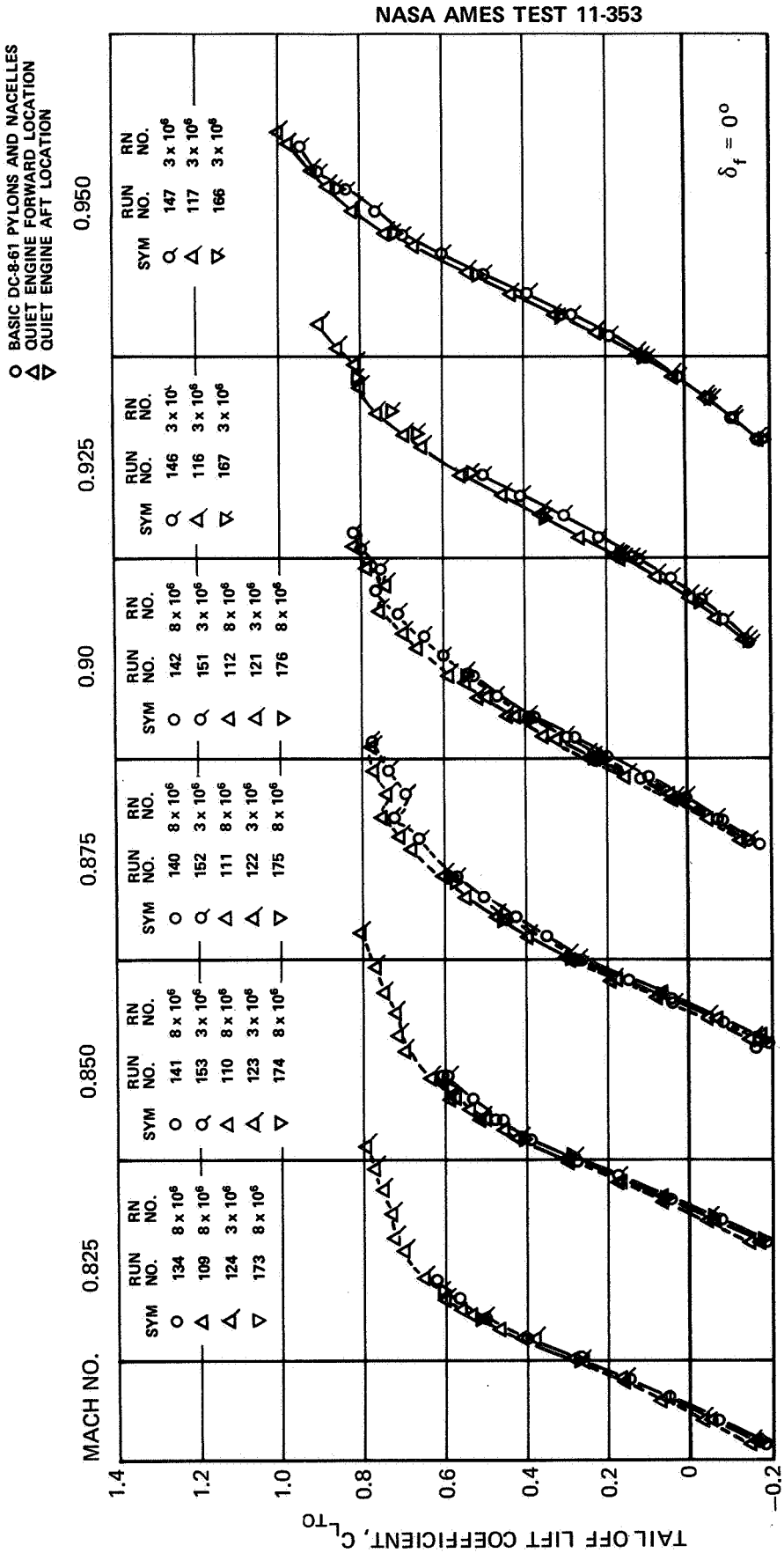

FIGURE III-6. EFFECT OF NACELLES AND PYLONS ON TAIL-OFF LIFT COEFFICIENT AT HIGH MACH NUMBER (SHEET 2 OF 2)

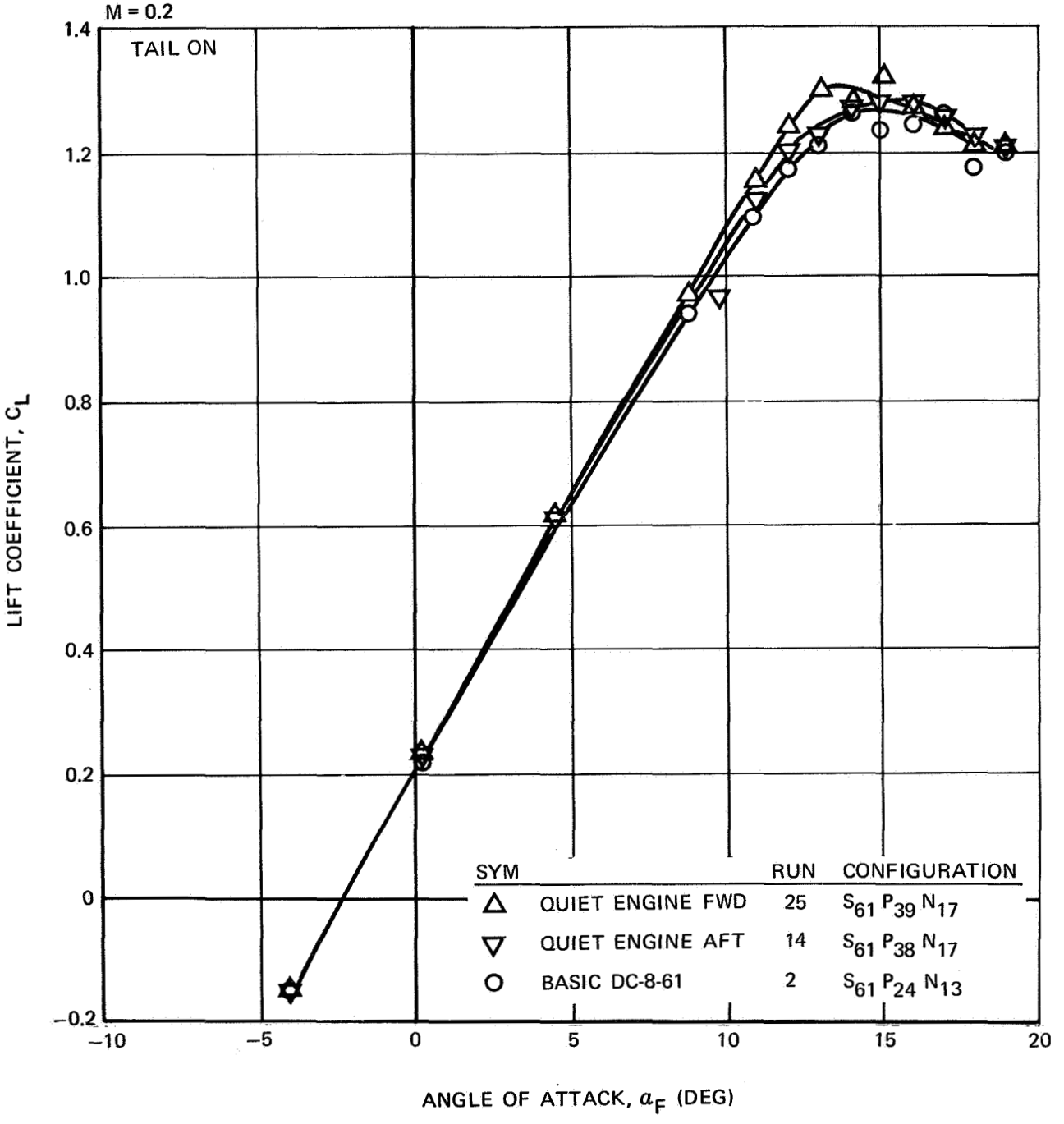

FIGURE III-7. EFFECT OF PYLONS AND NACELLES ON LIFT COEFFICIENT – $\delta_f = 0^o$, $i_H = 5^o$

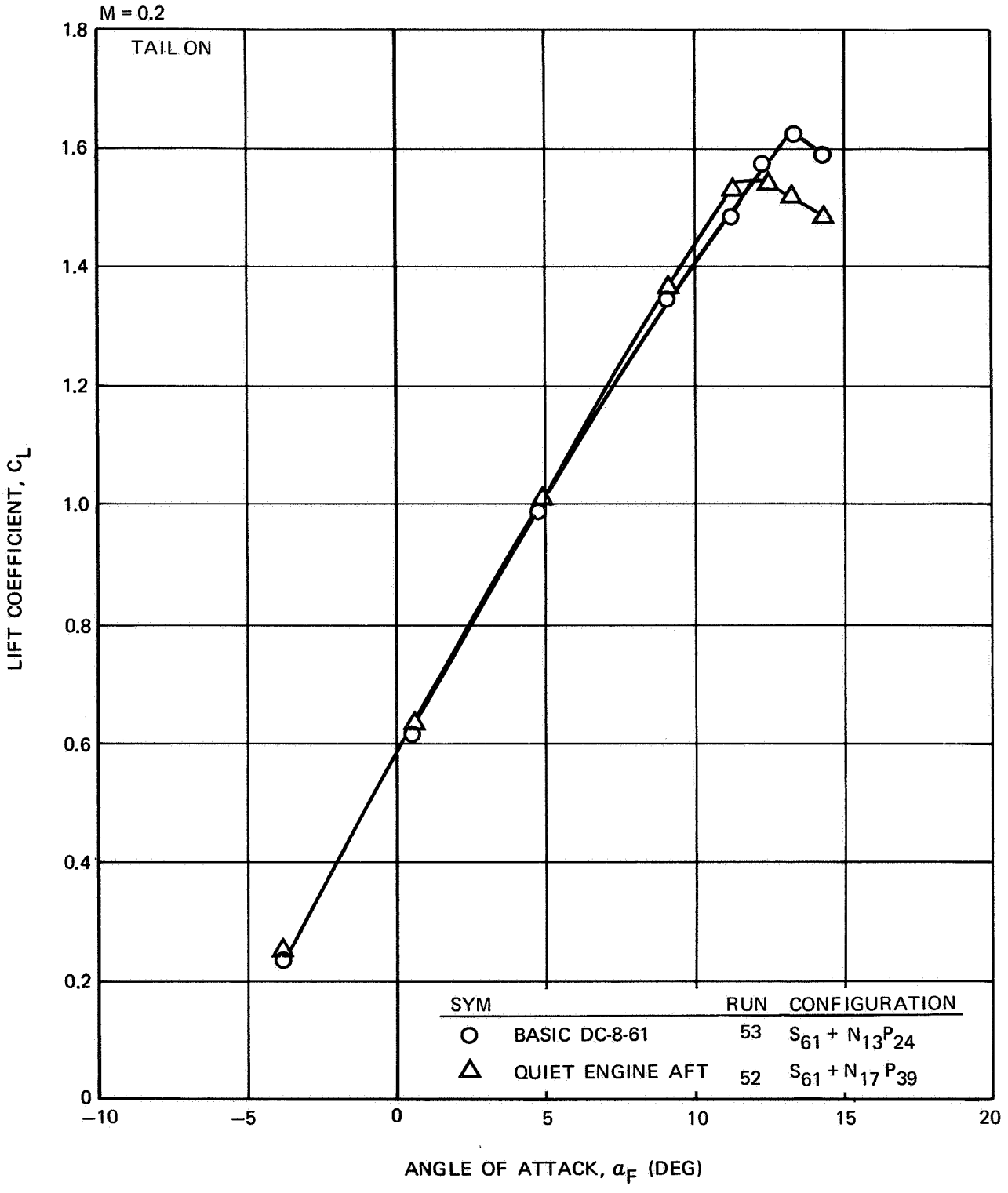

FIGURE III-8. EFFECT OF PYLONS AND NACELLES ON LIFT COEFFICIENT – $\delta_f = 15^o$, $i_H = 0^o$

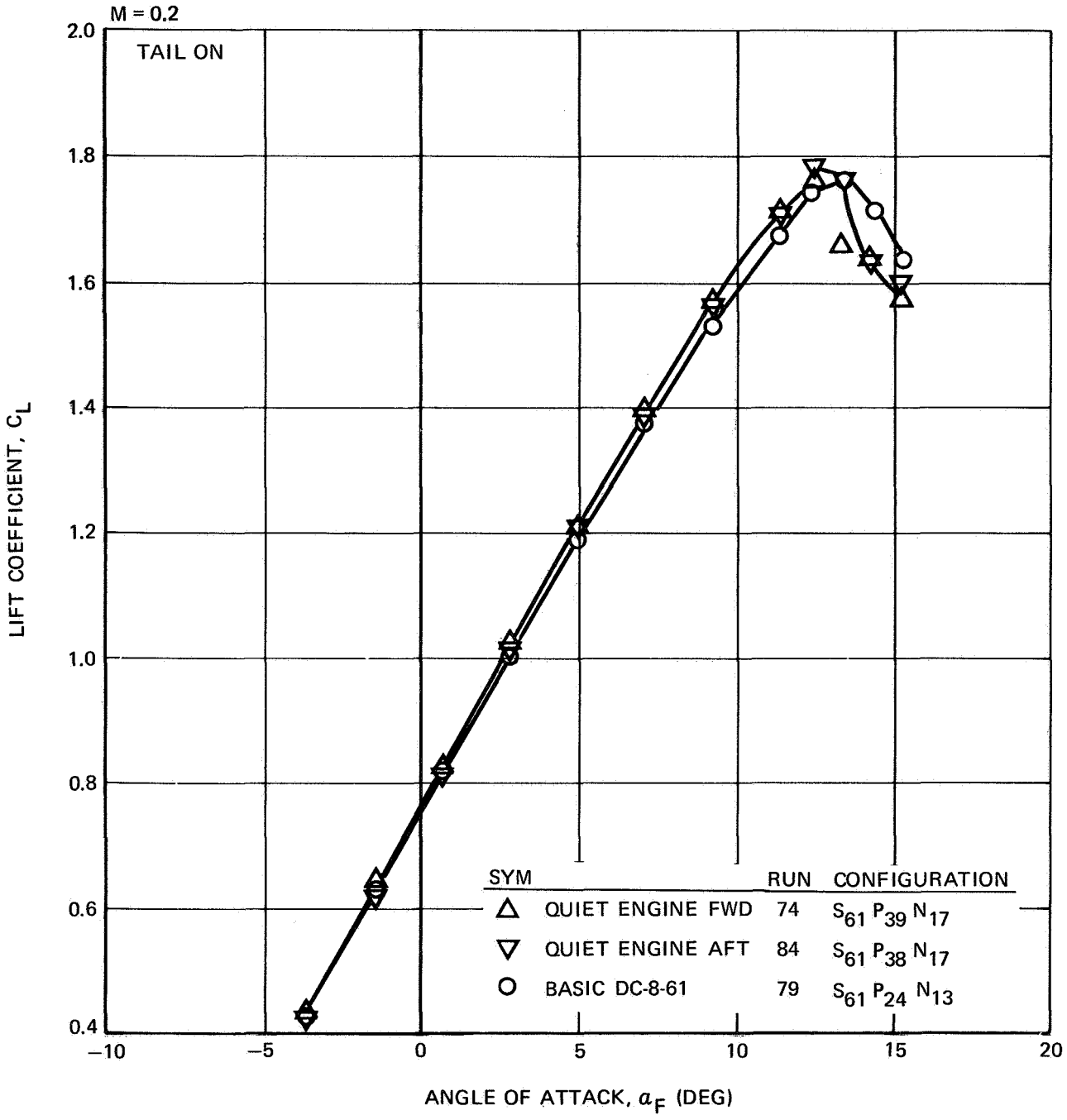

FIGURE III-9. EFFECT OF PYLONS AND NACELLES ON LIFT COEFFICIENT – $\delta_f = 25^o$, $i_H = -5^o$

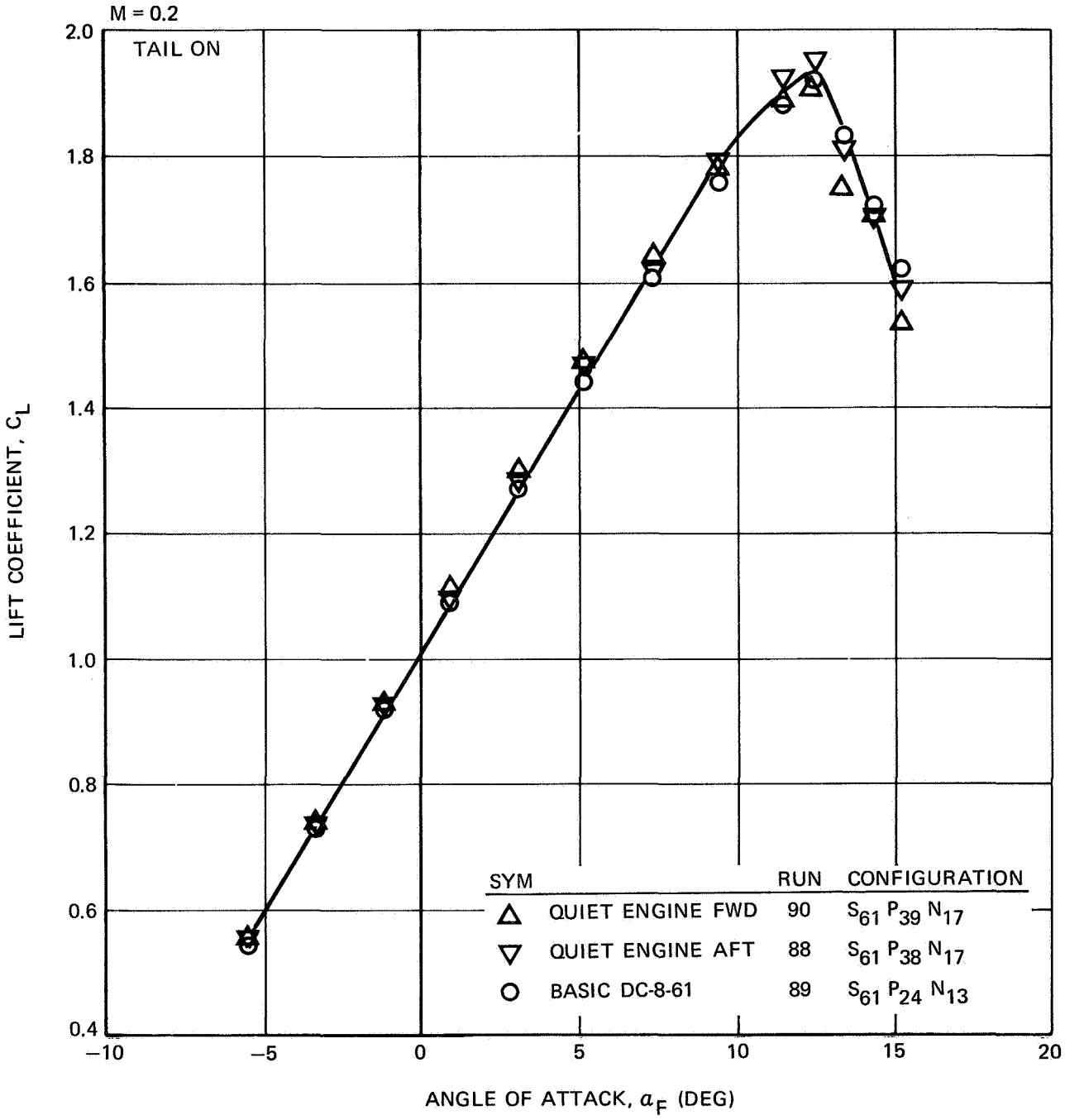

FIGURE III-10. EFFECT OF PYLONS AND NACELLES ON LIFT COEFFICIENT – $\delta_f = 35^o$, $i_H = 0^o$

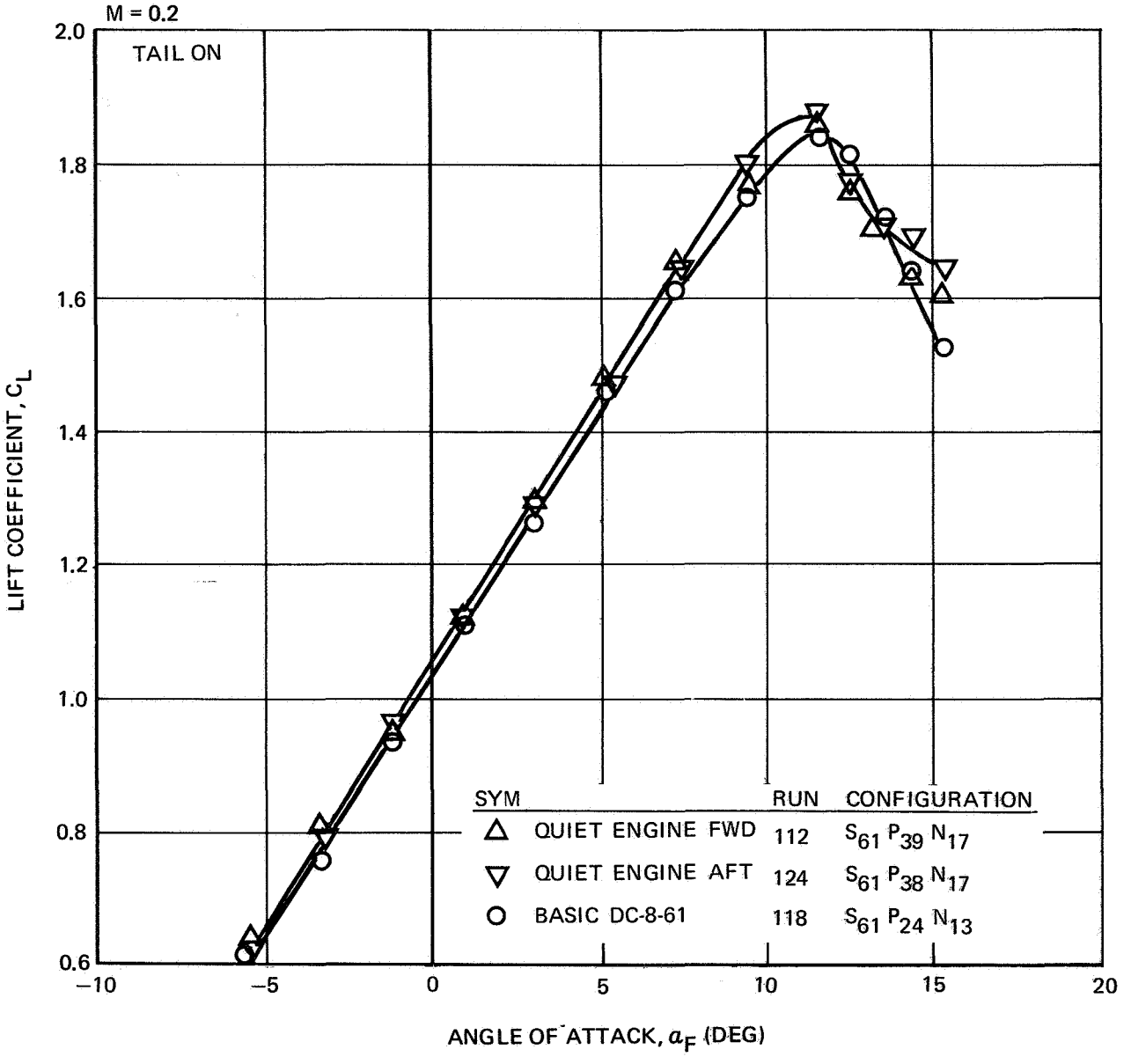

FIGURE III-11. LIFT COEFFICIENT VERSUS ANGLE OF ATTACK – $\delta_f = 50^o$, $i_H = -5^o$

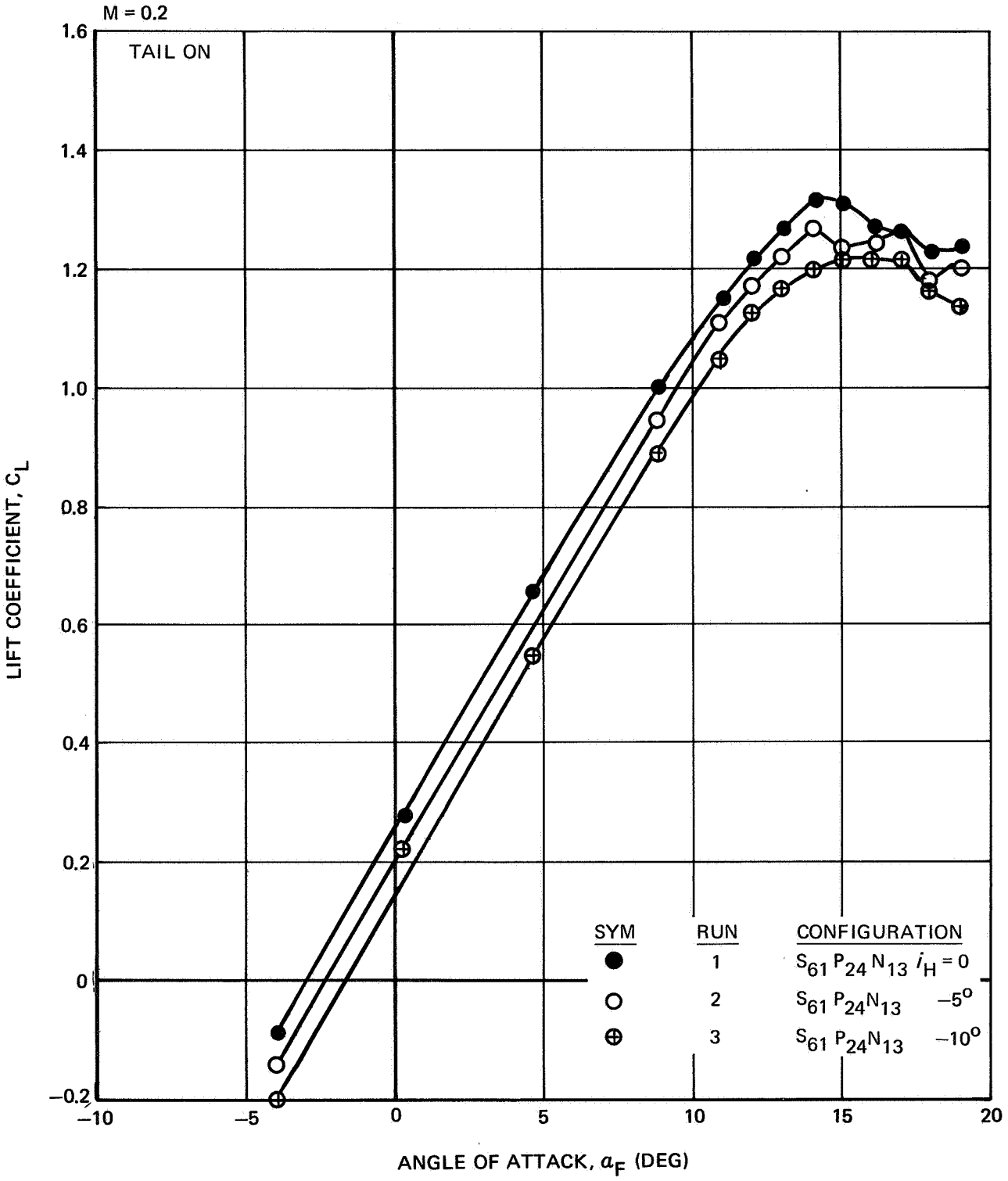

FIGURE III-12. EFFECT OF STABILIZER ANGLE ON LIFT COEFFICIENT, BASIC DC-8-61 – $\delta_f = 0^o$

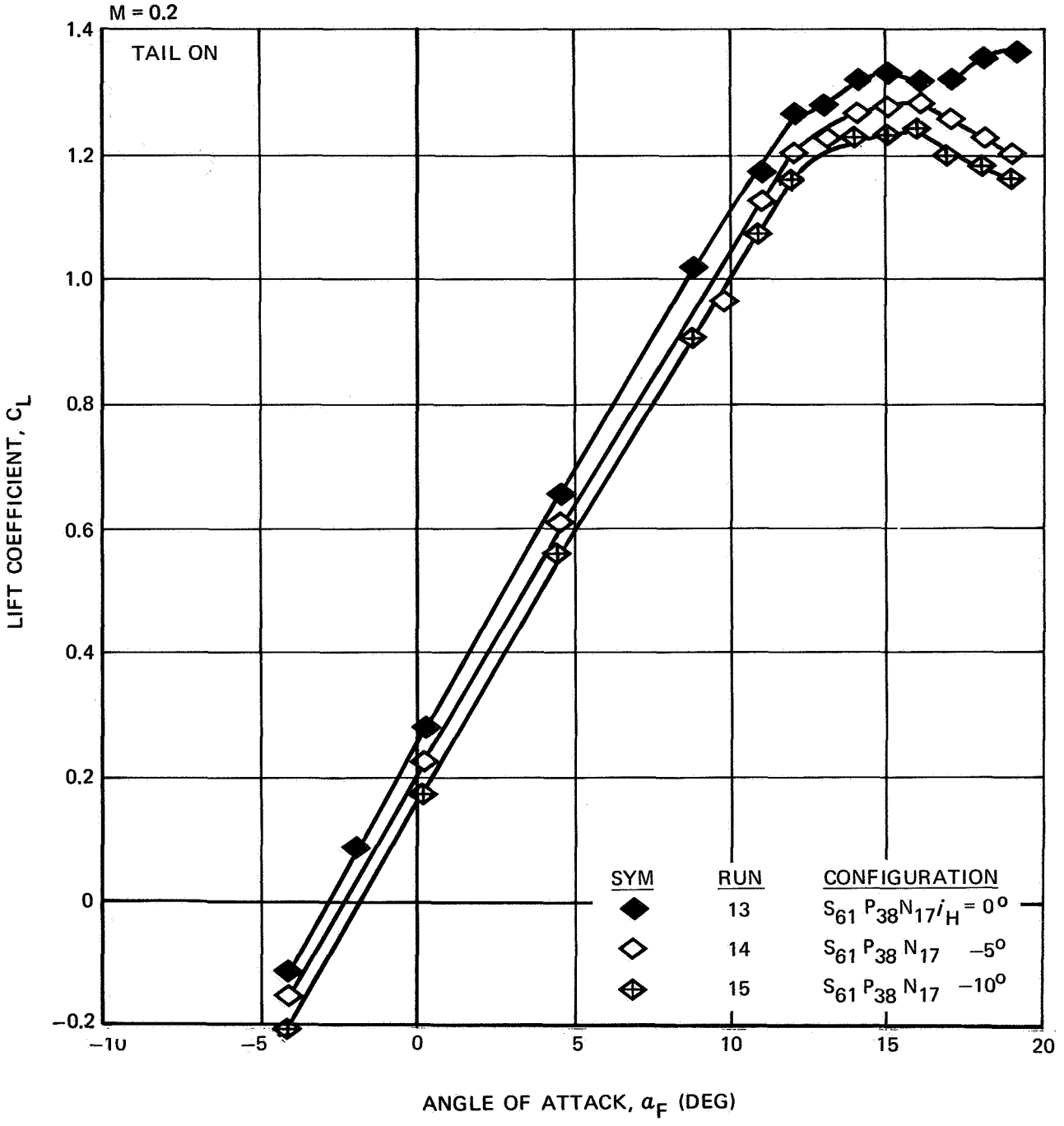

FIGURE III-13. EFFECT OF STABILIZER ANGLE ON LIFT COEFFICIENT, QUIET ENGINE AFT – $\delta_f = 0^o$

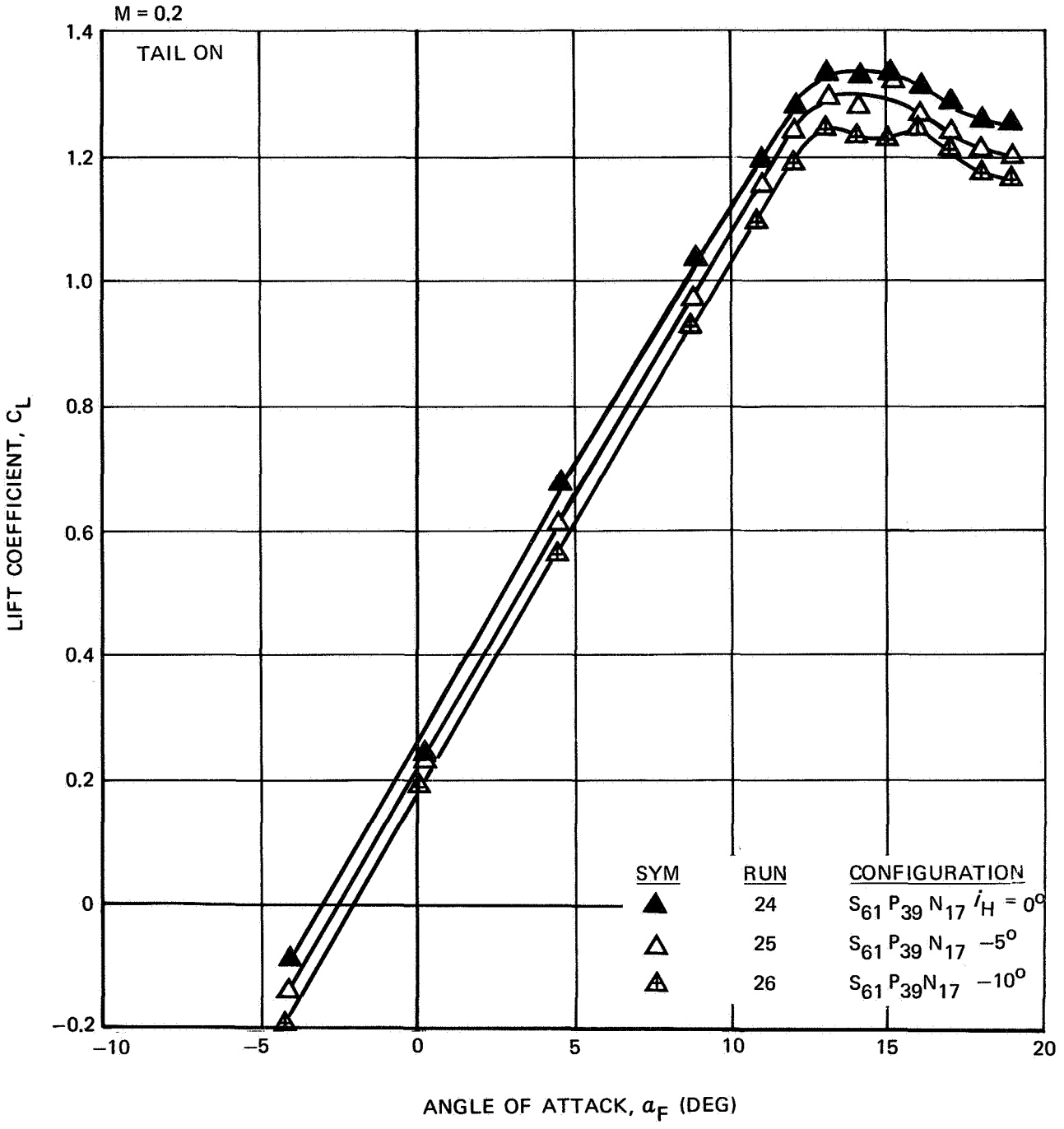

FIGURE III-14. EFFECT OF STABILIZER ANGLE ON LIFT COEFFICIENT, QUIET ENGINE FORWARD – $\delta_f = 0^o$

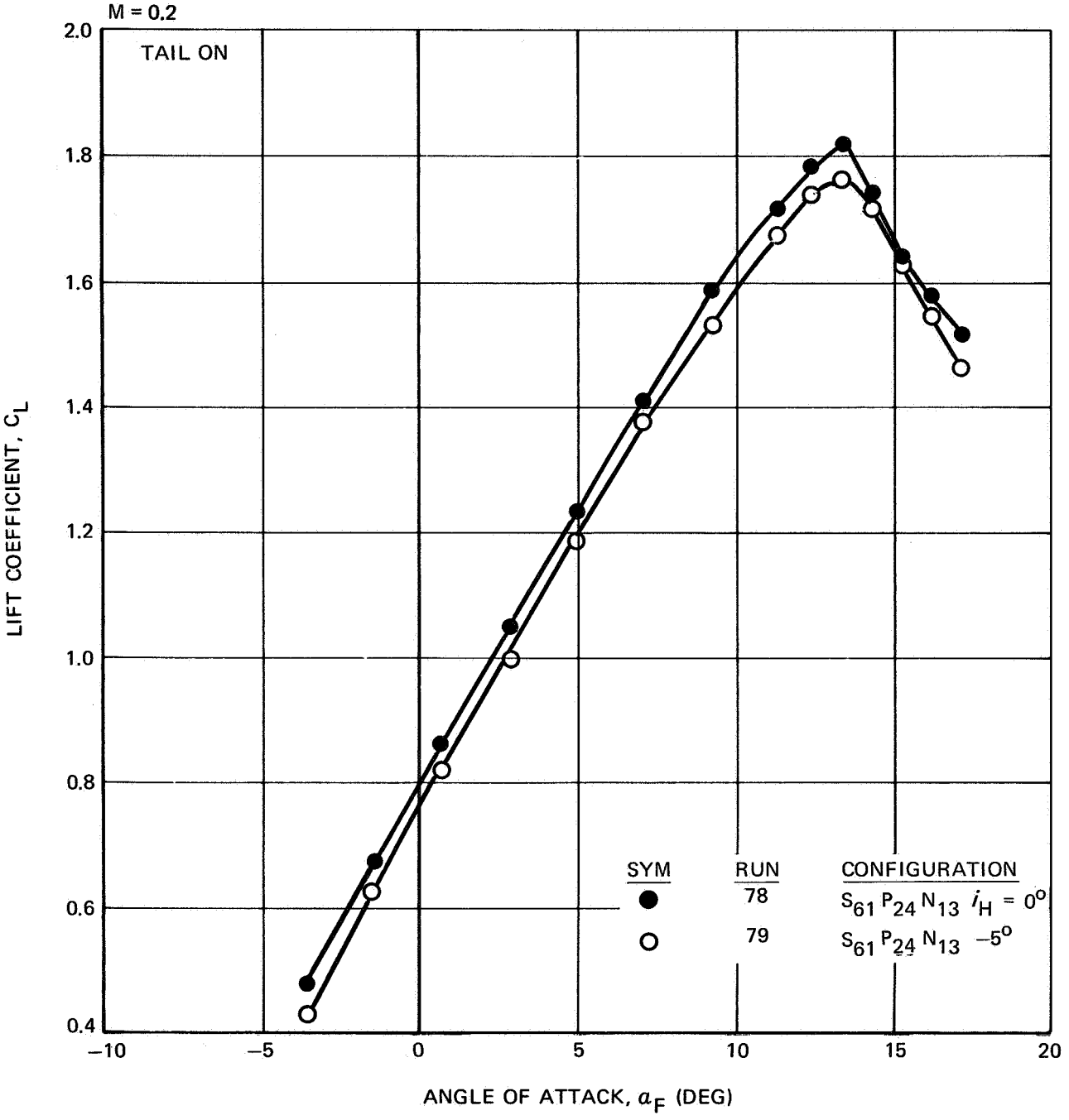

FIGURE III-15. EFFECT OF STABILIZER ANGLE ON LIFT COEFFICIENT, BASIC DC-8-61 – $\delta_f = 25^o$

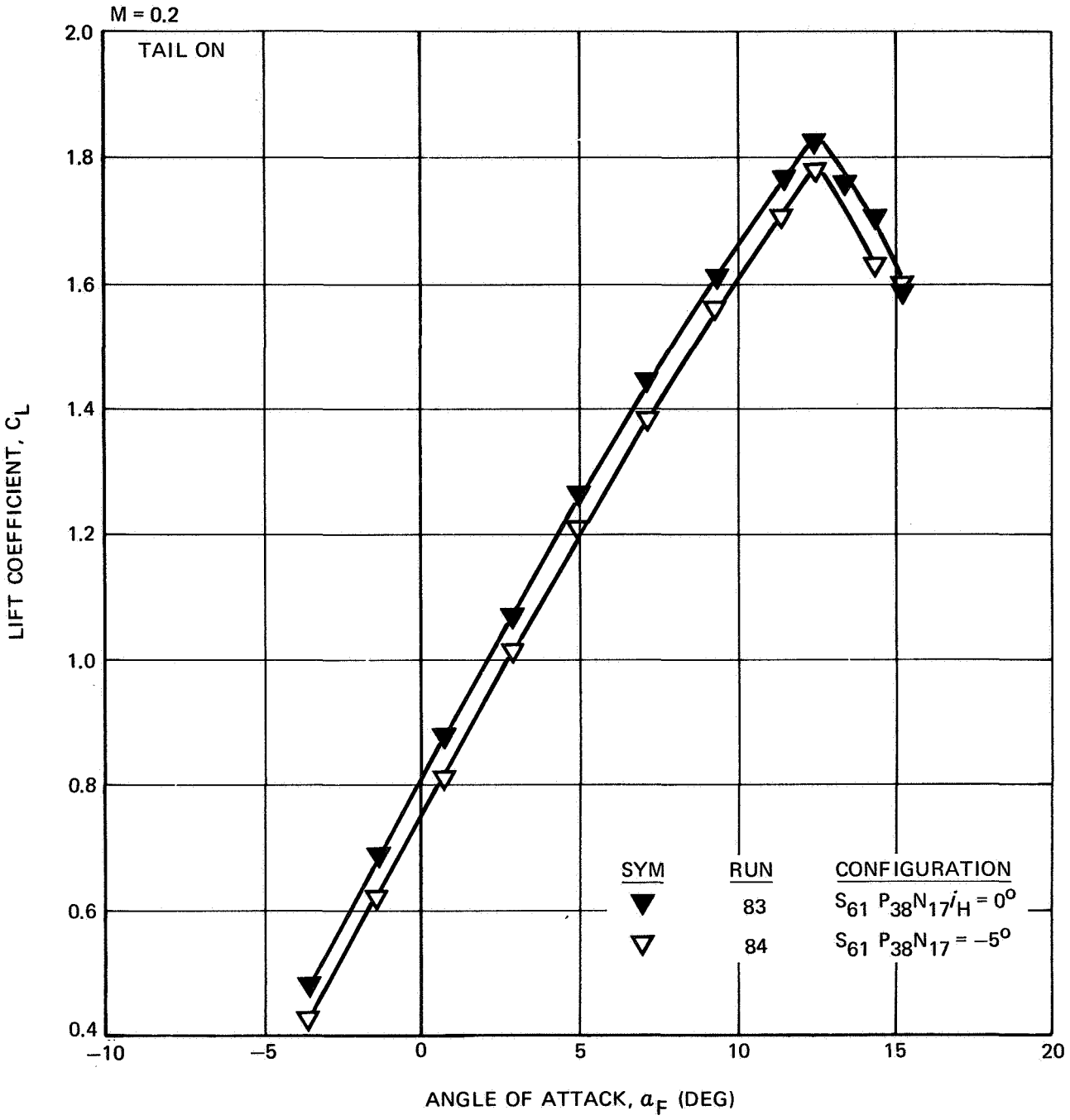

FIGURE III-16. EFFECT OF STABILIZER ANGLE ON LIFT COEFFICIENT, QUIET ENGINE AFT – $\delta_f = 25^o$

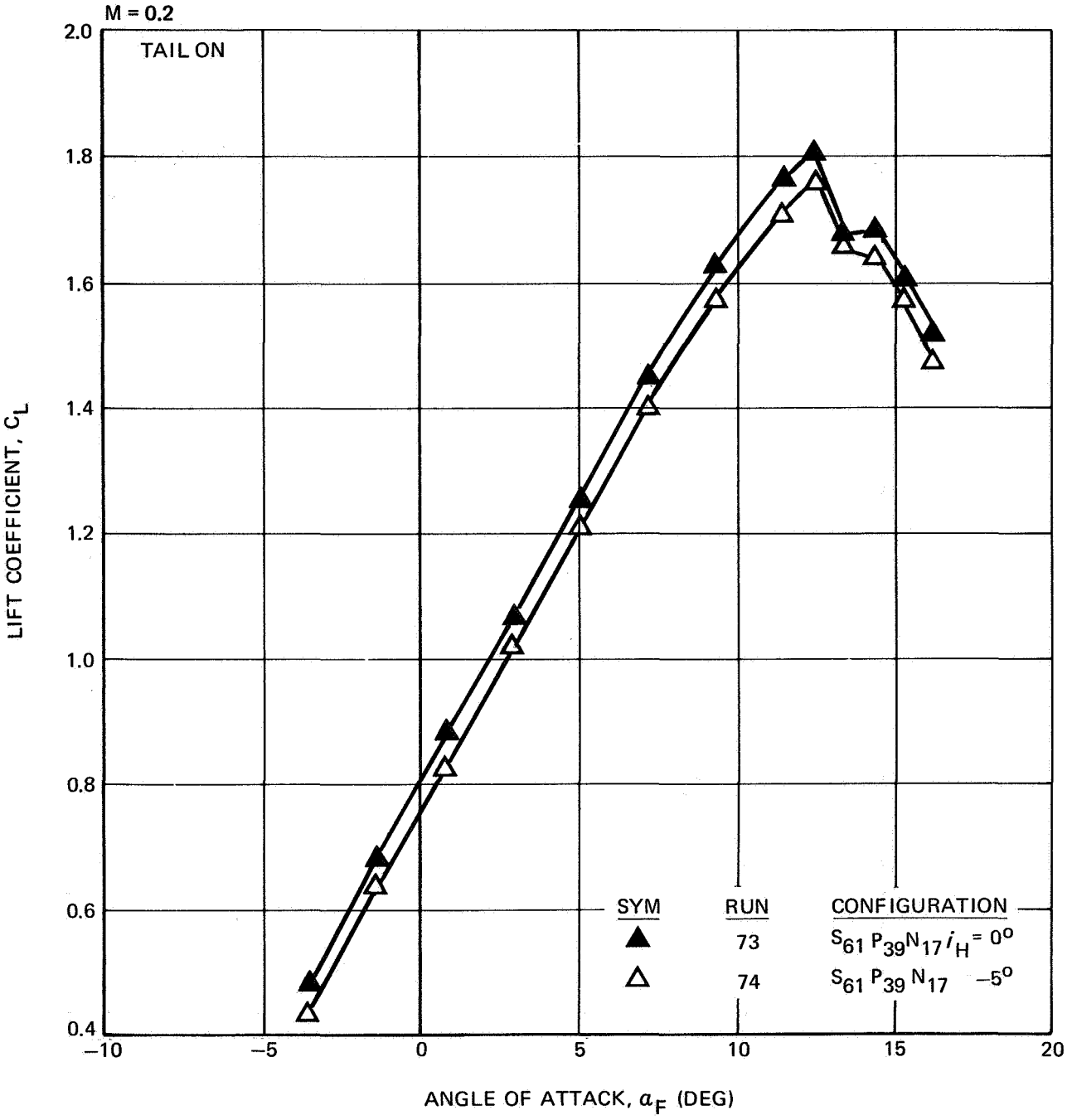

FIGURE III-17. EFFECT OF STABILIZER ANGLE ON LIFT COEFFICIENT, QUIET ENGINE FORWARD – $\delta_f = 25^o$

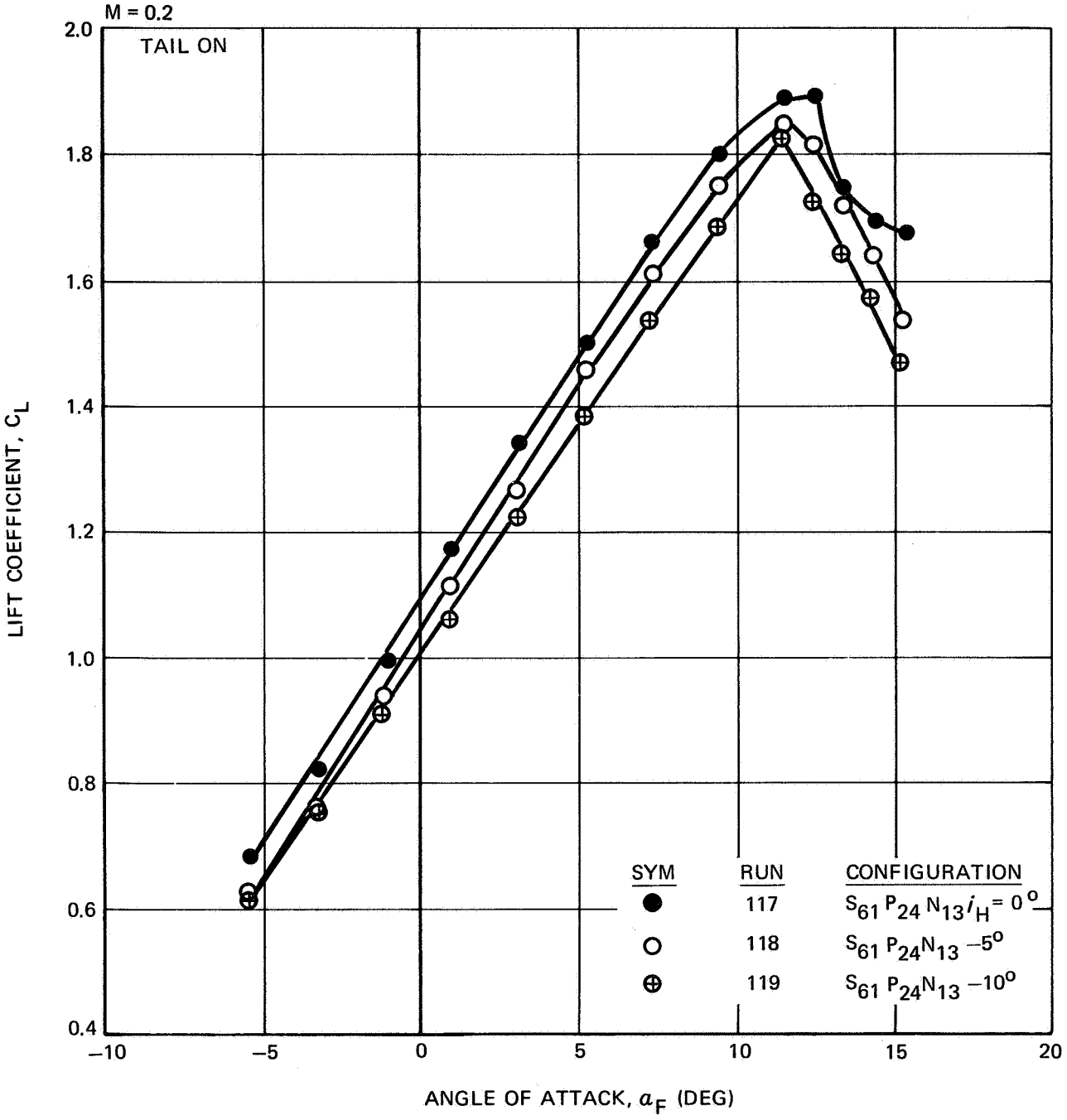

FIGURE III-18. EFFECT OF STABILIZER ANGLE ON LIFT COEFFICIENT, BASIC DC-8-61 – $\delta_f = 50^o$

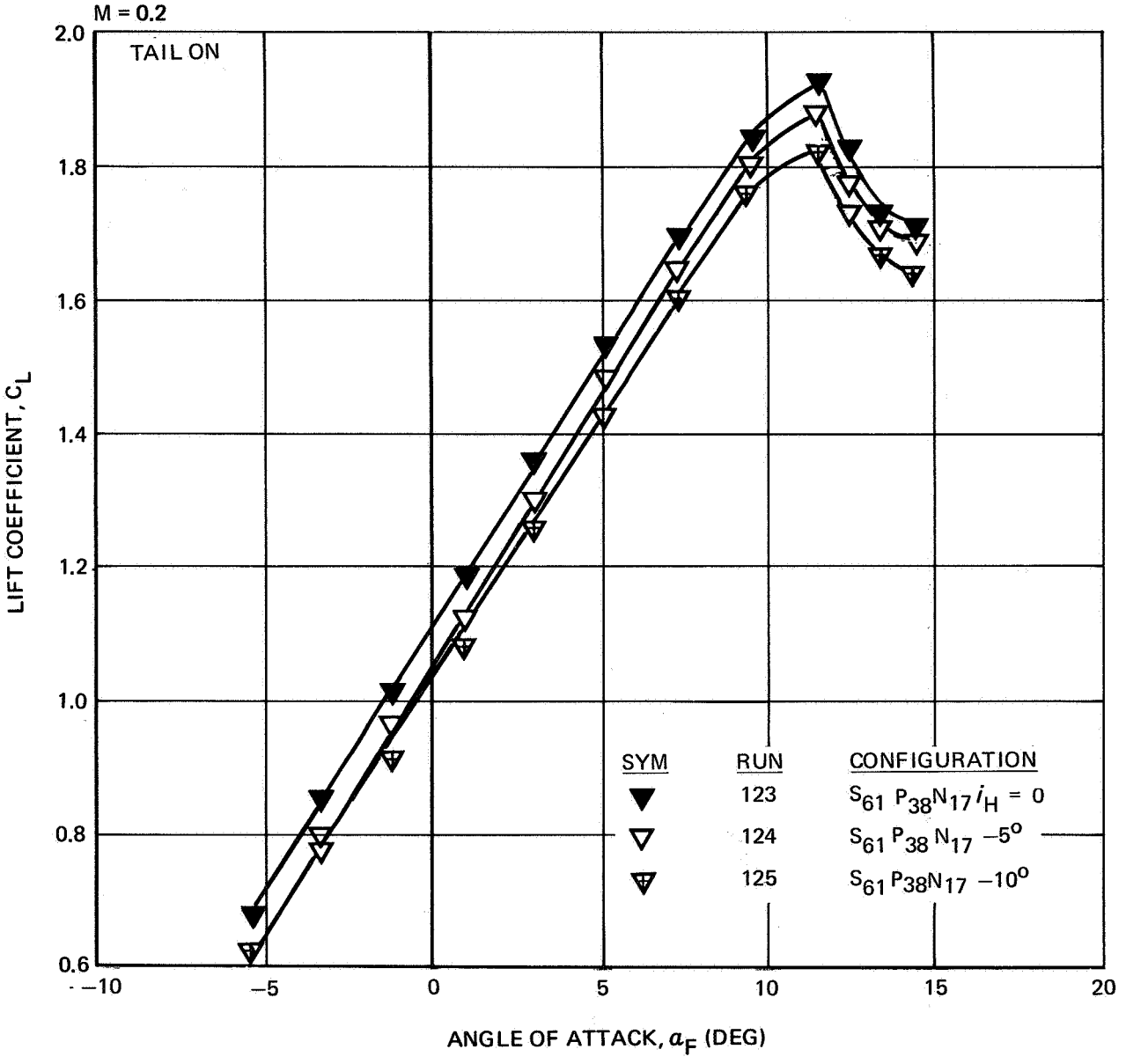

FIGURE III-19. EFFECT OF STABILIZER ANGLE ON LIFT COEFFICIENT, QUIET ENGINE AFT – $\delta_f = 50^o$

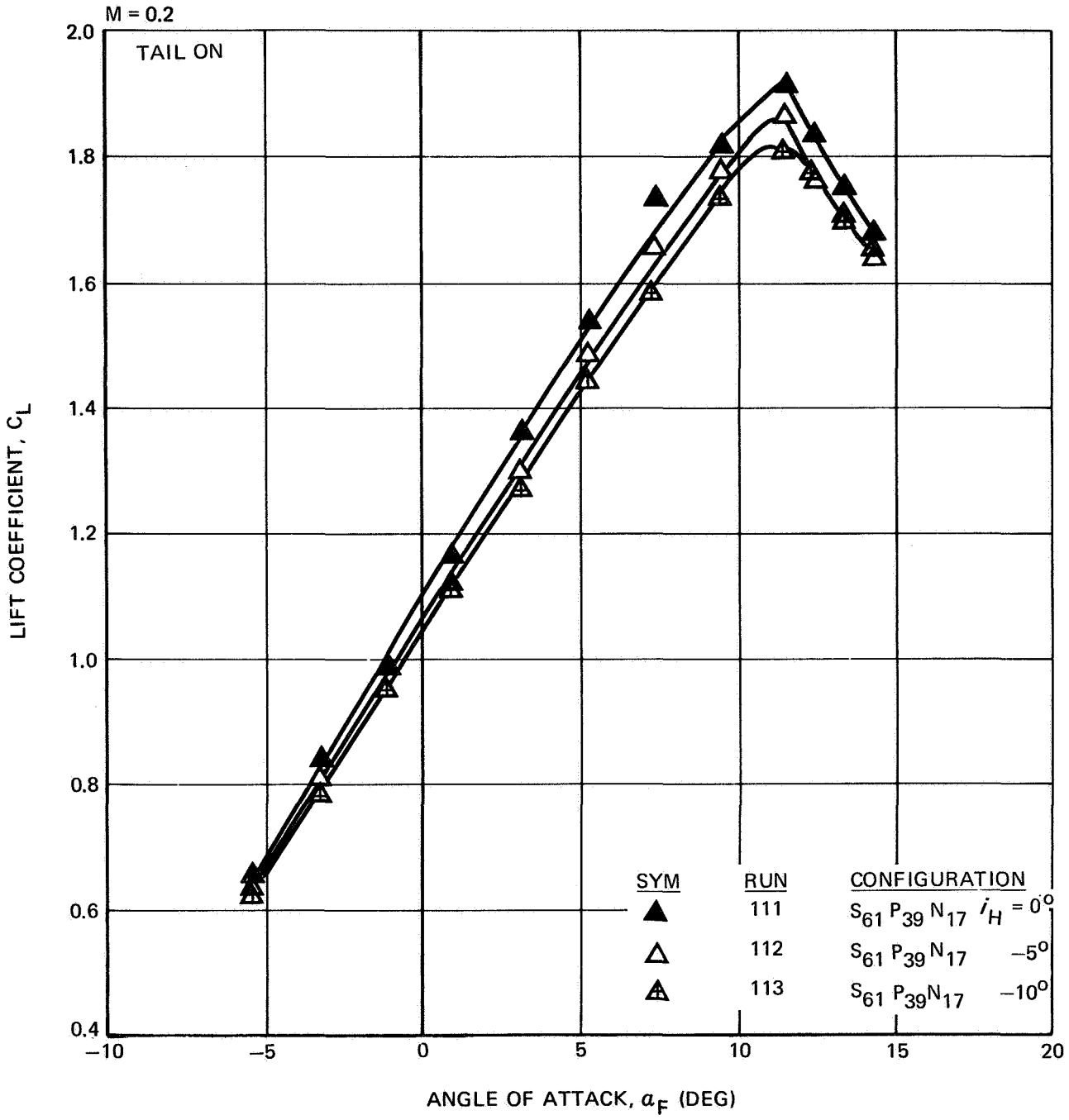

FIGURE III-20. EFFECT OF STABILIZER ANGLE ON LIFT COEFFICIENT, QUIET ENGINE FORWARD – $\delta_f = 50^o$

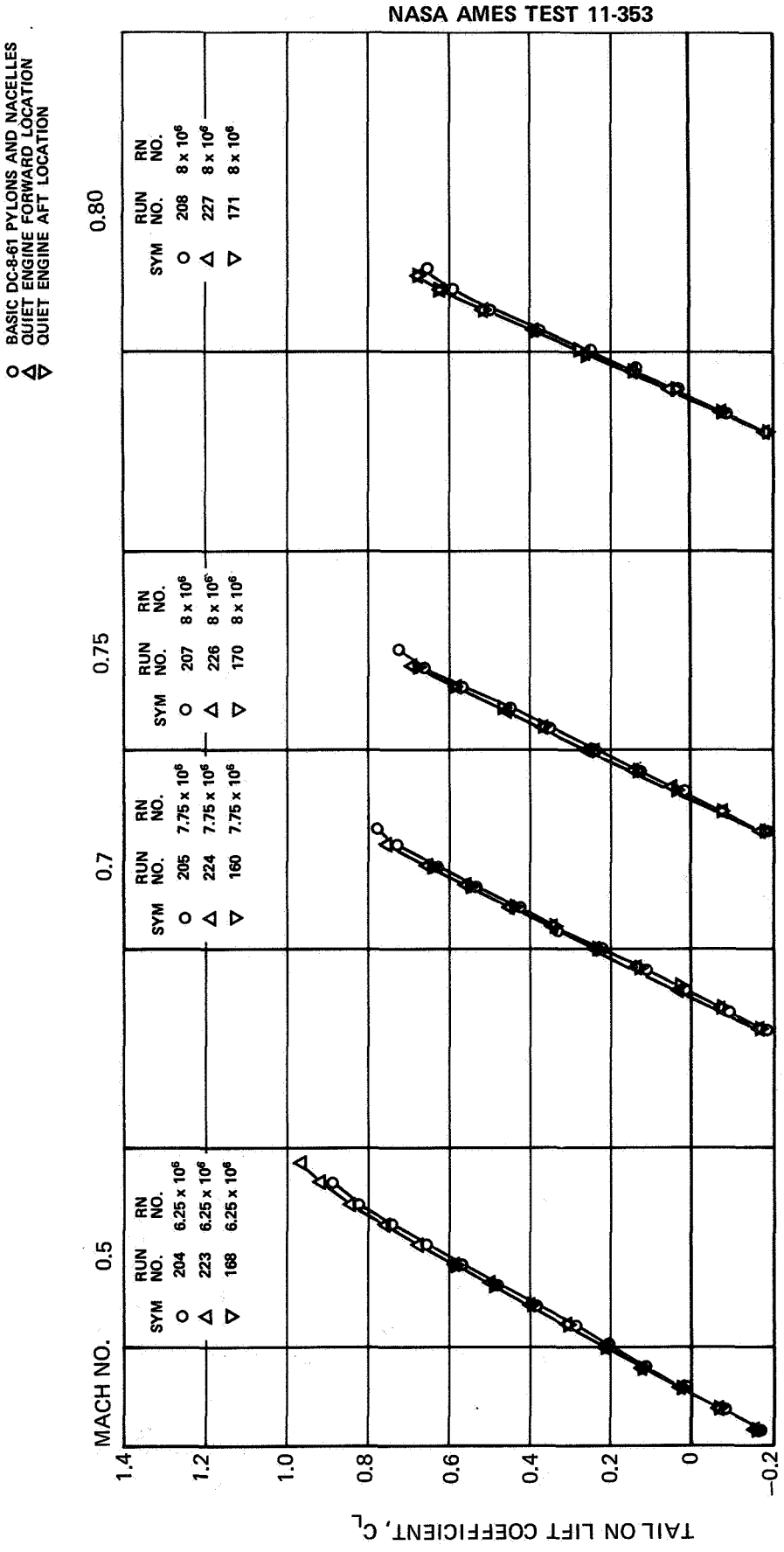

FIGURE III-21. EFFECT OF NACELLES AND PYLONS ON TAIL-ON LIFT COEFFICIENT – $\delta_f = 0^o$
(SHEET 1 OF 2)

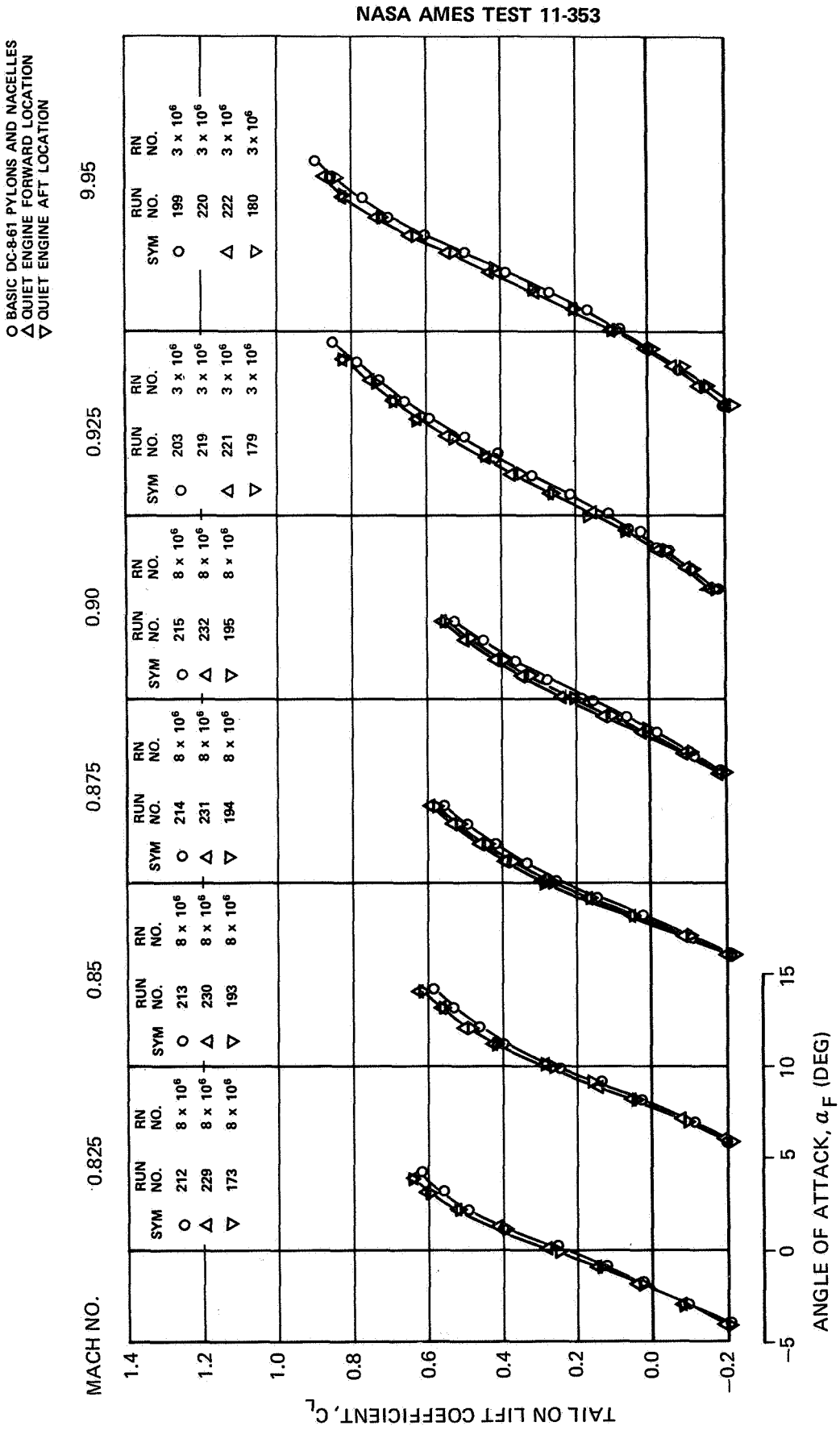

FIGURE III-21. EFFECT OF NACELLES AND PYLONS ON TAIL-ON LIFT COEFFICIENT – $\delta_f = 0^o$
(SHEET 2 OF 2)

NASA AMES TEST 12-361

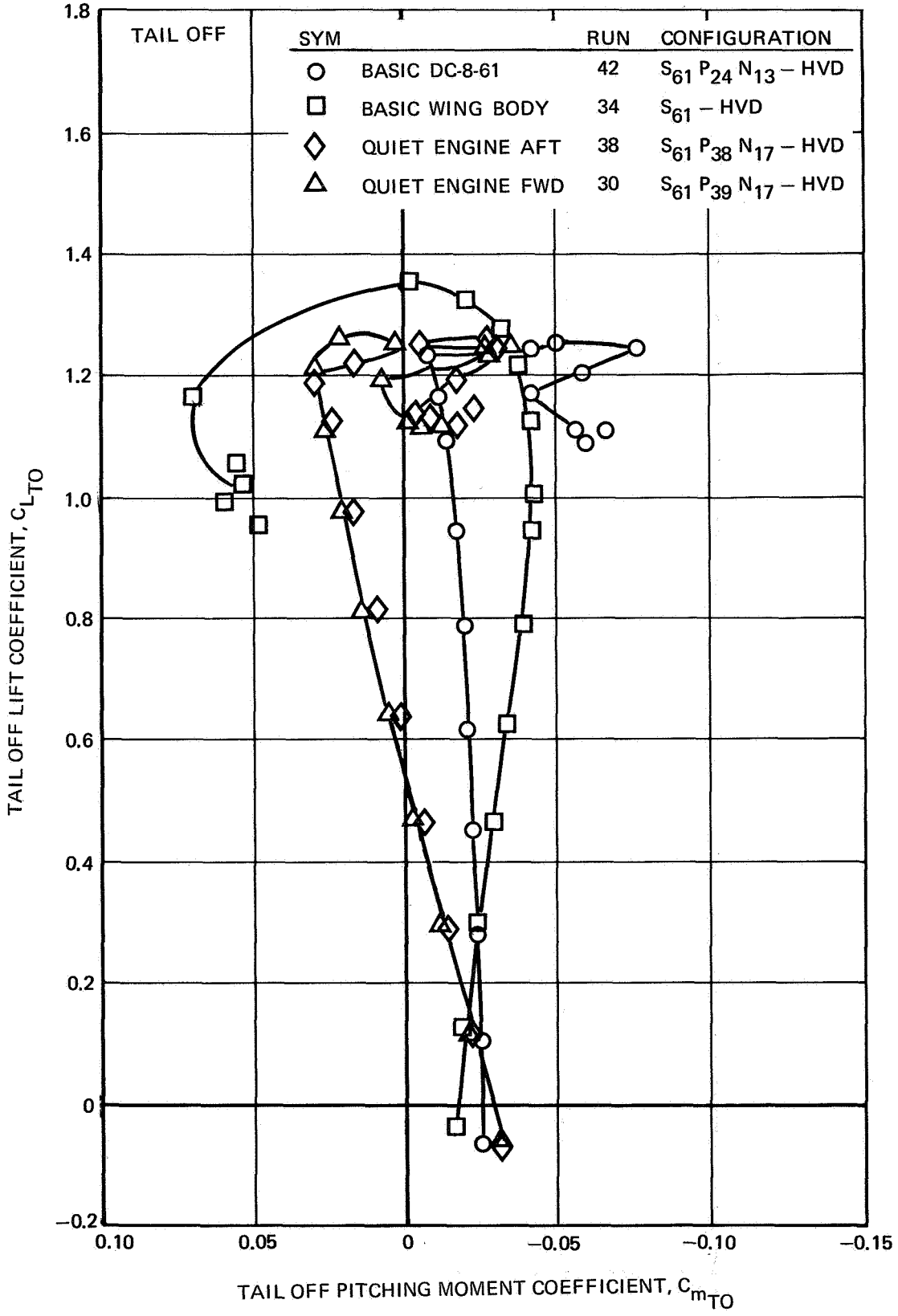

FIGURE III-22. EFFECT OF PYLONS AND NACELLES ON PITCHING MOMENTS – $\delta_f = 0^o$

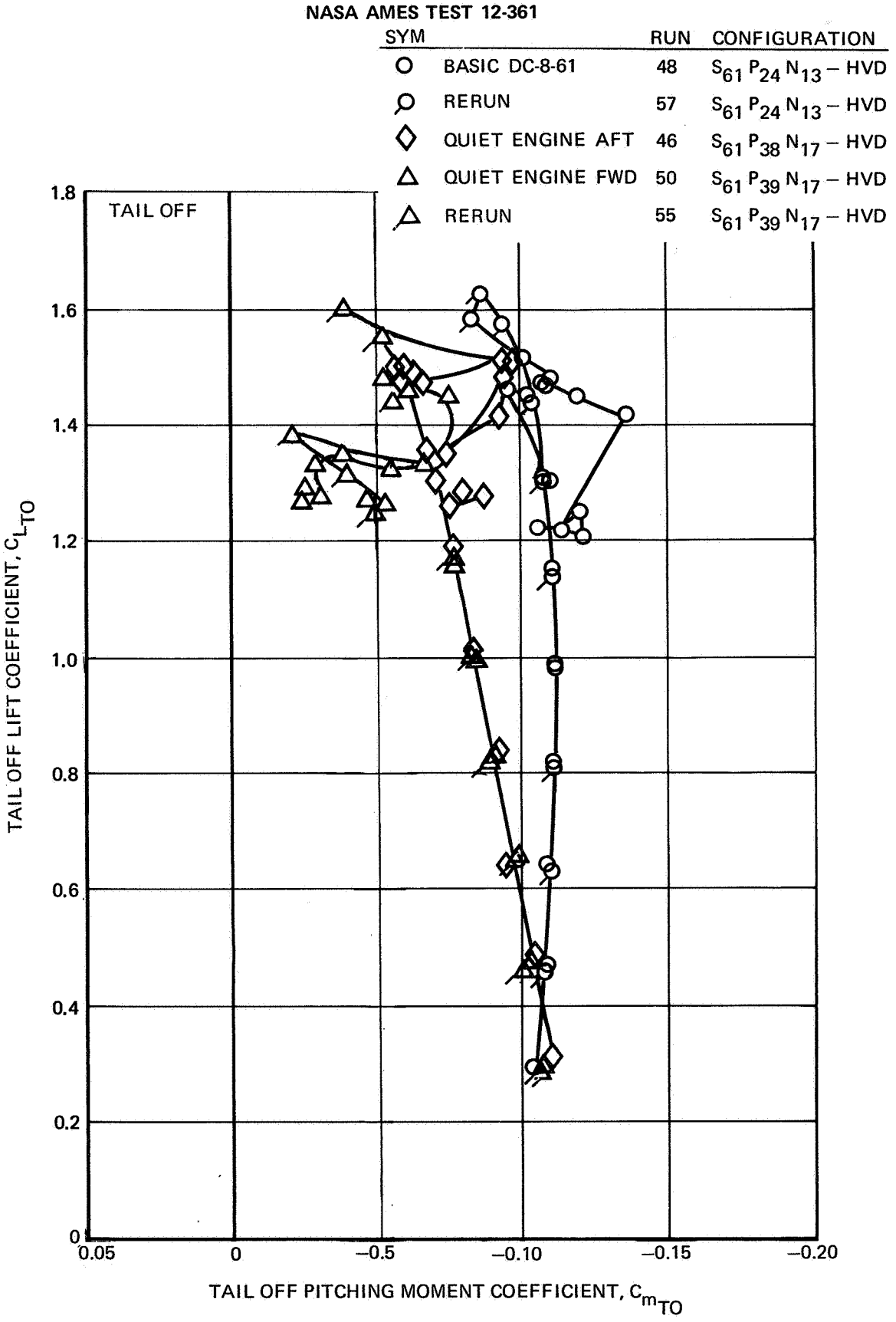

FIGURE III-23. EFFECT OF PYLONS AND NACELLES ON PITCHING MOMENTS – $\delta_f = 15^o$

NASA AMES TEST 12-361

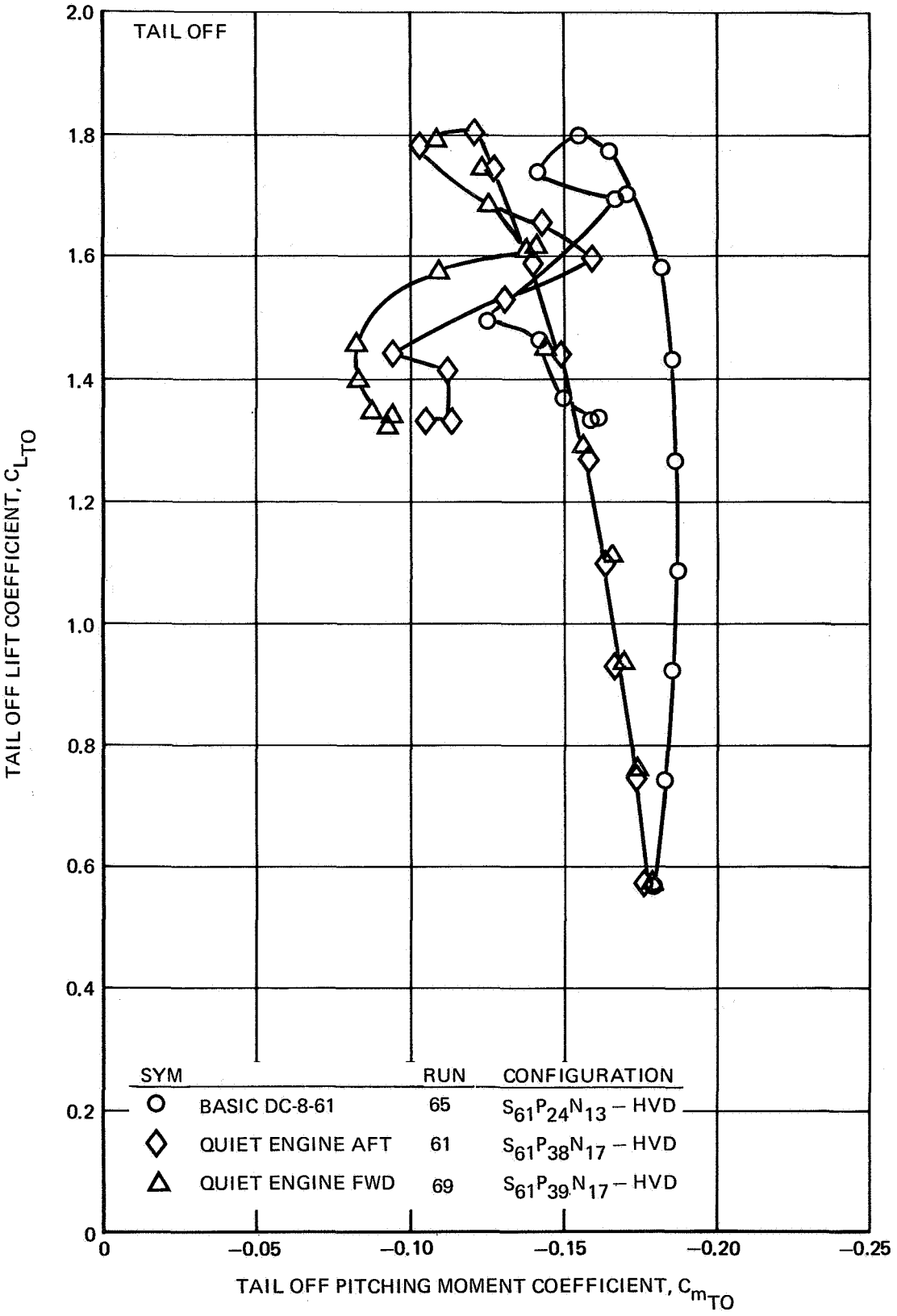

FIGURE III-24. EFFECT OF PYLONS AND NACELLES ON PITCHING MOMENTS – $\bar{\delta}_f = 25^o$

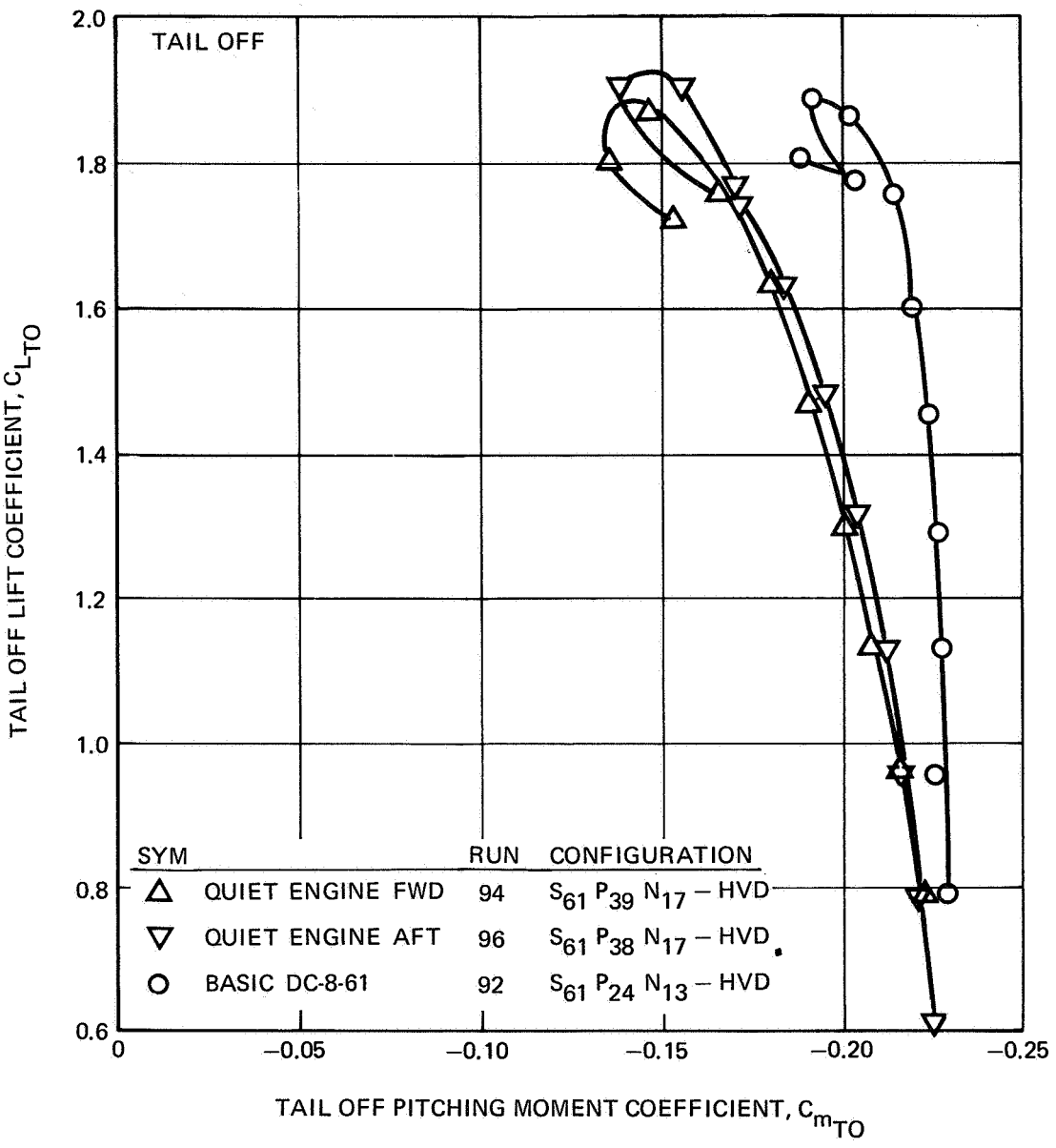

FIGURE III-25. EFFECT OF PYLONS AND NACELLES ON PITCHING MOMENTS – $\delta_f = 35^o$

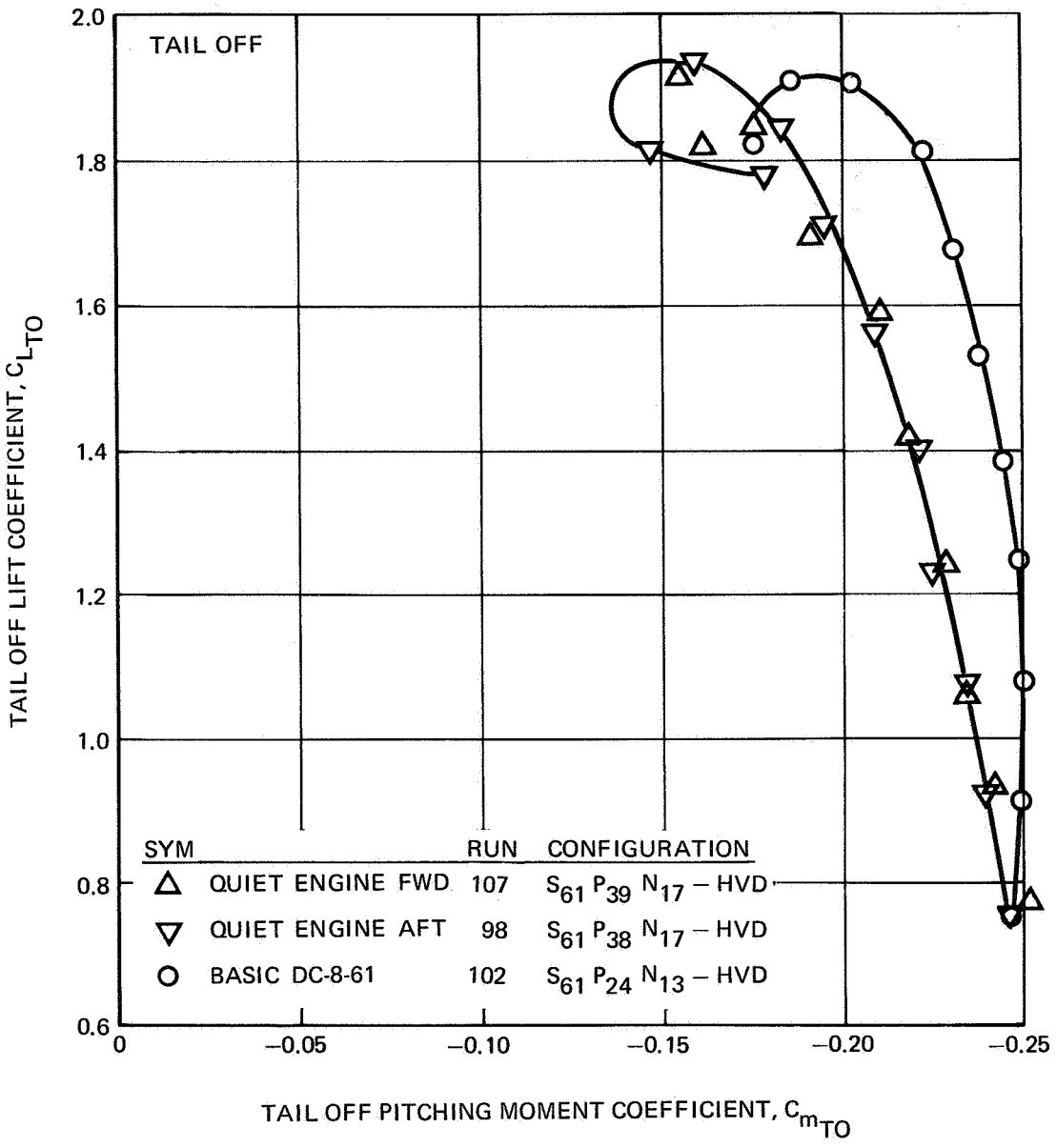

FIGURE III-26. EFFECT OF PYLONS AND NACELLES ON PITCHING MOMENTS – δ_f = 50°

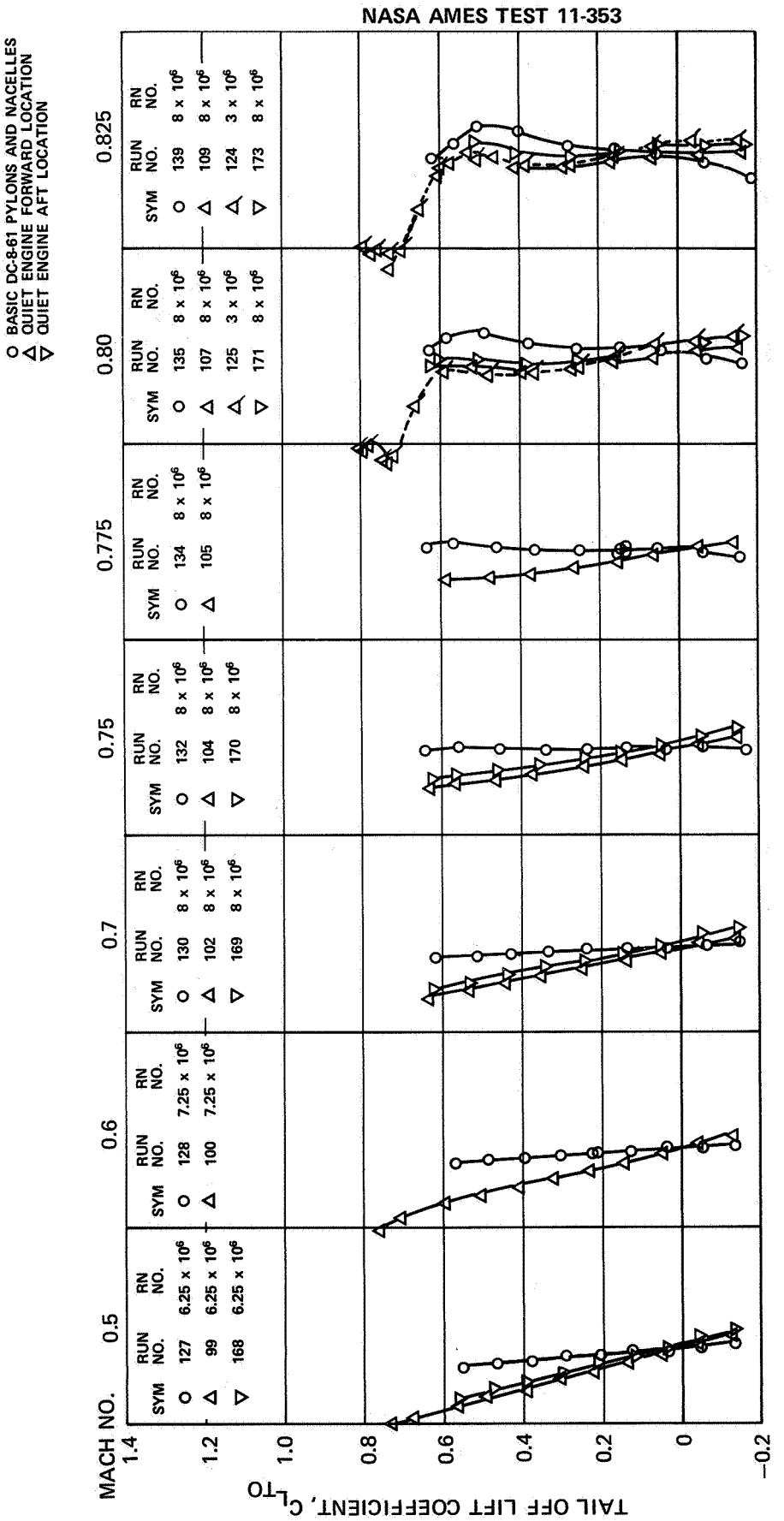

FIGURE III-27. EFFECT OF NACELLES AND PYLONS ON TAIL-OFF PITCHING MOMENT COEFFICIENT AT HIGH MACH NUMBER — $\delta_f = 0^0$ (SHEET 1 OF 2)

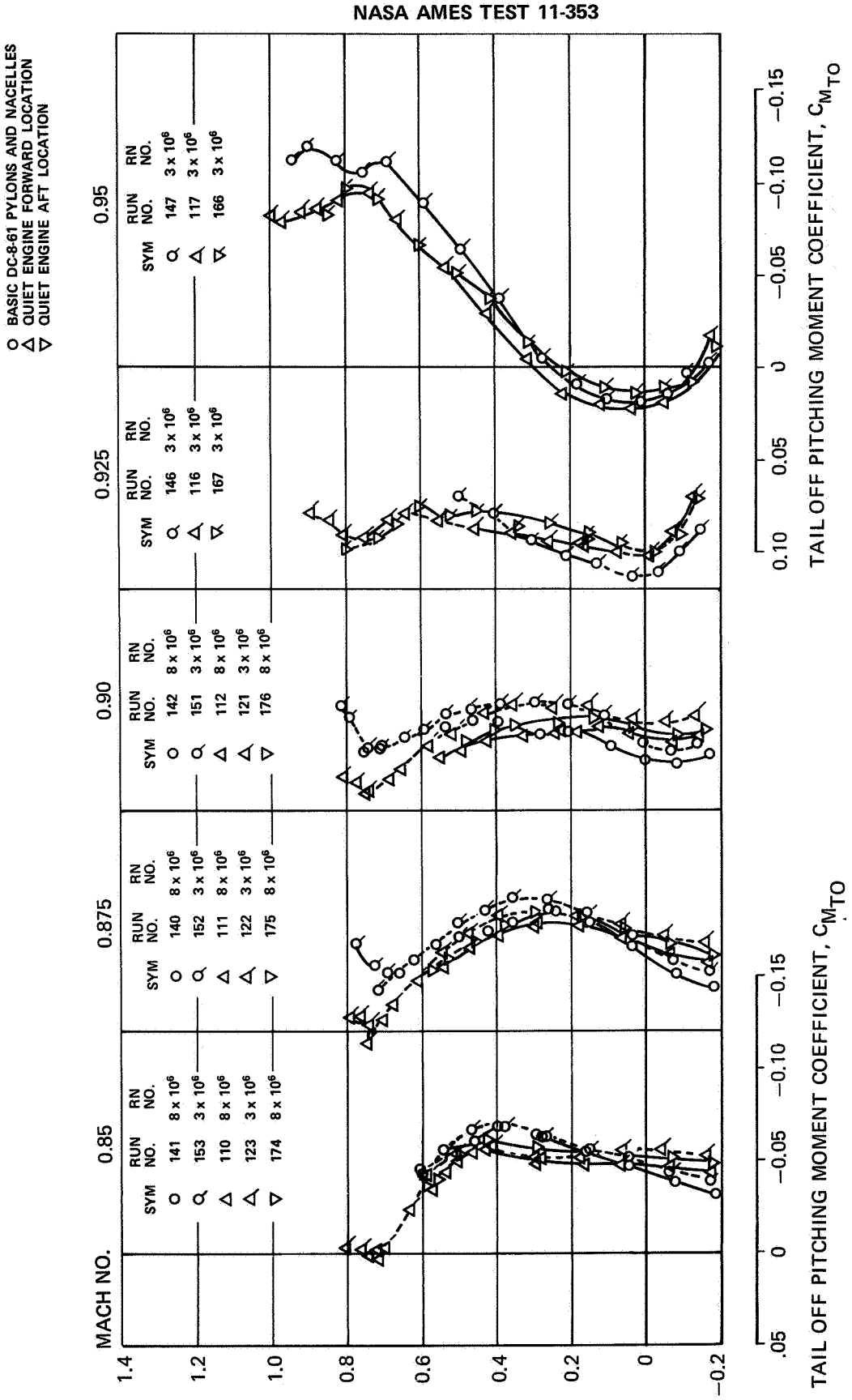

FIGURE III-27. EFFECT OF NACELLES AND PYLONS ON TAIL-OFF PITCHING MOMENT COEFFICIENT AT HIGH MACH NUMBER – $\delta_f = 0^o$ (SHEET 2 OF 2)

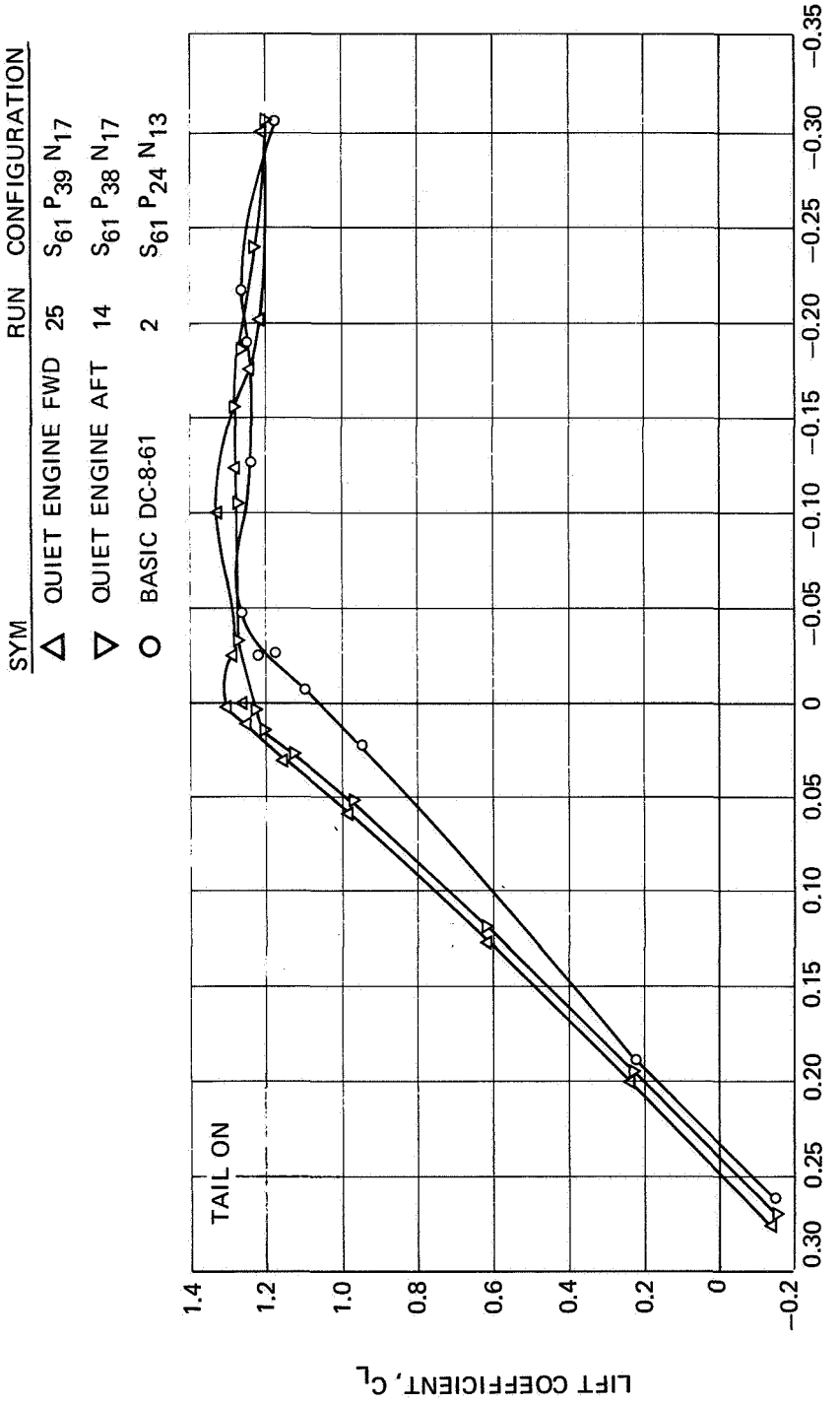

FIGURE III-28. EFFECT OF PYLONS AND NACELLES ON PITCHING MOMENT – $\delta_f = 0^o$, $i_H = 5^o$

NASA AMES TEST 12-361

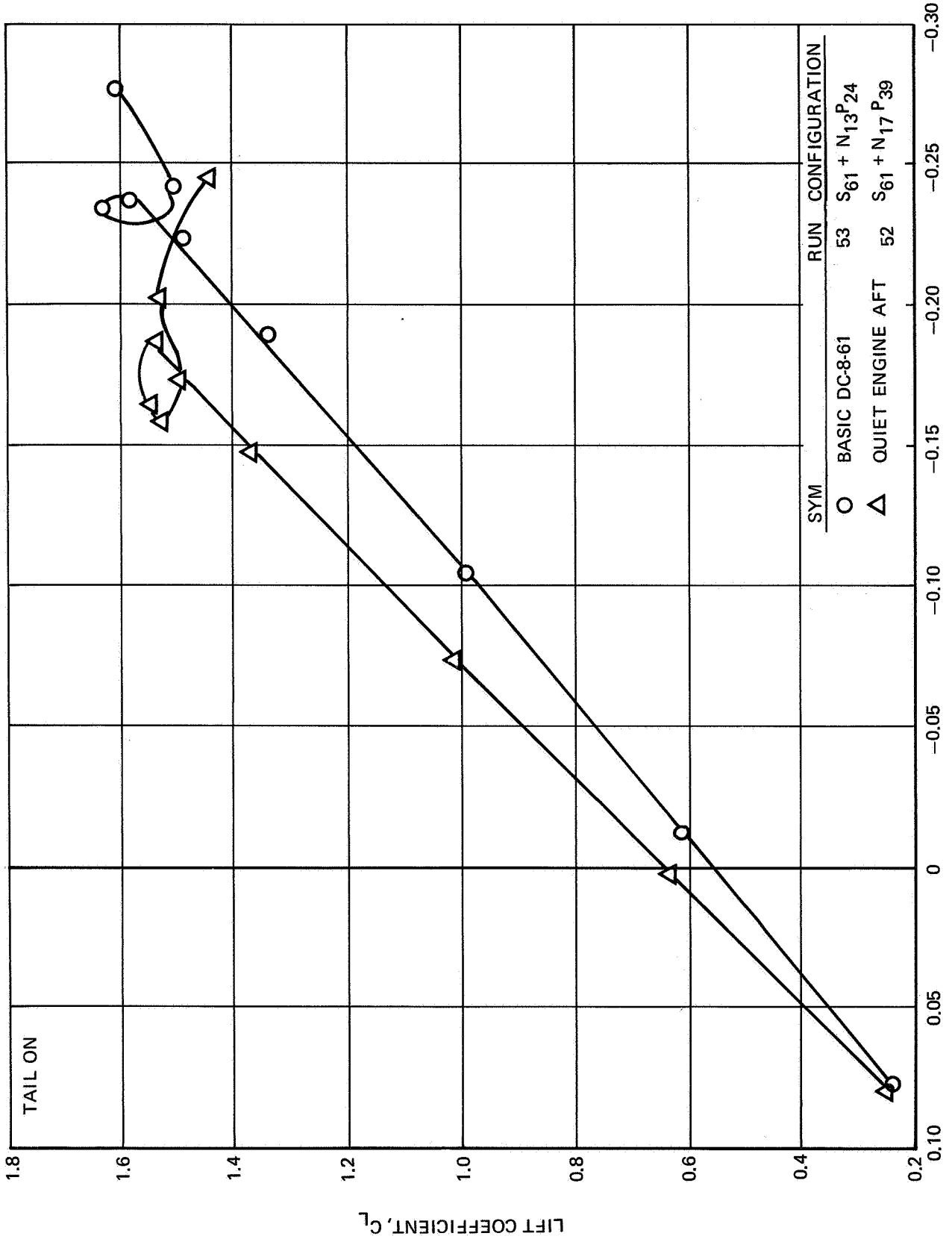

FIGURE III-29. EFFECT OF PYLONS AND NACELLES ON PITCHING MOMENT – $\delta_f = 15^o$, $i_H = 0^o$

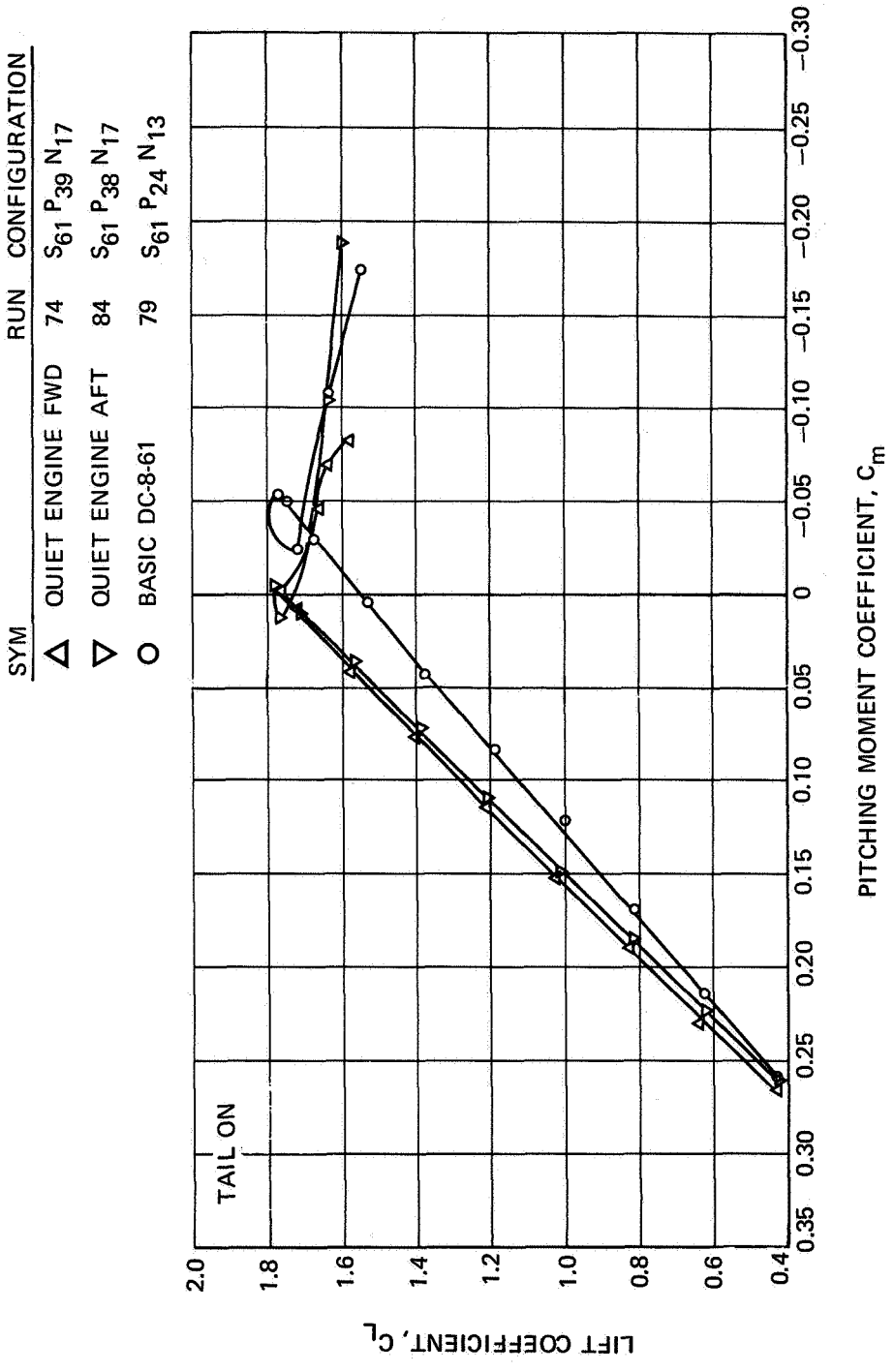

FIGURE III-30. EFFECT OF PYLONS AND NACELLES ON PITCHING MOMENT – $\delta_f = 25^o$, $i_H = -5^o$

NASA AMES TEST 12-361

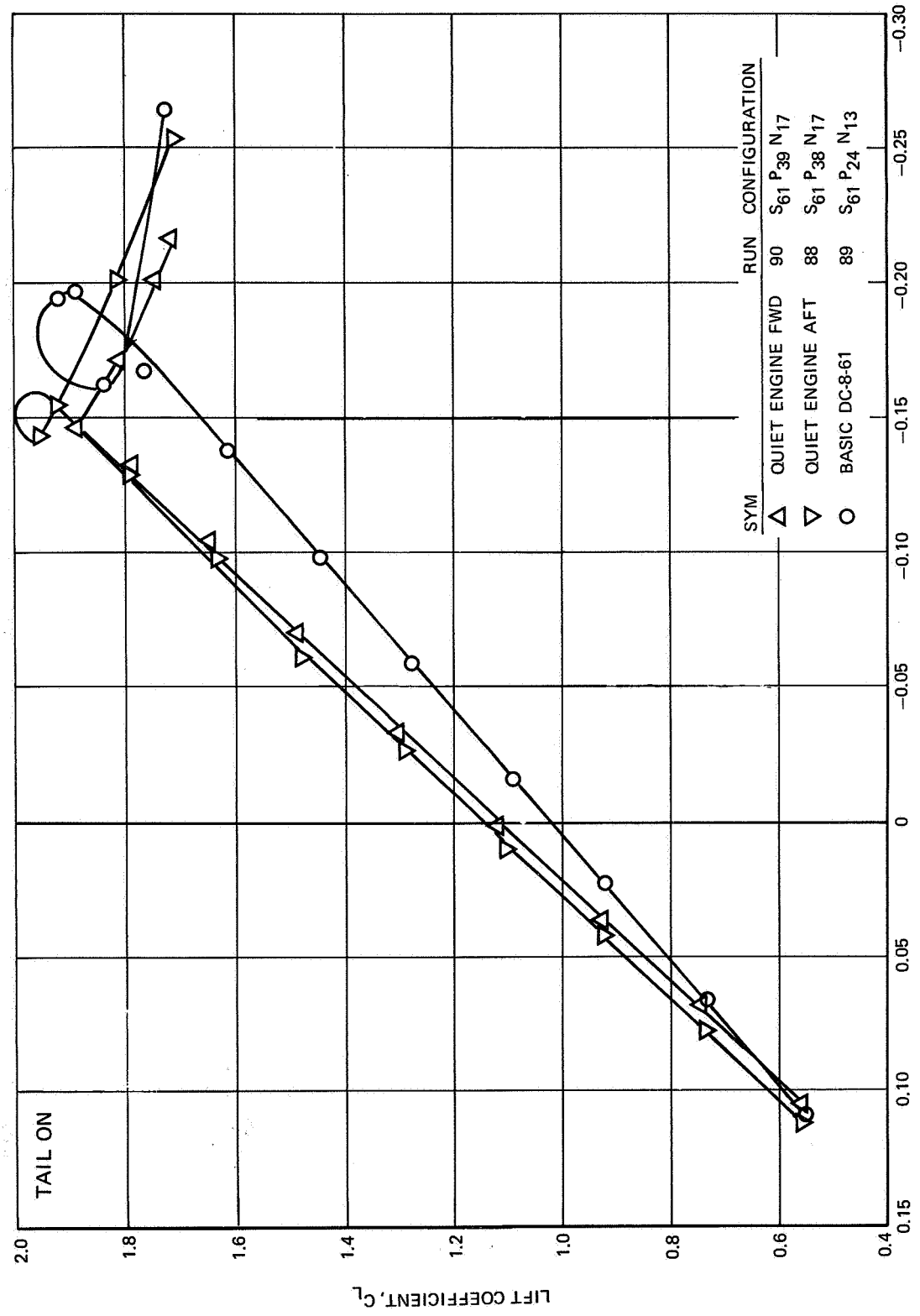

FIGURE III-31. EFFECT OF PYLONS AND NACELLES ON PITCHING MOMENT – $\delta_f = 35^o$, $i_H = 0^o$

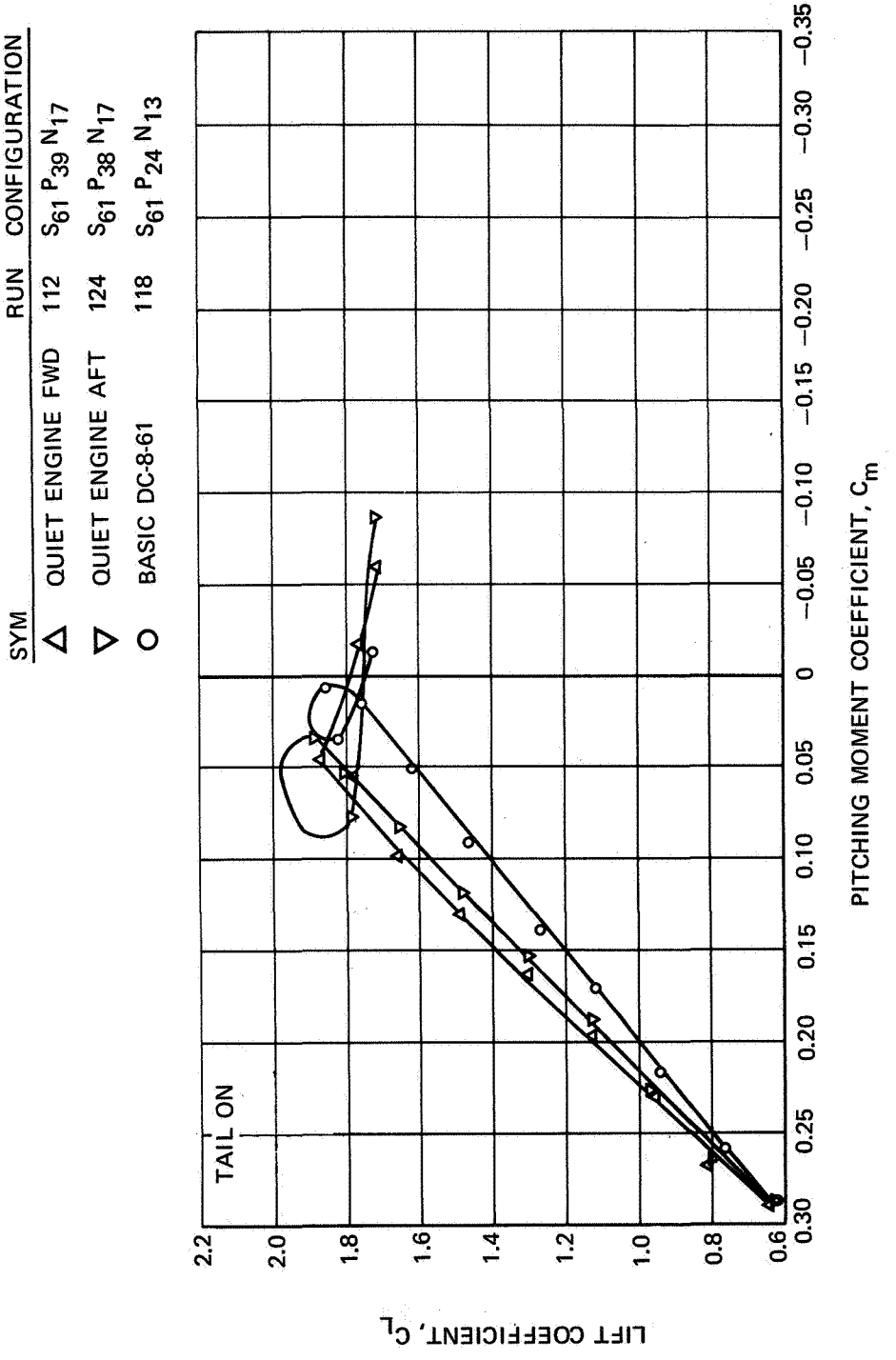

FIGURE III-32. EFFECT OF PYLONS AN D NACELLES ON PITCHING MOMENT – $\delta_f = 50^o$, $i_H = -5^o$

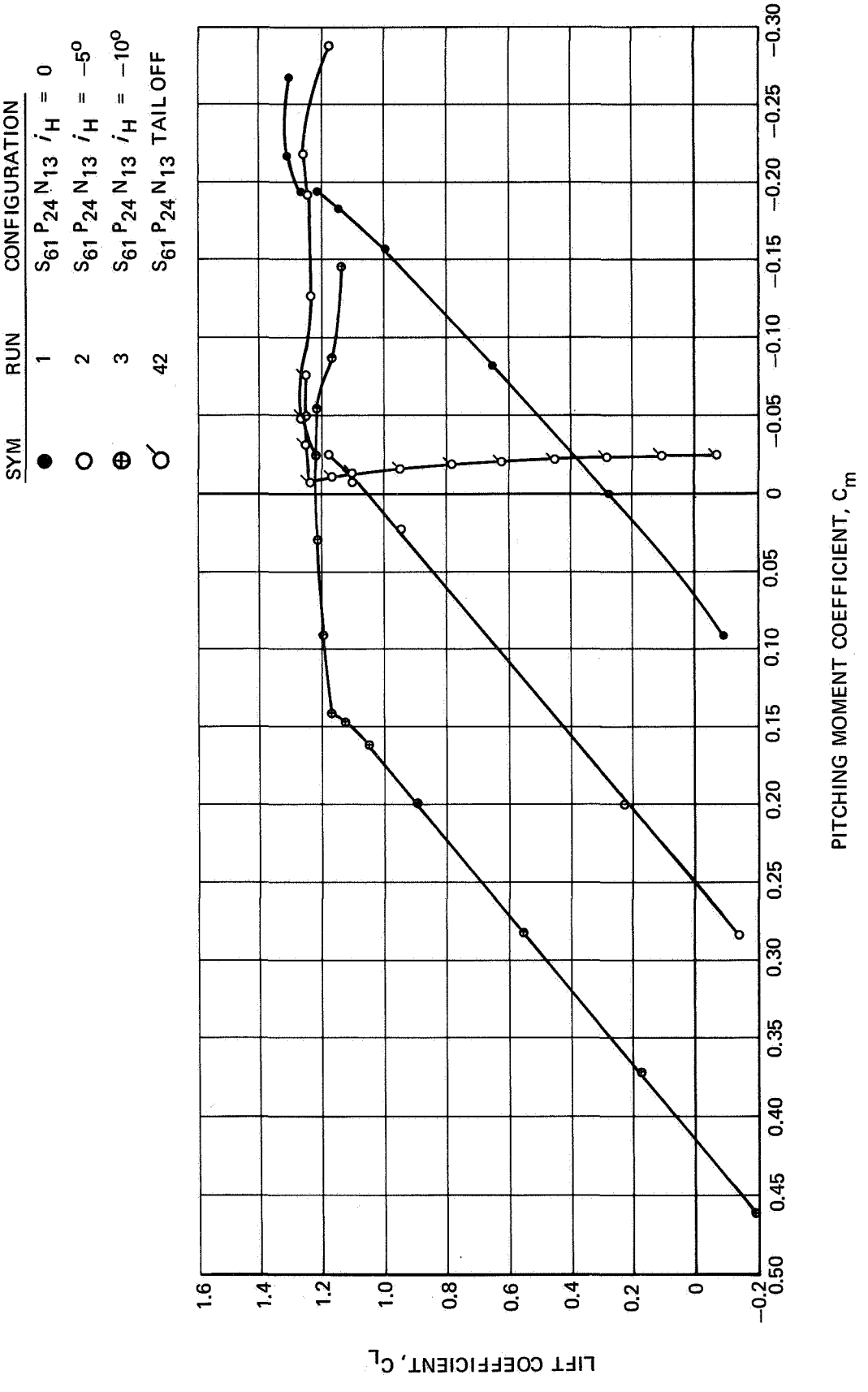

FIGURE III-33. EFFECT OF STABILIZER ANGLE ON PITCHING MOMENT COEFFICIENT, BASIC DC-8-61 – δ_f = 0°

NASA AMES TEST 12-361

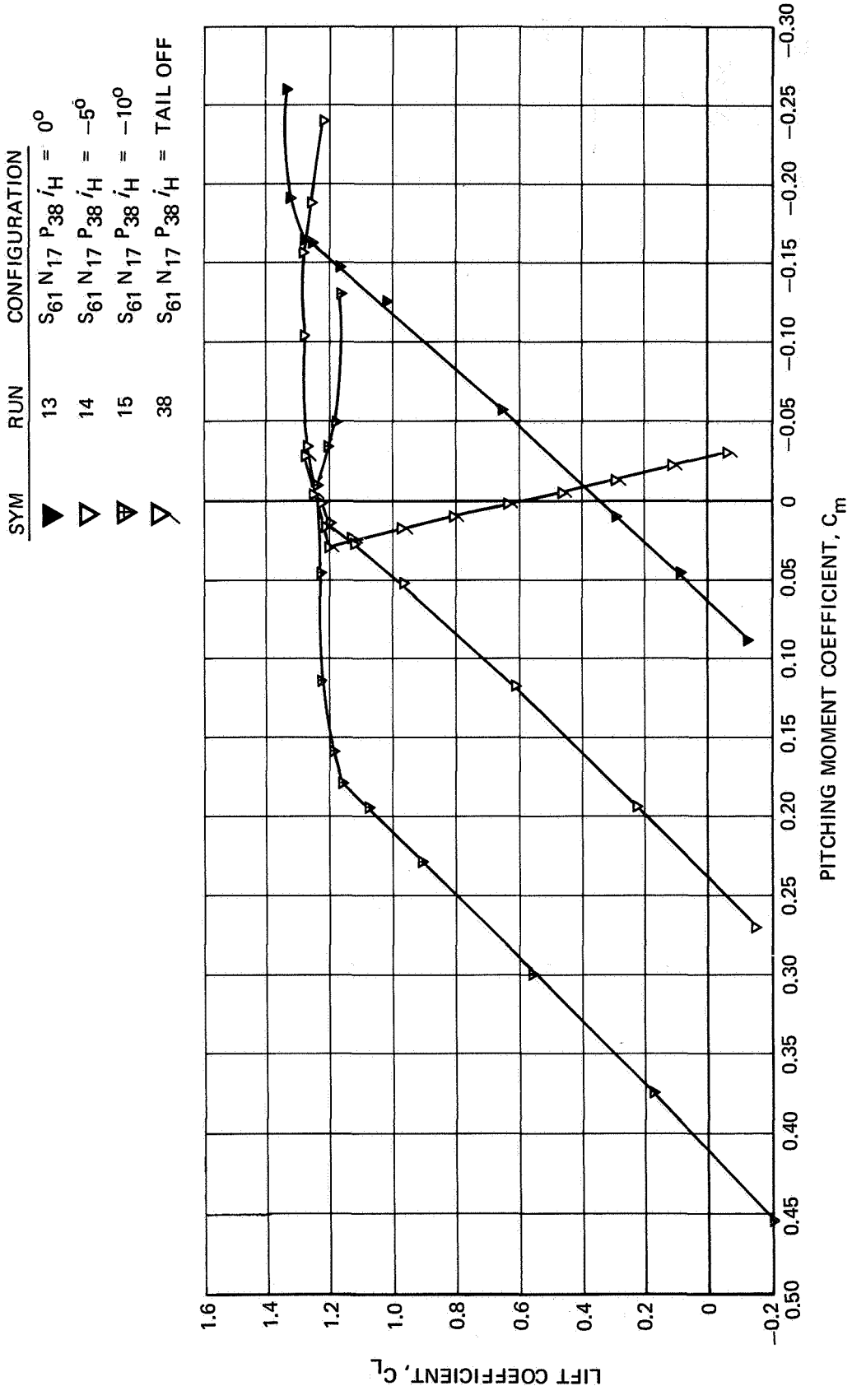

FIGURE III-34. EFFECT OF STABILIZER ANGLE ON PITCHING MOMENT COEFFICIENT, QUIET ENGINE AFT – $\delta_f = 0^o$

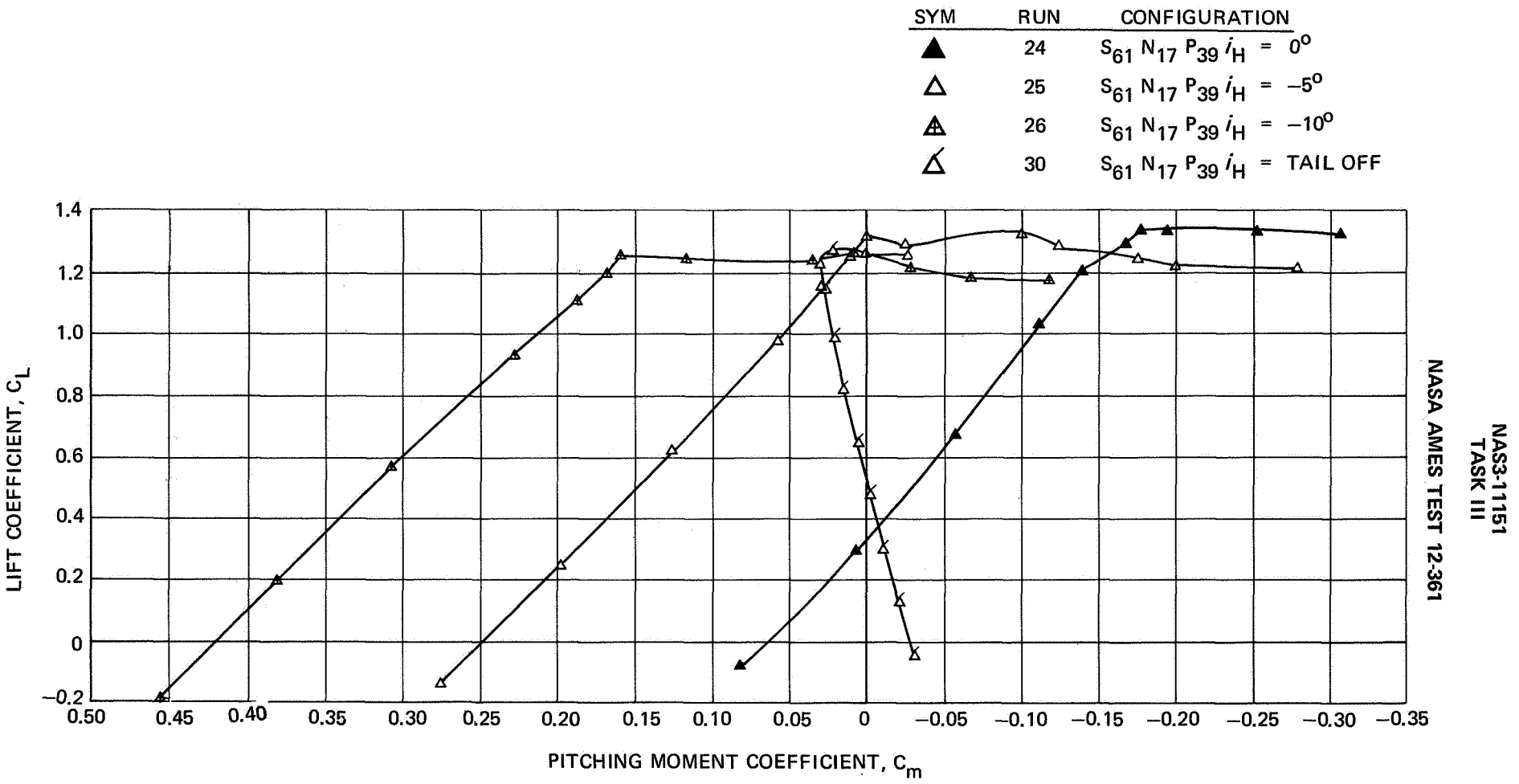

FIGURE III-35. EFFECT OF STABILIZER ANGLE ON PITCHING MOMENT COEFFICIENT, QUIET ENGINE FORWARD – $\delta_f = 0^o$

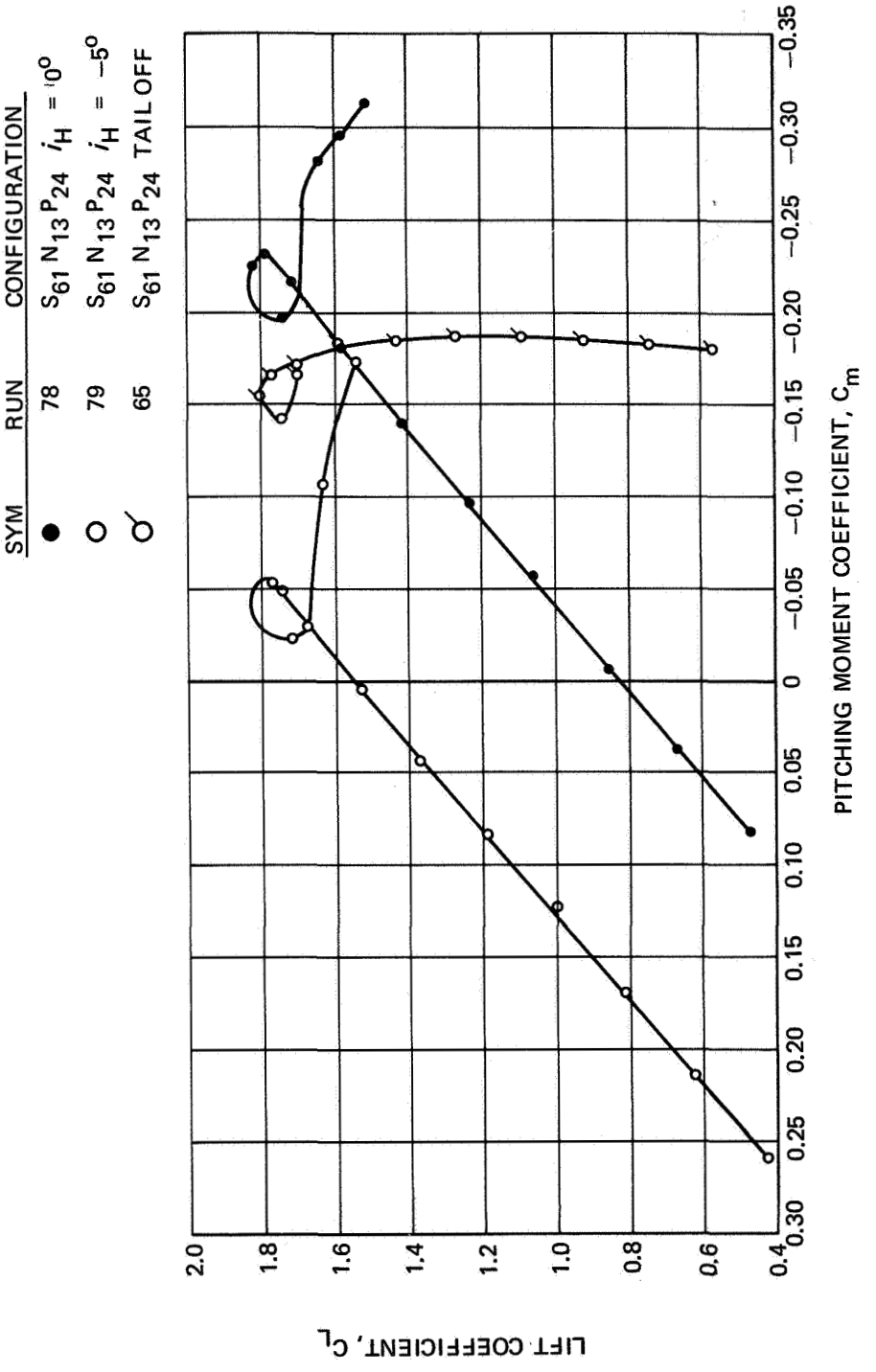

FIGURE III-36. EFFECT OF STABILIZER ANGLE ON PITCHING MOMENT COEFFICIENT, BASIC DC-8-61 – $\delta_f = 25^o$

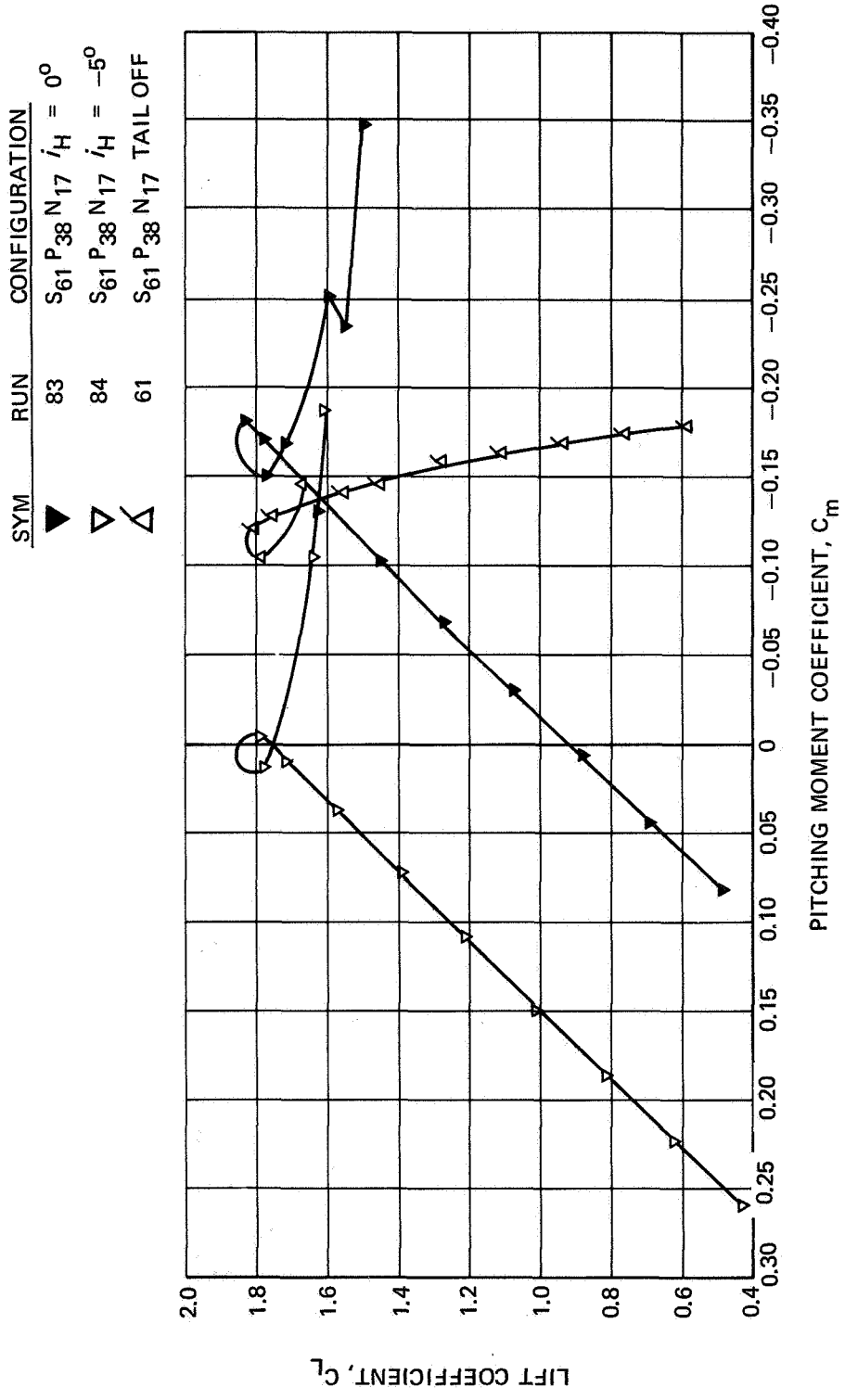

FIGURE III-37. EFFECT OF STABILIZER ANGLE ON PITCHING MOMENT COEFFICIENT, QUIET ENGINE AFT – $\delta_f = 25^o$

NASA AMES TEST 12-361

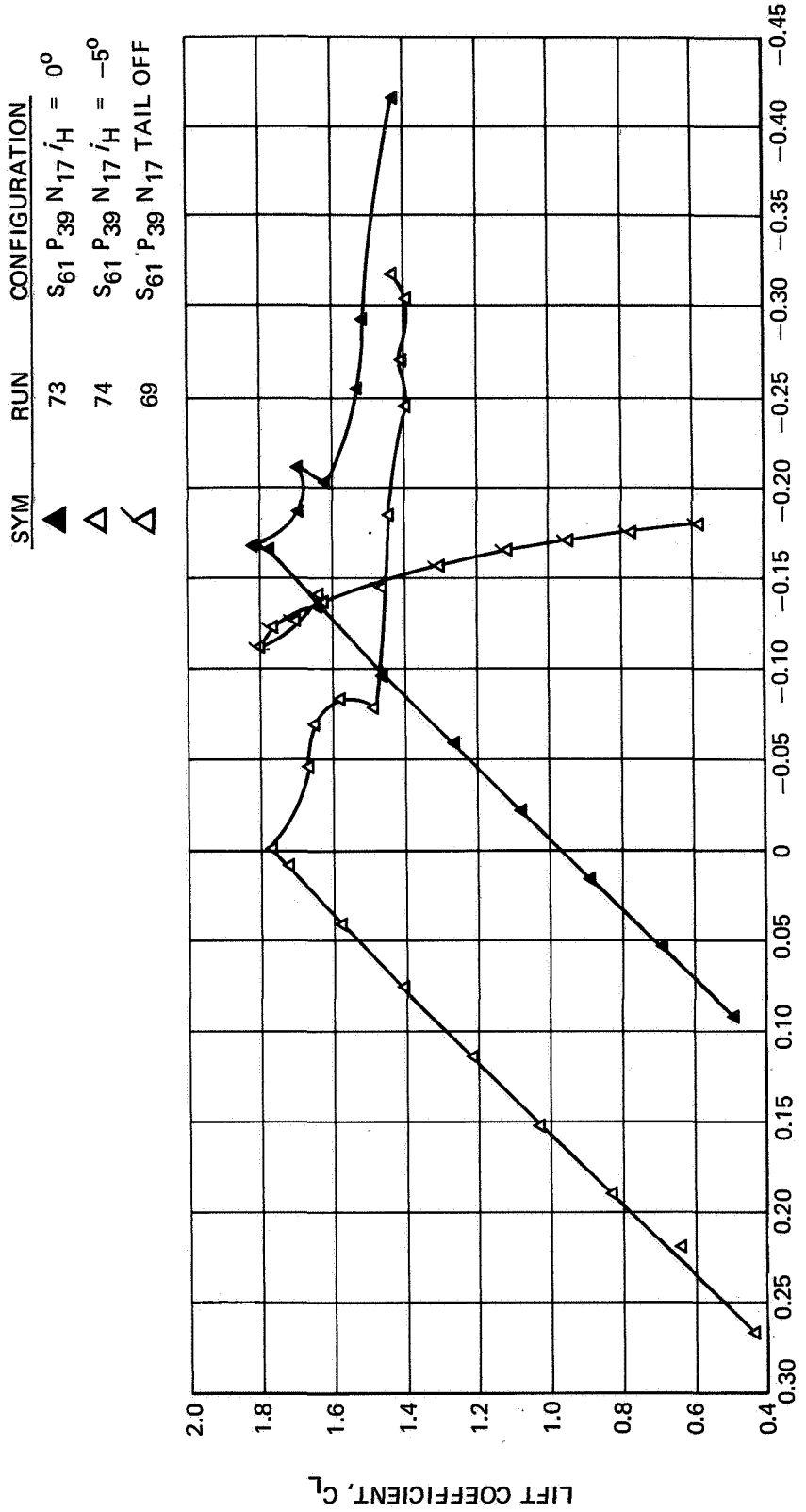

FIGURE III-38. EFFECT OF STABILIZER ANGLE ON PITCHING MOMENT COEFFICIENT, QUIET ENGINE FORWARD – $\delta_f = 25^o$

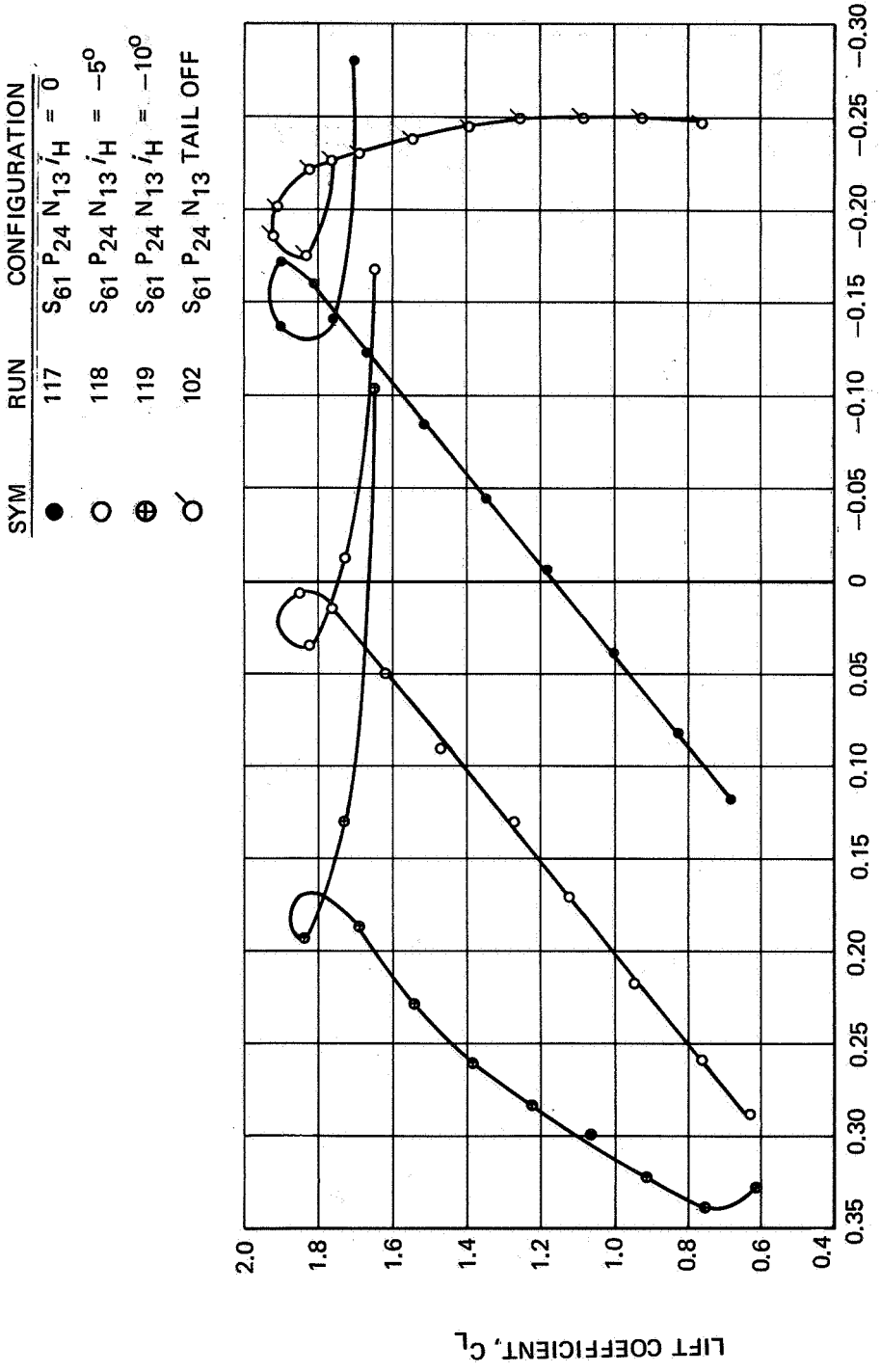

FIGURE III-39. EFFECT OF STABILIZER ANGLE ON PITCHING MOMENT COEFFICIENT, BASIC DC-8-61 – δ_f = 50°

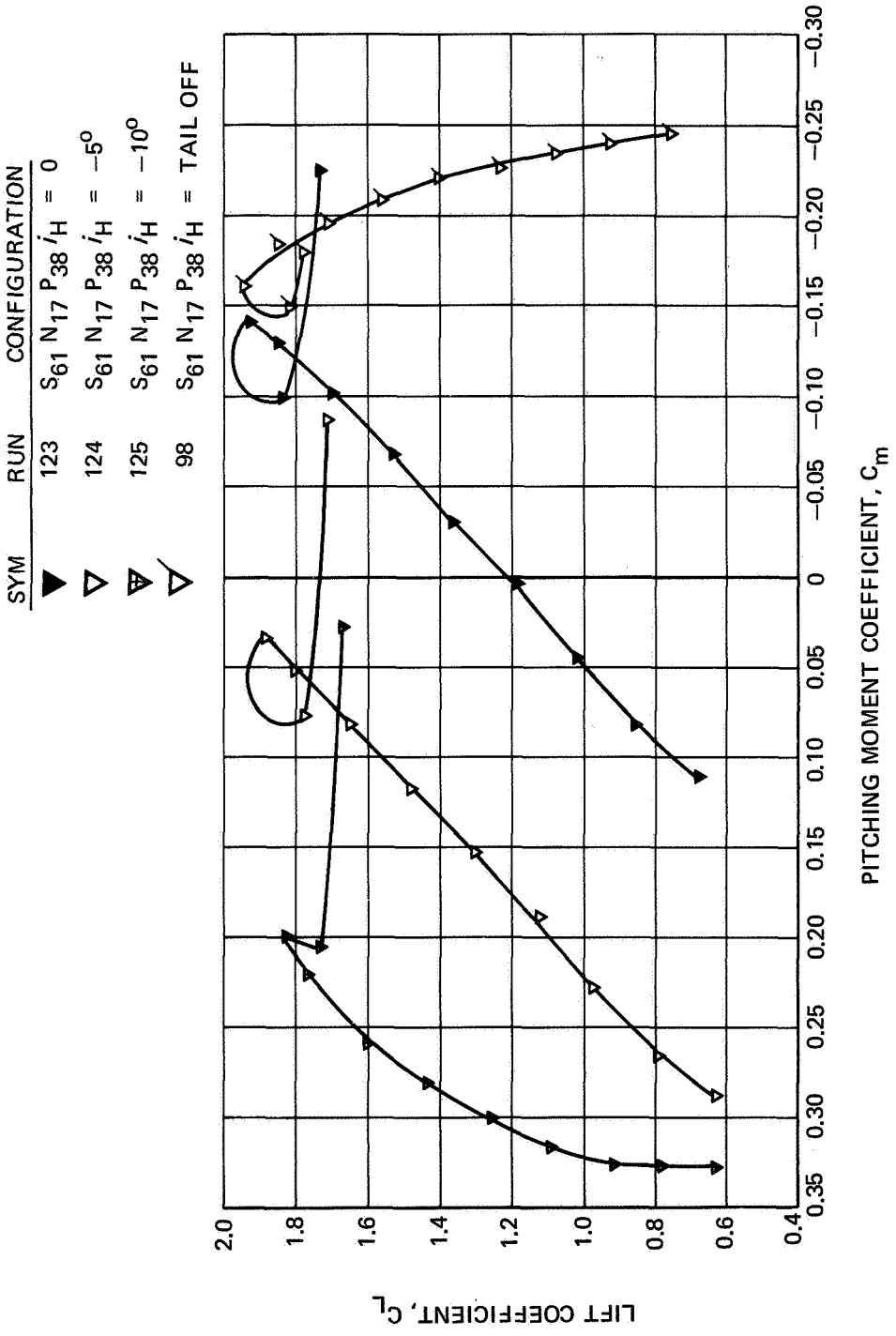

FIGURE III-40. EFFECT OF STABILIZER ANGLE ON PITCHING MOMENT COEFFICIENT, QUIET ENGINE AFT – $\delta_f = 50^o$

NASA AMES TEST 12-361

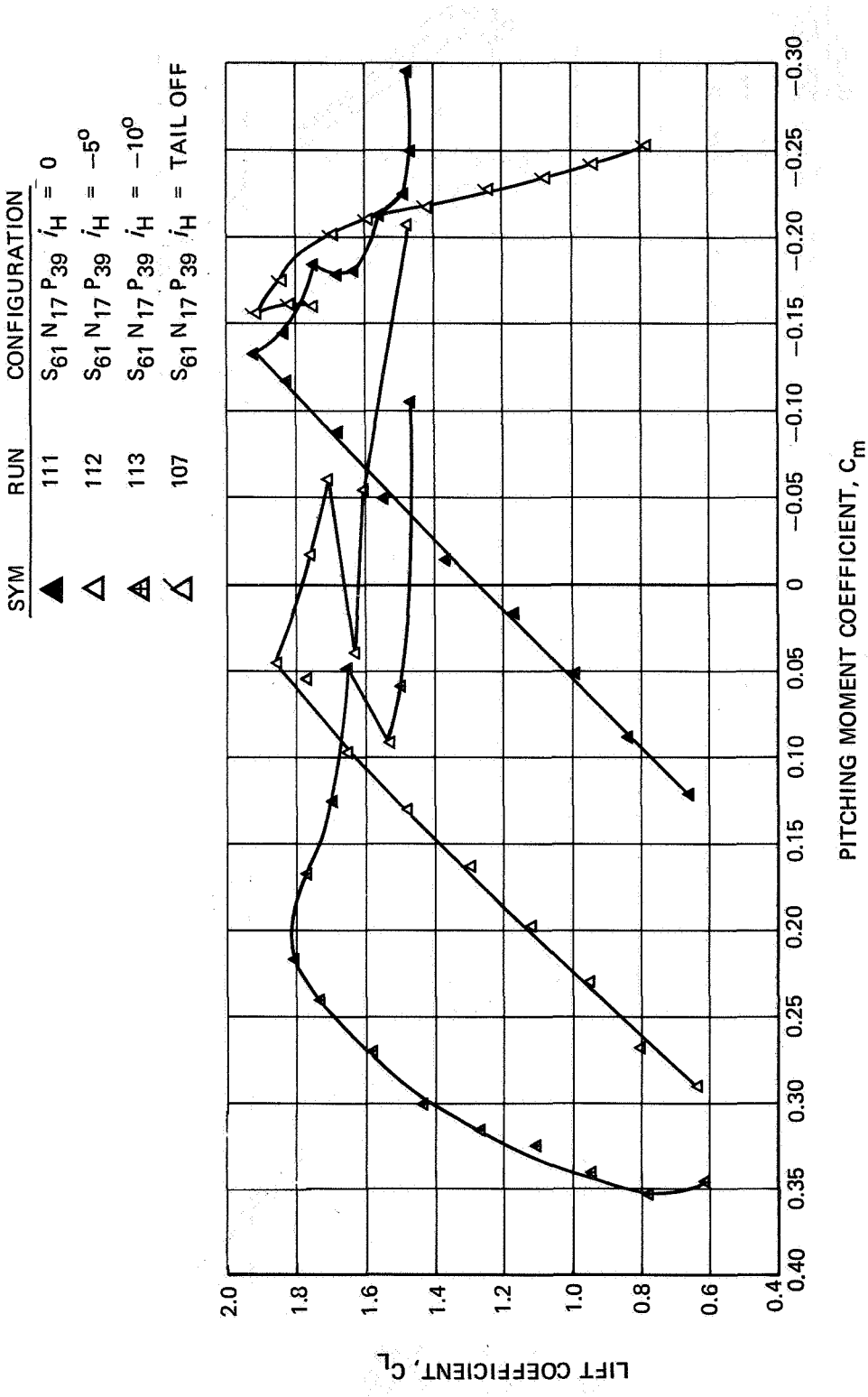

FIGURE III-41. EFFECT OF STABILIZER ANGLE ON PITCHING MOMENT COEFFICIENT, QUIET ENGINE FORWARD – $\delta_f = 50^o$

NASA AMES TEST 11-353

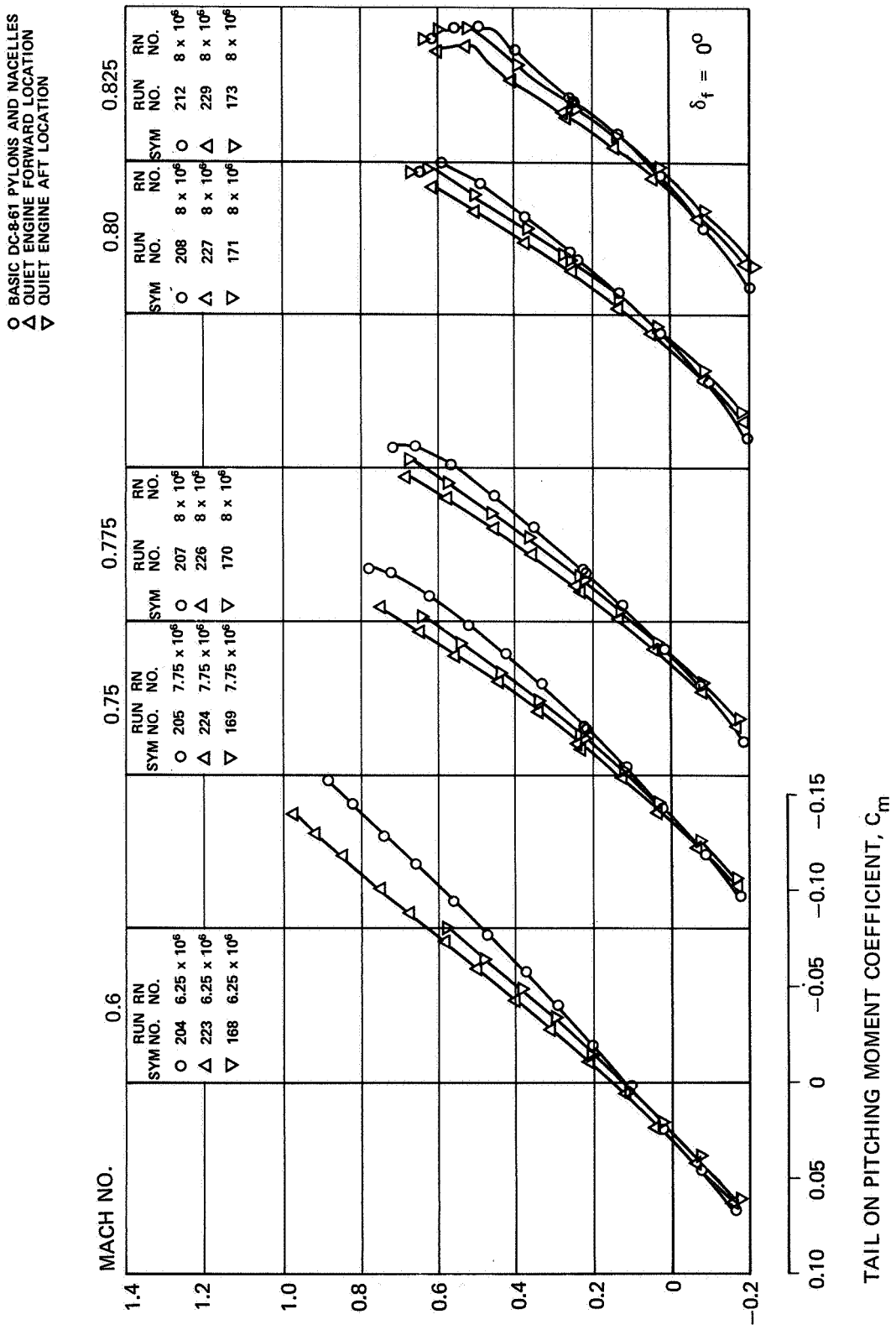

FIGURE III-42. EFFECT OF NACELLES AND PYLONS ON TAIL-ON PITCHING MOMENT COEFFICIENT – M_o = 0.6 THROUGH 0.825

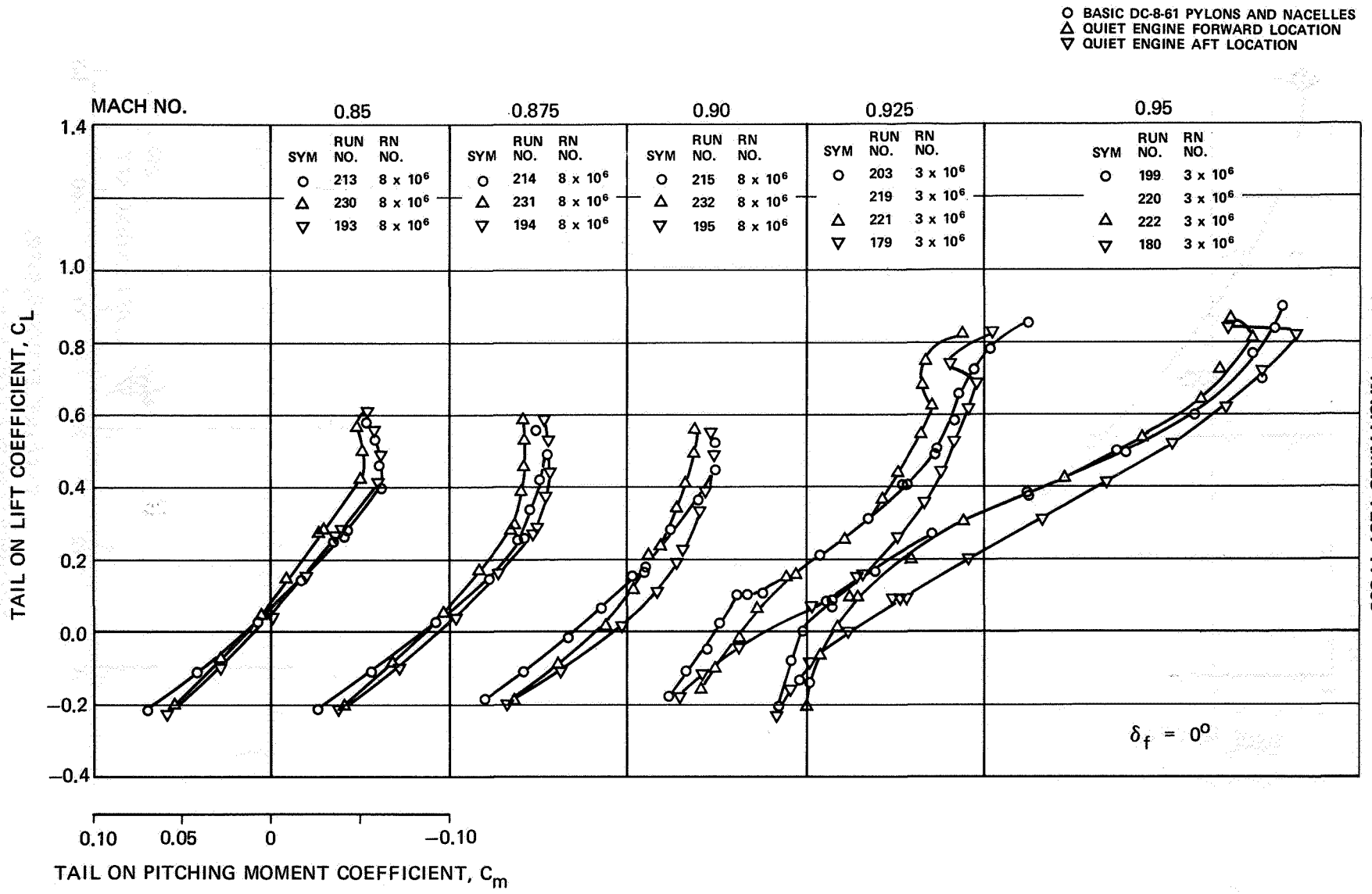

NAS3-11151
TASK III

NASA AMES TEST 11-353

III-55

FIGURE III-43. EFFECT OF NACELLES AND PYLONS ON TAIL-ON PITCHING MOMENT COEFFICIENT – M_o = 0.85 THROUGH 0.95

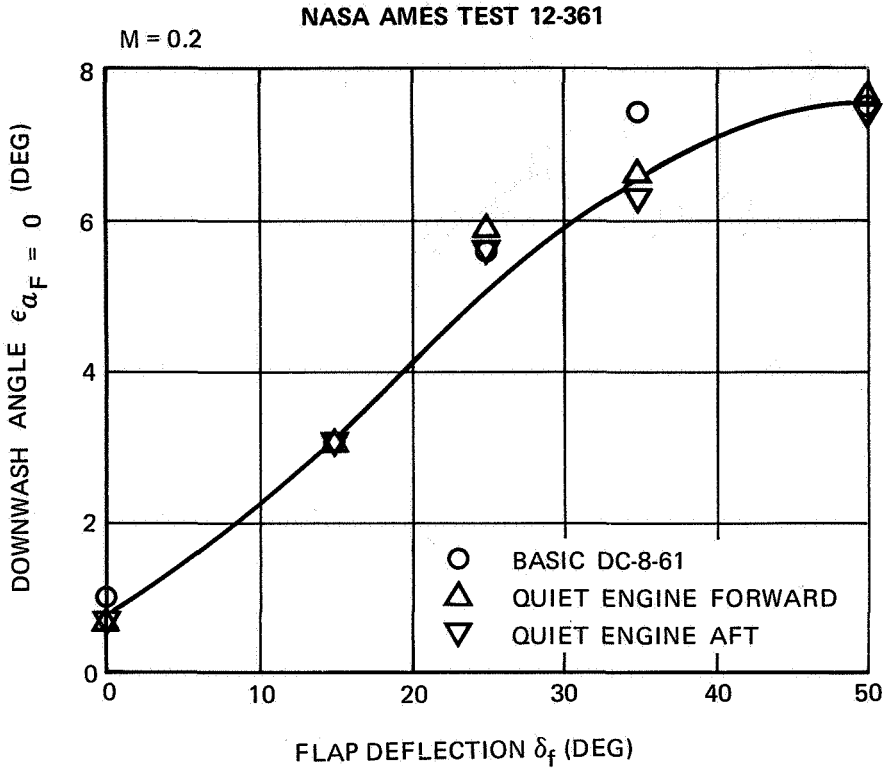

FIGURE III-44. ESTIMATED DOWNWASH ANGLE AT ZERO ANGLE OF ATTACK

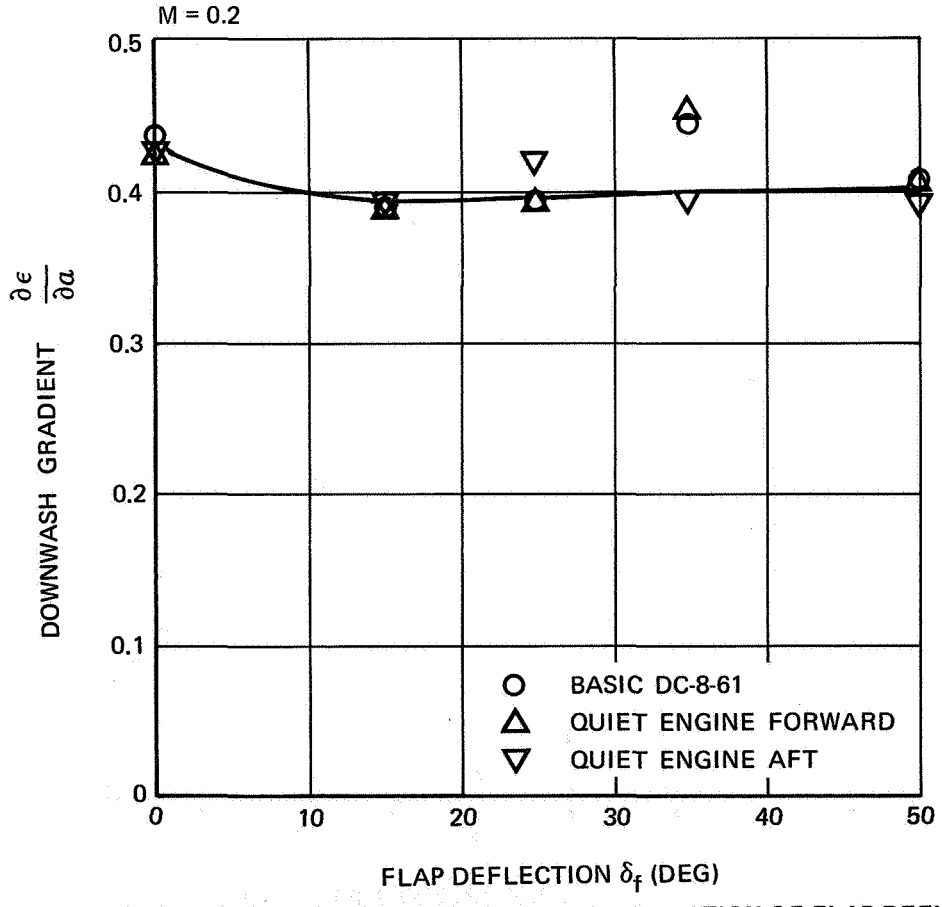

FIGURE III-45. ESTIMATED DOWNWASH GRADIENT AS A FUNCTION OF FLAP DEFLECTION

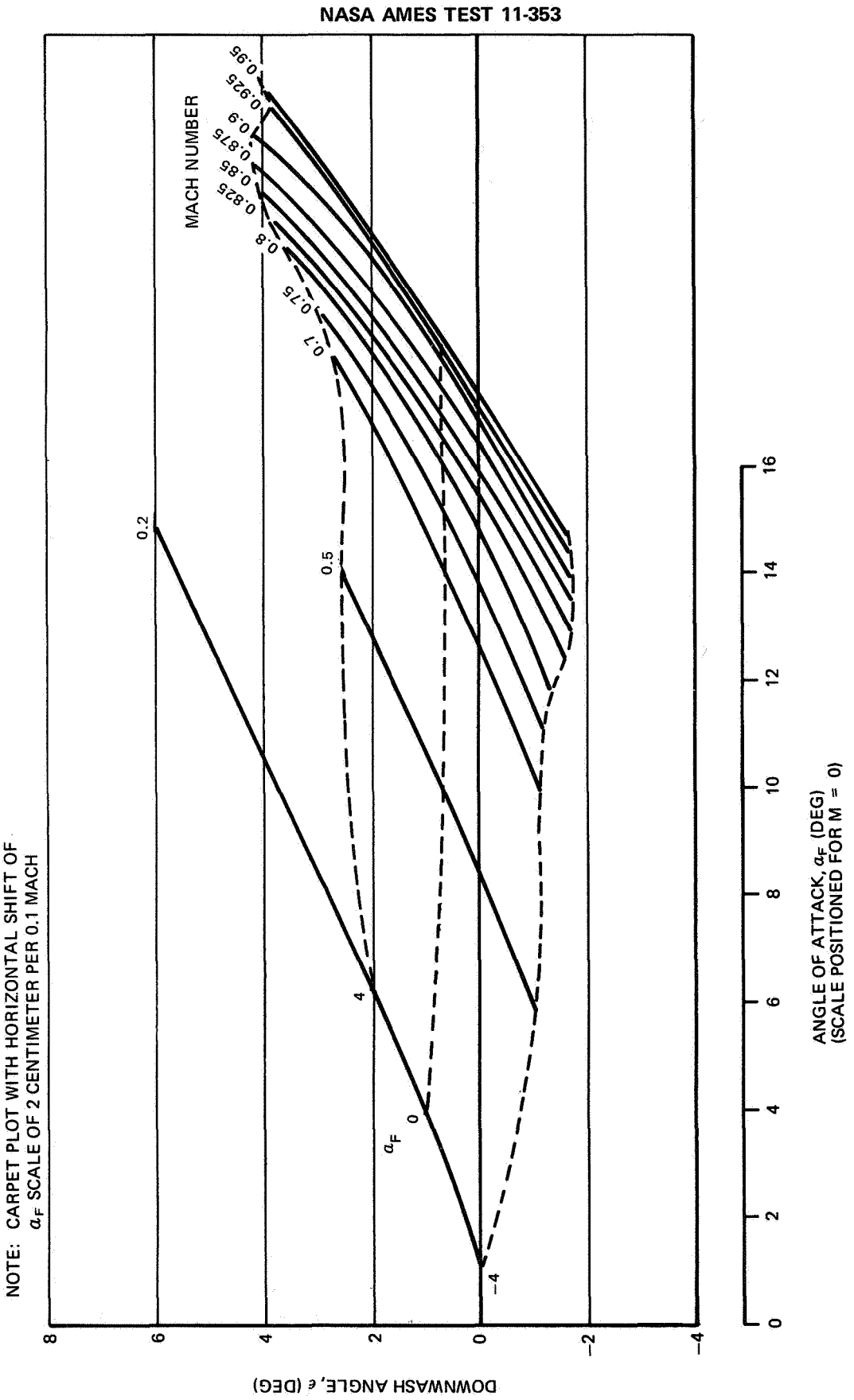

FIGURE III-46. ESTIMATED DOWNWASH AS A FUNCTION OF ANGLE OF ATTACK AND MACH NUMBER – BASIC DC-8-61

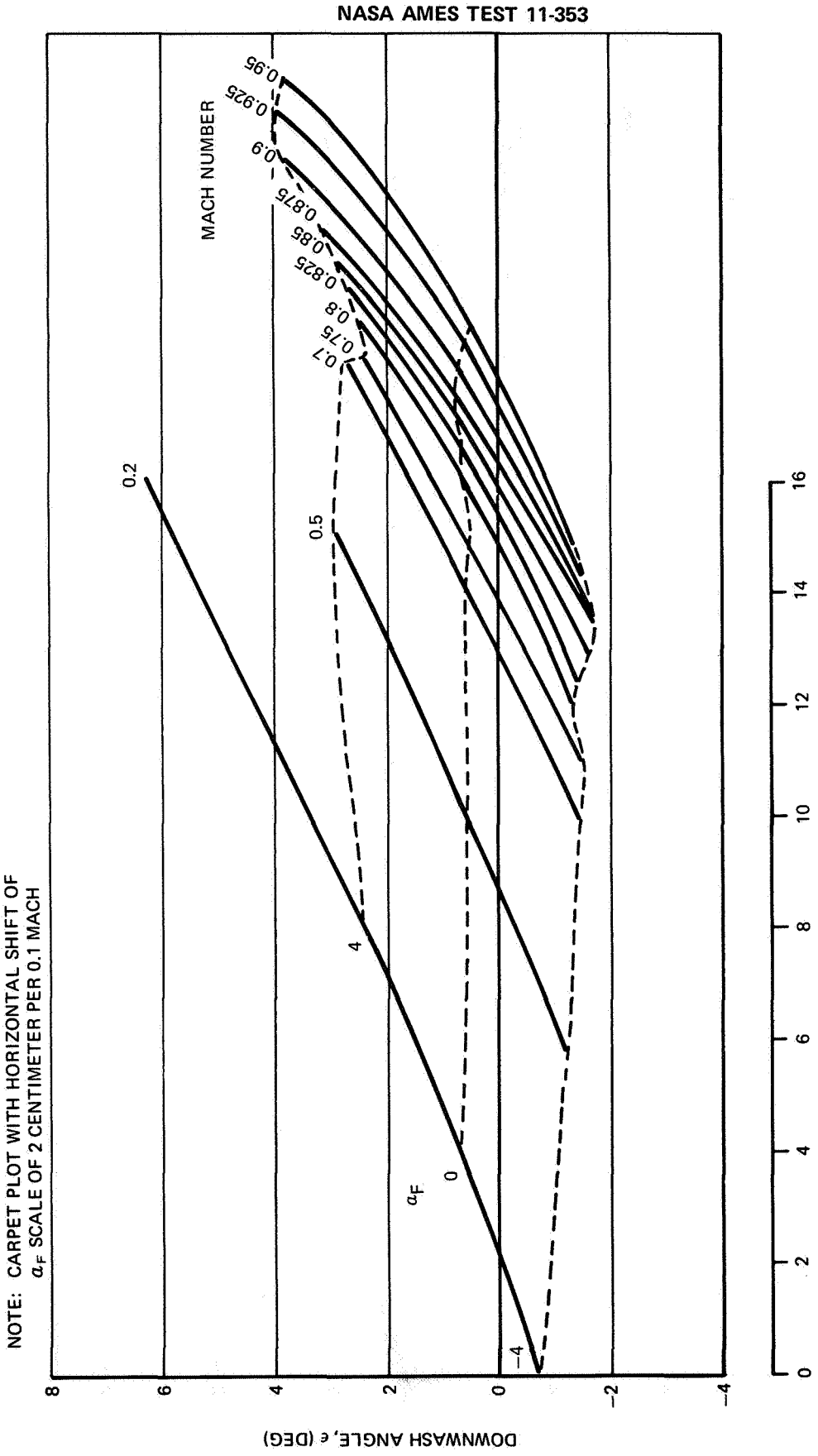

FIGURE III-47. ESTIMATED DOWNWASH AS A FUNCTION OF ANGLE OF ATTACK AND MACH NUMBER – QUIET ENGINE FORWARD LOCATION

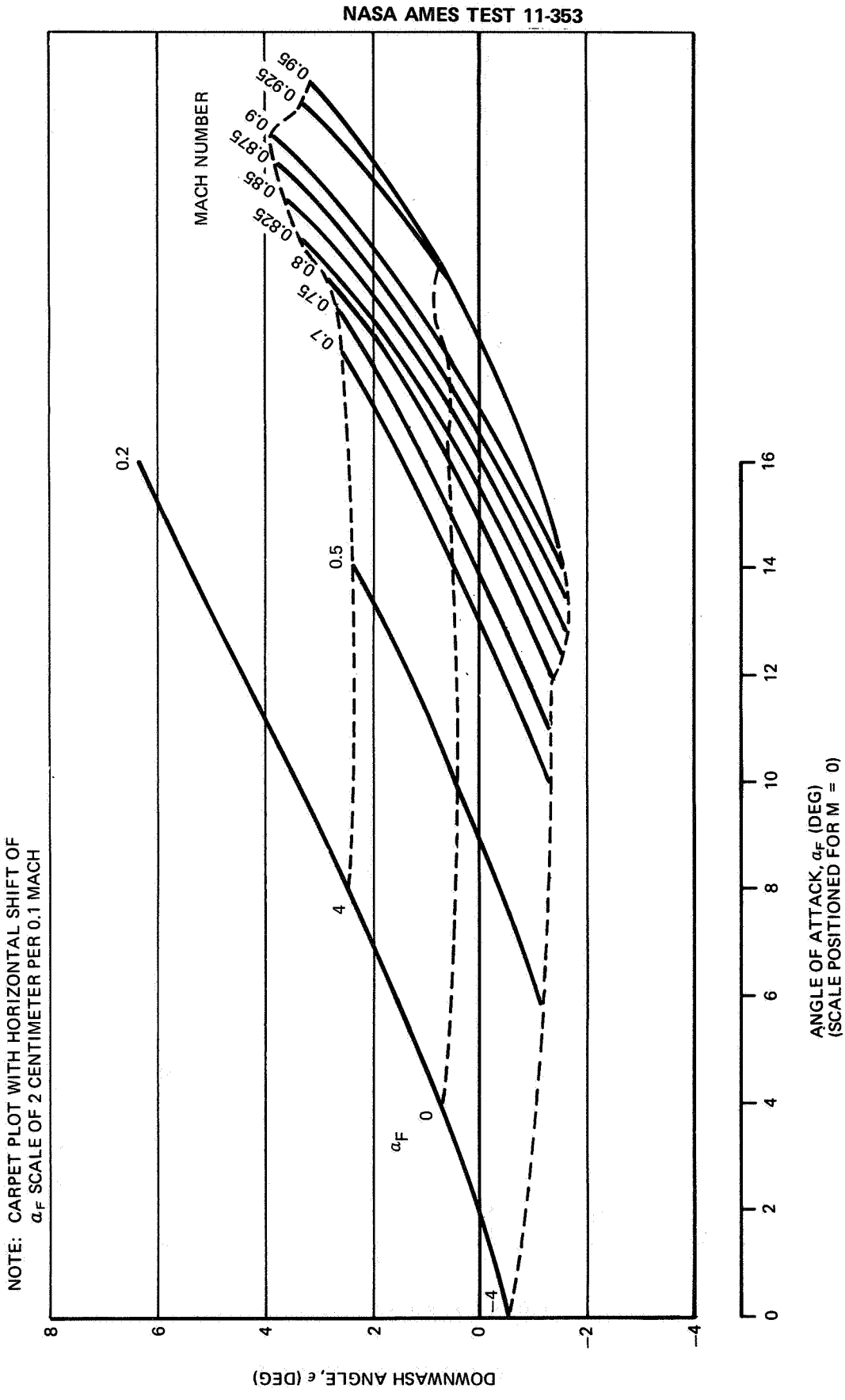

FIGURE III-48. ESTIMATED DOWNWASH AS A FUNCTION OF ANGLE OF ATTACK AND MACH NUMBER – QUIET ENGINE AFT LOCATION

NASA AMES TEST 12-361

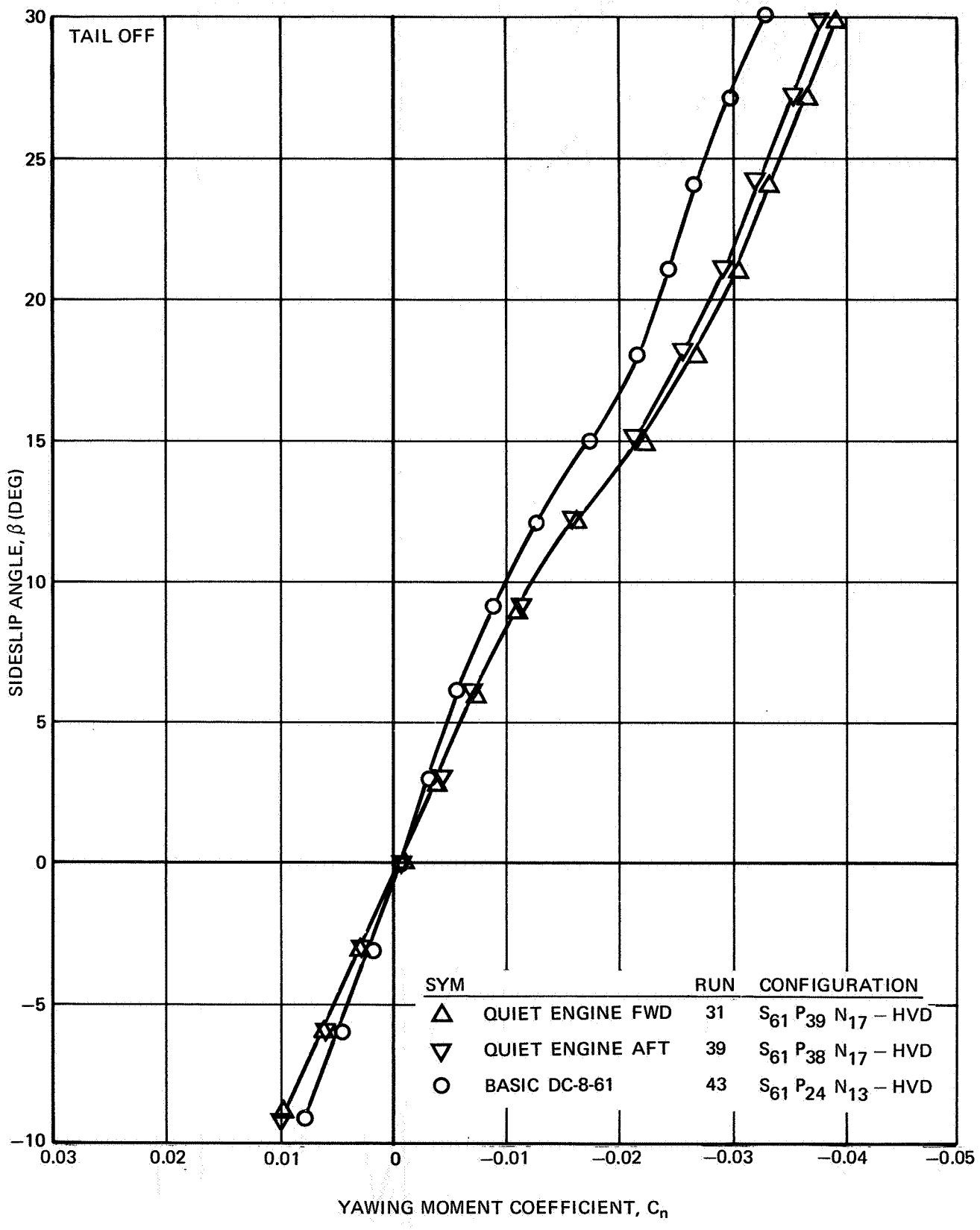

FIGURE III-49. EFFECT OF PYLONS AND NACELLES ON YAWING MOMENT – $\delta_f = 0^o$, $\alpha_F = 0^o$

NASA AMES TEST 12-361

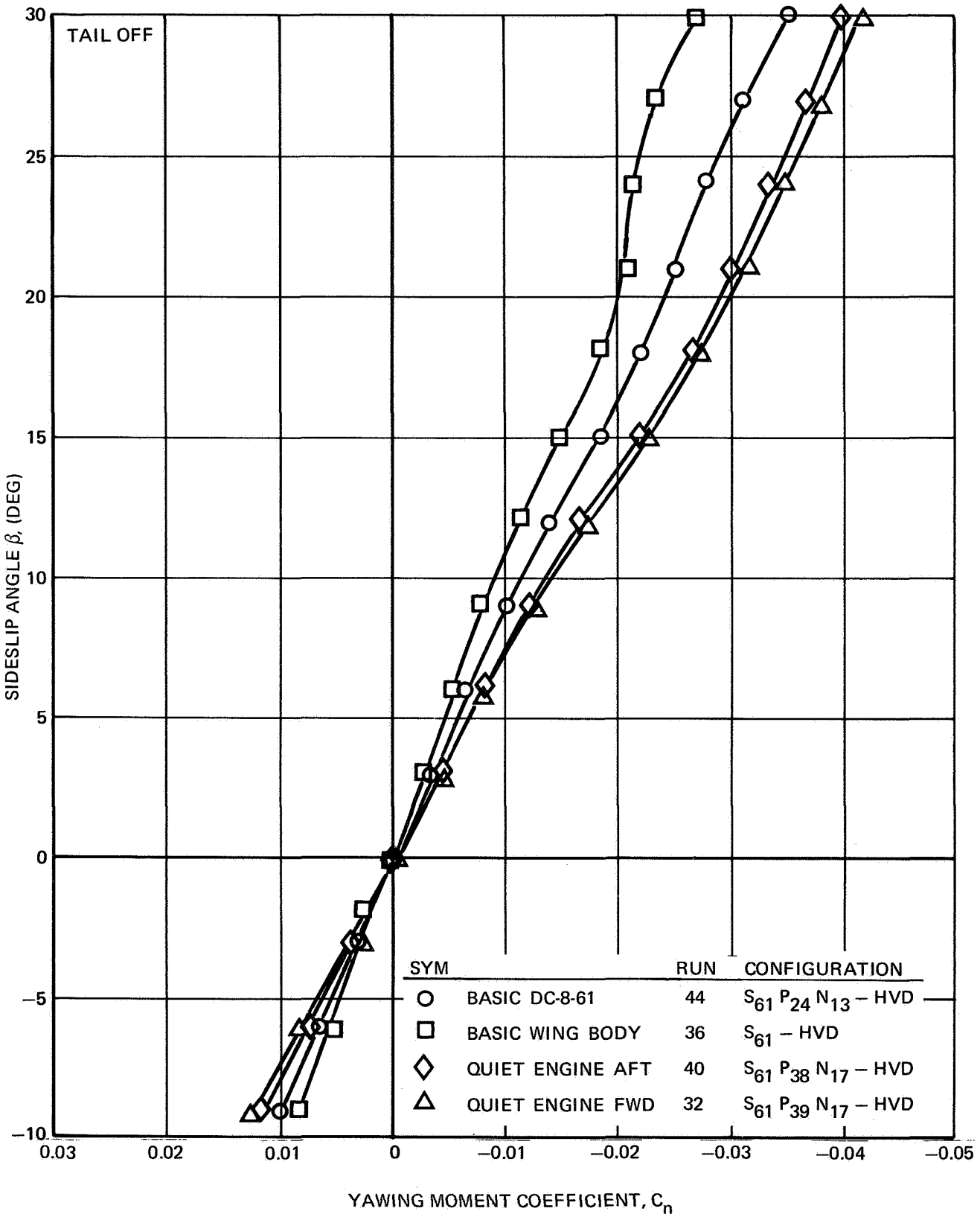

FIGURE III-50. EFFECT OF PYLONS AND NACELLES ON YAWING MOMENT – $\delta_f = 0^o$, $a_F = 4^o$

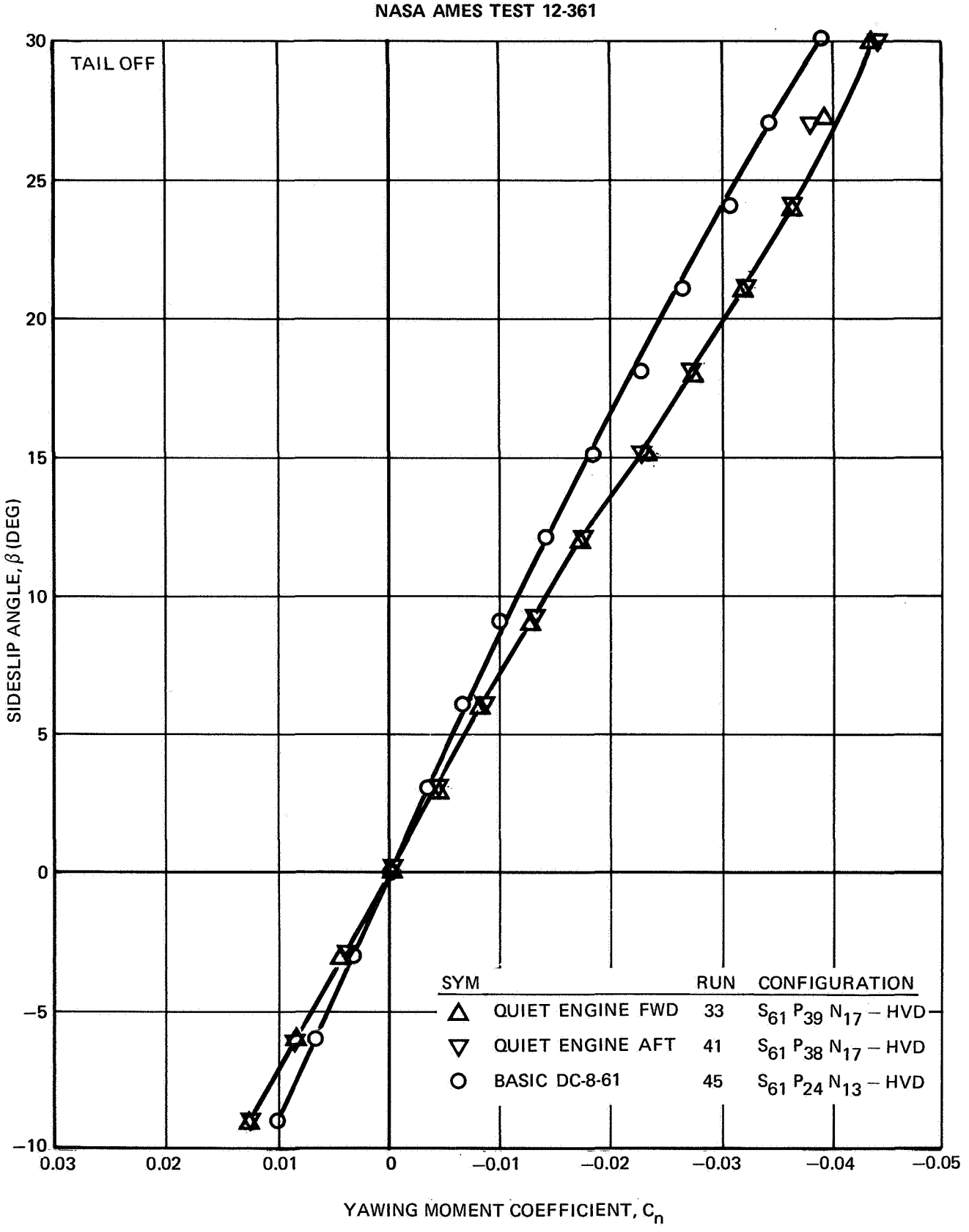

FIGURE III-51. EFFECT OF PYLONS AND NACELLES ON YAWING MOMENT – $\delta_f = 0^o$, $\alpha_F = 8^o$

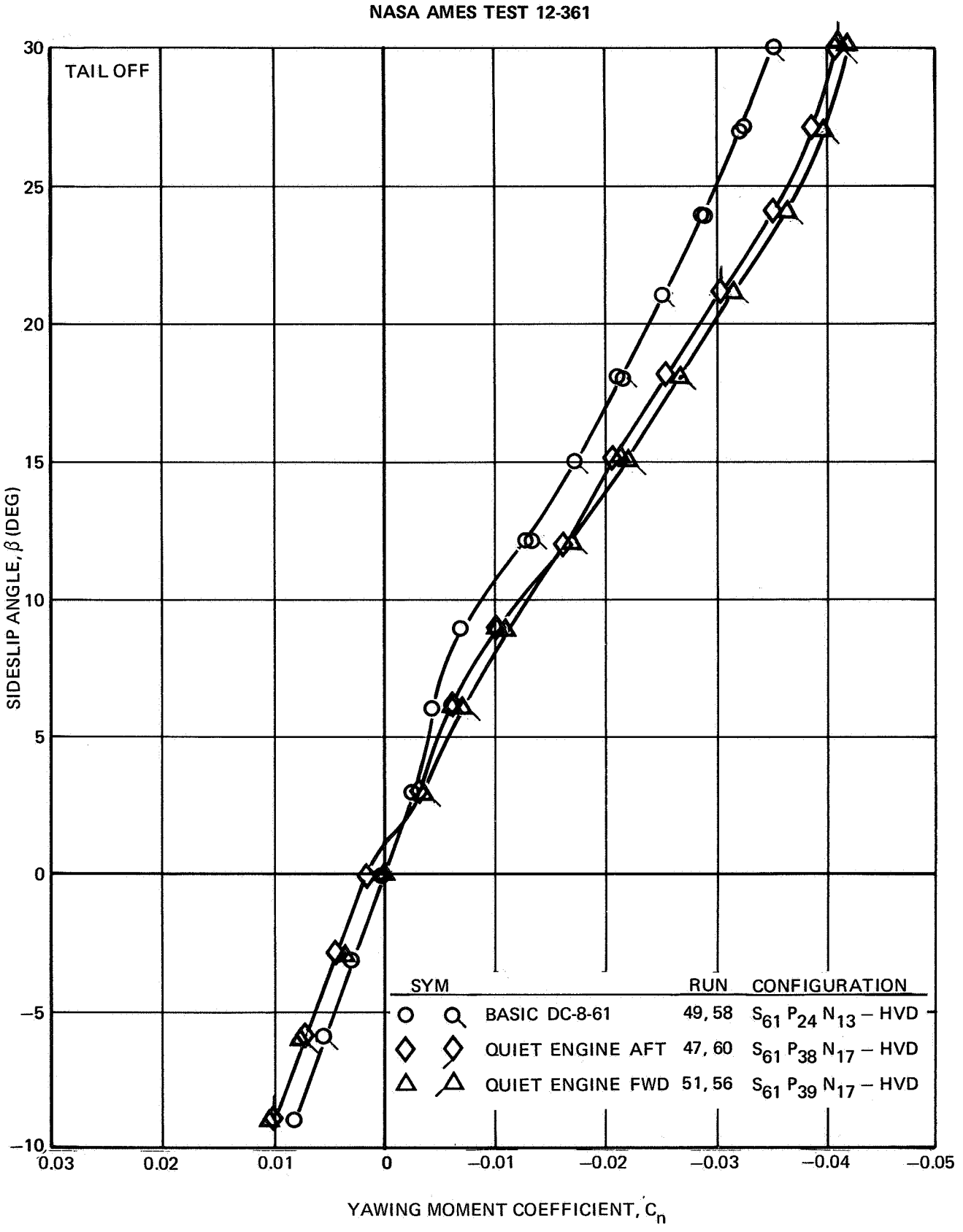

FIGURE III-52. EFFECT OF PYLONS AND NACELLES ON YAWING MOMENT $\delta_f = 15^o$, $\alpha_F = 0^o$

NASA AMES TEST 12-361

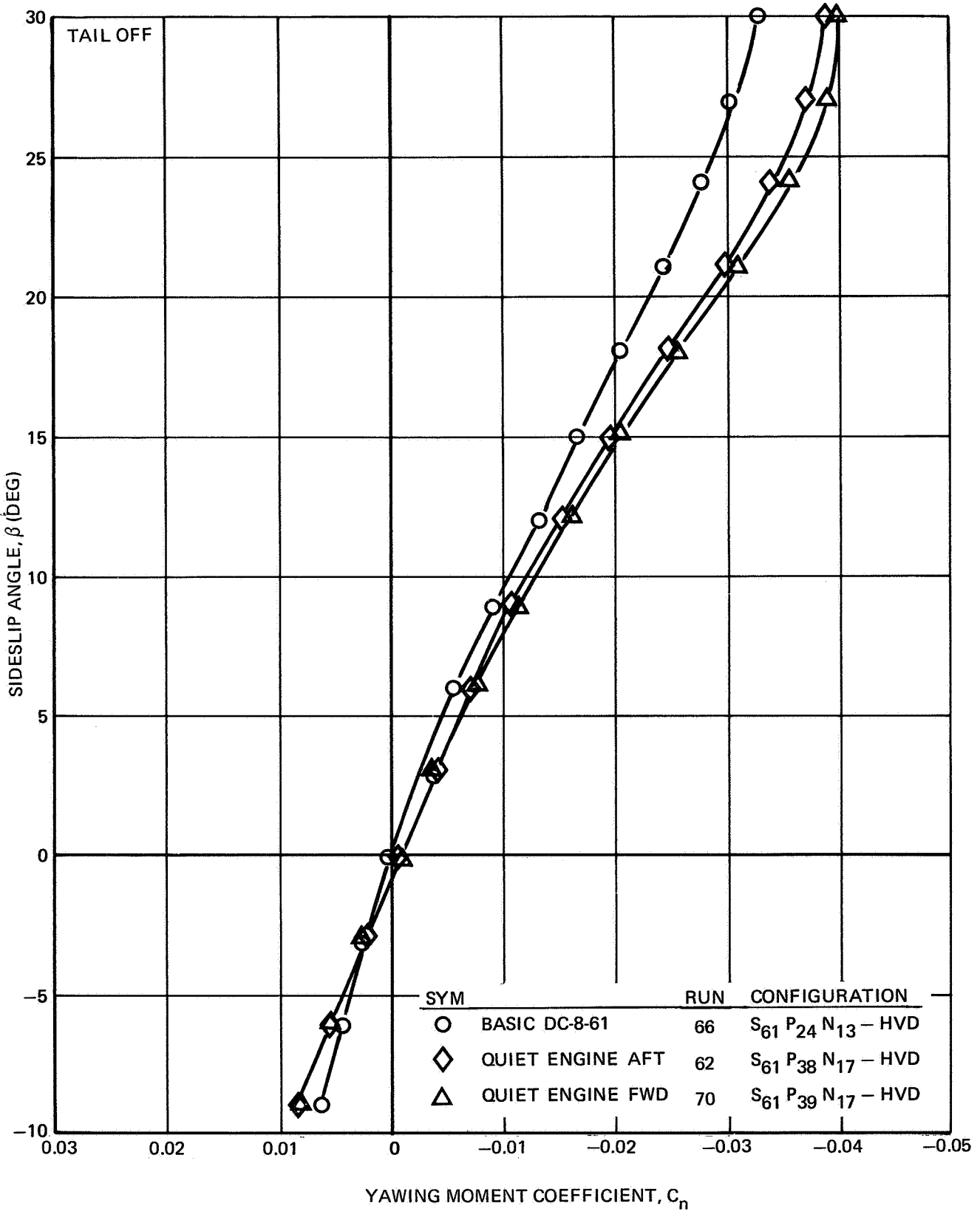

FIGURE III-53. EFFECT OF PYLONS AND NACELLES ON YAWING MOMENT – $\delta_f = 25^o$, $\alpha_F = 0^o$

NASA AMES TEST 12-361

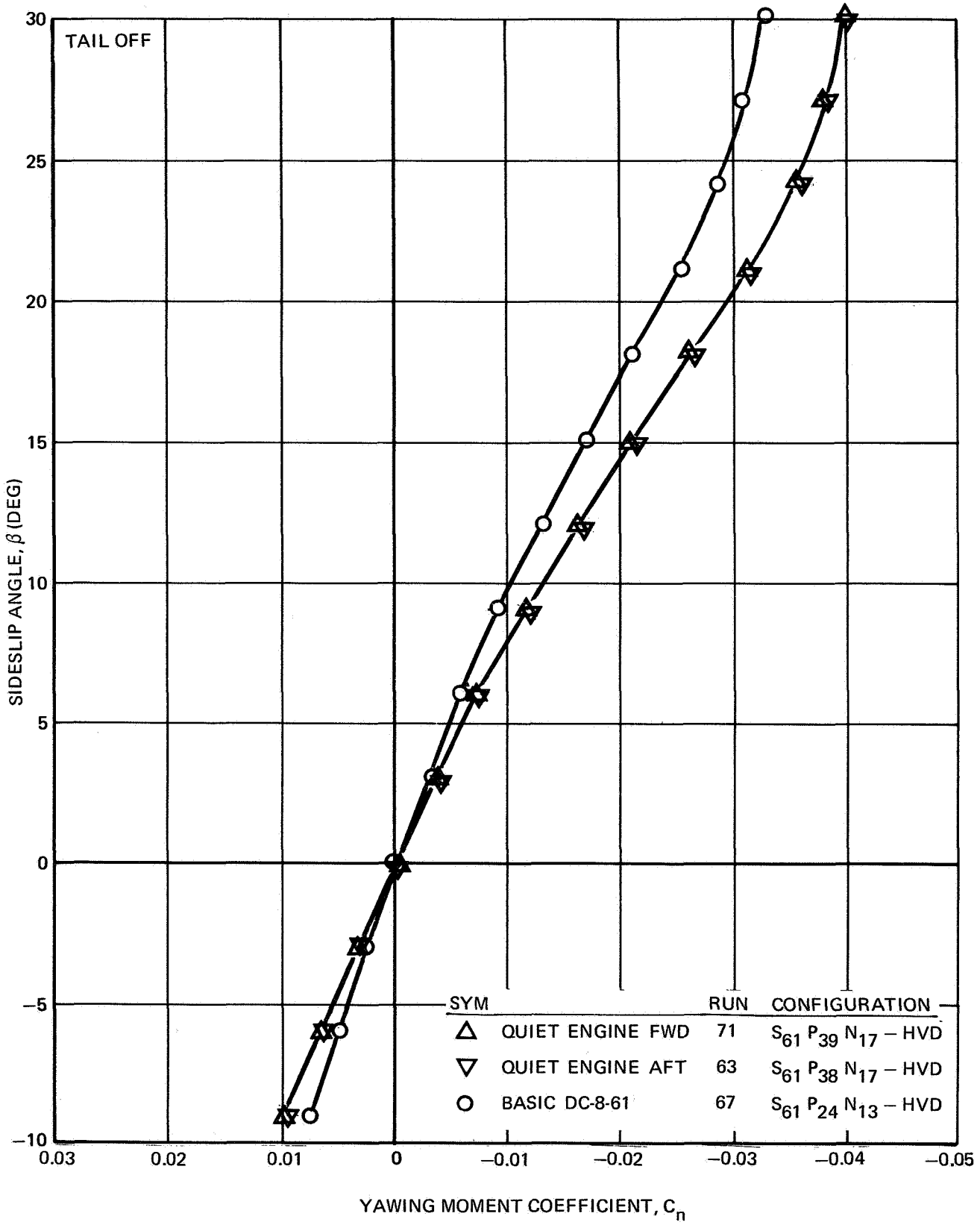

FIGURE III-54. EFFECT OF PYLONS AND NACELLES ON YAWING MOMENT – $\delta_f = 25^o$, $a_F = 4^o$

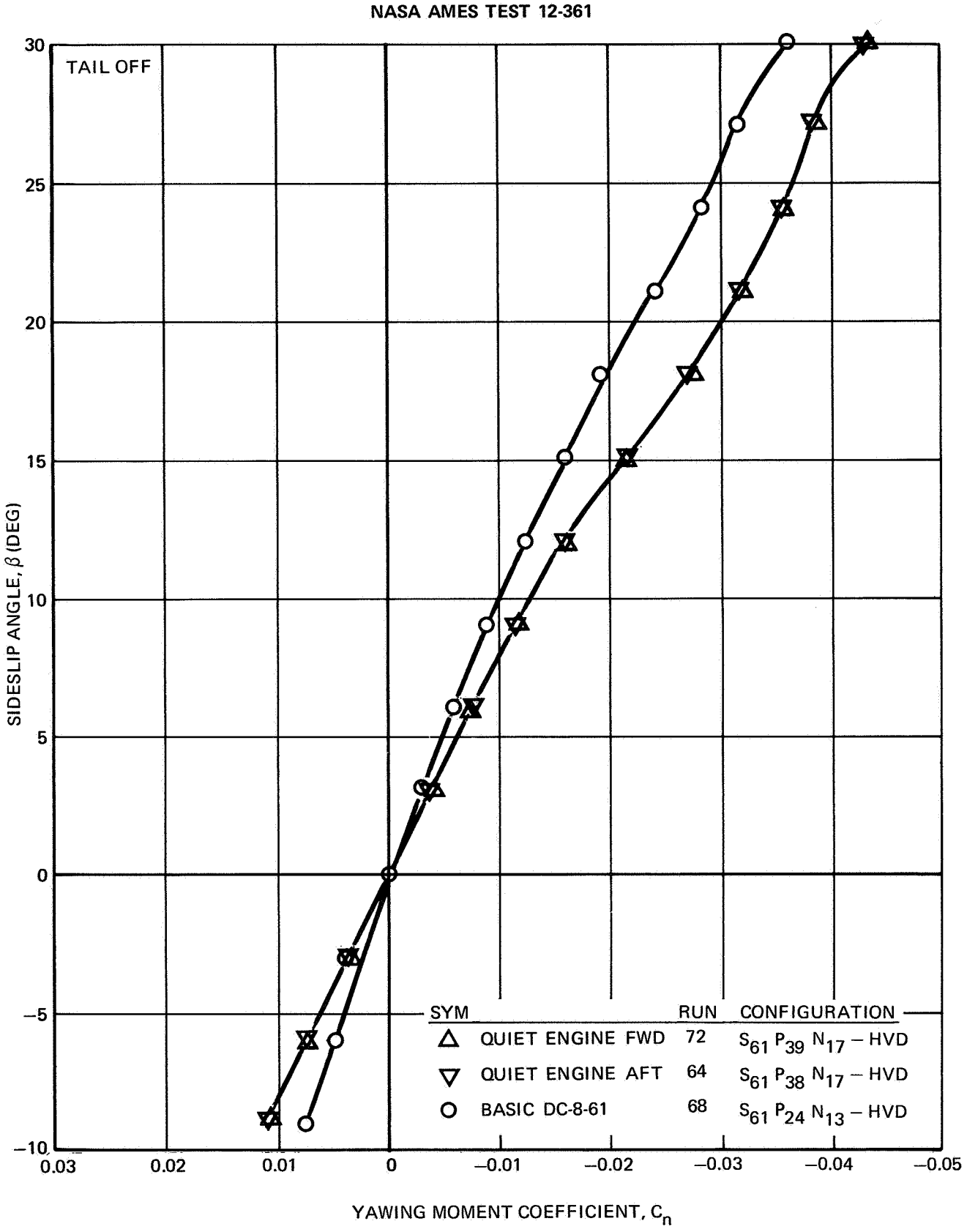

FIGURE III-55. EFFECT OF PYLONS AND NACELLES ON YAWING MOMENT – $\delta_f = 25^o$, $\alpha_F = 8^o$

NASA AMES TEST 12-361

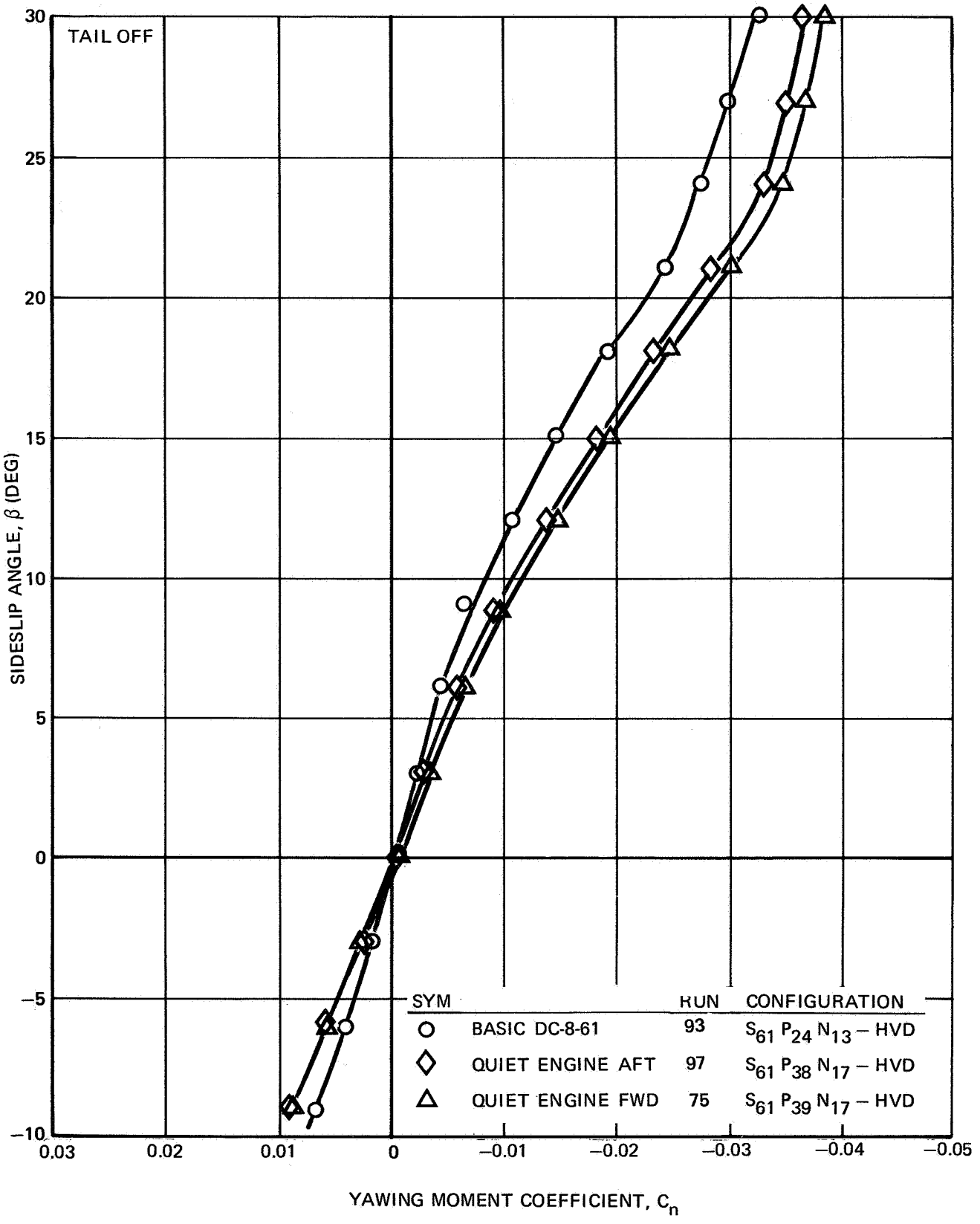

FIGURE III-56. EFFECT OF PYLONS AND NACELLES ON YAWING MOMENT – $\delta_f = 35^o$, $\alpha_F = 0^o$

NASA AMES TEST 12-361

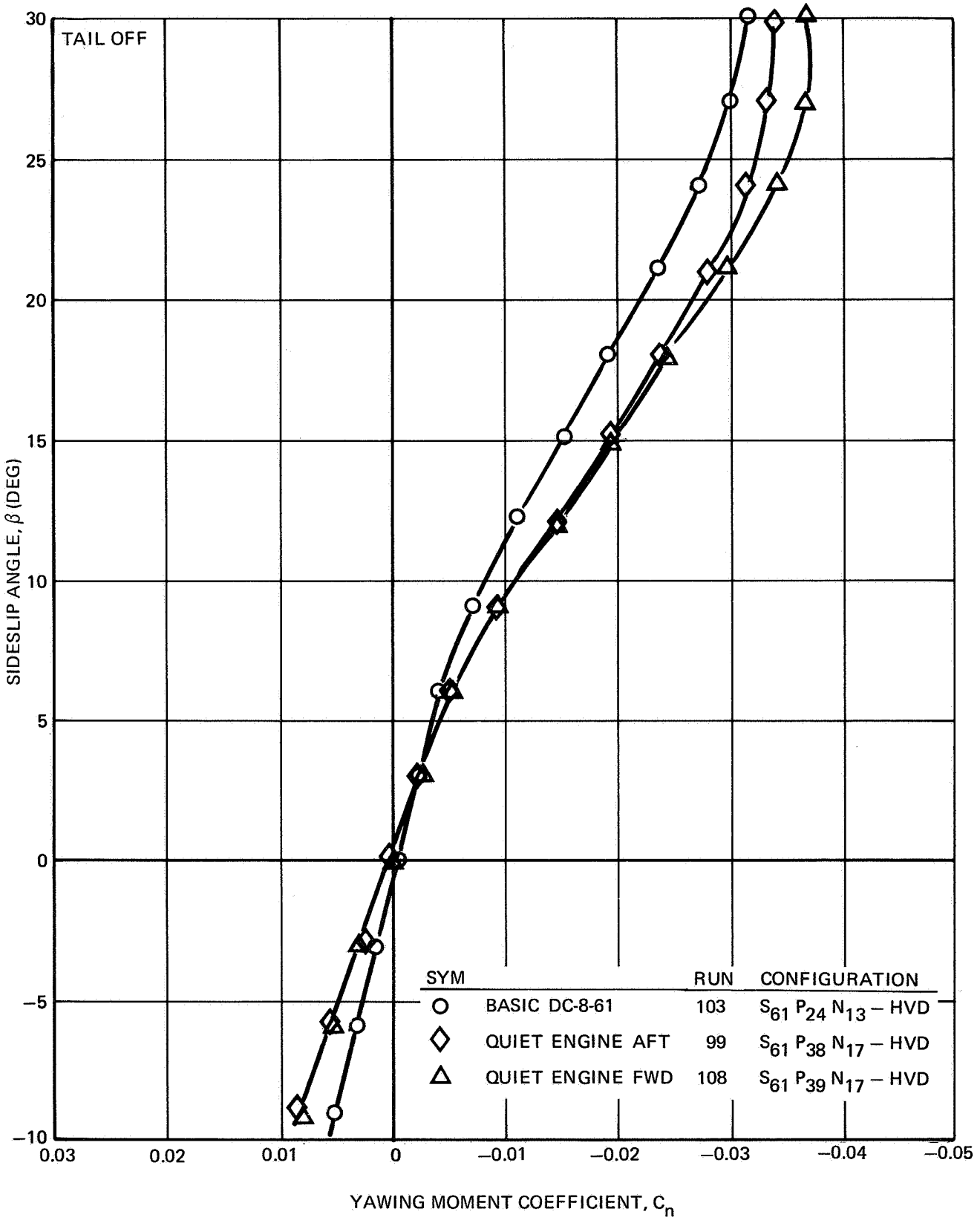

FIGURE III-57. EFFECT OF PYLONS AND NACELLES ON YAWING MOMENT – $\delta_f = 50^o$, $\alpha_F = 0^o$

NASA AMES TEST 12-361

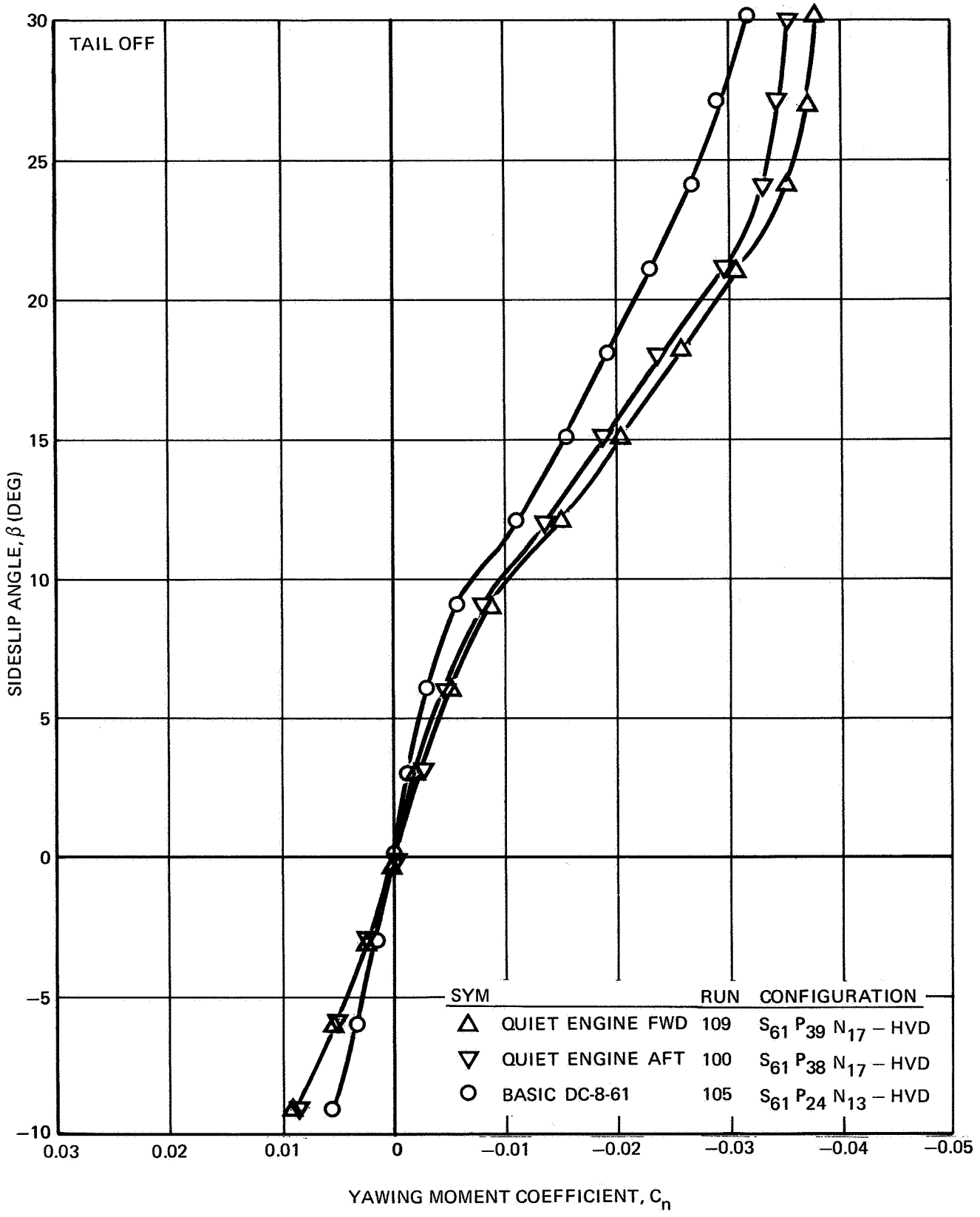

FIGURE III-58. EFFECT OF PYLONS AND NACELLES ON YAWING MOMENT – $\delta_f = 50^o$, $\alpha_F = 4^o$

NASA AMES TEST 12-361

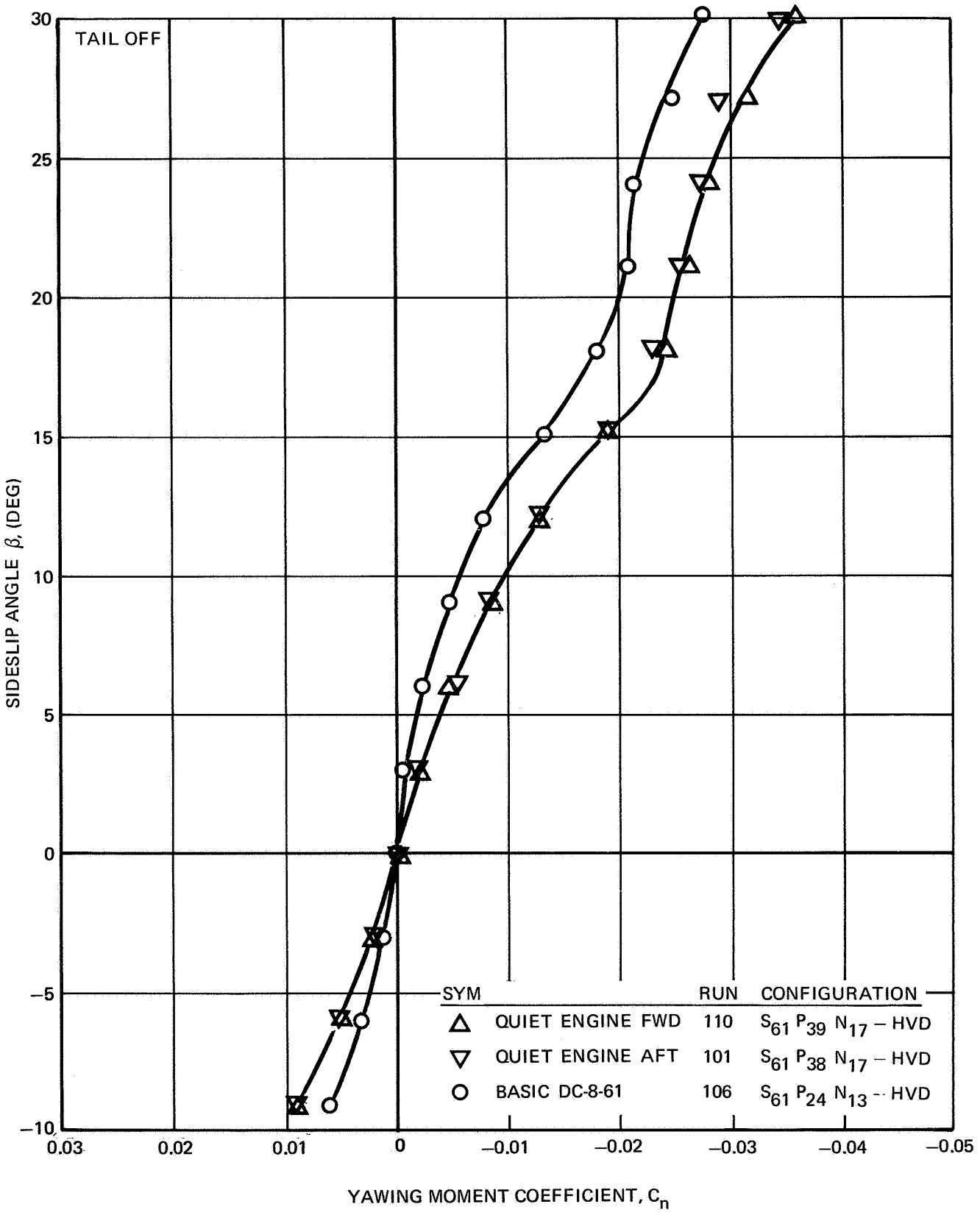

FIGURE III-59. EFFECT OF PYLONS AND NACELLES ON YAWING MOMENT – $\delta_f = 50^o$, $a_F = 8^o$

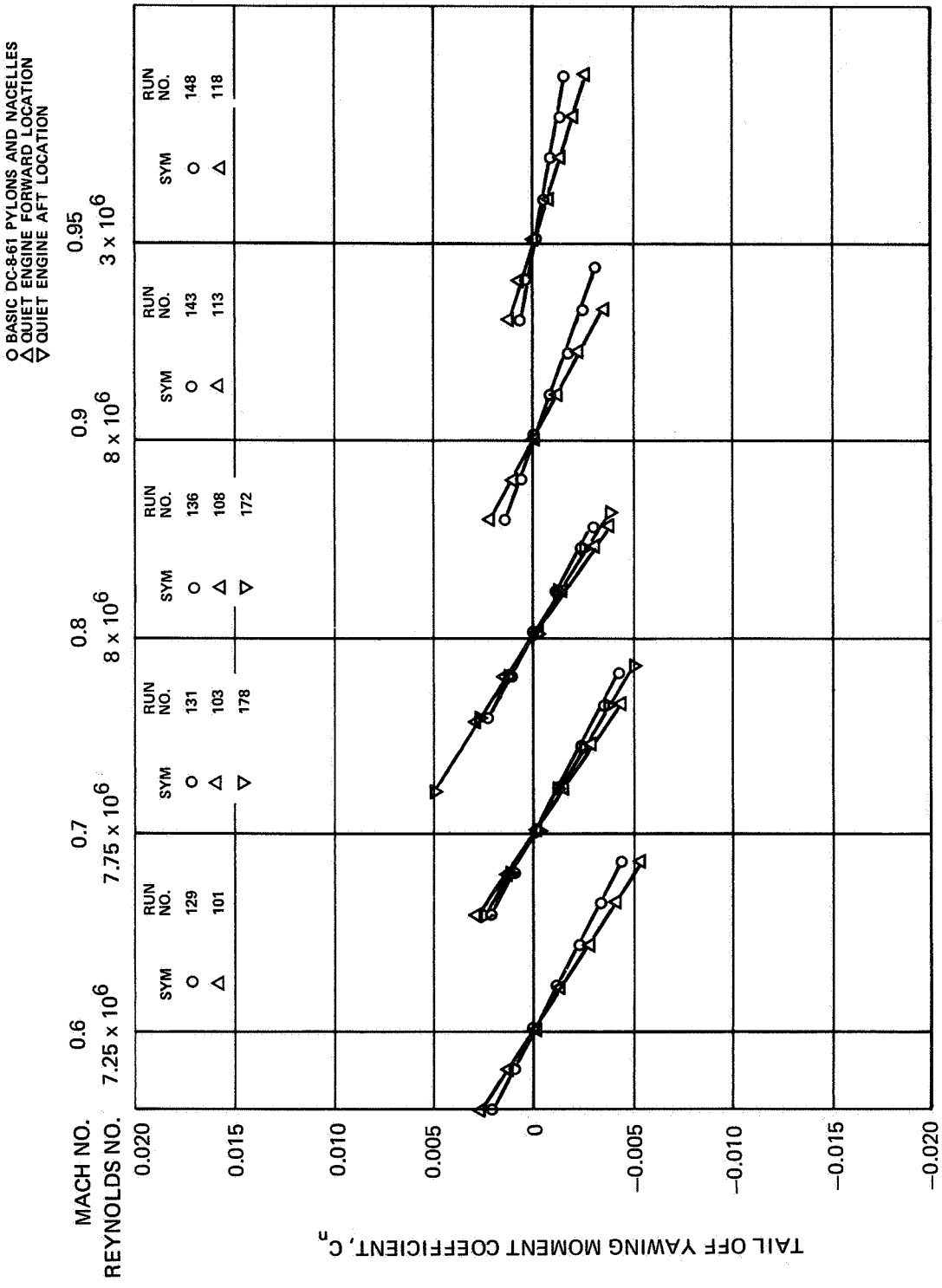

FIGURE III-60. EFFECT OF NACELLES AND PYLONS ON TAIL-OFF YAWING MOMENT DUE TO SIDESLIP – $\delta_f = 0^o$, $\alpha_F = 0^o$

The tail-on data, presented in Figures III-61 through III-72, show the same reduction in stability, $\Delta C_{n_c} = 0.0002$ to -0.0003, as the tail-off data, thus indicating an undiminished tail contribution. This reduction in complete aircraft stability amounts to approximately 10 percent of the basic level throughout the Mach number range.

Side-force coefficients due to sideslip angle are presented in Figures III-73 through III-96 for both low Mach numbers and high Mach numbers. These data show an increase of 0.0015 in side force due to the larger quiet-engine nacelles at low Mach numbers and 0.0005 at high Mach numbers. The value of 0.0005 is believed to be representative of the true effect.

Data on rolling-moment coefficient due to sideslip, presented in Figures III-97 through III-120, generally show a negligible effect on the quiet-engine nacelles. However, the reduction in roll due to sideslip at the higher Mach numbers appears to have been delayed or lessened somewhat.

ANALYSIS OF DATA

The effects of engine thrust and mass flow are generally considered in DC-8 stability and control calculations. The effects of engine-inlet normal force on pitching and yawing moments are particularly important in obtaining accurate calculated results. In order to accomplish the calculation in the most efficient way, the effects of the model-nacelle mass flow on the characteristics are removed by means of the following equations:

$$\Delta C_{m_{NF}} = \frac{2Wa\ Ve\ (a_F + i_t)\ [(\partial\beta/\partial a)_{INB}\ (\ell_N/C_w)_{INB} + (\partial\beta/\partial a)_{OUTB}\ (\ell_N/C_w)_{OUTB}]}{57.3gq\ S_w\ \sqrt{\sigma}}$$

$$\Delta C_{n_{NF}} = \frac{2Wa\ Ve\beta\ \ (\ell_N/bw)_{INB} + (\ell_N/bw)_{OUTB}]}{57.3gq\ S_w\ \sqrt{\sigma}}$$

$$\Delta C_{L_{NF}} = \frac{2Wa\ Ve(a_F + i_t)\ [(\partial\beta/\partial a)_{INB} + (\partial\beta/\partial a)_{OUTB}]}{57.3gq\ S_w\ \sqrt{\sigma}}$$

$$\Delta C_{Y_{NF}} = \frac{4Wa\ Ve\beta}{57.3gq\ S_w\ \sqrt{\sigma}}$$

The same equations may be used to calculate the effects of engine mass flow on the actual airplane characteristics.

In the analyses of pitching-moment and yawing-moment data, the mass-flow effects have been taken into consideration. The results of the analyses are shown in Figures III-121 and III-122. Longitudinal stability with the quiet engines is reduced by an amount equivalent to a forward shift of the aerodynamic center (neutral point) as large as 8-percent mean aerodynamic chord.

Static directional stability with the quiet engines is reduced by as much as 10 percent.

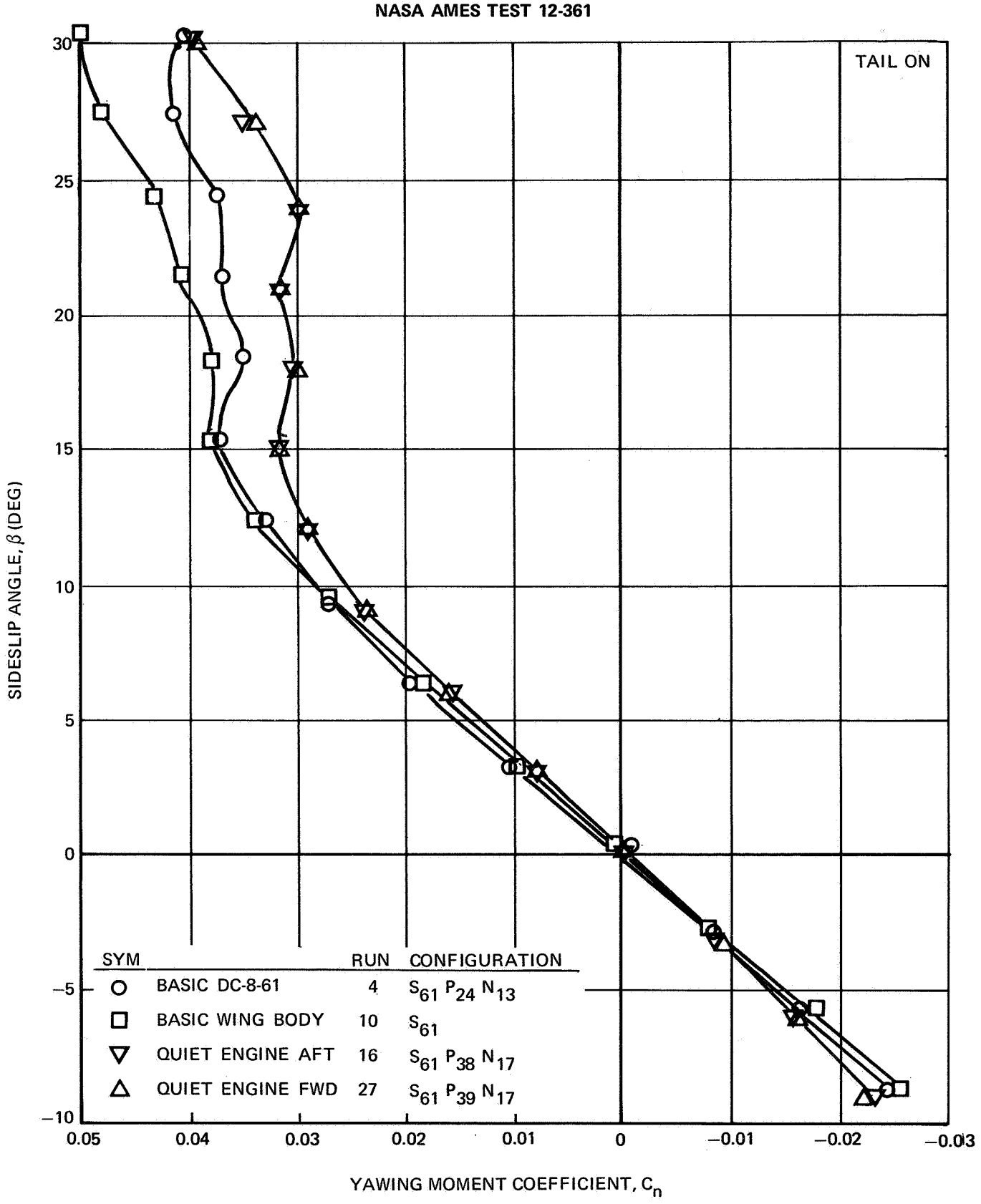

FIGURE III-61. EFFECT OF PYLONS AND NACELLES ON YAWING MOMENT – δ_f = 0°, i_H = 0°, α = 0°

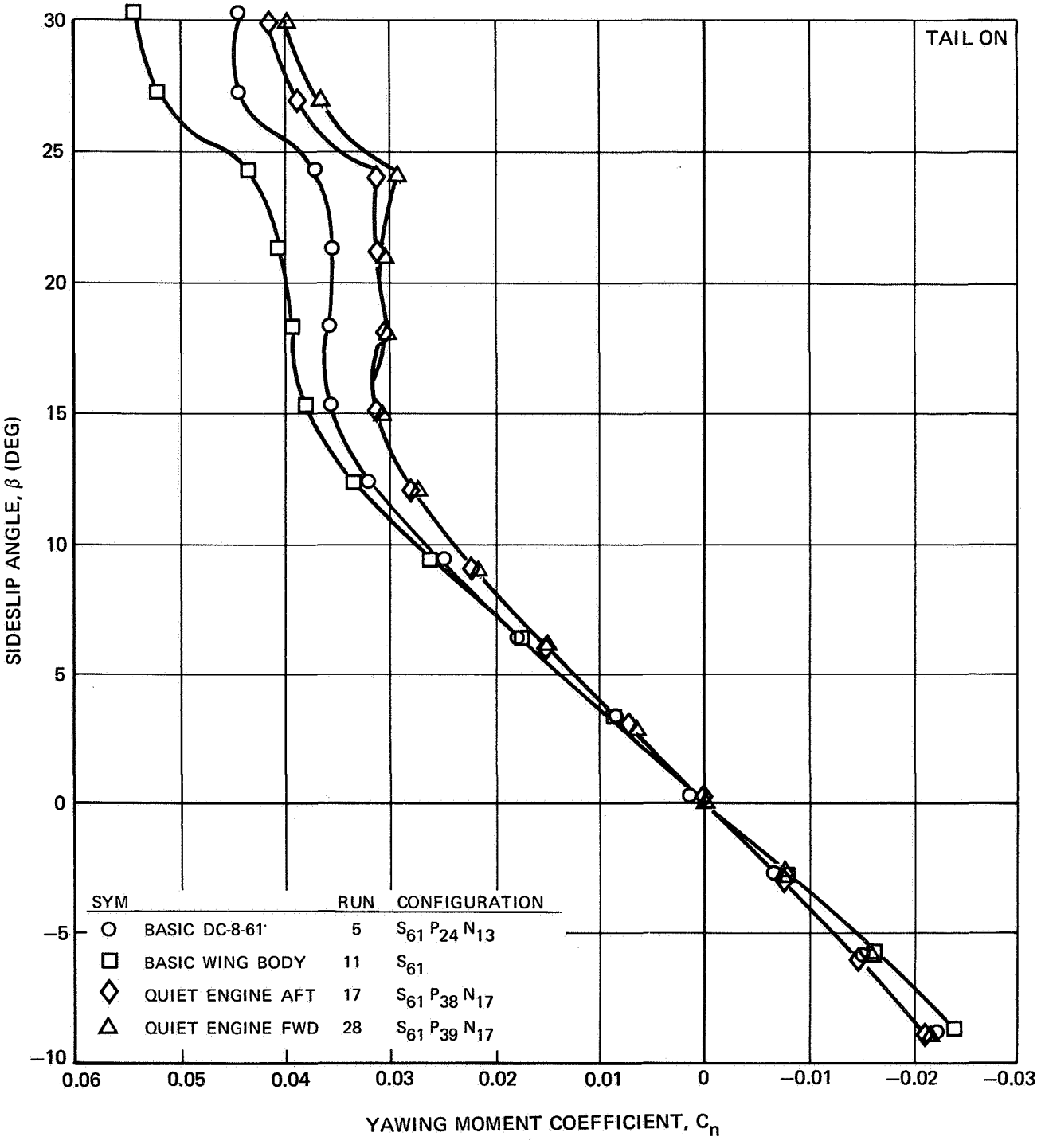

FIGURE III-62. EFFECT OF PYLONS AND NACELLES ON YAWING MOMENT – $\delta_f = 0^o$, $i_H = 0^o$, $\alpha = 4^o$

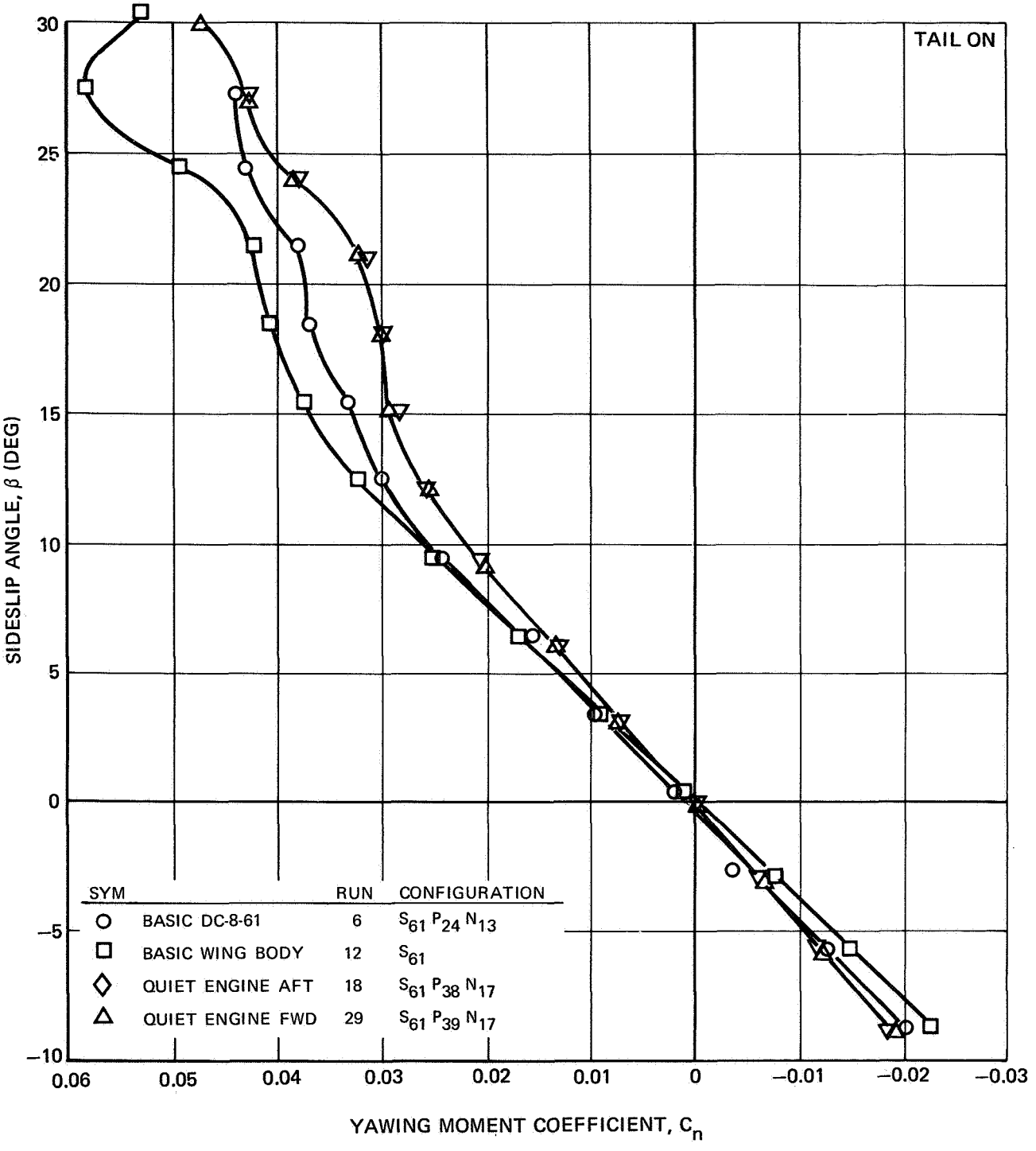

FIGURE III-63. EFFECT OF PYLONS AND NACELLES ON YAWING MOMENT – $\delta_f = 0^o$, $i_H = 0^o$, $\alpha = 8^o$

NAS AMES TEST 12-361

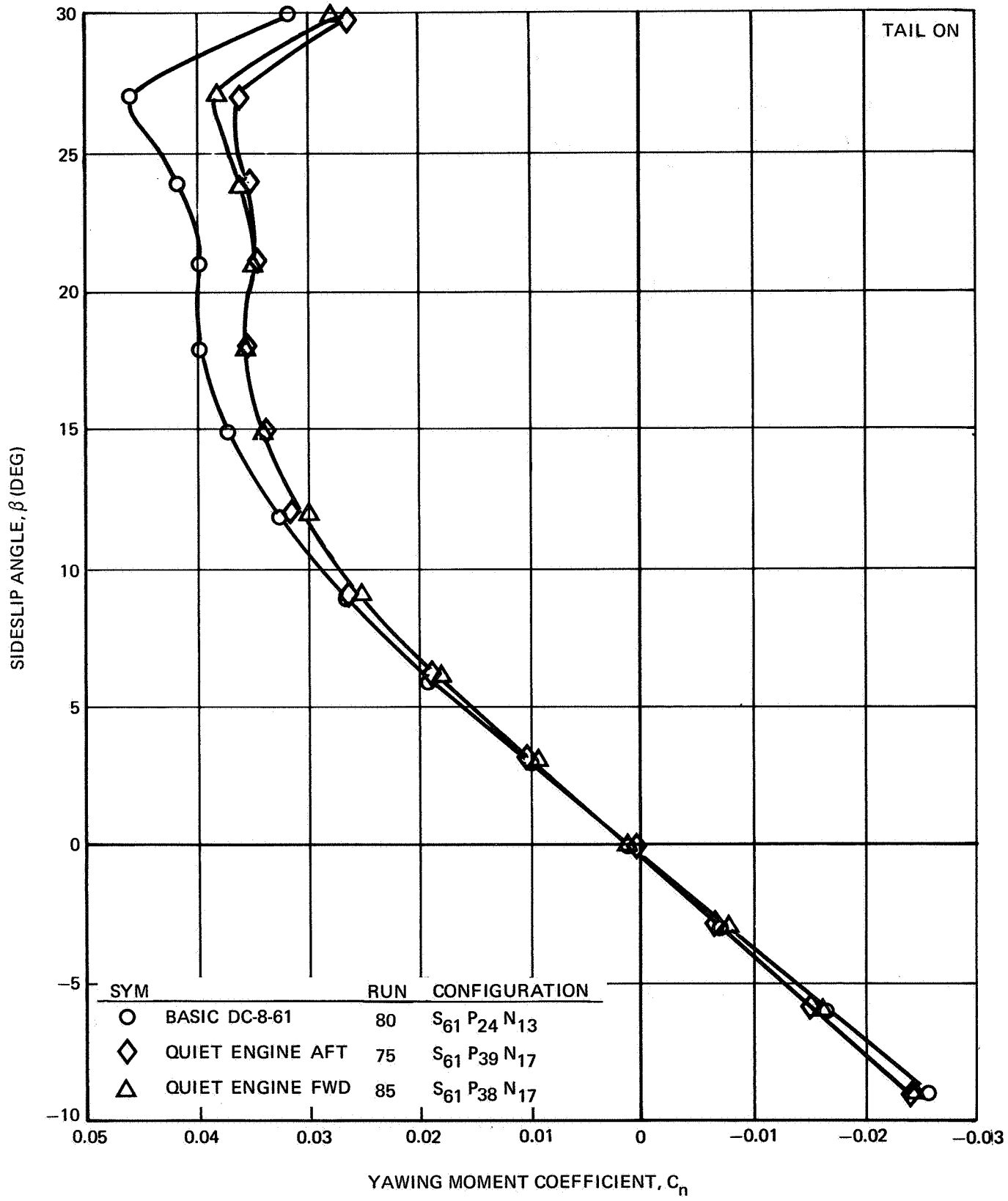

FIGURE III-64. EFFECT OF PYLONS AND NACELLES ON YAWING MOMENT – $\delta_f = 25^o$, $i_H = 0^o$, $\alpha = 0^o$

NASA AMES TEST 12-361

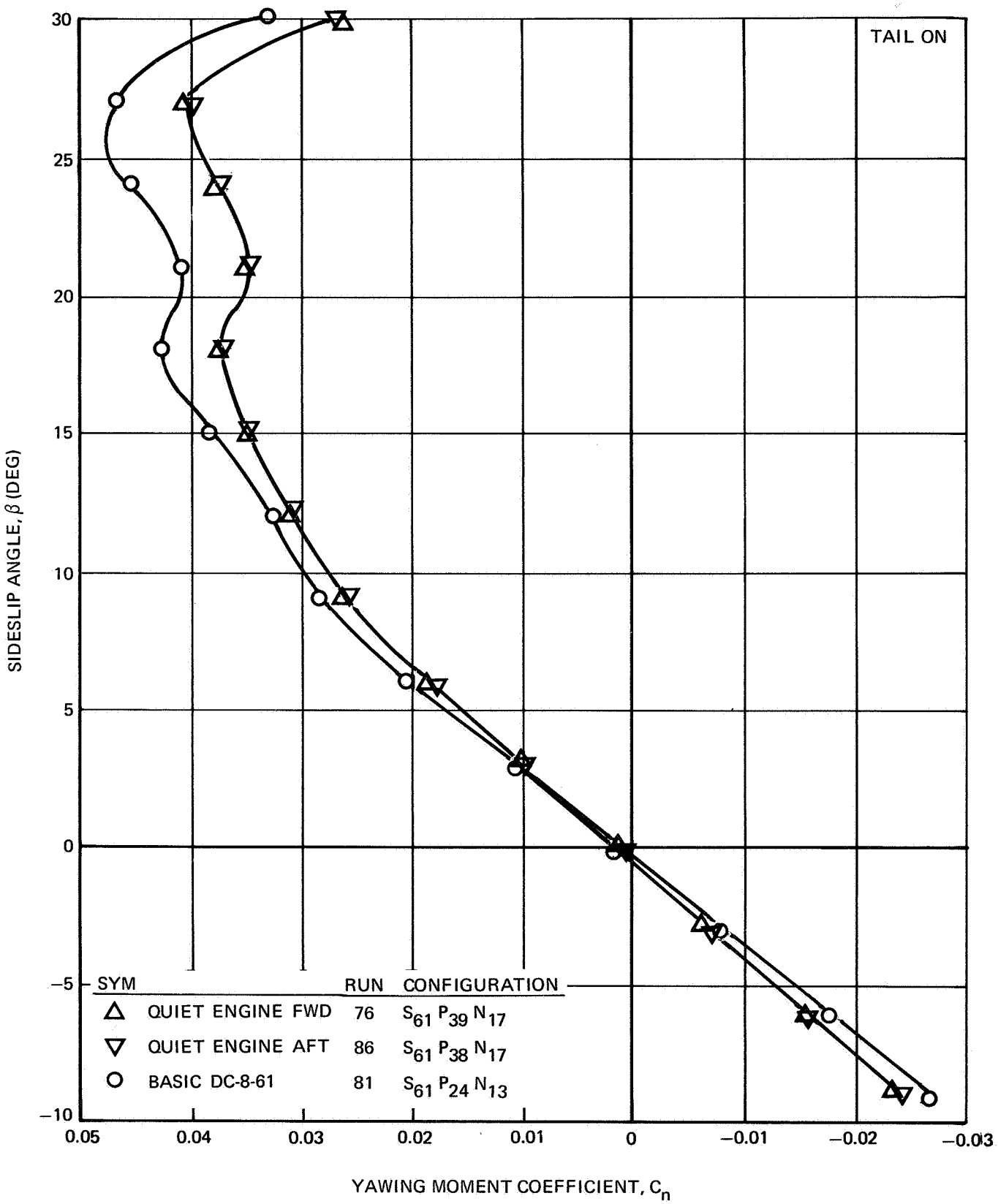

FIGURE III-65. EFFECT OF PYLONS AND NACELLES ON YAWING MOMENT – $\delta_f = 25^o$, $\alpha_F = 4^o$, $i_H = 0^o$

NASA AMES TEST 12-361

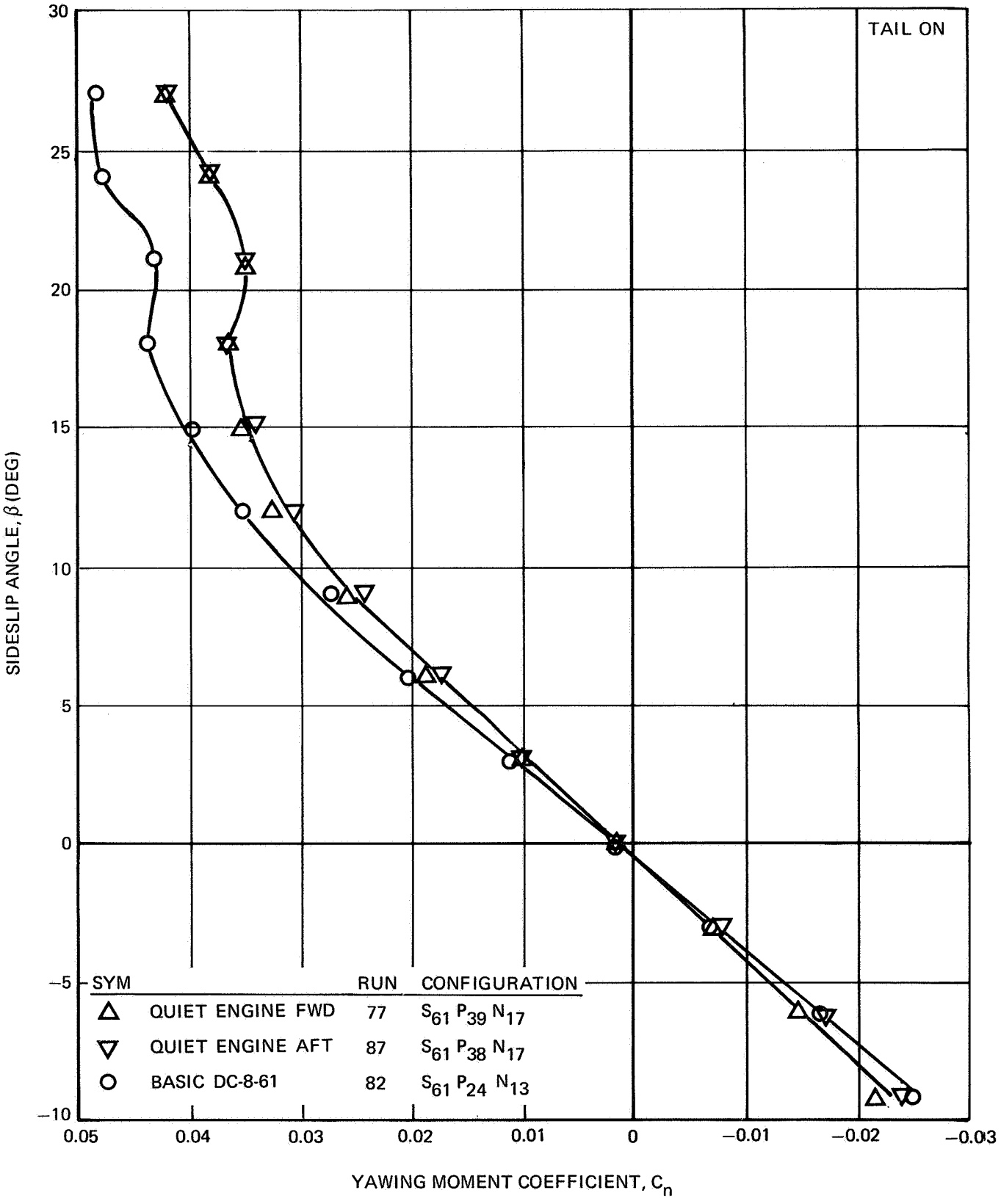

FIGURE III-66. EFFECT OF PYLONS AND NACELLES ON YAWING MOMENT – $\delta_f = 25^o$, $\alpha_F = 8^o$, $i_H = 0^o$

NASA AMES TEST 12-361

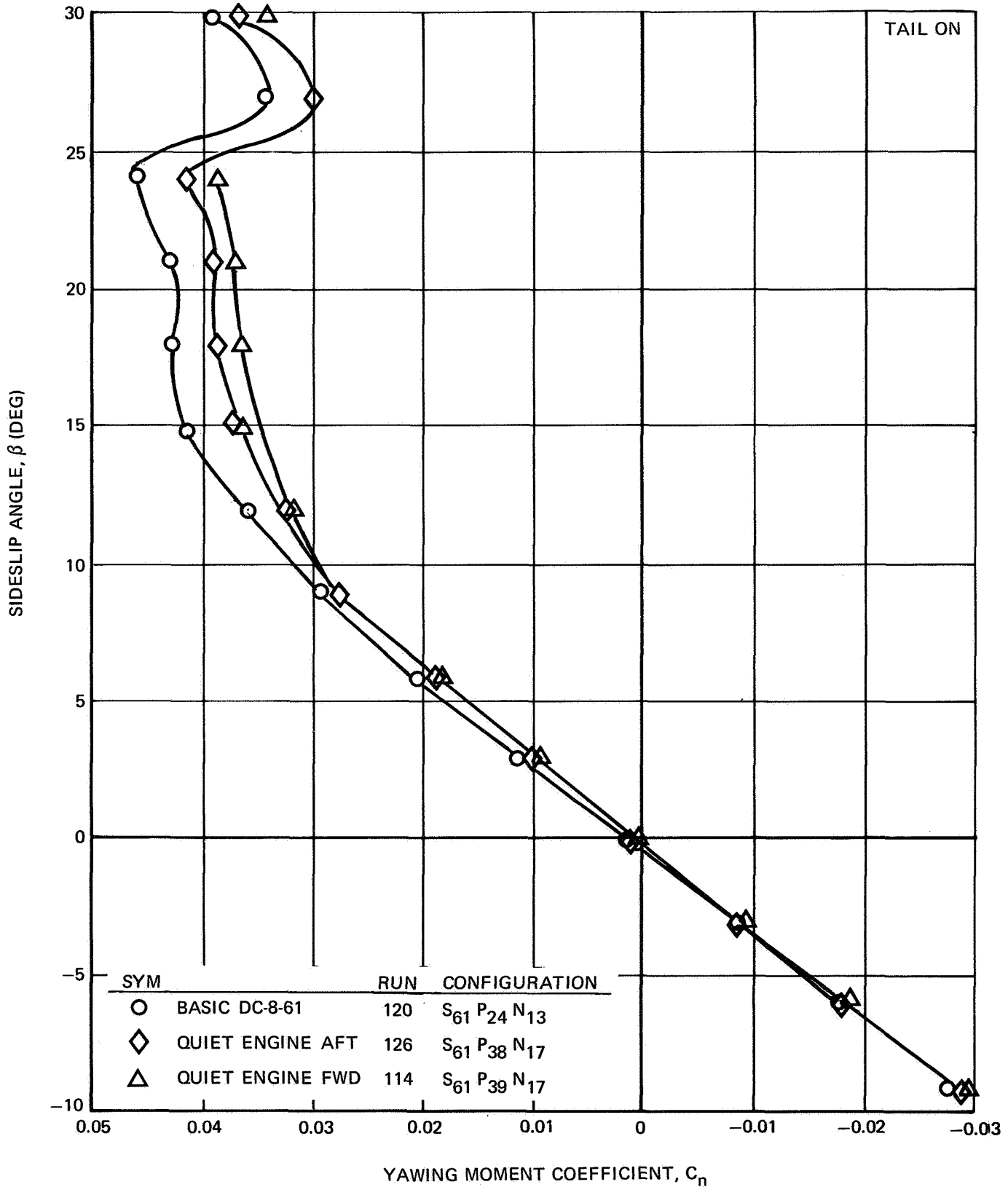

FIGURE III-67. EFFECT OF PYLONS AND NACELLES ON YAWING MOMENT – $\delta_f = 50^o$, $\alpha_F = 0^o$, $i_H = 0^o$

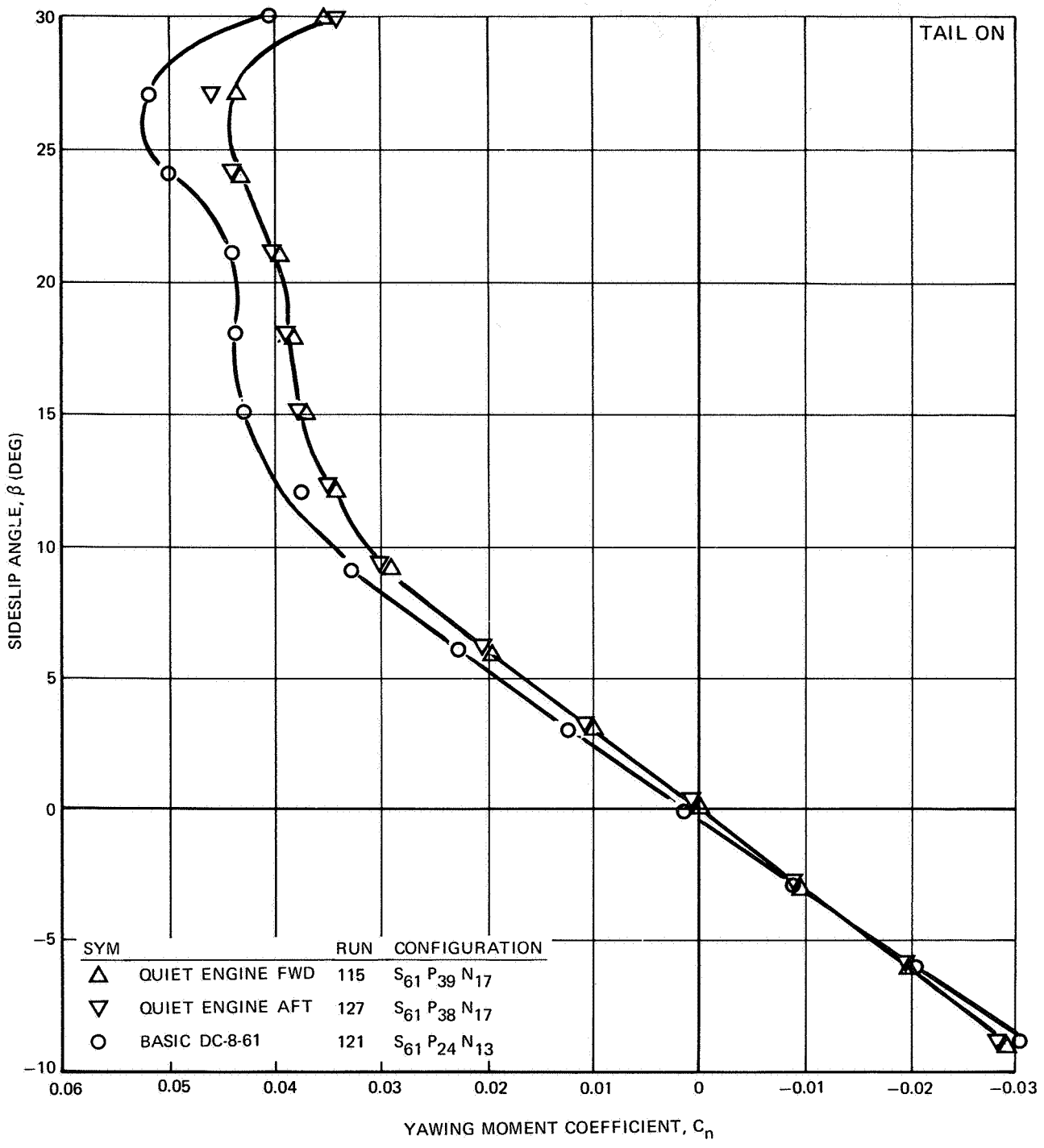

FIGURE III-68. EFFECT OF PYLONS AND NACELLES ON YAWING MOMENT – $\delta_f = 50^o$, $\alpha_F = 4^o$, $i_H = 0^o$

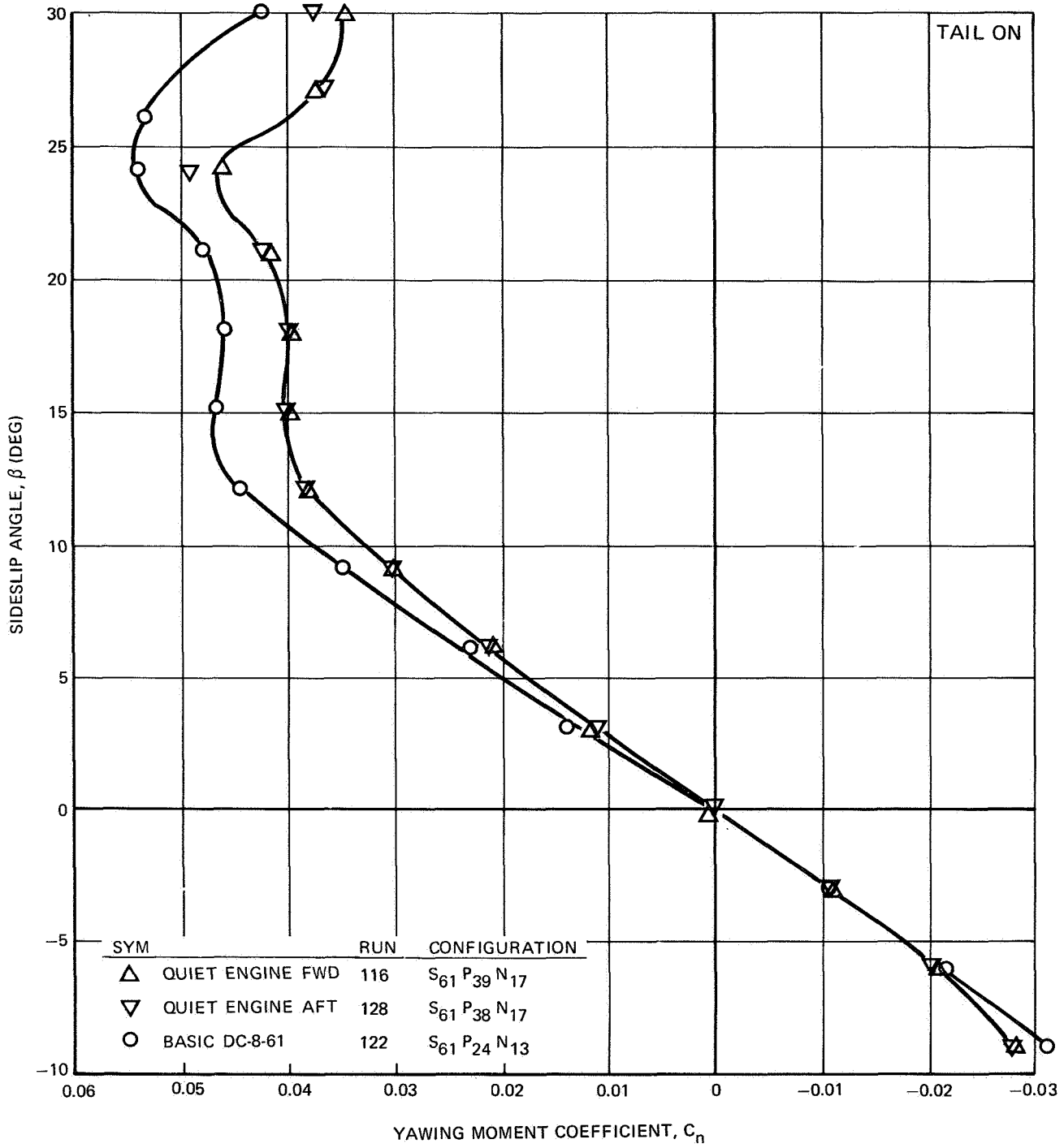

FIGURE III-69. EFFECT OF PYLONS AND NACELLES ON YAWING MOMENT – $\delta_f = 50^o$, $\alpha_F = 8^o$, $i_H = 0^o$

NASA AMES TEST 11-353

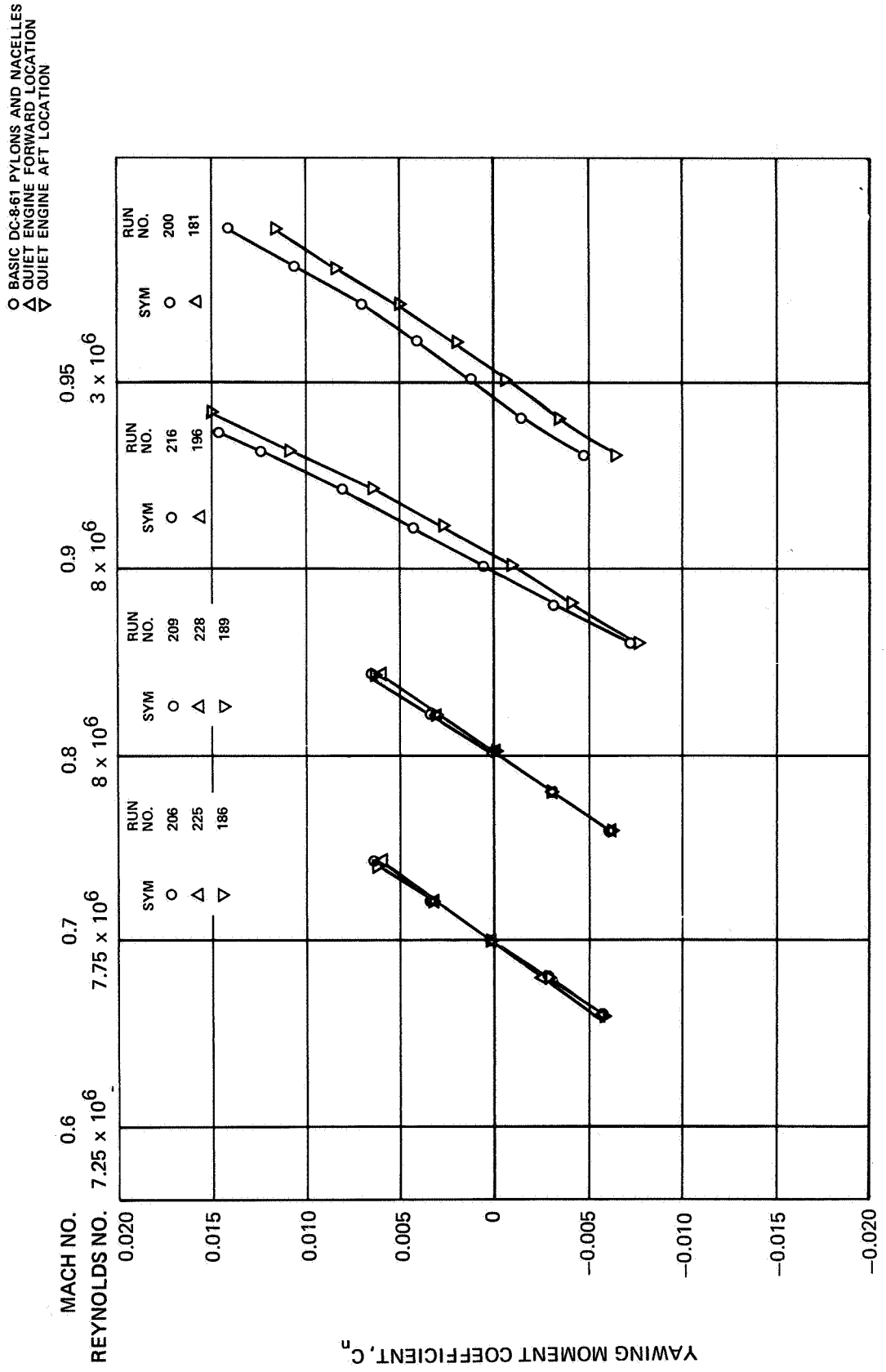

FIGURE III-70. EFFECT OF NACELLES AND PYLONS ON YAWING MOMENT DUE TO SIDESLIP – $\delta_f = 0^o$, $\alpha_F = 0^o$

NASA AMES TEST 11-353

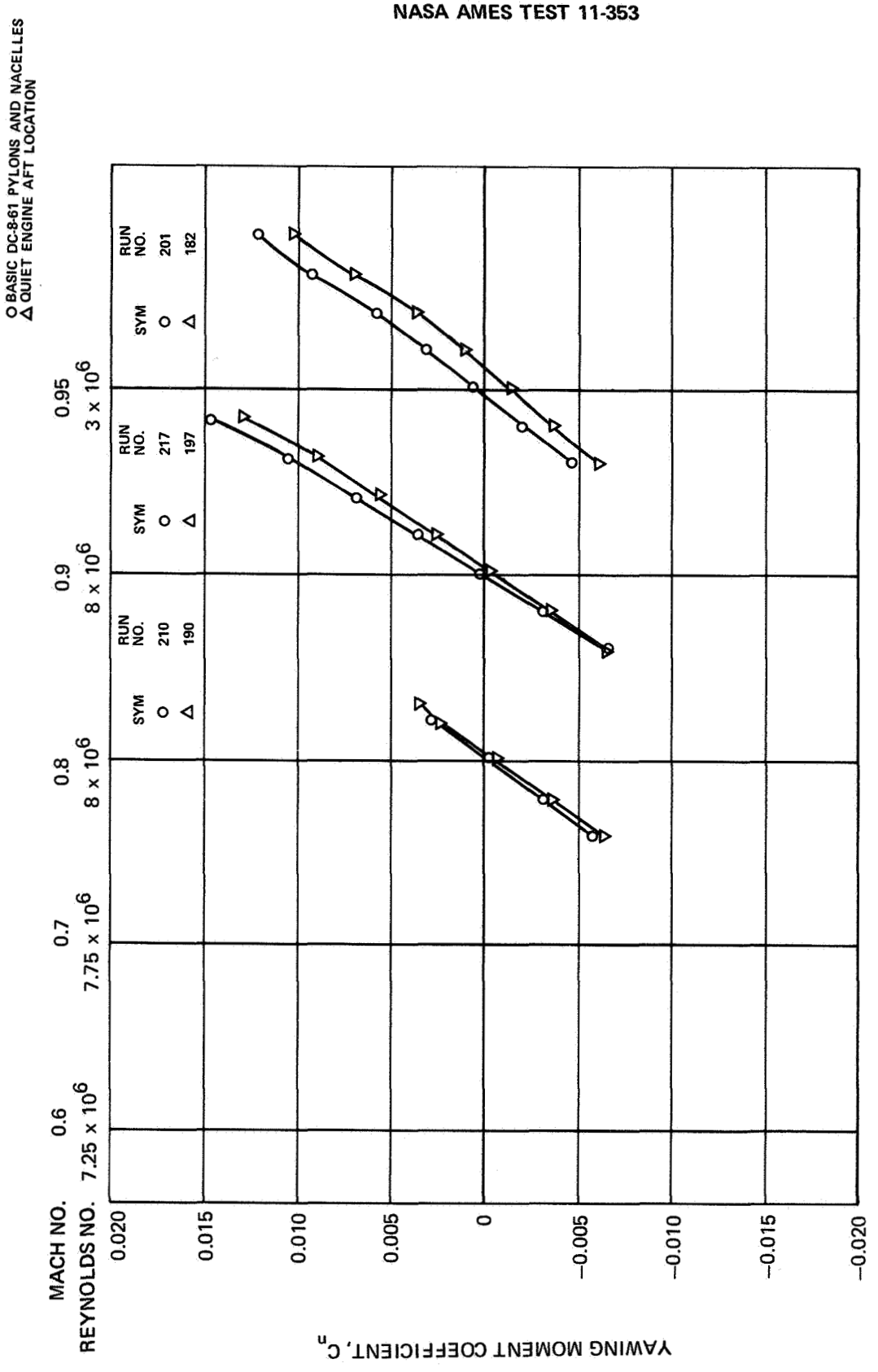

FIGURE III-71. EFFECT OF NACELLES AND PYLONS ON YAWING MOMENT DUE TO SIDESLIP – $\delta_f = 0^o$, $\alpha_F = 2.1^o$

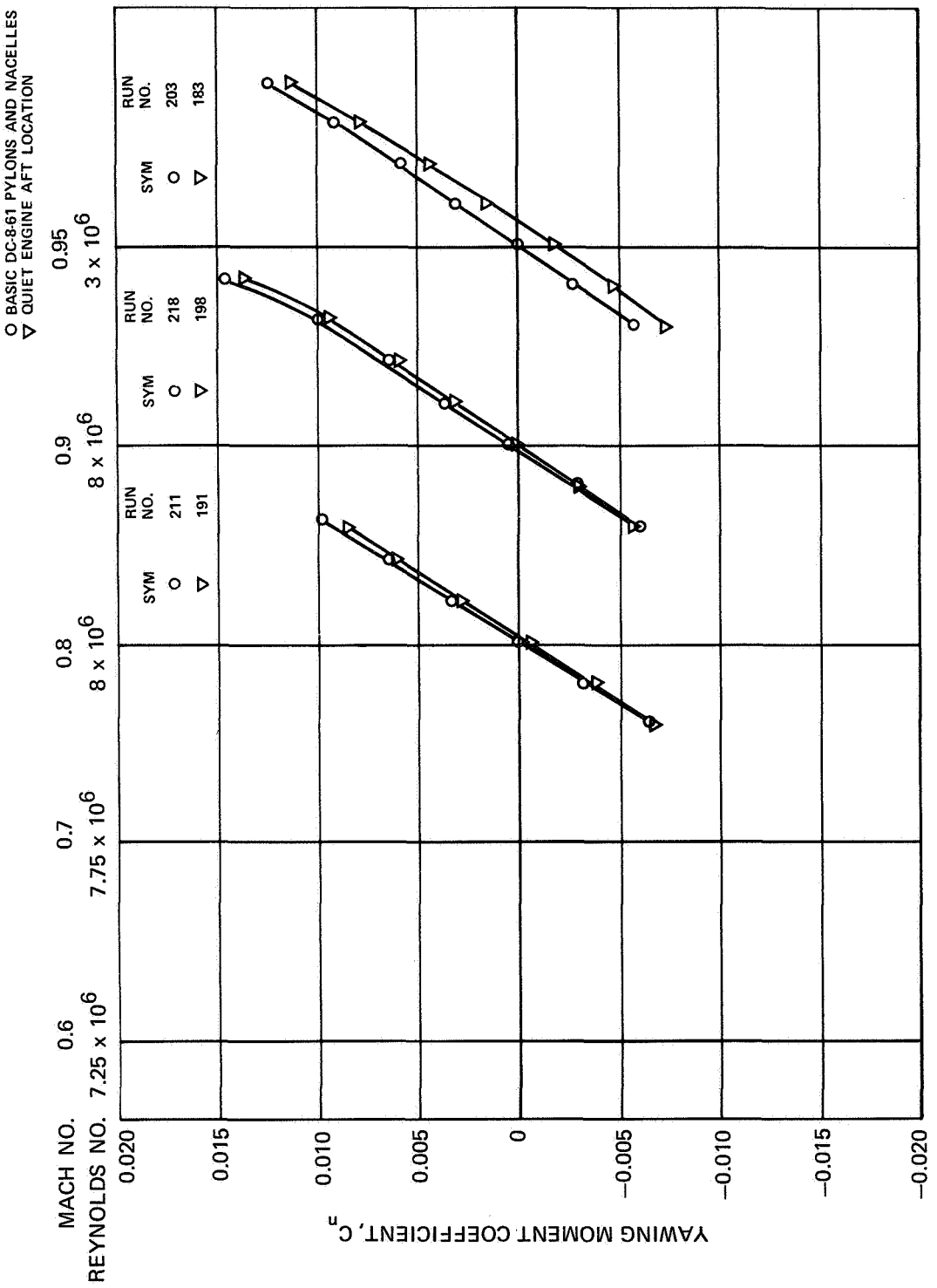

FIGURE III-72. EFFECT OF NACELLES AND PYLONS ON YAWING MOMENT DUE TO SIDESLIP – $\delta_f = 0^o$, $\alpha_F = 4.1^o$

NASA AMES TEST 12-361

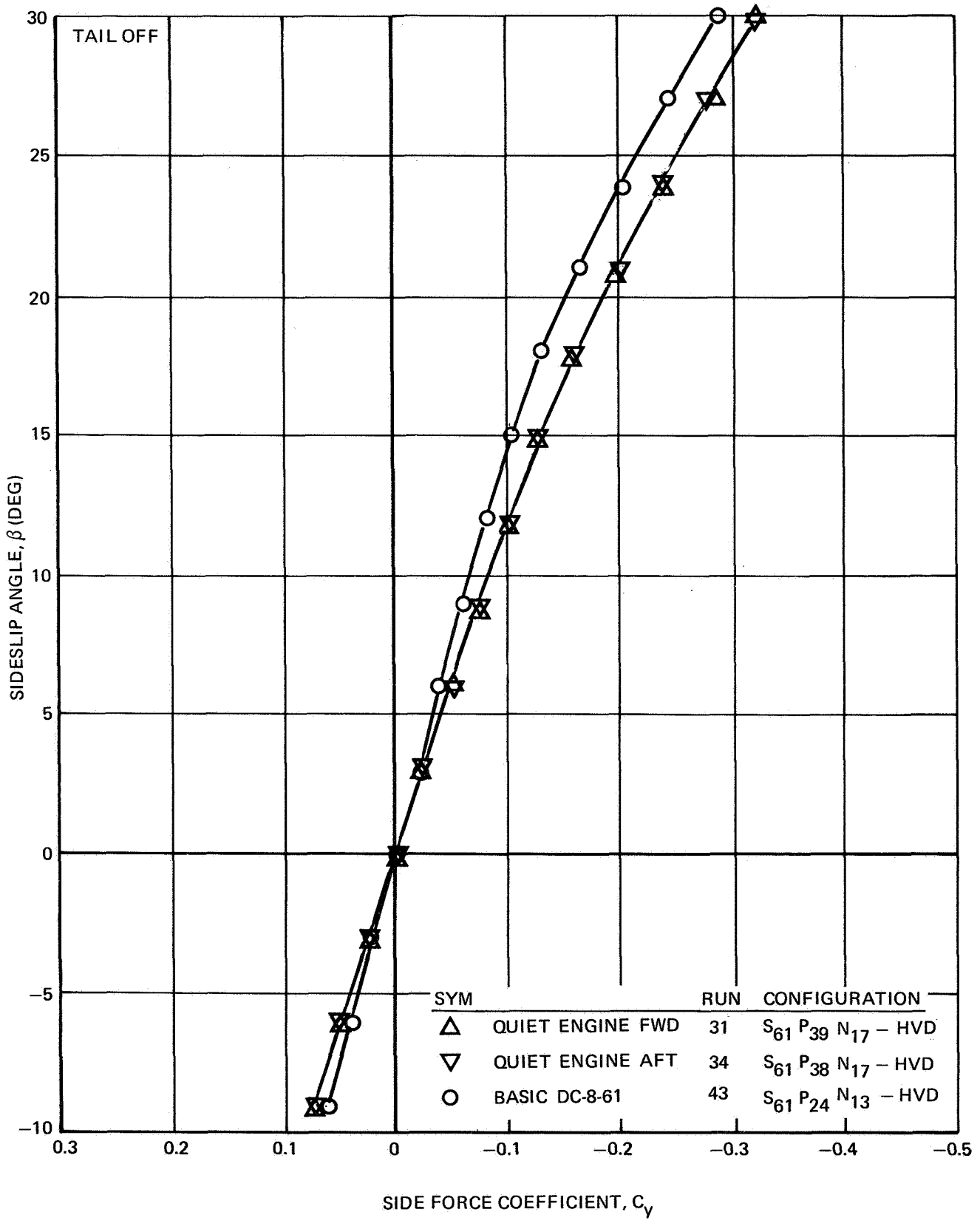

FIGURE III-73. EFFECT OF PYLONS AND NACELLES ON SIDE FORCE – $\delta_f = 0^o$, $\alpha_F = 0^o$

NASA AMES TEST 12-361

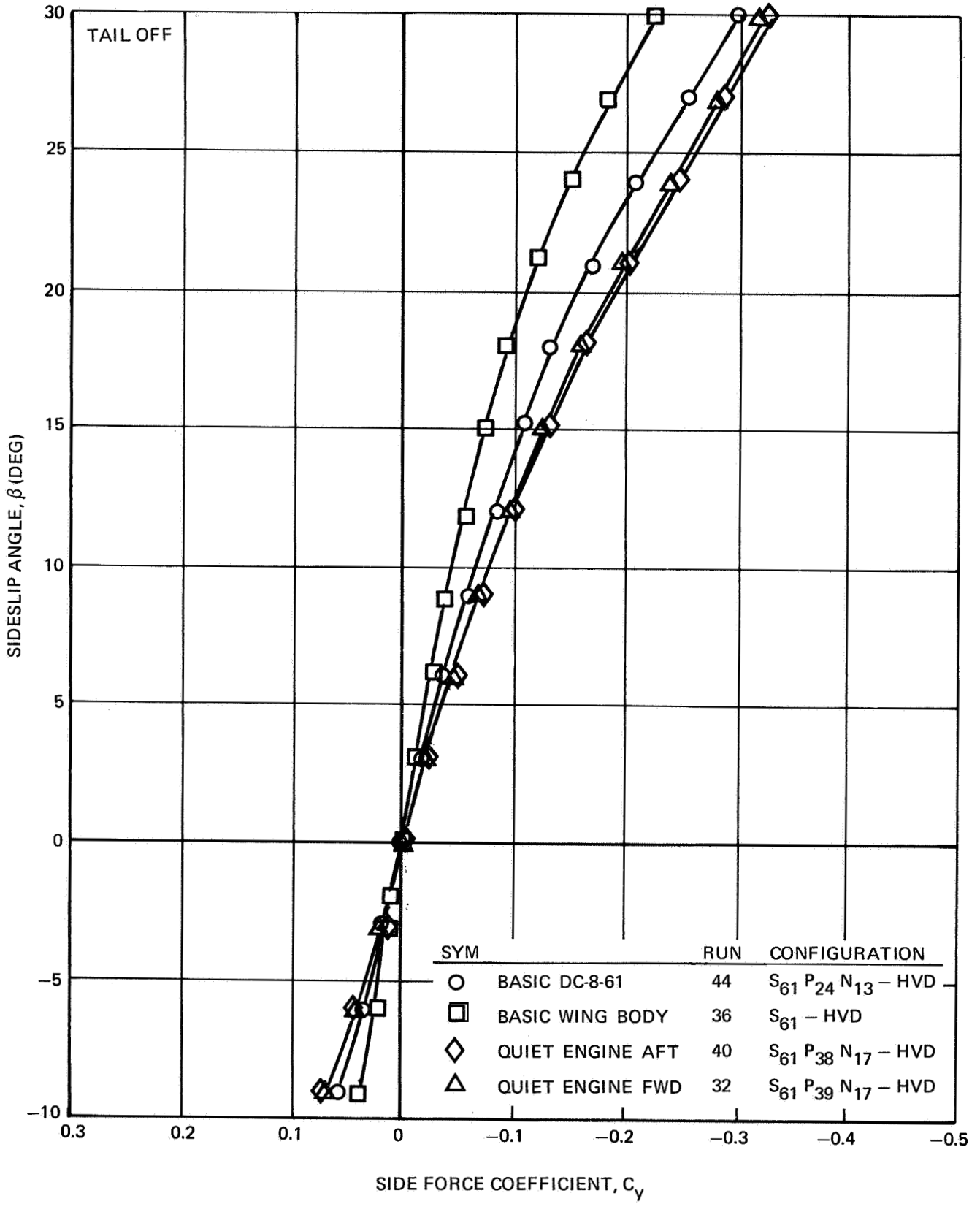

FIGURE III-74. EFFECT OF PYLONS AND NACELLES ON SIDE FORCE – $\delta_f = 0^o$, $\alpha_F = 4^o$

NASA AMES TEST 12-361

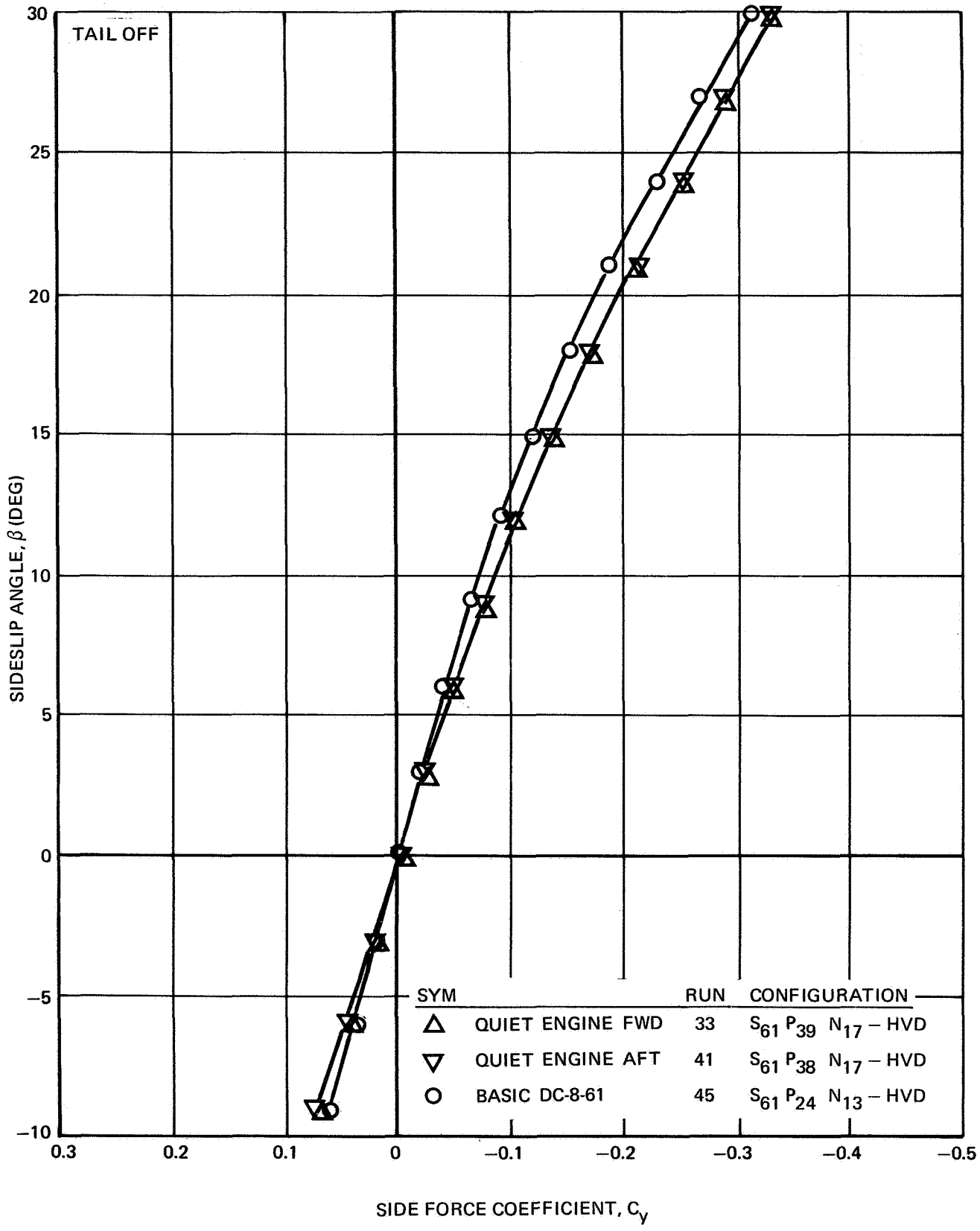

FIGURE III-75. EFFECT OF PYLONS AND NACELLES ON SIDE FORCE – $\delta_f = 0^o$, $\alpha_F = 8^o$

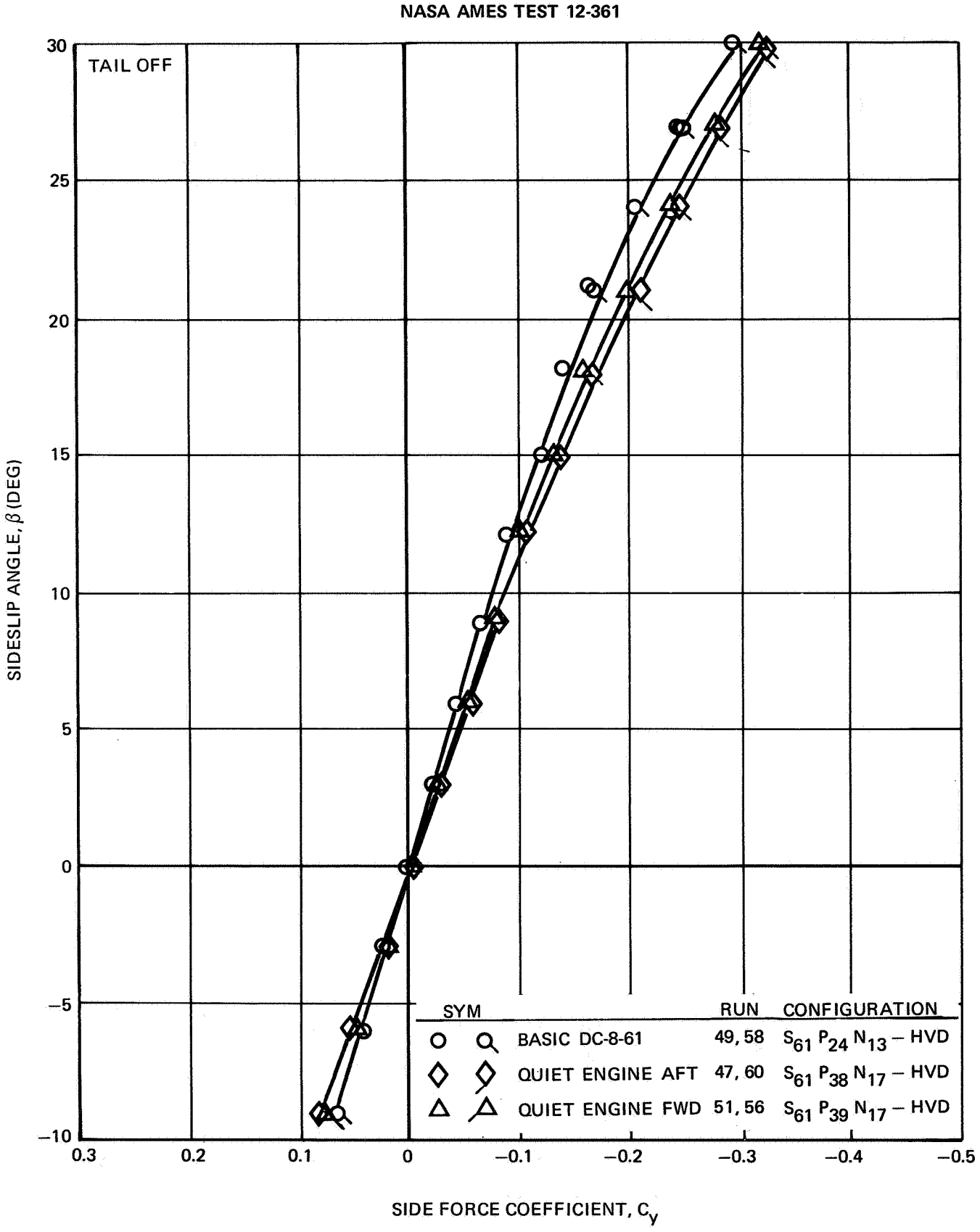

FIGURE III-76. EFFECT OF PYLONS AND NACELLES ON SIDE FORCE – $\delta_f = 15^o$, $a_F = 0^o$

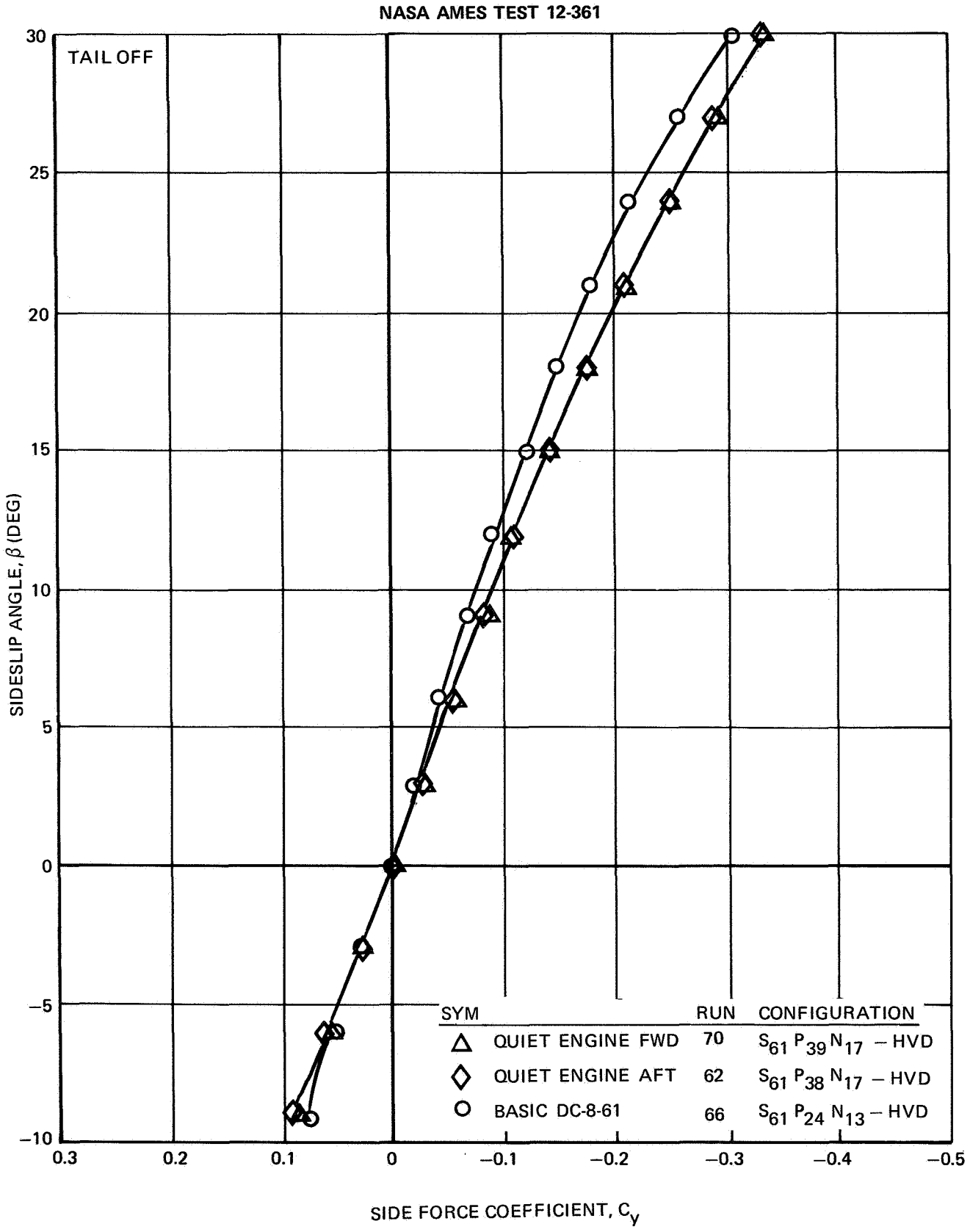

FIGURE III-77. EFFECT OF PYLONS AND NACELLES ON SIDE FORCE – $\delta_f = 25^o$, $a_F = 0^o$

NASA AMES TEST 12-361

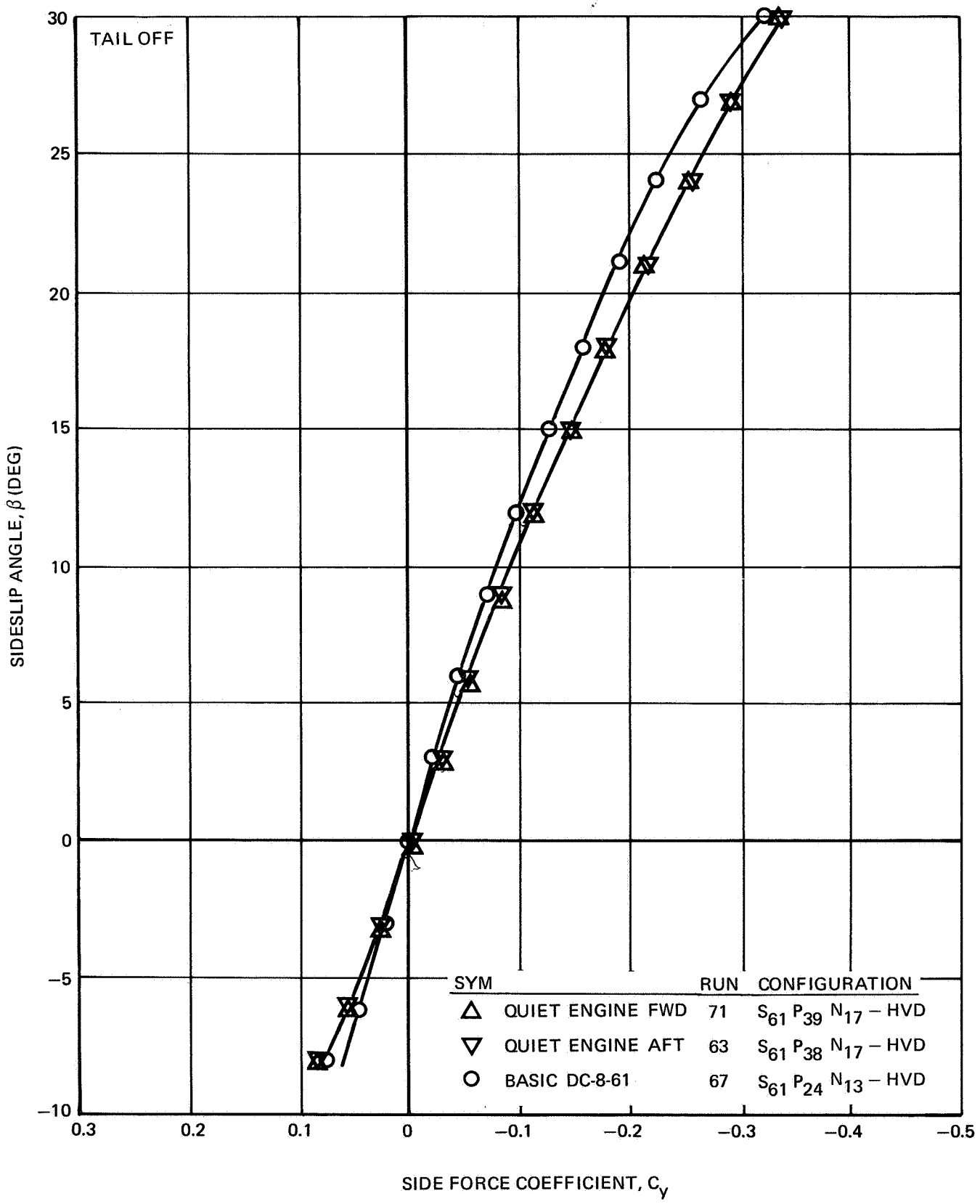

FIGURE III-78. EFFECT OF PYLONS AND NACELLES ON SIDE FORCE – $\delta_f = 25^o$, $a_F = 4^o$

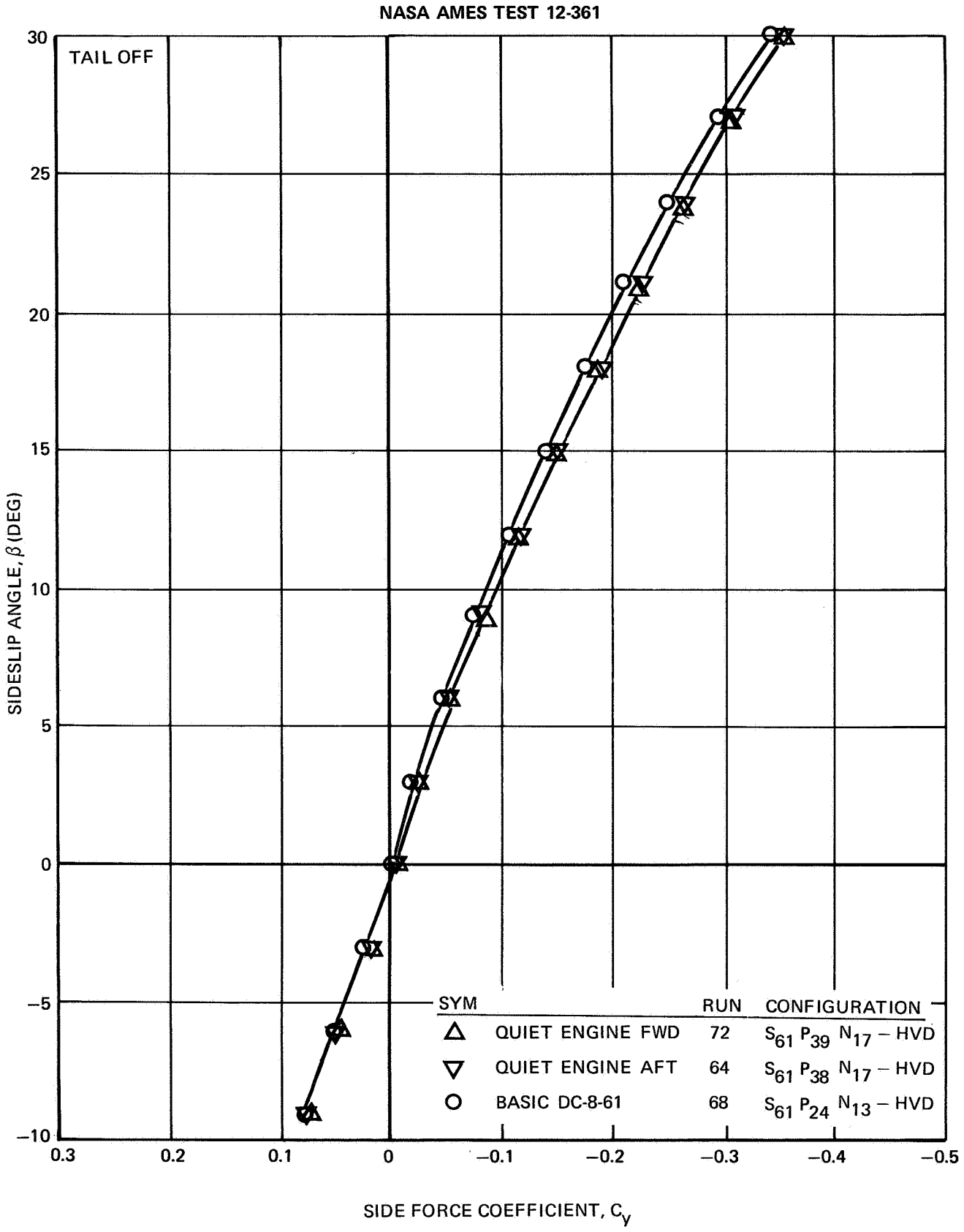

FIGURE III-79. EFFECT OF PYLONS AND NACELLES ON SIDE FORCE – $\delta_f = 25^o$, $\alpha_F = 8^o$

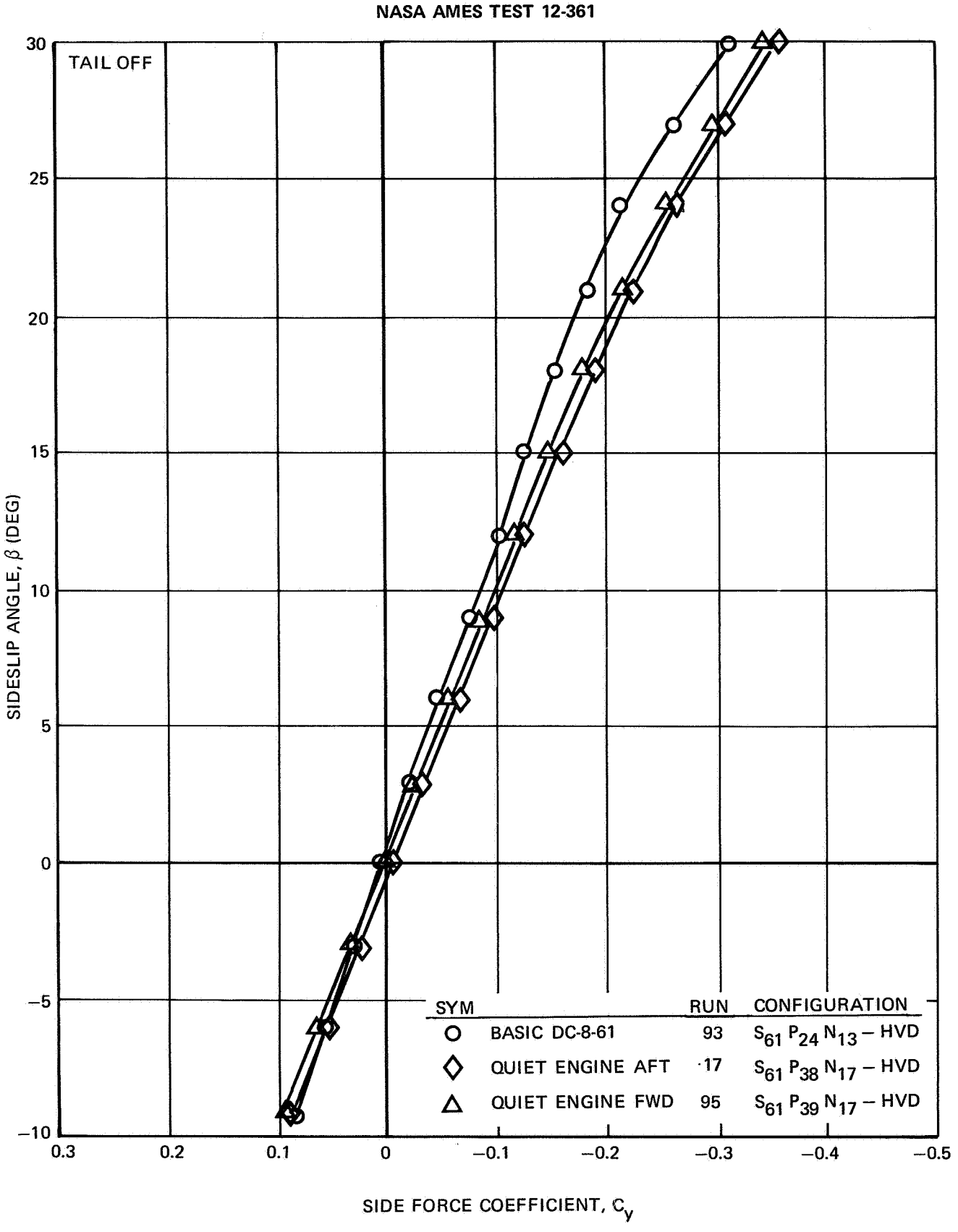

FIGURE III-80. EFFECT OF PYLONS AND NACELLES ON SIDE FORCE – $\delta_f = 35^o$, $\alpha_F = 0^o$

NASA AMES TEST 12-361

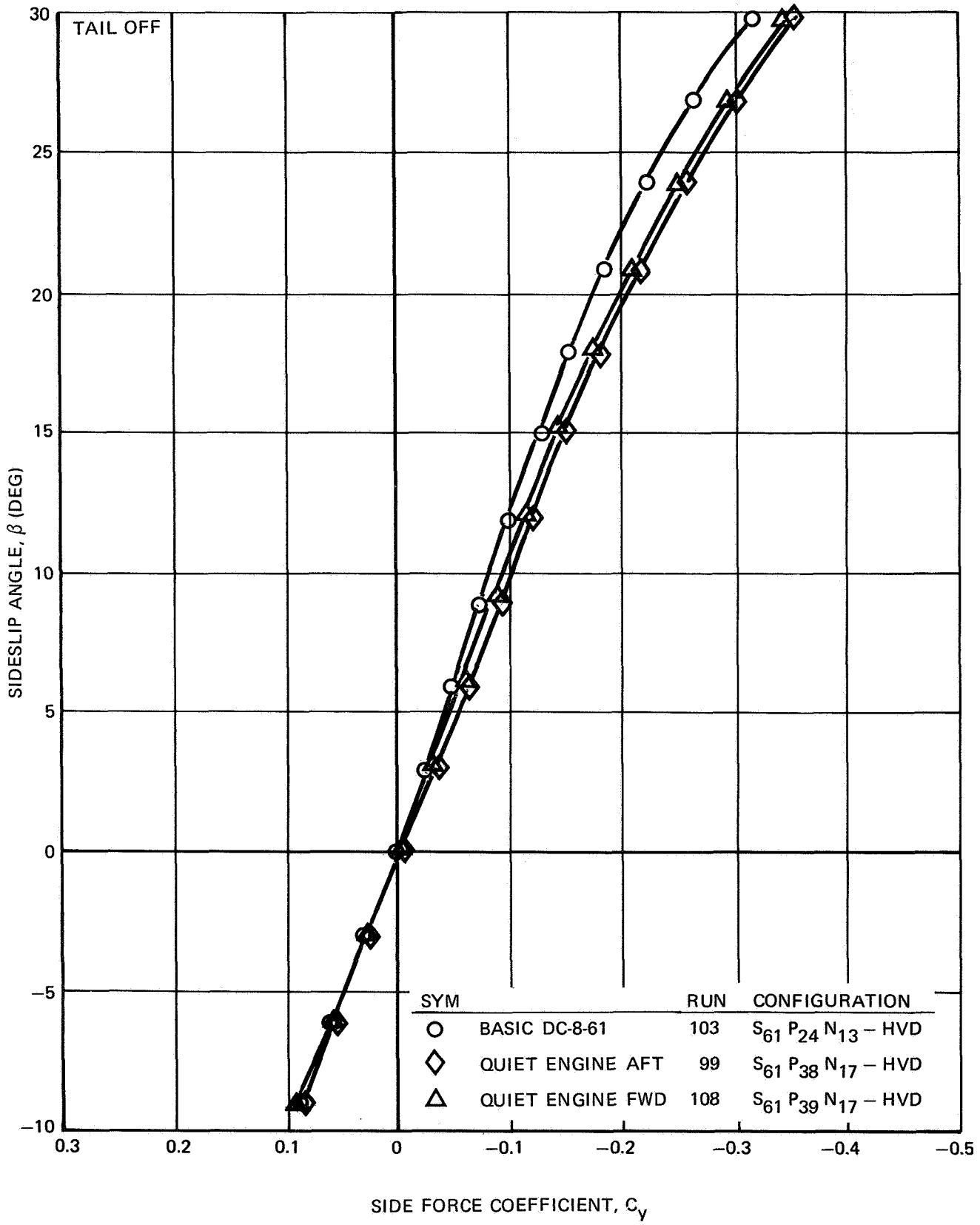

FIGURE III-81. EFFECT OF PYLONS AND NACELLES ON SIDE FORCE – $\delta_f = 50^o$, $a_F = 0^o$

NASA AMES TEST 12-361

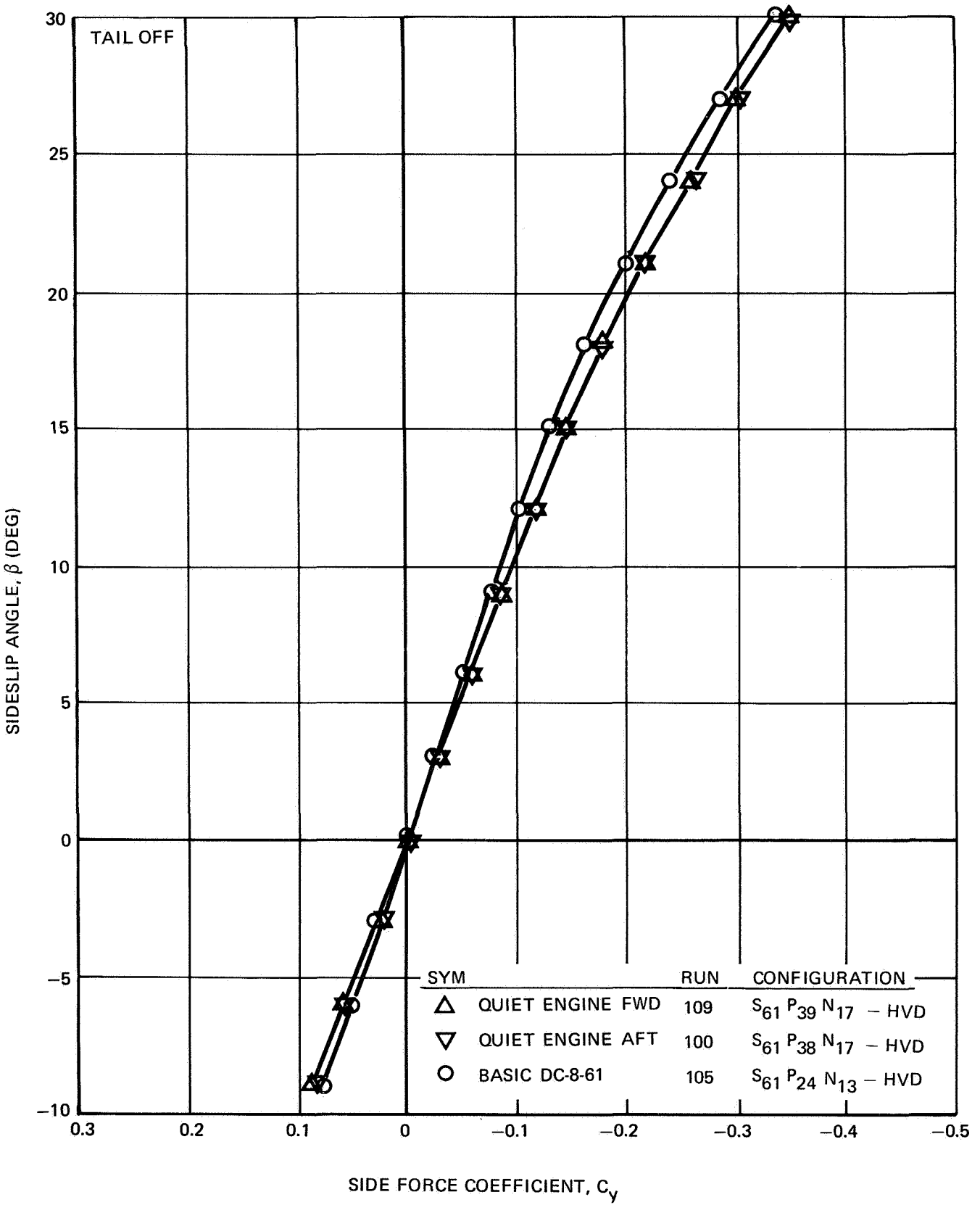

FIGURE III-82. EFFECT OF PYLONS AND NACELLES ON SIDE FORCE – $\delta_f = 50^o$, $\alpha_F = 4^o$

NASA AMES TEST 12-361

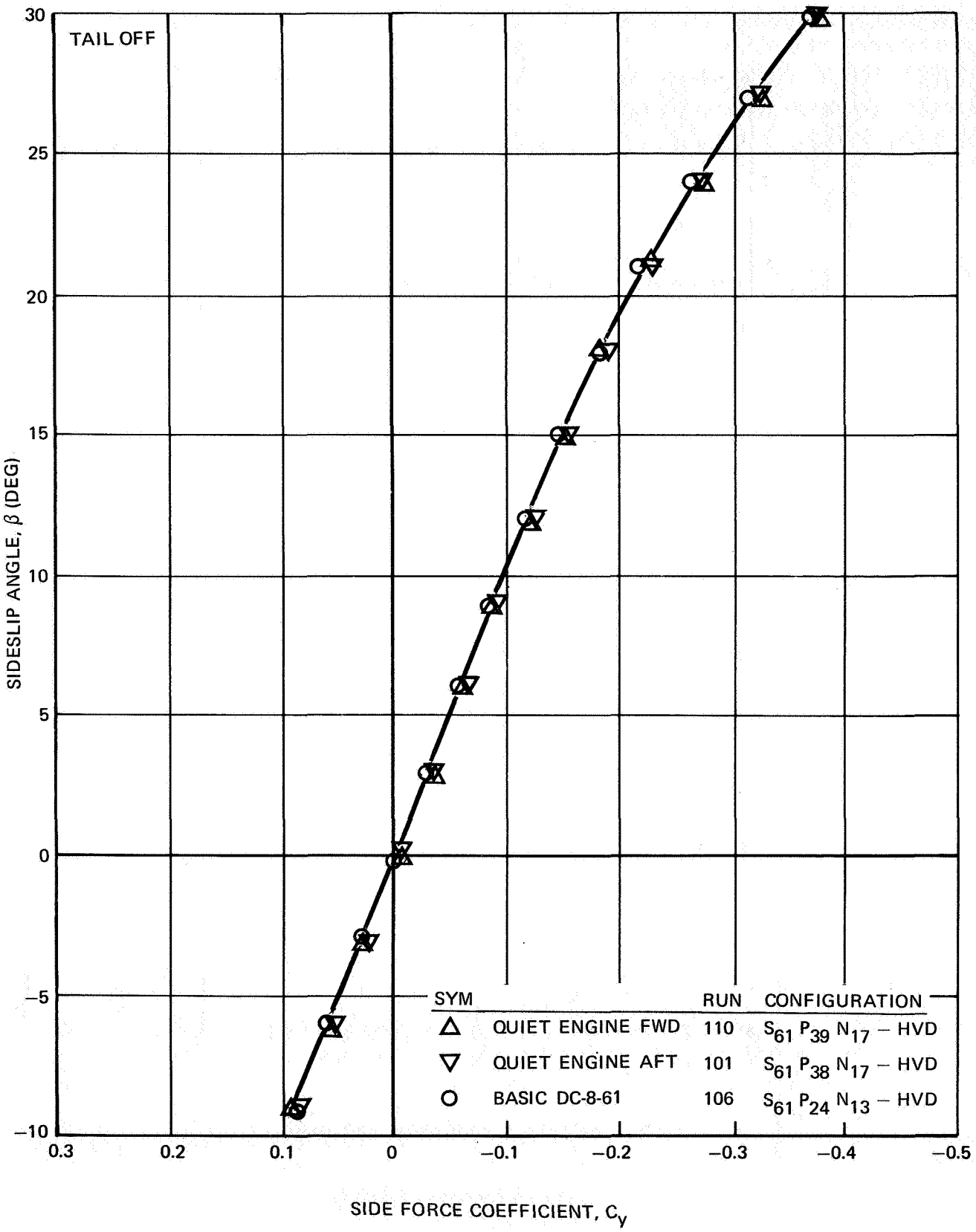

FIGURE III-83. EFFECT OF PYLONS AND NACELLES ON SIDE FORCE – $\delta_f = 50^o$, $\alpha_F = 8^o$

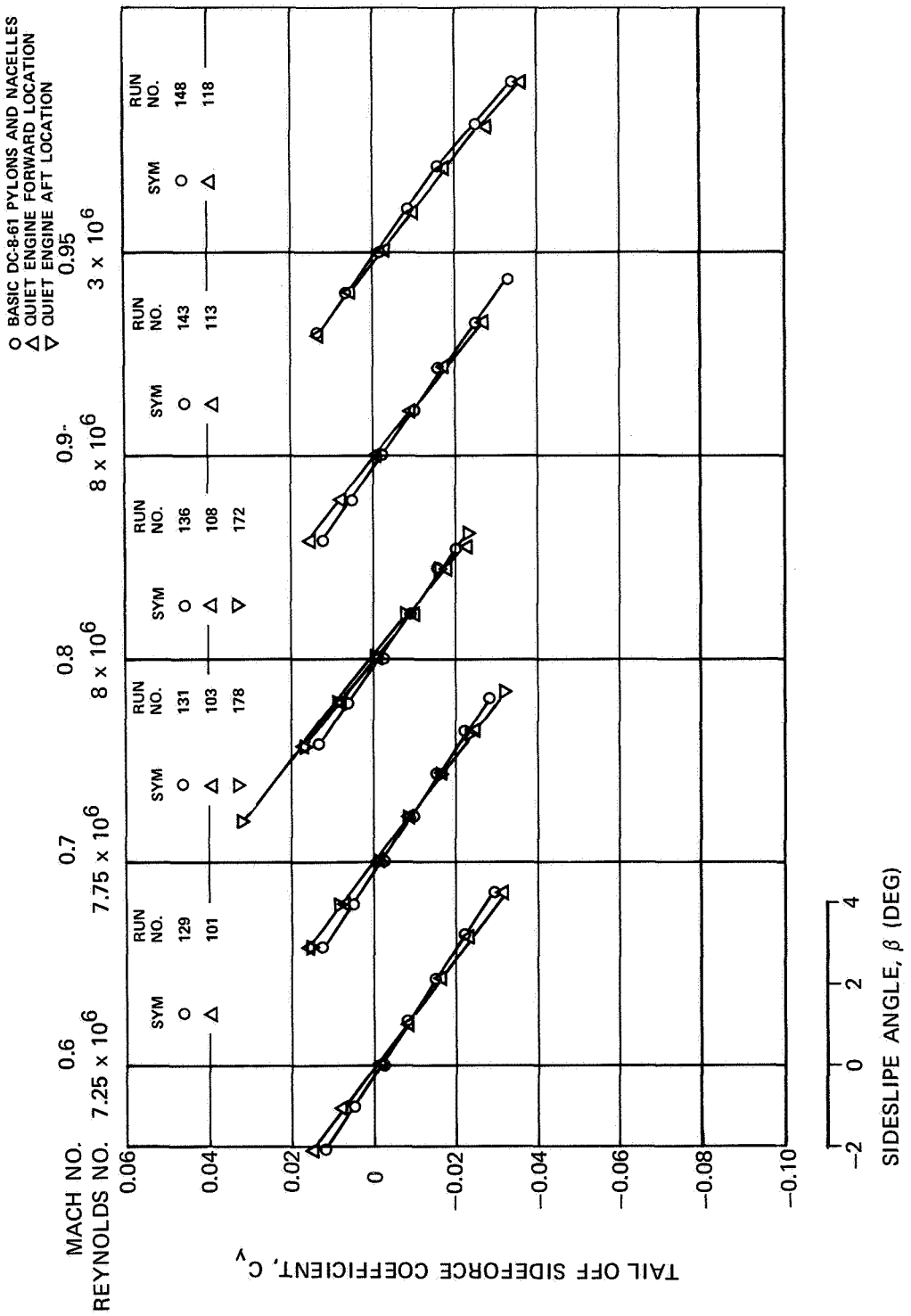

FIGURE III-84. EFFECT OF NACELLES AND PYLONS ON TAIL-OFF SIDE FORCE DUE TO SIDESLIP – $\delta_f = 0^o$, $\alpha_F = 0^o$

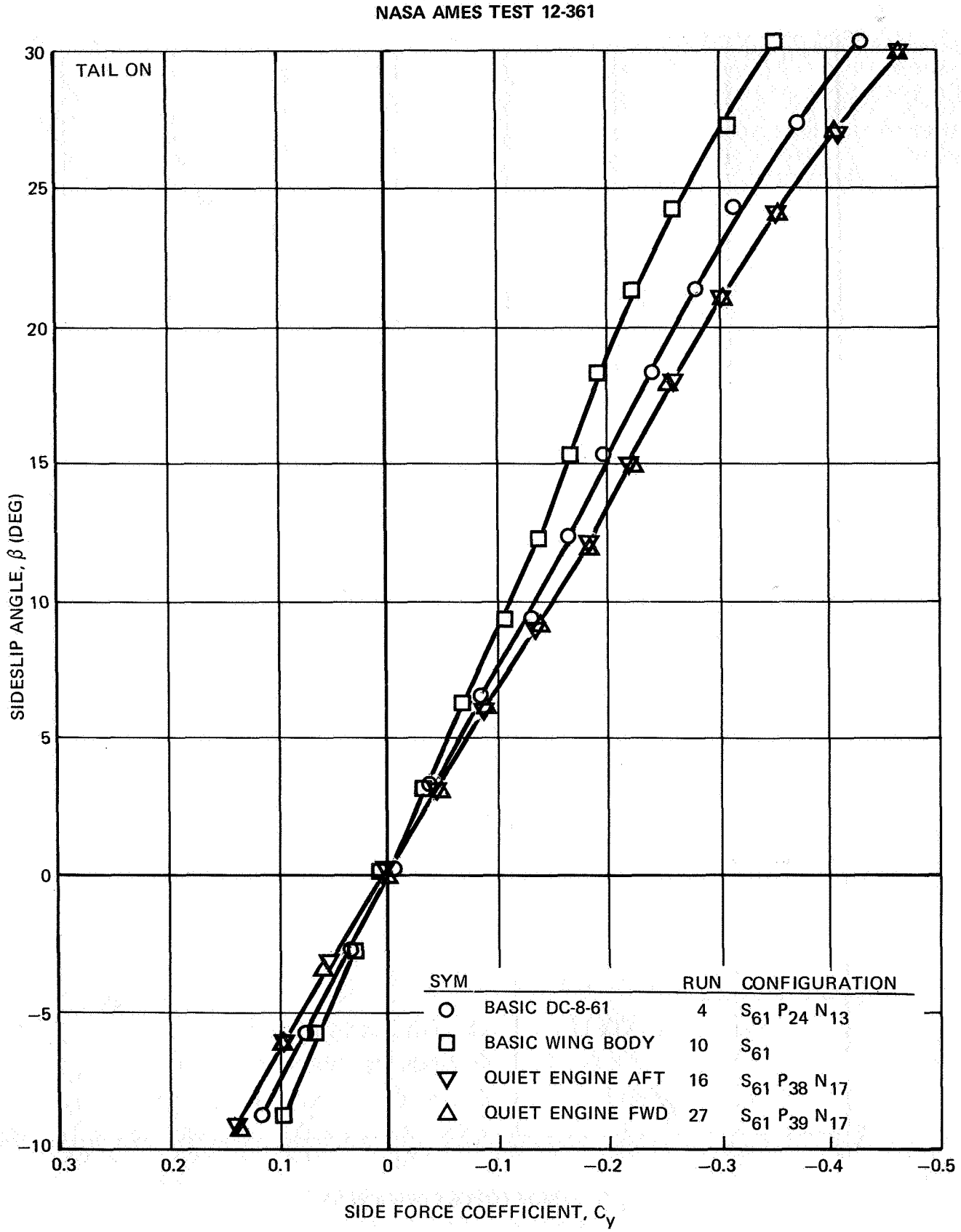

FIGURE III-85. EFFECT OF PYLONS AND NACELLES ON SIDE FORCE – $\delta_f = 0^o$, $i_H = 0^o$, $\alpha = 0^o$

NASA AMES TEST 12-361

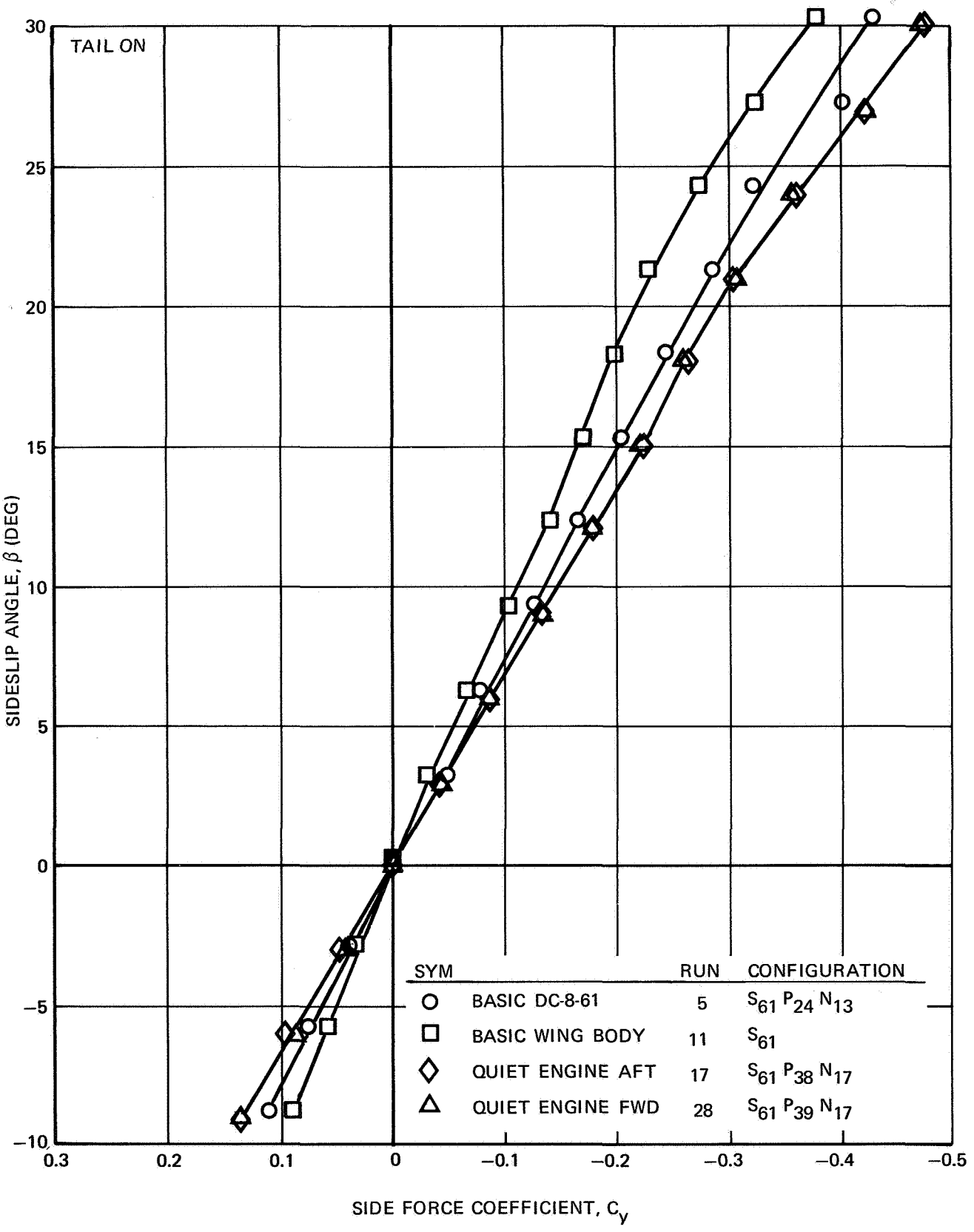

FIGURE III-86. EFFECT OF PYLONS AND NACELLES ON SIDE FORCE – $\delta_f = 0^o$, $i_H = 0^o$, $\alpha = 4^o$

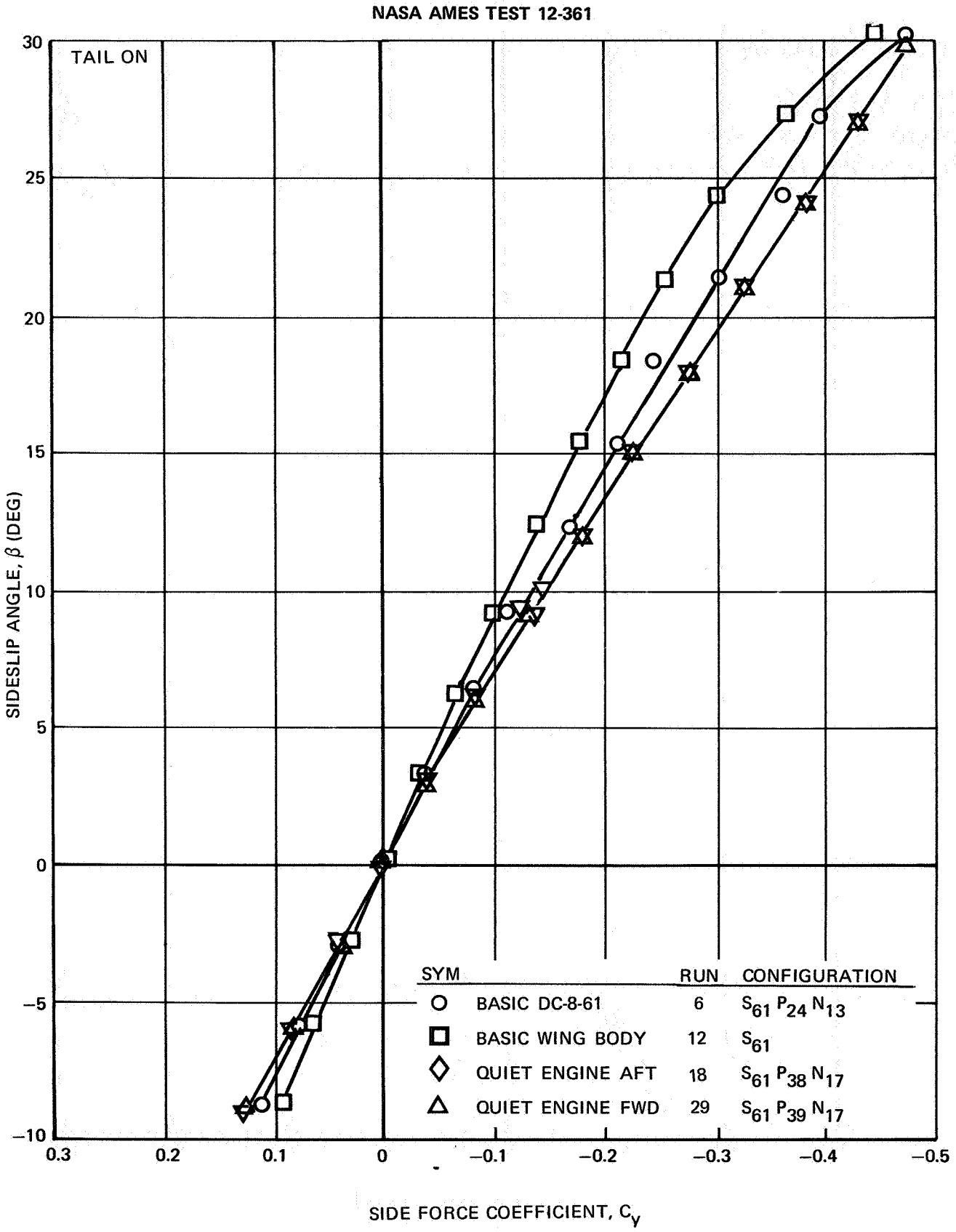

FIGURE III-87. EFFECT OF PYLONS AND NACELLES ON SIDE FORCE – $\delta_f = 0^o$, $i_H = 0^o$, $\alpha = 8^o$

NASA AMES TEST 12-361

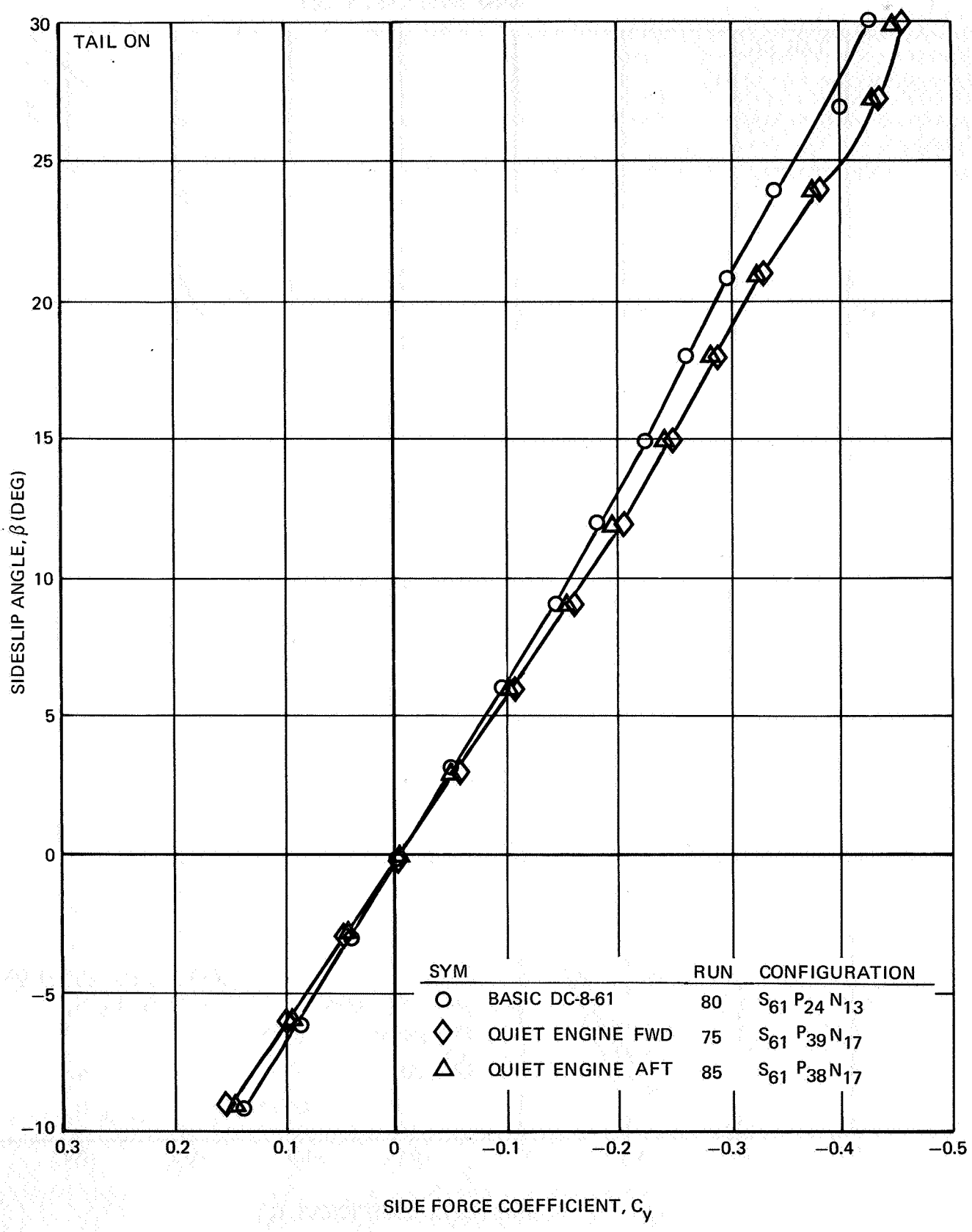

FIGURE III-88. EFFECT OF PYLONS AND NACELLES ON SIDE FORCE – $\delta_f = 25^o$, $i_H = 0^o$, $\alpha = 0^o$

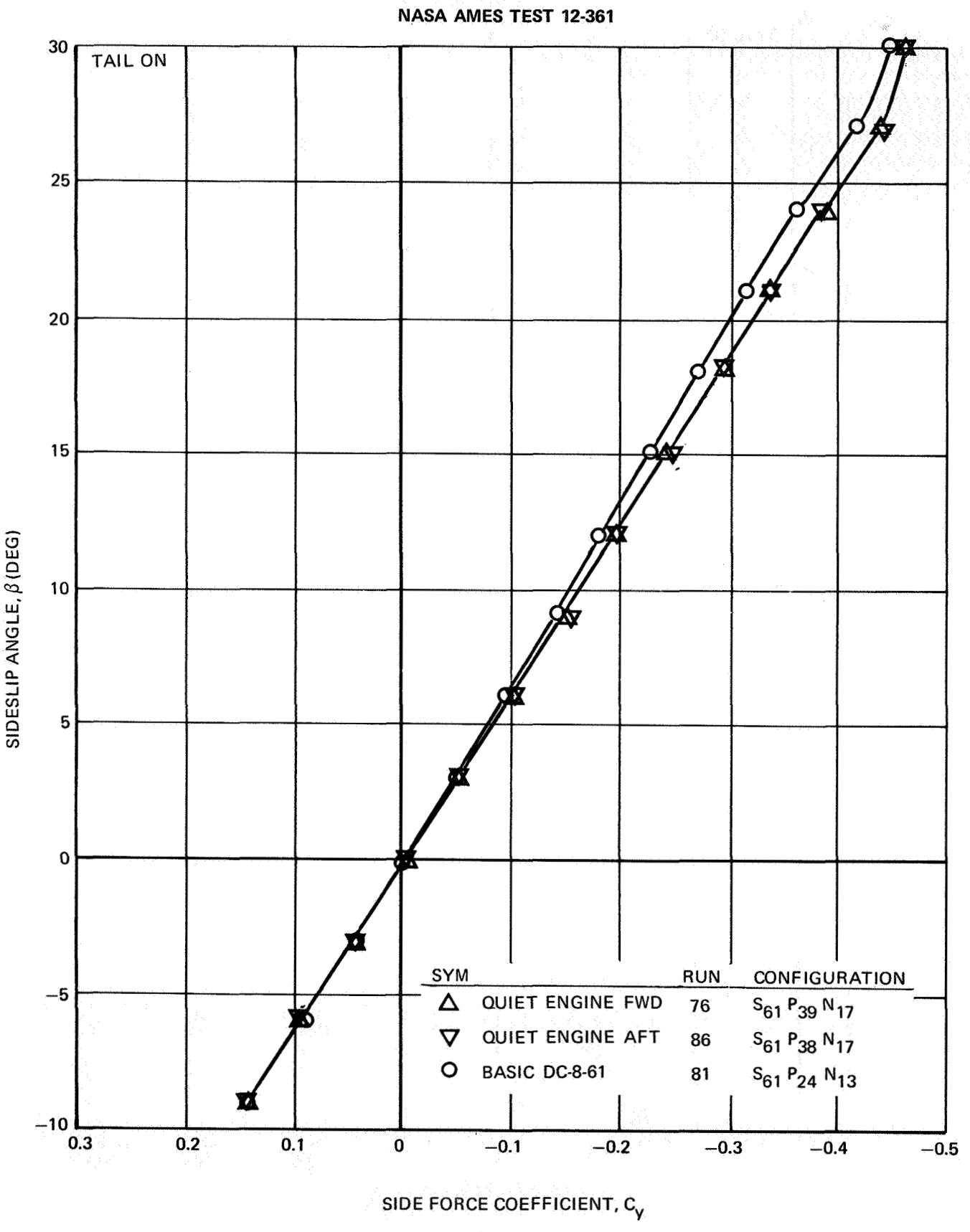

FIGURE III-89. EFFECT OF PYLONS AND NACELLES ON SIDE FORCE – $\delta_f = 25^o$, $\alpha_F = 4^o$, $i_H = 0^o$

NASA AMES TEST 12-361

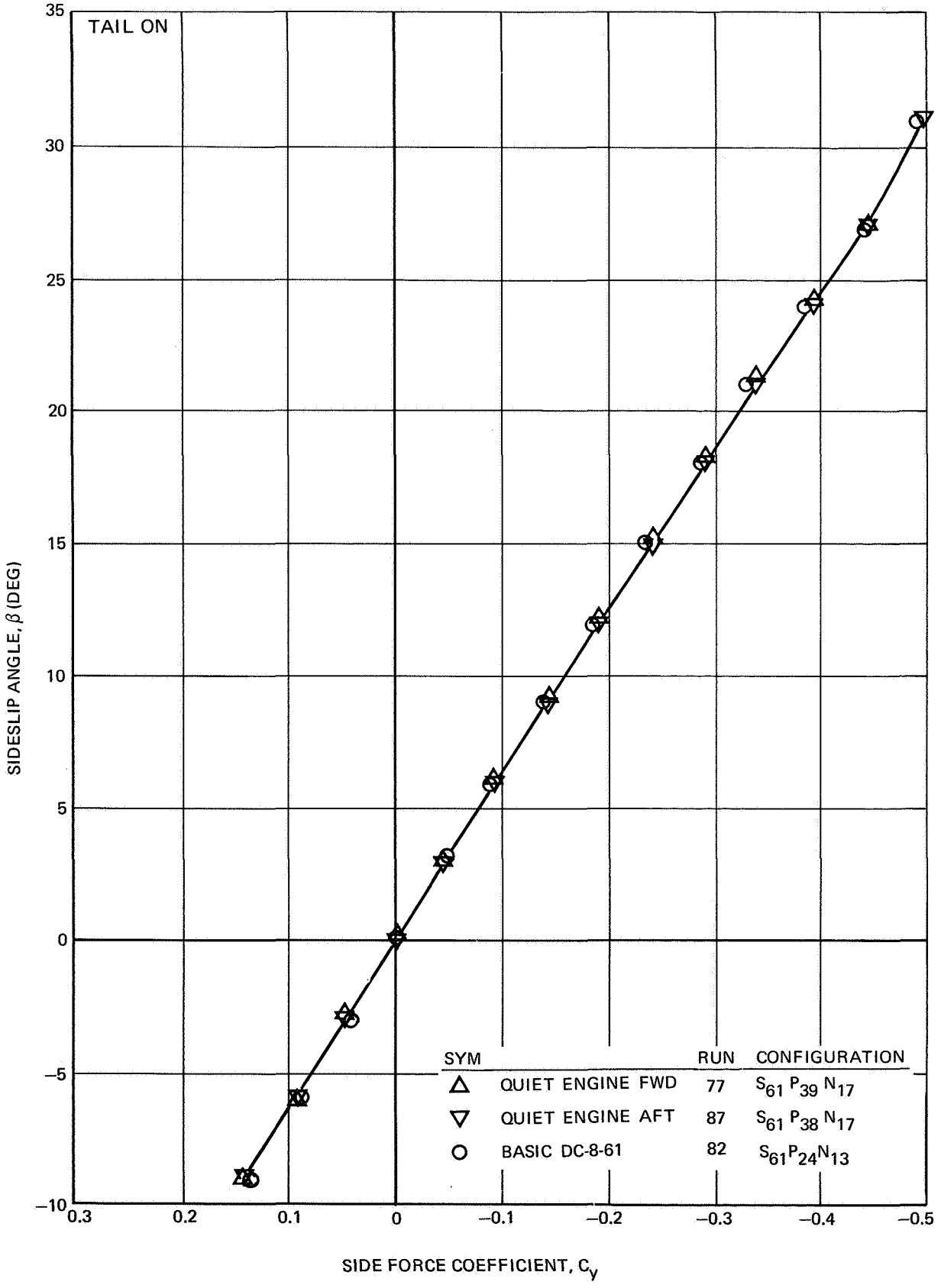

FIGURE III-90. EFFECT OF PYLONS AND NACELLES ON SIDE FORCE – $\delta_f = 25^o$, $a_F = 8^o$, $i_H = 0^o$

NASA AMES TEST 12-361

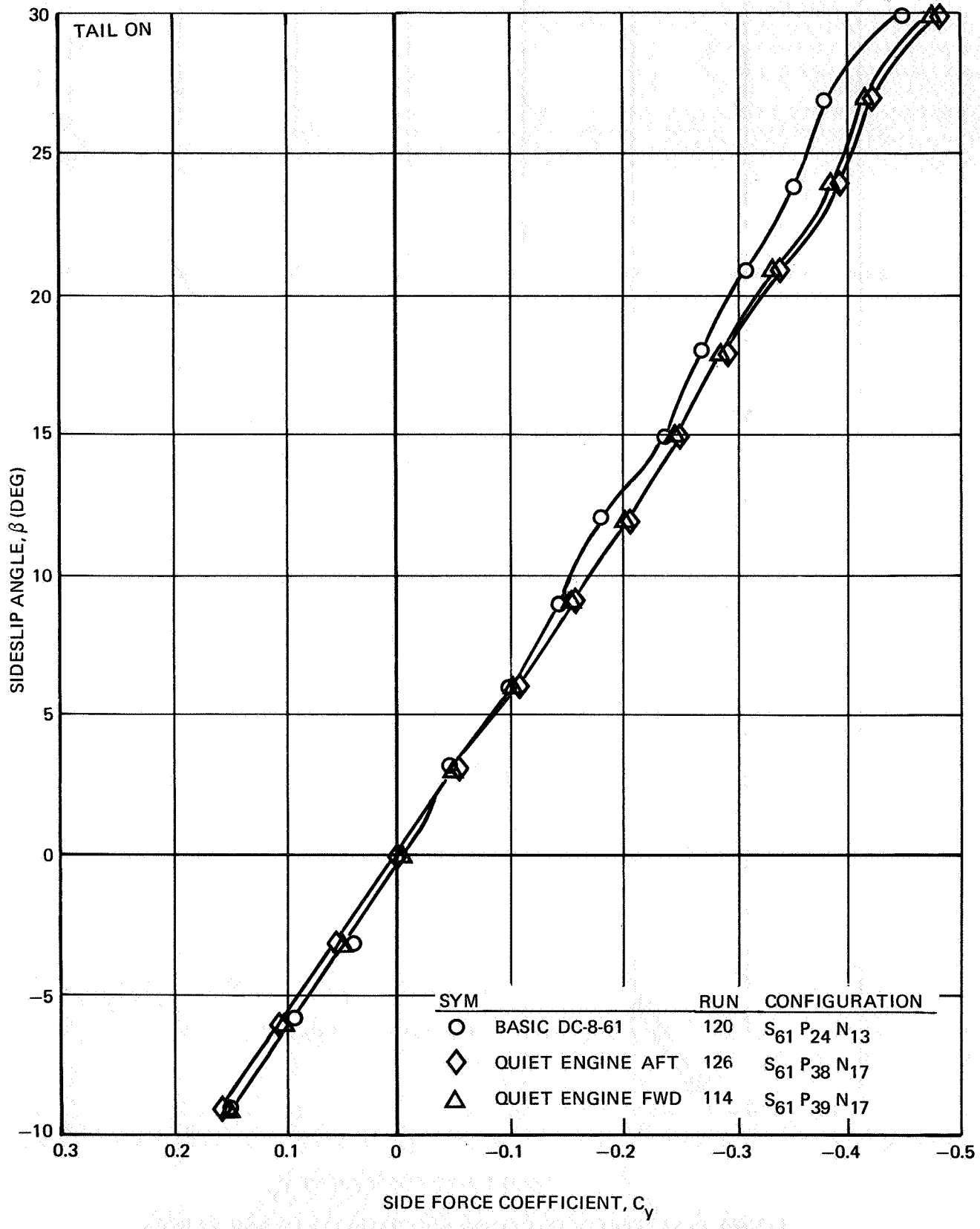

FIGURE III-91. EFFECT OF PYLONS AND NACELLES ON SIDE FORCE – $\delta_f = 50^o$, $\alpha_F = 0^o$, $i_H = 0^o$

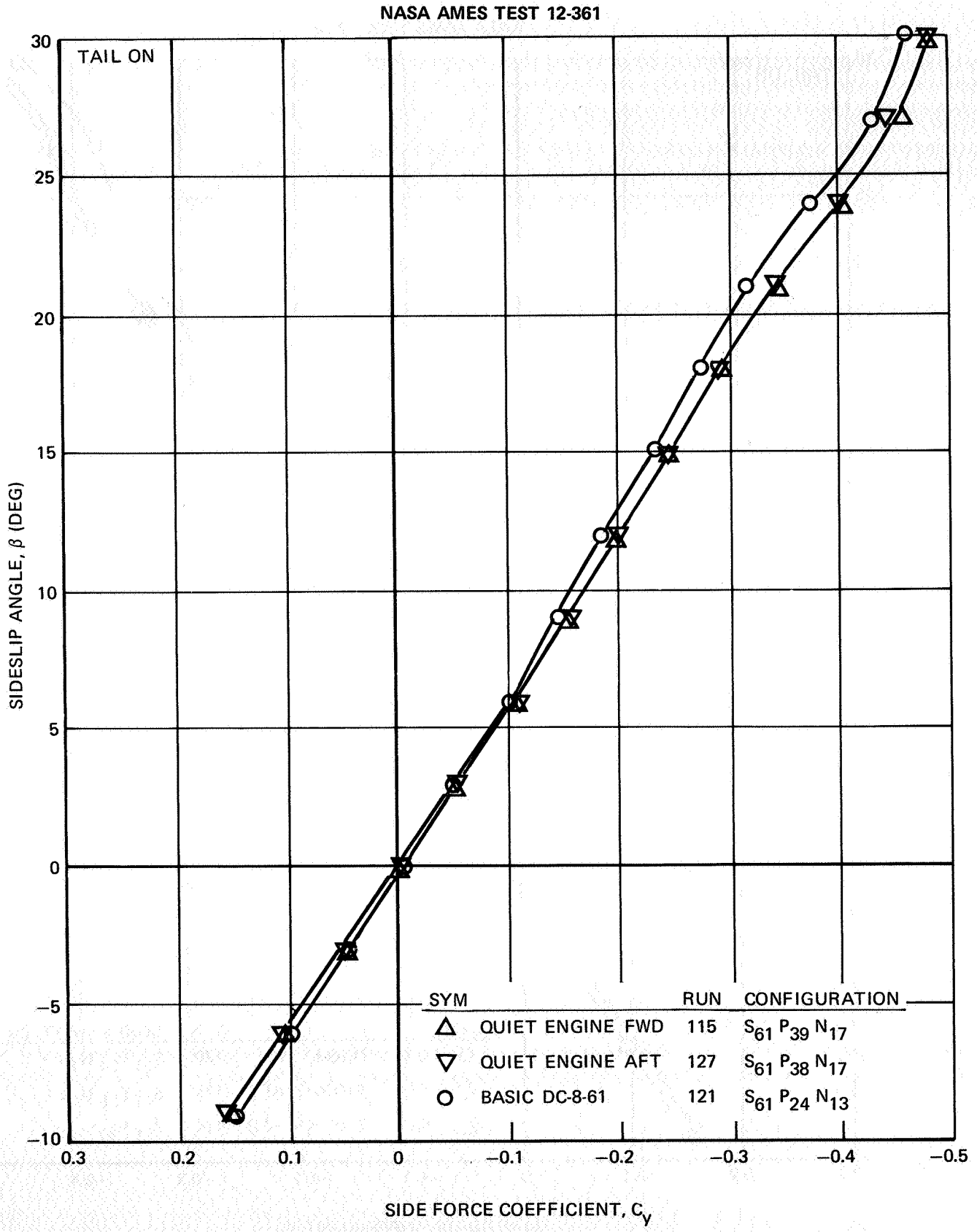

FIGURE III-92. EFFECT OF PYLONS AND NACELLES ON SIDE FORCE– $\delta_f = 50^o$, $\alpha_F = 4^o$, $i_H = 0^o$

NASA AMES TEST 12-361

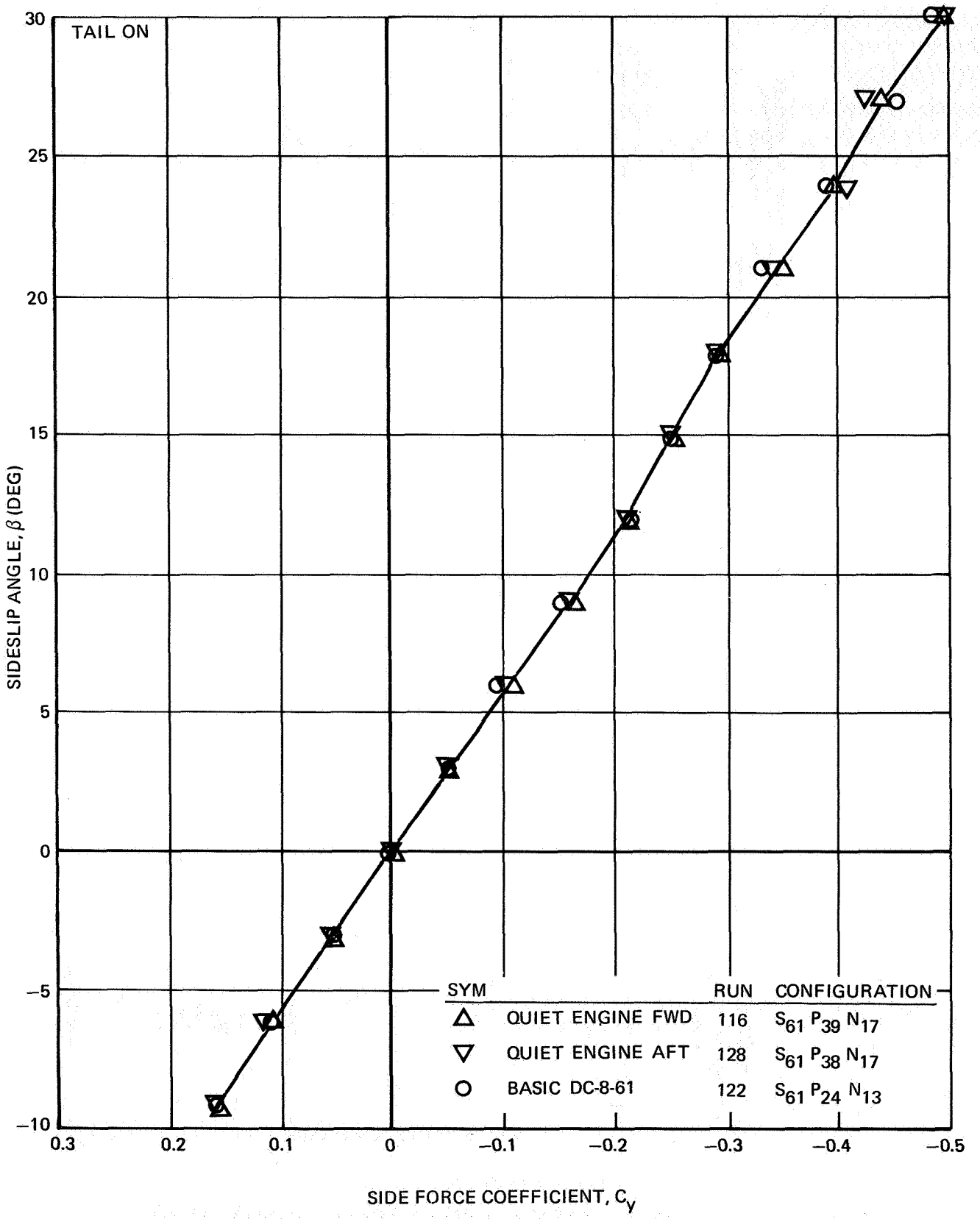

FIGURE III-93. EFFECT OF PYLONS AND NACELLES ON SIDE FORCE – $\delta_f = 50^o$ $\alpha_F = 8^o$, $i_H = 0^o$

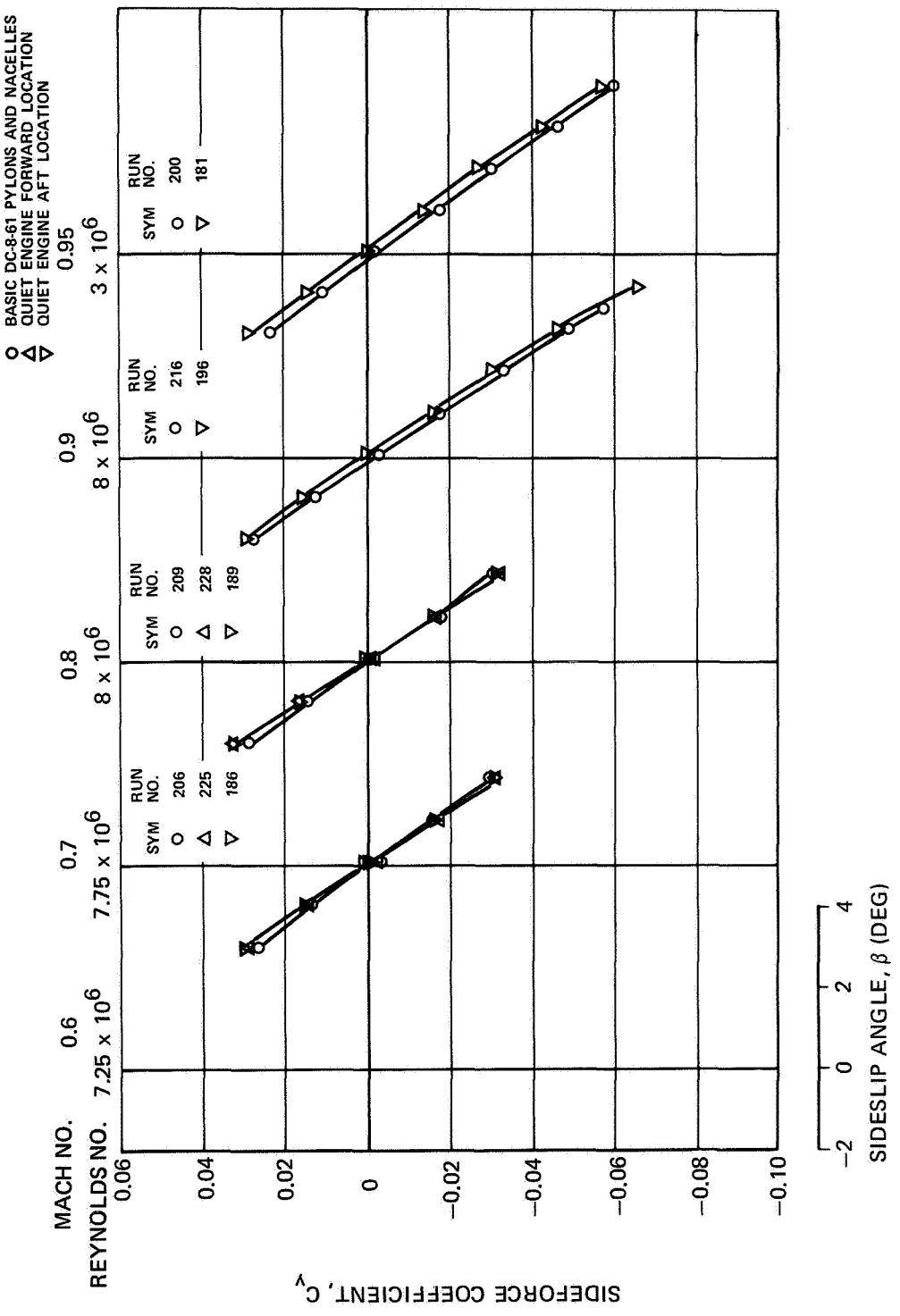

FIGURE III-94. EFFECT OF NACELLES AND PYLONS ON SIDE FORCE DUE TO SIDESLIP – $\delta_f = 0^o, \alpha_F = 0^o$

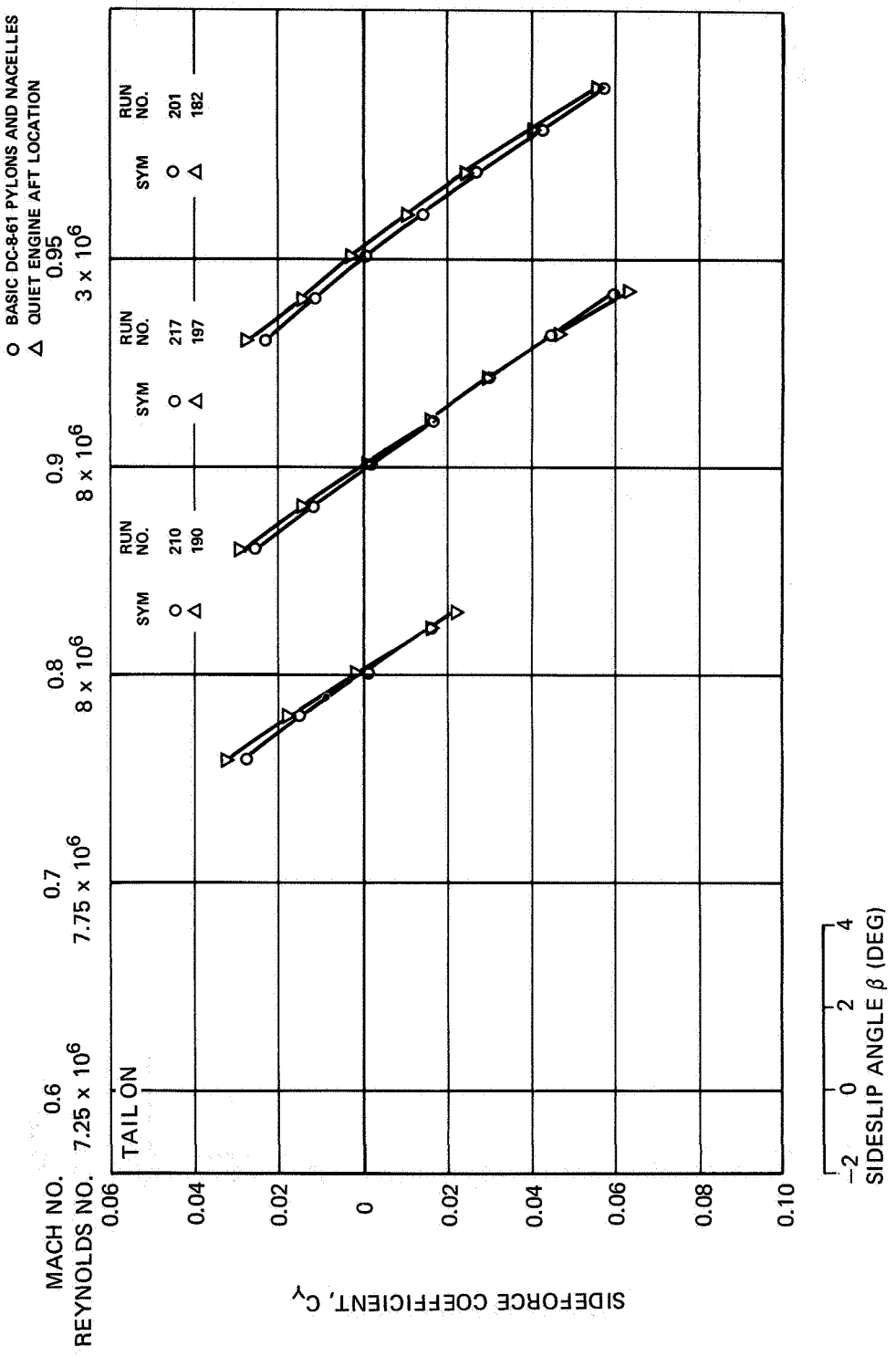

FIGURE III-95. EFFECT OF NACELLES AND PYLONS ON SIDE FORCE DUE TO SIDESLIP – $\delta_f = 0^o$, $\alpha_F = 2.1^o$

NASA AMES TEST 11-353

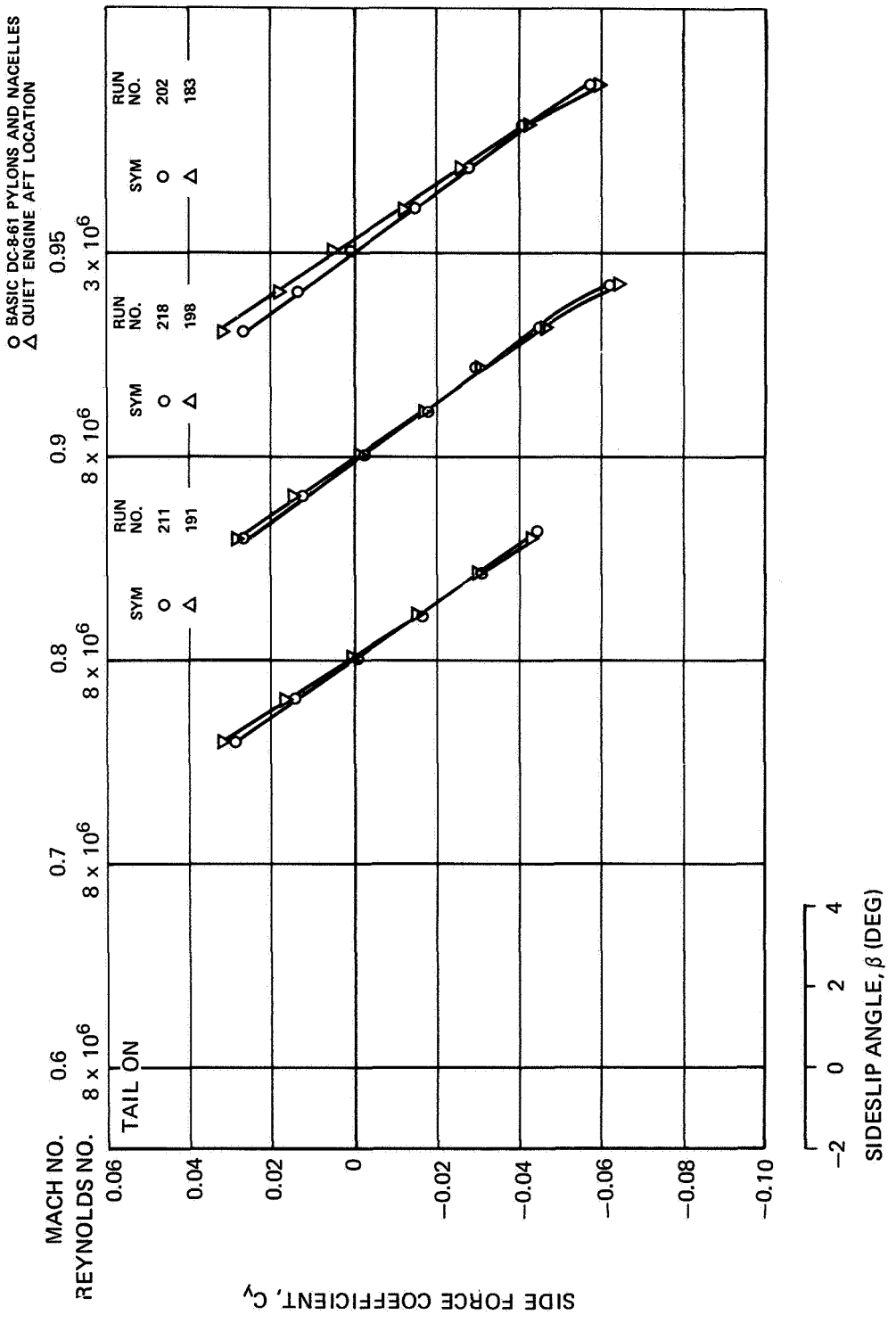

FIGURE III-96. EFFECT OF NACELLES AND PYLONS ON SIDE FORCE DUE TO SIDESLIP — $\delta_f = 0^o$, $\alpha_F = 4.1^o$

NASA AMES TEST 12-361

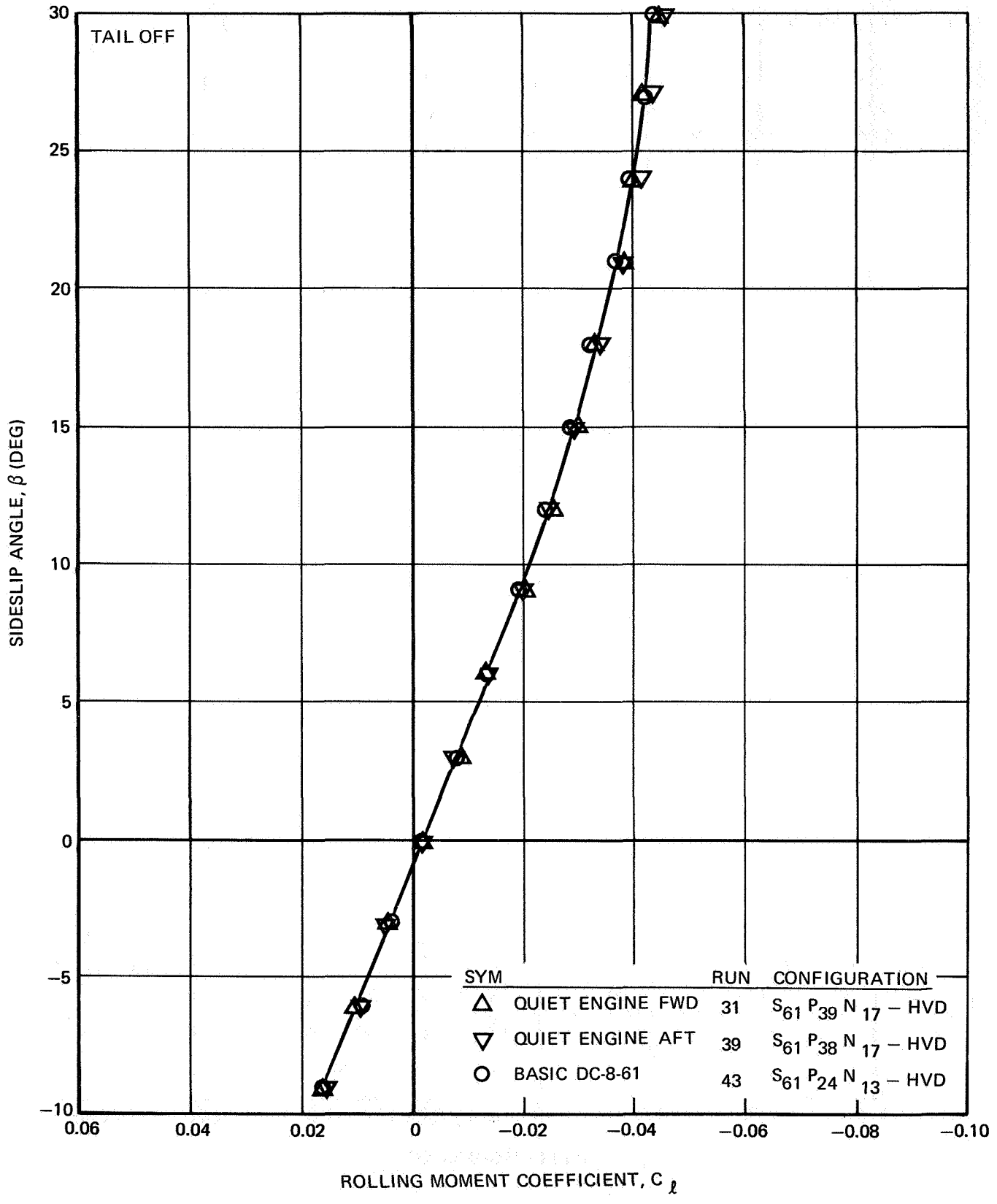

FIGURE III-97. EFFECT OF PYLONS AND NACELLES ON ROLLING MOMENT – $\delta_f = 0^o$, $\alpha_F = 0^o$

NASA AMES TEST 12-361

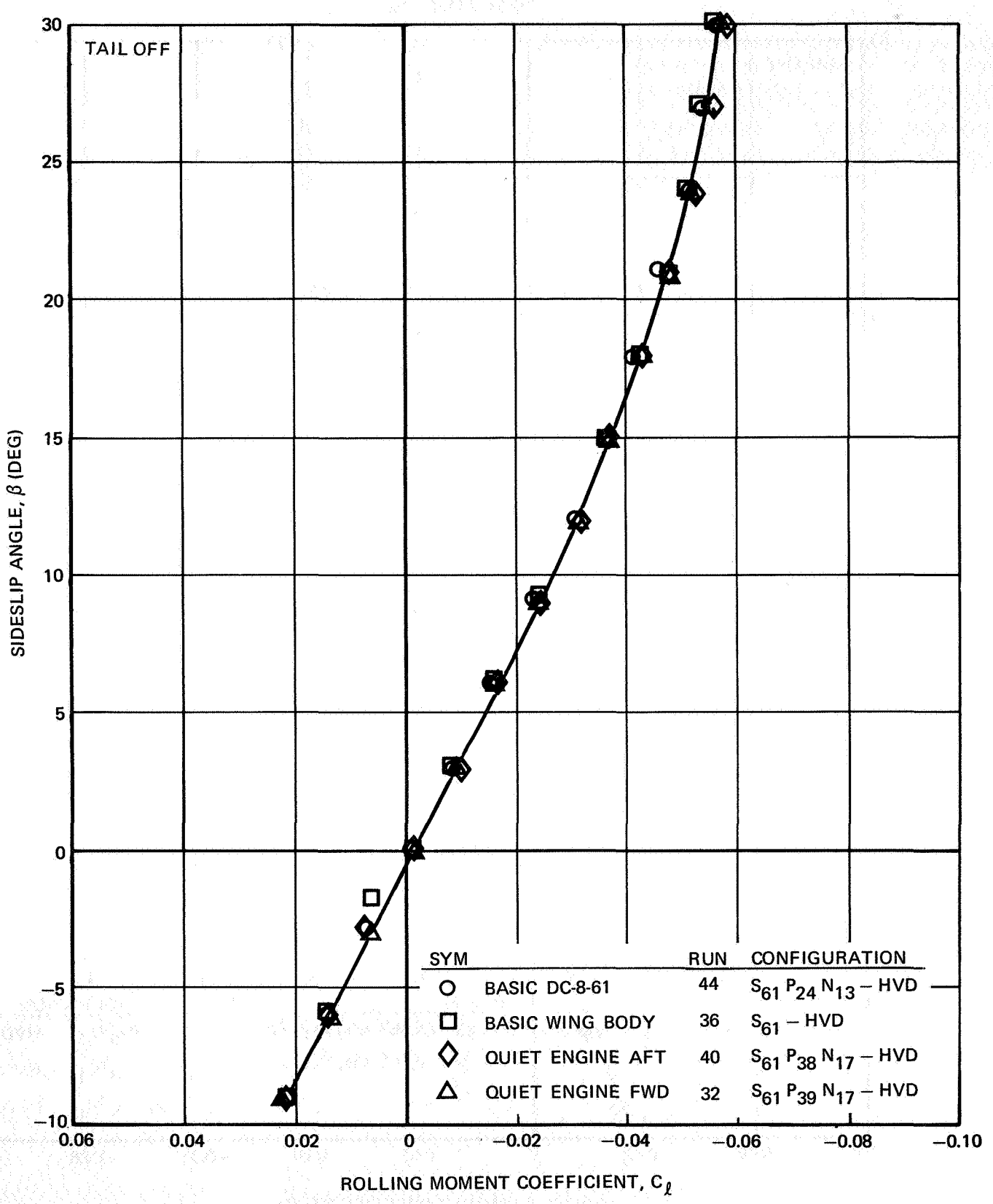

FIGURE III-98. EFFECT OF PYLONS AND NACELLES ON ROLLING MOMENT – δ_f = 0°, a_F = 4°

NASA AMES TEST 12-361

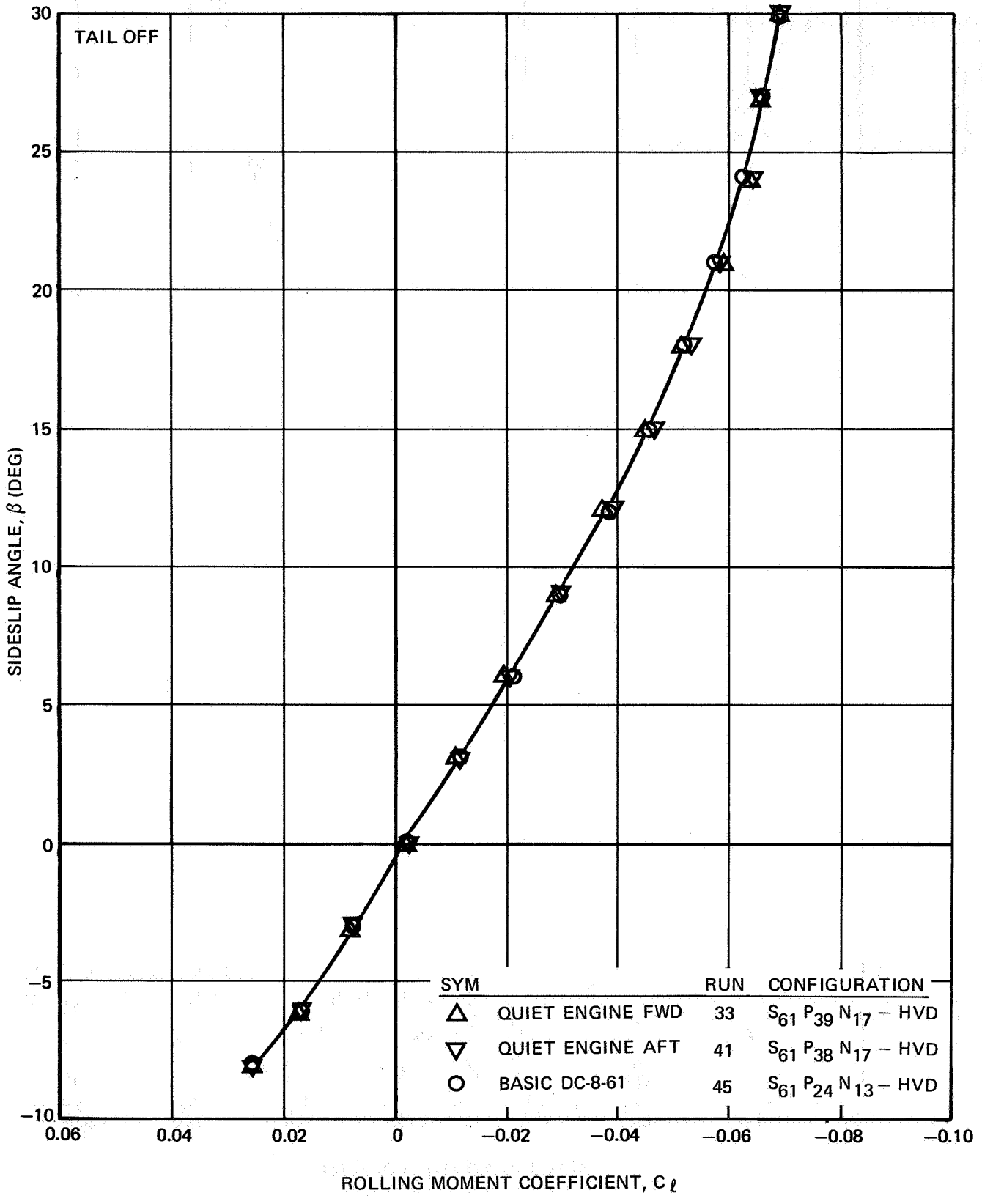

FIGURE III-99. EFFECT OF PYLONS AND NACELLES ON ROLLING MOMENT – $\delta_f = 0^o$, $a_F = 8^o$

NASA AMES TEST 12-361

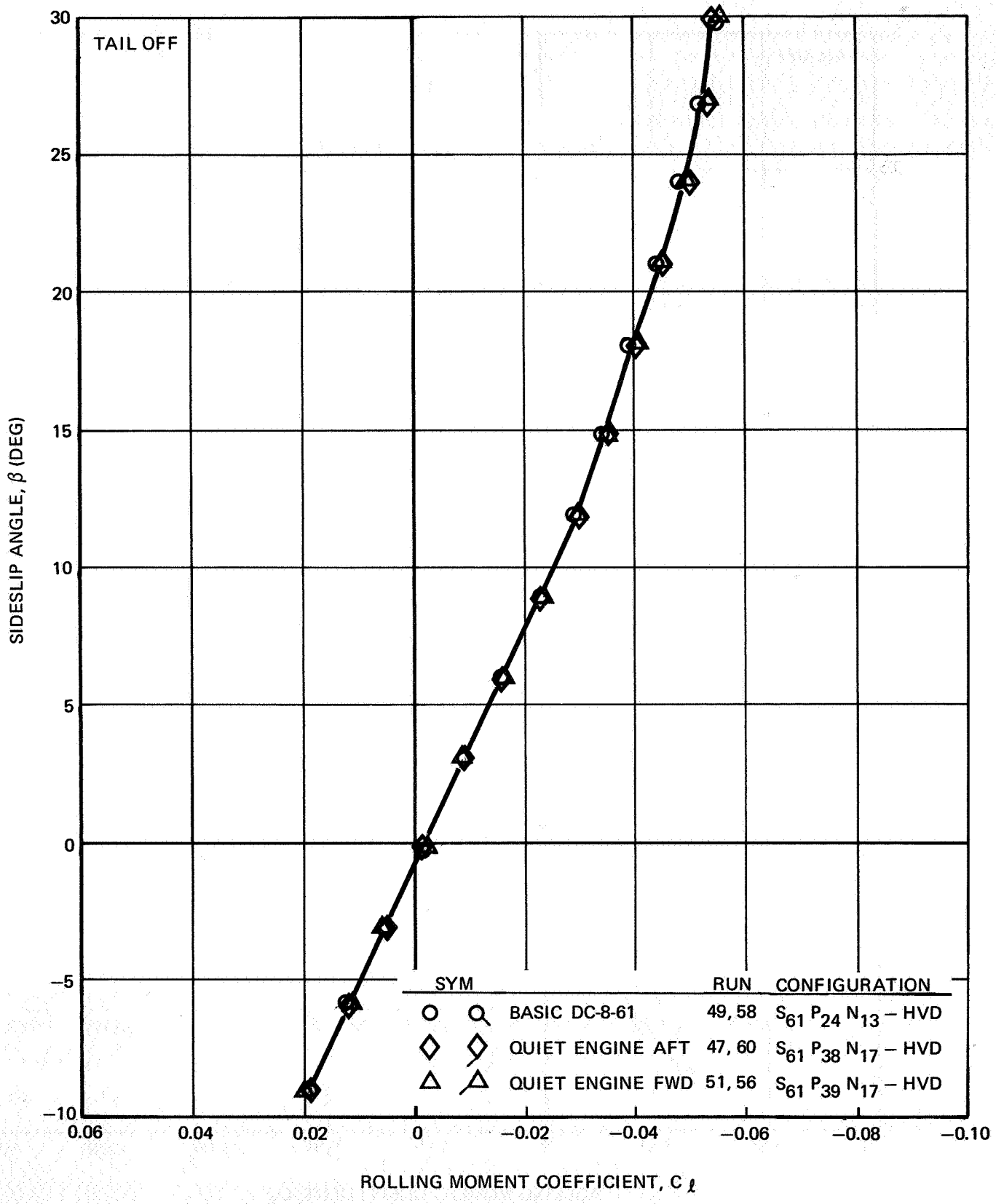

FIGURE III-100. EFFECT OF PYLONS AND NACELLES ON ROLLING MOMENT – δ_f 15°, a_F = 0°

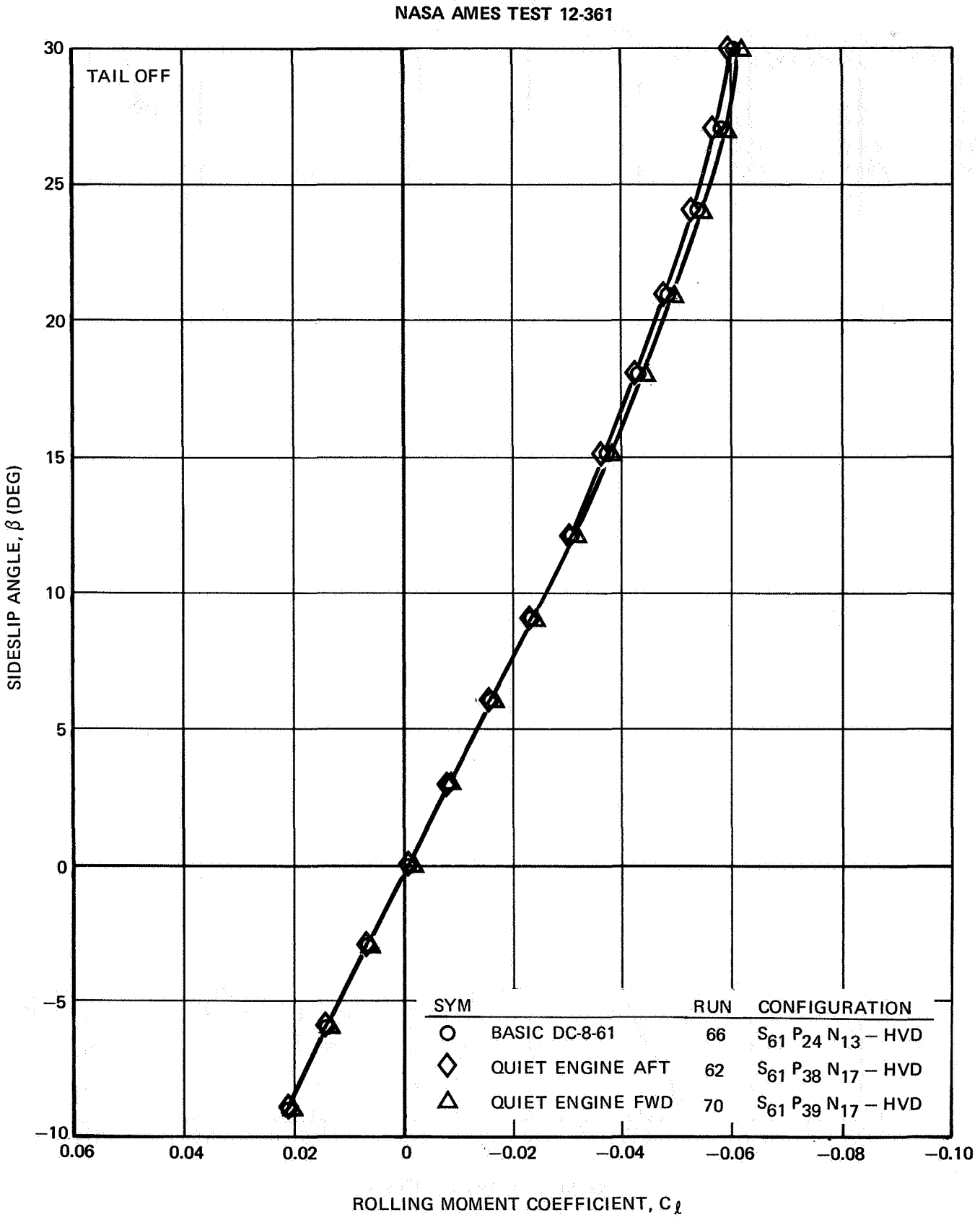

FIGURE III-101. EFFECT OF PYLONS AND NACELLES ON ROLLING MOMENT – $\delta_f = 25^o$, $a_F = 0^o$

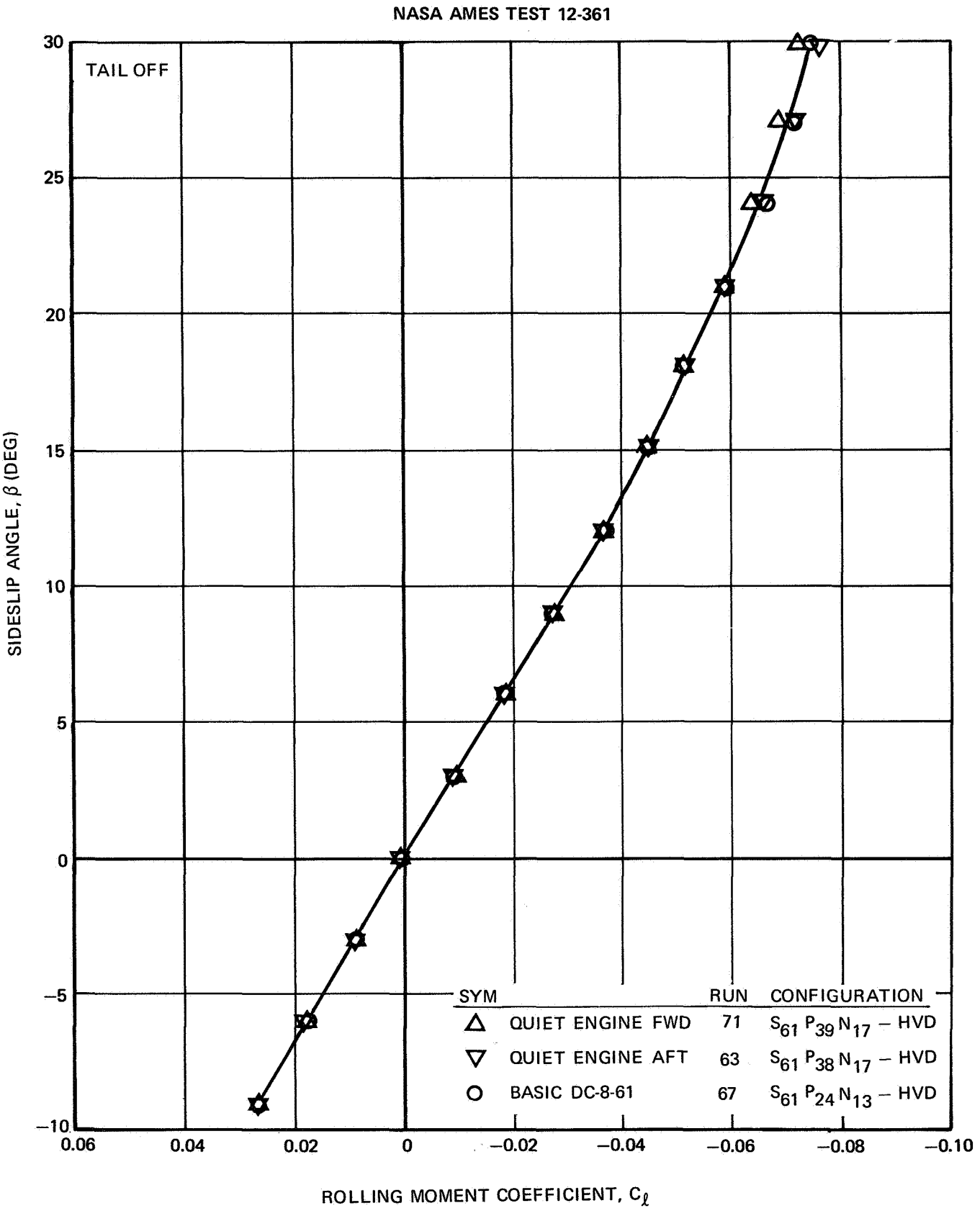

FIGURE III-102. EFFECT OF PYLONS AND NACELLES ON ROLLING MOMENT – $\delta_f = 25^o$, $a_F = 4^o$

NASA AMES TEST 12-361

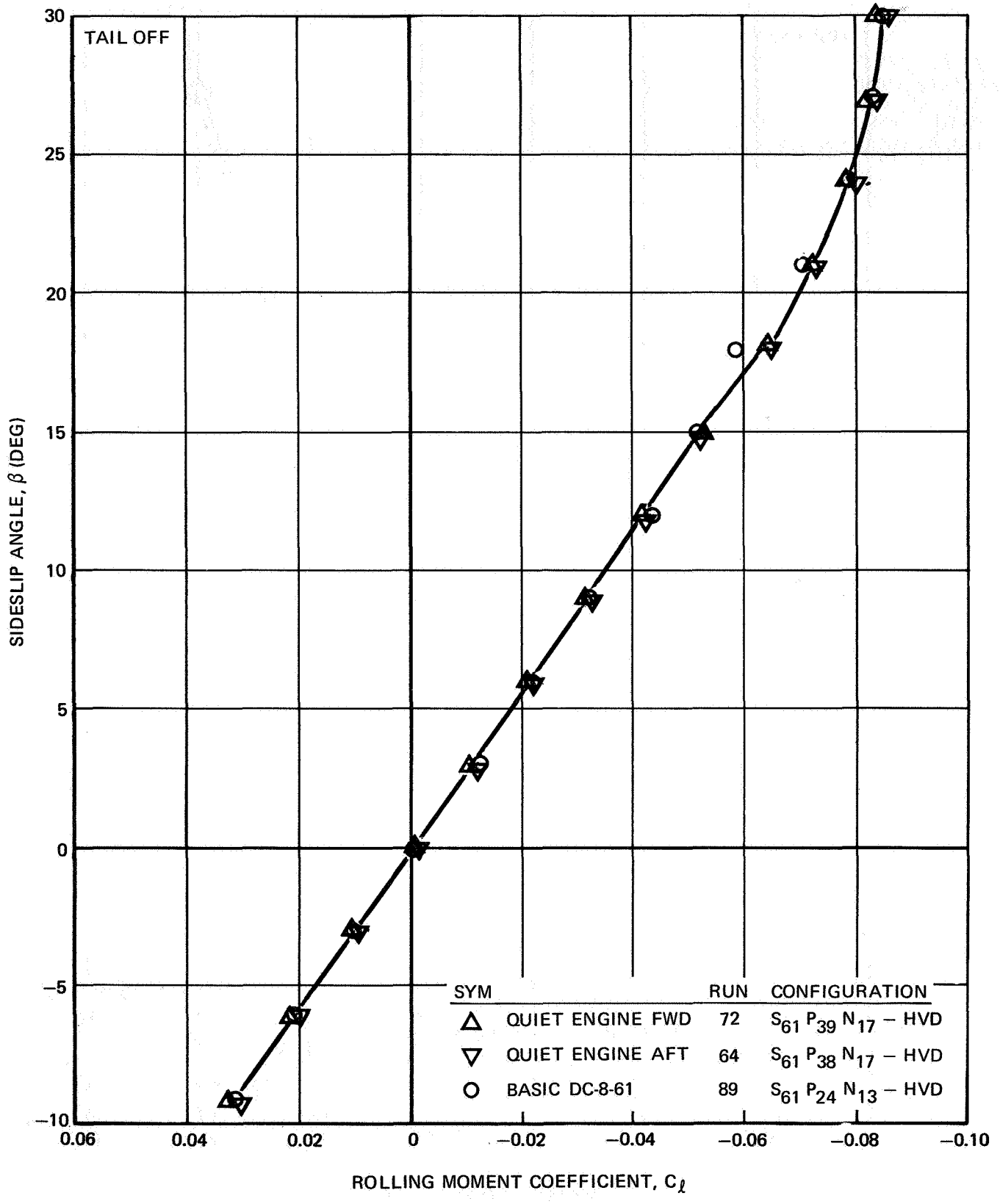

FIGURE III-103. EFFECT OF PYLONS AND NACELLES ON ROLLING MOMENT – $\delta_f = 25^o$, $\alpha_F = 8^o$

NASA AMES TEST 12-361

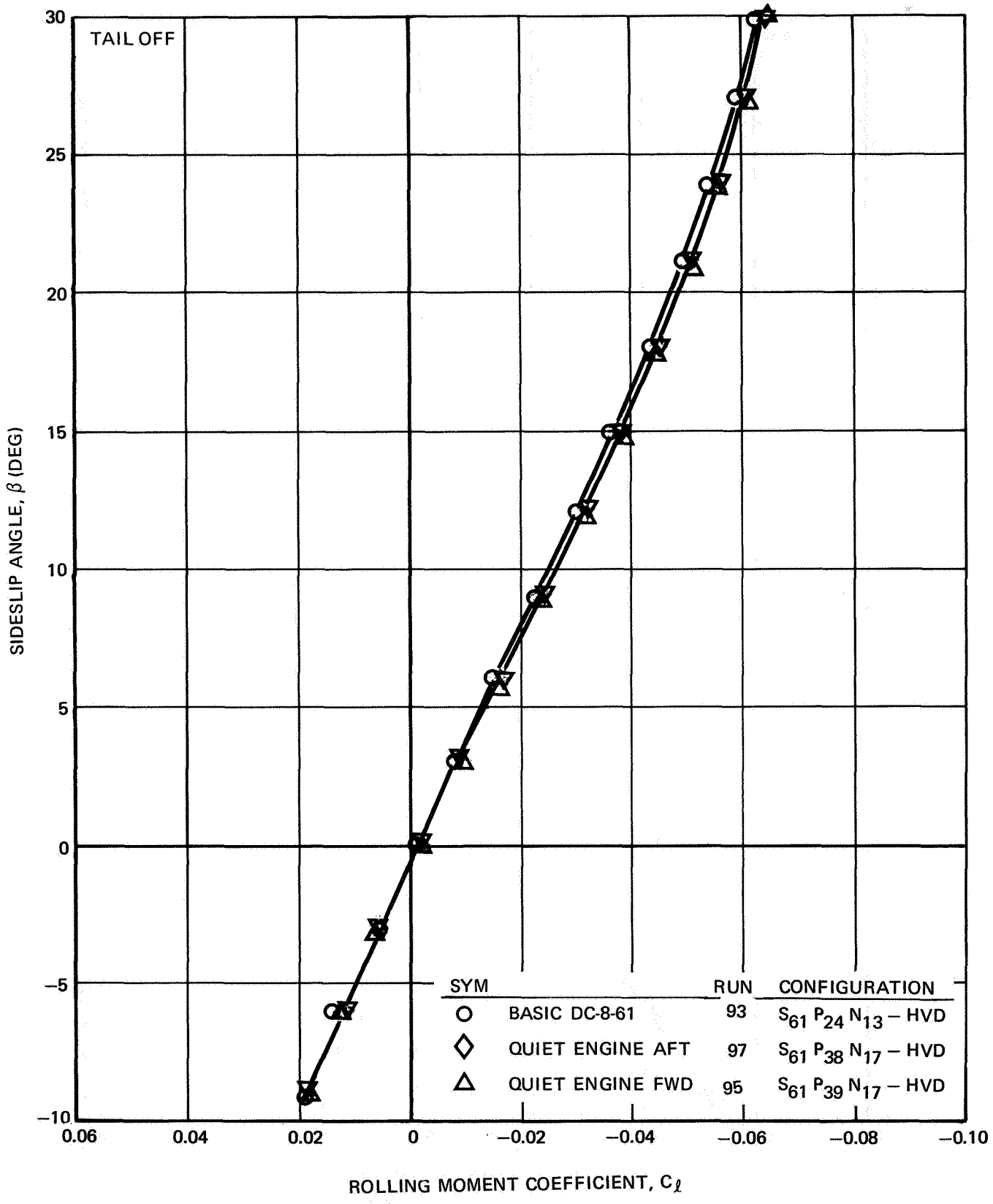

FIGURE III-104. EFFECT OF PYLONS AND NACELLES ON ROLLING MOMENT – $\delta_f = 35^o$, $a_F = 0^o$

NASA AMES TEST 12-361

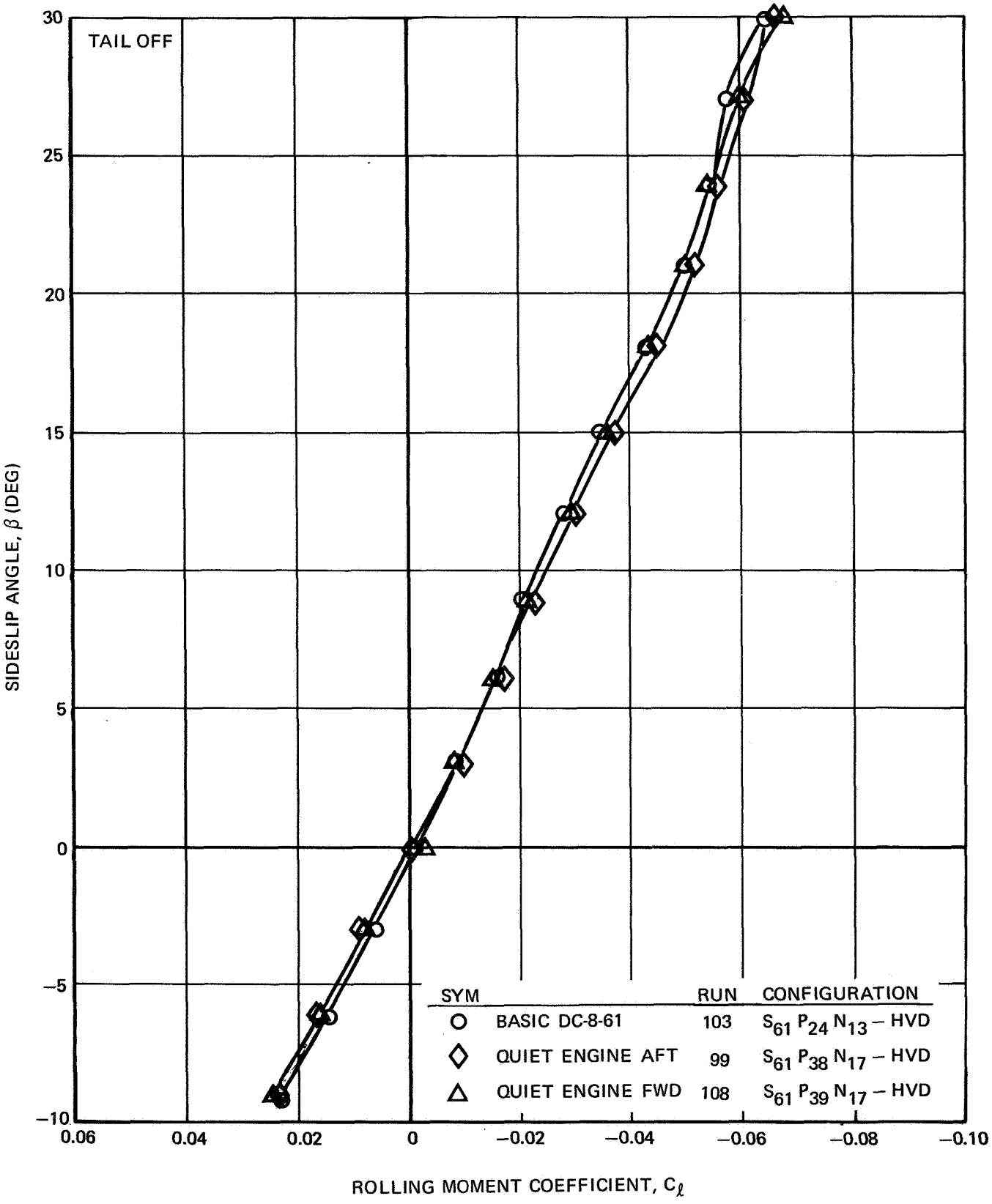

FIGURE III-105. EFFECT OF PYLONS AND NACELLES ON ROLLING MOMENT – $\delta_f = 50^o$, $a_F = 0^o$

NASA AMES TEST 12-361

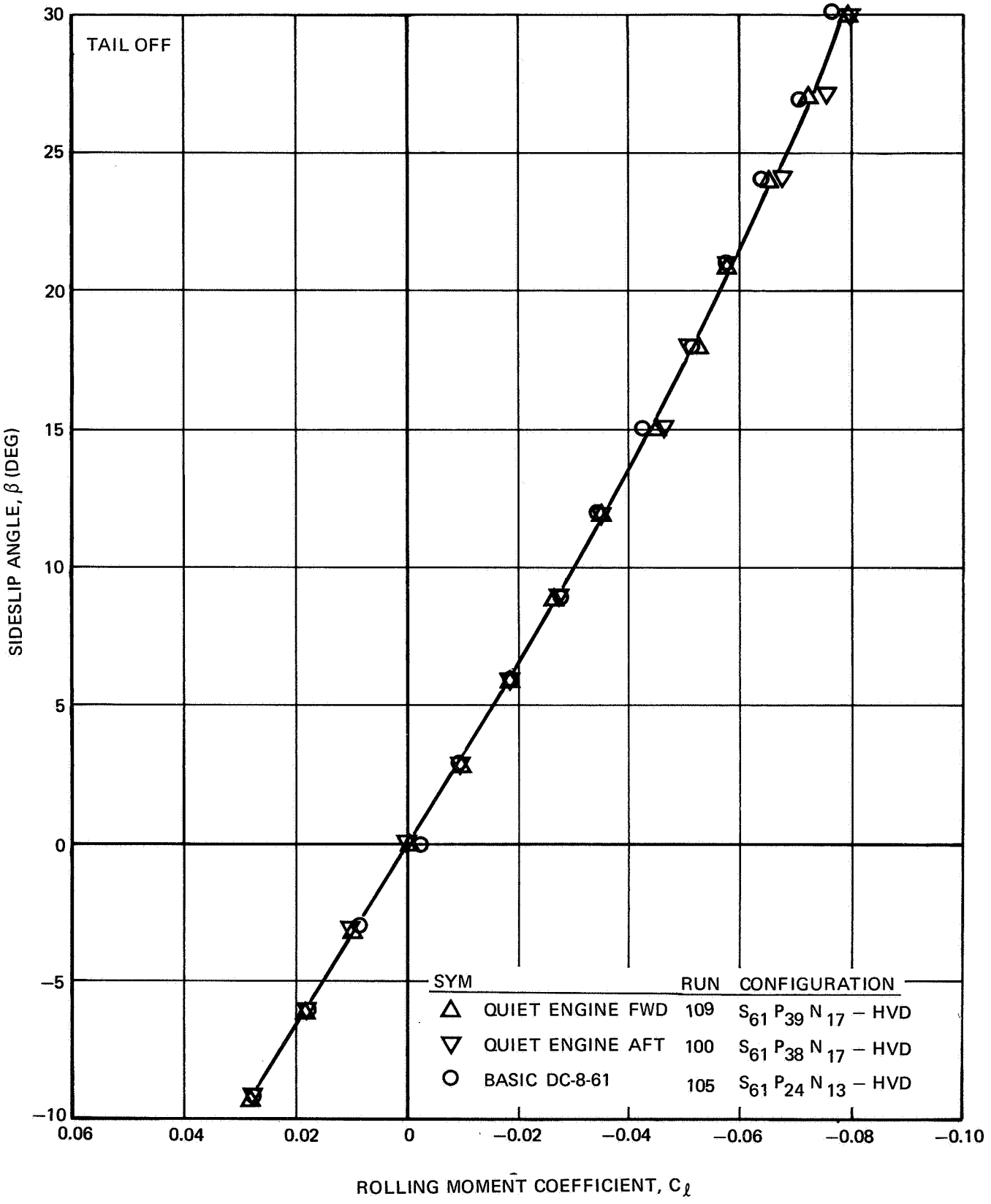

FIGURE III-106. EFFECT OF PYLONS AND NACELLES ON ROLLING MOMENT – δ_f = 50°, α_F = 4°

NASA AMES TEST 12-361

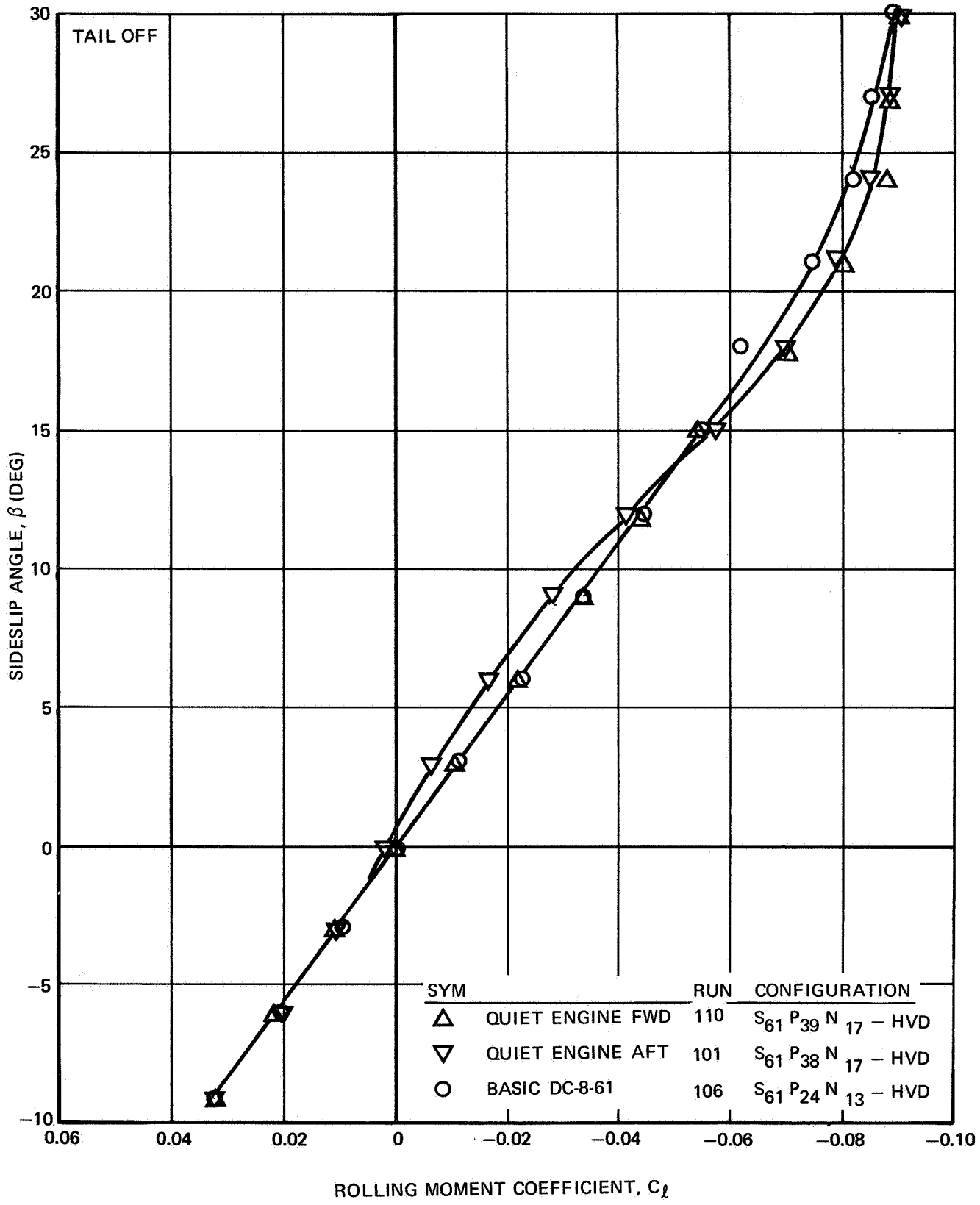

FIGURE III-107. EFFECT OF PYLONS AND NACELLES ON ROLLING MOMENT – $\delta_f = 50^o$, $a_F = 8^o$

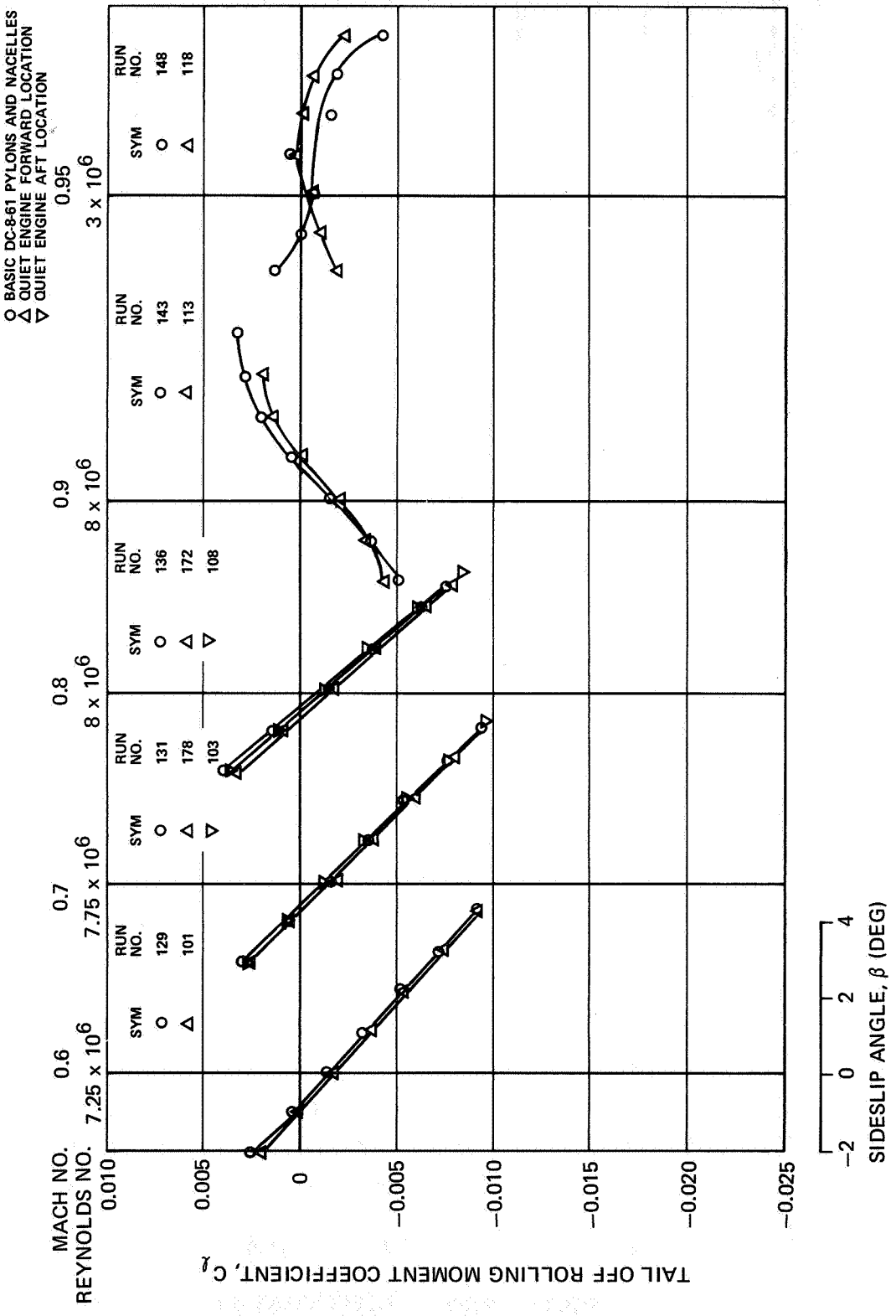

FIGURE III-108. EFFECT OF NACELLES AND PYLONS ON TAIL-OFF ROLLING MOMENT DUE TO SIDESLIP – $\delta_f = 0^o$, $\alpha_F = 0^o$

NASA AMES TEST 12-361

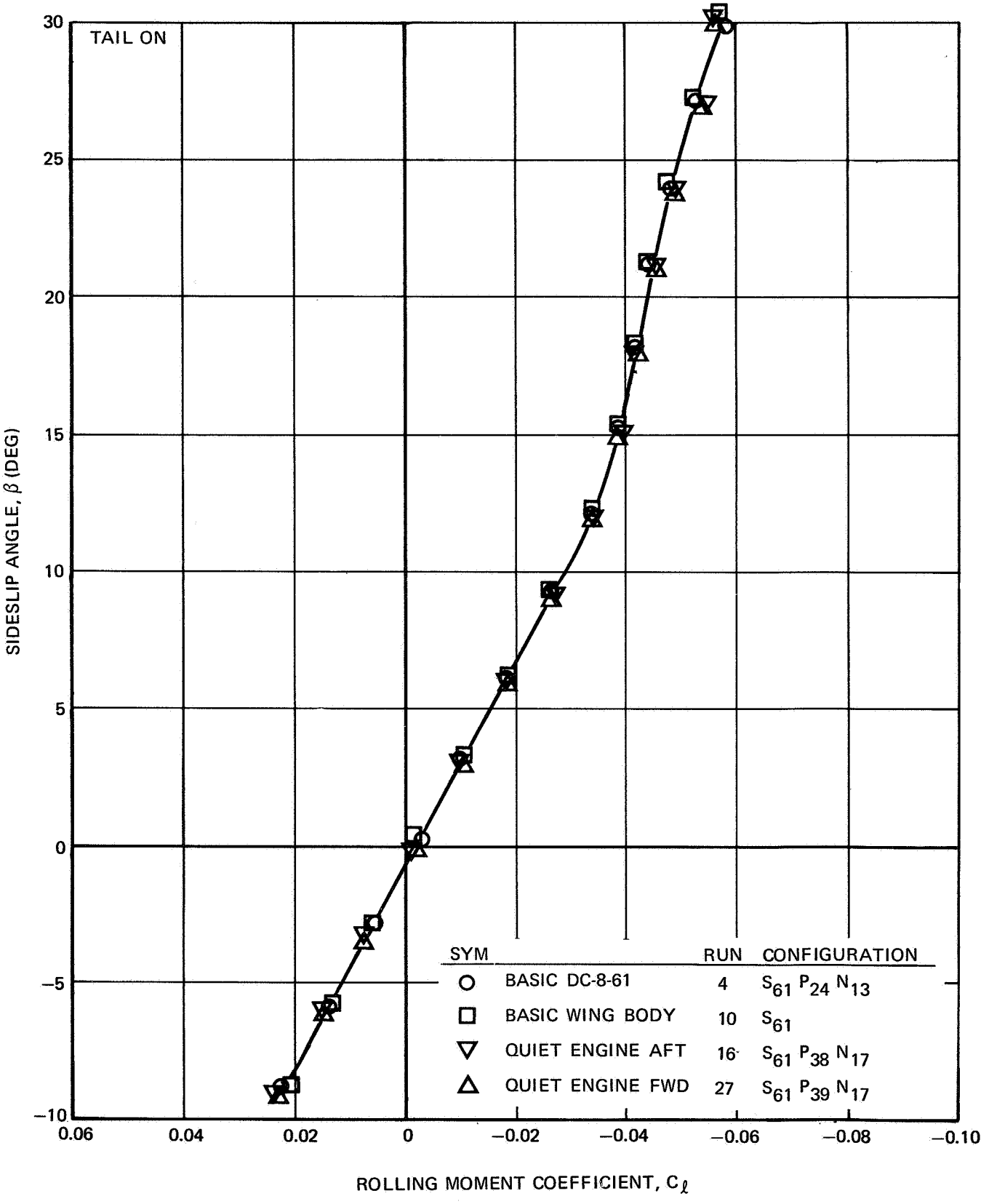

FIGURE III-109. EFFECT OF PYLONS AND NACELLES ON ROLLING MOMENT – δ_f = 0°, i_H = 0°, a = 0°

NASA AMES TEST 12-361

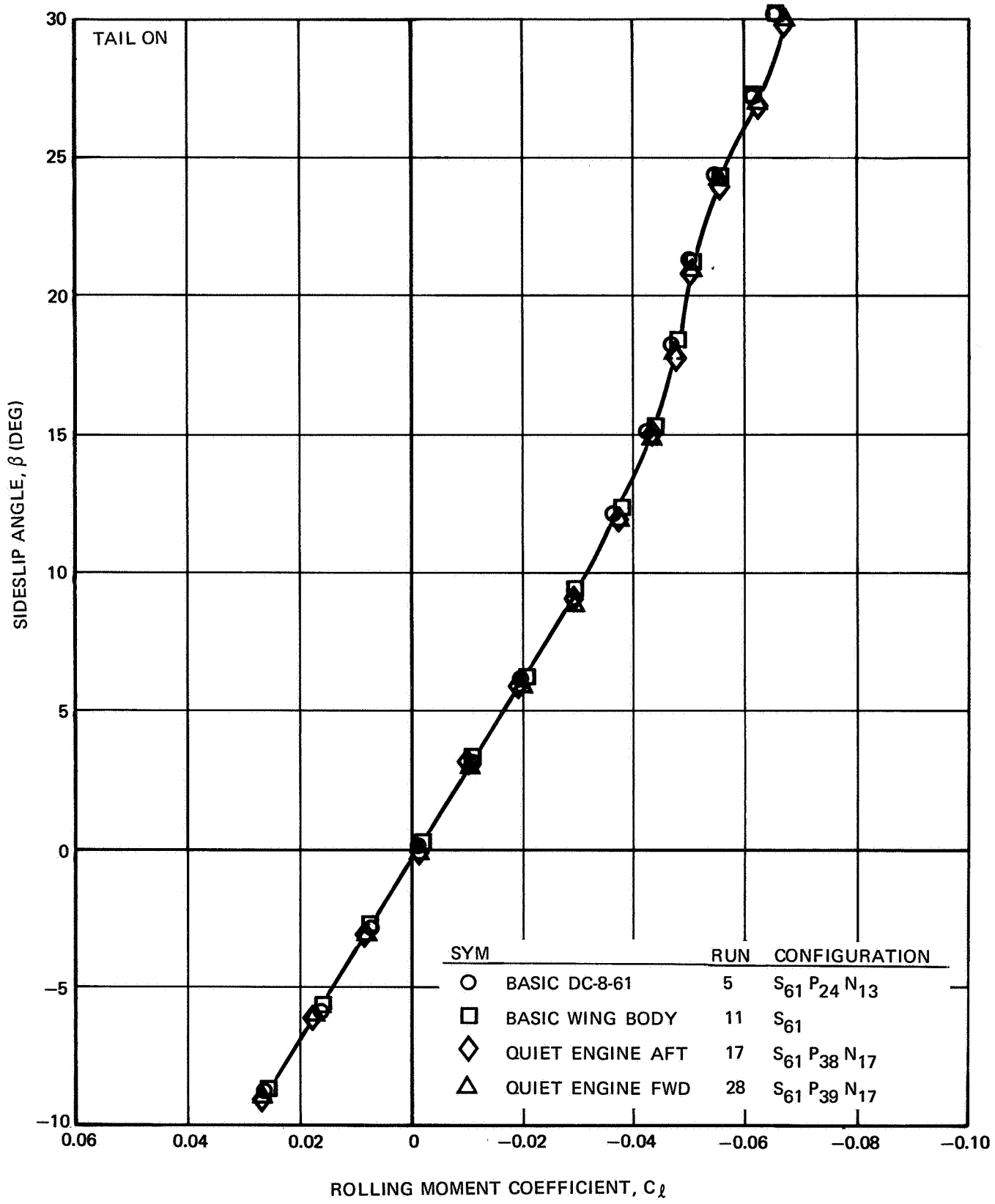

FIGURE III-110. EFFECT OF PYLONS AND NACELLES ON ROLLING MOMENT – $\delta_f = 0^o$, $i_H = 0^o$, $\alpha = 4^o$

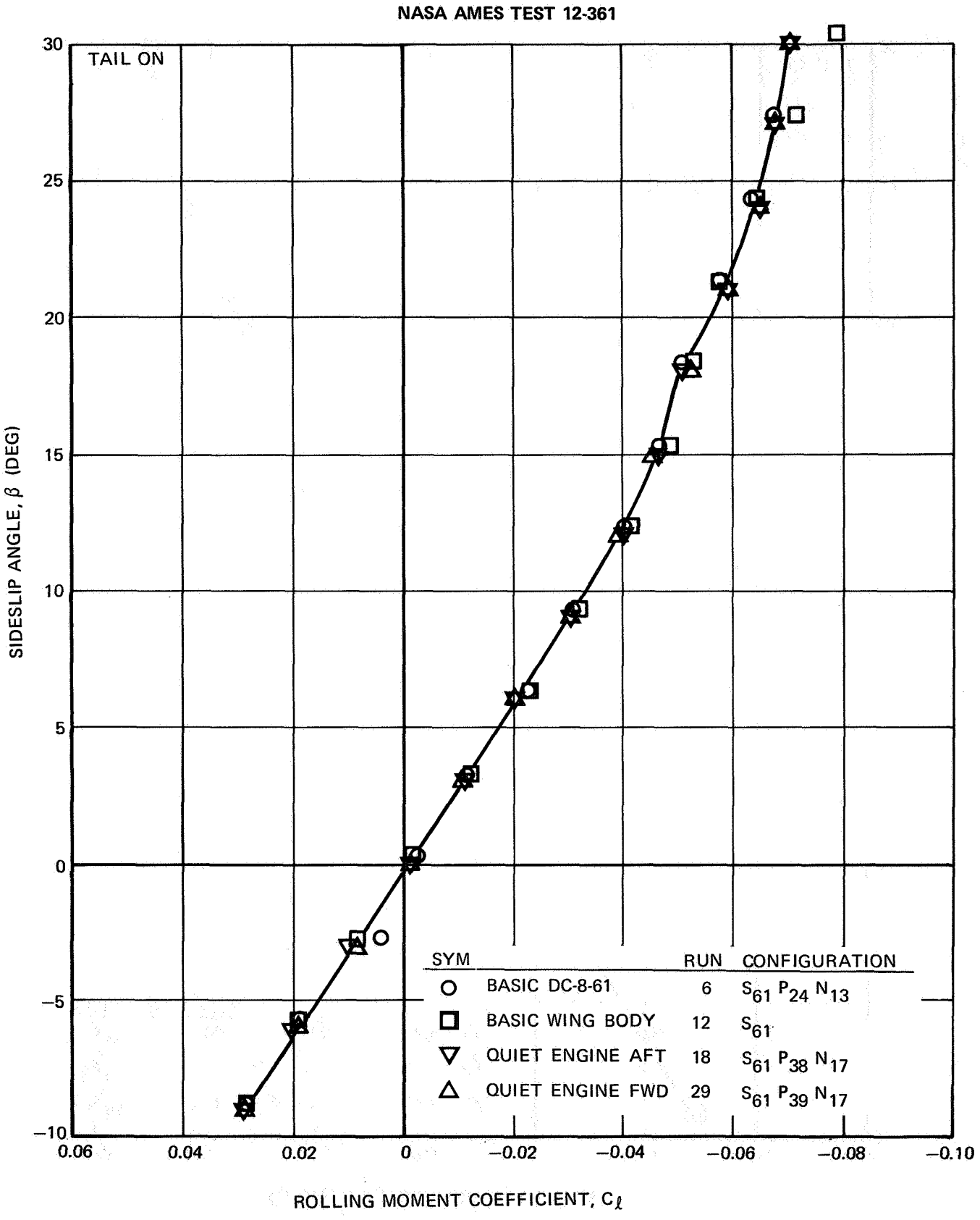

FIGURE III-111. EFFECT OF PYLONS AND NACELLES ON ROLLING MOMENT – $\delta_f = 0^o$, $i_H = 0^o$, $\alpha = 8^o$

NASA AMES TEST 12-361

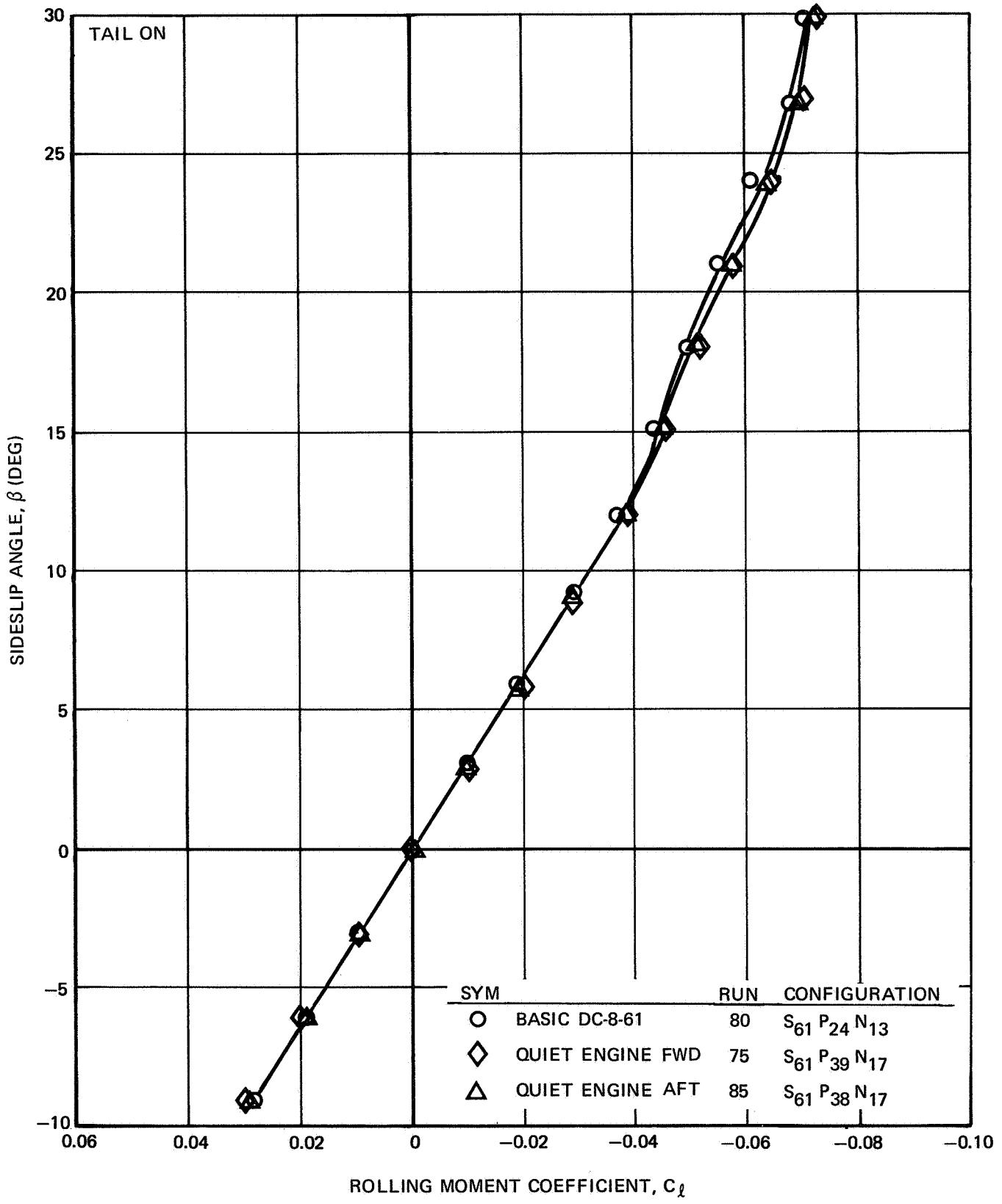

FIGURE III-112. EFFECT OF PYLONS AND NACELLES ON ROLLING MOMENT – δ_f = 25°, i_H = 0°, α = 0°

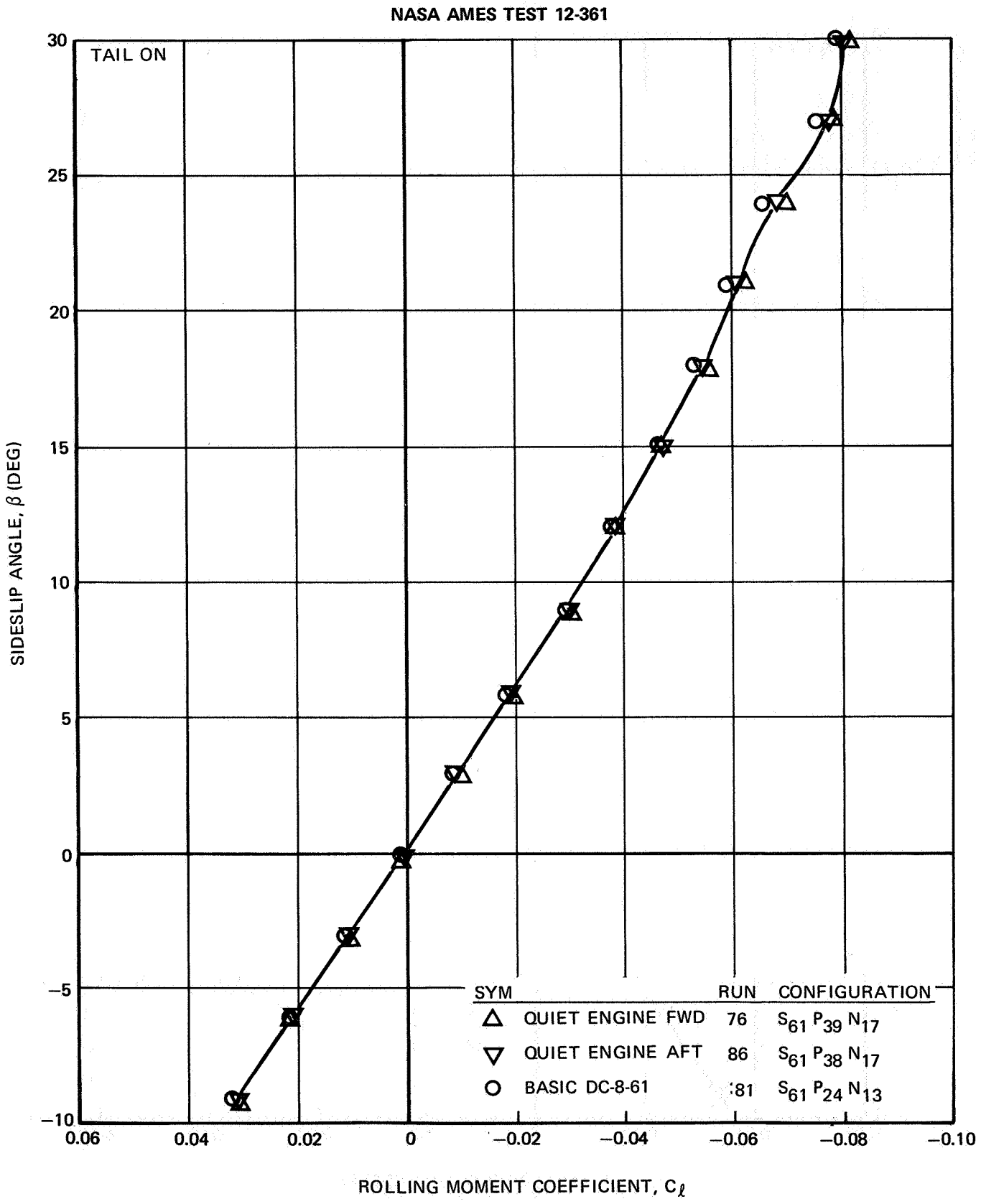

FIGURE III-113. EFFECT OF PYLONS AND NACELLES ON ROLLING MOMENT – δ_f = 25°, a_F = 4°, i_H = 0°

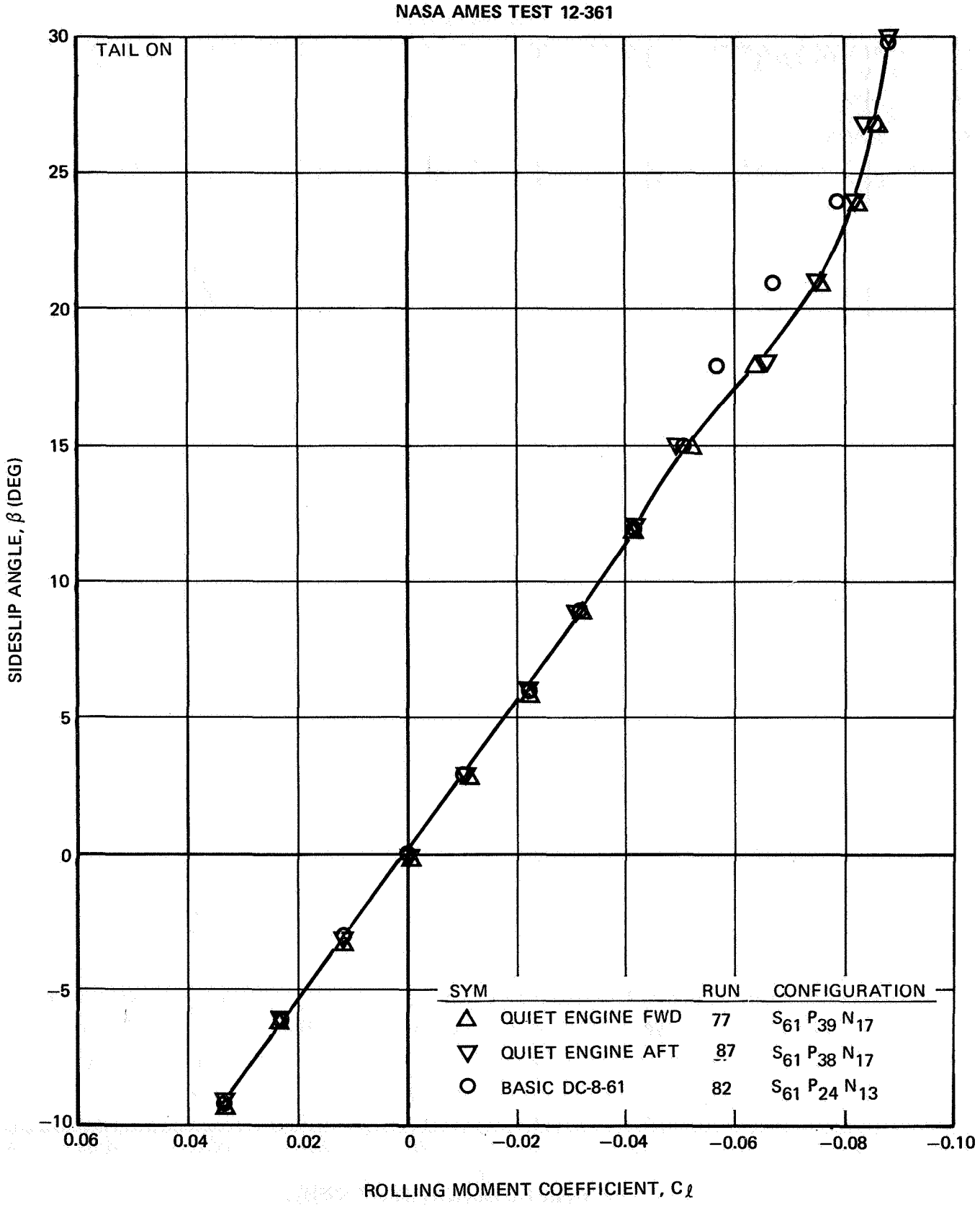

FIGURE III-114. EFFECT OF PYLONS AND NACELLES ON ROLLING MOMENT – $\delta_f = 25^o$, $\alpha_F = 8^o$, $i_H = 0^o$

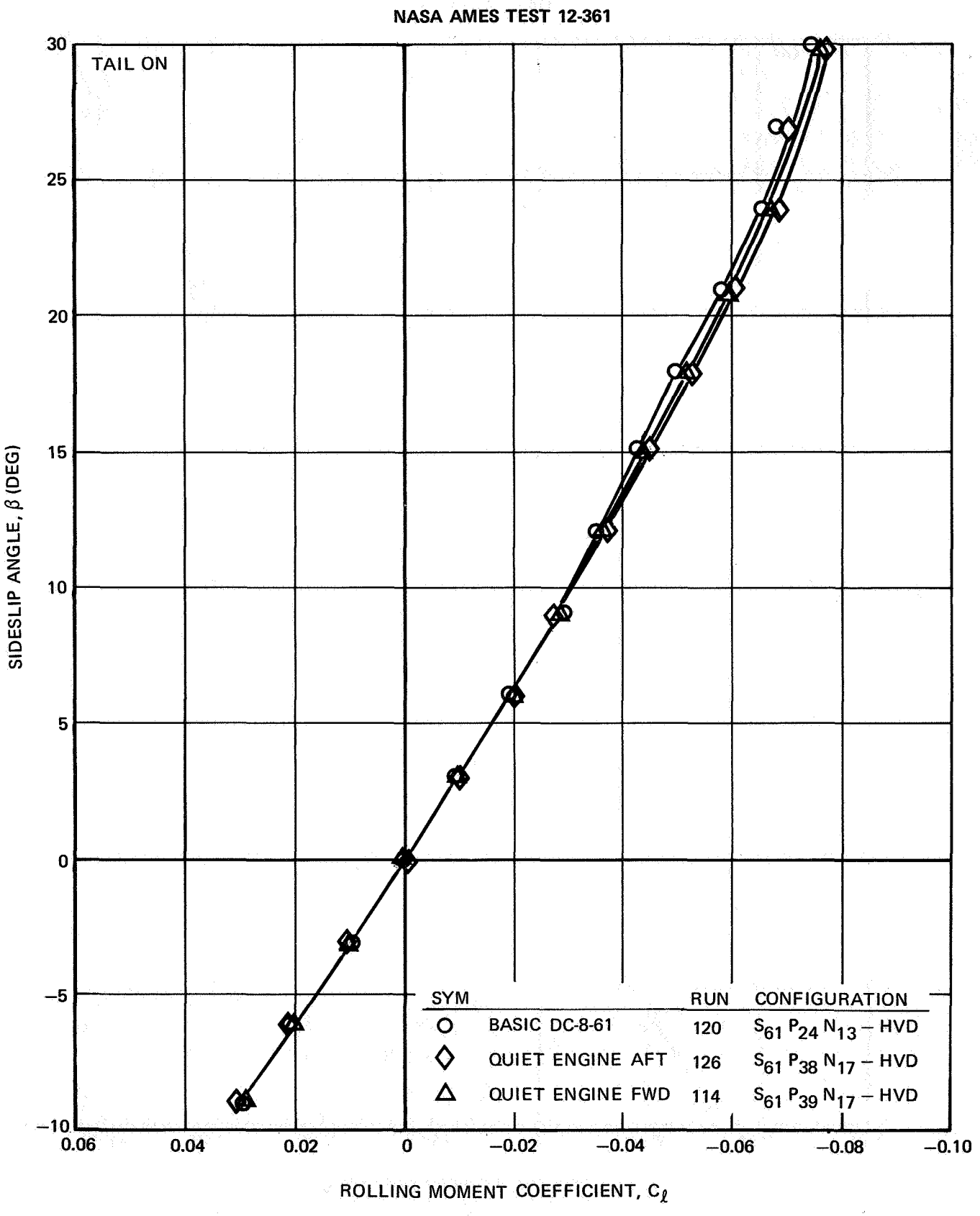

FIGURE III-115. EFFECT OF PYLONS AND NACELLES ON ROLLING MOMENT – δ_f = 50°, α_F = 0°, i_H = 0°

NASA AMES TEST 12-361

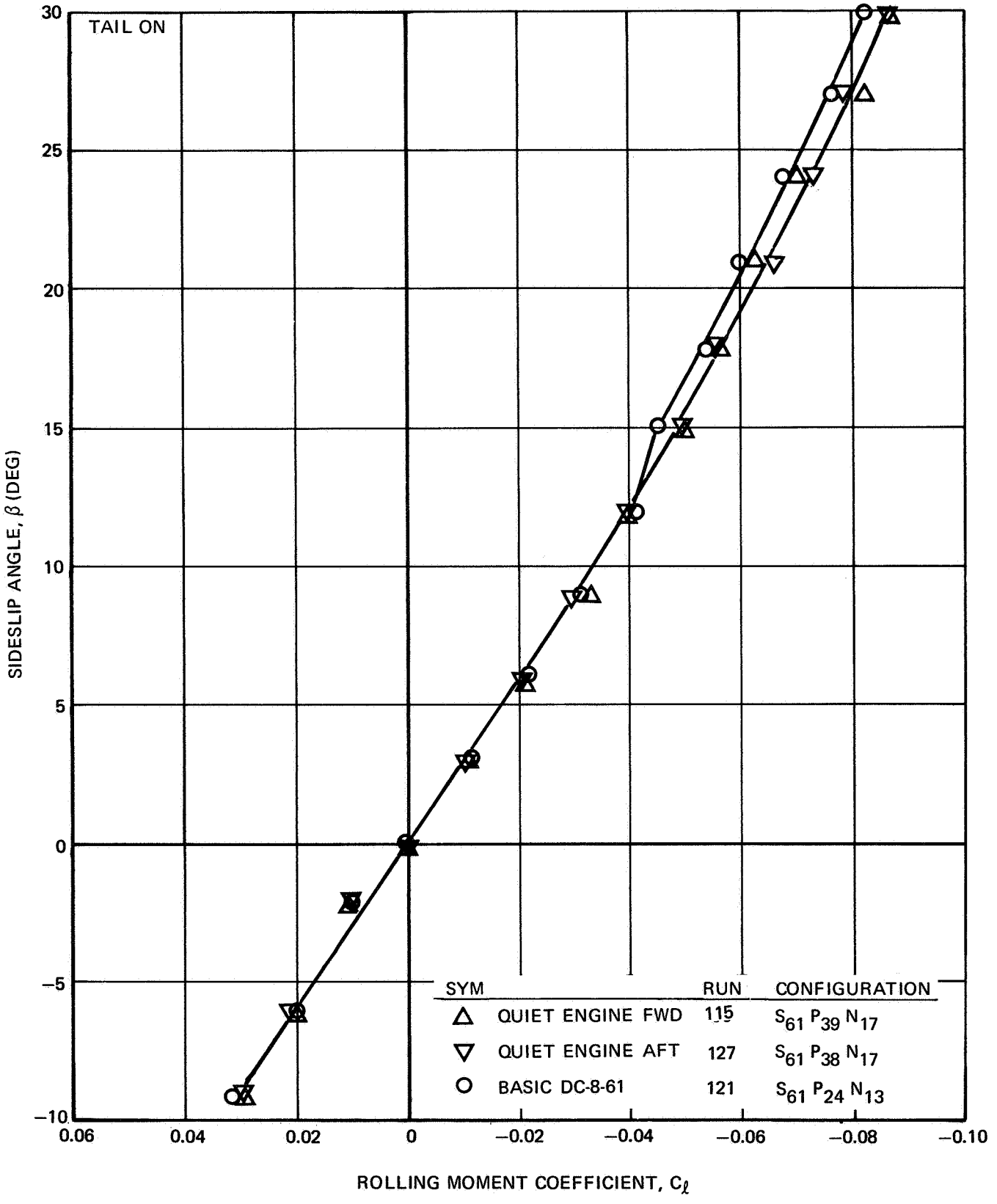

FIGURE III-116. EFFECT OF PYLONS AND NACELLES ON ROLLING MOMENT – $\delta_f = 50^o$, $\alpha_F = 4^o$, $i_H = 0^o$

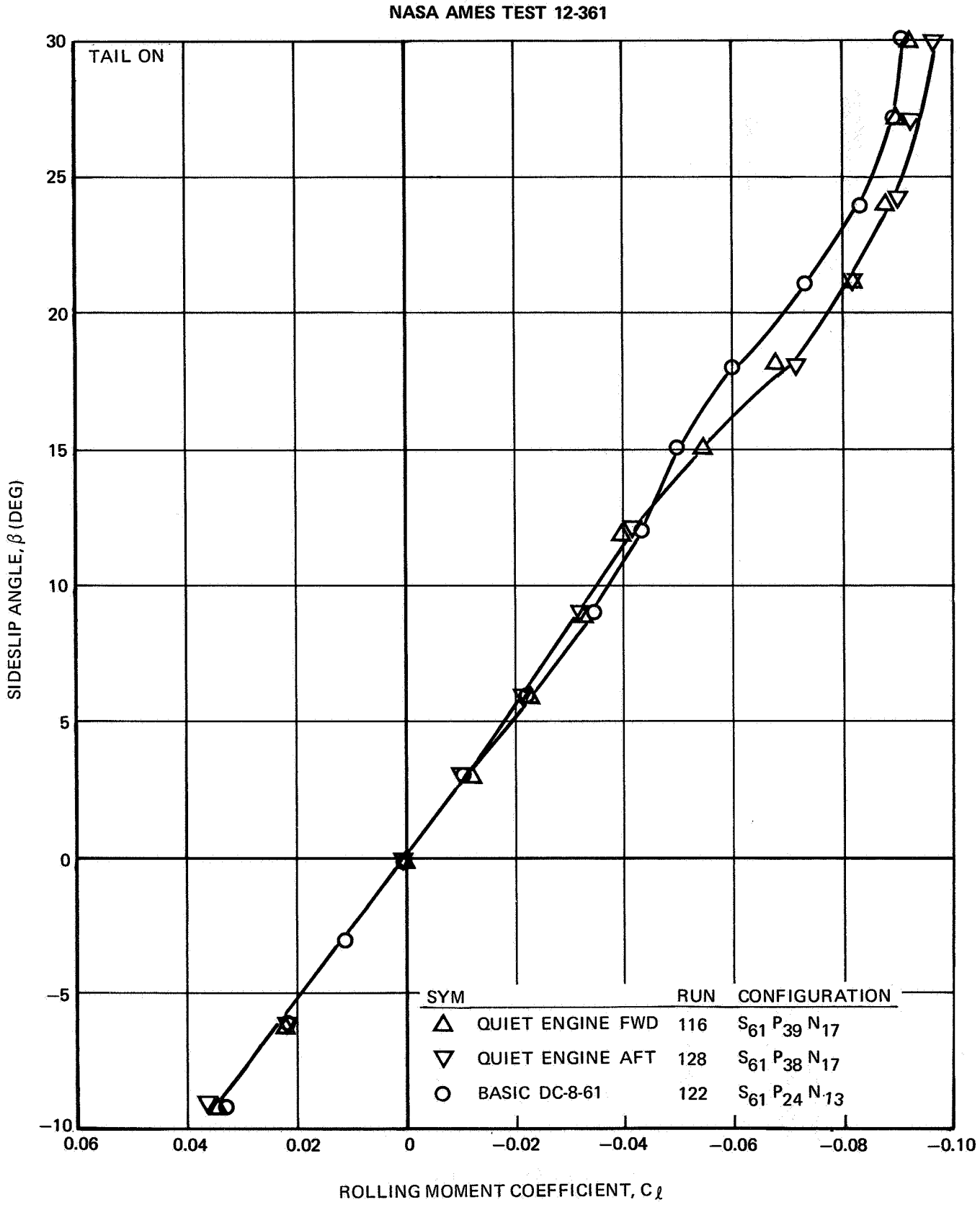

FIGURE III-117. EFFECT OF PYLONS AND NACELLES ON ROLLING MOMENT – δ_f = 50°, α_F = 8°, i_H 0°

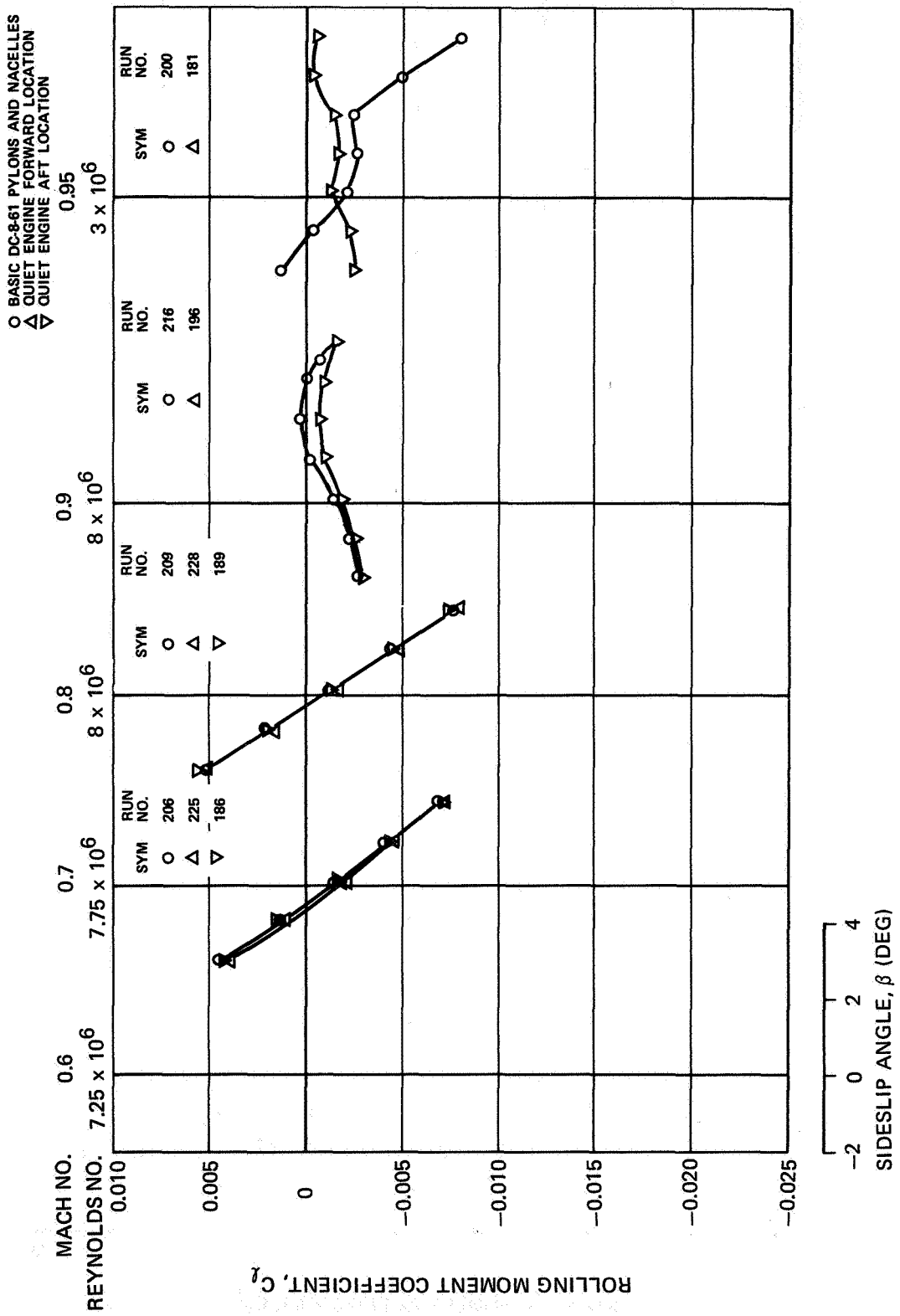

FIGURE III-118. EFFECT OF NACELLES AND PYLONS ON ROLLING MOMENT DUE TO SIDESLIP – $\delta_f = 0^o$, $\alpha_F = 0^o$

NASA AMES TEST 11-353

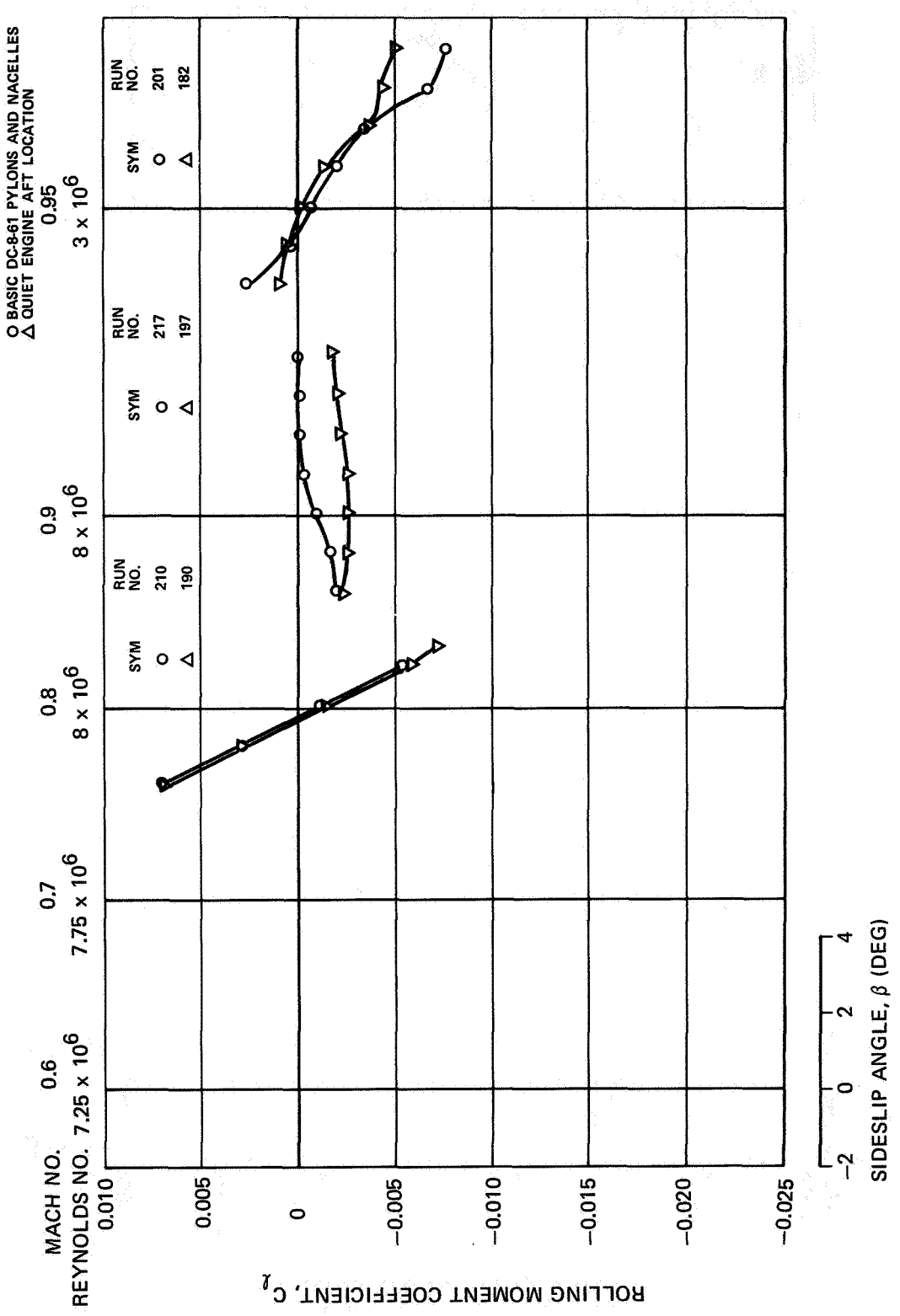

FIGURE III-119. EFFECT OF NACELLES AND PYLONS ON ROLLING MOMENT DUE TO SIDESLIP – $\delta_f = 0^o$, $\alpha_F = 0^o$

NASA AMES TEST 11-353

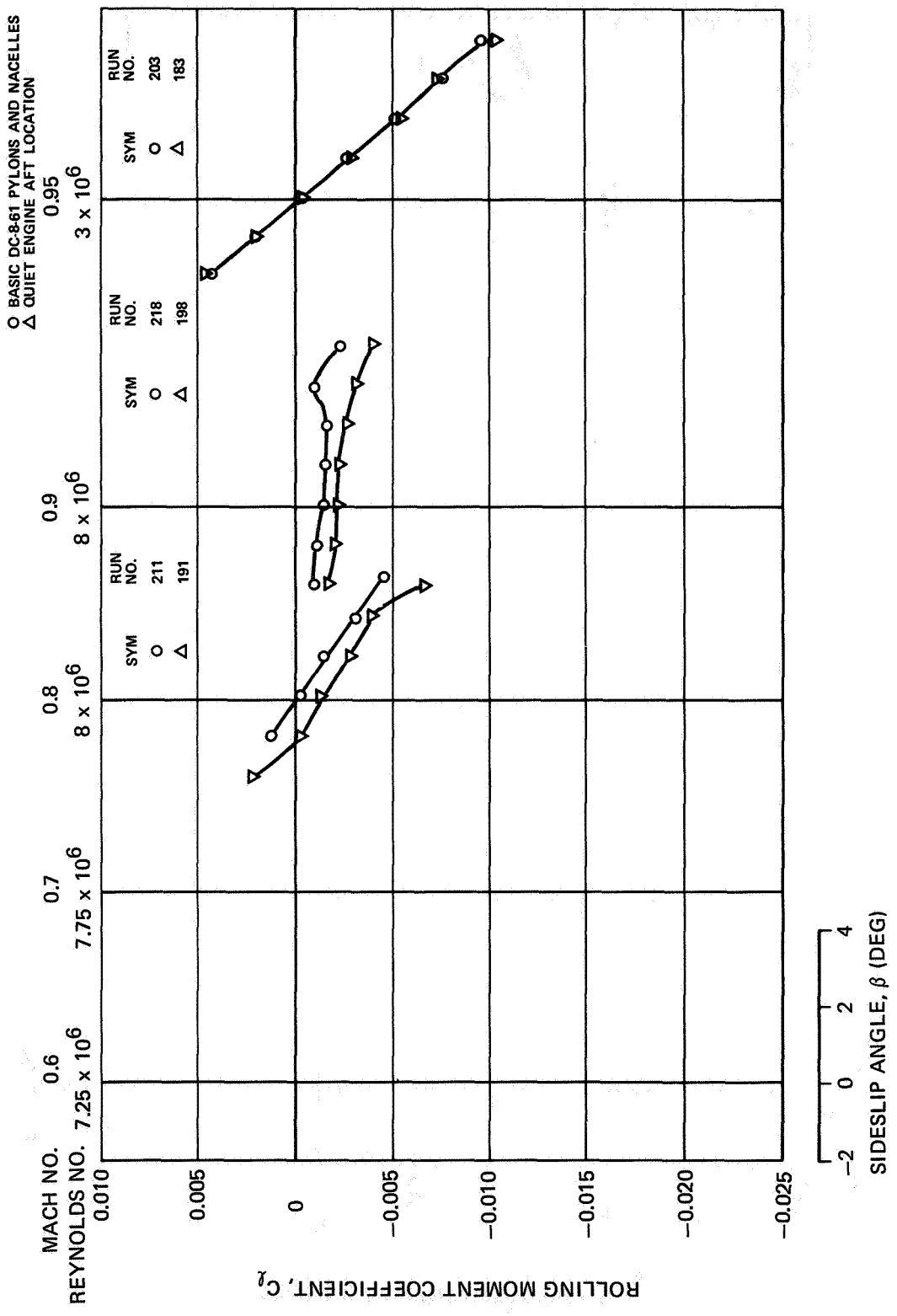

FIGURE III-120. EFFECT OF NACELLES AND PYLONS ON ROLLING MOMENT DUE TO SIDESLIP – $\delta_f = 0^o$, $\alpha_F = 4.1^o$

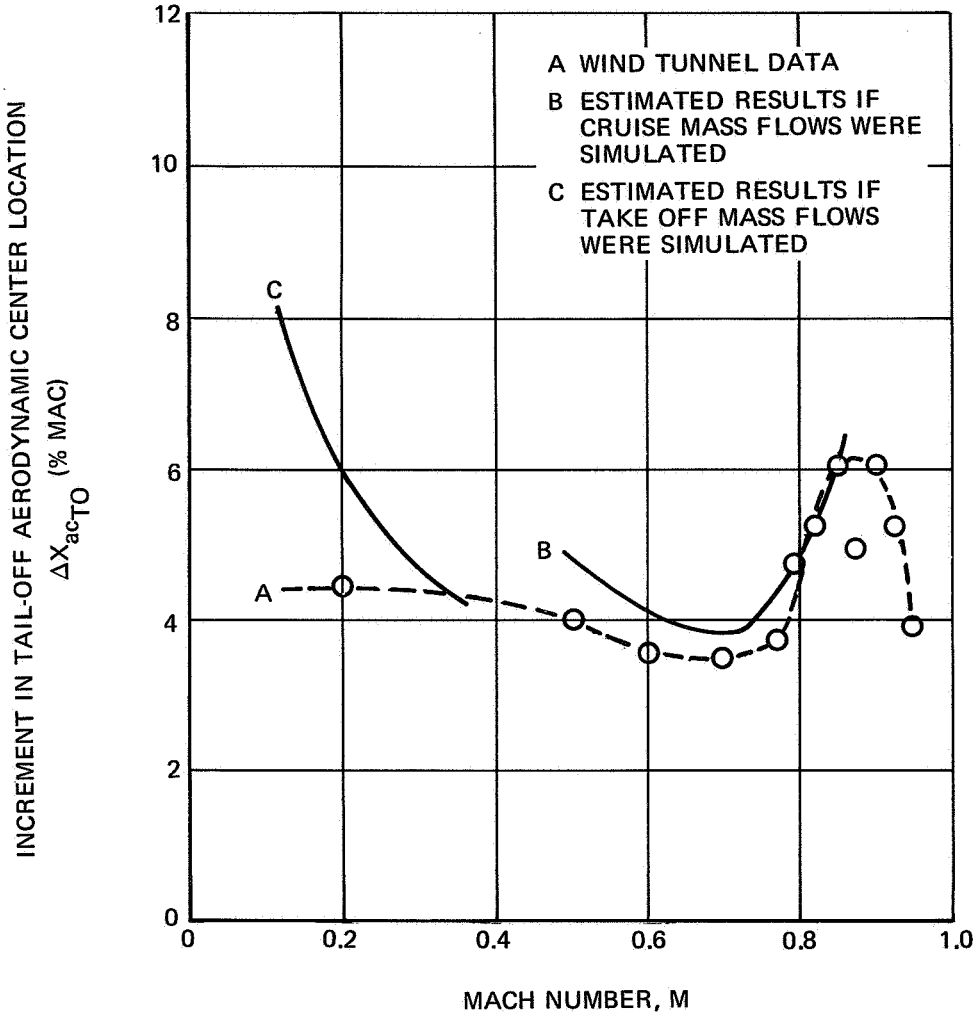

FIGURE III-121. EFFECT OF QUIET ENGINE INSTALLATION ON AERODYNAMIC CENTER LOCATION

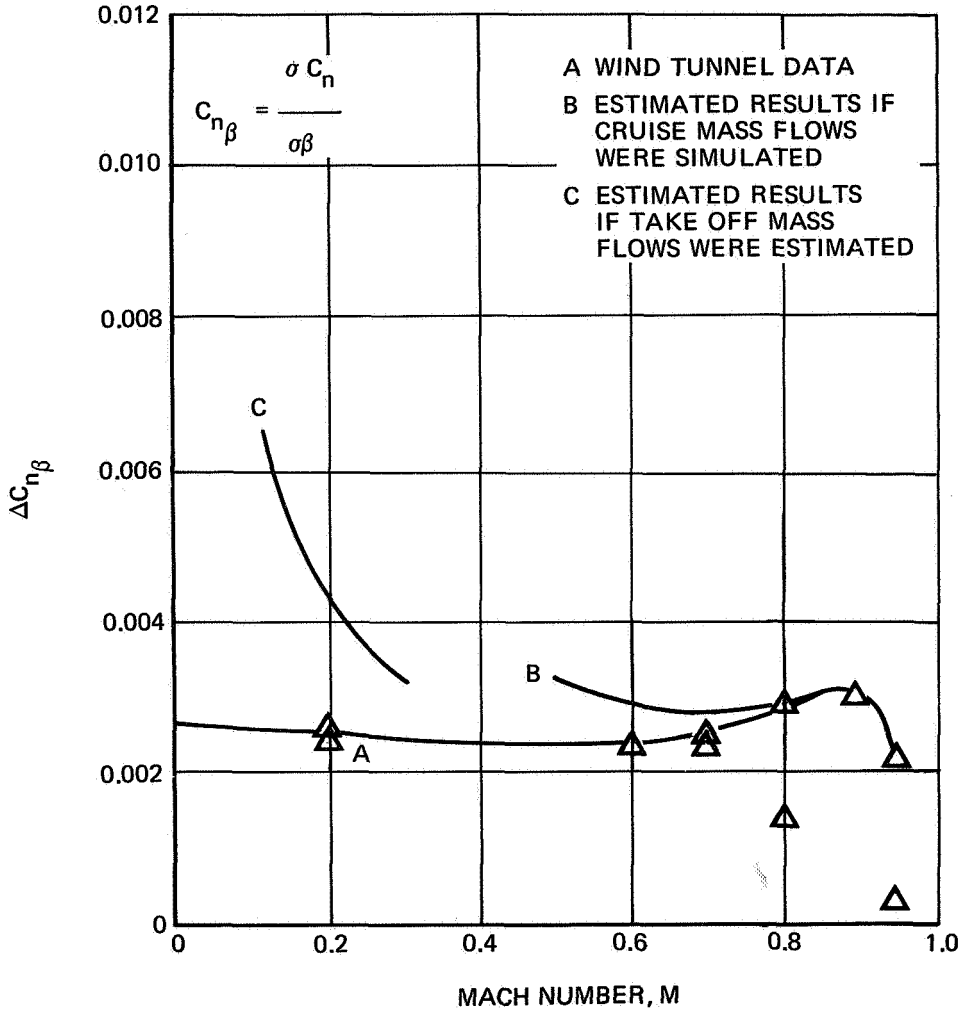

FIGURE III-122. EFFECT OF QUIET ENGINE INSTALLATION ON C_{n_β}

RESULTS OF THE DRAG TESTS

The evaluation of the wind-tunnel drag of the quiet-engine installation on the DC-8 used the DC-8-63 long-duct nacelle and cutback pylon as the base case. This was done because of the impossibility of simulating the flight characteristics of the DC-8-61 bifurcated-short-duct nacelle with a flow-through nacelle in the wind tunnel. Measured flight-test drag increments between the DC-8-61 and the DC-8-63 can be used to relate the wind-tunnel results to the DC-8-61.

The quiet-engine nacelle-pylon configurations were expected to have significantly higher drag than the DC-8-63 nacelle-pylon configuration, simply because of the skin-friction drag associated with the greater wetted area of the much larger nacelle. The estimated drag increase at the wind-tunnel test conditions, including an increase in the internal drag of the wind-tunnel nacelles, was a total $\Delta C_D = 0.0014$ for all four nacelles. The wind-tunnel incremental drags due to replacing the DC-8-63 nacelle-pylon configuration by the quiet-engine configurations are shown in Figure III-123 for airplane lift coefficients of 0.30 and 0.45. It can be seen that the measured incremental drags are significantly greater than the estimated values. The difference between any one of these drags and the estimated drag will hereafter be called the excess drag. The chief distinguishing features of the excess drag are the increase with increasing lift coefficient and the decrease with increasing Mach number, particularly at the higher lift coefficient. This behavior indicates that the excess drag is largely related to the lift-dependent drag of the nacelle.

The induced drag of the wind-tunnel model quiet-engine nacelle is much higher at a given angle of attack than either that of the DC-8-63 nacelle or of the retrofitted airplane. This is caused by the large amount of camber introduced by the warping of the fan cowl and gas generator to properly simulate the inlet mass-flow ratio. This can be seen from the results of the isolated quiet-engine nacelle-and-pylon test shown in Figure III-124. At an angle of attack of 0^o, the nacelle-induced drag is 2 drag counts ($\Delta C_D = 0.0002$) per nacelle or a total of 8 drag counts for all four nacelles. Having the nacelles carry lift reduces the required wing lift for a fixed total airplane drag; however, the nacelle is an inefficient lifting surface, because of its very low aspect ratio compared to the wing, and for practical purposes none of the nacelle-induced drag is offset by a reduction in the wing-induced drag.

The induced drag of the warped quiet-engine wind-tunnel-model nacelles increases much more rapidly with increasing angle of attack (airplane lift coefficient) than with the actual airplane nacelles or with the DC-8-63 wind-tunnel-model nacelles. The reason is that the induced drag is proportional to the square of the lift and, at the high level of lift on the warped nacelle, the increment in the square of the lift for a given change in angle of attack is much greater than at the much lower lift level that would exist with the actual airplane nacelles. This large increase in nacelle induced drag with increases in angle of attack also explains why the excess drag seen in Figure III-123 decreases with increasing Mach number, since the airplane angle of attack (and hence nacelle angle of attack) for a constant airplane lift coefficient decreases with increasing Mach number.

Some of the excess drag, measured with the quiet-engine nacelle-and pylon installation, is probably due to the over-the-wing pylons (the DC-8-63 has cutback pylons), and to an increased side load on the nacelle and pylon due to the greater planform area. The higher side load results in an increased induced drag. DC-8 wind-tunnel measurements have shown drag penalties of about five drag counts for over-the-wing pylons compared to cutback pylons Further wind-tunnel testing would be required to determine what part of the excess drag of quiet-engine installation is due to these design features, and what part is due to the warping of the wind-tunnel-model nacelles. Part of the additional wind-tunnel data needed would be direct measurement of the nacelle lift, from which the nacelle-induced drag could be assessed.

A comparison of the static-pressure distributions on the DC-8-63 wing upper and lower surfaces with those on the wing surfaces of the quiet-engine configurations is shown in Figure III-125. Although the pressures indicate that the local loading on the wing is changed when the DC-8-63 nacelles and pylons are replaced by the quiet-engine nacelles and pylons, the change appears to have caused no flow separations or serious interference problems.

The incremental drags caused by moving the quiet-engine nacelle 31 inches (79 cm) aft from the forward (DC-8-63) location are shown in Figure III-126. A small improvement is indicated. Since the improvement is generally greater at the higher lift coefficients, a reduction in nacelle-induced drag is probably the cause. If so, very little difference should occur in the drag for either of the nacelle locations with the actual airplane nacelle. The aft location was expected to produce supersonic flows and shock waves in the channel between the wing and the nacelles, but the static-pressure distributions on the wing lower surface, shown in Figure III-125, indicate no supersonic flow. The velocities are well below sonic at the inboard nacelle and become sonic at the outboard nacelle location. The absence of supersonic velocities at the aft location may be attributable to the cambered pylons, which were used for this location in an attempt to minimize the high velocities.

An attempt to determine the effect of engine power on the drag characteristics of the quiet-engine installation was also made during the test. The fan-exhaust jet was simulated by a solid extension of the nacelle fan cowl to represent a constant-area fan-exhaust jet. It was hoped that the displacement flow about the solid body would be similar to the displacement flow around the jet. However, subsequent testing of powered nacelle models by Douglas has shown that the solid-body technique of jet simulation is not at all representative. Consequently, the data from this part of the test are not considered meaningful and are not presented here.

The drag characteristics shown in Figure III-124 for the isolated quiet-engine nacelle-pylon configuration indicate that the zero-lift nacelle-pylon drag matches the estimated drag throughout the Mach number range. This indicates that the basic nacelle design is satisfactory.

The increase in drag of the quiet-engine installation (relative to the present engine installation on DC-8-63) that was measured in the wind-tunnel tests is essentially the same as the increase in DC-8-61 drag relative to the DC-8-63 that was determined from flight tests. It can therefore be concluded that the drag of the quiet-engine installation on the DC-8-61 will be essentially the same as the drag of the present JT3D-3B installation on that airplane. If any of the excess drag described above can be eliminated, the drag of the quiet-engine installation will be lower than that of the JT3D-3B.

NASA AMES TEST 11-353

NOTE: 1. THE REFERENCE CONFIGURATION FOR THE INCREMENTAL DRAGS IS THE DC-8-63 CONFIGURATION (N_{12} P_{35})

2. ESTIMATED INCREMENTAL DRAG INCLUDES THE NACELLE INTERNAL DRAG. NO INTERFERENCE FACTORS ARE USED

SYMBOL	NACELLE-PYLON	NACELLE LOCATION
○	N_{17A} P_{39}	FORWARD LOCATION
△	N_{17A} P_{38}	AFT LOCATION

$R_{N_{MAC}} \approx 6.2 \times 10^6$

$S_{W_{REF}} = 2926.8$ SQ FT

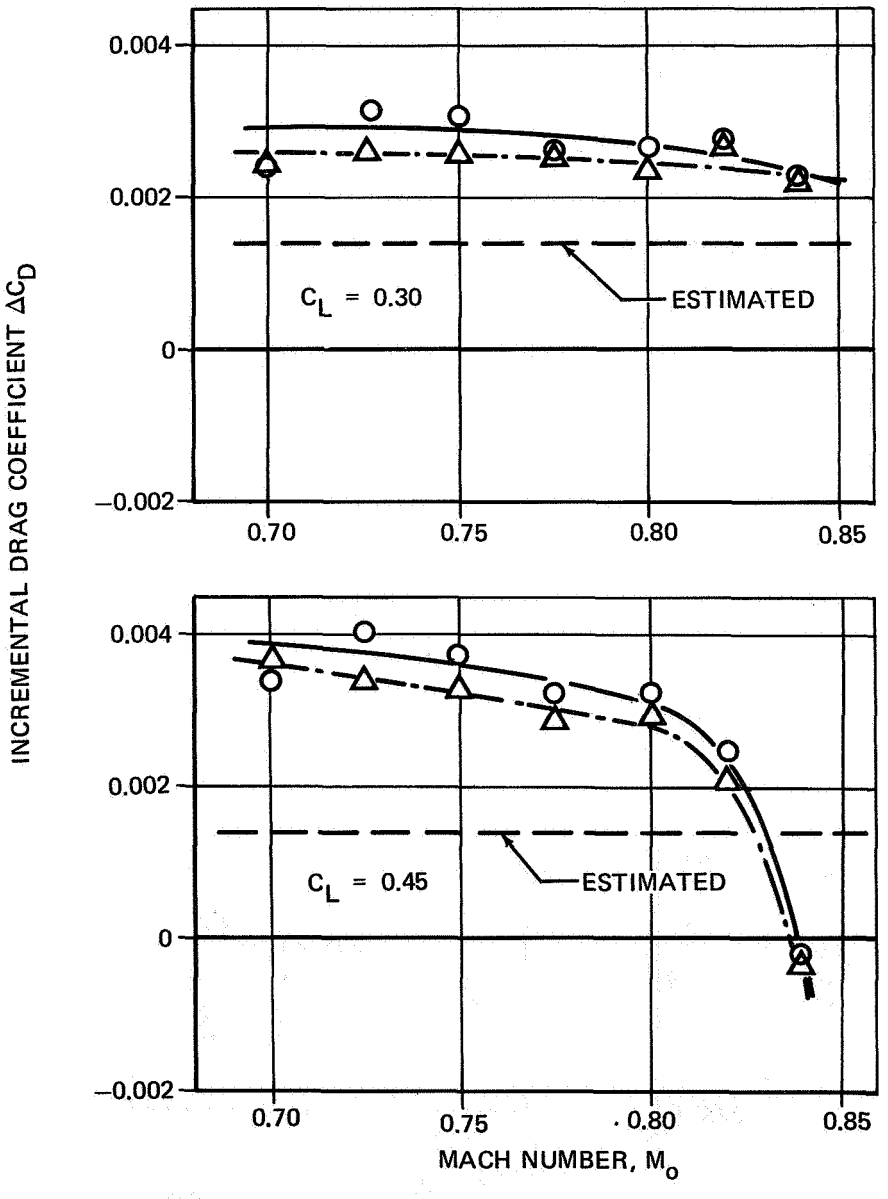

FIGURE III-123. CHANGE IN DRAG DUE TO REPLACING DC-8-63 NACELLE-PYLON CONFIGURATION BY QUIET-ENGINE CONFIGURATION

DAL TEST NO. 7-152

NOTE: 1. ESTIMATED DRAG INCLUDES THE NACELLE INTERNAL DRAG. NO INTERFERENCE FACTORS ARE USED.
2. DRAG IS FOR ONE NACELLE AND PYLON.

$R_{N_{MAC\ WING}} \approx 6.2 \times 10^6$ $S_{W_{REF}}$ = 2926.8 SQ FT

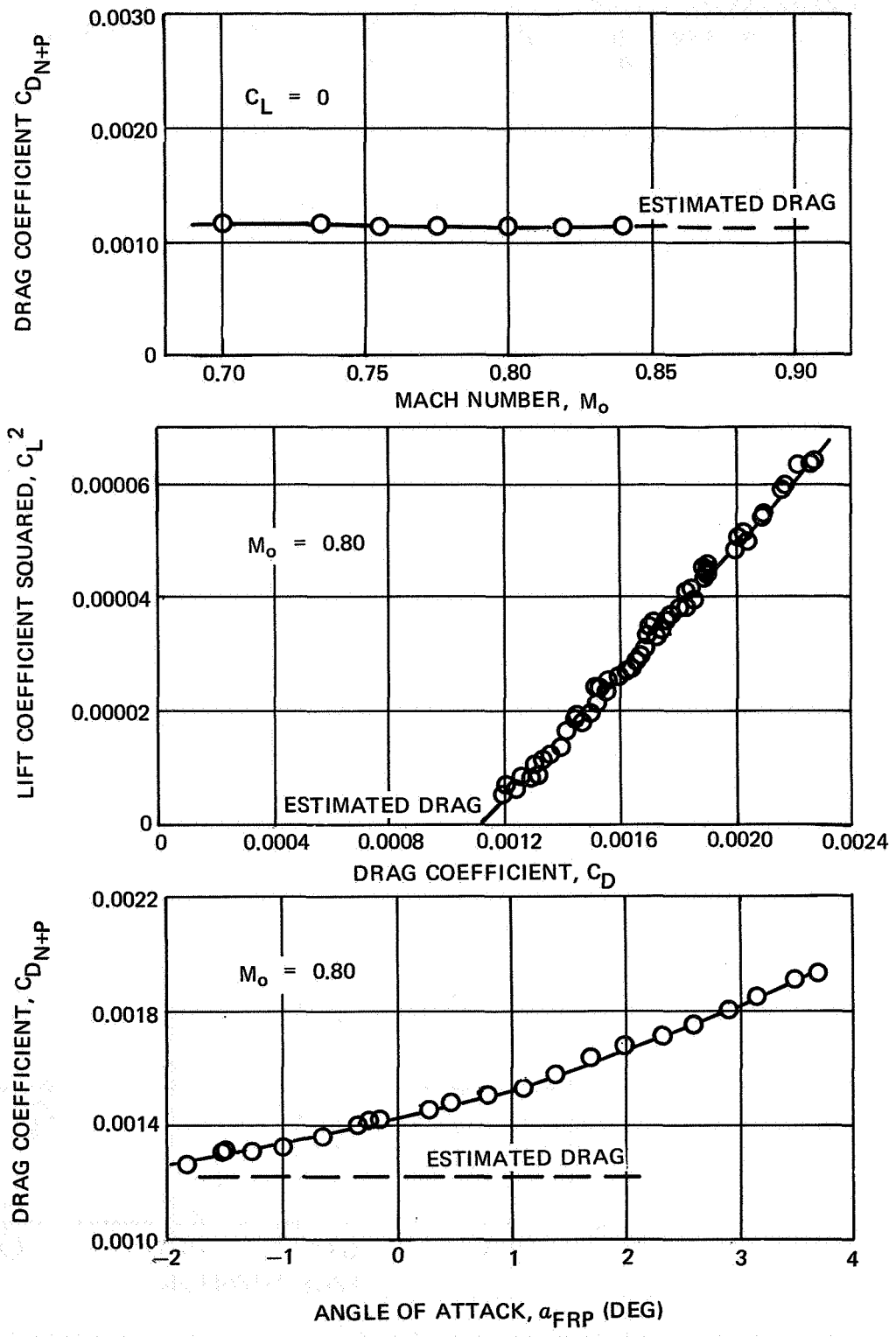

FIGURE III-124. DRAG CHARACTERISTICS OF ISOLATED QUIET-ENGINE NACELLE-PYLON CONFIGURATION

NAS3-11151
TASK III

NASA AMES TEST 11-353

SYMBOL	NACELLE-PYLON
○	DC-8-63
△	QUIET-ENGINE, FORWARD LOCATION
□	QUIET-ENGINE, AFT LOCATION

$R_{N_{MAC}} \approx 6.2 \times 10^6$ $C_L = 0.40$

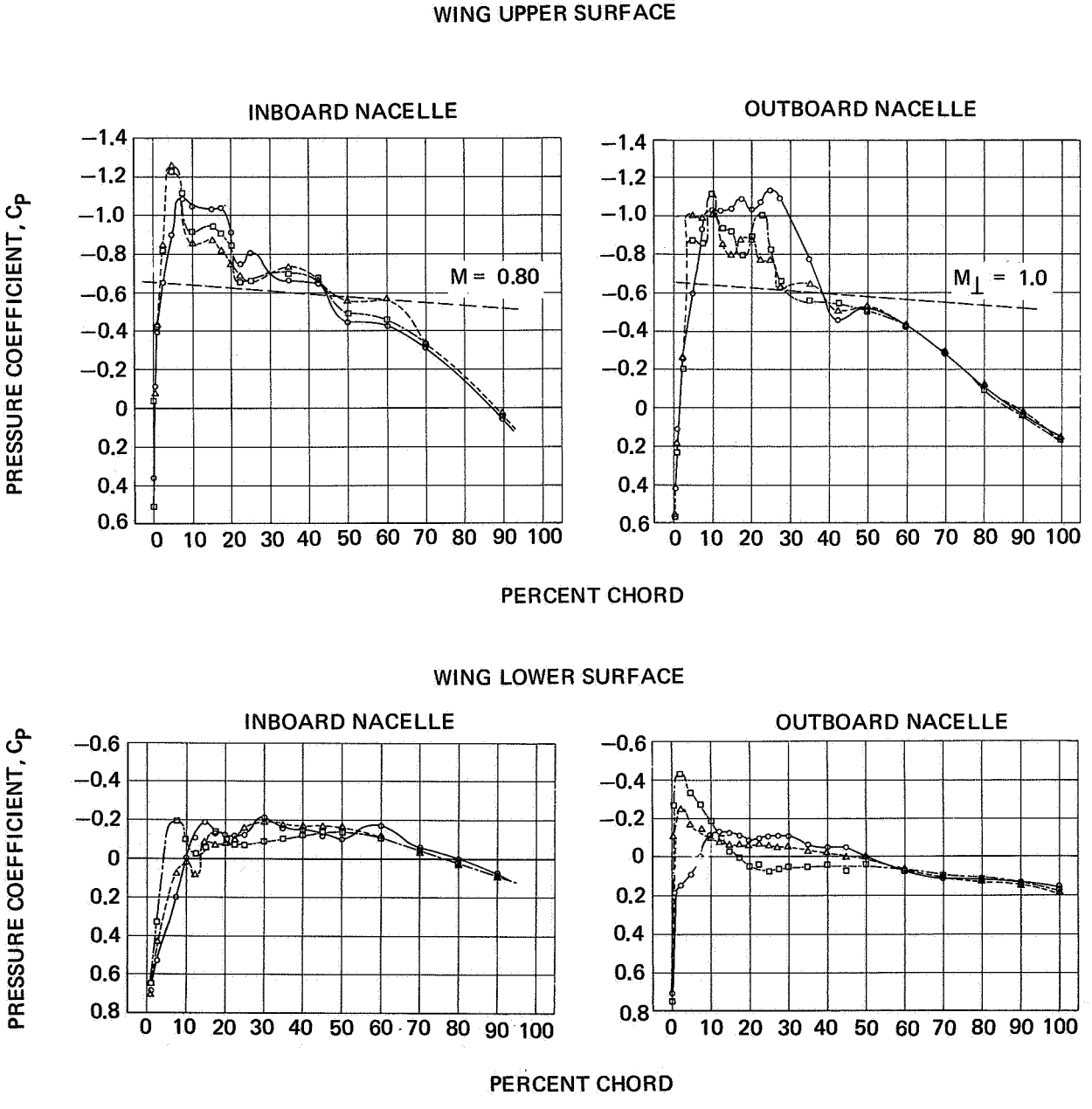

FIGURE III-125. EFFECT OF NACELLE-PYLON INSTALLATION ON WIND-TUNNEL PRESSURE DISTRIBUTION ON WING SURFACE

NASA AMES TEST 11-353

NOTE: 1. FORWARD NACELLE LOCATION:

INBOARD NACELLE T.E. AT 10-PERCENT POINT OF LOCAL WING CHORD
OUTBOARD NACELLE T.E. AT 6.8-PERCENT POINT OF LOCAL WING CHORD

2. DISTANCE MOVED: 31 INCHES AFT OF FORWARD LOCATION
3. ESTIMATED INCREMENTAL DRAG INCLUDES THE NACELLE INTERNAL DRAG. NO INTERFERENCE FACTORS ARE USED

$R_{N_{MAC}} \approx 6.2 \times 10^6$ $S_{W_{REF}} = 2926.8$ SQ FT

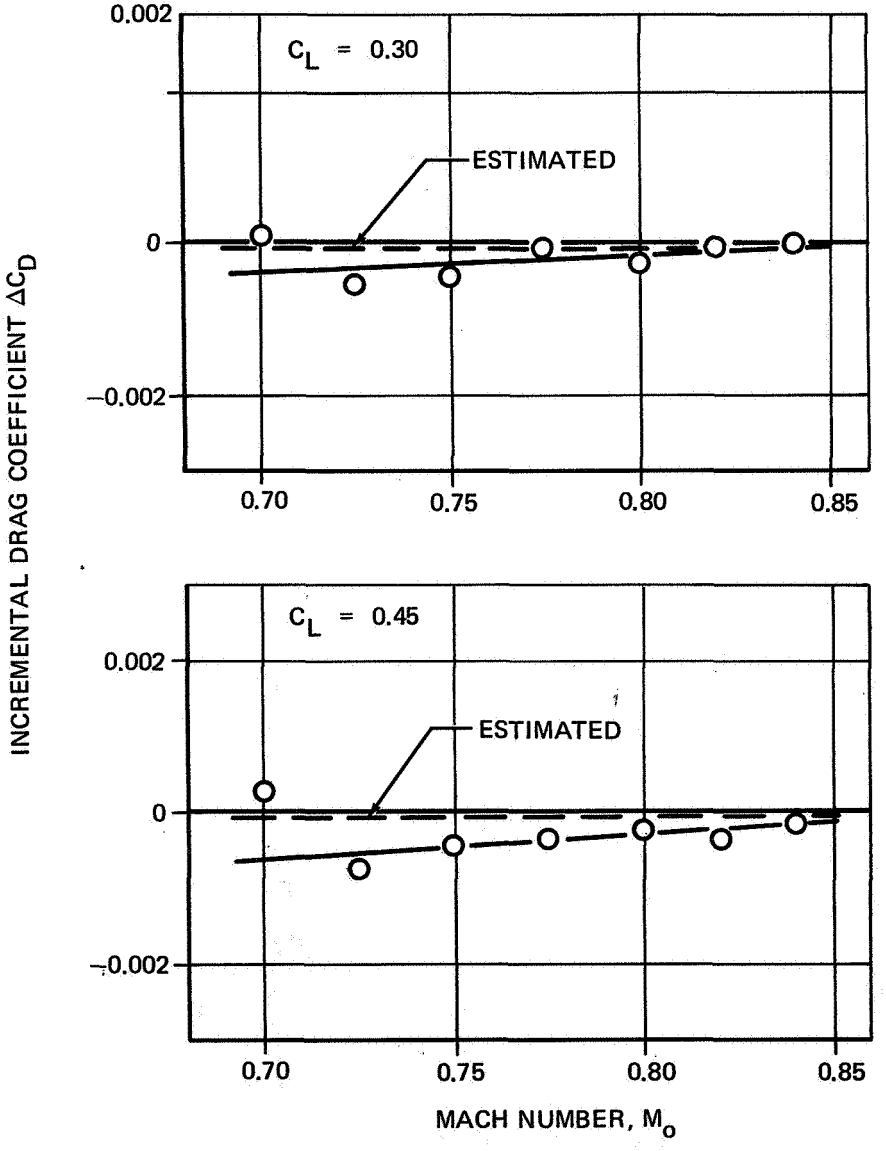

FIGURE III-126. INCREMENTAL DRAG DUE TO MOVING THE NACELLES AFT

CONCLUSIONS

STABILITY AND CONTROL CHARACTERISTICS

The test results can be summarized as follows:

1. The effects of the quiet engine on the aerodynamic characteristics are essentially independent of flap position.

2. The maximum lift coefficient and thus the stall speed are unaffected.

3. Lift-curve slope is increased approximately 2.5 percent.

4. A destabilizing effect on pitching moment is produced, amounting to the equivalent of at least a 4 percent forward shift of the neutral point.

5. The tail-on directional stability is decreased by 5 to 10 percent.

6. The side-force coefficients are increased by approximately 5 percent.

7. Rolling moments are unaffected.

8. The forward engine location affects the pitching and yawing moments more than does the aft location. Both affect the lift and side force data to approximately the same extent.

DRAG CHARACTERISTICS

The following conclusions result from the high-speed drag-test program:

1. The incremental drags resulting from the installation of the quiet-engine nacelle and pylon are significantly greater than the estimated drags. The excess drag (the difference between the measured drag and the estimated drag of a quiet-engine nacelle) amounts to from 10 to 20 drag counts, depending on the airplane lift coefficient and Mach number.

2. The drag of the quiet-engine installation on the DC-8-61 is essentially the same as the drag of the present JT3D-3B installation.

3. A significant part of the excess drag is thought to be the result of high-induced drag of the nacelle, which is brought about by the warping of the wind-tunnel-model nacelles for simulation of inlet conditions. The actual airplane installation probably will not exhibit much excess drag.

4. Pressure distributions on the wing show no separations or serious interference problems associated with the installation of the quiet-engine nacelle and pylon.

5. No interference problems were encountered when the quiet-engine nacelle was moved 31 inches (79 cm) aft of the basic location.

6. The isolated nacelle has no excess drag other than the previously mentioned induced drag.

7. Further testing would be required to determine how much of the measured excess drag can be eliminated.

IMPLICATIONS

The work accomplished during Tasks I and II of this contract indicated that the wing of the DC-8-61 airplane might require extensive reskinning in order to prevent wing flutter. Flutter model tests subsequently conducted as part of the work required in Task VI showed that the forward quiet-engine-nacelle location was significantly superior to the aft location and also that the wing reskinning would not be required. The wind-tunnel test results reported herein show that there is a less significant difference in aerodynamic performance between the forward and aft nacelle locations. Consequently, the forward nacelle location has been selected as the configuration to be studied during the remainder of the contract.

The results of the stability and control tests indicate that the DC-8 flying qualities would be adversely affected, mainly in the area of static longitudinal stability. Other affected areas are static directional stability and lateral-directional dynamic stability. The implications are discussed further in the following paragraphs.

LONGITUDINAL CHARACTERISTICS

The aerodynamic aft center of gravity limit on the DC-8-61 is determined primarily by static longitudinal stability requirements in the critical enroute climb condition (FAR 25.171). The effects of nacelle size, engine thrust, and mass flow are all destabilizing and, since these parameters are all increased with the quiet engines, the aft center of gravity limit would be adversely affected. Preliminary analyses indicate that a restriction of the aft center of gravity of as much as 8 percent MAC may be necessary to achieve satisfactory stability levels. Alternatively, a large horizontal tail and/or a powered elevator system might be developed to reduce or eliminate the loading restrictions. These items would have an adverse effect on cost and weight.

DIRECTIONAL CHARACTERISTICS

The increased engine thrust and slightly reduced directional stability will increase the minimum control speeds with one engine inoperative. As a result, minimum takeoff field lengths will be increased, and vertical tail loads may be increased because of higher speeds.

The effects of the quiet engine on these items and on dynamic lateral-directional stability (Dutch roll damping) are described in Task VI.

DRAG CHARACTERISTICS

The results of the drag tests show that the drag of the DC-8-61 airplane with the quiet engine is essentially the same as the drag of the airplane with the JT3D-3B engine installation.

The work accomplished in Tasks V and VI include the results of the wind-tunnel test programs.

REFERENCES

III-1. Lalor, David P., *Quiet Engine Study Operating Report for the Wind Tunnel Test of the Model DC-8 Six-Percent-Scale HRN Complete Model LB-161L in the NASA Ames 12-Foot Pressure Tunnel,* Douglas Aircraft Company Report DAC-67240, 22 August 1968.

III-2. Baden, Marvin W., *Quiet Engine Study Operating Report for the Wind Tunnel Test of the Model DC-8 3.429%-Scale High Speed Model LB-184L in the NASA Ames 11-foot Transonic Tunnel,* Douglas Aircraft Company, Report DAC-67296, 27 September 1968.

III-3. Grogan, Martin L., *Operating Report for the Test of the Isolated DC-8 Quiet Engine Nacelle-Pylon Model LB-265B in the Four-Foot Transonic Wind Tunnel,* Douglas Aerophysics Laboratory, Douglas Aircraft Company Report DAC-67481, 18 November 1968.

TASK IV

DESIGN OF THE NACELLE AND PYLON FOR THE SELECTED ENGINE CONFIGURATION

LIST OF ILLUSTRATIONS

LIST OF TABLES

TASK IV

DESIGN OF NACELLE AND PYLON FOR THE SELECTED CONFIGURATION

A nacelle design was initiated that used the engine configuration defined by the NASA Project Manager (refer to Table IV-I). Because the primary subject of the contract was noise reduction, initial design emphasis was placed on the acoustic-treatment requirements for the nacelle and on the installation problems associated with this treatment.

Figure IV-1 shows the nacelle design that resulted from this study.

DEFINITION OF SELECTED ENGINE CONFIGURATION

The definition of selected engine configuration is shown in Table IV-1.

TABLE IV-I
ENGINE DEFINITION

		SI UNITS*
1. BYPASS RATIO	5.5:1	
2. FAN PRESSURE RATIO	1.5:1	
3. CRUISE THRUST (M = 0.82, 35,000 FT – 10,668 M)	4,900 LB (41,769 N/SFC)	21,796 N
4. TOTAL CORRECTED AIRFLOW	939 LB/SEC	KG (MASS)/SEC
5. FAN TIP DIAMETER	74.6 IN.	1.89 M
6. FAN HUB-TO-TIP RATIO	0.47	
7. FAN STAGES	ONE	
8. DRY UNINSTALLED ENGINE WEIGHT	5,100 LB MAX	2313 KG
9. FLOW DIMENSIONS:		
FAN NOZZLE AREA	11.67 SQ FT	1.08 SQ M
ENGINE NOZZLE AREA	3.60 SQ FT	0.33 SQ M
FAN-EXHAUST-CASE FLOW PATH:	(33.4 SQ CM)	
OUTER DIAMETER	73.0 IN.	1.85 M
INNER DIAMETER	50.0 IN.	1.27 M
10. ENGINE PERFORMANCE	ALLISON PD 218-Q**	
11. ENGINE MOUNTING	TAKE THRUST AT REAR MOUNT. FORWARD MOUNT ON FAN CASE OR ON ENGINE CASE AT DOUGLAS DISCRETION.	
12. ENGINE SELLING PRICE (APPROX)	$523,000	
13. SUPPRESSOR CRITERIA – FAN NOISE SUPPRESSION UPSTREAM AND DOWNSTREAM	10 PNdB	

* STANDARD INTERNATIONAL UNITS
**FROM THE NASA QUIET ENGINE DEFINITION PROGRAM

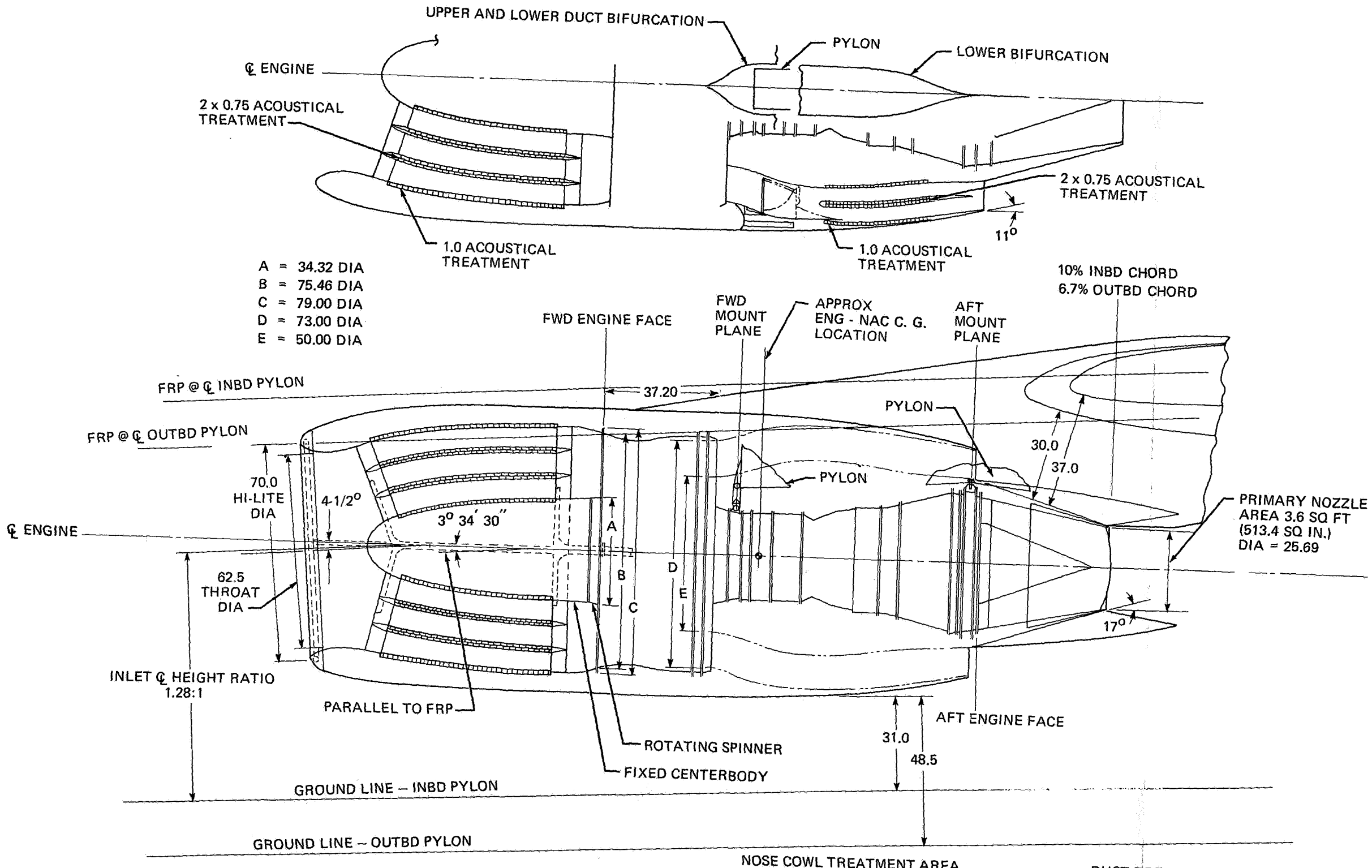

NOSE COWL TREATMENT AREA

INLET DUCT	13,200	SQ IN.
OUTER RING	20,700	SQ IN.
INNER RING	14,300	SQ IN.
BULLET	4,600	SQ IN.
TOTAL	52,800	SQ IN. = 367 SQ FT

DUCT TREATMENT AREA

INNER WALL	5,700 SQ IN.
SPLITTER	13,700 SQ IN.
OUTER WALL	8,000 SQ IN.
TOTAL	27,400 SQ IN. = 190.2 SQ FT

FIGURE IV-1. NACELLE AND PYLON DESIGN

NACELLE DESIGN

INLET DESIGN

Acoustics

The acoustical design is based on the analysis and assumptions reported in Task I. The equivalent acoustical design parameters for Task IV are:

1. A referred speed of the fan rotor shaft of 2132 rpm (36 Hz) during landing approach at 5225 pounds (23,242 N) of referred net thrust per engine.

2. Sixty-two blades on the single-stage fan.

3. A fundamental blade passage frequency, (BPF), of 2203 Hz.

4. A wavelength of the fundamental BPF of 0.526 feet (16 cm) for a speed of sound of 1160 feet (354 m) per second in both the inlet and fan-exhaust ducts.

5. A noise-source area of 23.6 square feet (2.19 m^2) at the annular opening immediately upstream of the fan blades. A 25-percent increase in treated area, to account for treatment made less effective by installation components such as attachments.

Examination of Figure I-5 of Task I reveals the strong interdependence of the height of the channel between the treated surfaces and the total treated area. Various inlet configurations based on the acoustic design parameters were evaluated. Only the following three configurations met the acoustic requirements and also had desirable nacelle and inlet aerodynamic characteristics:

1. An inlet having five concentric rings supported by a cruciform frame.

2. A multiple-radial-vane inlet.

3. An inlet having two concentric rings and an extended, treated centerbody.

The first two designs were thought to be acoustically marginal, and they could introduce extensive disturbances into the inlet flow field. The inlet design with two concentric rings and the extended centerbody showed the greatest promise of achieving the 10 PNdb goal with minimum flow disturbance. With this configuration, 366 square feet (34 m^2) of treatment can be accommodated on the cowl wall, both faces of each concentric ring, and the extended centerbody.

The acoustic treatment assumed is of the resistive resonant cavity type developed under the auspices of the NASA-Langley Research Center (Contract NAS1-7130). The treatment consisted of a sandwich constructed of a 0.020-inch (0.5 mm) aluminum-alloy backing sheet, a 0.75-inch (1.9 cm) nominal cell fiberglass honeycomb, and a 0.040-inch (1 mm) fibermetal facing sheet. The sandwich was assembled by mechanical bonding with an epoxy resin adhesive. The depth of the honeycomb cell was 1.0 inch (2.5 cm) on the cowl wall and centerbody and 0.75 inch (1.9 cm) on both faces of the concentric rings. The flow resistance of the fibermetal facing sheet was 100 MKS rayls.

Although this type of acoustic treatment has undergone extensive structural testing to validate its safety for use in flight testing, much more extensive investigation would be required to validate its use as a structural design material for production usage. For this reason, conventional skin and

stringer construction was assumed throughout the cowl design, although limited use of structural honeycomb also was considered. The acoustic treatment was designed for nonstructural application only.

The porous facing sheet of the acoustic treatment introduces the probability of liquid entrapment in the honeycomb cell structure. A drainage scheme developed for the flight test phase of the previously noted NASA-Langley contract was used in the design. Alternate honeycomb cell rows were connected circumferentially by small (1/8 by 1/4 inch – 3 by 6 mm) drain holes located midway between cell nodes. Liquid contaminants were drained to a collection manifold and vented overboard. Using this drainage scheme, no cell interconnection exists in the direction of a positive pressure gradient in the inlet.

The rotation of the centerbody, necessitated by the absence of inlet guide vanes, introduced considerable difficulty in providing acoustic treatment for the centerbody. A centerbody long enough to provide adequate treatment area would greatly overload the engine front bearing. In addition, there was doubt about the ability of the acoustical treatment to sustain the centrifugal loads introduced by rotation. It was therefore decided to provide a fixed, treated, long centerbody supported by the same two sets of four radial struts that support the concentric rings. A short rotating spinner would replace the standard centerbody. Providing a seal for this large-diameter spinner would require a development effort, but it is not considered to be beyond the present state of the art.

Aerodynamics

The design of the inlet lip was based on recent design data developed for new installations of high-bypass-ratio engines. The aerodynamic design of the inlet duct was based on the results of the analyses and tests conducted under NASA Contract NAS1-7130. The method consists of enlarging the inlet inner barrel to compensate for the area taken up by the rings and vanes. The rings are then positioned by trial and error based on potential-flow analysis until the rings have good pressure distributions and are in hoop tension. If the leading edges of the rings are at least two-thirds of an inlet radius aft of the inlet leading edge, they will be insensitive to changes in inlet angle of attack, and they will sense only changes in the velocity of the inlet duct flow.

The test program conducted under Contract NAS1-7130 for a two-ring inlet confirmed the validity of the design method. Therefore, the design data used in that program were used to design the inlet duct for the quiet engine. Exact positioning of the concentric rings by trial and error based on potential flow was not accomplished, because of the large number of man-hours and computing time involved in that process.

Figure IV-2 shows the inlet-duct area distribution for the quiet engine installation.

Figure IV-3 shows the pressure distributions of a two-ring inlet designed by the potential-flow technique for the DC-8 with the JT3D-3B engine.

Fan-Exhaust-Duct Design

Essentially the same acoustic design parameters were used for the fan-exhaust ducts and inlet duct, with the exception of the noise-source area.

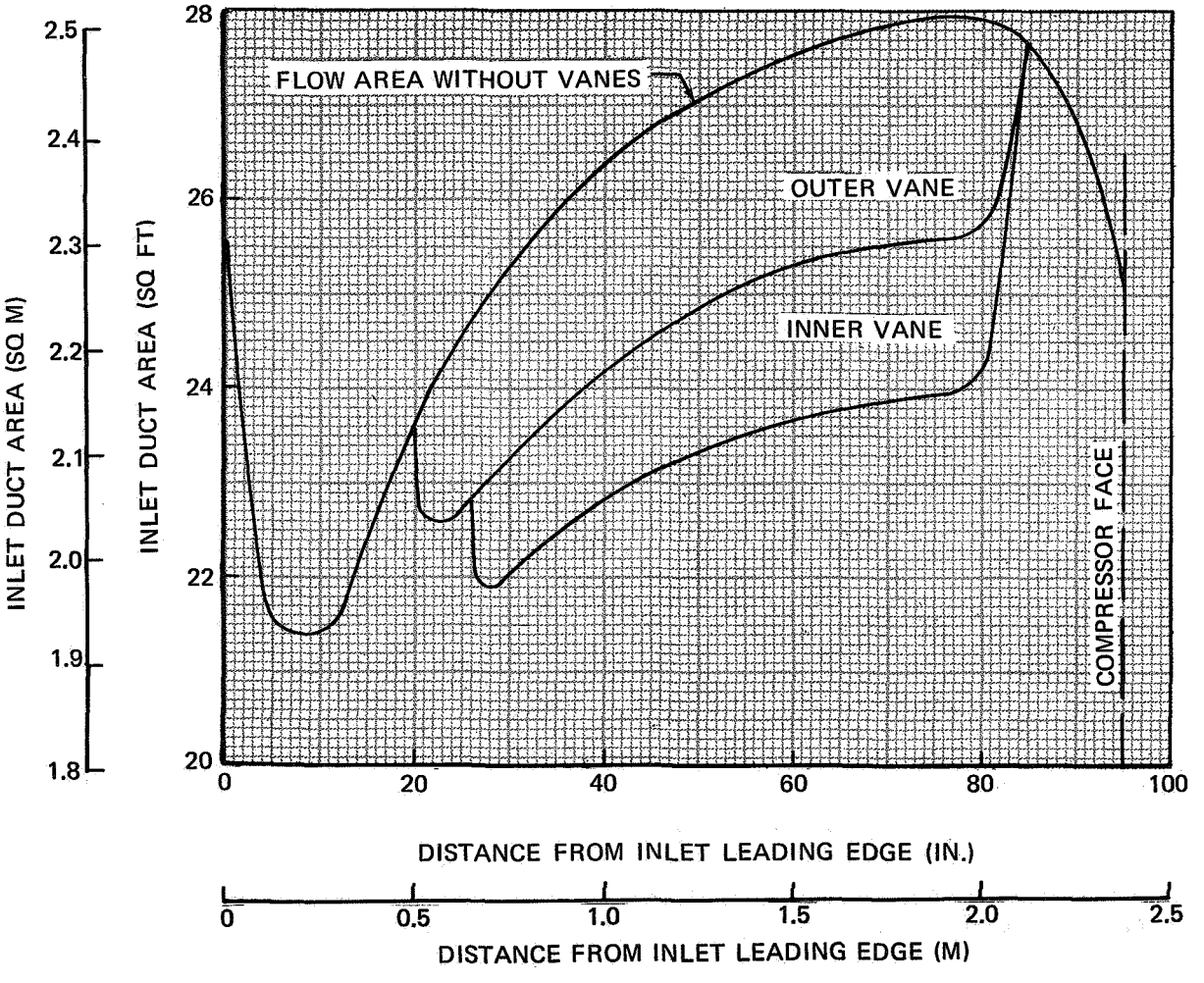

FIGURE IV-2. INLET DUCT AREA DISTRIBUTION

The fan-duct bifurcation necessary to provide structural access to the engine mount from the pylon had an unfavorable aerodynamic contour, because of the large fan diameter and the position of the forward engine mount on the engine core. After consultation with several engine manufacturers, it was decided to extend the bifurcation forward approximately 10 inches (25 cm) into the aft end of the fan case. Prior experience with fan-exit pressure distributions resulting from duct bifurcations strongly suggests that the proximity of the duct bifurcation to the fan-exit guide vanes will be more than compensated for by the much more favorable bifurcation contour. This design decision also reduces the fan-exhaust-duct inlet area from 15.4 square feet (1.43 m^2) with the usual bifurcation to 13.8 square feet (1.28 m^2) with the extended bifurcation. The noise-source area was assumed to be identical to the actual duct inlet area, that is, 13.8 square feet (1.28 m^2).

In an effort to minimize the acoustic treatment required, a circumferential splitter was provided to reduce the effective channel height to approximately 6 inches (15 cm). The acoustic treatment was similar to that provided for the inlet duct, with the following exceptions:

1. The aluminum backing sheet used for the inlet duct was replaced by titanium for the fan-exhaust ducts to ensure adequate fire protection.

2. The depth of the honeycomb cell for the fan exhaust ducts was 1.0 inch (2.5 cm) for the inner and outer duct interior walls and 0.75 inch (1.9 cm) for both faces of the circumferential splitter.

3. No acoustic treatment was provided in the fan thrust reverser.

4. The longitudinal splitters used to support the circumferential splitter were not treated.

For reasons outlined in Task II the fan exhaust ducts were made as short as was consistent with provision for the required 190 square feet (18 m^2) of acoustic treatment. Figure IV-4 shows the fan-exhaust-duct area distribution. Prior experience has shown that it is desirable to maintain an essentially constant flow area through the forward half of the duct and then to decrease the area gradually to the exit area. For this reason, a relatively constant area was maintained through the bifurcated section of the ducts and through the fan thrust reverser.

Nacelle Aerodynamics

The external nacelle lines were established to enclose the engine and its associated accessories in the most efficient manner. Current aerodynamic design practice was used to establish the proper inlet cowling shape and the proper ratio of inlet diameter to maximum nacelle diameter. The design includes the latest wind-tunnel test results conducted on other installations with high-bypass-ratio engines. The radial dimensions of fan-duct exhaust nozzle were sized by varying the fan exit diameter and gas-generator nacelle diameter within the constraints set by engine size to produce the best compromise in the afterbody shapes of both fan and gas generator.

The final nacelle design, which is axisymmetric aft of the inlet droop, was then checked by the automatic computing program for axisymmetric potential flow.

For the calculations, the drooped section of the cowl was replaced by an axisymmetric section with the maximum-half-breadth profile of the actual cowl. The fan and core exhaust flow boundaries were simulated by assuming a constant-area jet exhaust flow. Figure IV-5 shows the axisymmetric-nacelle pressure distribution along the top and bottom meridians of the nacelle for the angle of attack and inlet mass-flow ratio corresponding to cruise.

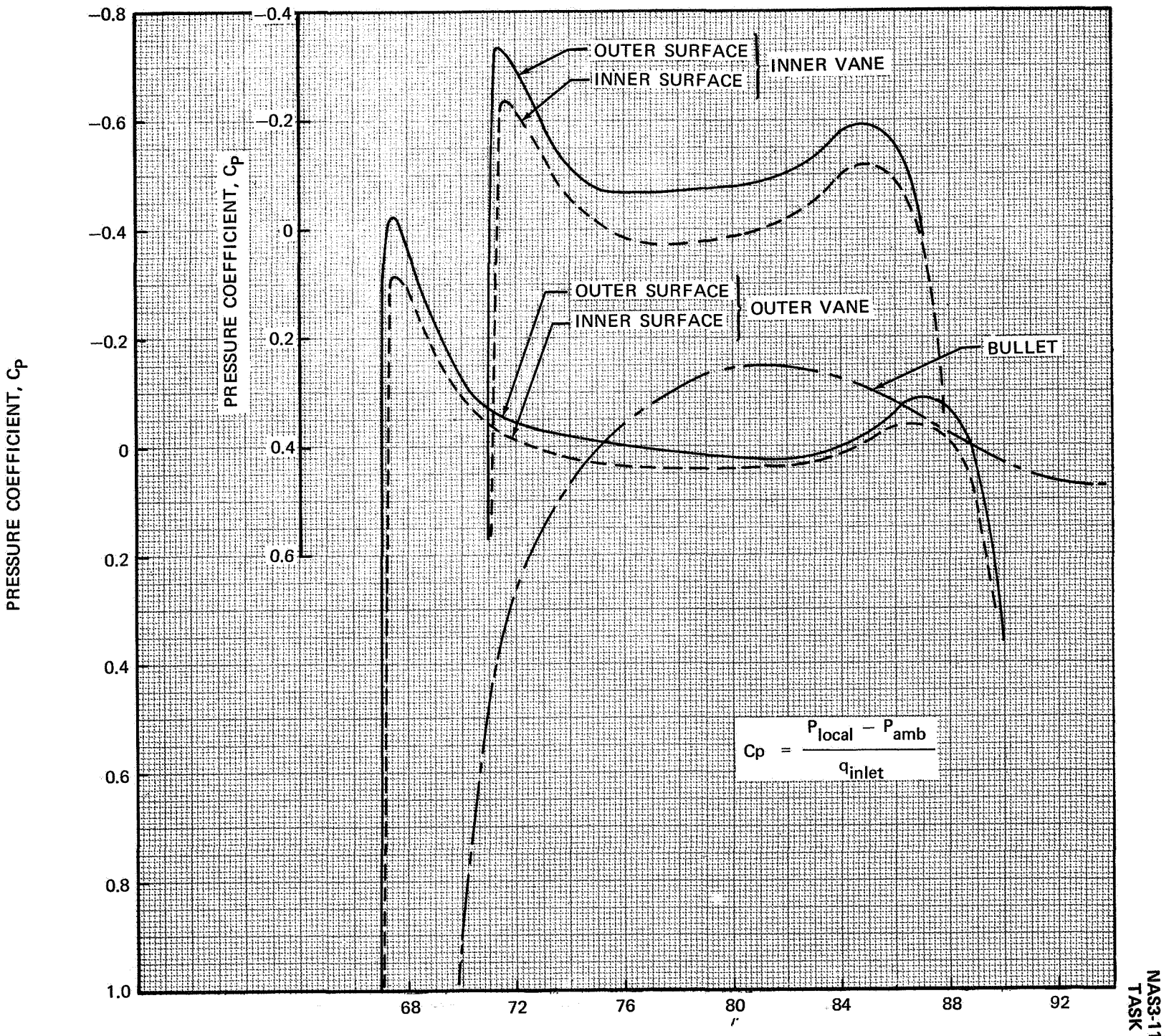

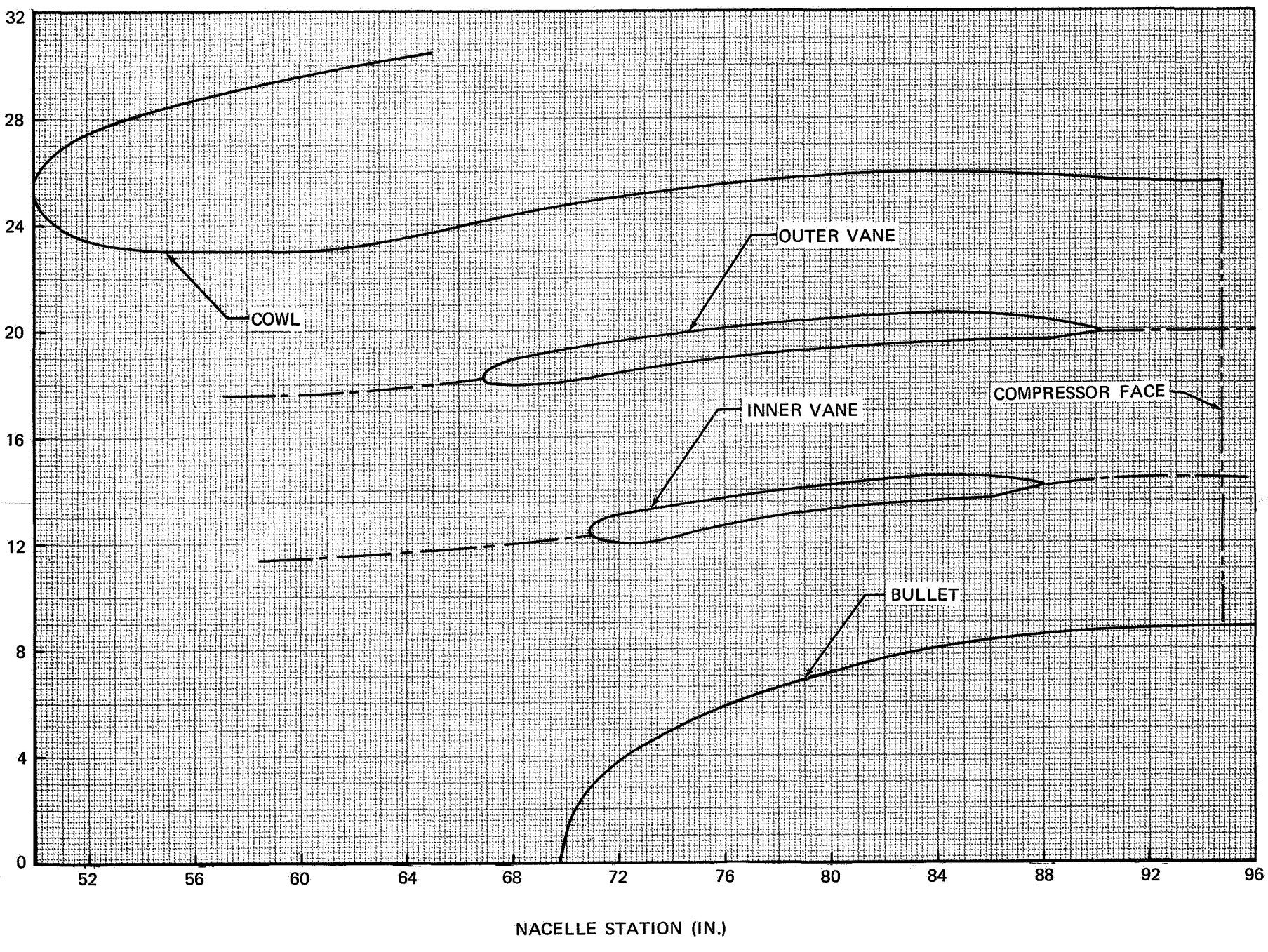

FIGURE IV-3. TWO-RING INLET PRESSURE DISTRIBUTIONS

Good nacelle design is characterized by small adverse pressure gradients as well as by low pressure peaks. The pressure gradient on the inlet cowl is good. The gradient on the afterbody is quite large, although the aft pressure peak is reasonable.

The unusually large turbine diameter that results from the relatively low rotor speeds in the quiet engine causes the beginning of the afterbody curvature of the gas-generator nacelle to be farther aft than desired. In turn, the fan-cowl afterbody curvature also must be farther aft to provide a satisfactory fan-duct area. The resulting nacelle boattail angle is 11 degrees (0.19 rad), which is satisfactory. The relatively small radius of curvature causes the large aft pressure gradient seen in Figure IV-5. Increasing the radius of curvature would improve the pressure gradient but would cause the nacelle to be longer, or would cause the core engine boattail angle to be increased to obtain the correct fan nozzle area. In addition, the difference between the nacelle and core-engine boattail angles would increase. A longer nacelle would cause the nacelle to be located farther forward in order to maintain the desired location of the exhaust relative to the wing. The resulting nacelle design is a compromise of all these effects.

The large adverse gradient is caused partly by the simulation of the fan exhaust boundary by a solid surface. In reality, probably neither the peak value nor the gradient would be as severe.

(The isolated nacelle-pylon wind-tunnel tests, reported in Task III, were conducted with the nacelle model based on the Task IV design. The results show that the nacelle drag was equal to the calculated value, which indicates that the nacelle aerodynamics are satisfactory.)

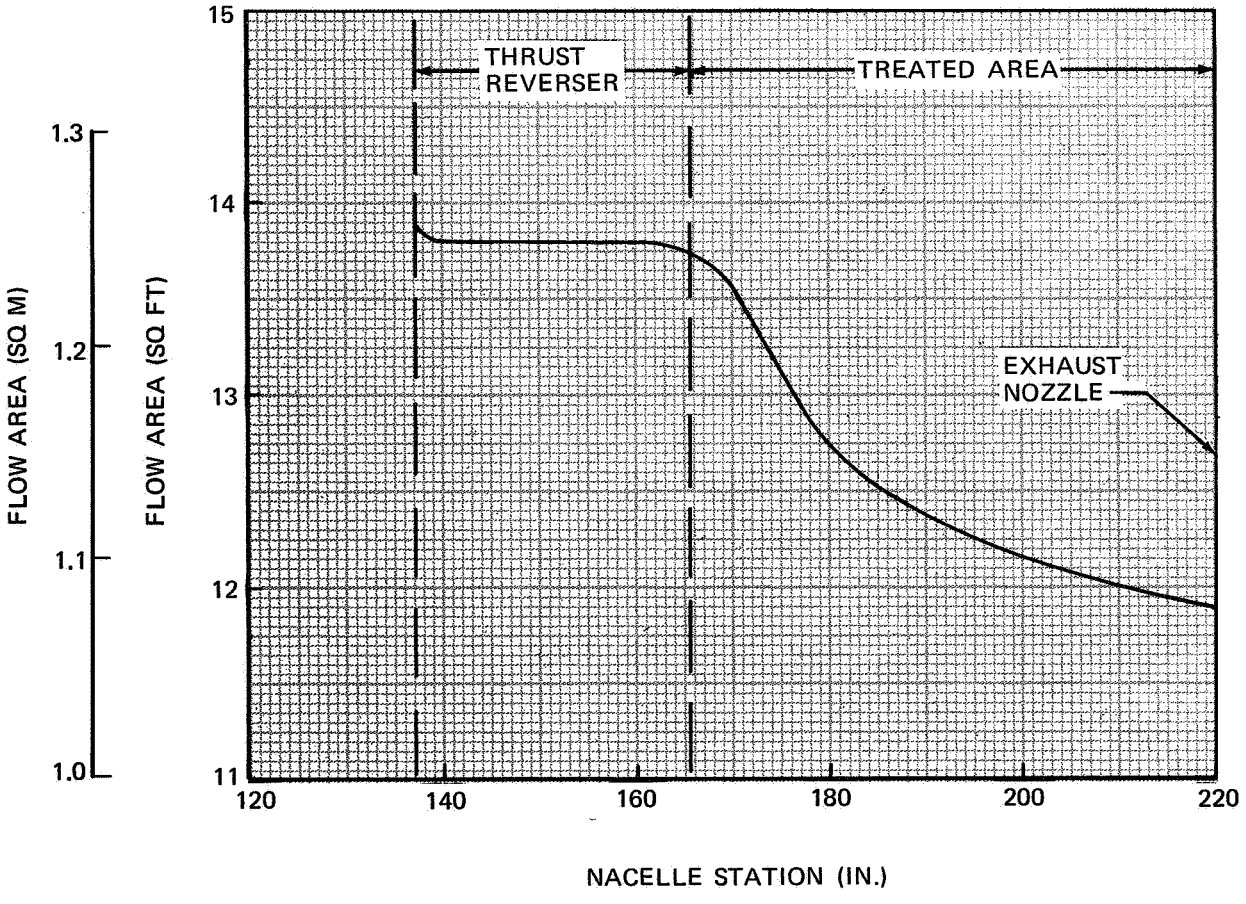

FIGURE IV-4. FAN-EXHAUST-DUCT AREA DISTRIBUTION

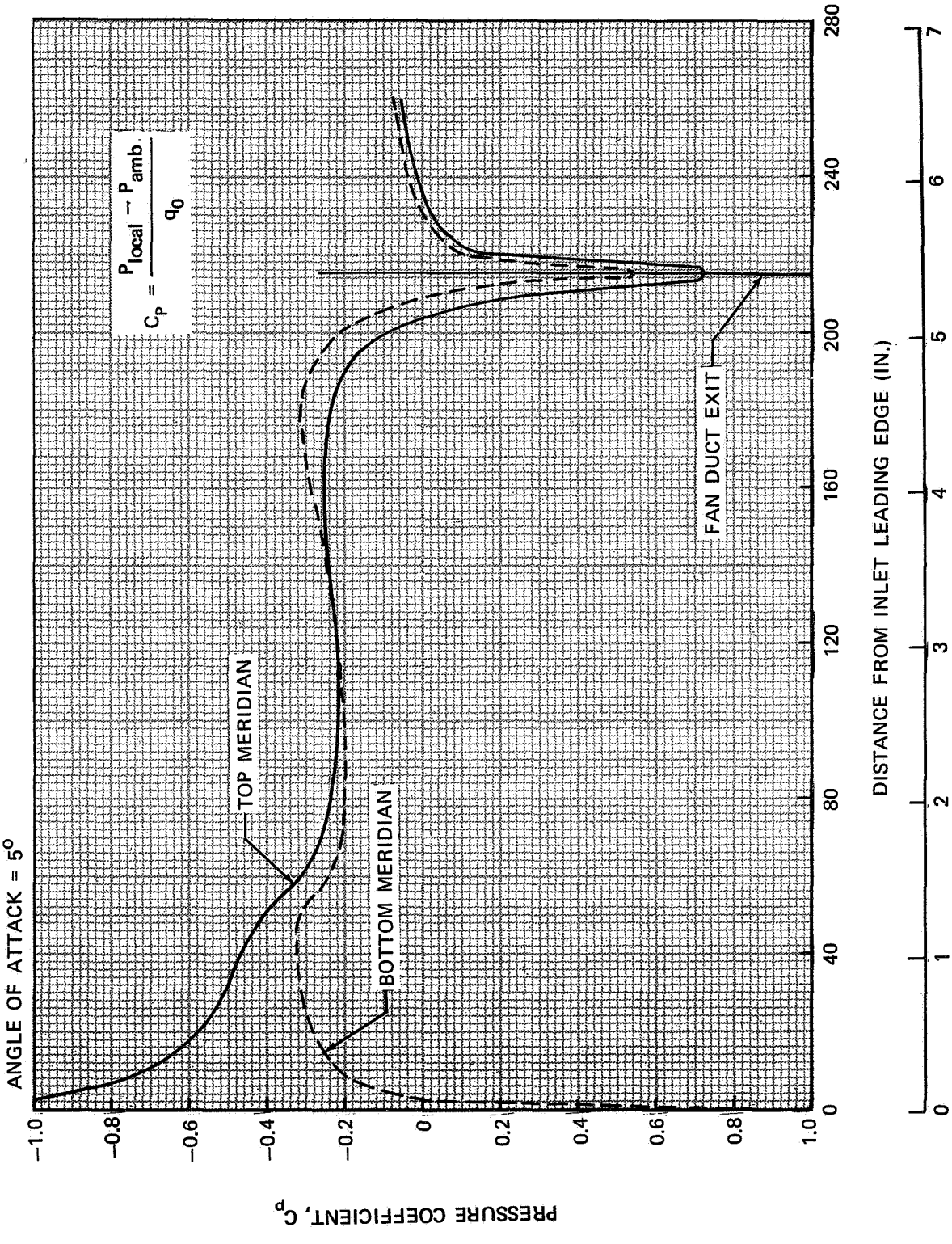

FIGURE IV-5. AXISYMMETRIC POTENTIAL FLOW PRESSURE DISTRIBUTION

ENGINE LOCATION

After establishment of the general configuration of the engine with both inlet and fan-exhaust ducts installed, the engine location required by the large nacelle diameter was examined. The ground-clearance and inlet-height criteria and the drag considerations outlined in Task II were reevaluated. The primary-nozzle exit was located at the 10-percent point of the local wing chord at the inboard nacelle location to minimize interference drag. The criterion defined as the ratio of inlet-centerline height to inlet diameter was relaxed from 1.30 to 1.28 to accommodate the increased nacelle diameter required by the increased fan diameter of the Task IV engine. Although this provision will permit the aspiration of slightly larger particles into the engine, the increase is not large enough to cause concern about decreased engine life. A minimum ground clearance of 31 inches (78 cm) was maintained to ensure compliance with ground-clearance criteria established during Task I.

PYLON DESIGN

The pylon design retains the basic three-spar box-beam concept developed for Task I. For simplicity of retrofit, the wing front spar fitting and the wing lower surface attach angles were not changed. The pylon contours are symmetrical in the region of the nacelle, but cambered in the region of the wing.

MECHANICAL DESIGN

Every effort was made to retain the maximum number of standard DC-8-61 engine accessories. By reorienting the gearbox-driven accessories relative to one another, it was possible to retain the standard alternator, hydraulic pump, tachometer, fuel boost pump, and fuel control. To provide access to the engine gearbox and accessories, the fan-air exit ducts were hinged at the top to permit approximately 30 degrees (0.52 rad) of opening on each side of the bottom. This opening provides sufficient space allowance to permit removal, replacement, and repair of all engine accessories, without the necessity for providing powered lifting devices to lift the relatively heavy weight of the fan-exhaust ducting.

Provision was made in the cowl exterior skin for access doors to service the nacelle ice-protection system. A brief examination of other doors brought no unusual problems to light. Standard top-hinged, skin-and-stringer construction doors were assumed for all aft applications.

Adequate space provisions were made both between the engine core and the fan exhaust ducts and between the front engine mount and the fan case to assume that control cables, linkage, and wiring could be satisfactorily accommodated. Conventional fire walls are provided, as well as the standard fire detection system now in use on the DC-8-61.

Uncertainties as to the heat load in the compartment between the engine core and the fan exhaust ducts made an analysis of compartment cooling and ventilating prohibitively difficult. Provision was made for both cooling and ventilating in the lower fan duct bifurcated section and for inlet and outlet of substantial quantities of ambient air.

ENGINE-MOUNTING PROVISIONS

In accordance with the Task I design criteria, the front mount was designed to attach to the gas-generator case. However, as a result of loads analysis and mechanical-design studies, a change was made in the load distribution between the front and rear mounts. Difficulties in carrying loads into the pylon through the rear mount, as well as mechanical assembly difficulties, led to a decision to design the rear mount for vertical loads only. The forward mount was designed to carry vertical, side, torque, and thrust loads.

THRUST REVERSER

Essentially the same design philosophy developed in Task I was applied to the thrust reverser design. Because of the requirement for a high-efficiency fan thrust reverser, design efforts were directed toward a cascade-type reverser employing a blocker-door arrangement to direct fan flow into a cascade mounted at the duct entrance. This design employs a total of 10 blocker-doors directing fan flow into 20 cascades. The blocker doors are interconnected with the wind sock to provide actuation by a common actuator. The interconnection permits actuation of all components of the reverser by only four hydraulic actuators. This design also benefits by a high degree of interchangeability, in that identical cascades, blocker doors, and flaps are used in both the right- and left-hand sides of the reverser.

A brief examination of reverser fore-and-aft location was conducted to assure optimum reverser positioning. The forward location (reverser upstream of the fan exhaust ducts) proved to be lighter in weight with comparable, or slightly improved, performance as compared with the aft location (reverser downstream of the fan exhaust ducts). Although the aft-location reverser was lighter in weight, as a result of the smaller diameter, the weight benefit was more than offset by the increased

structure required to carry the reversing loads into the engine case. A small performance benefit would be expected for the forward-location reverser as a result of the slightly smaller amount of turning required in the cascades of the forward design as compared with that required in the aft design.

Although surface area for acoustic treatment was available in the fan thrust reverser additional weight would be required to provide for reasonable life of the acoustic treatment. For this reason, no acoustic treatment was provided in the fan thrust reverser.

The gas-generator exhaust spoiler is of the simple target type, deflecting the gas-generator-exhaust flow 90 degrees (1.6 rad). It is similar in concept to the reverser now in service on the DC-9. A four-bar linkage deploys two panels that normally form the aft tailcone fairing into the gas-generator exhaust stream, deflecting the flow stream horizontally to reduce the probability of foreign-object damage resulting from ingestion of ground debris disturbed by the reversed flow.

An alternate spoiler design also was investigated. This concept proposed using the aft pylon panels as the flow deflectors. The primary advantage of this concept was the possibility of carrying a large portion of the gas-generator reversing loads directly into the pylon structure, relieving the engine mounts of this load. It also offered the possibility of stowing the operating mechanism (linkage, actuators, etc.) in the relatively unencumbered space of the aft section of the pylon. A brief examination of this concept suggested that validation of the design would extend the effort beyond the program goals. For this reason, the concept was abandoned in favor of the already proven DC-9 concept.

PNEUMATIC SYSTEM

An examination of those aircraft services requiring engine bleed air revealed the following:

1. Nacelle ice-protection requirements were substantially increased.

2. All other aircraft pneumatic services were relatively unchanged.

Analysis of nacelle ice-protection requirements resulted in a decision to continue to use engine bleed air for nacelle anti-icing, although approximately 3.4 pounds kg mass per second of engine air flow would be required for each engine. This requirement is based on the most severe icing environment foreseen, which occurs during a 45-minute hold at 15,000 feet (4572 m) in a continuous maximum cloud. A limited water runback was allowed to form an ice buildup with a triangular shape 0.152-inch high (3.86 mm) and 6 inches (15 cm) long. An air distribution system is necessary to provide anti-icing air to the cowl lip, the leading edges of both concentric rings, and the leading edges of both fore and aft supporting struts. Ice protection for the centerbody was assumed to be provided by the engine manufacturer. Evaluations of other methods of ice protection, notably electrical heating, were abandoned because power requirements were prohibitively large.

In addition, aircraft pneumatic services, that is, cabin pressurization and air conditioning, airframe ice protection, windshield rain removal, etc., required a maximum of 2.9 pounds kg mass per second of engine airflow per engine. Although the total quantity of engine bleed flow was relatively large in terms of common design practice, coordination with various engine manufacturers suggested that adequate engine design provisions could be made if the engine bleed-flow requirements were established during the early stages of the engine design.

TASK V

AIRPLANE PERFORMANCE AND OPERATING COST ANALYSIS

LIST OF ILLUSTRATIONS

LIST OF TABLES

TASK V

AIRPLANE PERFORMANCE AND OPERATING COST ANALYSIS

The aerodynamic performance and direct operating cost (DOC) for the DC-8-61 powered with the JT3D-3B and with the retrofitted quiet engine defined in Task IV are presented in this section. The results of the work done in Tasks III, IV, and VI are incorporated into the performance and costs shown herein for the airplane powered by the quiet engine.

Performance for the present DC-8-61 is shown in Figures II-10 through II-17 of Task II. These data are not shown separately in this section, but instead are shown on the same figures that present the performance of the DC-8-61 with the quiet engine (DC-8-61-Q2). The following comments apply equally to both airplanes.

1. As in Task II, the performance is calculated for a passenger airplane. A survey showed that a typical payload, hereafter referred to as the normal payload, consists of 193 passengers with baggage and a nominal cargo load. Each passenger is assumed to weigh 165 pounds (75 kg) and his baggage is assumed to weigh 35 pounds (16 kg). The cargo volume is based on using 25 percent of the space available after subtracting a 25-percent stacking loss (625 cubic feet – 18 m^3) and baggage space equal to 4.5 cubic feet (0.127 m^3) per passenger (868 cubic feet – 25 m^3). A cargo density of 10 pounds per cubic foot (159 kg/m^3) is assumed. On this basis, the passengers and baggage weigh 38,600 pounds (17,509 kg) and the cargo weighs 2516 pounds (1141 kg), for a total payload of 41,116 pounds (18,650 kg).

2. The airplane is operated at 0.82 Mach number for ranges less than those corresponding to maximum takeoff gross weight (TOGW), because the operators prefer to fly fast and pay the resulting penalty in specific range. For ranges corresponding to maximum TOGW, the operators prefer to fly at the speed for nearly optimum specific range in order to reduce the fuel load and increase the payload. They therefore must fly slower.

3. FAA field length is based on four-engine operation and is defined as 1.15 times the distance measured from the start of roll to the point where the airplane is 35 feet (11 m) above the runway.

4. Initial cruise altitude is defined as the highest altitude at which the airplane can cruise at 0.82 Mach number, including a margin for maneuvering before buffet onset.

5. Approach characteristics are calculated at sea level and at 1.3 times stall airspeed with full flaps.

DC-8-61 PERFORMANCE WITH THE JT3D-3B ENGINE

The performance for the present airplane with the JT3D-3B engine is the same as the performance shown for the airplane in the section covering Task II work. It is based on flight-test results. The engine performance is based on test-stand and flight-test results for engines with the Douglas production-inlet hardware and exhaust-system hardware installed. The performance shown is the same as that presented in the FAA-approved flight manual and in the Douglas performance report for the DC-8-61 airplane.

Table V-I is a weight statement for the airplane with JT3D-3B engines. The maximum design takeoff weight, zero fuel weight, and landing weights are FAA limiting weights. The operational empty weight (OEW or OWE) includes the items the operator requires.

TABLE V-I
DC-8-61 WEIGHT STATEMENT JT3D-3B ENGINES

	WEIGHT			
	LB	KG	LB	KG
MAXIMUM DESIGN TAKEOFF WEIGHT, MAXIMUM TOGW			325,000	147,420
MAXIMUM DESIGN ZERO FUEL WEIGHT			224,000	101,606
MAXIMUM DESIGN LANDING WEIGHT			240,000	108,864
OPERATIONAL EMPTY WEIGHT, OWE			156,803	71,126
MANUFACTURER'S EMPTY WEIGHT, MWE	149,339	67,740		
OPERATIONAL ITEMS	7,464	3,386		
SPACE-LIMITED PAYLOAD			56,845	25,785
PASSENGERS (193 AT 165 LB – 75 KG)	31,845	14,445		
BAGGAGE AND CARGO	25,000	11,340		
NORMAL PAYLOAD			41,116	18,650
PASSENGERS (193 AT 165 LB – 75 KG)	31,845	14,445		
BAGGAGE (35 LB – 16 KG/PASSENGER)	6,755	3,064		
CARGO (251.6 CU FT AT 10 LB/CU FT – 7.36 CU M AT 162 KG/CU M)	2,516	1,141		

DC-8-61 PERFORMANCE WITH THE QUIET ENGINE

The performance shown herein is for the DC-8-61 airplane powered by the quiet engines. The airplane is designated the DC-8-61-Q2 to differentiate it from the DC-8-61-Q1 used in Task II. The performance shown in Task II was based on preliminary quiet-engine physical and performance characteristics that were somewhat different from those selected for Tasks IV, V, and VI. The performance of the DC-8-61-Q2 airplane was obtained by calculating (by consistent methods) the differences between the installed performance of the quiet engine and that of the JT3D-3B and by then applying these differences to the performance of the DC-8-61 having the JT3D-3B engine.

AIRPLANE WEIGHT AND PAYLOAD

Table V-II shows the changes in DC-8-61 manufacturers empty weight and OWE due to retrofitting the quiet engines. The increase shown is 1359 pounds (616 kg) per airplane less than the increase indicated in Task II. The results of the flutter testing reported in Task VI shows that wing reskinning will not be necessary. The saving in weight that results is more than the weight increase caused by the addition of a powered elevator and redundant yaw damper indicated to be necessary by the wind-tunnel tests reported in Task III.

The work in Task II showed that the FAA-certified Maximum Design Zero Fuel Weight of 224,000 pounds (101,606 kg) would be exceeded by about 800 pounds (363 kg). The final analysis presented in Table V-III shows that the certified value will not be exceeded.

TABLE V-II
WEIGHT-CHANGE SUMMARY

	WEIGHT REMOVED		WEIGHT ADDED		ΔWEIGHT	
	LB	KG	LB	KG	LB	KG
ENGINE AND NACELLE INBOARD	6876	3119	8986	4076	2110	957
ENGINE AND NACELLE INBOARD	6876	3119	8986	4076	2110	957
ENGINE AND NACELLE OUTBOARD	6819	3093	8929	4050	2110	957
ENGINE AND NACELLE OUTBOARD	6819	3093	8929	4050	2110	957
PYLON INBOARD	798	362	1102	500	304	138
PYLON INBOARD	798	362	1102	500	304	138
PYLON OUTBOARD	808	367	1119	508	311	141
PYLON OUTBOARD	808	367	1119	508	311	141
ELEVATOR	0	0	115	52	115	52
RUDDER	0	0	20	9	20	9
TOTAL PER AIRPLANE					9805	4448

TABLE V-III
WEIGHT STATEMENT

	DC-8-61 (JT3D-3B)				DC-8-61-Q2 QUIET ENGINE			
	LB	KG	LB	KG	LB	KG	LB	KG
MAXIMUM DESIGN TAKEOFF WEIGHT			325,000	147,420			325,000	147,420
MAXIMUM DESIGN ZERO FUEL WEIGHT			224,000	101,606			224,000	101,606
MAXIMUM DESIGN LANDING WEIGHT			240,000	108,864			240,000	108,864
OPERATIONAL EMPTY WEIGHT			166,608	75,573			156,803	71,126
MANUFACTURER'S EMPTY WEIGHT	149,339	67,740			159,144	72,188		
OPERATIONAL ITEMS	7,464	3,386			7,464	3,386		
SPACE-LIMITED PAYLOAD			56,845	25,785			56,845	25,785
PASSENGERS (193 AT 165 LB 75 KG)	31,845	14,445			31,845	14,445		
BAGGAGE AND CARGO	25,000	11,340			25,000	11,340		
NORMAL PAYLOAD			41,116	18,650			41,116	18,650
PASSENGERS (193 AT 165 LB 75 KG)	31,845	14,445			31,845	14,445		
BAGGAGE (35 LB 16 KG/ PASSENGER)	6,755	3,064			6,755	3,064		
CARGO (251.6 FT^3 AT 10 LB/FT^3 7 M^3 AT 4.536 KG/M^3)	2,516	1,141			2,516	1,141		

INSTALLED-ENGINE PERFORMANCE

The installed-engine performance of the quiet engine is based on the engine configuration and performance specified in Task IV. The engine performance shown is for the Allison PD-218-Q study engine (from the NASA Quiet Engine Definition Program), which was considered representative of the selected engine configuration. The basic engine performance is taken from Allison PD-218-Q automatic computing card deck for EDR 5846-A, dated July 5, 1968.

INSTALLATION LOSSES

A description of the engine-installation assumptions used for the quiet engine installation in the DC-8-61 is presented in the following paragraphs:

Inlet and Exhaust Total Pressure Losses

The total-pressure losses resulting from acoustic treatment in the inlet and exhaust ducts were analytically determined by calculating the drag of the internal surfaces and then equating that drag to an equivalent total-pressure change. Wind-tunnel tests at Douglas show that acoustically treated surfaces are approximately 40 percent rougher than smooth aluminum. A friction factor of 0.0039 was therefore used for these calculations.

Airbleed and Shaft-Power Extraction

DC-8-61 values of airbleed and shaft-power extraction were used.

Nacelle Cooling

Fan bleed was assumed for cooling the accessories and engine compartment. No thrust recovery is assumed for exhausting the flow overboard.

Thrust-Reverser Leakage

Analysis shows that the leakage that can be expected through the reverser cascade causes a loss of 0.14 percent of fan gross thrust. This value has been used to account for thrust-reverser leakage.

Nacelle-Pylon Drag

The drag of the nacelle and pylon is based on the Task III wind-tunnel test results. Those results show that the drag of the DC-8-61-Q2 is essentially the same as the drag of the production DC-8-61 at cruise conditions.

The results of the high-speed wind-tunnel drag tests are applicable only for high speed or for cruise conditions. To use the wind-tunnel data at other flight conditions the measured drags were reduced to the following coefficients, which were in turn incorporated into the installed-engine performance computing program:

D/q_o – the drag of those components that are subjected to free-stream dynamic pressure, including the excessive drag effects described in Task III.

D/q_F – the drag of those components over which the fan exhaust flows.

D/q_G – the drag of those components over which the gas-generator exhaust flows.

The following method was used to determine these coefficients.

The scrubbing drag, D/q_F and D/q_G, of the JT3D-3B and quiet-engine nacelles and pylons were calculated at cruise. The value of free-stream drag for the quiet engine was then adjusted so that the total drag for the installation was equal to the drag of the JT3D-3B installation at cruise. The free-stream drag then includes the excess drag effects discussed in Task III. The final drag coefficients used to calculate airplane performance are shown in Table V-IV.

TABLE V-IV
DRAG COEFFICIENTS

	JT3D-3B	QUIET ENGINE
FREE STREAM, D/q_0	1.1274	1.420
SCRUBBING		
FAN JET, D/q_F	0.4090	0.2850
PRIMARY JET, D/q_G	0.0134	0.0206

These values were used at all flight conditions. As is indicated in Task III, the source of the excess drag is not evident. There are indications that it may be a model effect. What part, if any, of the excess drag is caused by interference is not clear. To be conservative, the values of drag shown were used for low-speed flight conditions as well as for high-speed. The effect of the excess drag on takeoff thrust is less than one-half percent.

COMPARISON OF INSTALLATION LOSSES

Table V-V shows a comparison of installation losses for the JT3D-3B and for the baseline quiet engine. The JT3D-3B values shown were calculated with the engine-specification data and installation-handbook correction factors. The fractional losses for both engines are essentially the same.

INSTALLED-ENGINE PERFORMANCE CALCULATION

The engine-performance automatic computing program supplied by Allison was used as a subroutine in Douglas Program Number J5CA, which was used to calculate the installed-engine performance for the quiet engine. The calculated performance includes the installation losses previously described, including the nacelle-pylon drag.

Similar performance was calculated for the present JT3D-3B installation. The differences in performance between the two installations were applied to the flight performance of the DC-8-61 to obtain performance for the DC-8-61-Q2.

TABLE V-V
COMPARISON OF INSTALLATION LOSSES,
MAX CRUISE POWER (35,000 FT – 10,668 M; M = 0.82)

	BASELINE QUIET ENGINE		JT3D-3B*	
	THRUST	FUEL FLOW	THRUST	FUEL FLOW
	$\Delta F_n/F_n$	$\Delta W_F/W_F$	$\Delta F_n/F_n$	$\Delta W_F/W_F$
INLET	0.0073	0	0	0
FAN EXHAUST	0.0038	0	0	0
AIRBLEED	0.0302	0.0164	0.0238	0.0175
SHAFT POWER	0.0020	–0.0001	0.0030	0.0010
NACELLE COOLING	0.0080	0	NEGLIGIBLE	0
THRUST-REVERSER LEAKAGE	0.0028	0	0.0013	0
TOTAL DRAG	0.0887	0	0.1154	0
FAN COWL	0.0536	0	0.0593	0
SCRUBBING	0.0351	0	0.0561	0
TOTAL LOSSES	0.1428	0.0163	0.1435	0.0185

*ASSUMES THE SAME CALCULATION METHOD AS FOR THE QUIET ENGINE.

AIRPLANE PERFORMANCE COMPARISONS

The following presentation of performance comparisons is in the same form as that shown in Task II. The comparisons are shown for three ranges: the range corresponding to maximum TOGW and two shorter ranges. The shortest range, 847 nautical miles, is the average domestic range for the DC-8.

The performance comparisons shown here are not vastly different from those of Task II, in spite of the significant differences in the quiet-engine-powered airplane structural changes that are indicated in the weight analysis sections of Tasks II and V.

PAYLOAD RANGE

The OWE of the quiet-engine-powered airplane is 9805 pounds (4448 kg) greater than the OWE of the present airplane. This means that for a given payload the fuel load must be less for operation at maximum TOGW. Figure V-1 compares the payload-range curves for the two airplanes. Note that in spite of the heavier OWE the airplane has a 650-nautical-mile longer range with the quiet engine. This is the direct result of the improved specific fuel consumption (SFC) shown in Figure V-2, which more than compensates for the increase in OWE.

It is to be expected then that the advantage gained from SFC improvement will be less and less as ranges become shorter. Figure V-3 shows that for ranges less than about 1250 nautical miles the OWE increase is the dominant factor and that the takeoff weight of the present airplane is less for a given range.

TAKEOFF

A comparison of installed takeoff thrust is shown in Figure V-4. The increase in quiet-engine thrust is due to sizing the engine for a high cruise thrust and also to the higher characteristic thrust lapse rate with speed and altitude for high-bypass-ratio engines.

The effect of the higher takeoff thrust on takeoff field length is shown in Figure V-5 for operation with 15- and 25-degree flaps. The improvement depends on TOGW and is of the order of 20 percent. Note the large increase in gross weight that is possible for operation from a given field length. The ranges indicated are for the DC-8-61-Q2 airplane. Figure V-6 shows the improvement in takeoff field length due to the quiet engines as a function of range.

The FAA requires that V_2 be equal to or greater than 1.1 times V_{MC_A}, the minimum control speed in the air. V_2 is the airspeed when the airplane is 35 feet (11 m) above the runway. The value of V_2 for the DC-8-61-Q2 is less than 1.1 V_{MC_A} for gross weights less than 230,000 pounds (104,328 kg) with a 25-degree flap angle. Takeoff performance for these cases is shown on Figure V-5. The value of V_{MC_A} for the DC-8-61-Q2 is 17 knots higher than that for the present DC-8-61. The DC-8-61 FAA-certified field length is based on DC-8-50 minimum control speed, which is 14 knots greater than the actual DC-8-61 V_{MC}. The increase in V_{MC} for the DC-8-61-Q2 for certification purposes is therefore only 3 knots (Figure VI-28 of Task VI).

Figure V-7 shows the increase in height above the runway that results from the higher takeoff thrust. The increase is approximately 250 feet (76 m), although it varies somewhat with gross weight.

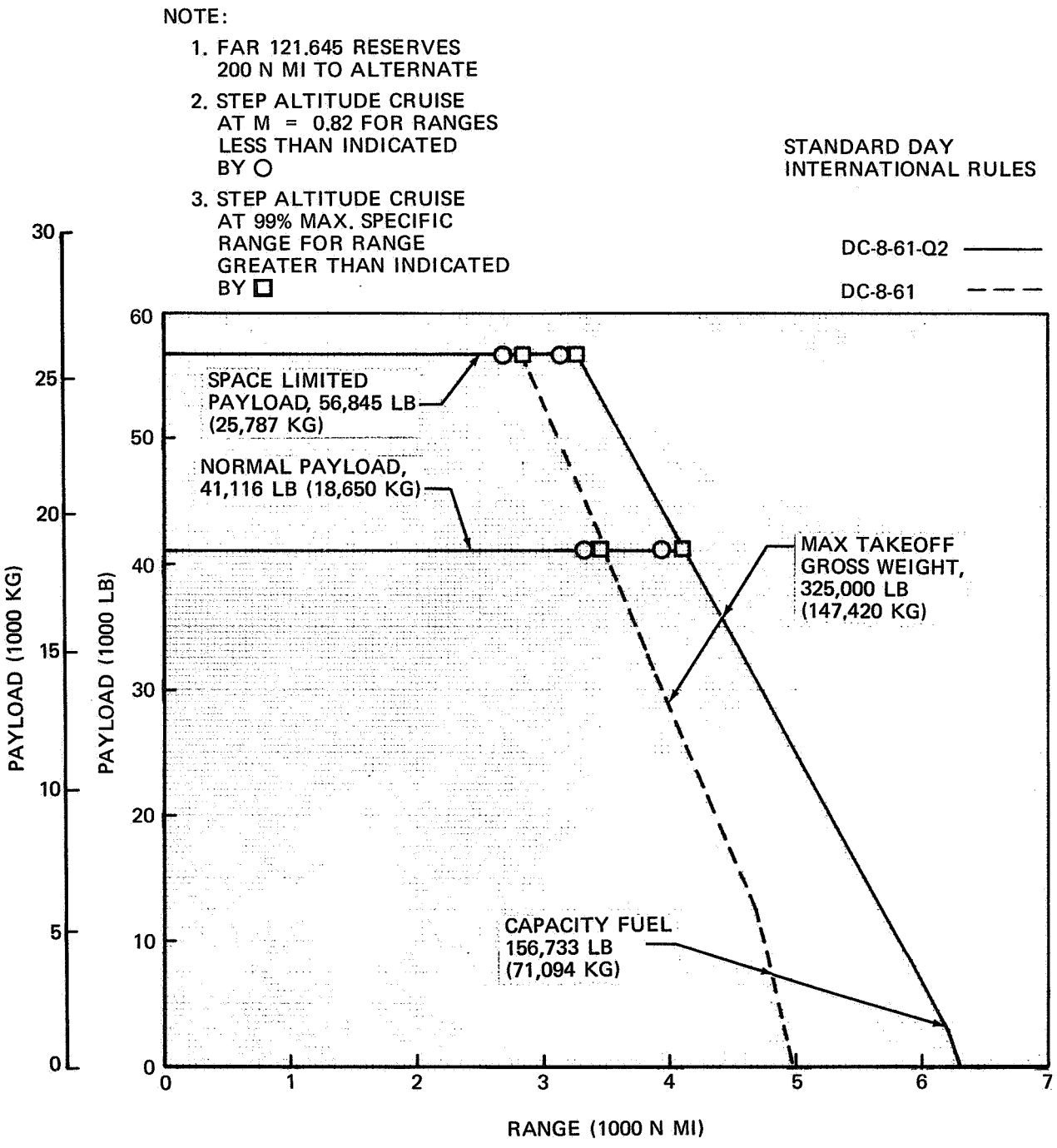

FIGURE V-1. PAYLOAD-RANGE CAPABILITIES

CLIMB

The available net thrust for climb is shown in Figure V-8 for a typical climb profile. The curves show that the quiet-engine-powered airplane can get to a given cruising altitude faster but will have to climb at a slightly steeper angle. The small increase in angle would not be objectionable to the passengers.

CRUISE

The comparison of initial cruise altitude is shown in Figure V-9. The three ranges previously mentioned are indicated. The advantage in initial cruise altitude for the maximum TOGW case is shown. Note that the quiet-engine powered airplane is about 4000 pounds (1814 kg) heavier at start of cruise. This tends to degrade the advantage in initial cruise altitude it enjoys because of its higher cruise thrust. Figure V-10 shows the improvement in initial cruise altitude as a function of range.

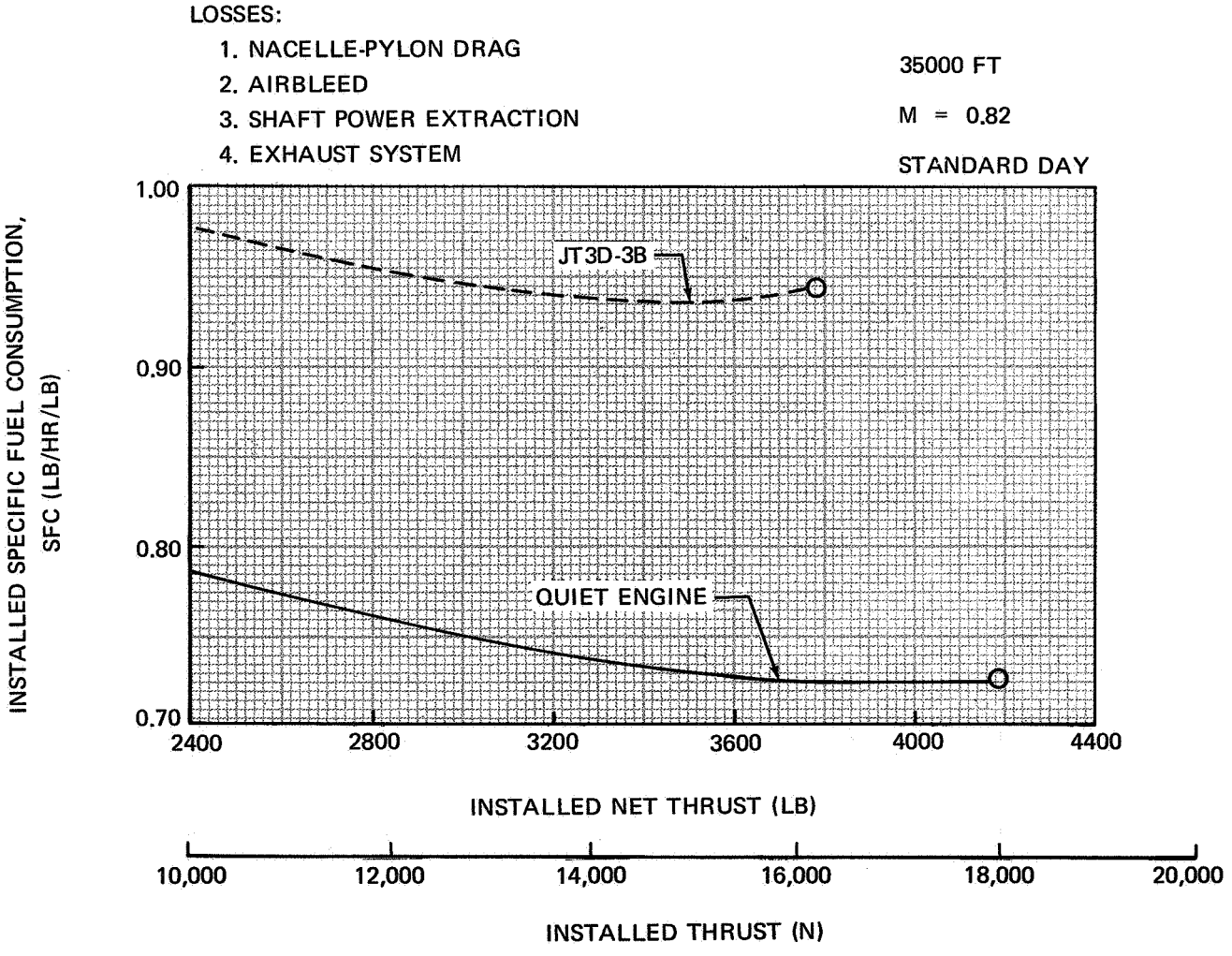

FIGURE V-2. CRUISE SPECIFIC FUEL CONSUMPTION

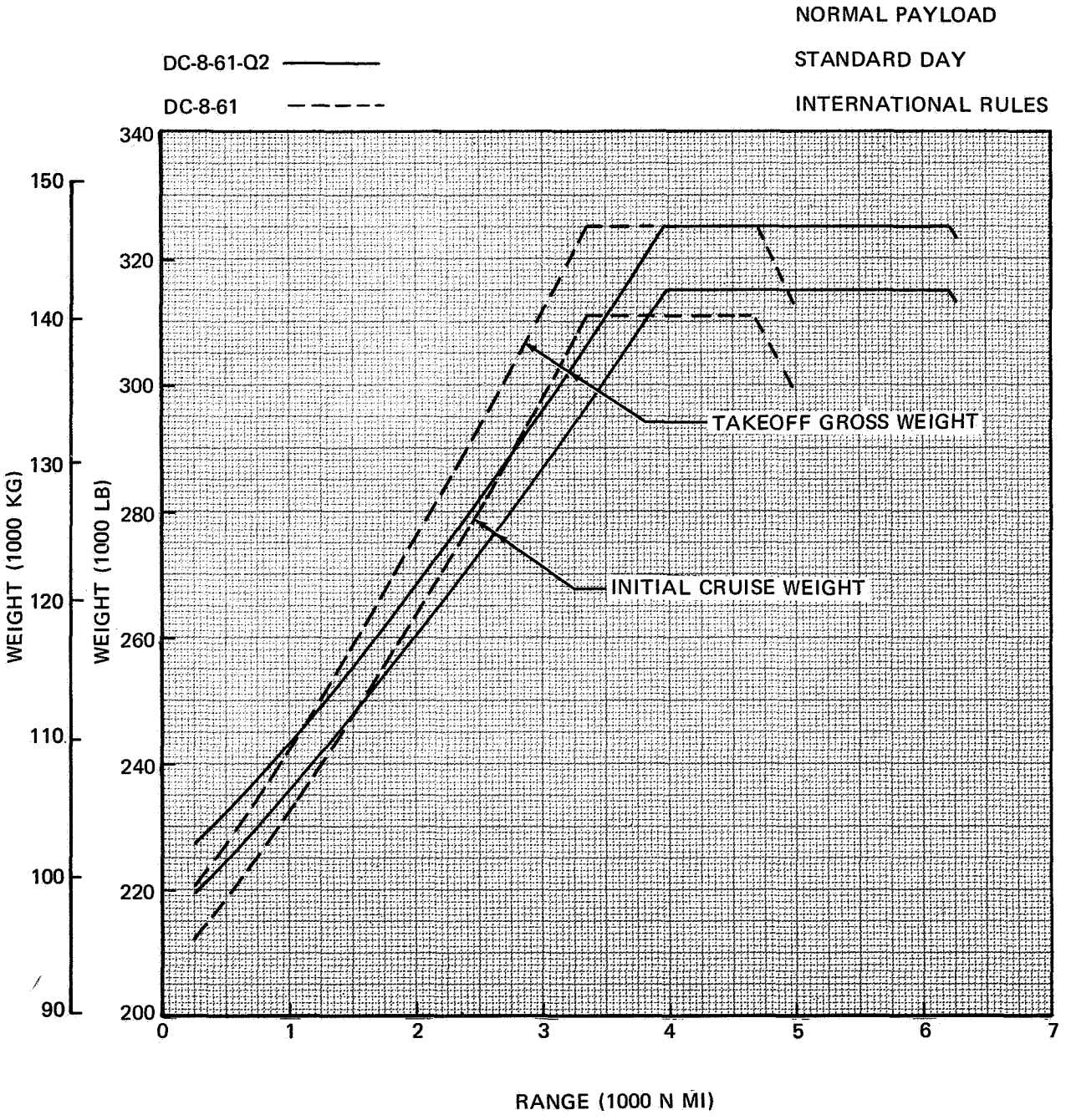

FIGURE V-3. TAKEOFF AND INITIAL CRUISE WEIGHT

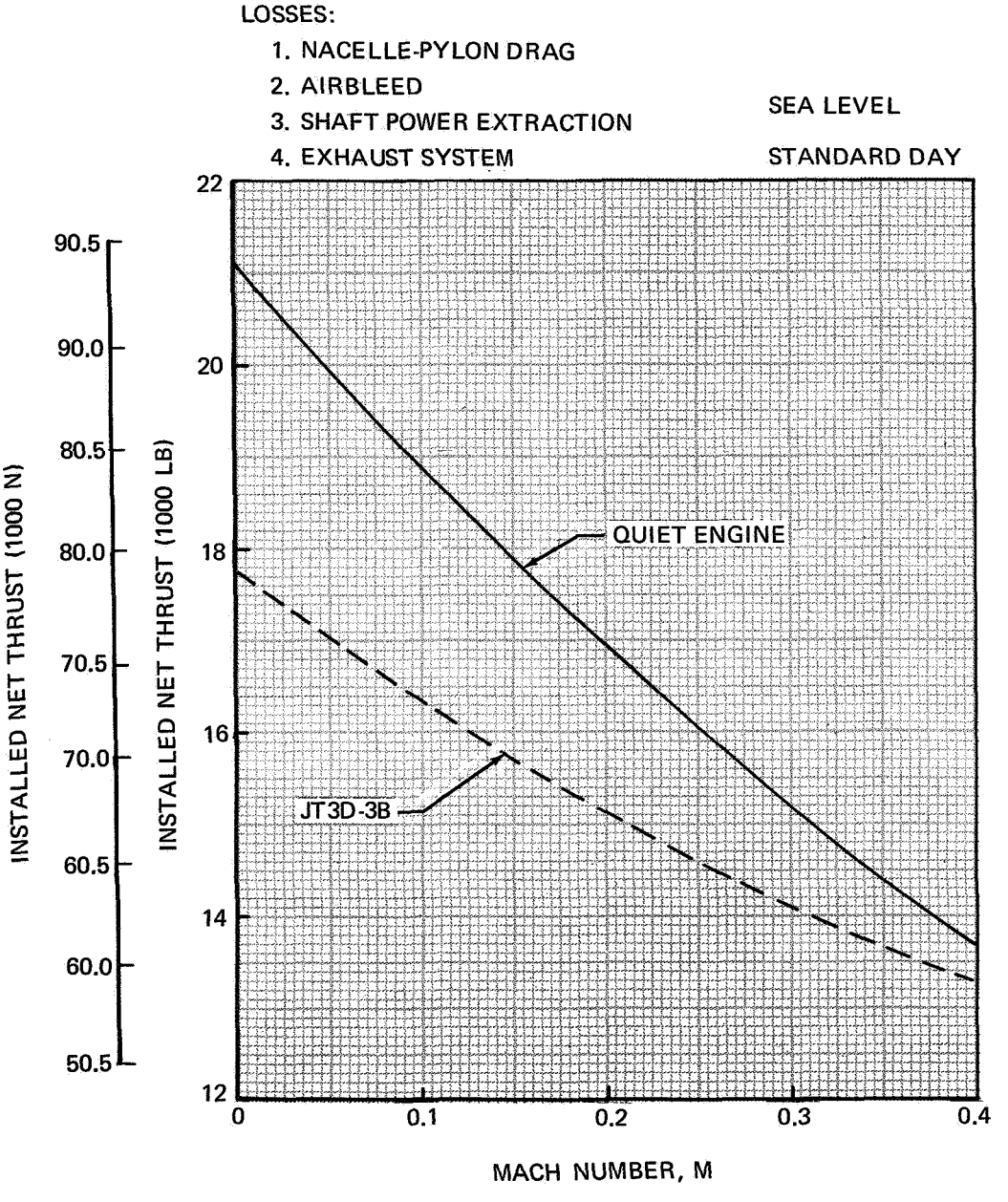

FIGURE V-4. TAKEOFF THRUST

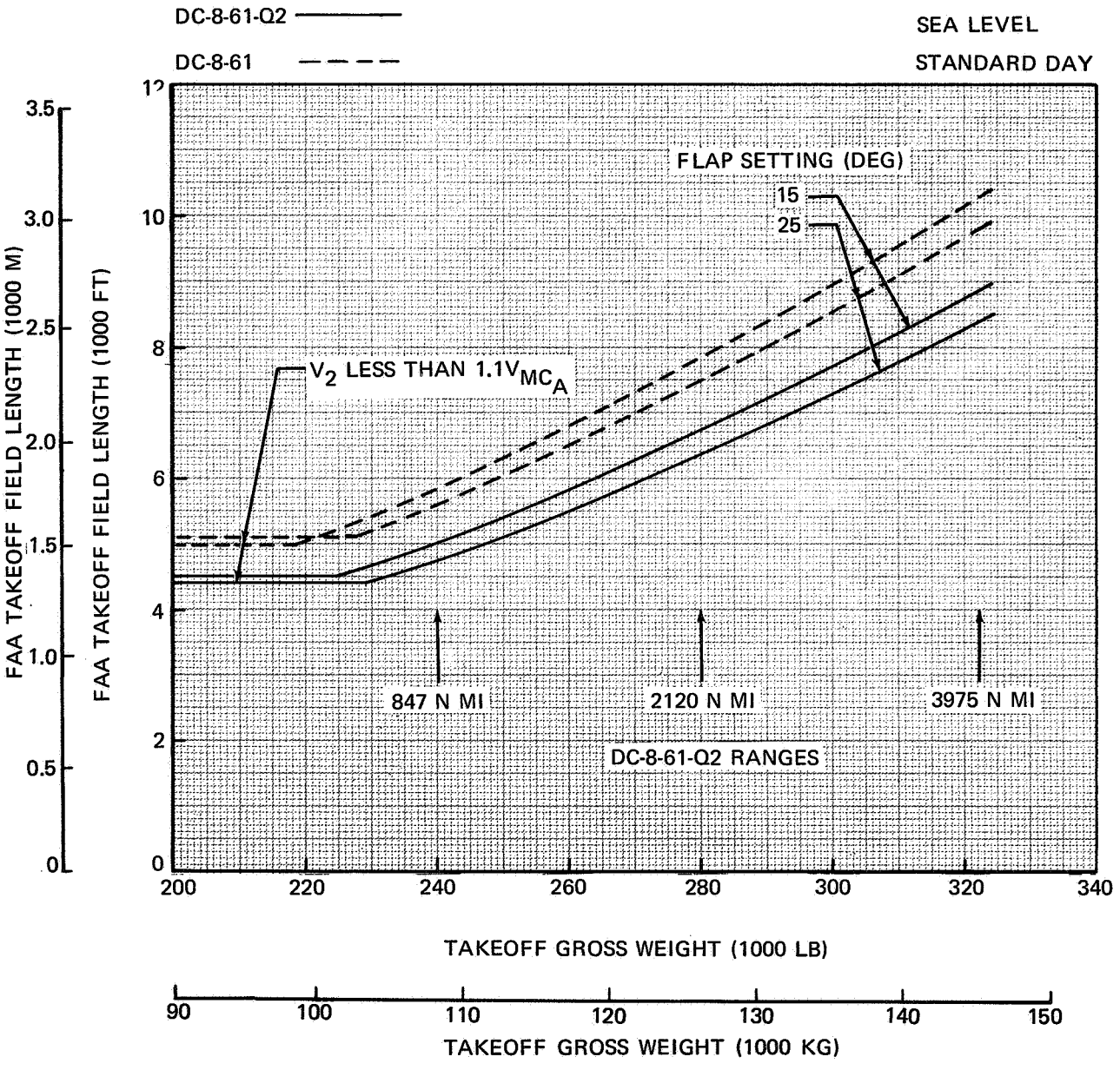

FIGURE V-5. EFFECT OF TAKEOFF GROSS WEIGHT ON FAA TAKEOFF FIELD LENGTH

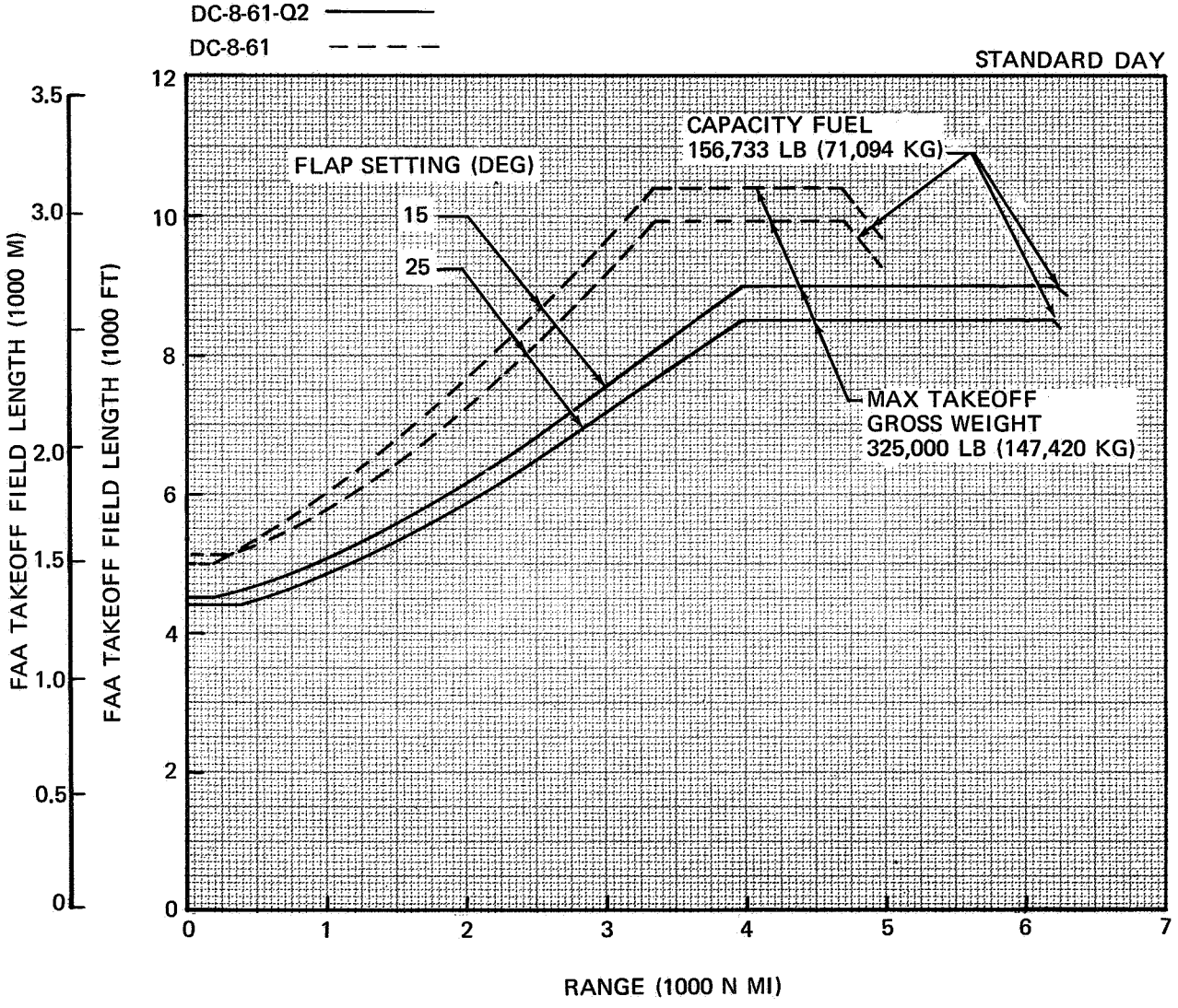

FIGURE V-6. FAA TAKEOFF FIELD LENGTH

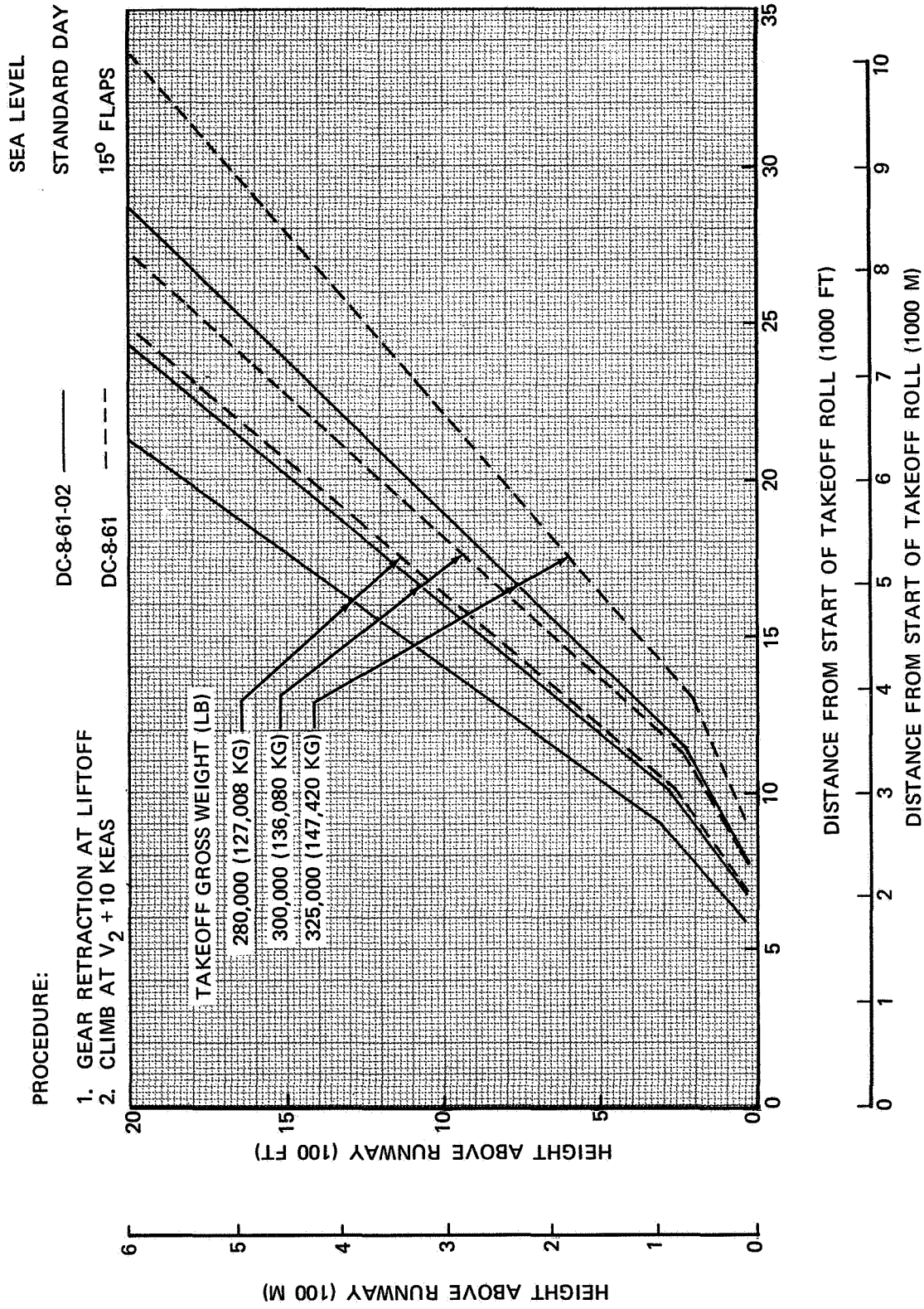

FIGURE V-7. FOUR-ENGINE FLIGHT PATH

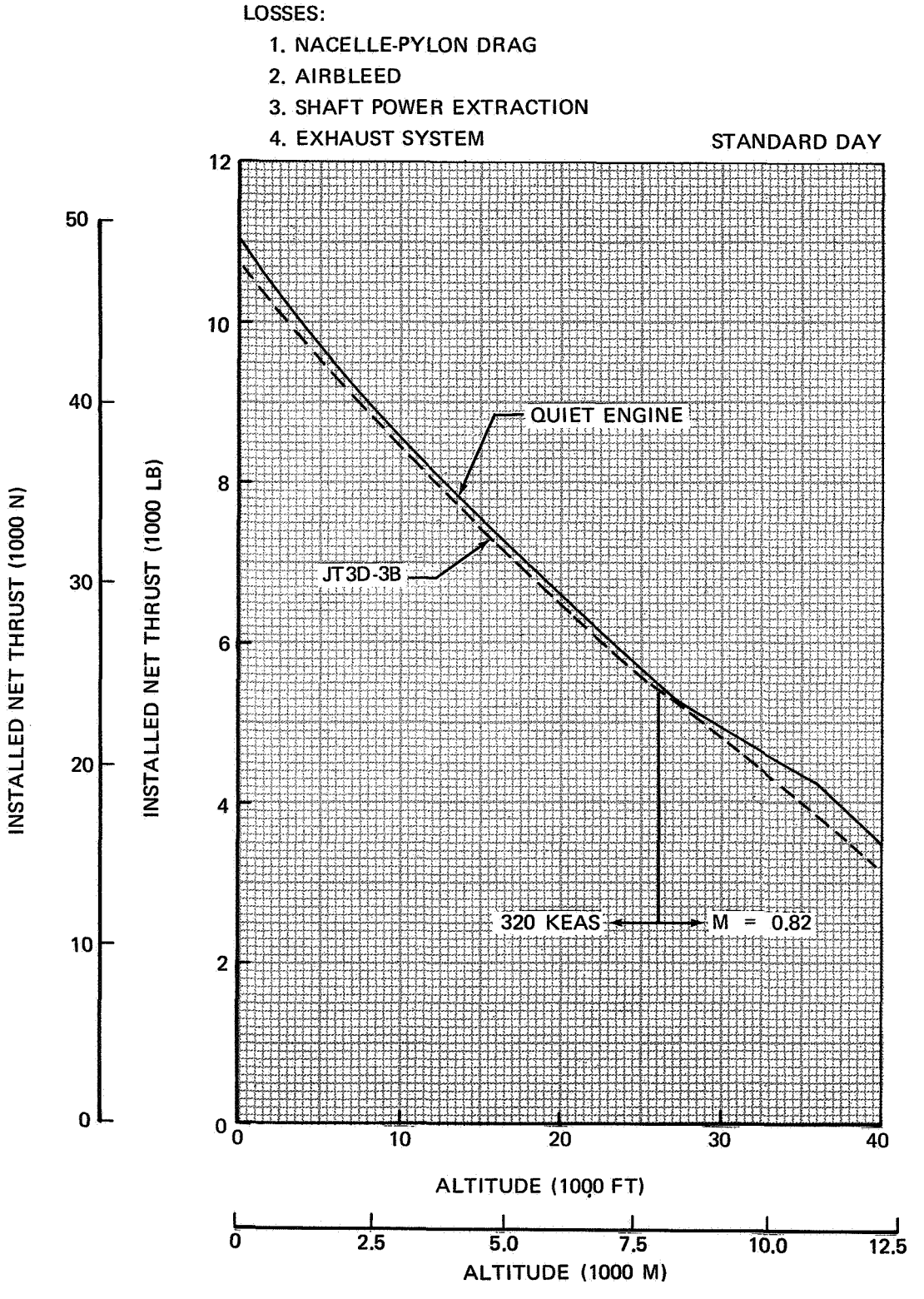

FIGURE V-8. CLIMB THRUST

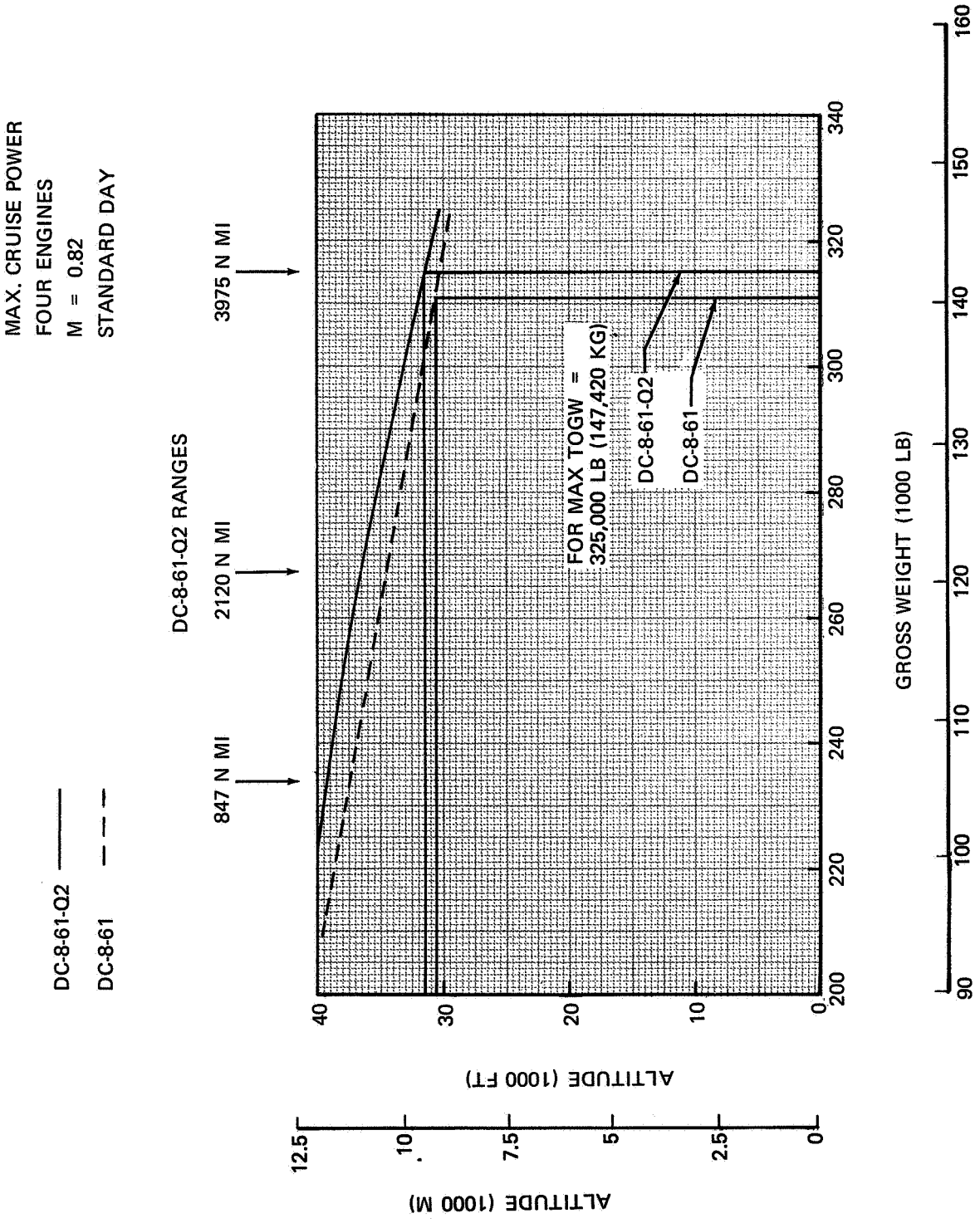

FIGURE V-9. EFFECT OF GROSS WEIGHT ON MAXIMUM RECOMMENDED INITIAL CRUISE ALTITUDE

APPROACH THRUST AND AIRSPEED

The approach airspeed and thrust required are the same for the DC-8-61-Q2 as for the DC-8-61 with the JT3D-3B engine. The installed thrust required will also be the same because the nacelle-pylon drag is included in the installation losses. Figure V-11 shows these data.

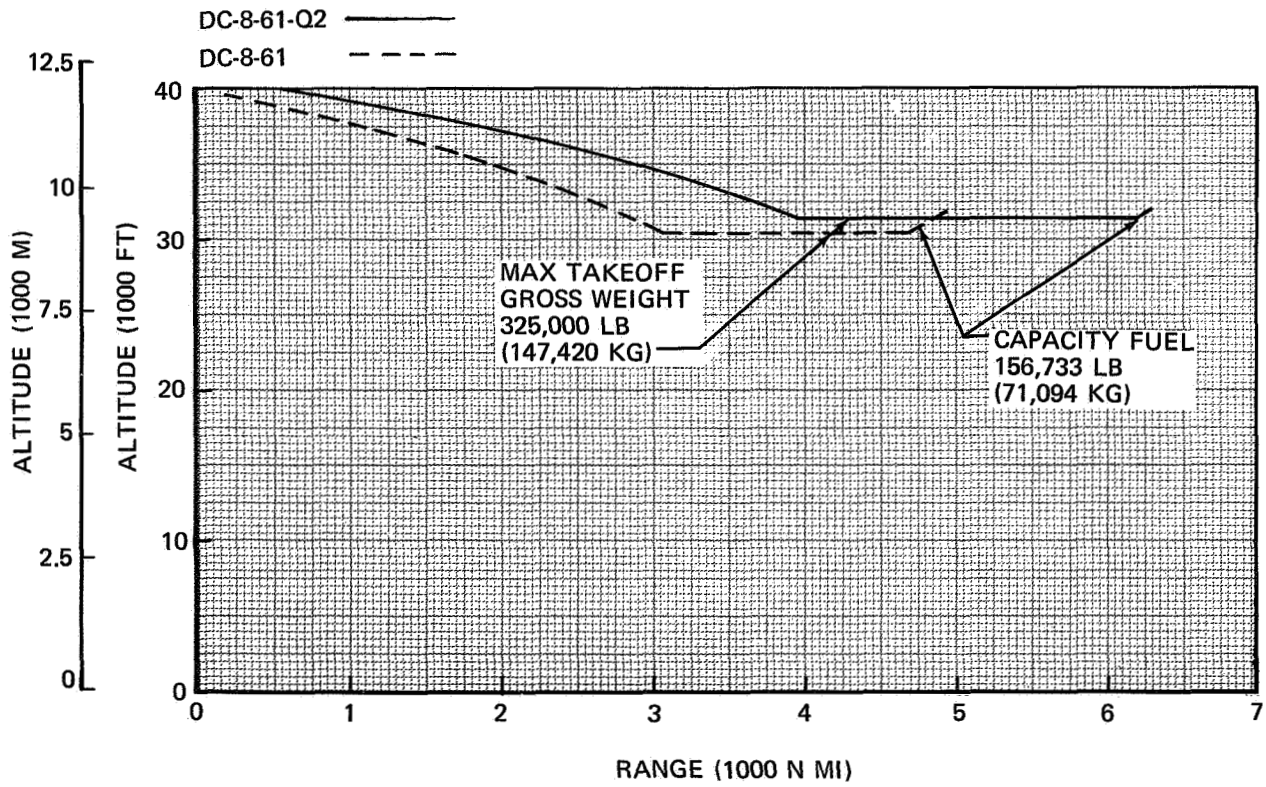

FIGURE V-10. MAXIMUM RECOMMENDED INITIAL CRUISE ALTITUDE

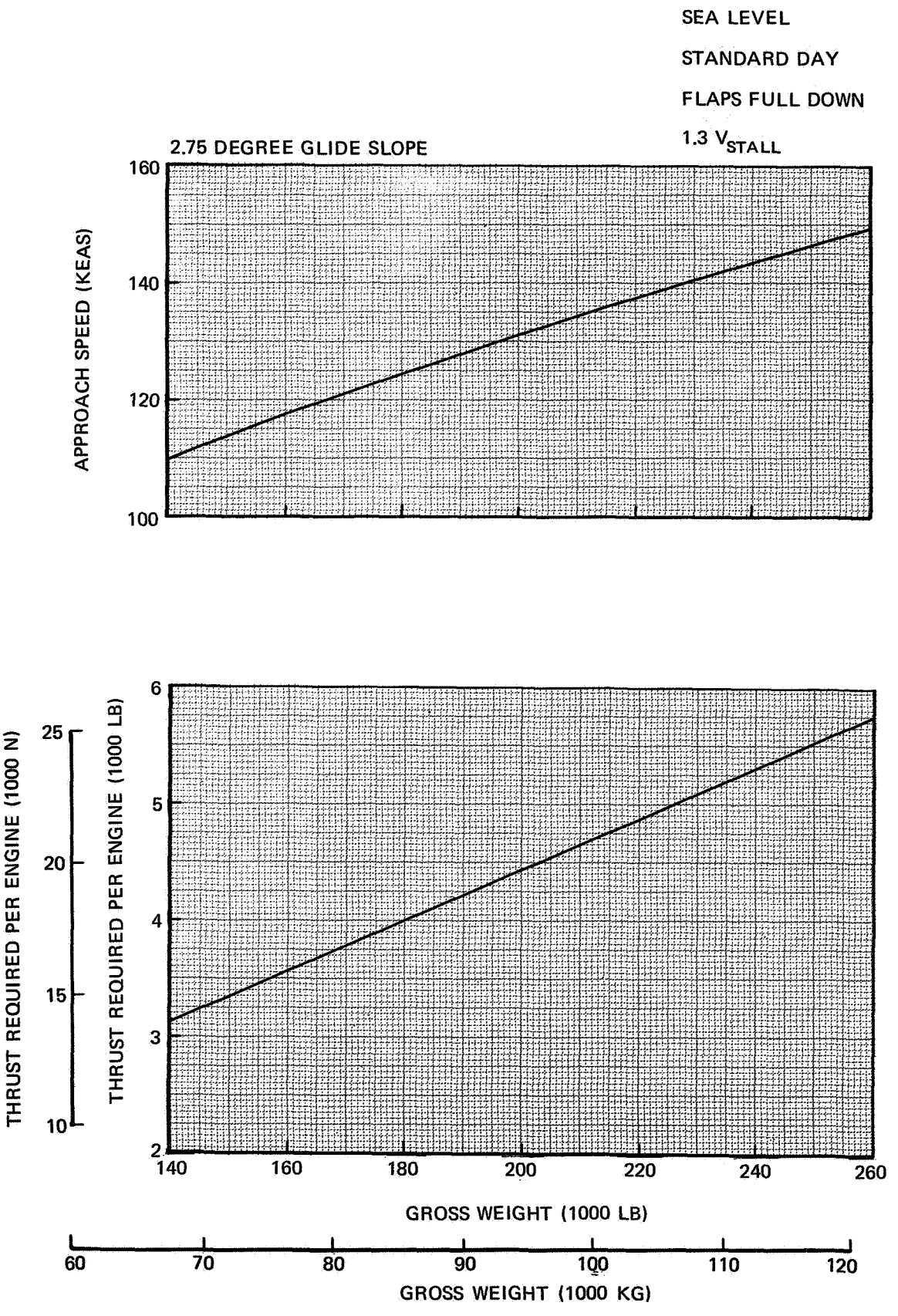

FIGURE V-11. APPROACH SPEED AND THRUST REQUIRED – DC-8-61 AND DC-8-61-Q2

DIRECT OPERATING COST

The procedure of calculating the DOC is the same as that described in Task II. The calculation is carried out in two stages. First, the DOC is calculated for the present DC-8-61 with the selected payloads. Then increments of cost elements that are specifically affected by the retrofit of a quiet engine and an acoustically treated nacelle are calculated. The two stages of the calculations are discussed separately in the following paragraphs. The 1967 ATA method of DOC calculations described in Reference V-1 was used.

PRESENT DC-8-61 DOC CALCULATIONS

The procedure for calculating DOC is shown in Table V-VI. Table V-VII summarizes the 1967 ATA formulas and defines the notation used. The cumulative costs evaluated by the ATA formulas, together with the pertinent parameters of payload-range, fuel burned, block speed, and block time, determined in separate performance calculations, are used to determine DOC in dollars per mile, or in cents per seat-mile, as functions of range. Results of DOC-versus-range calculations for the DC-8-61 (standard day and International Fuel Reserves) using representative 1968 prices (for the aircraft, for maintenance labor rate, and for maintenance material costs) are displayed in Figure V-12 for the specified flight conditions.

DC-8-61-Q2 DOC CALCULATION

The elements of operating costs affected by retrofit of a quiet engine are as follows:

1. Flying operation
    a. Fuel consumption
    b. Insurance
2. Maintenance
    a. Airframe maintenance labor
    b. Airframe maintenance material
    c. Maintenance labor for quiet engine
    d. Maintenance material for quiet engine
3. Depreciation
    a. For cost of retrofit-kit acquisition
    b. For cost of retrofit-kit installation

The incremental changes in these elements can be evaluated by the formulas of the 1967 ATA Method. The incremental formulas are summarized in Table V-VIII. Some pertinent points to be noted relative to these formulas are considered under separate headings in the following paragraphs.

TABLE V-VI
1967 ATA DIRECT OPERATING COST, SUBSONIC JET AIRCRAFT, 1968 PRICES

			DC-8-61	DC-8-61-Q2
AIRCRAFT TYPE				
ENGINE TYPE			JT3D-3B	QUIET ENGINE
$TOGW_{MAX}$ (MAX CERTIFIED TAKEOFF GROSS WT)		(LB)	325,000	325,000
MWE (MANUFACTURER'S WEIGHT EMPTY)		(LB)	149,339	159,144
W_e (DRY WEIGHT OF ENGINE)		(LB)	4,260	5,100
N_e (NUMBER OF ENGINES)			4	4
$W_3 = [MWE - (N_e \ W_w)]$		(LB)	132,299	138,744
NUMBER IN CREW			3	3
T (MAX STATIC TAKEOFF THRUST/ENGINE)		(LB)	18,000	22,000
U (ANNUAL UTILIZATION)		(HR/YR)	3,800	3,800
C_t (TOTAL AIRCRAFT PRICE)		($)	9,200,000	*
C_e (ENGINE PRICE)		($)	302,000	523,000
$C_a = [C_t - (N_e \ C_e)]$		($)	7,992,000	*
D_a (DEPRECIATION PERIOD)		(YR)	12	VARIABLE
R (RESIDUAL VALUE)		($)	0	0
IR_a (ANNUAL INSURANCE RATE)			0.02	0.02
t_{gm} (GROUND MANEUVER TIME)		(HR)	0.25	0.25
$K = (0.05 \ W_a/1000) + 6 - \left(\frac{630}{120 + W_a/1000}\right)$			10.12	11.673
FLYING OPERATIONS (LESS FUEL)				
CREW	2-MAN CREW	$0.05 \ (TOGW_{MAX}/1000) + 100.0$		
	3-MAN CREW	$0.05 \ (TOGW_{MAX}/1000) + 135.0$		
	ADD 20.0 FOR INTERNATIONAL OPERATION			
	ADDITIONAL CREW MEMBER	35.0		
OIL		$0.125N_e$		
HULL INSURANCE		$IR_a \cdot C_1/U$		
(A)	TOTAL	($/BLK HR)		
DEPRECIATION FLIGHT EQUIPMENT				
COMPLETE AIRCRAFT		$(C_t - R) \ (D_a \cdot U)$		
AIRFRAME SPARES		$(0.1) \ C_a/(D_a \cdot U)$		
ENGINE SPARES		$(0.4) \ N_e \cdot C_e/(D_a \cdot U)$		
(B)	TOTAL	($/BLK HR)		
HOURLY MAINTENANCE, FLIGHT EQUIPMENT				
LABOR, AIRFRAME		2.36 K		
LABOR, ENGINES		$(2.4 + 0.108 \ T/1000) \ N_e$		
MATERIAL, AIRFRAME		$3.08 \ C_a/10^6$		
MATERIAL, ENGINES		$2.5 \ N_e \cdot C_e/10^5$		
BURDEN		1.8 (TOTAL LABOR)		
(C)	TOTAL	($/FLT HR)		
CYCLIC MAINTENANCE, FLIGHT EQUIPMENT				
LABOR, AIRFRAME		4.0 K		
LABOR, ENGINES		$(1.2 + 0.12 \ T/1000) \ N_e$		
MATERIAL, AIRFRAMES		$6.24 \ C_a/10^6$		
MATERIAL, ENGINES		$2.0 \ N_e \cdot C_e/10^5$		
BURDEN		1.8 (TOTAL LABOR)		
(D)		($/FLT CYCLE)		
FOR COMPUTATION				
(A)+(B)+(C)		($/BLK HR)		
(D) $- (t_{gm} \cdot$ (C))		($/FLT CYCLE)		

*FOR THE INCREMENTAL VALUES OF C_t AND C_a REQUIRED TO CALCULATE THE INCREMENTAL COST ELEMENTS, REFER TO TABLES II-VIII AND II-IX

TABLE V–VII
BASE-CASE DOC – SUMMARY OF THE 1967 ATA FORMULAS

	$/BLOCK HOUR
CREW PAY – DOMESTIC:	5×10^{-5} (MAX TOGW) + 100 2-MAN CREW
	5×10^{-5} (MAX TOGW) + 135 3-MAN CREW
CREW PAY – INTERNATIONAL:	ADD $20.00
OIL	$0.125\ N_e = 0.5\ N_e$ = NUMBER OF ENGINES = 4
INSURANCE	$0.02\ C_t \div U$
FUEL	(FUEL BURNED LB/BLK HR) x (FUEL COST $/LB)
DEPRECIATION – AIRFRAME: (12-YEAR PERIOD)	AIRCRAFT SPARES: $C_t \div 12U$
	$0.1\ C_a \div 12U$
DEPRECIATION – ENGINES:	$0.4\ N_e C_e \div 12U$

MAINTENANCE	$/FLIGHT HOUR	$/FLIGHT CYCLE
LABOR – AIRFRAME	3.K	5.08K
LABOR – ENGINES	$(3.05+1.08 \times 10^{-4}T)N_e$	$(1.52 + 0.12\ T/100)N_e$
BURDEN	1.8 x TOTAL LABOR	1.8 x TOTAL LABOR
MATERIAL – AIRFRAME	$3.08 \times 10^{-6}\ C_a$	$6.24 \times 10^{-6}\ C_a$
MATERIAL – ENGINES	$25 \times 10^{-6}\ N_e C_e$	$20 \times 10^{-6}\ N_e C_e$
TOTAL $/BLK HR = ($/FLT HR) ÷ (BLK HR/FLT HR) + ($/FLT CY) ÷ (BLK HR)		

NOTATION

C_t = TOTAL AIRPLANE PRICE

C_e = ENGINE PRICE

N_e = NUMBER OF ENGINES

C_a = $C_t - C_e N_e$

$K = 5 \times 10^{-5} W_a + 6 - \left(\frac{630}{120 + 10^{-3} W_a}\right)$

TOGW = TAKEOFF GROSS WEIGHT

W_e = ENGINE WEIGHT

MEW = MANUFACTURER'S EMPTY WEIGHT

W_a = MEW – $W_e N_e$

U = UTILIZATION. ASSUMED 3800 HR/YR

T = ENGINE TAKEOFF THRUST

BASE LABOR RATE = $4.0/HR

NOTE:
1. OWE = 156,803 LB (71,126 KG)
2. FAR 121.645 RESERVES
   200 N MI TO ALTERNATE
3. 193 PASSENGERS PLUS
   9271 LB (4,205 KG) BAGGAGE AND CARGO
4. STEP ALTITUDE CRUISE AT MACH
   0.82 FOR RANGES SHORTER THAN
   INDICATED BY ○
5. STEP ALTITUDE CRUISE AT 99%
   MAX N MI/LB FOR RANGES
   LONGER THAN INDICATED BY □

INTERNATIONAL OPERATION
STANDARD DAY

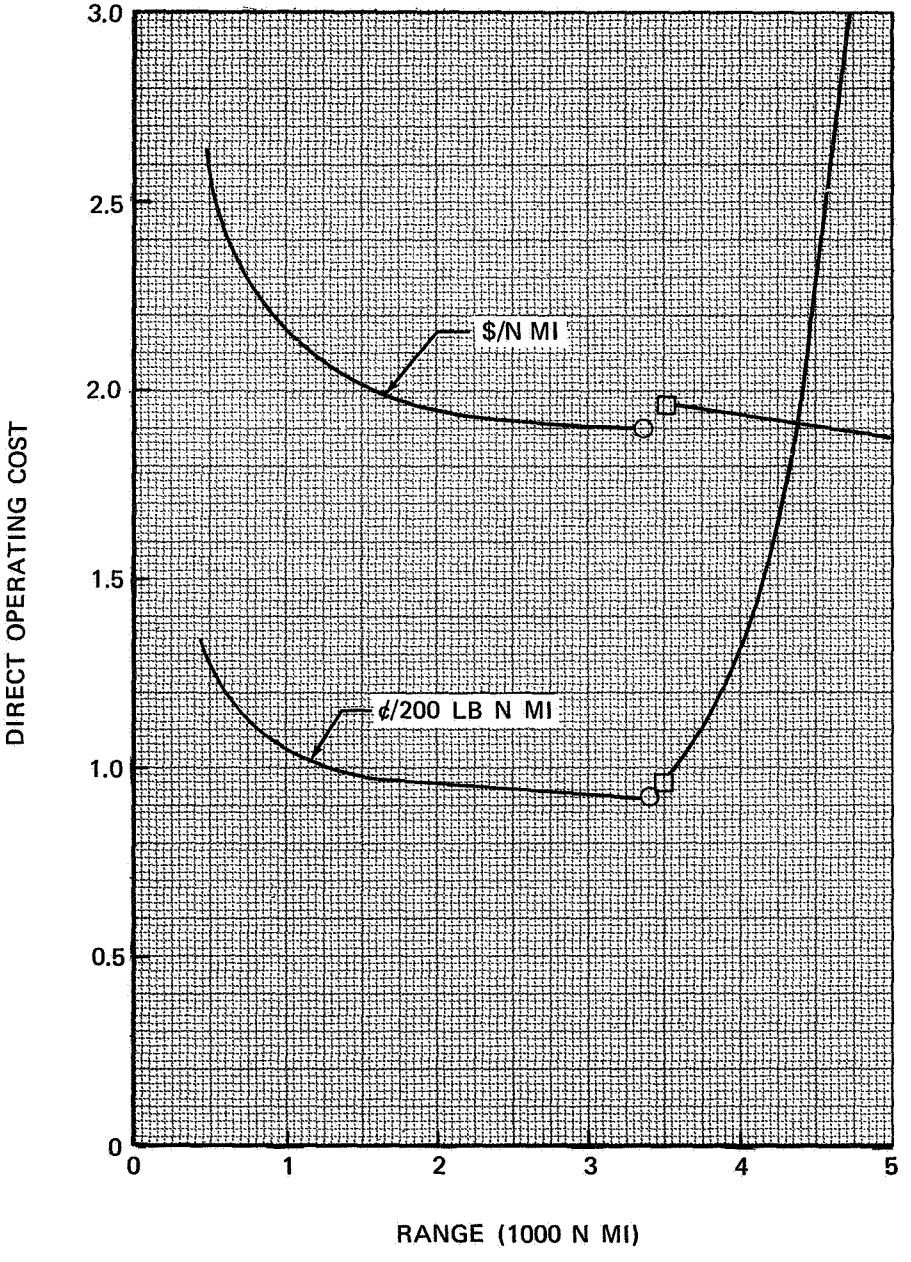

FIGURE V-12. DC-8-61 DIRECT OPERATING COST

TABLE V–VIII
INCREMENTAL OPERATING COSTS FOR DC-8-61 WITH RETROFITTED QUIET ENGINE AND NACELLE

	$/BLOCK HOUR
Δ CREW PAY – DOMESTIC	0
Δ CREW PAY – INTERNATIONAL	0
Δ OIL	0
Δ INSURANCE	$0.02 (C_K + N_e C_{e_1} - N_e C_e) \div U$
Δ FUEL	Δ (FUEL BURNED LB/BLK HR) x (FUEL COST $/LB)
Δ DEPRECIATION – AIRFRAME	$1.1\, C_K \div (D_K U)$
Δ DEPRECIATION – ENGINES	$1.4\, N_e C_{e_1} \div (D_K U)$

MAINTENANCE	$/FLIGHT HOUR	$/FLIGHT CYCLE
Δ LABOR – AIRFRAME	$2.36(K_1 - K) + 0.3$*	$4(K_1 - K)$
Δ LABOR – ENGINE	$1.08 \times 10^{-4} \Delta T\, N_e$	$1.2 \times 10^{-4} \Delta T\, N_e$
Δ BURDEN	1.8 (TOTAL LABOR)	1.8 (TOTAL LABOR)
Δ MATERIAL – AIRFRAME	$3.08 \times 10^{-6} \Delta C_a$	$6.24 \times 10^{-6} \Delta C_a$
Δ MATERIAL – ENGINES	$25 \times 10^{-6} N_e (C_{e_1} - C_e)$	$20 \times 10^{-6} N_e (C_{e_1} - C_e)$
Δ TOTAL $/BLK HR = (Δ $/FLT HR) ÷ (BLK HR/FLT HR) + (Δ $/FLT CY) ÷ (BLK HR)		

C_K = COST OF AIRFRAME KIT INCLUDING INSTALLATION

C_{e_1} = COST OF QUIET ENGINE

D_K = RETROFIT-KIT USE PERIOD EXPRESSED IN YEARS

ΔT = THRUST INCREMENT FOR QUIET ENGINE

$$K_1 = 5 \times 10^{-5} W_{a_1} + 6 - \left(\frac{630}{120 + 10^{-3} W_{a_1}} \right)$$

W_{e_1} = WEIGHT OF QUIET ENGINE

MEW_1 = MANUFACTURER'S EMPTY WEIGHT FOR RETROFITTED AIRPLANE

$W_{a_1} = MEW_1 - W_{e_1} N_e$

$\Delta C_a = C_K - 57 \Delta W_a$ = NET INCREASE IN COST OF RETROFITTED AIRPLANE FOR MAINTENANCE-MATERIAL CALCULATION

ΔW_a = DECREASE IN TOTAL WEIGHT OF WING, NACELLE, AND PYLON PARTS DUE TO RETROFIT KIT (APPROX 14,000 LB). THIS IS PRICED AT $57/LB FOR CALCULATION OF ΔC_a.

*DOUGLAS ESTIMATES FOR MAINTENANCE OF ACOUSTICAL LININGS.

DEFINITION OF RETROFITTED AIRPLANE

Price for Insurance Calculations

The total airplane price C_{t_1} used in insurance calculations for the retrofitted airplane is taken as the sum of the original airframe cost, C_a, the airframe retrofit kit cost, C_K, and the cost of the kit of four quiet engines, $N_e C_{e_1}$, as follows:

$$C_{t_1} = C_a + C_K + N_e C_{e_1} = (C_t - N_e C_e) + C_K + N_e C_{e_1}$$

OR

$$\Delta C_t = C_{t_1} - C_t = C_K + N_e C_{e_1} - N_e C_e$$

This definition of ΔC_t, which deducts the cost of the replaced JT3D-3B engines, is used to calculate the increment in insurance costs.

MAINTENANCE LABOR COSTS

It was assumed that the quiet-engine retrofit program would be introduced in 1975. The labor costs were increased at a rate of 4 percent per year for the 6-year period between 1969 and 1975. The total increase is 26.5 percent.

DEPRECIATION

The DOC increment for kit acquisition, which is by far the largest cost increment in this study, required definition of the following:

1. The total number of airplanes to be retrofitted (to evaluate unit kit cost).

2. The retrofitted airplanes' effective operating period of depreciation. Calculations were made for fleets of 100, 200, and 300 aircraft. The mean operating period would vary according to each airline's fleet retrofit schedule and the retrofitted airplanes' retirement dates. The airline industry does not appear to have established retirement plans for the present subsonic turbofan-powered transport fleets. To resolve this difficulty, a parametric approach has been adopted, wherein kit depreciation charges are presented for a series of assumed operating periods ranging from 1 to 6 years. With these data, each operator can assess the magnitude of the cost according to his individual projections on retirement dates. In the event that greater operating periods are considered, the corresponding depreciation increment can be calculated by prorating the data for 6-year intervals.

RETROFIT COSTS

The retrofit costs were based on the engine configuration of Task IV and on the results of Task VI, Retrofit Analysis.

Table V-IX shows the retrofit costs for 100, 200, and 300 airplanes.

DOC COMPARISONS

The change in DOC shown is essentially the same as that shown in Task II. The increase in the DOC per mile resulting from retrofit of the quiet engine is shown in Figure V-13. Data are shown for two different fleet sizes for which retrofit was assumed. The two lowest curves show the increase in operating cost arising from all sources other than depreciation. The increments shown thus account for the effects of changes in weight, drag, installed-engine performance, insurance, and maintenance costs.

As the no-depreciation curves indicate, the quiet engine causes little or no increase in DOC (less depreciation) over a large part of the DC-8-61 range. This means that the improved fuel economy of the quiet engine compensates approximately for increases in all items except depreciation.

The other curves of Figure V-13 include the increment in depreciation resulting from retrofit and thus show the total increase in DOC. Curves are presented for several depreciation periods, because of the previously discussed uncertainty about the length of the depreciation period.

Effects of the retrofit on DOC per passenger mile are shown in Figure V-14. Since the range of the DC-8-61 is extended by the quiet engine, the seat-mile costs are improved at ranges beyond that at which, for the DC-8-61, passengers must be off-loaded in favor of fuel. This advantage is not likely to be important, however, since it represents an improvement in a relatively unprofitable operation that is normally avoided.

Because of the changes in the monetary value with time, a parametric study was made to determine the effect of retrofit cost on DOC. Figure V-15 shows the effect of retrofit cost on DOC; it is essentially independent of range. The data are shown for a depreciation period of 5 years.

TABLE V-IX
ESTIMATED RETROFIT COSTS IN 1975 DOLLARS

NUMBER OF AIRPLANE KITS	100	200	300
AIRFRAME KIT PRICE	4,047,000	3,216,000	2,918,000
INSTALLATION COST	80,000	73,000	67,000
PRICE OF 4 ENGINES	2,646,000	2,646,000	2,646,000
SPARES			
ENGINE (40%)	1,059,000	1,059,000	1,059,000
AIRFRAME (10%)	405,000	321,000	292,000
TOTAL	8,237,000	7,315,000	6,982,000

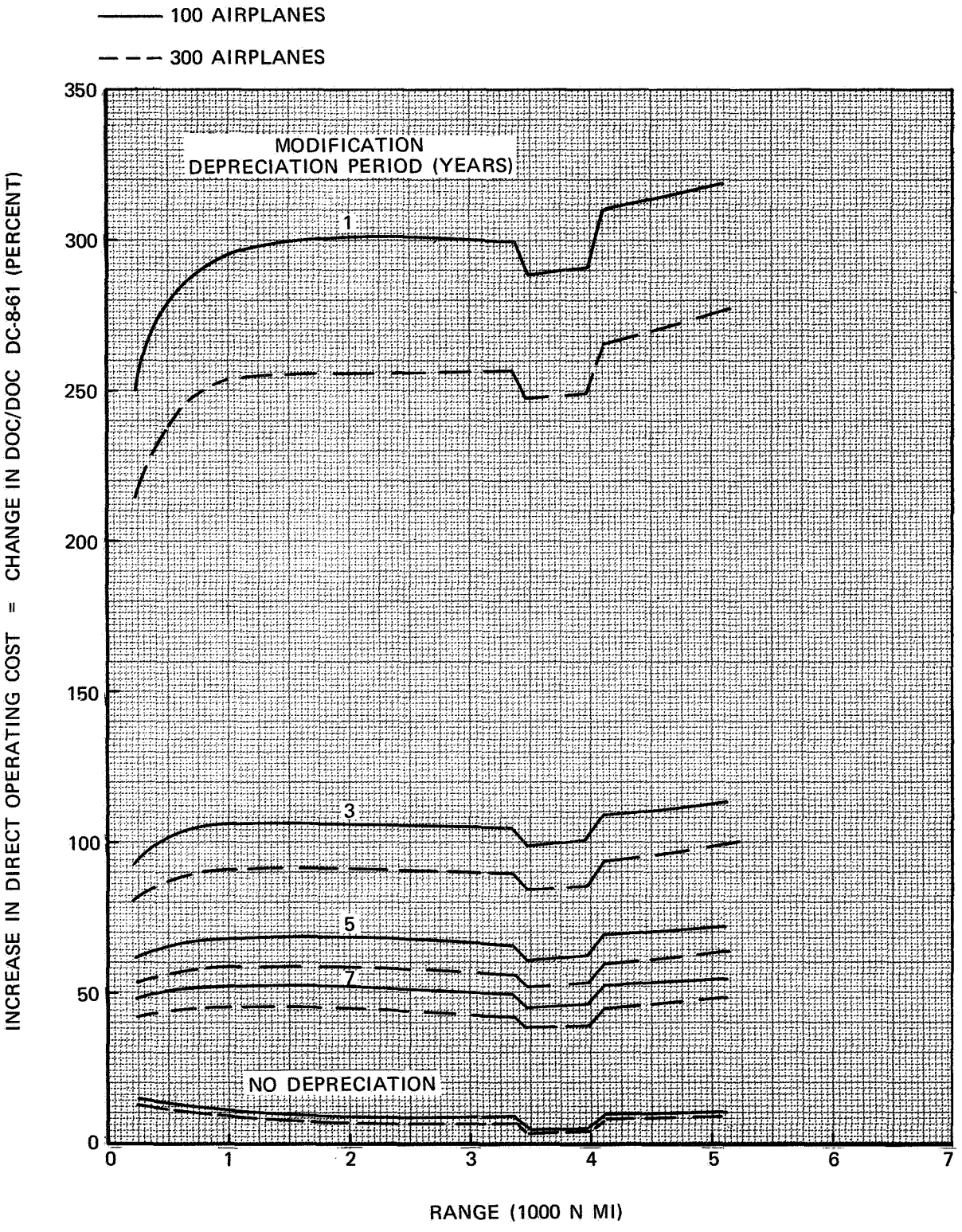

FIGURE V-13. INCREASE IN DIRECT OPERATING COST BASED ON $/N MI

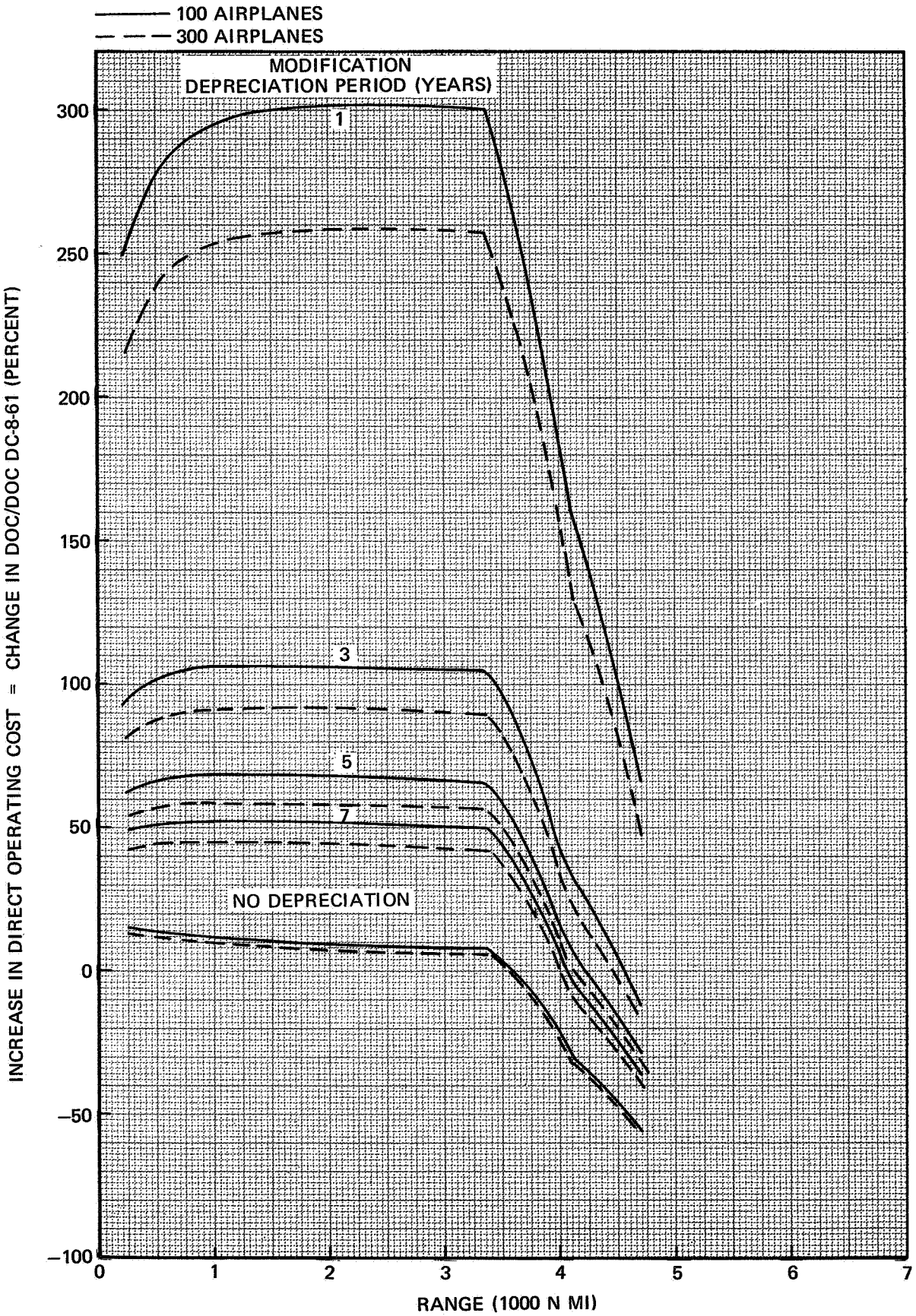

FIGURE V-14. INCREASE IN DIRECT OPERATING COST BASED ON ¢/200 LB/N MI

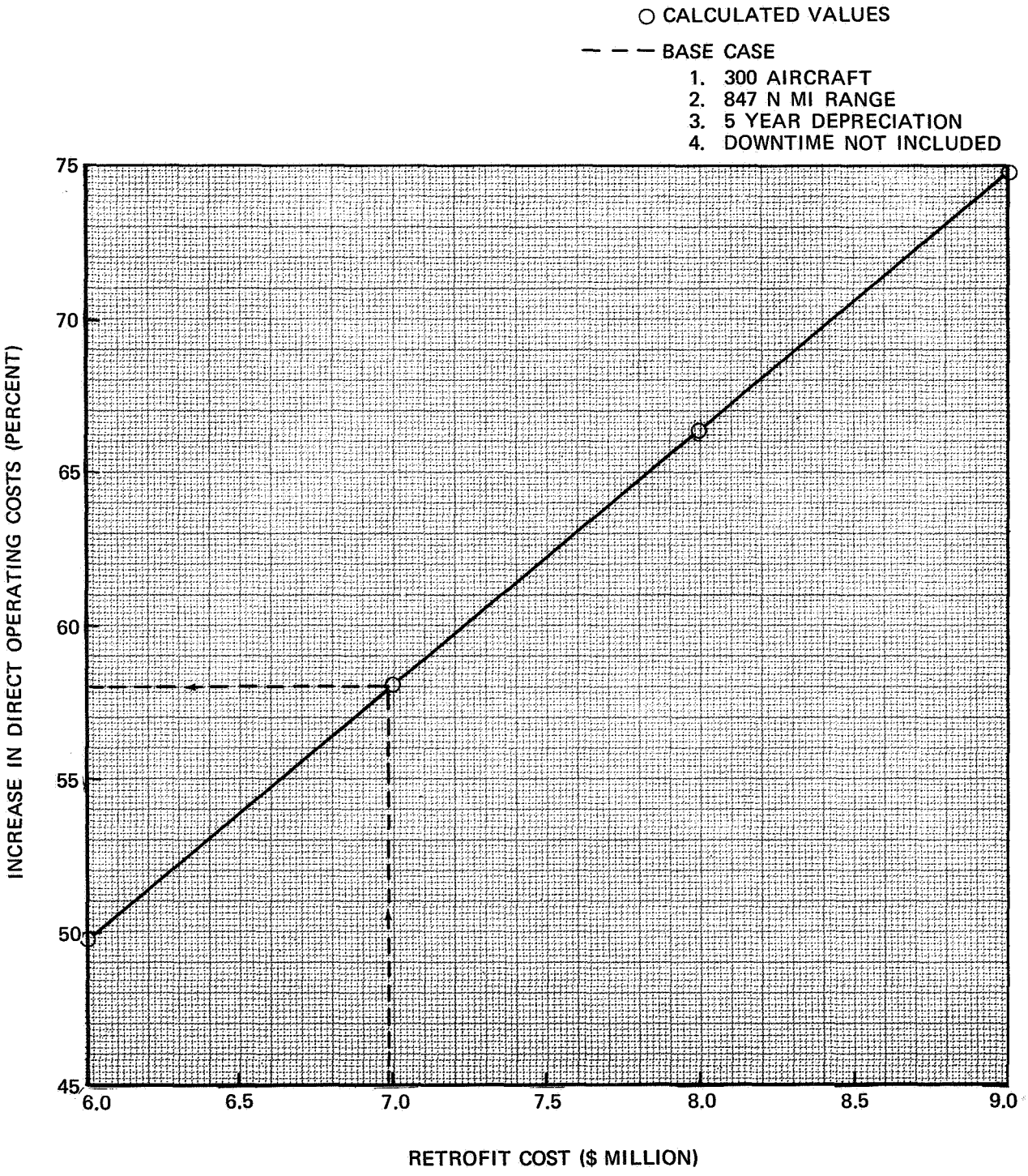

FIGURE V-15. EFFECT OF RETROFIT COST ON DIRECT OPERATING COST

REFERENCE

V-1 Anon: Standard Method of Estimating Comparative Direct Operating Costs of Turbine Powered Transport Airplanes. Air Transport Association, December 1967.

TASK VI
RETROFIT ANALYSIS

LIST OF ILLUSTRATIONS

LIST OF ILLUSTRATIONS (Continued)

Figure Page

LIST OF TABLES

TASK VI

RETROFIT ANALYSIS

The feasibility of retrofitting the quiet engine to the DC-8-61 airplane is evaluated in this section. The strength and flutter characteristics were analyzed to determine if any structural or operational changes in the airplane are required.

The retrofit costs were calculated, and the impact on the operator's return on investment was determined.

Definition of symbols used in this task are shown in Appendix A.

LOADS ANALYSIS

The loads supplied by the quiet-engine installation to the wing and vertical tail were evaluated.

WING LOADS

Both external and internal loads were calculated. The external loads were calculated in accordance with Civil Air Regulations (C.A.R.) paragraph 4b. Internal loads were determined by applying the external loads to an idealized structure consisting of skin stringer elements. The wing loads were calculated for the critical flight and groundborne conditions.

Structural Criteria

The following design data were the basis for the loads analysis.

Design Load Factors – The DC-8-61 airplane is designed for limit symmetrical vertical maneuver load factors of 2.5 g and – 1.0 g. Design load factors for roll conditions are 1.67 g and 0 g. The load factors are applied at the center of gravity. Figure VI-1 shows the airplane load factors at 325,000 pounds (147,420 kg) gross weight for the limiting airspeeds shown in Figure VI-2.

Airplane gust load factors were determined at V_{dive}, V_{cruise}, and V_b airspeeds as functions of airplane gross weight and altitude from the mass-parameter equations of C.A.R. paragraph 4b. The V_b airspeed-altitude profile is a constant 300 KEAS until the V_{cruise} limit is reached. These factors are based on a flexible lift-curve slope for the wing, but the analysis assumes that the tail, the fuselage, and the nacelle-pylon combination are rigid. Figure VI-1 shows that the V_b gust load factors for a 66 (20 m) feet-per-second gust exceed the load factors corresponding to V_{cruise} and V_{dive} airspeeds. Figure VI-3 shows the gust load factor at V_b airspeeds.

Design Gross Weight – Airplane maximum gross weight, 325,000 pounds (147,420 kg), was used for all groundborne conditions. Maximum gross weight less fuel burnoff was the airplane weight assumed for flight conditions. Since the DC-8-61 is maneuver-critical, gust conditions are not limiting.

Aileron roll was analyzed at an intermediate gross weight corresponding to a value of V_{dive}, 415 KEAS, at an altitude of 18,580 feet (5663 m). This condition produces a high rolling acceleration and only small fuel inertial relief.

Design Speed – The design level-flight and dive speeds, V_{cruise} and V_{dive}, respectively, are the same for the DC-8-61-Q2 as for the DC-8-61. A change in placard speed, such as was considered in Task II, is not required in view of the results of the flutter tests discussed later in this report.

Center of Gravity – The center-of-gravity position was determined in the following way. Forward and aft limits were established for the airplane with no fuel on board. The center of gravity at any gross weight including fuel then depends on the fuel load and the fuel loading schedule. The fuel loading schedule is based on a fuel slosh angle of 10 degrees (0.17 rad), which corresponds to a forward and inboard loading of fuel and low dead-weight fuel.

Aerodynamics – All aerodynamic parameters, two dimensional and three dimensional, are the same as those used for the Model DC-8-61.

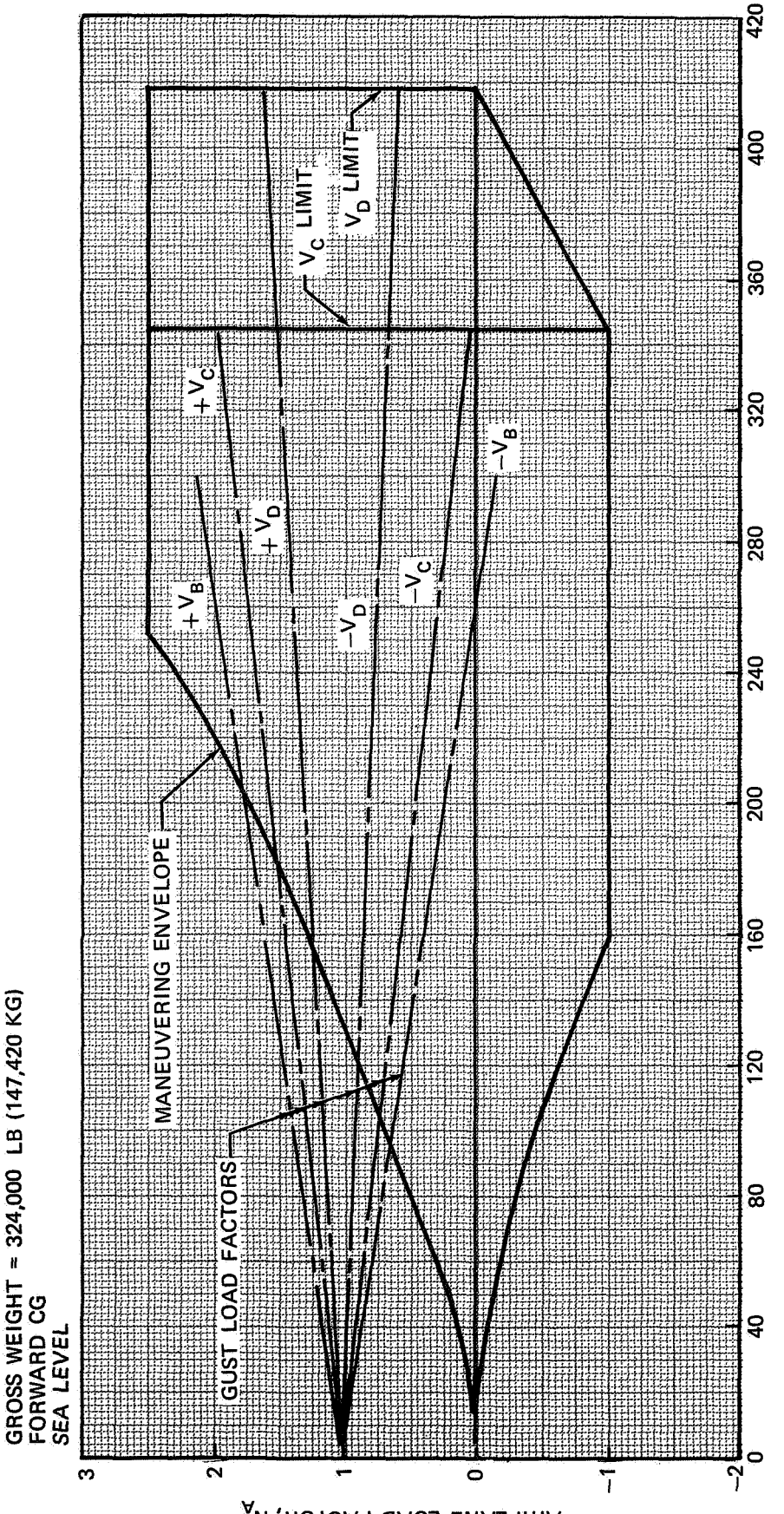

FIGURE VI-1. AIRSPEED-LOAD FACTOR DIAGRAM

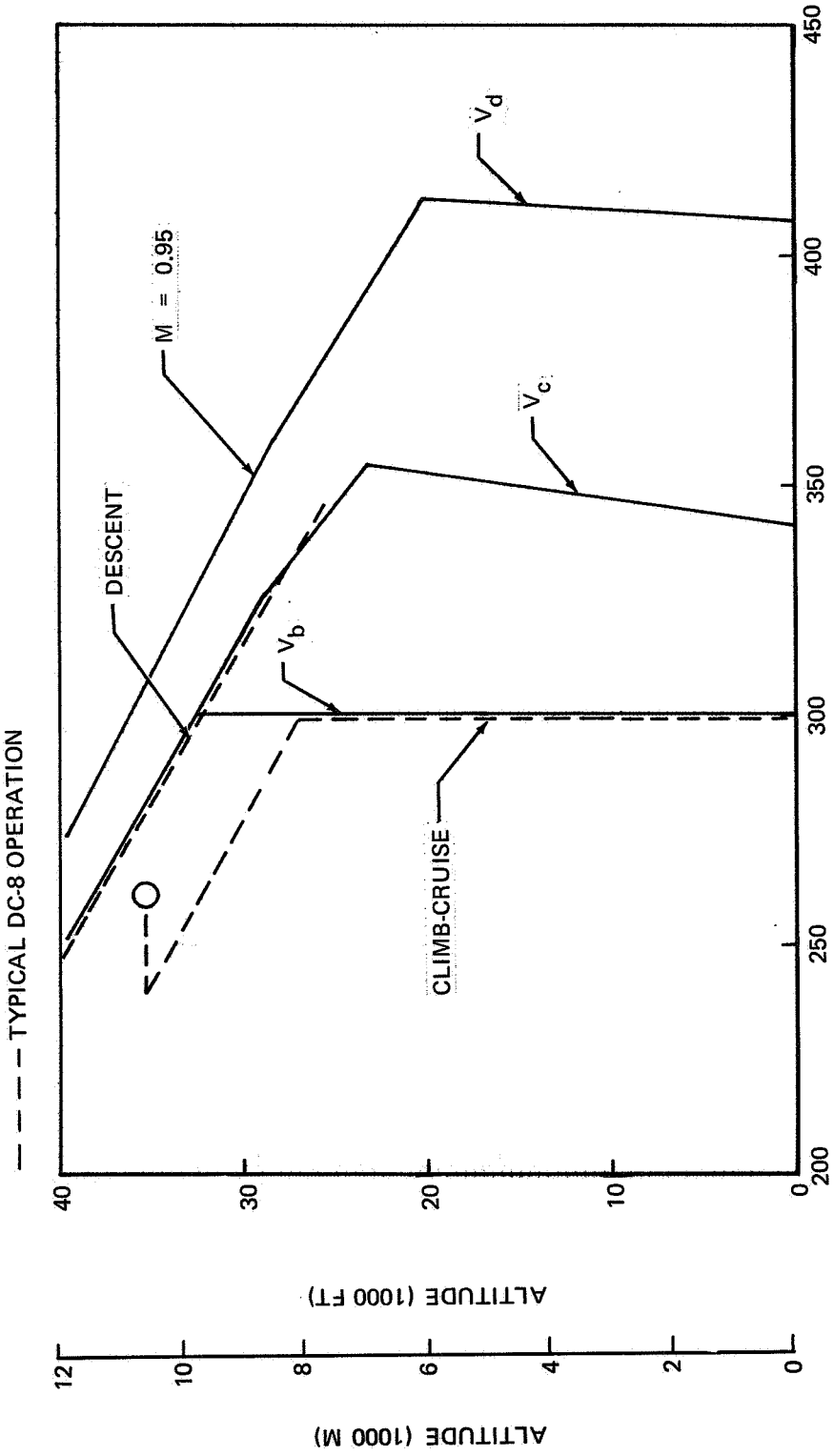

FIGURE VI-2. PLACARD AIRSPEED – DC-8-61

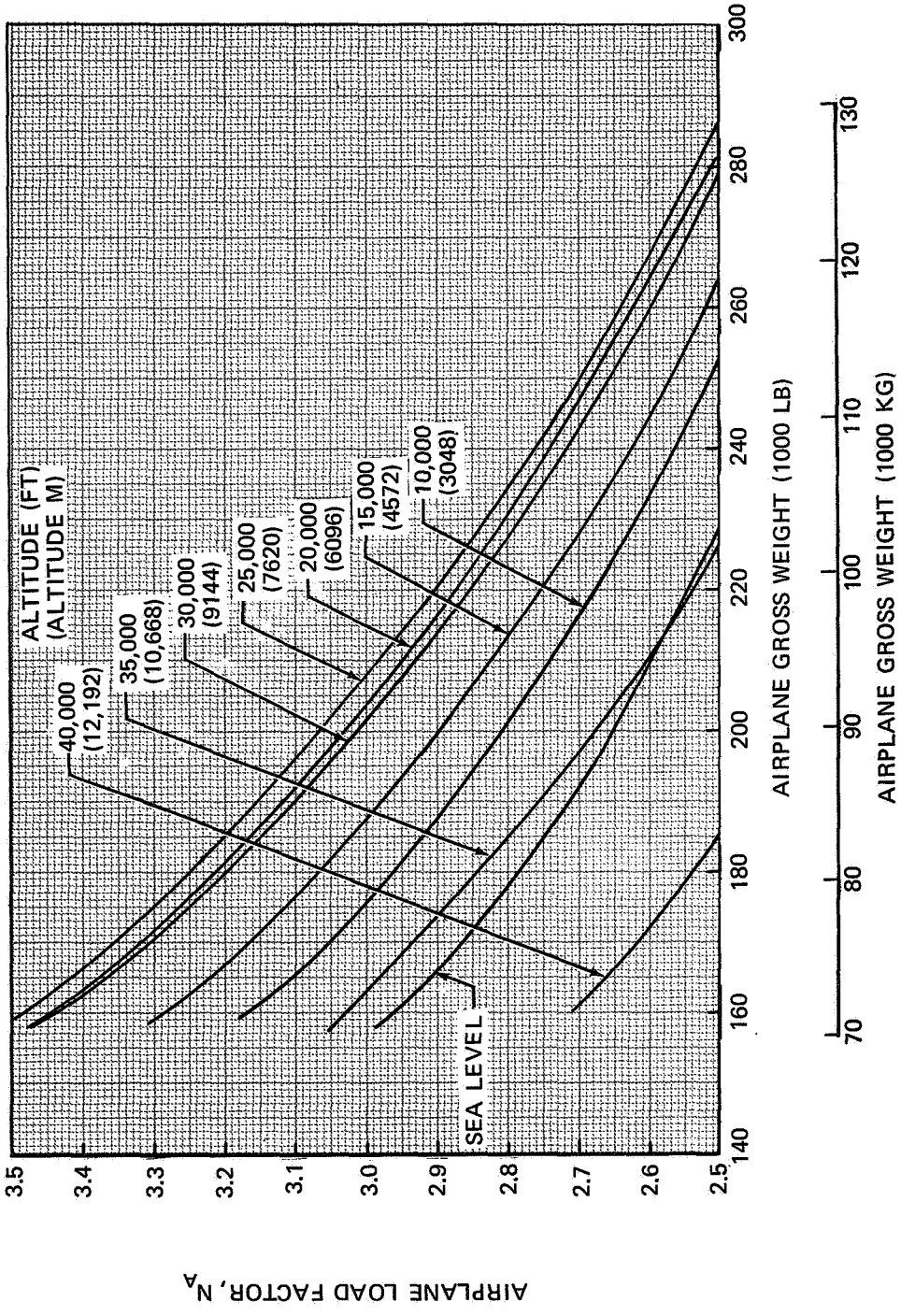

FIGURE VI-3. GUST LOADS AT V_B

Balancing tail loads are also taken from DC-8-61 data and are in a direction that increases the wing lift coefficient.

For flight conditions, the airloads are distributed along the span essentially in accordance with the Weissinger theory.

Aeroelasticity is considered by allowing the wing to cycle until the deflections between the last two cycles run have closed. Allowance was made for both forward and reverse thrust where pertinent.

Weights – The weights used in determining wing loads were separated into concentrated weights and distributed weights. Weight items such as fuel, structure, and aileron balance weights were distributed spanwise. Pods, pylons, and main-gear fitting weights were applied as concentrated loads. Both concentrated and distributed weights are influenced by airplane load factor. Fuel weights were distributed at a slosh angle that gives the most forward and inboard distribution of fuel.

Forces – Engine thrust and aerodynamic effects of the nacelles were applied as forces to the pylons and nacelles. Thrust was applied to the engine-nacelle center of gravity, and the aerodynamic forces were applied to the nacelle leading edge.

Gust Load Factors

Gust load factors were calculated in accordance with C.A.R. paragraph 4b.211. The equation used for the gust load factor is

$$n = 1 + \frac{K_g \, Ude \, V_a}{498 \, (w/s)}$$

where

n	=	gust load factor
K_g	=	gust alleviation factor
Ude	=	derived gust velocities in feet per second
V	=	airplane speed in knots
a	=	slope of airplane normal-force coefficient
(W/S)	=	wing loading in pounds per square foot

Figure VI-4 shows the FAA derived gust velocities for the limiting airspeeds, V_b, V_{cruise}, and V_{dive}. For wing design cases the V_b-value was used. The gust load factors for V_b speeds are shown in Figure VI-3.

Nacelle-Pylon Loads

The loads on the DC-8-61-Q2 nacelle were generated by modifying existing DC-8-61 data. New load analyses were required because of significant differences in length, c.g., and planform areas. Figures VI-5 and VI-6 show baseline DC-8-61-Q2 locations relative to the wing.

Airloads acting on the quiet engine were developed by using the aerodynamic coefficients from DC-8 external-stores design criteria. The nacelle-pylon balance equations were modified to account for the increased areas of the quiet-engine nacelle and pylon. The DC-8-61-Q2 engine loads are summarized in Table VI-I. No lift or pitching-moment loads are included. Lift and pitching-moment loads are computed for every case run by the wing-loads program. The resulting loads are transferred to the wing elastic axis for use in computing stresses.

The lift that was calculated for the nacelles was divided by qS_W and subtracted from the wing lift coefficient, C_{ℓ_W}. The reduced coefficient ($C_{\ell_W} - C_{\ell_{NP}}$) was then to determine the spanwise lift distribution of the wing.

Figures VI-5 and VI-6 show the geometry and aerodynamic load points of the quiet-engine nacelle-pylon combination. Weights were applied at the c.g., and the aerodynamic loads were applied at the noted aero-load reference point.

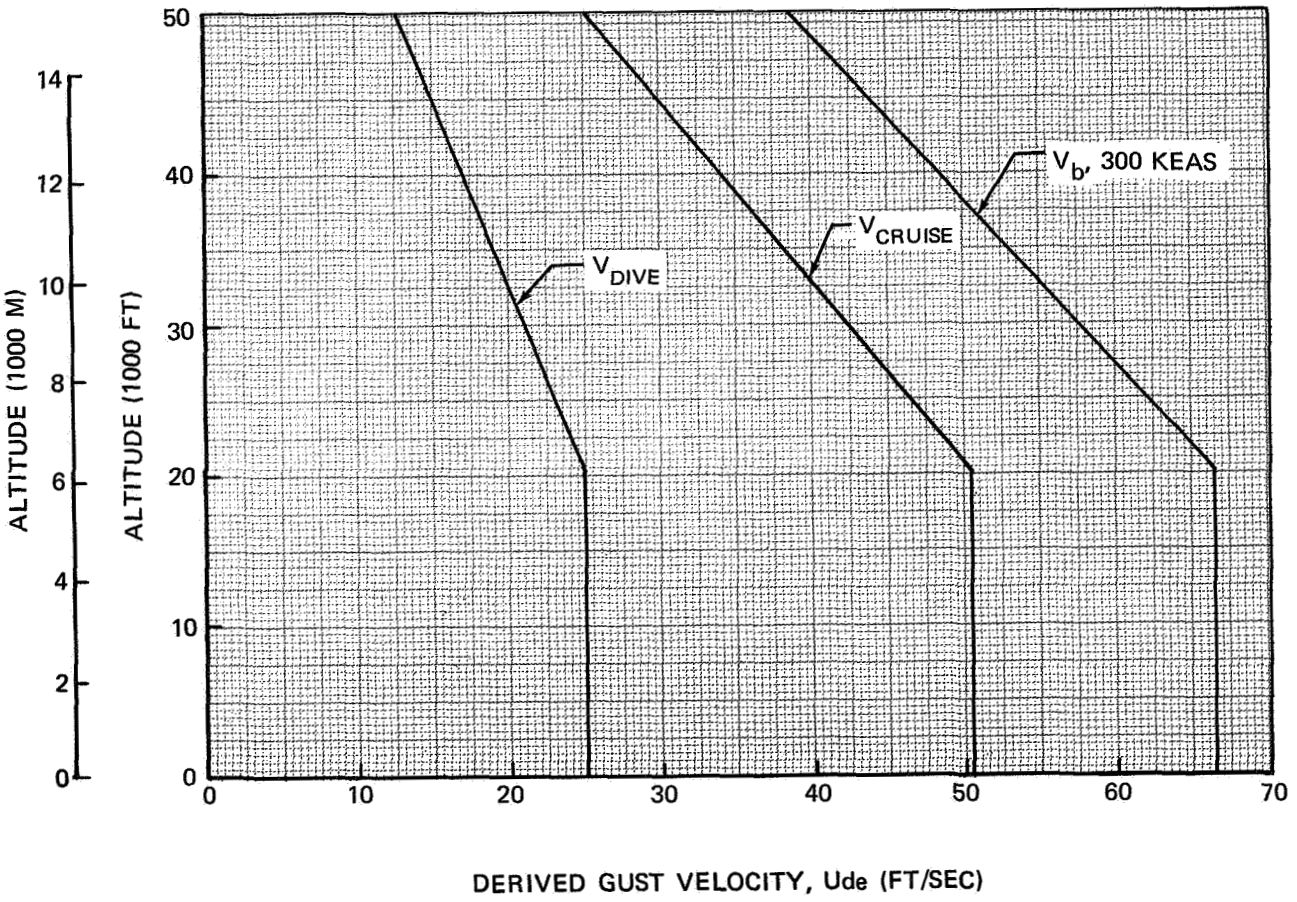

FIGURE VI-4. GUST INTENSITIES

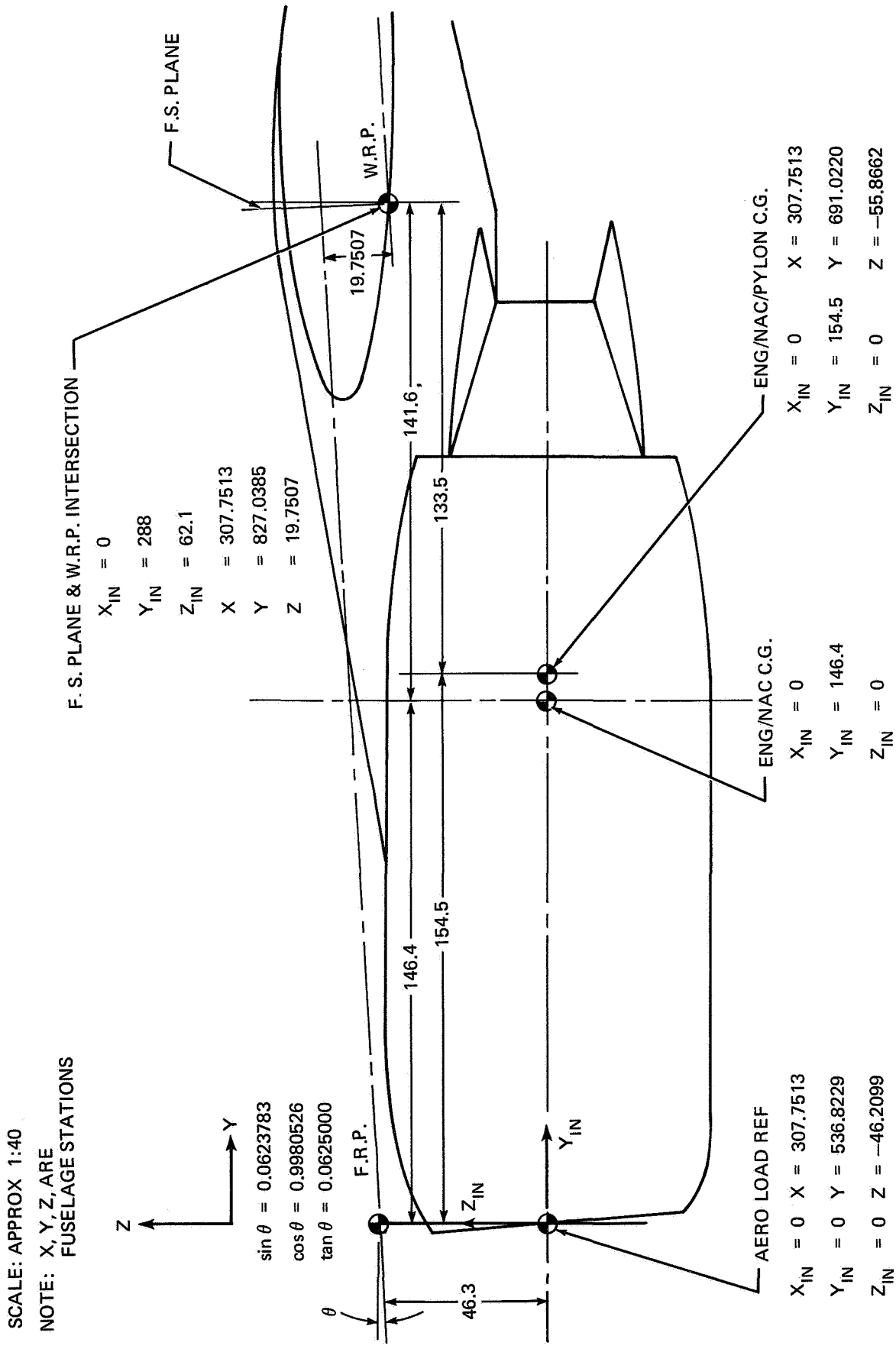

FIGURE VI-5. INBOARD NACELLE

SCALE: APPROX 1:40

NOTE: X, Y, Z, ARE
FUSELAGE STATIONS

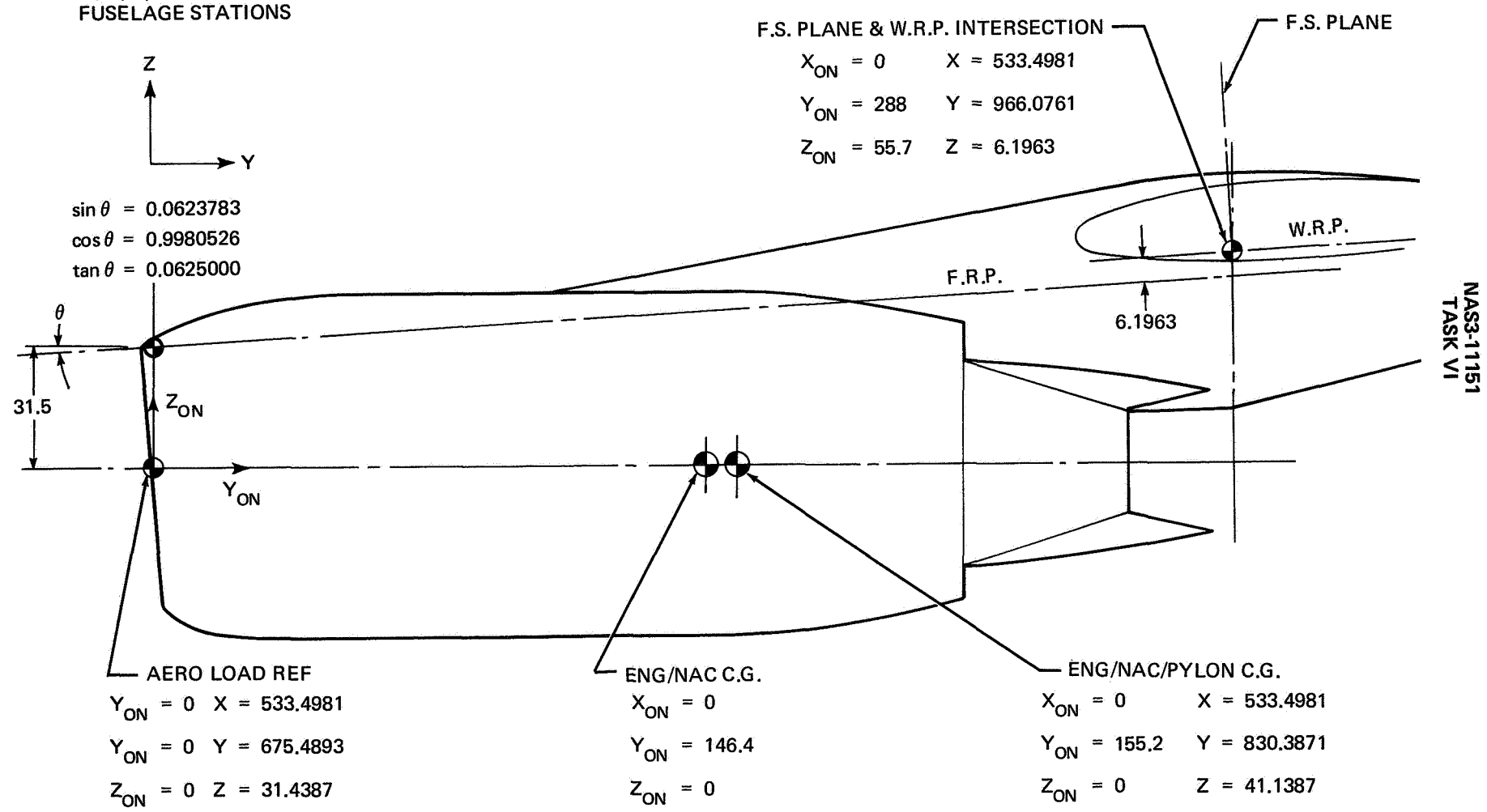

FIGURE VI-6. OUTBOARD NACELLE

TABLE VI-I
NACELLE-PYLON QUIET-ENGINE LOADS

YAWING MOMENT = C_{X_q} 24,884)

PYLON POSITION	COND	COEFFICIENT YAW, C_x	N/SQ M	DYNAMIC PRESSURE q, LB/SQ FT	MOMENT IN./LB	M_4 (M–Kg)
INBOARD	20	0.235	12,401	259	2,506,656	218×10^6
	30	0.11	16,902	353	1,599,045	139×10^6
	38	–0.002	28,010	585	–48,026	-418×10^4
OUTBOARD	20	0.265	12,401	259	2,826,596	246×10^6
	30	0.153	16,902	353	2,224,253	194×10^6
	38	0.020	28,010	585	481,841	419×10^5

SIDE FORCE NACELLE PYLON

	COND	SIDE FORCE, C_y	N/SQ M	q	SIDE (IN.-LB)	(M–Kg)
INBOARD	20	–0.31	12,401	259	–16,050	-140×10^4
	30	–0.190	16,902	353	–13,407	-117×10^4
	38	–0.075	28,010	585	– 8,748	-761×10^3
OUTBOARD	20	0.335	12,401	259	–17,375	-151×10^4
	30	–0.22	16,902	353	–15,551	-135×10^4
	38	–0.10	28,010	585	–11,694	-102×10^4

ROLLING MOMENT

	COND	ROLLING, C_ℓ	N/SQ M	q	ROLL. MOM. (IN.-LB)	(M–Kg)
BOTH INBD AND OUTBD	20	–0.042	12,401	259	–270,688	-235×10^6
	30	–0.027	16,902	353	–237,169	-206×10^5
	38	–0.008	28,010	585	–116,457	-101×10^5

C_{ℓ_q} 24,884 = ROLL ON N.P. q = LB/SQ FT (N/SQ M)

Figure VI-7 shows the terminology and sign convention used in the analysis.

Results

The results of the wing loading analysis are presented for three flight conditions and for groundborne operation. The flight conditions considered are for symmetrical flight, aileron roll, and landing. Shear, torque, and bending forces are shown for these four operational conditions.

Symmetrical Flight – This condition was evaluated in accordance with C.A.M. paragraph 4b-21b. Two critical flight conditions described in Table VI-II were analyzed.

Figures VI-8 through VI-10 show the shear, torque, and bending loads at the critical flight conditions for the DC-8-61 and DC-8-61-Q2 airplanes.

Aileron Roll – The effects of aileron roll were calculated in accordance with C.A.M. paragraph 4b.214a. In computing the spanwise distribution of loads, allowance was made for aeroelastic-alleviation effects, load distribution, and angle of attack. The critical condition for aileron roll is shown in Table VI-III.

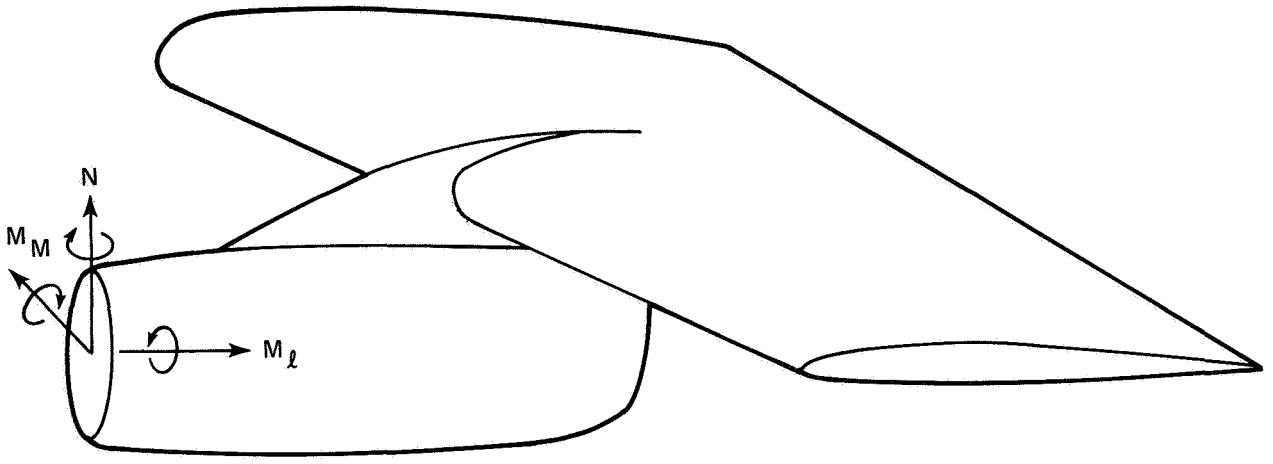

FORCES AND MOMENTS
ARE SHOWN ACTING
IN A POSITIVE DIRECTION

DEFINITIONS:

M_ℓ	=	ROLLING MOMENT IN INCH-LB
M_M	=	PITCHING MOMENT IN INCH-LB
M_N	=	YAWING MOMENT IN INCH-LB
N	=	NORMAL FORCE IN LB
y	=	SIDE FORCE IN LB
q	=	DYNAMIC PRESSURE IN LB/FT SQ

NACELLE AND PYLON BALANCE EQUATIONS:

SIDE FORCE	Y_{N_p}	=	120.79 q C_y
YAWING MOMENT	M_{N_p}	=	24,884 q C_N
ROLLING MOMENT	$M_{\ell_{N_p}}$	=	24,884 q C_ℓ

FIGURE VI-7. SIGN CONVENTION NACELLE-PYLON

TABLE VI-II
CRITICAL SYMMETRICAL-FLIGHT CONDITIONS

STALL

CRITICAL CONDITION	1		2	
	USC UNITS*	SI UNITS**	USC UNITS*	SI UNITS**
GROSS WEIGHT (LB)	342,000	146,966	314,050	142,453
ALTITUDE (FT)	SEA LEVEL		27,970	8,525
MACH NUMBER	0.4181		0.88	
LOAD FACTOR (N_A)	2.5		2.5	
TOTAL FUEL (LB)	100,000	45,360	90,050	41,051
LIFT COEFFICIENT	1.117		0.745	
FUSELAGE ANGLE OF ATTACK (DEG)	13.20		8.16	
CHORDWISE LOAD FACTOR (N_{YF})	−0.530		0.319	

TABLE VI-III
CRITICAL AILERON-ROLL FLIGHT CONDITION

V_{DIVE}

	USC UNITS*	SI UNITS**
GROSS WEIGHT (LB)	317,900	144,199 KG
ALTITUDE (FT)	18,580	5663 M
MACH NUMBER	0.90	
LOAD FACTOR	1.667	
CENTER OF GRAVITY (% MAC)	20.74	
LIFT COEFFICIENT	0.3366	
FUSELAGE ANGLE OF ATTACK (DEG)	2.43	
CHORDWISE LOAD FACTOR	0.3825	

* UNITED STATES CUSTOMARY UNITS
** STANDARD INTERNATIONAL UNITS

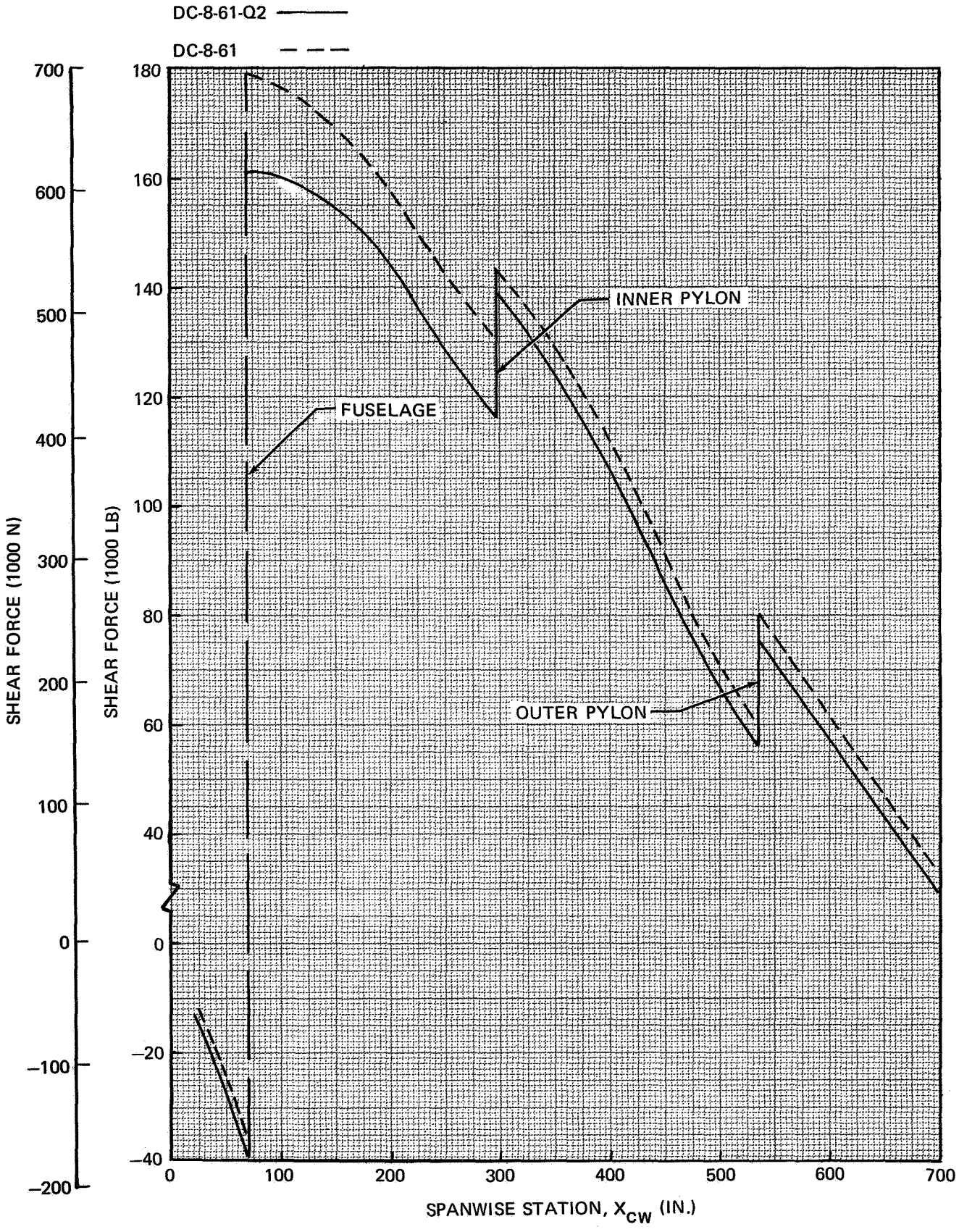

FIGURE VI-8. SYMMETRICAL FLIGHT SHEAR

Figures VI-11 through VI-13 show the external loads for the critical aileron roll condition. Large increases in torque are evident. These are primarily attributed to the geometry and increased weight of the quiet-engine nacelle.

Landing – C.A.M. paragraph 4b.23b was the basis for the landing-loads analysis. The critical landing case is for maximum landing weight, 240,000 pounds (108,864 kg), and a sink speed of 10 feet (3 m) per second. One-g airloads, acting in conjunction with the inertia forces and landing-gear reaction, result in the net wing loads. The landing loads are shown in Figures VI-14 through VI-16.

Groundborne Operation – C.A.M. paragraph 4b.235 was the basis for this analysis. The critical conditions exist during the takeoff run. To simulate the dynamic taxi case, the takeoff run was analyzed at a 2 g static load factor. A gross weight of 328,000 pounds (148,780 kg) was assumed. A vertical load factor of 2 g and a horizontal load factor (ratio of thrust minus landing-gear drag to gross weight) of 0.243 was used.

Figures VI-17 through VI-19 compare the groundborne loads for the DC-8-61 and DC-8-61-Q2.

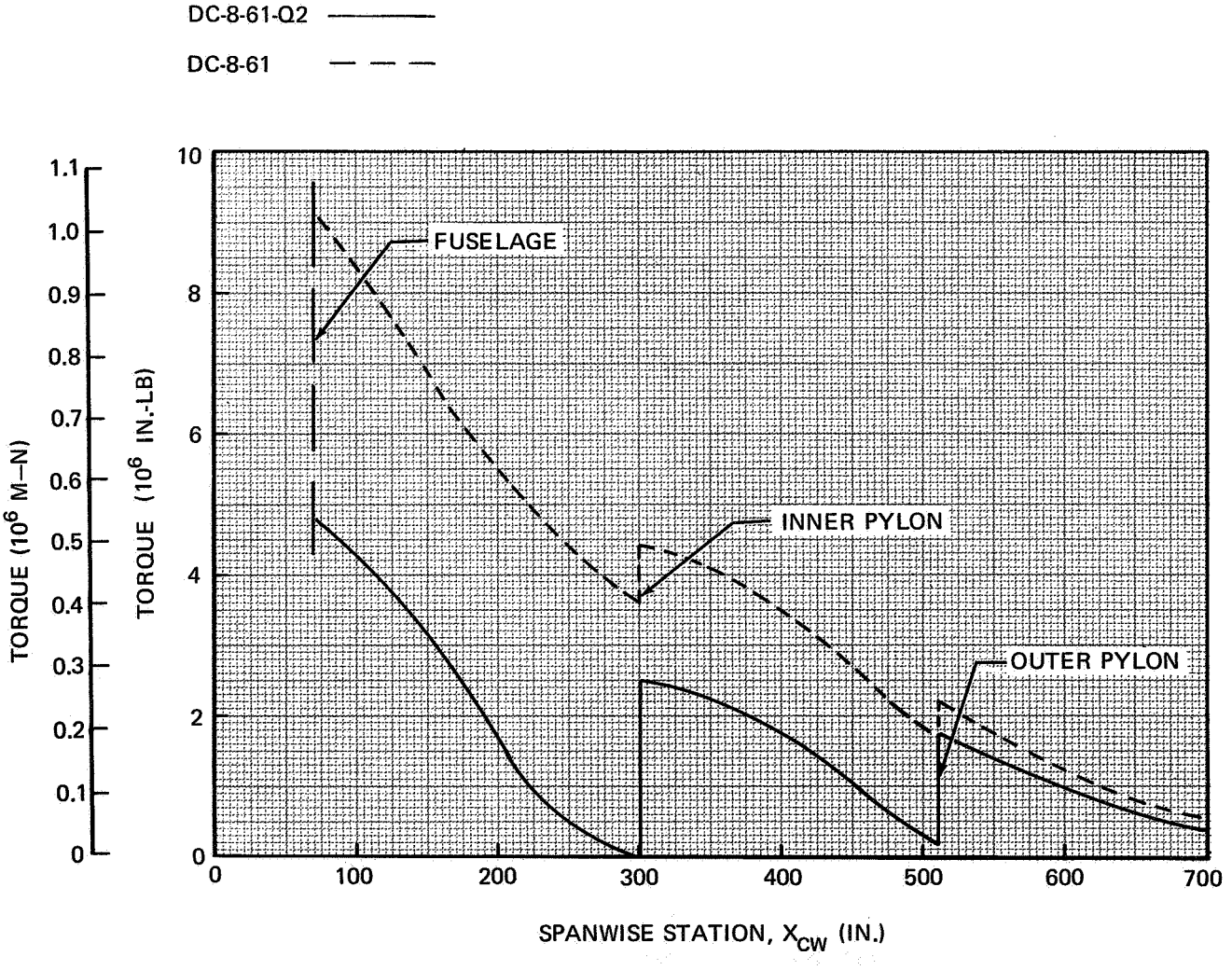

FIGURE VI-9. SYMMETRICAL FLIGHT TORQUE

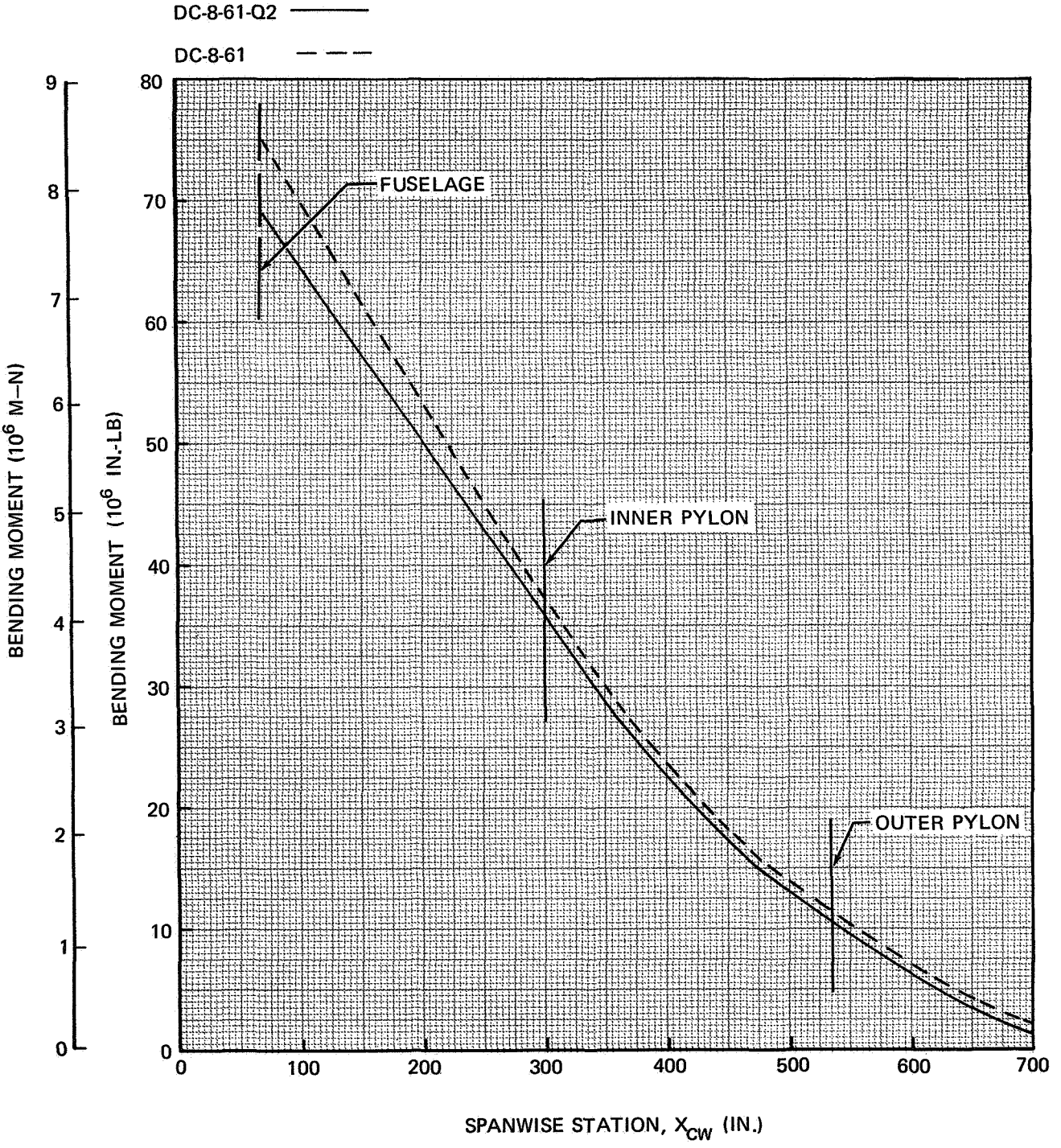

FIGURE VI-10. SYMMETRICAL FLIGHT BENDING MOMENT

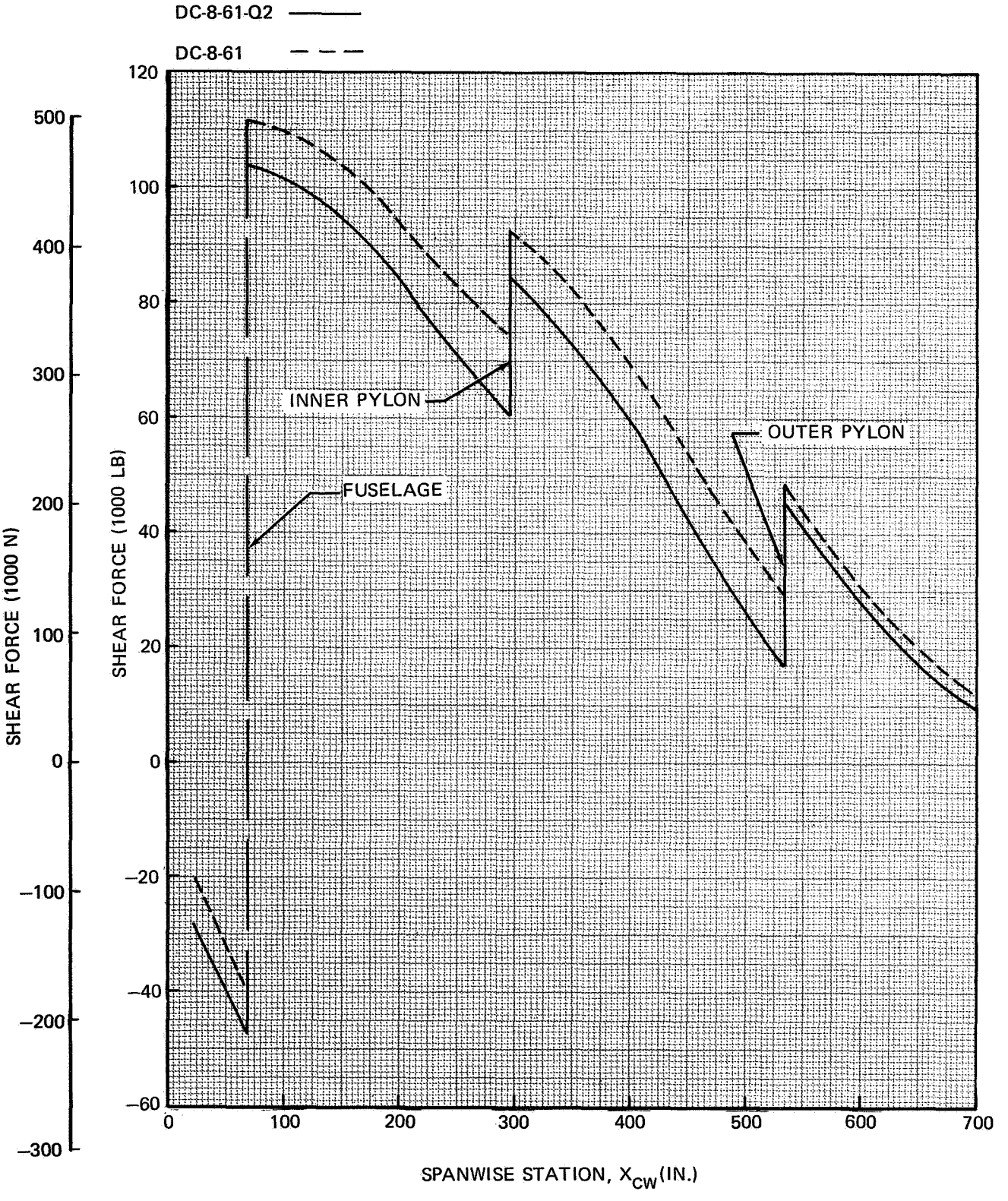

FIGURE VI-11. AILERON ROLL SHEAR

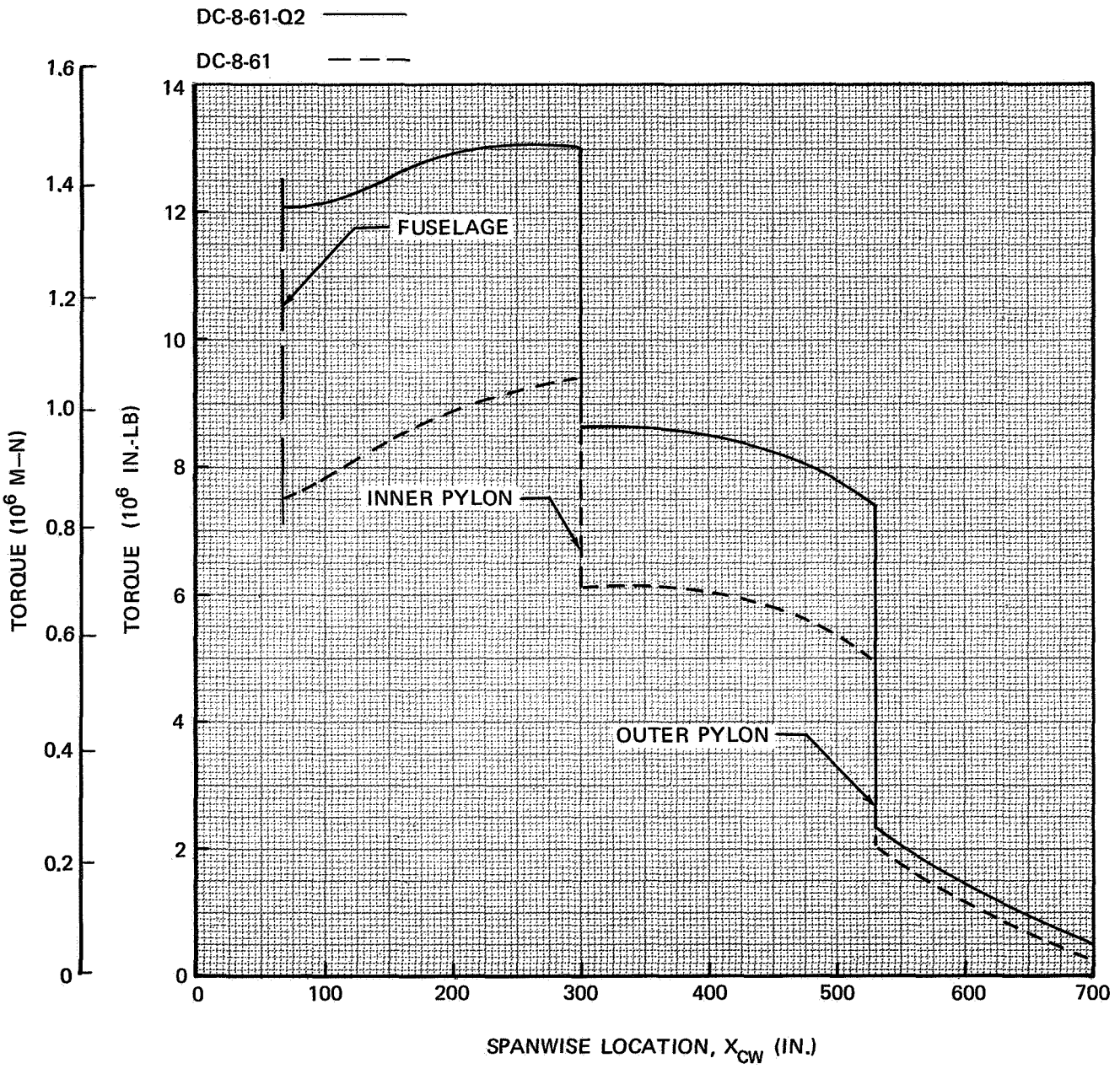

FIGURE VI-12. AILERON ROLL TORQUE

VERTICAL-TAIL LOADS

A study of tail-load conditions of the DC-8-61 showed that the vertical tail was affected by changes in engine thrust.

The horizontal tail is not structurally critical for changes in engine characteristics.

The critical vertical-tail condition that is affected by the installation of a quiet engine on the DC-8-61 is unsymmetrical thrust caused by a thrust-reverser malfunction during high speed flight at sea level. A thrust-reverser malfunction occurs when the buckets will not actuate and move to the aft position in flight. Outboard reversers cannot be actuated in flight.

The DC-8-61 vertical-tail design load is 40,100 pounds (178,373 N). Dynamic overswing caused by a quiet engine-thrust-reverser malfunction produces a vertical-tail load of 37,716 pounds (167,768 N) on a normal DC-8-61 installation. Therefore, the present tail structure will allow a loads increase for dynamic overswing of 16 percent. Table VI-IV defines the critical flight condition and shows the calculation of the load.

Figure VI-20 illustrates the dynamic-overswing forces.

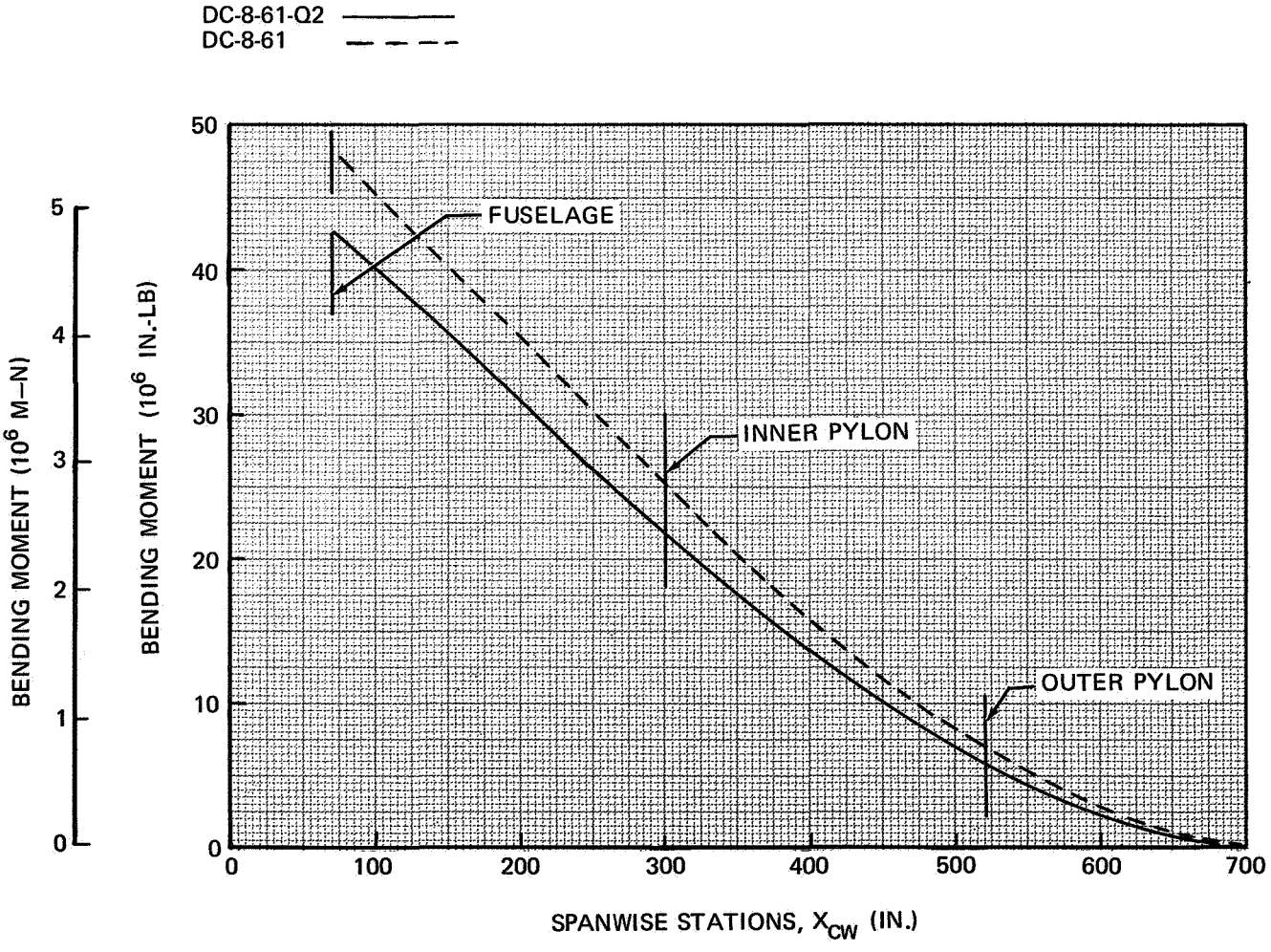

FIGURE VI-13. AILERON ROLL BENDING MOMENT

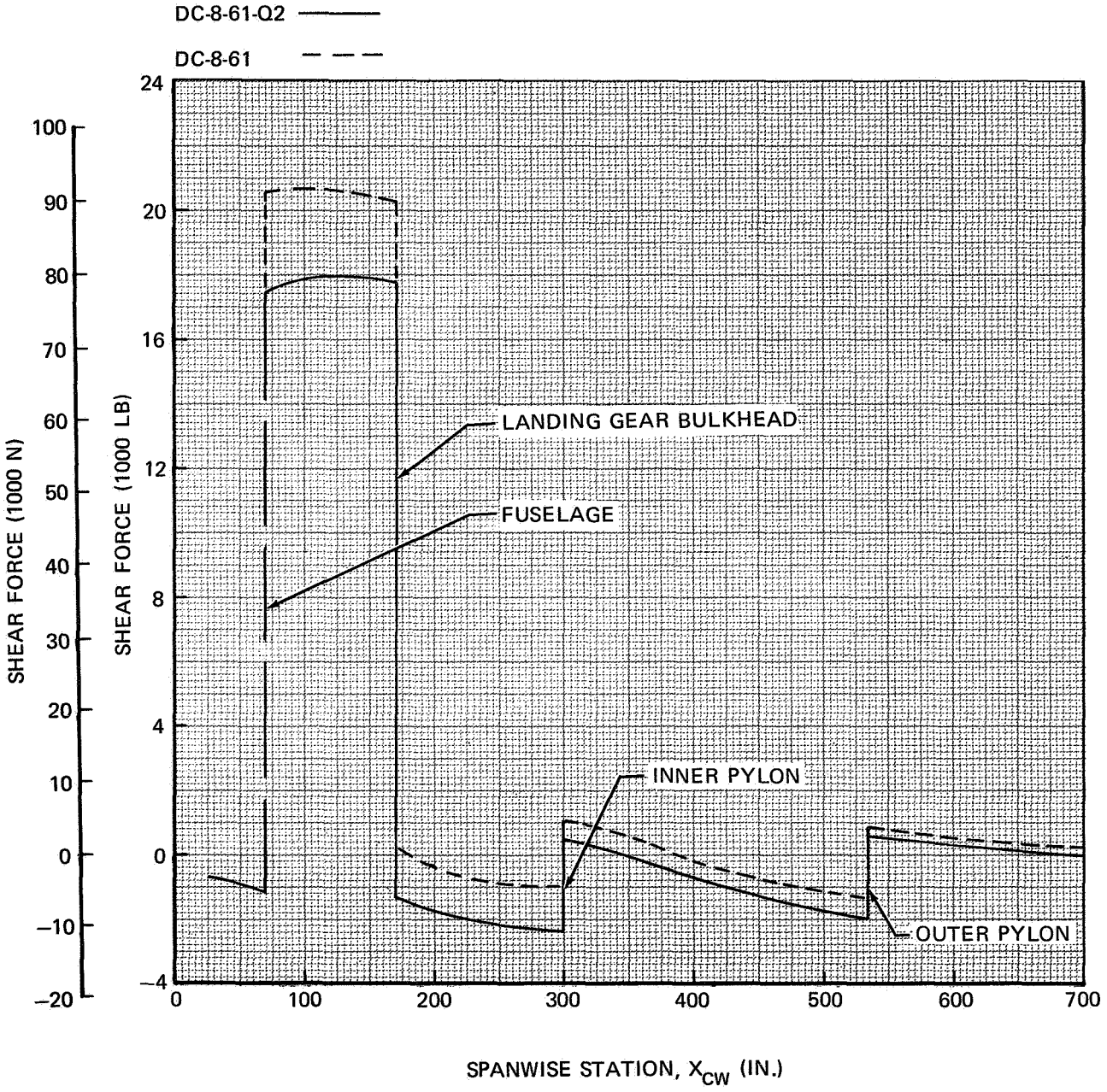

FIGURE VI-14. LANDING SHEAR

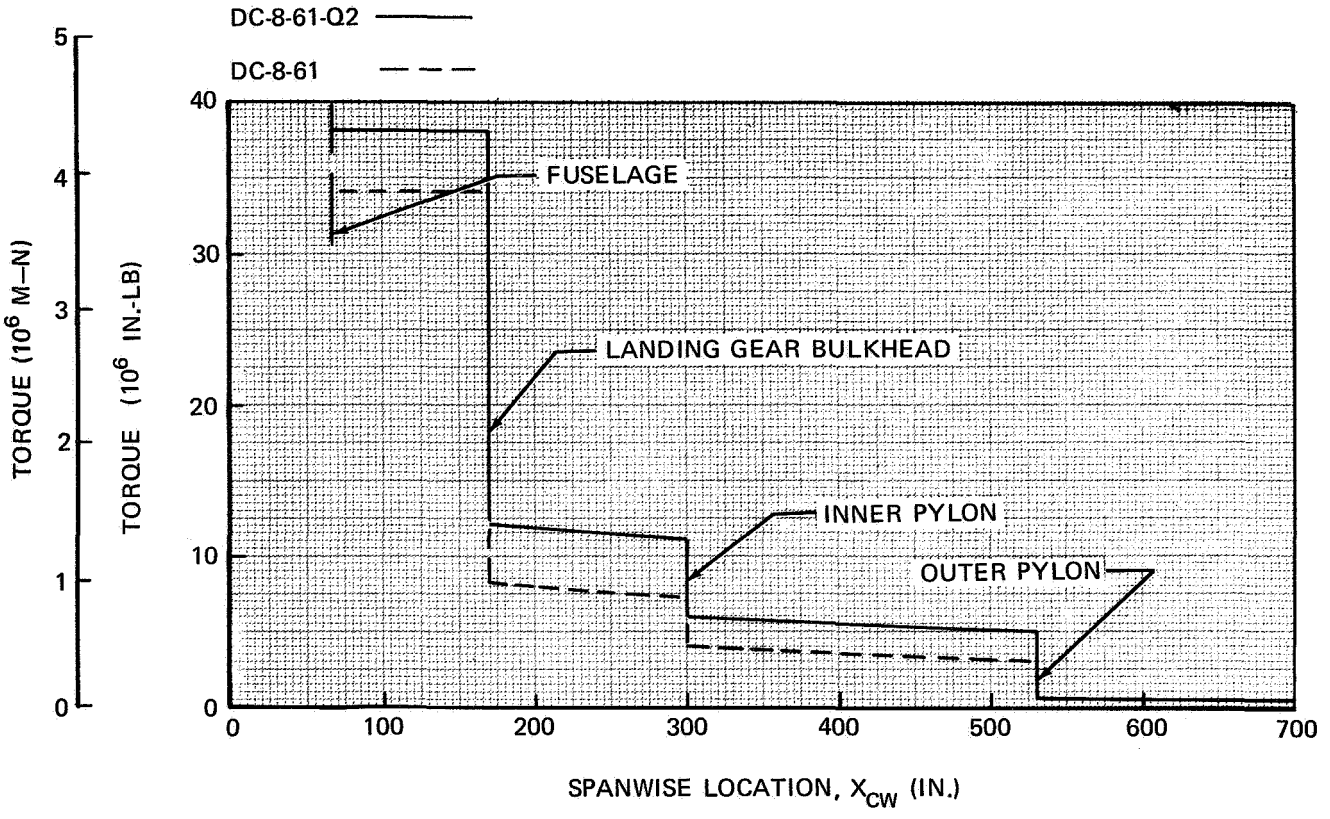

FIGURE VI-15. LANDING TORQUE

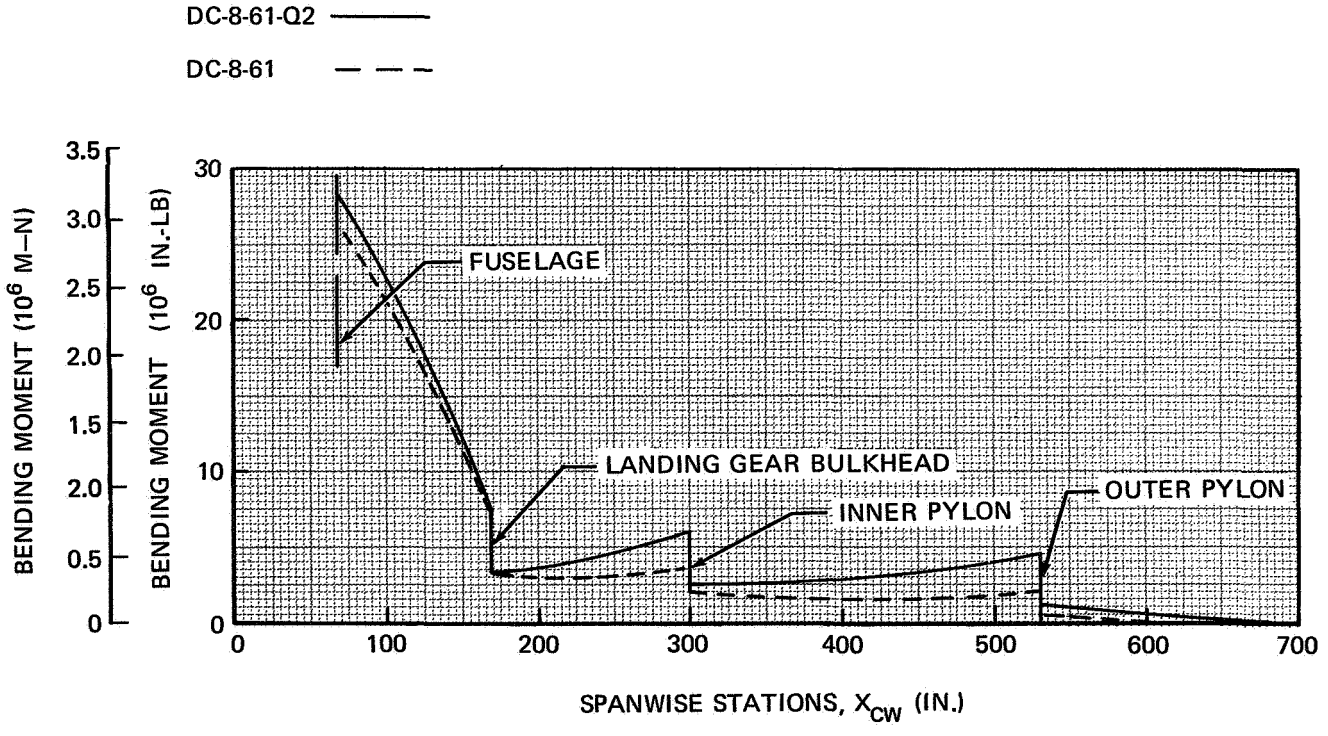

FIGURE VI-16. LANDING BENDING MOMENT

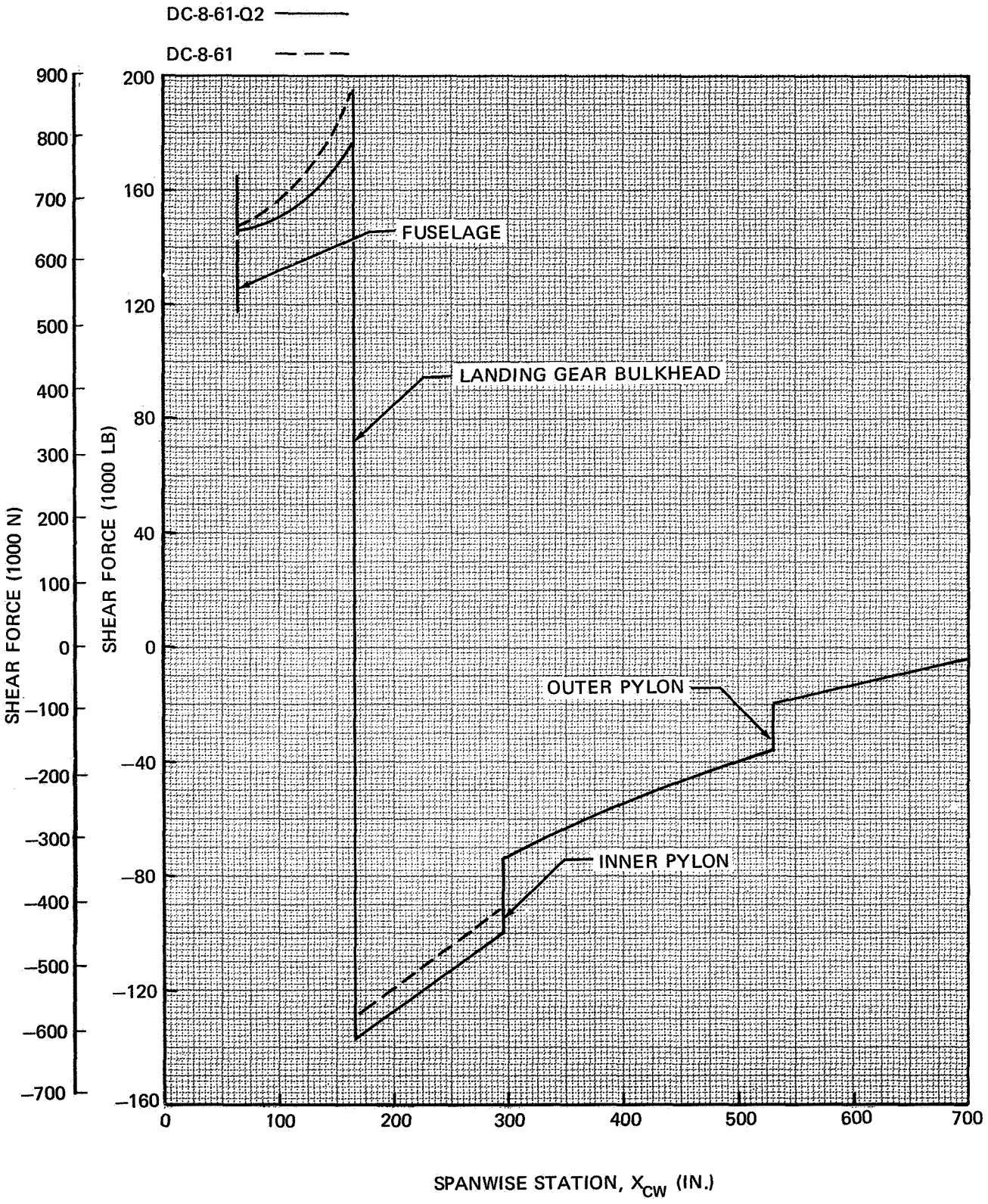

FIGURE VI-17. GROUNDBORNE SHEAR

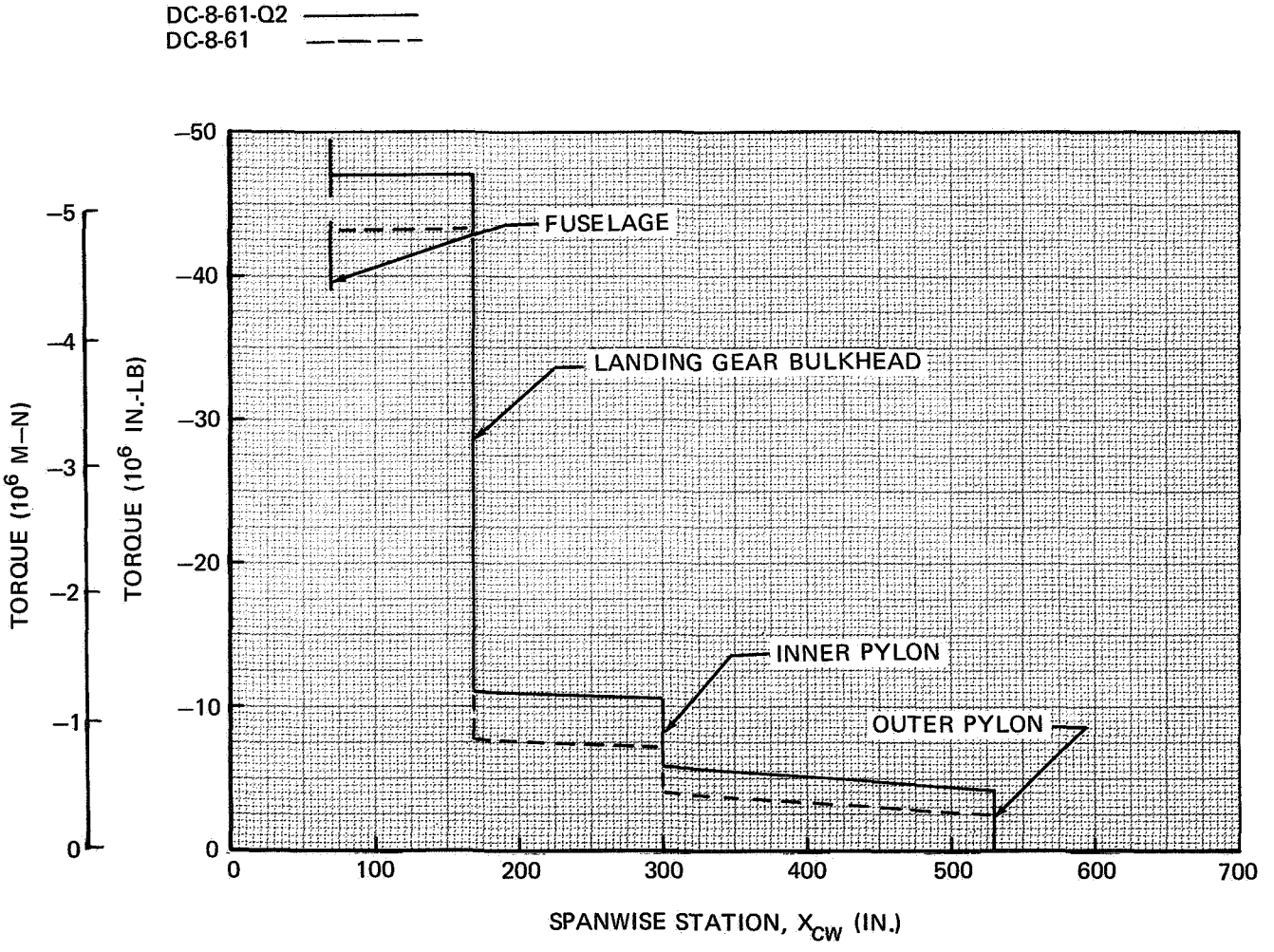

FIGURE VI-18. GROUNDBORNE TORQUE

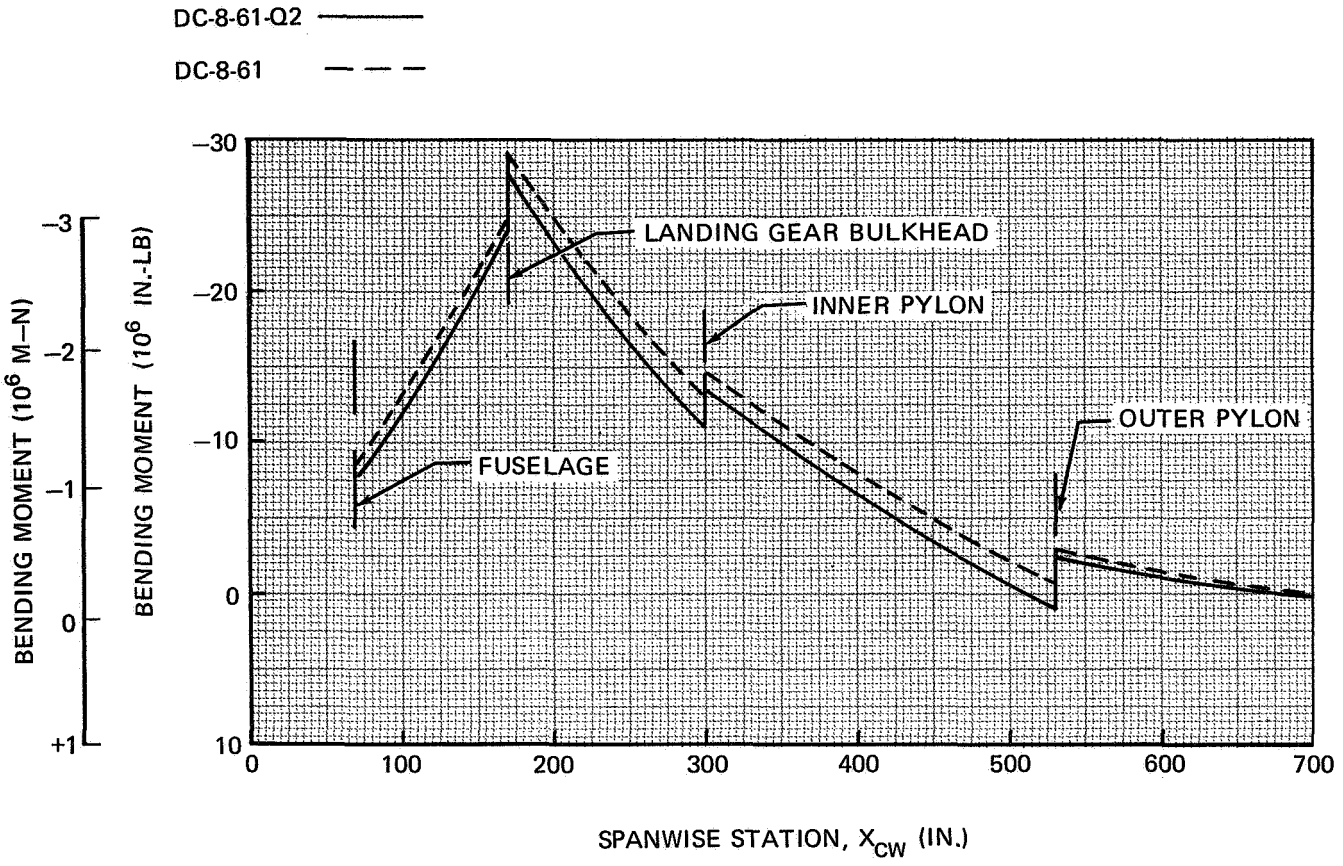

FIGURE VI-19. GROUNDBORNE BENDING MOMENT

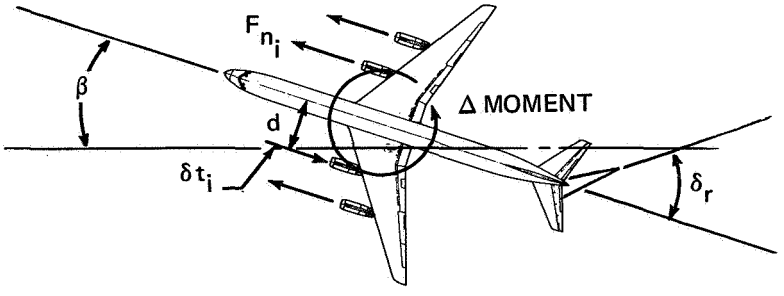

δ_r = RUDDER DEFLECTION

FIGURE VI-20. DYNAMIC-OVERSWING FORCES

TABLE VI-IV
DYNAMIC-OVERSWING LOADS

CONDITION			
M	–	0.514	
V_c	(KEAS)	340	
ALTITUDE	(FT)	SEA LEVEL	
Δt_i (REVERSER THRUST)	(LB)	26,500	117,877 N
F_{N_i} (NET THRUST)	(LB)	11,500	51,154 N
d (MOMENT ARM)	(IN.)	308.5	7.8 M
UNBALANCE DUE TO THRUST REVERSER MALFUNCTION			
$\Delta MOM = \left[\Delta t_i + F_{N_i}\right]\left(\frac{d}{12}\right)$	(FT/LB) FT/LB (M–N)	977,000 (1,328,720)	656,502 M/KG
g (SIDEWASH FACTOR)	–	–1.25	
$\alpha V = g\beta$ (VERTICAL-TAIL ANGLE)	(DEG)	4.738	
δR_{MAX} (MAXIMUM CORRECTIVE RUDDER DEFLECTION)	(DEG)	2.8	
$C_{L_{V(\alpha V)}}$ (VERTICAL-TAIL LIFT COEFFICIENT DUE TO αV)	–	0.265	
$C_{L_{V(\delta R)}}$ (VERTICAL-TAIL LIFT COEFFICIENT DUE TO δR)	–	0.093	
S_V (VERTICAL-TAIL EXPOSED AREA)	(SQ FT) (SQ M)	268.7 (25)	24.9 SQ M
VERTICAL-TAIL LOAD			
$N_V = \left[C_{L_{V(\alpha V)}} + C_{L_{V(\delta R)}}\right] q \cdot S_V$	(LB) (N)	37,716 (167,768) LIMIT	17,107 KG
VERTICAL-TAIL DESIGN N_V	(LB) (N)	40,100 178,373 LIMIT	18,189 KG

STRESS ANALYSIS

The external loads presented in the previous paragraphs were used to develop margins of safety on the main-wing-box structure. An idealized structural model was used to determine the stresses with a computer program. The skin and stringers were idealized into spanwise structural elements and shear panels to form a multi-cell box beam. The results of the stress analysis are summarized by the margin-of-safety plot of Figure VI-21. All margins are positive, but the rear-spar web is marginal for the aileron-roll conditions.

The interface structure connecting the pylon to the wing was analyzed for higher load factors than the wing, because of the dynamic amplification effect of the flexible wing. Therefore, the pylon support structure was analyzed separately. For the external loads, the load factor acting at the engine-nacelle center of gravity was predominant. This load factor was assumed to be similar to the Model DC-8-62 engine-nacelle load factors because the center of gravity locations are approximately the same (Figure VI-22).

The inboard-engine load factor is 5 g ultimate. The outboard is 7 g ultimate. Because the inboard pylon is located where the wing box section and skin gages are considerably larger than at the outboard pylon and because the inboard pylon loads are less, the interface structure of the DC-8-61 was found to be adequate for the inboard quiet engine pylon.

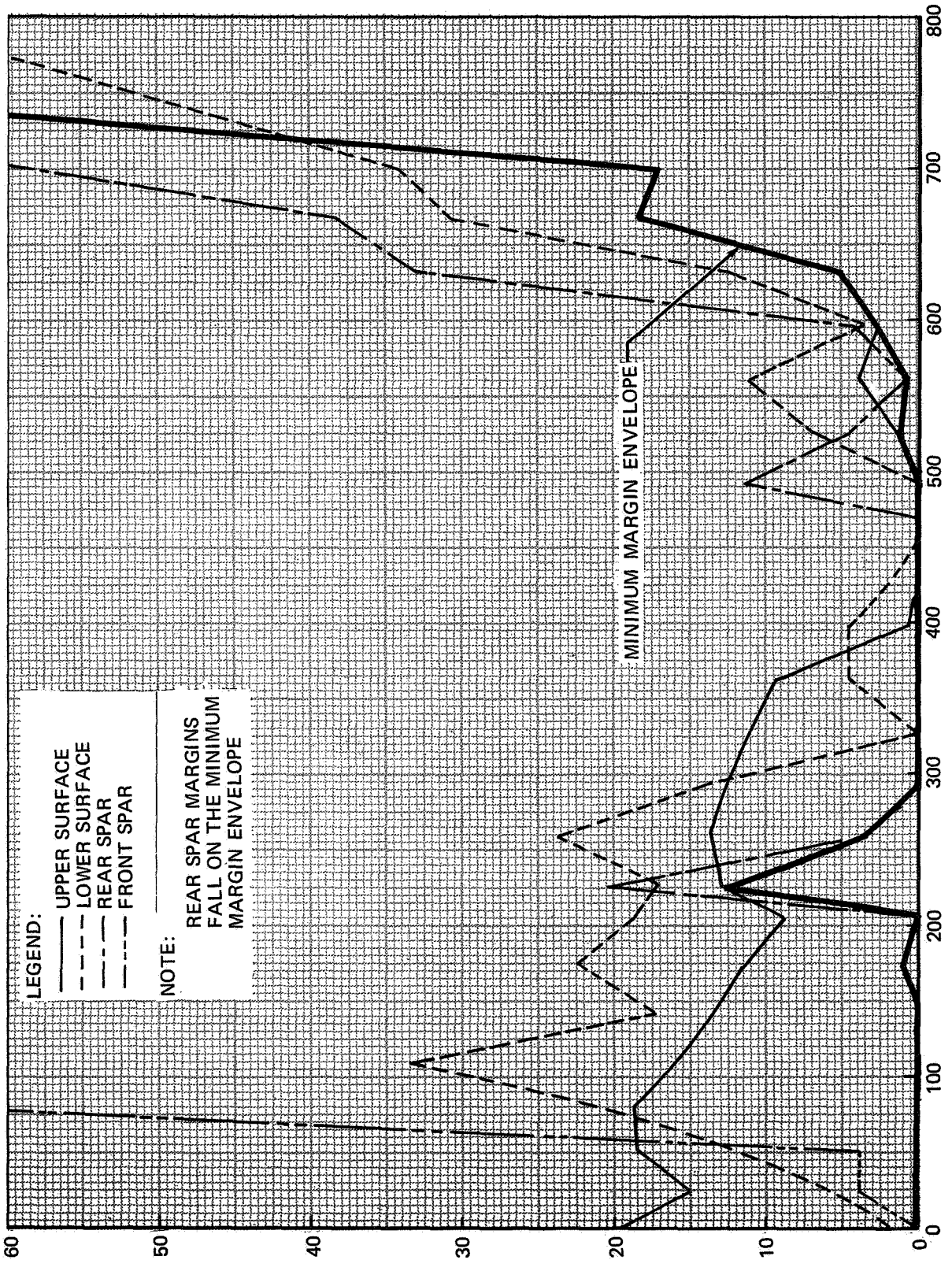

FIGURE VI-21. MINIMUM MARGINS OF SAFETY

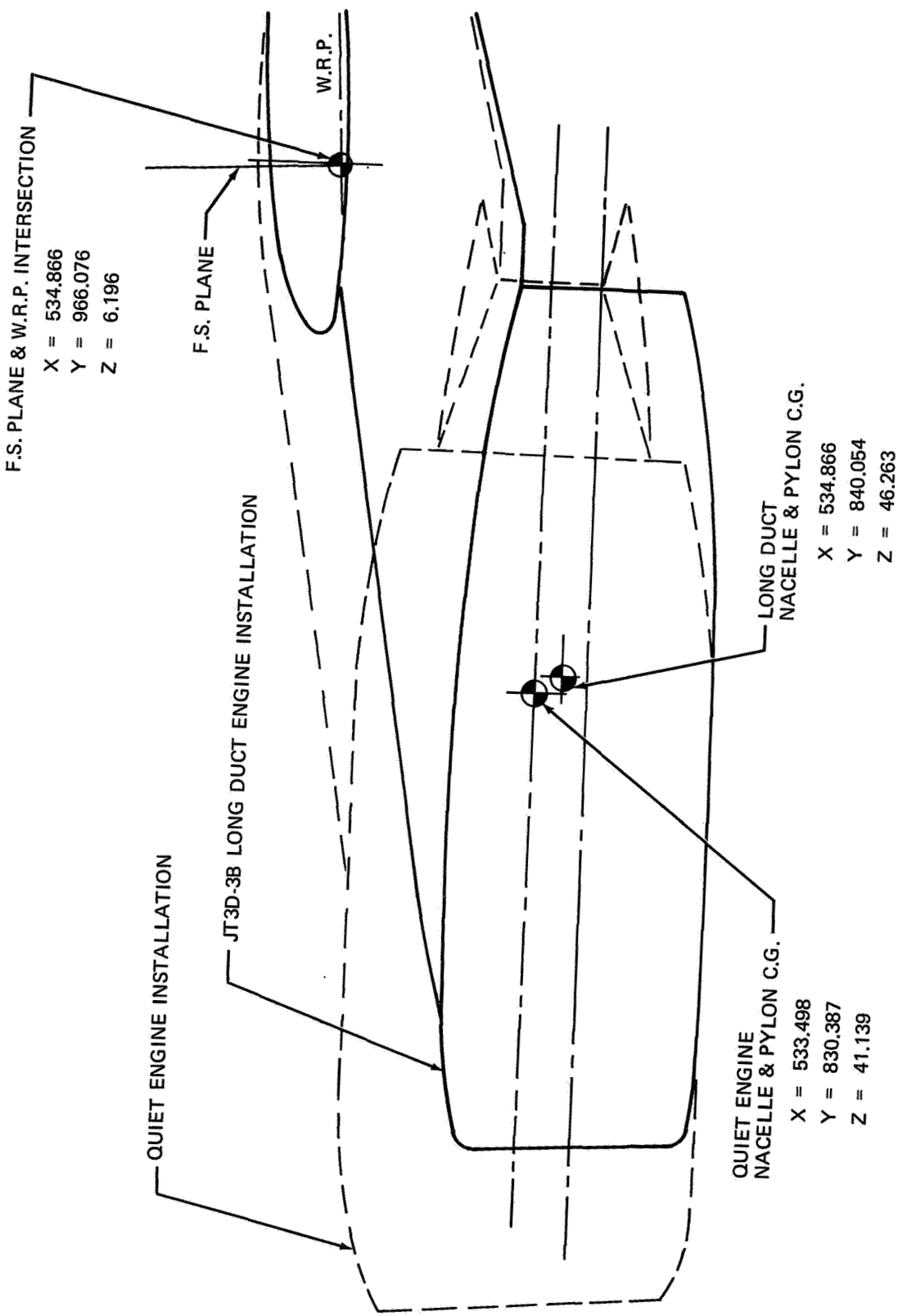

FIGURE VI-22. NACELLE COMPARISON WITH DC-8-62

STRUCTURAL CHANGES

The outboard-pylon interface structure requires the modifications described in the following paragraphs.

1. The vertical pylon loads are reacted directly into the front-spar web by a "horseshoe" fitting and a "zee" stiffener. The attachments between these fittings and the front spar must be replaced by the next larger standard-diameter bolt.

2. Within the wing tank, the webs on the canted support bulkheads require a 0.125-inch (3.1 mm) doubler from the front to the center spar. A 0.090-inch (2.2 mm) doubler now exists on the bulkhead at cant station 509 and will have to be removed. This 0.090 (2.2 mm) doubler extends only 11 inches (28 cm) aft of the front spar.

3. The forward-lower-bulkhead cap attachments to the center spar will be increased to 3/8-inch-diameter (9.5 mm) bolts, for both bulkheads.

4. The attachments of the forward webs to the front and center spars, and to the upper and lower caps, will be changed to 1/4-inch-diameter (6.3 mm) lockbolts on both bulkheads.

5. All stringer shear clips will be double back-to-back clips from the front to the center spar for the upper and lower surfaces. This also applies to both bulkheads.

Figures VI-23 through VI-25 show these changes in detail.

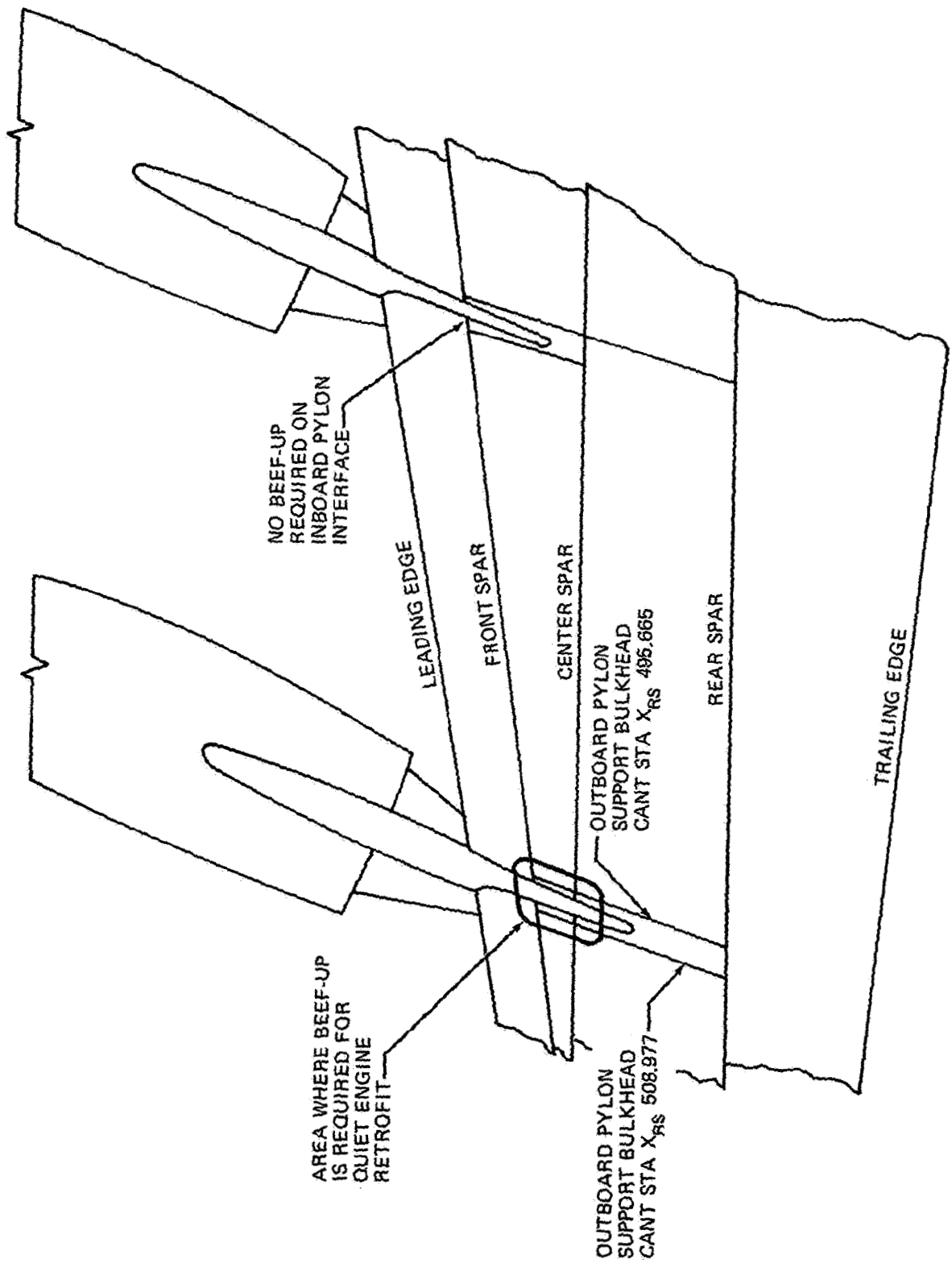

FIGURE VI-23. WING STRUCTURAL CHANGES

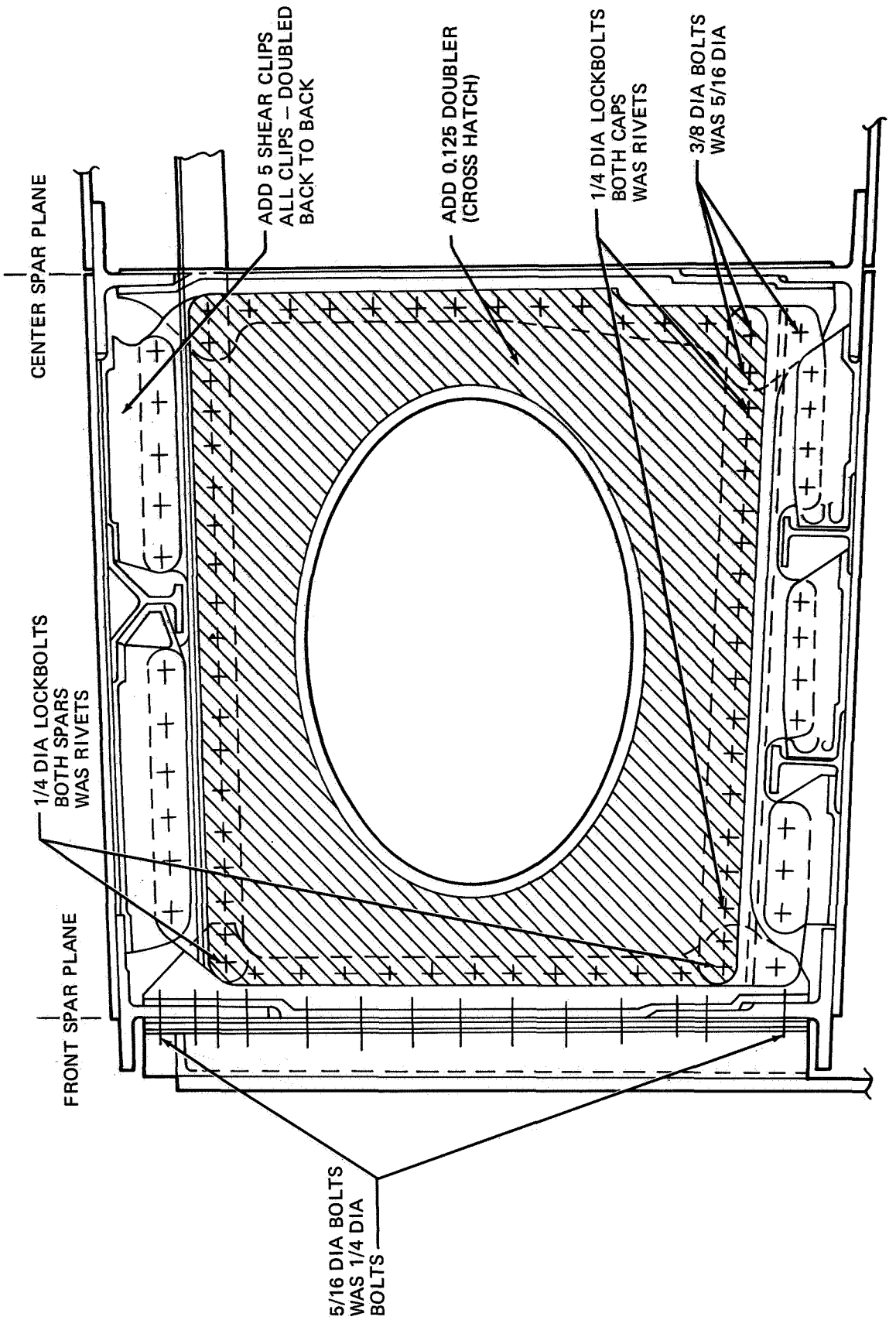

FIGURE VI-24. STRUCTURAL CHANGES AT STATION X_{RS} = 495.665

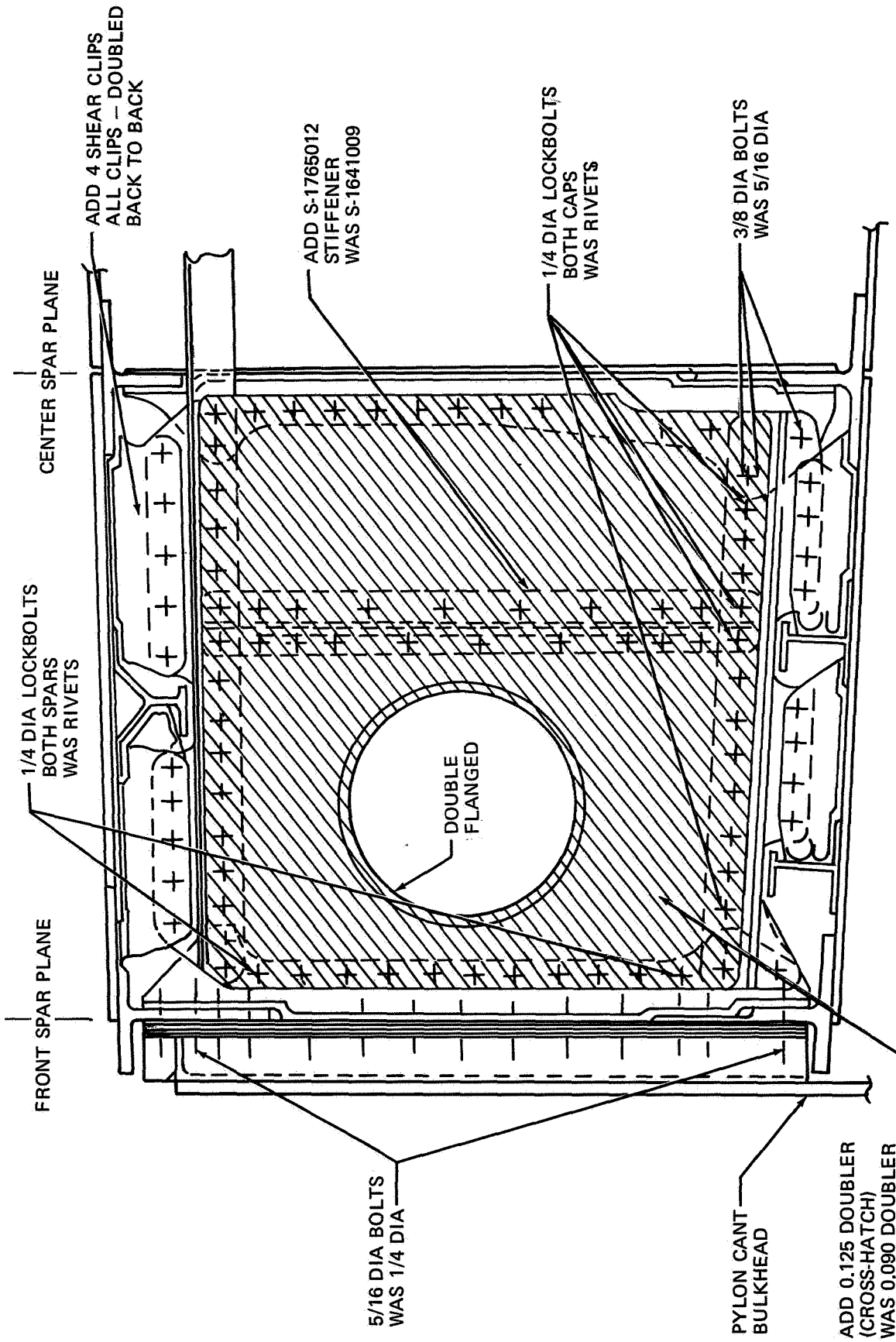

FIGURE VI-25. STRUCTURAL CHANGES AT STATION X_{RS} = 508.977

CONTROL-SYSTEM CHANGES

The results of the aerodynamic wind-tunnel test program reported in Task III show that a powered-elevator system and a redundant yaw-damper system would have to be added to the DC-8-61-Q2 to obtain acceptable stability and control characteristics. The system changes are described below.

POWERED ELEVATOR

The existing aerodynamic elevator control would be replaced by an hydraulically powered system. The design would provide for reversion to manual control using the aerodynamic tab in the event of hydraulic failure. The reversion mechanism would be similar to the existing DC-8 aileron reversion mechanism.

The addition of powered elevators requires an elevator load-feel mechanism that would be programed as a function of free-stream dynamic pressure and horizontal-stabilizer position.

A system similar to the DC-10 design will be used. This elevator load feel changer system has dual dynamic-pressure inputs, dual signal processors, and a dual servo actuator. In the event of system malfunction, manual programing of the feel mechanism is provided by a control switch accessible to the pilot. An indicator to monitor the system operation will be provided.

Figure VI-26 is a block diagram of the elevator load feel changer.

REDUNDANT YAW DAMPER

The following changes must be incorporated in this system:

1. The existing rudder hydraulic actuator will be revised to add a second electrical input value.

2. The existing pilot controller will be revised to add the second yaw-damper engage lever.

3. The existing automatic-pilot trim indicator will be revised to add a trim indicator for the second yaw damper. The existing yaw channel computer would be revised to add the second yaw-damper functions.

The operation will allow either yaw damper to be engaged separately or simultaneously with the other. In the event of a failure of the hydraulic actuator, reversion to manual control with an aerodynamic tab will be possible.

Figure VI-27 is a block diagram of the dual yaw-damper system.

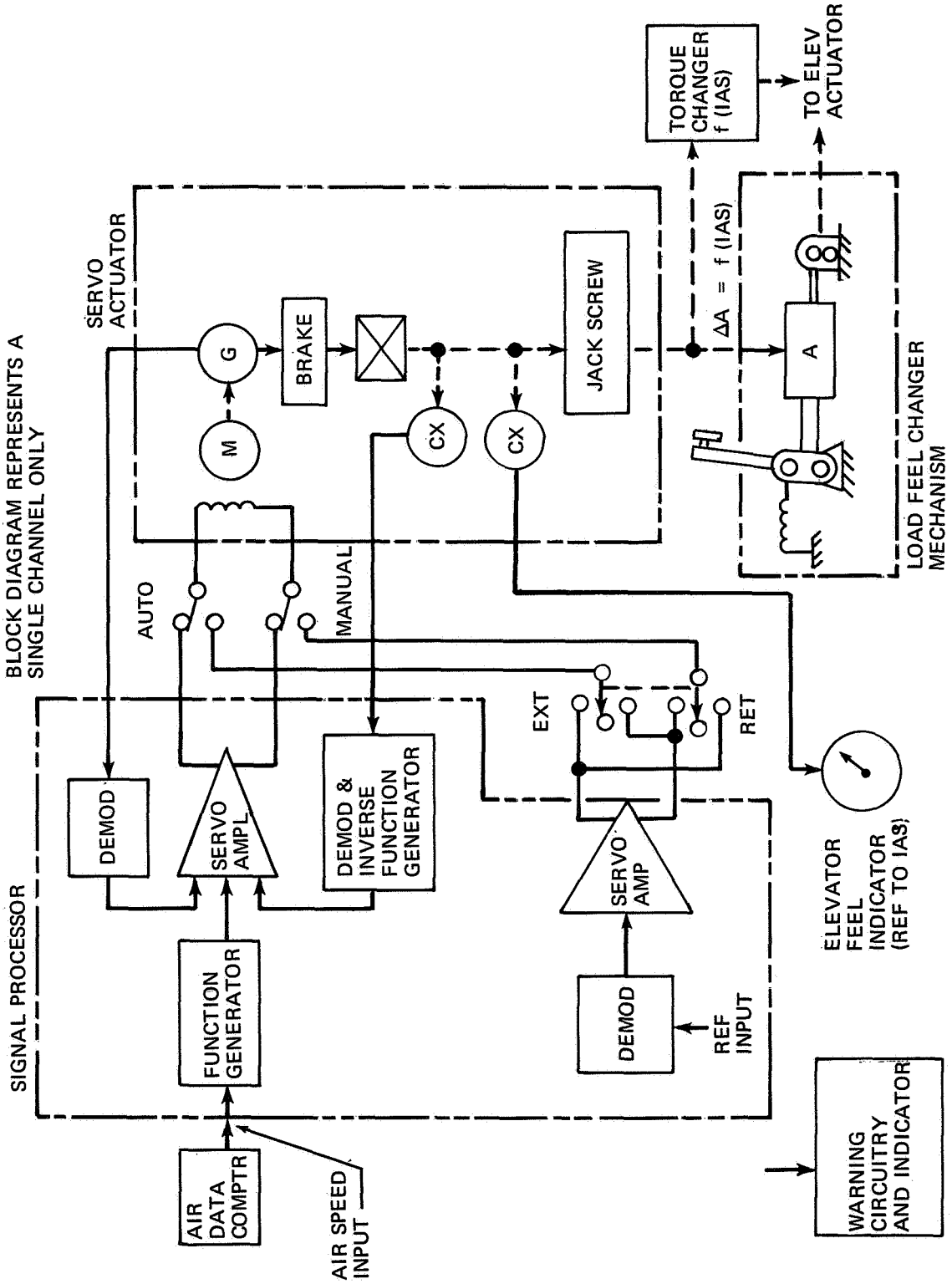

FIGURE VI-26. ELEVATOR LOAD FEEL CHANGER BLOCK DIAGRAM

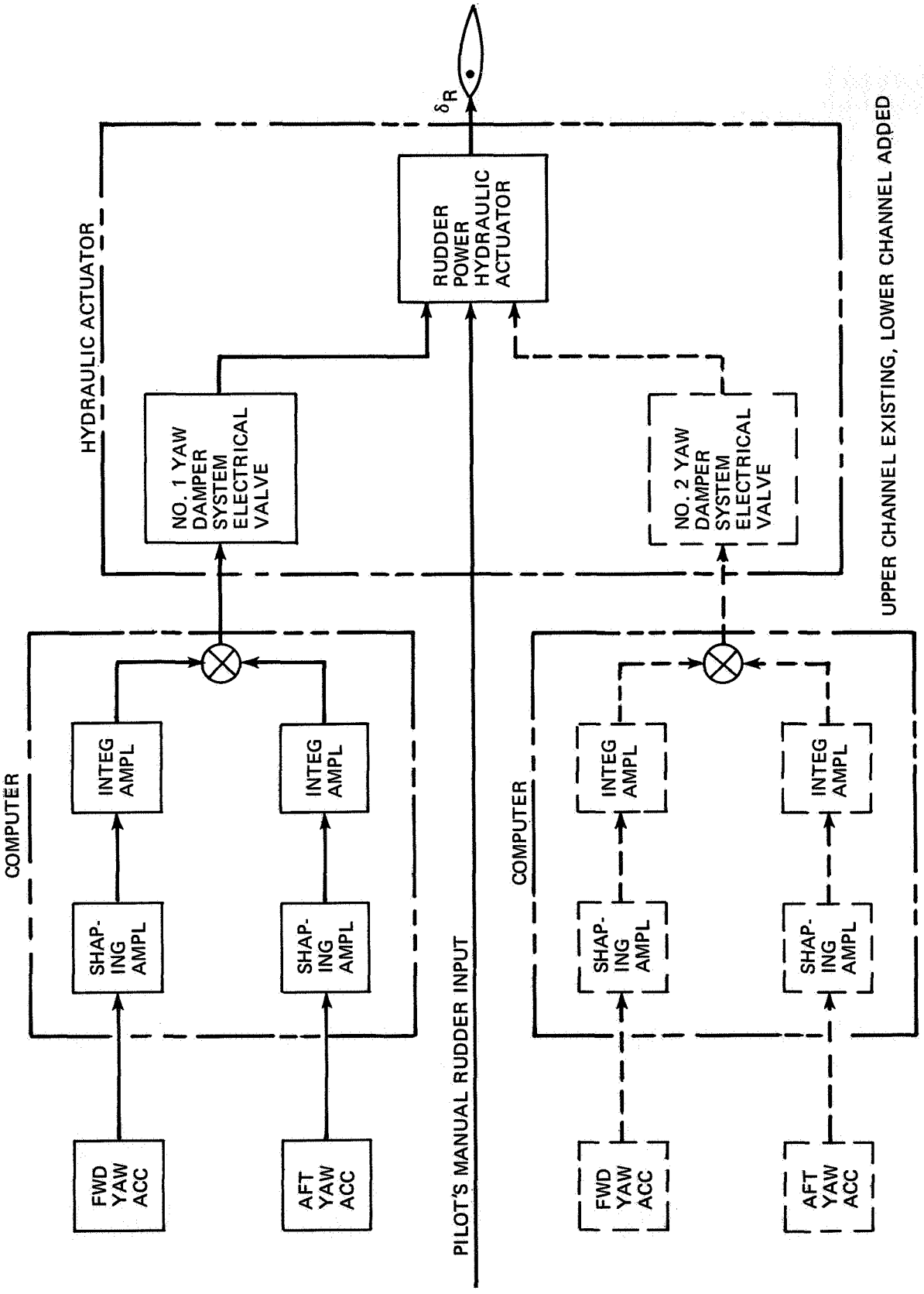

FIGURE VI-27. SERIES YAW DAMPER SYSTEM

STABILITY AND CONTROL ANALYSIS

Task III shows the results of the low- and high-speed wind-tunnel tests of the quiet-engine installation on the DC-8-61. The significant effects on stability and control parameters were as follows:

1. A reduction in static longitudinal stability equivalent to only slightly more than a 4 percent MAC forward movement of the neutral point.

2. A reduction of 5 to 10 percent in static directional stability.

3. An increase of 5 percent in side force caused by sideslip.

Preliminary analyses to determine the implications of the data, which were reported in Task III, identified the following three affected problem areas:

1. Static longitudinal stability and the aft center-of-gravity limit.

2. Minimum control speeds with one engine inoperative.

3. Dutch roll damping with the yaw damper inoperative.

These problem areas have been analyzed in more detail and are discussed below.

DUTCH ROLL CHARACTERISTICS

Analyses of the effects of the quiet-engine installation on DC-8-61 Dutch roll characteristics have been made for takeoff, cruise, and landing-approach conditions, for extremes of gross weight, and center-of-gravity position. The results indicate a generally uniform increase in Dutch roll period of 1/3 to 1/2 second, and a reduction of 0.01 in damping ratio, compared to the basic DC-8-61.

All DC-8 aircraft have Dutch roll characteristics that allow dispatch and operation without a yaw damper, with no flight-envelope restrictions. However, a yaw damper is provided for improved damping during normal operation. Any changes that reduce the inherent Dutch roll damping significantly would imperil this dispatch capability. A redundant yaw damper is therefore deemed necessary.

MINIMUM CONTROL SPEEDS

The reduction in static directional stability caused by the larger nacelles has an adverse effect on minimum control speed in the air. Calculations indicate that the air minimum control speed, V_{MC_A}, would be increased by 8 knots at JT3D-3B thrusts and 5.5 knots at quiet-engine thrusts, as is shown in Figure VI-28. However, the air minimum control speeds being used for the DC-8-61 are those of the shorter DC-8-50. Advantage has not been taken of the gains due to the increased tail arm of the Series 61. The minimum-control-speed capabilities with the quiet engines will still be better than the presently certificated version.

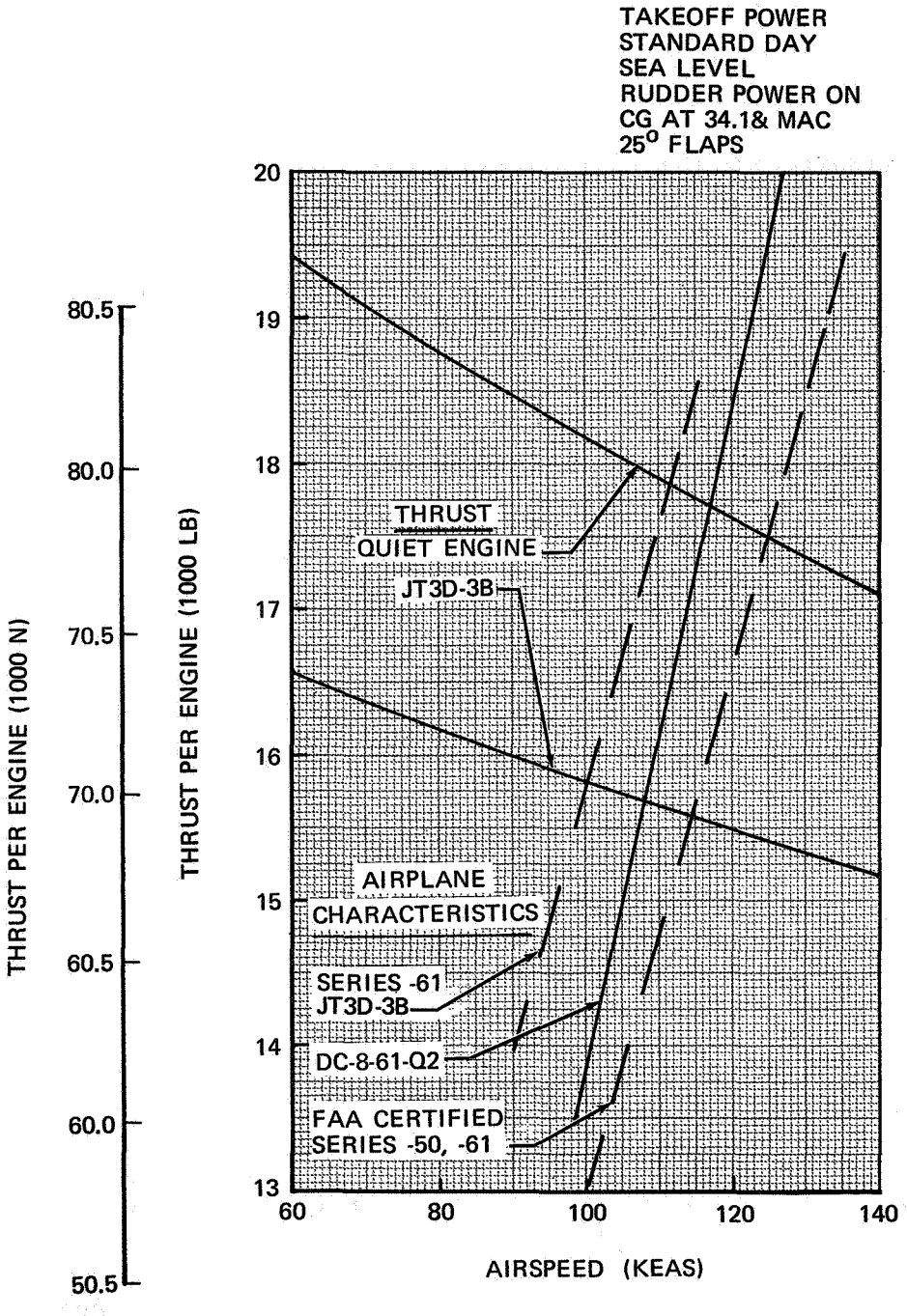

FIGURE VI-28. ESTIMATED AIR MINIMUM CONTROL SPEEDS

STATIC LONGITUDINAL STABILITY

As is explained in Task III, the aft center-of-gravity limit on the DC-8-61 is determined by the static-longitudinal stability requirements of F.A.R. 25.171. Stability is critical in the enroute climb condition with maximum climb thrust. The increased nacelle size, thrust, and mass flow of the quiet engine are all destabilizing, and can cause as much as an 8-percent MAC shift of the neutral point. The resulting static stability characteristics are shown in Figures VI-29 and VI-30.

Three possible solutions to this problem have been considered, as follows:

1. Restrict the aft center-of-gravity limit to approximately 26 percent MAC.

2. Increase the size of the horizontal tail.

3. Install a powered elevator system.

A restriction of the necessary magnitude on the loading envelope may prove unacceptable to the operators; hence only the last two possible solutions were considered.

Increasing the tail size offers a straightforward solution. However, an increase of approximately 30 percent in area might be required, with resulting adverse effects on weight and retrofit cost.

Analysis of the estimated characteristics indicates a stable, though slight, variation of elevator angle with airspeed. It is possible that the installation of an elevator power system would eliminate elevator floating and, through the use of artificially generated forces, create a stable condition. It is proposed that the present manual elevator system be retained as a backup system in the event of hydraulic system failure. An artificial feel system utilizing airspeed and stabilizer position inputs would have to be developed to provide the desired pilot forces. Detailed design of such a feel system would be required to determine whether the desired pilot forces and satisfactory stability can be obtained without restricting the aft center of gravity limit or increasing the size of the horizontal tail.

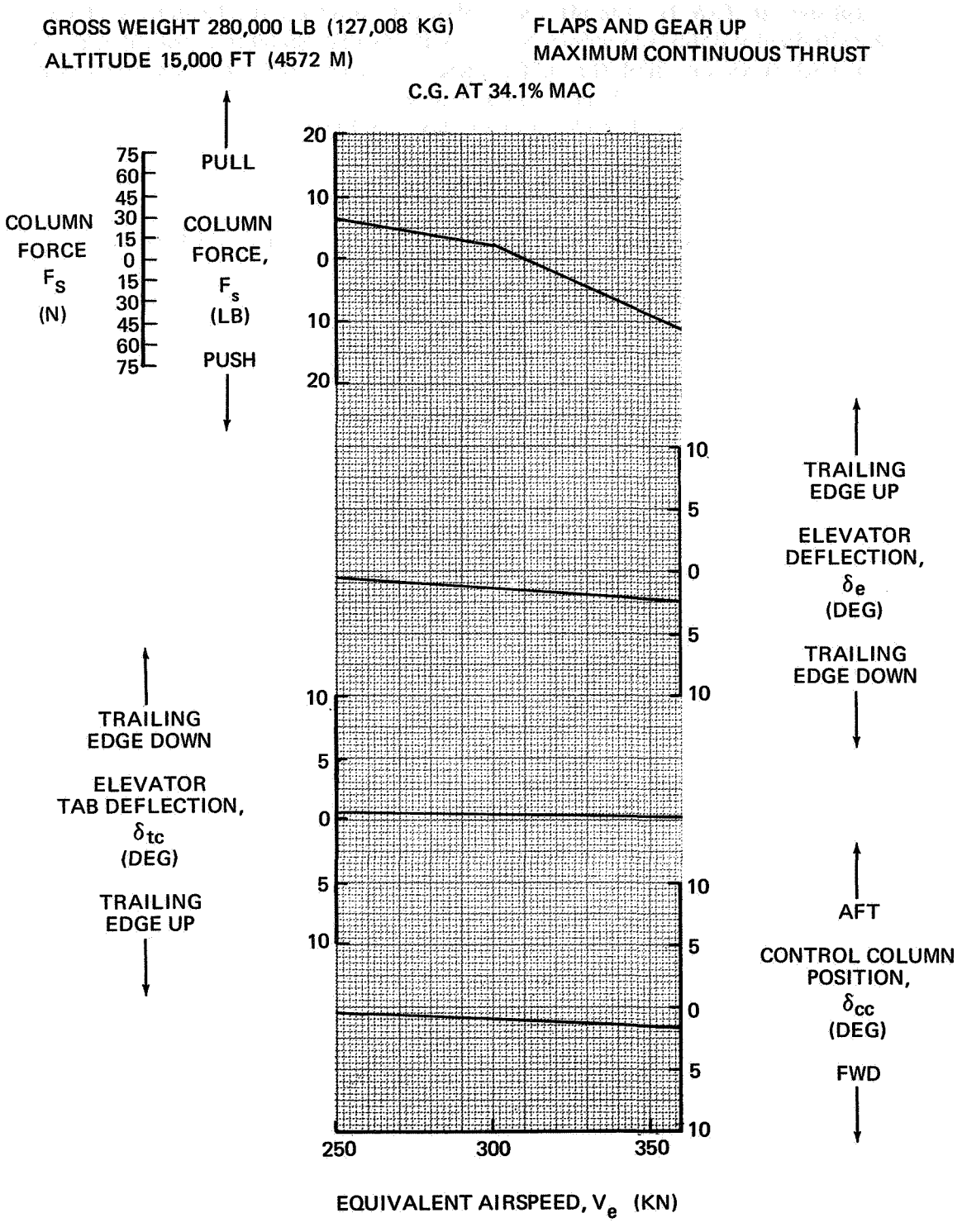

FIGURE VI-29. ESTIMATED LONGITUDINAL STABILITY DURING CLIMB – DC-8-61

GROSS WEIGHT 280,000 LB (127,008 KG)
ALTITUDE 15,000 FT (4572 M)

FLAPS AND GEAR UP
MAXIMUM CONTINUOUS THRUST

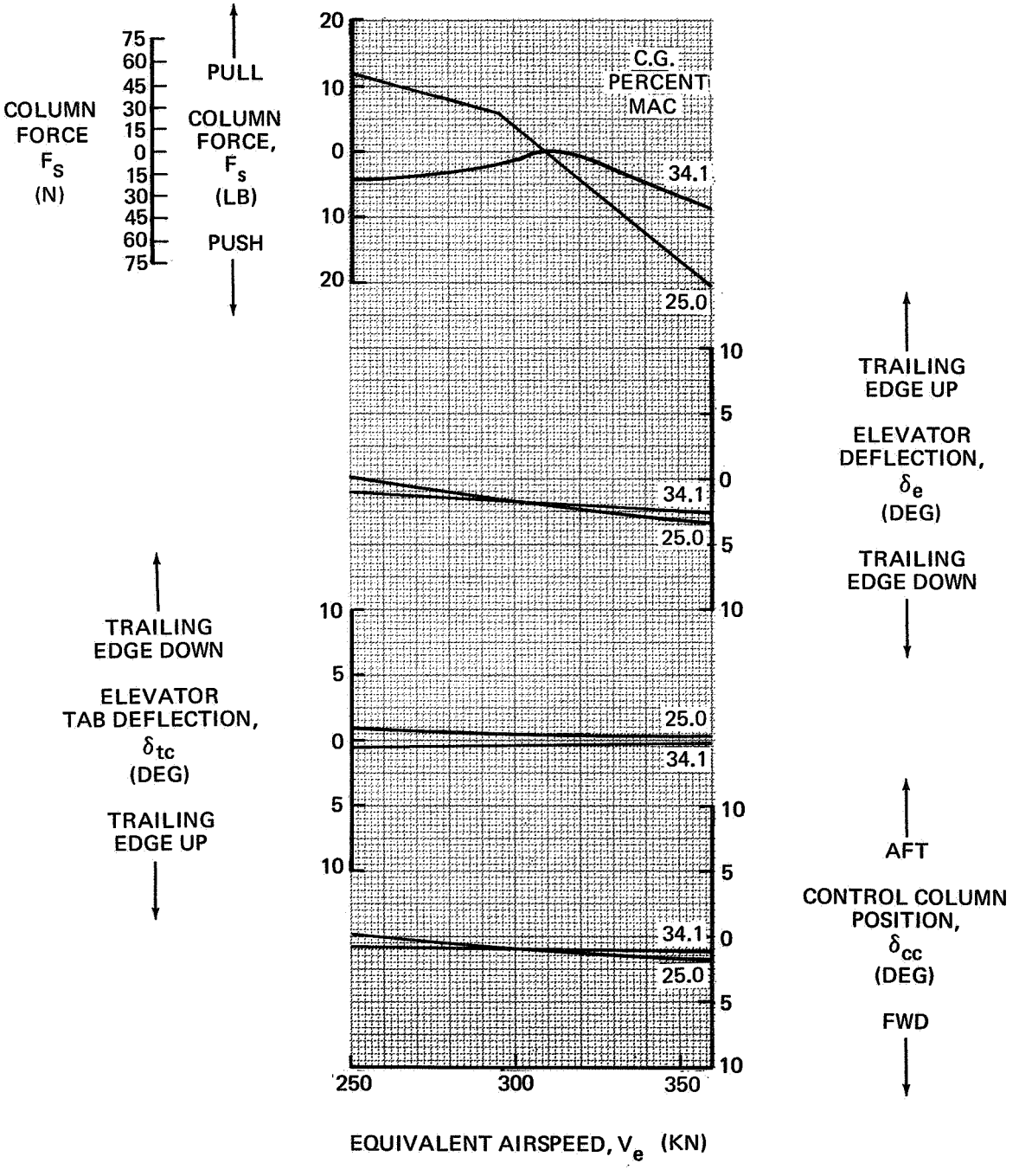

FIGURE VI-30. ESTIMATED LONGITUDINAL STABILITY DURING CLIMB – DC-8-61-Q2

FLUTTER TESTS AND ANALYSIS

This section discusses the flutter tests and analyses that were made to determine the flutter characteristics of the DC-8-61 aircraft retrofitted with the nacelles and pylons designed in Task IV. This part of the study consisted of flutter-model testing and analysis for several airplane configurations.

Previous tests and analyses of the DC-8-61 aircraft had established the geometric and structural characteristics that would significantly alter the flutter characteristics if they were changed. The addition of the quiet engine required detailed study of these items: wing fuel loadings, engine mass and center of gravity locations, and engine-pylon stiffnesses.

The flutter-model program included design and construction of quiet-engine nacelles and pylons. These were fitted to the existing DC-8-61 flutter model. The testing was performed in the Northrop 7- by 10-foot wind tunnel from 2 August 1968 through 12 August 1968. Eighty-eight airplane configurations were tested during 54 hours of tunnel operation.

The flutter analyses were performed on the IBM 360/65 digital computer by using the Douglas flutter program C4EB. The best available wind-tunnel tests and ground vibration test data were used in the analyses.

FLUTTER-MODEL TESTS

Previous tests of low-speed flutter models have shown that they give reliable flutter results. For this reason, low-speed flutter-model testing was chosen as the most reliable method of investigating the flutter problems that might arise if the DC-8-61 aircraft were to be fitted with the quiet engine. The model used for testing was the original DC-8-61 flutter model, which was refitted with new nacelles and pylons. A description of the construction is included in this report. A picture of the model mounted in the tunnel is shown in Figure VI-31.

The model was a 5-percent-scale low-speed model of the DC-8-61 aircraft with the stiffness and mass distributions simulated to be consistent with a 0.183 speed scale and a 1.44 density scale.

The primary design features of the DC-8-61 flutter model are as follows:

1. Single aluminum spars are used to represent the stiffness of the wing, vertical stabilizer, and fuselage.

2. The aerodynamic properties are simulated by rigidly attaching sections or bays to the spars. The sections are constructed of balsa wood, mylar, and fiber glass. The bay construction is necessary to preclude any additional stiffness due to the balsa wood. The gaps between bays are sealed with very thin rubber.

3. Mass properties are simulated by removable lead weights.

4. The model is designed to be as versatile as possible, so that many parameters and airplane configurations can be simulated.

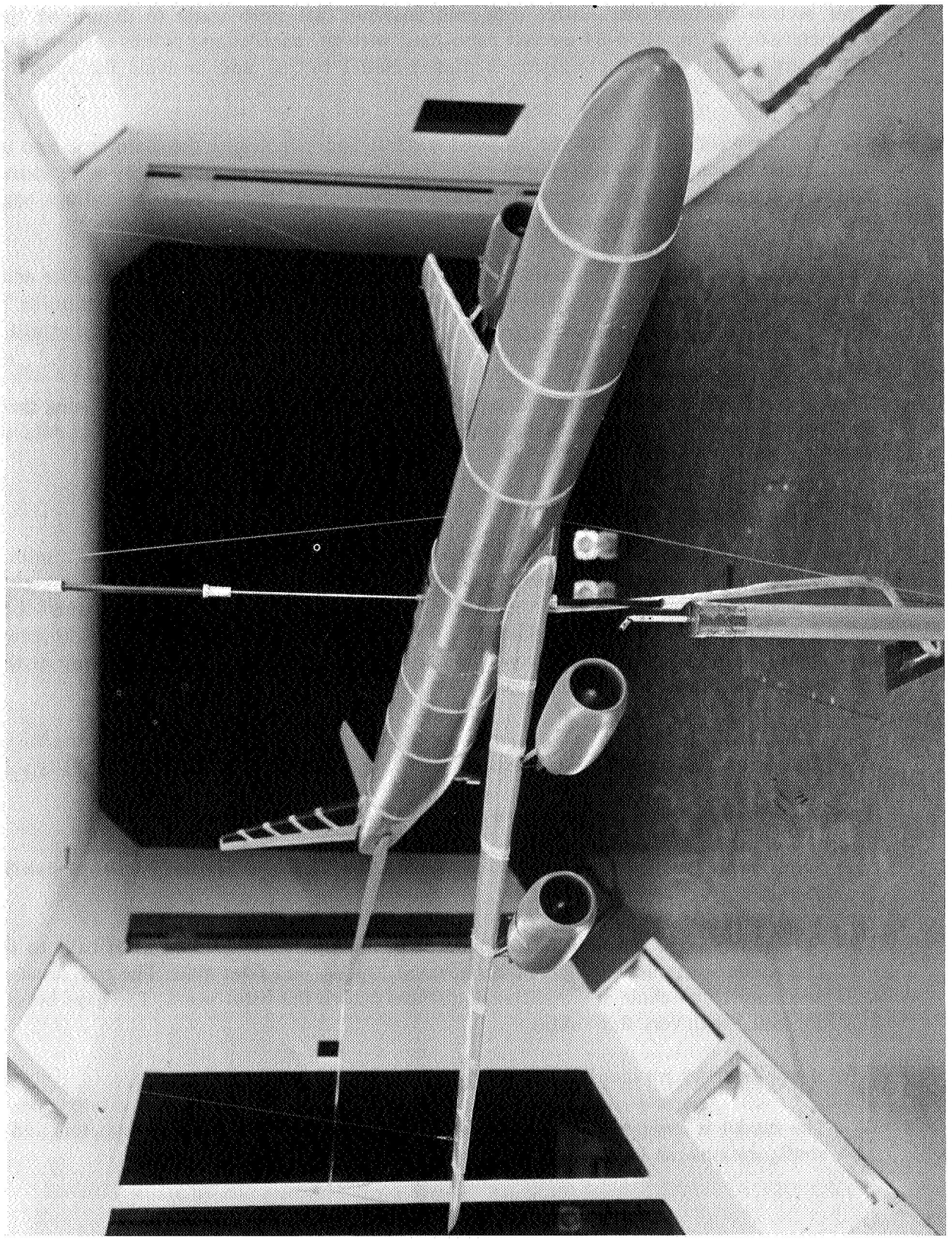

FIGURE VI-31. DC-8-61 FLUTTER MODEL

The quiet-engine nacelles were constructed of aluminum and balsa wood with lead to simulate inertia properties. The pylon was a uniform aluminum beam. A picture of the nacelle mounted on the wing is shown in Figure VI-32. The nacelle was movable forward and aft such that four center of gravity positions could be tested, the design position and positions 16.25 inches (41.27 cm), 32.5 inches (82.5 cm), and 48.75 inches (1.24 m) aft of the design position. Five sets of pylons were designed, which gave five possible frequency variations for each nacelle position. Thus, 20 combinations of frequency and nacelle location could be simulated for each pylon.

The nacelle geometry matched the primary dimensions of the Task IV engine. These included outside diameter, length, exposed area, and flow-through area. The simulated inertial properties were mass, pitch, yaw, and roll inertia about the engine center of gravity.

The model was free flying in the wind tunnel. It was restrained in the fore and aft and lateral directions by a steel rod. A damper was attached between the nose and tunnel floor to stabilize the rigid-body longitudinal mode. Snubber cables were attached to the forward fuselage and operated from outside the tunnel. The model was excited from outside the tunnel by means of small-diameter cables attached to the wing, nacelles, and stabilizer. A schematic of the installation is shown in Figure VI-33.

The instrumentation of the model included accelerometers and strain gages attached to the model spars and components. The output of these gages were recorded on an oscillograph. Frequencies and decay damping coefficients following cable excitation were measured from the oscillograph traces while the tests were in progress. The tunnel speed was increased until the model showed zero damping when excited. The tunnel was then shut down and the configuration changed.

FLUTTER ANALYSES

The flutter analyses were similar to the previous analyses used on all the DC-8-60 series aircraft. The analyses were updated to include the most recent wind-tunnel data and ground vibration test data. All vibration and flutter analyses were performed on the IBM 360/65 computer with Douglas Programs D7QA and C4EB.

The modes of vibration were calculated by using cantilevered component modes and the Mykelstad method. The cantilevered modes were coupled with rigid-body modes to generate the free-free modes of the airplane. The original vibration analyses of the DC-8-61 were revised in such a way that the frequencies, mode shapes, and node lines of the analyses matched those that had been measured on the ground vibration test (Reference VI-2). The revisions were made by altering the frequencies of the cantilevered component modes. The process is explained in detail in Reference VI-3. The correction factors used in Reference VI-3 were applied to the computed modes of the quiet-engine configurations.

Vibration analyses of the Task IV quiet-engine retrofit were performed for two airplane fuel configurations, 20 percent and 100 percent fuel, and two pylon stiffnesses. All the analyses were performed with the engines at the design center of gravity location. The aerodynamic theory used was a modified strip theory similar to that developed by Yates in Reference VI-3. It is essentially a modified version of Theodorsen's strip theory. Aerodynamic centers and lift coefficients were based upon results of wind-tunnel model tests. These were used instead of Theodorsen's theoretical values. The F and G circulation functions were not changed from Theodorsen's theoretical values.

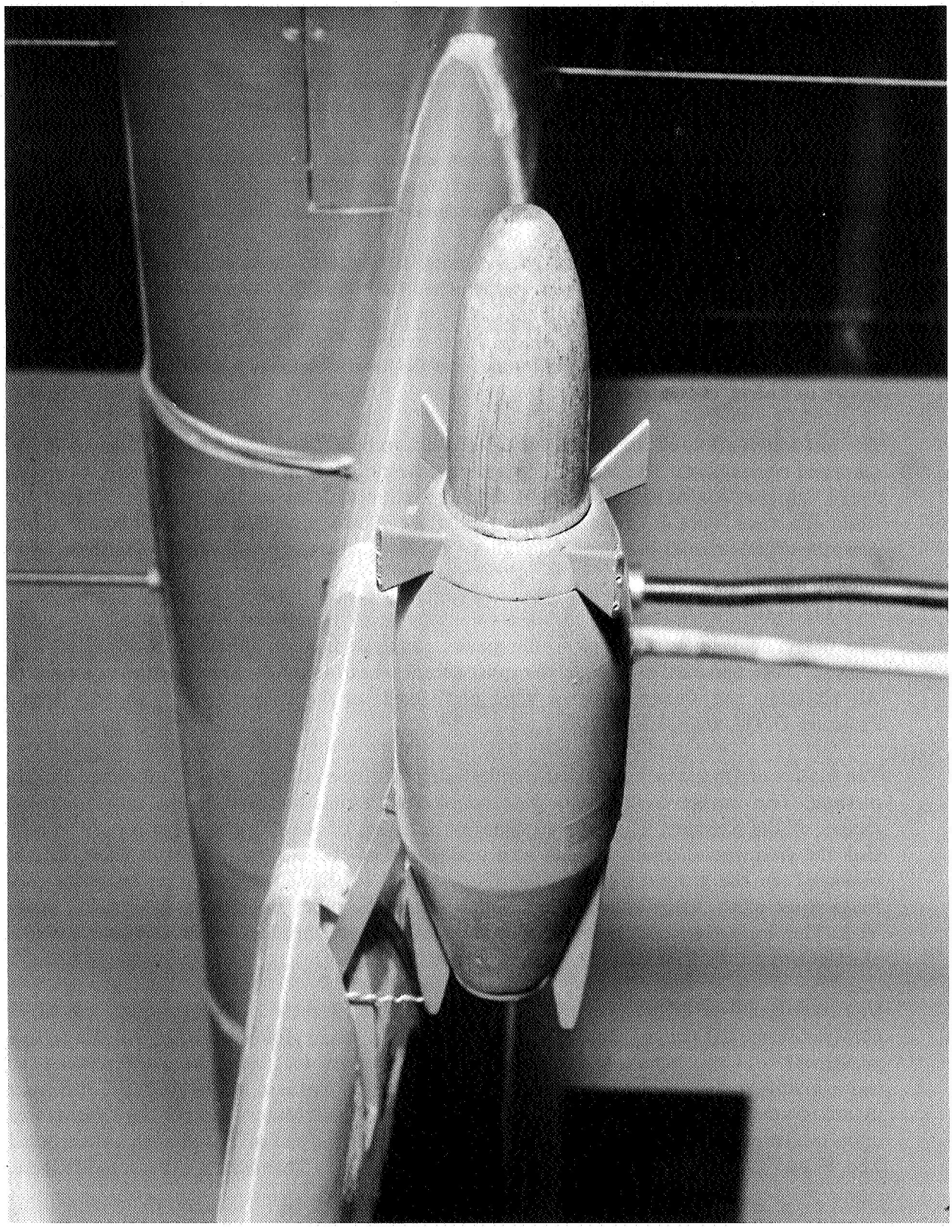

FIGURE VI-32. FLUTTER MODEL NACELLE CONFIGURATION (COWLING REMOVED)

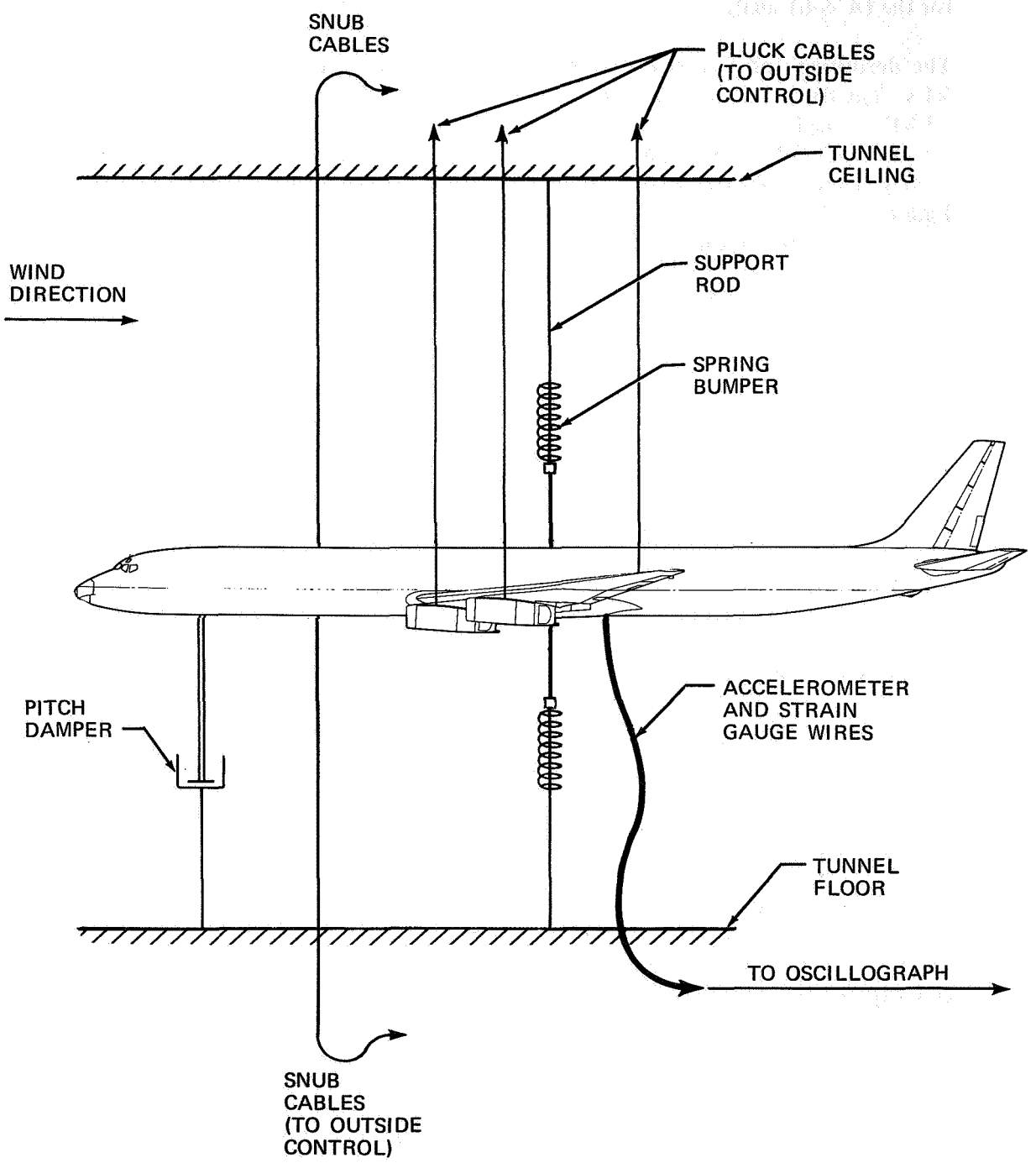

FIGURE VI-33. FLUTTER MODEL TEST SETUP

Basic Data

The basic structural data required for the flutter analyses are mass data, geometric data, and stiffness data. Except for the engines and pylons, these data were the same as all previous data used for the DC-8-61 analyses.

The definition and sign convention of the coordinates used in flutter analysis are given in Table VI-V. The discrete bay-stations used in representing the airplane are shown in Table VI-VI. Tables VI-VII through VI-XI give the weight and inertia data for the standard JT3D-3B engine as well as for the Task IV quiet engine. Both the design center of gravity case and aft-of-design center of gravity cases are shown. The coordinate system used to represent the elastic structure is defined in Figure VI-34. A comparison of analysis, flutter-model, and DC-8-61 engine center of gravity locations is shown in Figure VI-35.

Four fuel configurations were tested in the wind tunnel: Empty, 20 percent, 60 percent, and 100 percent fuel. Fuel loads of 100 percent and 20 percent were considered during the flutter analysis.

RESULTS

Flutter-Model Data

The structural data were scaled down, and the scaled values were simulated in the flutter model. Model vibration tests of the flutter model were performed during and after the wind-tunnel tests. These tests measured the important frequencies of the model and also located the wing node lines of these modes. Tables VI-XII and VI-XIII summarize the frequencies that were measured. Figures VI-36 through VI-40 show the important wing antisymmetric node lines for three airplane configurations, as follows:

1. Standard DC-8-61, 100 percent fuel.

2. Quiet engine, nacelles at design center of gravity, 100 percent fuel, inboard-pylon pitch frequency 3.04 Hz, and outboard-pylon pitch frequency 2.78 Hz.

3. Quiet engine, nacelles at design center of gravity, 100 percent fuel, inboard-pylon pitch frequency 4.59 Hz, and outboard-pylon pitch frequency 4.33 Hz.

The structural data also were used in the vibration analyses. The cantilevered variable pylon frequencies are given in Table VI-XIV. The output modes of the vibration analyses were used as inputs to the flutter program C4EB. The vibration results also can be compared to the flutter-model and airplane ground-vibration-test results. The following configurations were analyzed for both 20 percent fuel and 100 percent fuel:

1. Standard DC-8-61.

2. Quiet engine, nacelles at design center of gravity, inboard-engine pitch frequency 3.5 Hz, and outboard-engine pitch frequency 3.2 Hz.

3. Quiet engine, nacelles at design center of gravity, inboard-engine pitch frequency 4.5 Hz, and outboard-engine pitch frequency 4.0 Hz.

TABLE VI-V
DEFINITION OF LOCAL COORDINATES

(a) STRUCTURAL COORDINATES (TM)

SYMBOL	DESCRIPTION	POSITIVE SENSE*
h	VERTICAL TRANSLATION	DOWN
a	PITCH	NOSE UP
θ	ROLL	RIGHT WING TIP DOWN
f	FORE AND AFT TRANSLATION	FORWARD
ℓ	LATERAL TRANSLATION	OUTBOARD
ψ	YAW	NOSE LEFT, RIGHT WING TIP FORWARD
β	CONTROL-SURFACE ROTATION	TRAILING EDGE DOWN RELATIVE TO a
δ	TAB ROTATION	TRAILING EDGE DOWN RELATIVE TO β

(b) AERODYNAMIC COORDINATES (TD)

SYMBOL	DESCRIPTION	POSITIVE SENSE*
h	VERTICAL TRANSLATION	DOWN
a	PITCH	NOSE UP
β	CONTROL-SURFACE ROTATION	TRAILING EDGE DOWN RELATIVE TO a
δ	TAB ROTATION	TRAILING EDGE DOWN RELATIVE TO β

*FOR RIGHT SIDE OF AIRPLANE

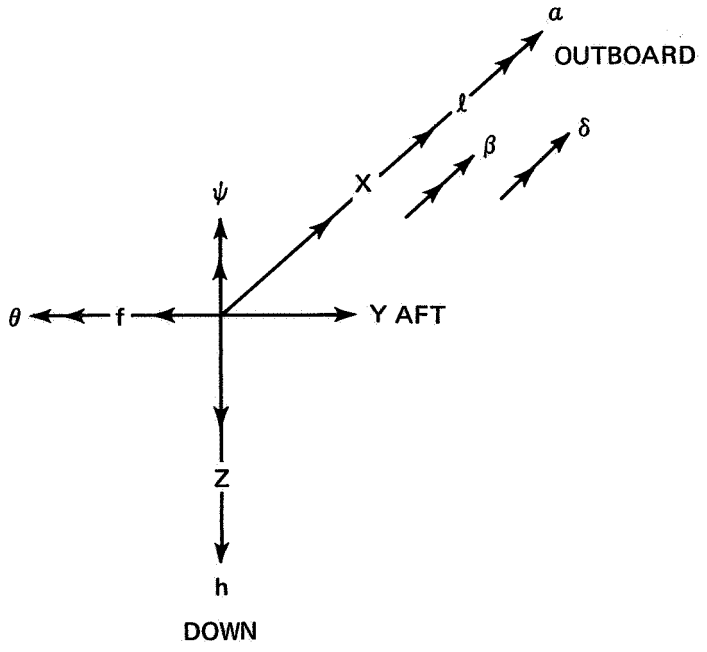

TABLE VI-VI
DC-8-61
BAY REFERENCE STATIONS IN FUSELAGE SYSTEM

COMPONENT	BAY	(OUTBOARD) X	Y	Z
VERTICAL STABILIZER	1	0	1804.227	–126.625
	2	↓	1830.852	–168.170
	3		1850.504	–198.835
	4		1879.368	–243.874
	5		1913.014	–296.374
	6	0	1941.614	–341.000
HORIZONTAL STABILIZER	7	69.606	1858.215	–59.274
	8	106.956	1883.278	–65.859
	9	146.004	1909.481	–72.744
	10	188.447	1937.962	–80.228
	11	227.494	1964.163	–87.113
	12	264.843	1989.226	–93.699
WING	13	103.592	783.098	43.012
	14	181.778	824.503	34.104
	15	288.601	881.074	21.933
	16	413.452	947.193	7.709
	17	491.122	988.326	–1.140
	18	540.174	1014.303	–6.729
	19	601.651	1046.860	–13.733
	20	664.759	1080.280	–20.923
	21	731.701	1115.731	–28.550
	22	808.833	1156.579	–37.338
INBOARD ENGINE	23	308.500	722.100	57.500
OUTBOARD ENGINE	24	534.500	860.300	42.400
FUSELAGE	25	0	–65.000	0
	26	↓	155.000	↓
	27		340.000	
	28		560.000	
	29		722.000	
	30		872.500	
	31		1080.000	
	32		1280.000	
	33		1460.000	
	34		1615.000	
	35	0	1842.000	0

TABLE VI-VII
STANDARD DC-8-61 ENGINE WEIGHT DATA JT3D-3B

INERTIAS ARE COMPUTED ABOUT THE ENGINE CENTER OF GRAVITY

ITEM	INBOARD ENGINE		OUTBOARD ENGINE	
	USC UNITS*	SI UNITS**	USC UNITS*	SI UNITS**
W	7477 LB	3392 KG	7385 LB	3350 KG
I_{xx} CG	16.36 x 10^6 LB-SQ IN.	0.00469 x 10^6 KG-SQ M	16.15 x 10^6 LB-SQ IN.	0.00468 x 10^6 KG-SQ M
I_{yy} CG	1.670 x 10^6 LB-SQ IN.	0.000484 x 10^6 KG-SQ M	1.679 x 10^6 LB-SQ IN.	0.000487 x 10^6 KG-SQ M
I_{zz} CG	14.77 x 10^6 LB-SQ IN.	0.00428 x 10^6 KG-SQ M	14.59 x 10^6 LB-SQ IN.	0.00423 x 10^6 KG-SQ M
I_{xy} CG	0.0	0.0	0.0	0.0
I_{yz} CG	0.160 x 10^6 LB-SQ IN.	0.0000464 x 10^6 KG-SQ M	0.158 x 10^6 LB-SQ IN.	0.0000458 x 10^6 KG-SQ M
I_{zx} CG	0.0	0.0	0.0	0.0

* UNITED STATES CUSTOMARY UNITS
**STANDARD INTERNATIONAL UNITS

TABLE VI-VIII
STANDARD DC-8-61 ENGINE MASS DATA JT3D-3B

DATA INCLUDE PYLONS. INERTIAS ARE ABOUT THE WING ELASTIC AXIS IN THE FUSELAGE COORDINATE SYSTEM

ITEM	INBOARD ENGINE VALUE		OUTBOARD ENGINE VALUE	
	USC UNITS*	SI UNITS**	USC UNITS*	SI UNITS**
W	7477 LB	3392 KG	7385 LB	3350 KG
Δx	0.0 IN.	0.0 M	0.0 IN.	0.0 M
Δy	−169.13 IN.	−4.295 M	−150.47 IN.	−3.821 M
Δz	−37.80 IN.	−0.960 M	−48.50 IN.	−1.231 M
$W\Delta x$	0.0 LB-IN.	0.0 KG-M	0.0 LB-IN.	0.0 KG-M
$W\Delta y$	−1.265 x 10^6 LB-IN.	0.0145 x 10^6 KG-M	1.111 x 10^6 LB-IN.	0.0128 x 10^6 KG-M
$W\Delta z$	−0.283 x 10^6 LB-IN.	0.00326 x 10^6 KG-M	0.358 x 10^6 LB-IN.	0.0041 x 10^6 KG-M
I_{xx}	2.410 x 10^8 LB-SQ IN.	0.000699 x 10^6 KG-SQ M	2.008 x 10^8 LB-SQ IN.	0.000595 x 10^8 KG-SQ M
I_{yy}	0.1235 x 10^8 LB-SQ IN.	0.0000358 x 10^8 KG-SQ M	0.9105 x 10^8 LB-SQ IN.	0.000264 x 10^8 KG-SQ M
I_{zz}	1.820 x 10^8 LB-SQ IN.	0.000528 x 10^8 KG-SQ M	1.818 x 10^8 LB-SQ IN.	0.000527 x 10^8 KG-SQ M
I_{xy}	0.0 LB-SQ IN.	0.0 KG-SQ M	0.0 LB-SQ IN.	0.0 KG-SQ M
I_{yz}	0.480 x 10^8 LB-SQ IN.	0.000139 x 10^8 KG-SQ M	0.541 x 10^8 LB-SQ IN.	0.000157 x 10^8 KG-SQ M
I_{zx}	0.0 LB-SQ IN.	0.0 KG-SQ M	0.0 LB-SQ IN.	0.0 KG-SQ M

*UNITED STATES CUSTOMARY UNITS
**STANDARD INTERNATIONAL UNITS

TABLE VI-IX

QUIET ENGINE WEIGHT DATA

INERTIAS ARE COMPUTED ABOUT THE ENGINE CENTER OF GRAVITY

	USC UNITS*	SI UNITS**
ENGINE WEIGHT	8800 LB	3992 KG
I_{xx} CG	26.7 x 10^6 LB-SQ IN.	0.00775 x 10^6 KG-SQ M
I_{yy} CG	3.48 x 10^6 LB-SQ IN.	0.00101 x 10^6 KG-SQ M
I_{zz} CG	26.2 x 10^6 LB-SQ IN.	0.00760 x 10^6 KG-SQ M
I_{xy} CG	−0.129 x 10^6 LB-SQ IN.	−0.0000374 x 10^6 KG-SQ M
I_{yz} CG	0.384 x 10^6 LB-SQ IN.	0.000111 x 10^6 KG-SQ M
I_{zx} CG	−0.113 x 10^6 LB-SQ IN.	0.0000328 x 10^6 KG-SQ M
PYLON WEIGHT	1000 LB	453.6 KG

* UNITED STATES CUSTOMARY UNITS
**STANDARD INTERNATIONAL UNITS

TABLE VI-X

QUIET ENGINE MASS DATA ENGINES AT DESIGN CG

DATA INCLUDE PYLONS. INERTIAS ARE ABOUT THE WING ELASTIC AXIS IN THE FUSELAGE COORDINATE SYSTEM

ITEM	INBOARD ENGINE VALUE		OUTBOARD ENGINE VALUE	
	USC UNITS*	SI UNITS**	USC UNITS*	SI UNITS**
W	9800 LB	4445 KG	9800 LB	4445 KG
Δx	0.0 IN.	0.0 M	0.0 IN.	0.0 M
Δy	−198.33 IN.	−5.037 M	−185.20 IN.	−4.704 M
Δz	−46.51 IN.	−1.181 M	−44.43 IN.	−1.128 M
$W\Delta x$	0.0 LB-IN.	0.0 KG-M	0.0 LB-IN.	0.0 KG-M
$W\Delta y$	−1.94 x 10^6 LB-IN.	0.0223 x 10^6 KG-M	−1.82 x 10^6 LB-IN.	0.0209 x 10^6 KG-M
$W\Delta z$	0.456 x 10^6 LB-IN.	0.00525 x 10^6 KG-M	−0.435 x 10^6 LB-IN.	−0.00501 x 10^6 KG-M
I_{xx}	4.45 x 10^8 LB-SQ IN.	0.00129 x 10^8 KG-SQ M	3.92 x 10^8 LB-SQ IN.	0.00113 x 10^8 KG-SQ M
I_{yy}	0.256 x 10^8 LB-SQ IN.	0.0000743 x 10^8 KG-SQ M	0.241 x 10^8 LB-SQ IN.	0.0000699 x 10^8 KG-SQ M
I_{zz}	4.23 x 10^8 LB-SQ IN.	0.00122 x 10^8 KG-SQ M	3.71 x 10^8 LB-SQ IN.	0.00107 x 10^8 KG-SQ M
I_{xy}	−0.129 x 10^6 LB-SQ IN.	−0.0000374 x 10^6 KG-SQ M	−0.129 x 10^6 LB-SQ IN.	0.0000374 x 10^6 KG-SQ M
I_{yz}	0.940 x 10^8 LB-SQ IN.	0.000272 x 10^8 KG-SQ M	0.842 x 10^8 LB-SQ IN.	0.000244 x 10^8 KG-SQ M
I_{zx}	−0.113 x 10^6 LB-SQ IN.	0.0000328 x 10^6 KG-SQ M	−0.129 x 10^6 LB-SQ IN.	0.0000374 x 10^6 KG-SQ M

* UNITED STATES CUSTOMARY UNITS
**STANDARD INTERNATIONAL UNITS

TABLE VI-XI
QUIET ENGINE MASS DATA ENGINES AT AFT CG

DATA INCLUDE PYLONS. INERTIAS ARE ABOUT THE WING ELASTIC AXIS IN THE FUSELAGE COORDINATE SYSTEM

ITEM	INBOARD ENGINE VALUE		OUTBOARD ENGINE VALUE	
	USC UNITS*	SI UNITS**	USC UNITS*	SI UNITS**
W	9800 LB	4445 KG	9800 LB	4445 KG
Δx	0.0 IN.	0.0 M	0.0 IN.	0.0 M
Δy	−168.66 IN.	−4.283 M	−142.55 IN.	−3.620 M
Δz	−49.38 IN.	−1.254 M	−51.38 IN.	−1.305 M
$W\Delta x$	0.0 LB-IN.	0.0 KG-M	0.0 LB-IN.	0.0 KG-M
$W\Delta y$	-1.65×10^6 LB-IN.	-0.0190×10^6 KG-M	-1.40×10^6 LB-IN.	-0.0161×10^6 KG-M
$W\Delta z$	-0.484×10^6 LB-IN.	-0.00557×10^6 KG-M	-0.504×10^6 LB-IN.	-0.00580×10^6 KG-M
I_{xx}	3.38×10^8 LB-SQ IN.	0.000981×10^8 KG-SQ M	2.58×10^8 LB-SQ IN.	0.000748×10^8 KG-SQ M
I_{yy}	0.285×10^8 LB-SQ IN.	0.0000827×10^8 KG-SQ M	0.307×10^8 LB-SQ IN.	0.0000891×10^8 KG-SQ M
I_{zz}	3.12×10^8 LB-SQ IN.	0.000905×10^8 KG-SQ M	2.30×10^8 LB-SQ IN.	0.000667×10^8 KG-SQ M
I_{xy}	-0.129×10^8 LB-SQ IN.	0.0000374×10^8 KG-SQ M	-0.129×10^8 LB-SQ IN.	0.0000374×10^8 KG-SQ M
I_{yz}	0.849×10^8 LB-SQ IN.	0.000246×10^8 KG-SQ M	0.747×10^8 LB-SQ IN.	0.000216×10^8 KG-SQ M
I_{zx}	-0.113×10^8 LB-SQ IN.	0.0000328×10^8 KG-SQ M	0.113×10^8 LB-SQ IN.	0.0000328×10^8 KG-SQ M

*UNITED STATES CUSTOMARY UNITS
**STANDARD INTERNATIONAL UNITS

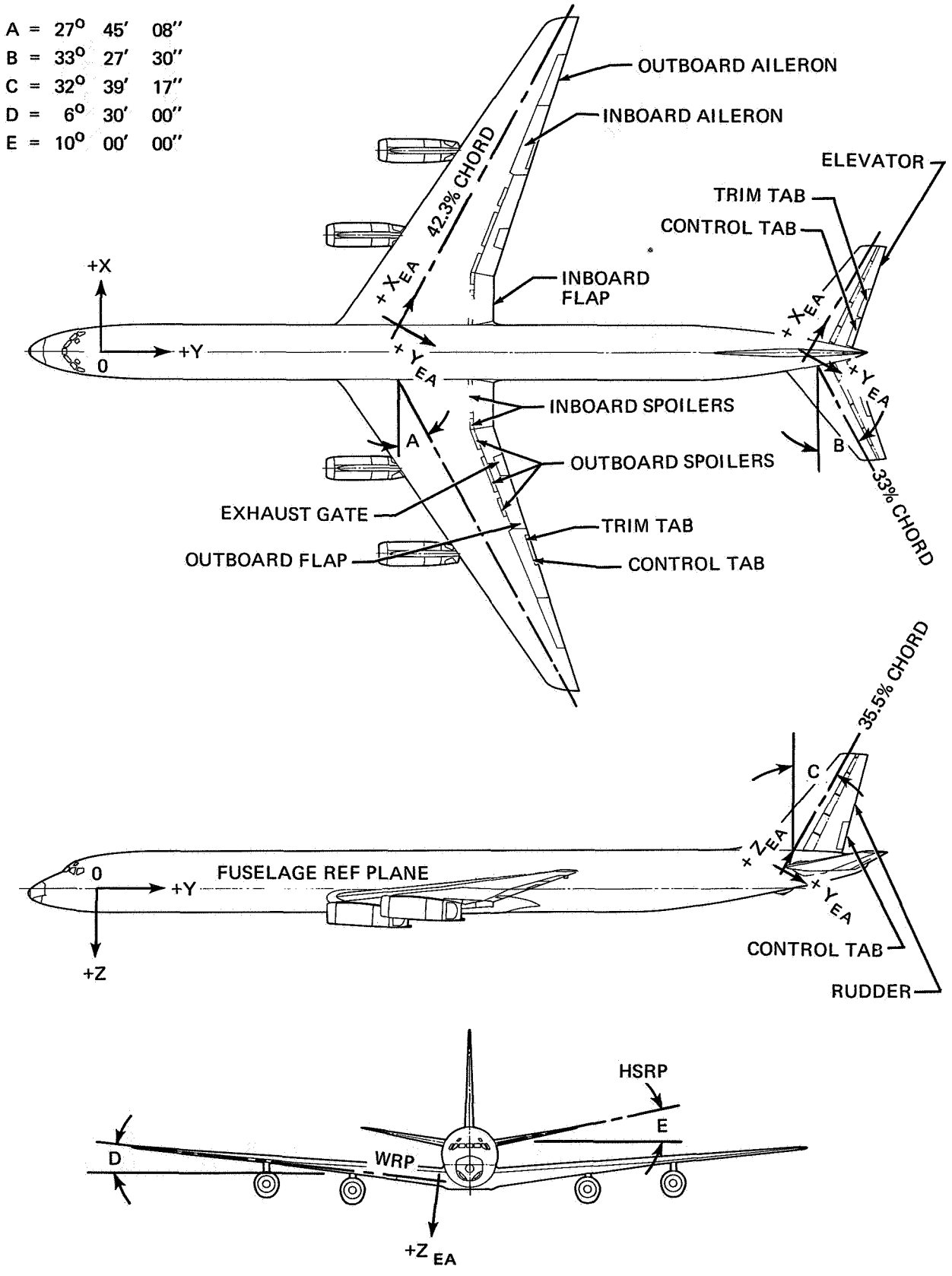

FIGURE VI-34. DC-8-61 ELASTIC AXIS REPRESENTATION

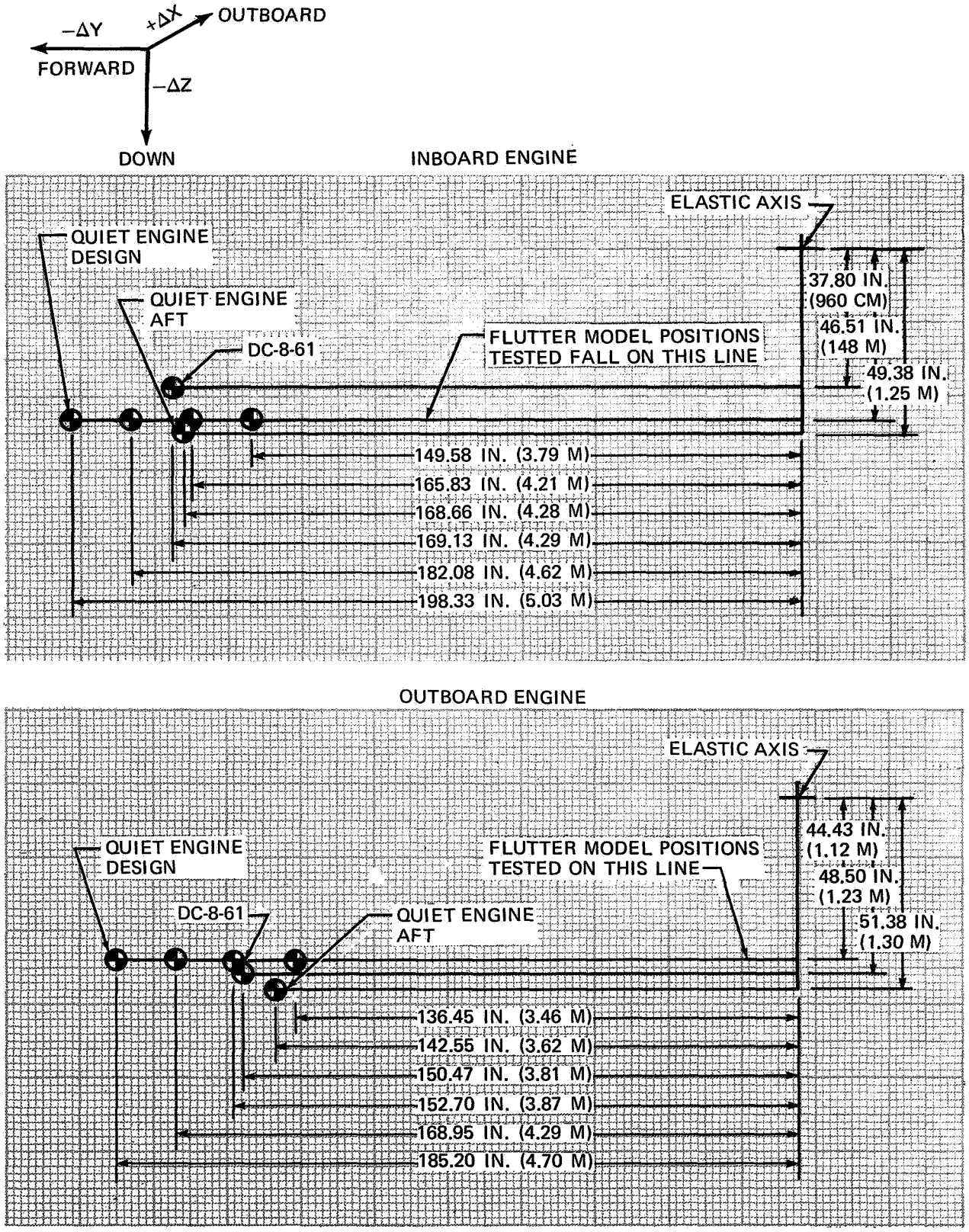

FIGURE VI-35. NACELLE-PYLON CENTER OF GRAVITY LOCATIONS RELATIVE TO THE WING ELASTIC AXIS

TABLE VI-XII
FLUTTER MODEL CANTILEVERED NACELLE PYLON
FREQUENCIES ABOUT THE WING ELASTIC AXIS

NACELLE POSITION	INBOARD PYLON PITCH FREQUENCY (Hz)	INBOARD PYLON YAW FREQUENCY (Hz)	OUTBOARD PYLON PITCH FREQUENCY (Hz)	OUTBOARD PYLON YAW FREQUENCY (Hz)
DESIGN	3.04	2.23	2.78	2.21
	3.66	2.22	3.47	2.20
	4.59	2.25	4.33	2.20
			3.05	2.20
16.25 IN. (41.27 CM) AFT OF DESIGN	3.32	2.56	3.05	2.58
	3.97	2.56	3.79	2.57
	4.93	2.58	4.69	2.57
			3.35	2.57
32.5 IN. (82.5 CM) AFT OF DESIGN	3.64	2.87	3.36	2.90
	4.41	2.87	4.14	2.90
	5.21	2.91	5.00	2.90
			3.69	2.90
48.75 IN. (123.82 CM) AFT OF DESIGN	4.00	3.20	3.71	3.23
	4.72	3.22	4.54	3.24
	5.46	3.27	5.27	3.24
			4.07	3.24

TABLE VI-XIII
FLUTTER MODEL GROUND VIBRATION TEST SUMMARY ANTI-SYMMETRIC MODES

MODE DESCRIPTION	STANDARD DC-8-61, 100% FUEL	QUIET ENGINE *IBf_a = 3.04 **OBf_a = 2.78 100% FUEL	QUIET ENGINE IBf_a = 4.59 OBf_a = 4.33 100% FUEL	QUIET ENGINE IBf_a = 3.04 OBf_a = 2.78 0% FUEL
FIRST WING BENDING	2.18 Hz	1.90 Hz	2.00 Hz	2.22 Hz
ENGINES YAWING OUT OF PHASE	2.54 Hz	2.08 Hz	2.16 Hz	2.06 Hz
ENGINES YAWING IN PHASE	2.80 Hz	2.14 Hz	2.66 Hz	2.64 Hz
OUTBOARD-ENGINE PITCH	3.32 Hz	2.55 Hz	2.92 Hz	3.26 Hz
INBOARD-ENGINE PITCH	4.52 Hz	3.32 Hz	3.72 Hz	4.43 Hz
AFT-FUSELAGE LATERAL BENDING	–	2.34 Hz	2.33 Hz	2.72 Hz

*IBf_a INBOARD PYLON PITCH FREQUENCY
**OBf_a OUTBOARD PYLON PITCH FREQUENCY

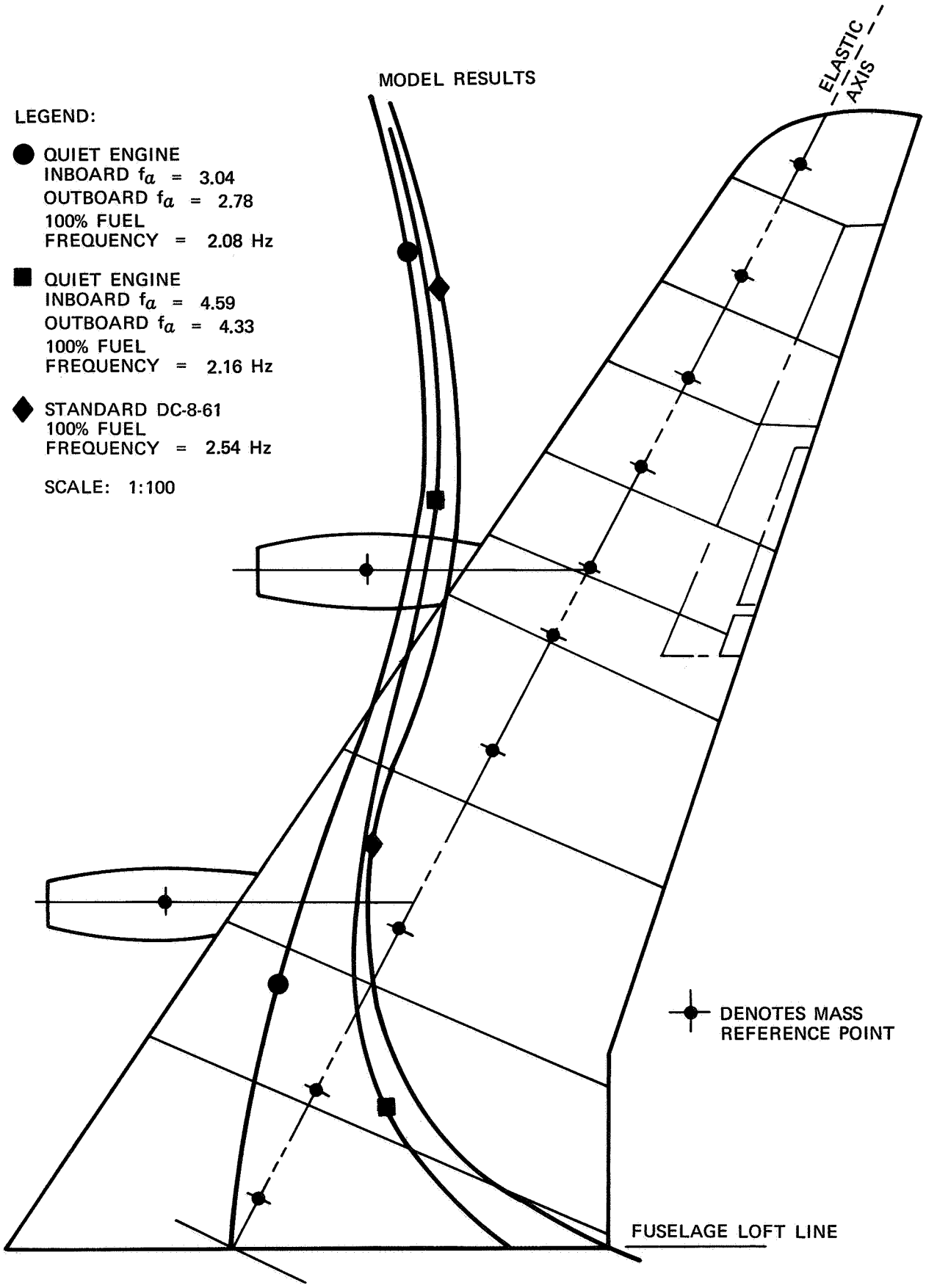

FIGURE VI-36. NODE LINES FOR ENGINES YAWING OUT OF PHASE

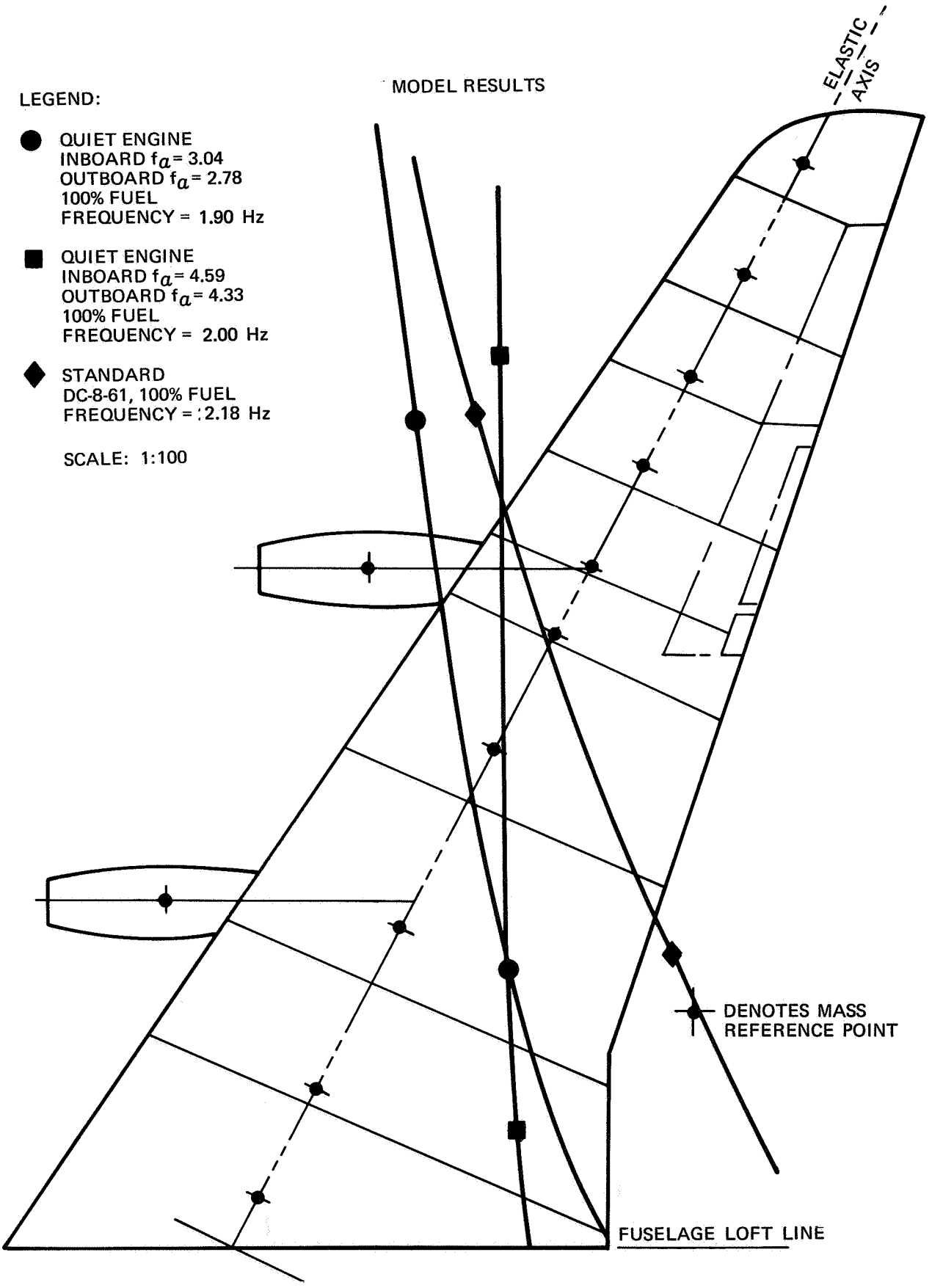

FIGURE VI-37. NODE LINES FOR FIRST WING-BENDING

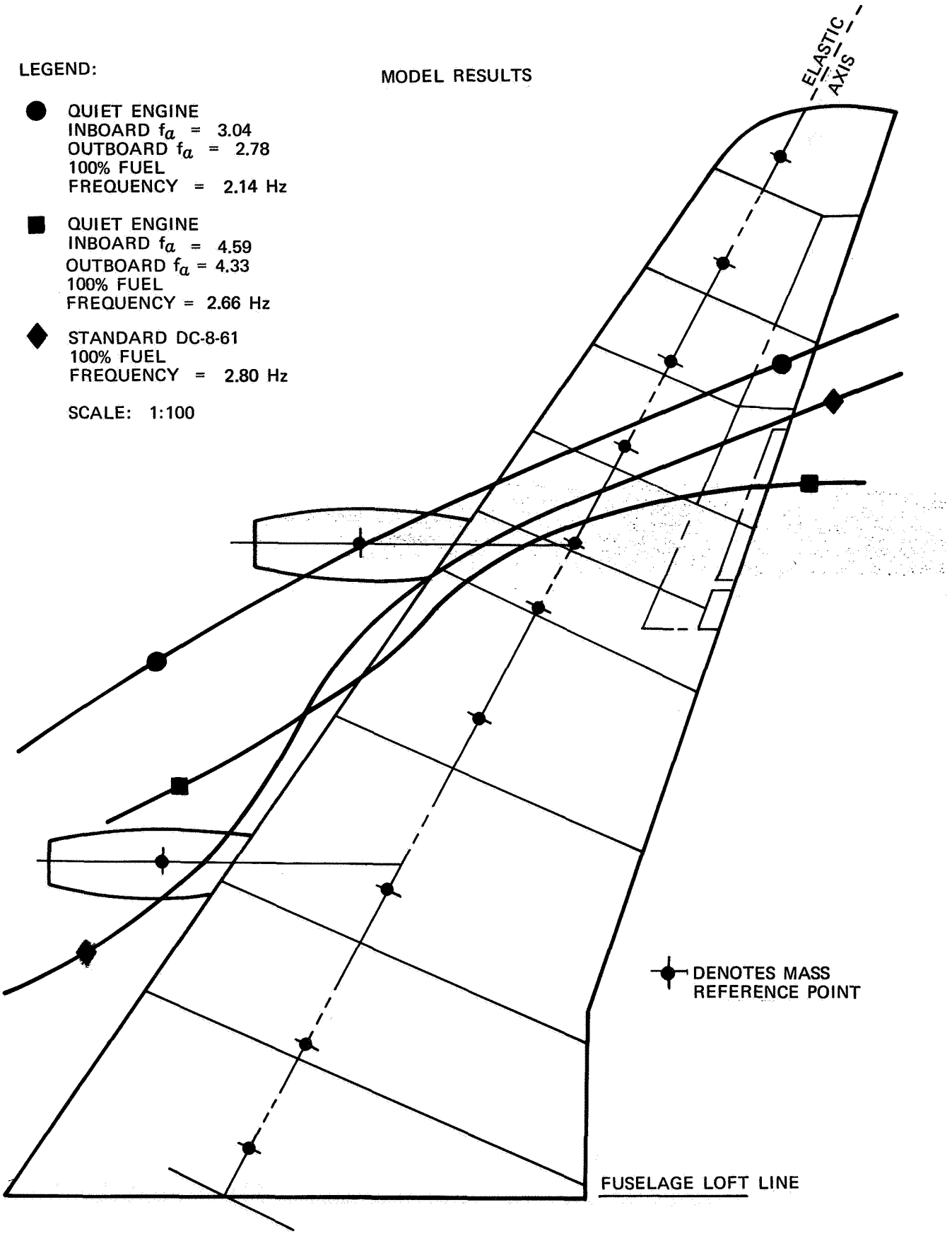

FIGURE VI-38. NODE LINES FOR ENGINES YAWING IN PHASE

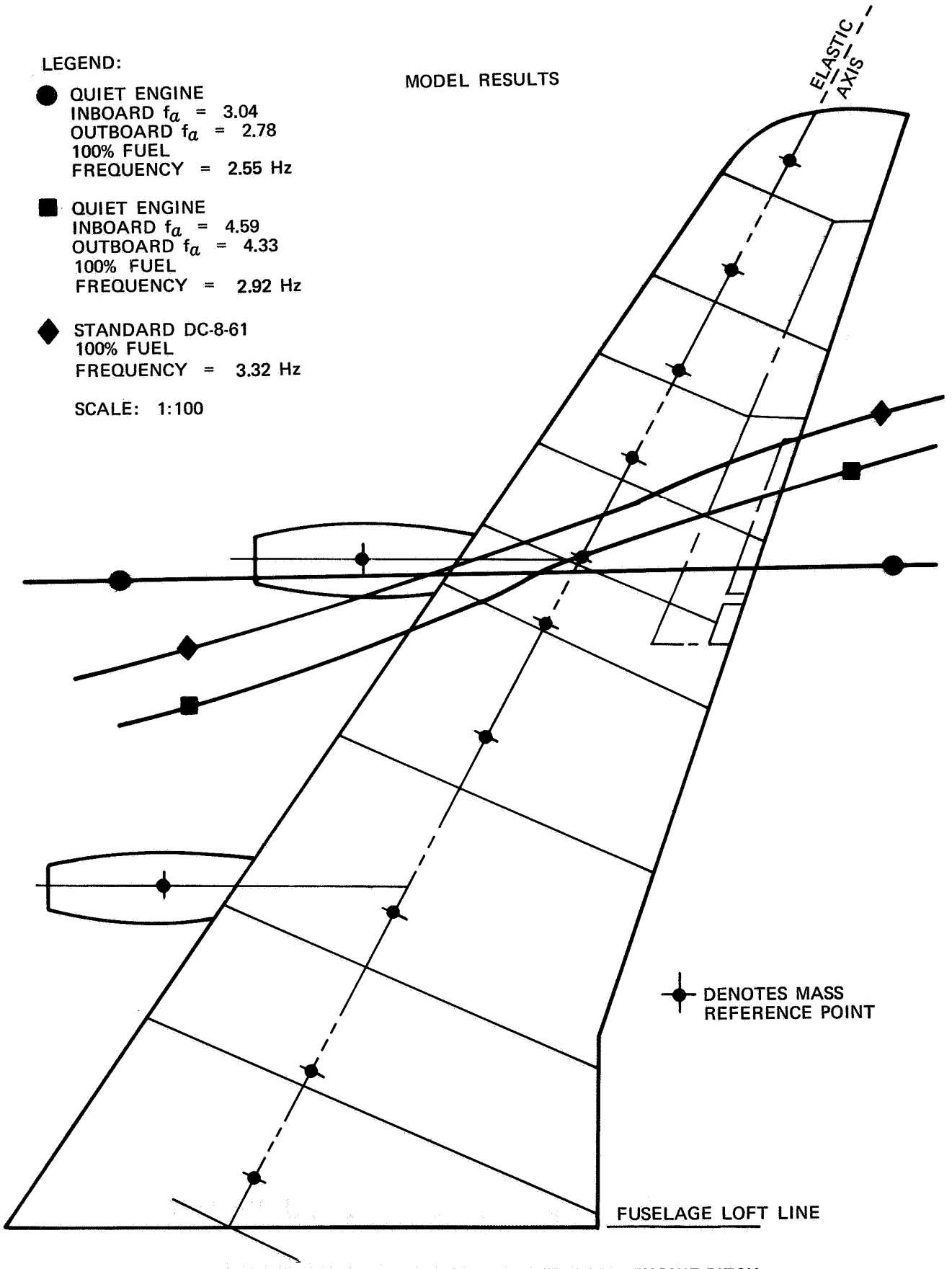

FIGURE VI-39. NODE LINES FOR OUTBOARD ENGINE PITCH

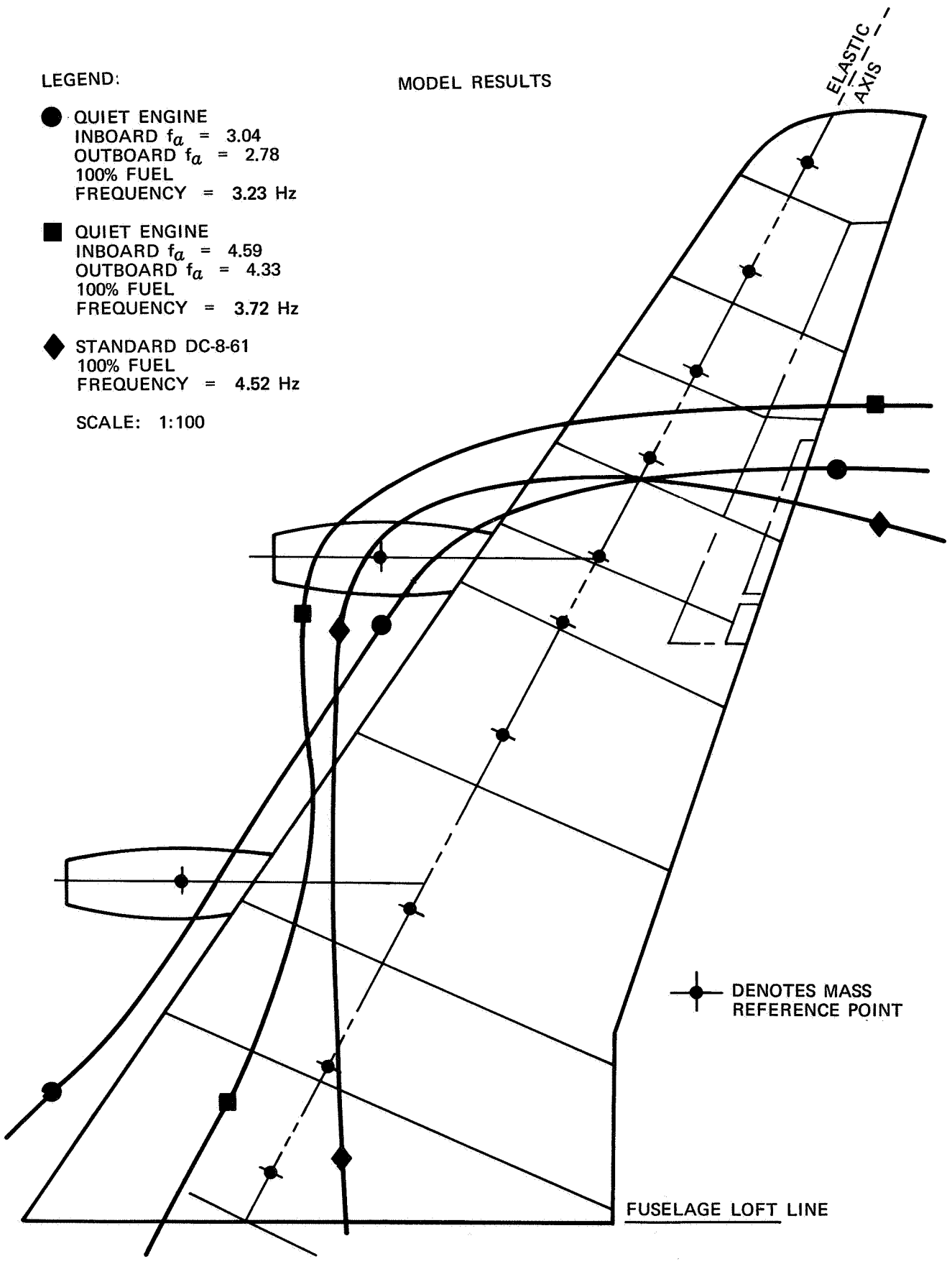

FIGURE VI-40. NODE LINES FOR INBOARD ENGINE PITCH

Frequencies, mode shapes, and mode lines were computed for these configurations. Frequency summaries are given in Tables VI-XV and VI-XVI. Computed wing node lines are shown for the 100 percent fuel configurations in Figures VI-41 through VI-45.

Flutter-Model Results

The results of the flutter-model tests are shown by plots in Figures VI-46 through VI-50. These plots show the effects of fuel quantity, engine-pod center of gravity position, nacelle-engine cantilever pitch frequency, and engine-cowling aerodynamics on the flutter speed (airplane velocity at which flutter develops).

TABLE VI-XIV
CANTILEVERED NACELLE-PYLON FREQUENCIES ABOUT THE WING ELASTIC AXIS

DESCRIPTION		PITCH FREQUENCY (Hz)	YAW FREQUENCY (Hz)	ROLL FREQUENCY (Hz)
STANDARD	INBOARD	7.00	2.88	11.00
DC-8-61	OUTBOARD	6.50	2.57	9.50
QUIET ENGINE	INBOARD	3.50	2.20	7.16
SOFT	OUTBOARD	3.20	2.20	5.77
QUIET ENGINE	INBOARD	4.50	2.20	7.16
STIFF	OUTBOARD	4.00	2.20	5.77

TABLE VI-XV
VIBRATION ANALYSIS MODE SUMMARY ANTISYMMETRIC MODES – 20% FUEL

	FREQUENCY (Hz)		
MODE DESCRIPTION	STANDARD DC-8-61	QUIET ENGINE IB f_a = 3.5 OB f_a = 3.2	QUIET ENGINE IB f_a = 4.5 OB f_a = 4.0
FIRST WING BENDING	2.59	2.12	2.37
ENGINES YAWING IN PHASE	2.44	2.31	2.25
ENGINES YAWING OUT OF PHASE	2.86	2.23	2.13
OUTBOARD-ENGINE PITCH	3.14	2.64	2.70
STABILIZER WING BENDING	3.78	3.75	3.79
FIRST HORIZONTAL-STAB. BENDING	3.99	3.94	3.97
INBOARD-ENGINE PITCH	4.32	2.84	3.13

TABLE VI-XVI
VIBRATION ANALYSIS MODE SUMMARY ANTISYMMETRIC MODES – 100% FUEL

	FREQUENCY (Hz)		
MODE DESCRIPTION	STANDARD DC-8-61	QUIET ENGINE IB f_a = 3.5 OB f_a = 3.2	QUIET ENGINE IB f_a = 4.5 OB f_a = 4.0
FIRST WING BENDING	2.06	1.82	1.86
ENGINES YAWING OUT OF PHASE	2.65	2.17	2.18
ENGINES YAWING IN PHASE	2.88	2.25	2.25
OUTBOARD-ENGINE PITCH	3.36	2.58	2.75
INBOARD-ENGINE PITCH	4.75	3.21	3.66
AFT-FUSELAGE LATERAL BENDING	2.36	2.38	2.40

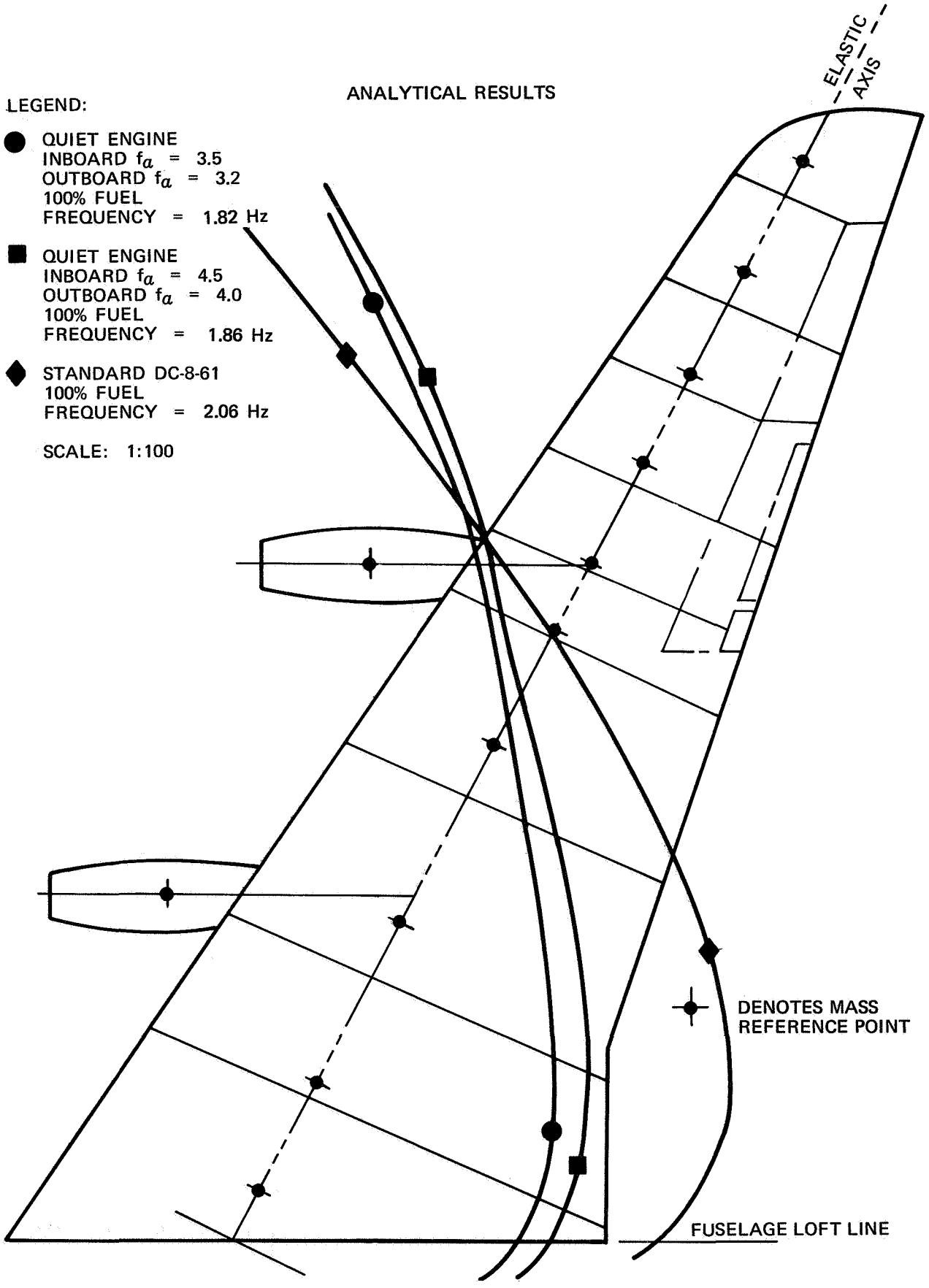

FIGURE VI-41. NODE LINES FOR FIRST WING-BENDING

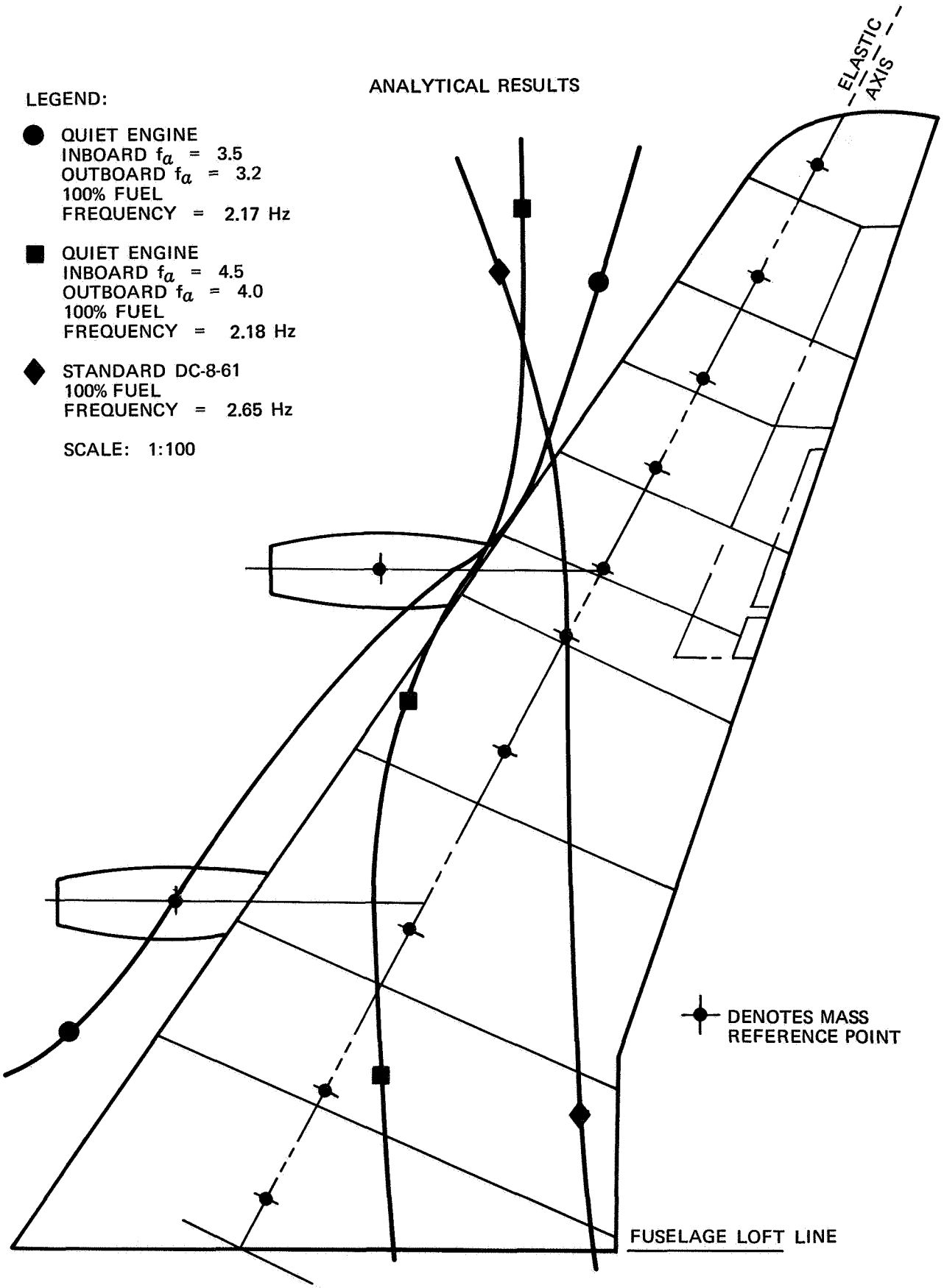

FIGURE VI-42. NODE LINES FOR ENGINES YAWING OUT OF PHASE

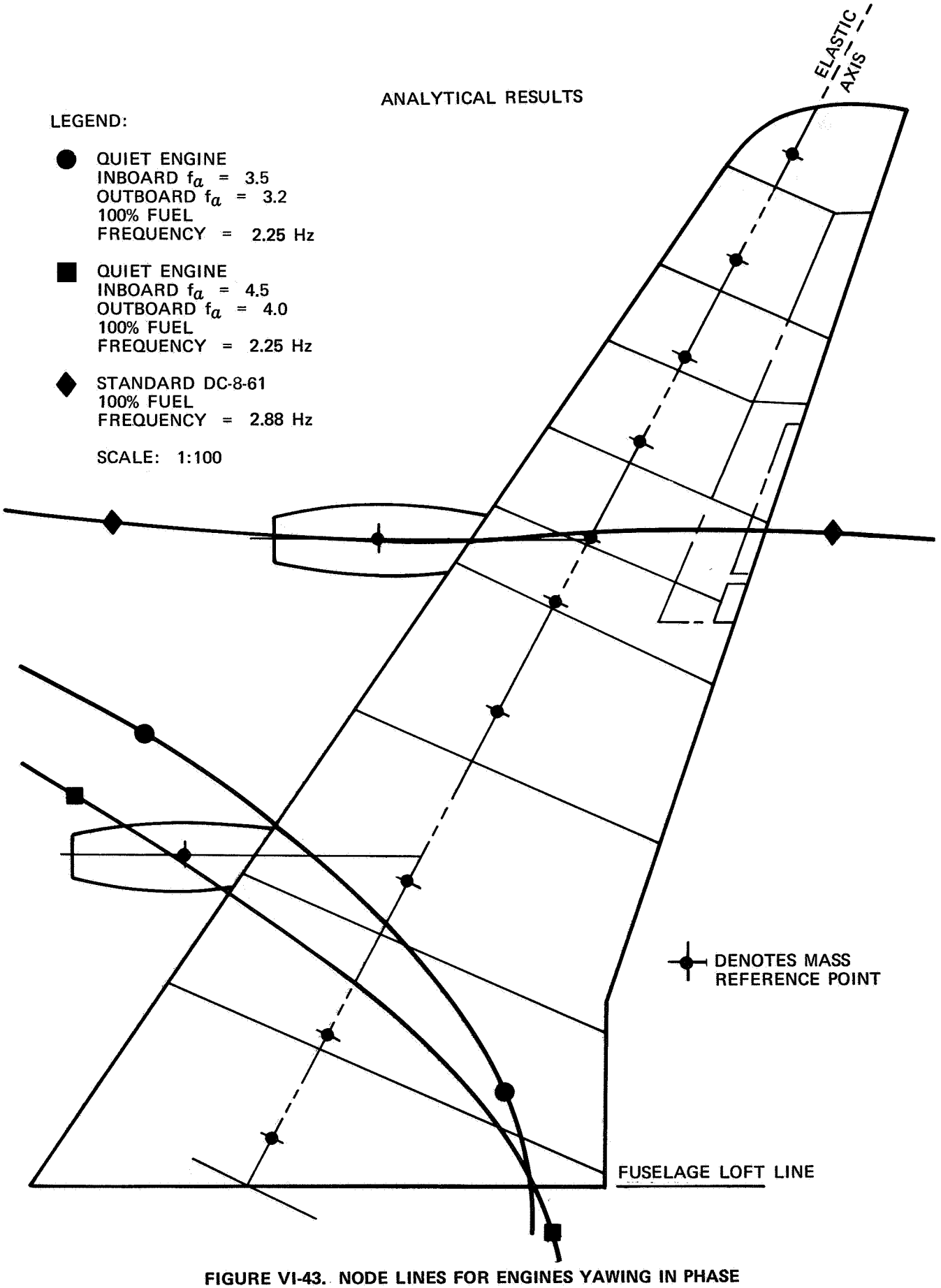

FIGURE VI-43. NODE LINES FOR ENGINES YAWING IN PHASE

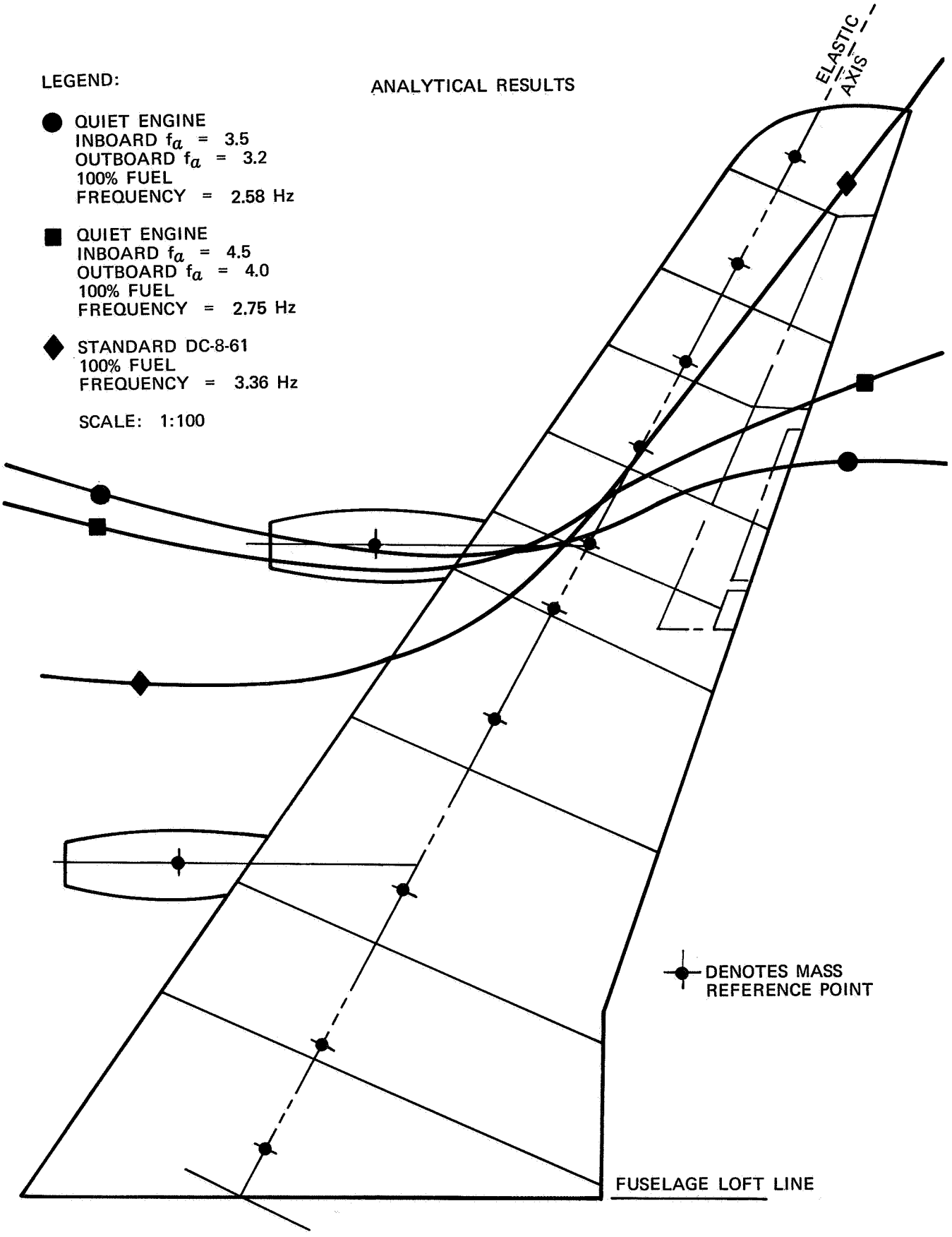

FIGURE VI-44. NODE LINES FOR OUTBOARD ENGINE PITCH

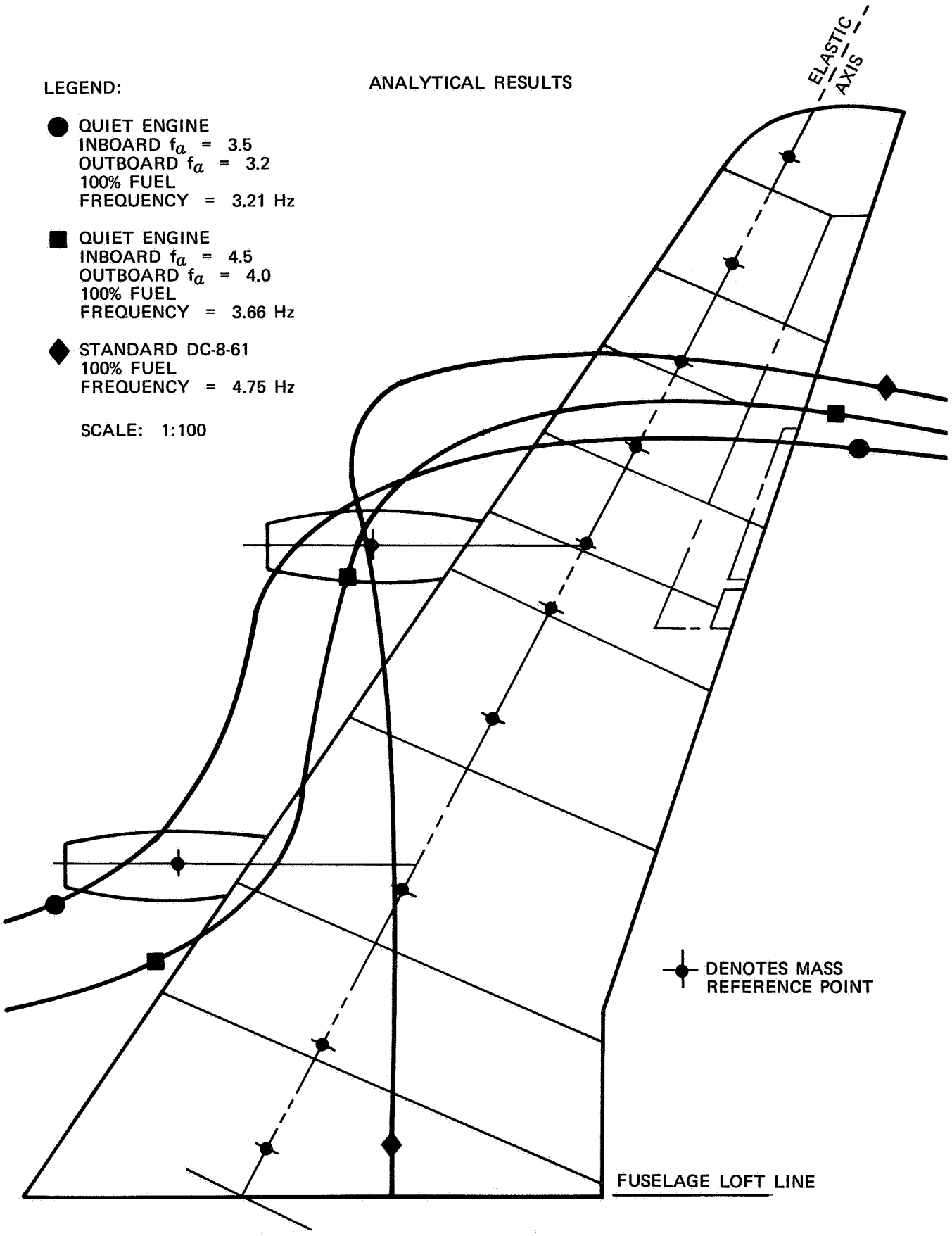

FIGURE VI-45. NODE LINES FOR INBOARD ENGINE PITCH

TEST DATA

LEGEND:

○ = STANDARD DC-8-61

□ = QUIET ENGINE, DESIGN CG
INBOARD PYLON 3.04 Hz, OUTBOARD PYLON 2.78 Hz

◇ = QUIET ENGINE, DESIGN CG
INBOARD PYLON 3.04 Hz, OUTBOARD PYLON 3.47 Hz

△ = QUIET ENGINE, DESIGN CG
INBOARD PYLON 3.04 Hz, OUTBOARD PYLON 4.33 Hz

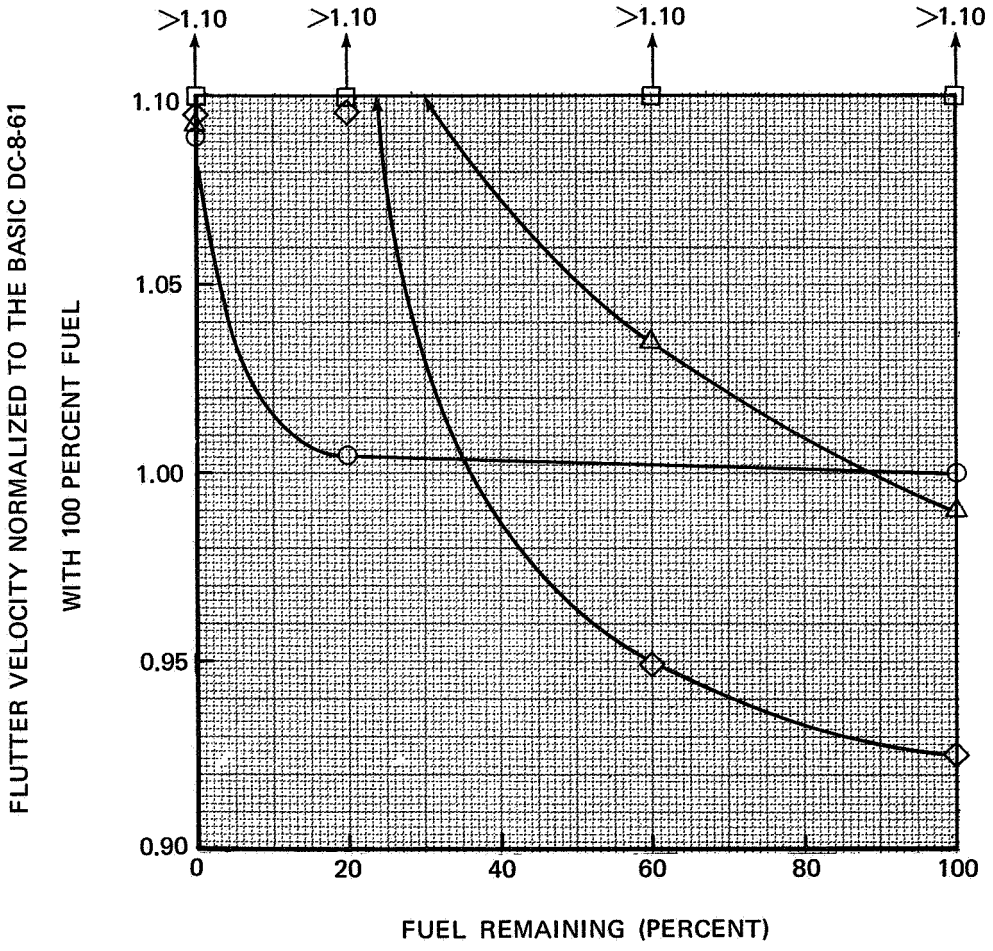

FIGURE VI-46. EFFECT OF FUEL LOAD ON FLUTTER VELOCITY

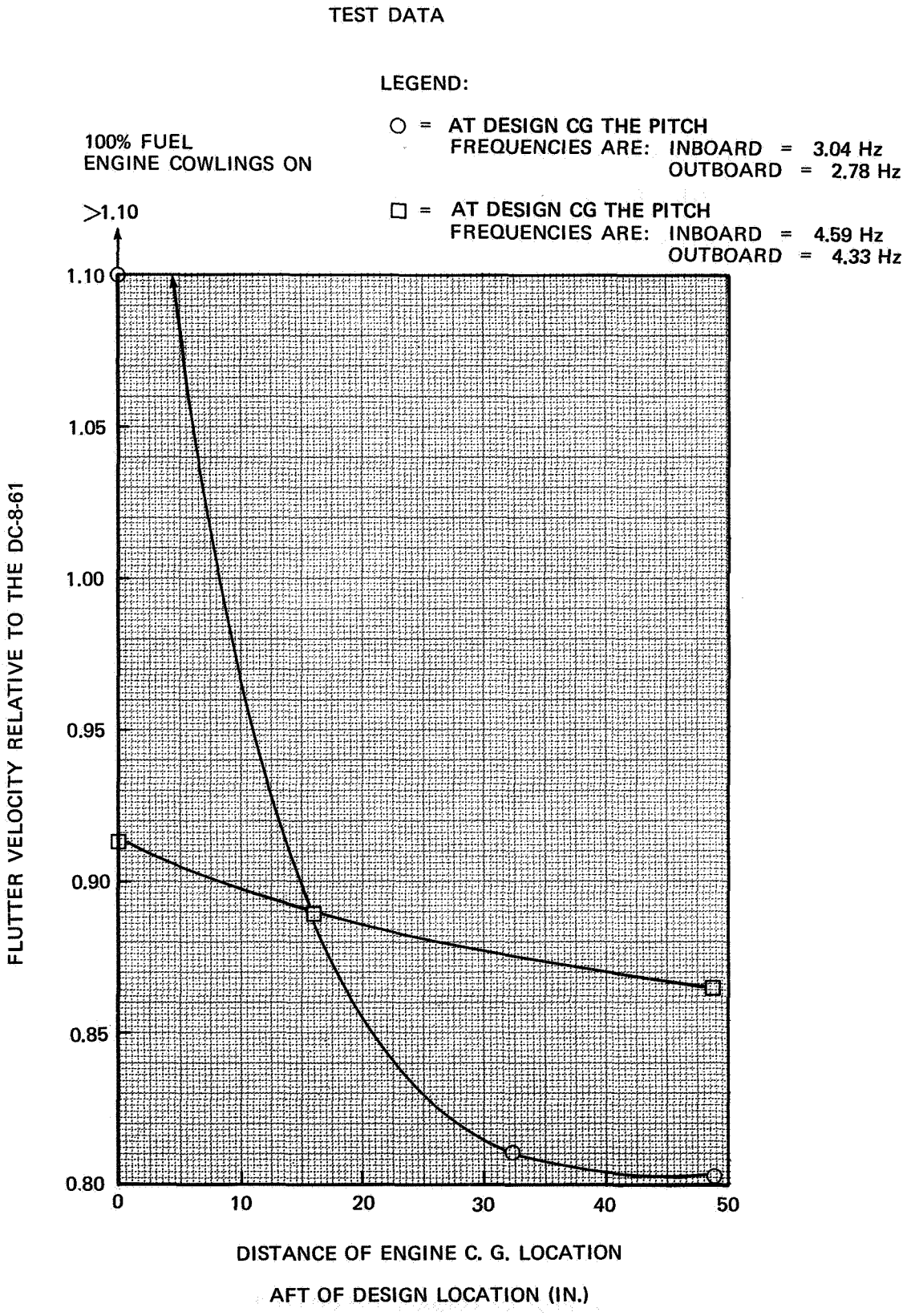

FIGURE VI-47. EFFECT OF CG LOCATION ON FLUTTER VELOCITY

TEST DATA

LEGEND:

△ = OUTBOARD PYLON PITCH FREQUENCY = 2.78 Hz

□ = OUTBOARD PYLON PITCH FREQUENCY = 3.47 Hz

○ = OUTBOARD PYLON PITCH FREQUENCY = 4.33 Hz

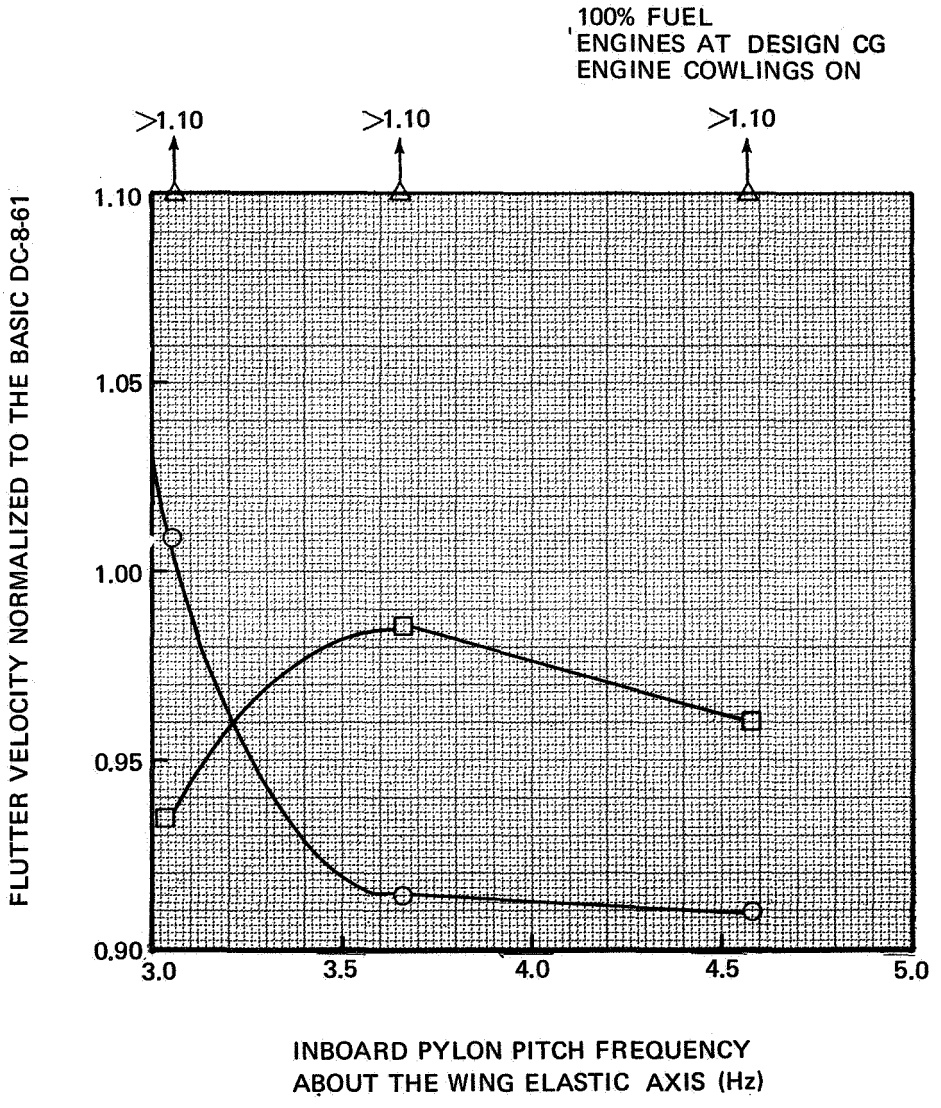

FIGURE VI-48. EFFECT OF INBOARD PYLON PITCH FREQUENCY ON FLUTTER VELOCITY

TEST DATA

LEGEND:

○ = INBOARD PYLON PITCH FREQUENCY = 3.04 Hz

□ = INBOARD PYLON PITCH FREQUENCY = 3.66 Hz

△ = INBOARD PYLON PITCH FREQUENCY = 4.59 Hz

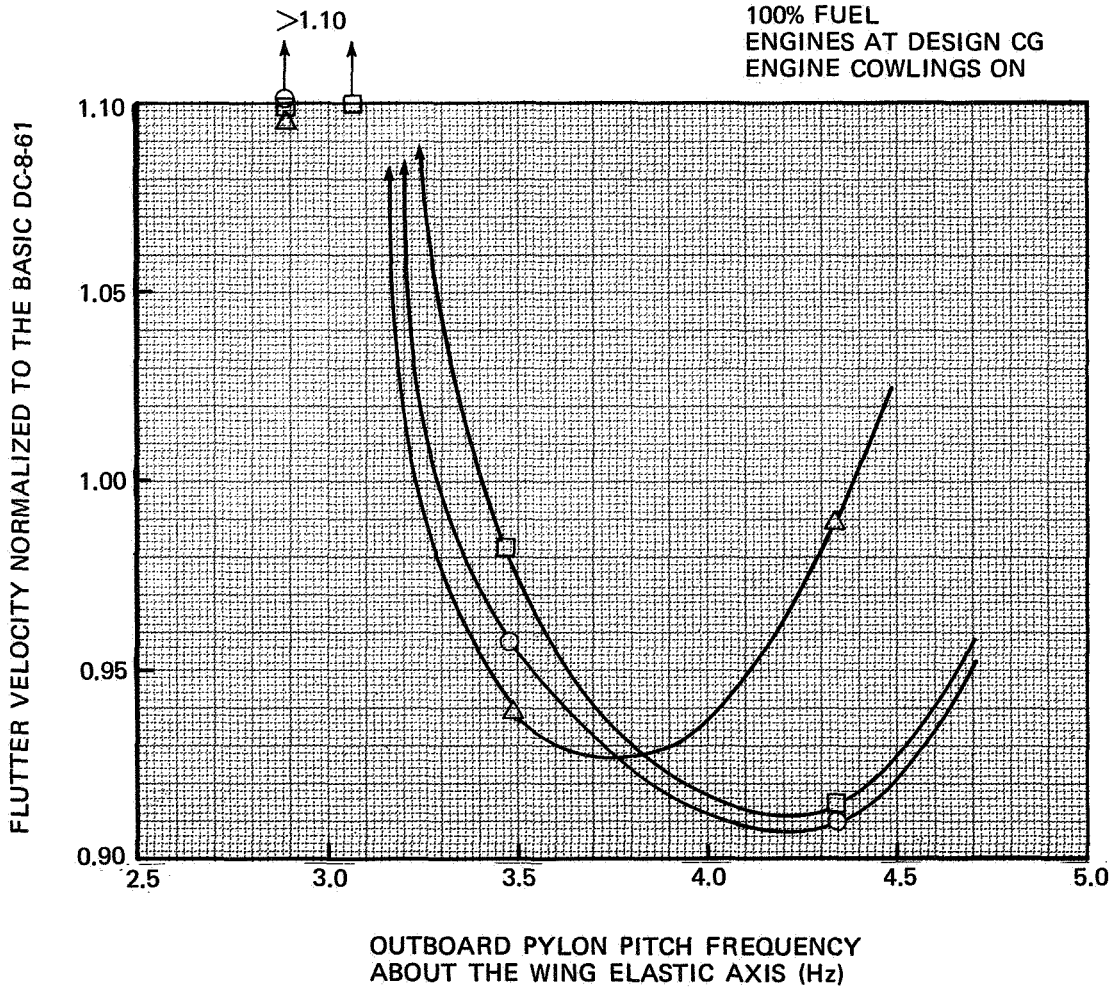

FIGURE VI-49. EFFECT OF OUTBOARD PYLON PITCH FREQUENCY ON FLUTTER VELOCITY

TEST DATA

LEGEND:

○ = INBOARD PYLON PITCH FREQUENCY = 3.66 Hz
ENGINE COWLINGS REMOVED

□ = INBOARD PYLON PITCH FREQUENCY = 3.66 Hz
ENGINE COWLINGS ON

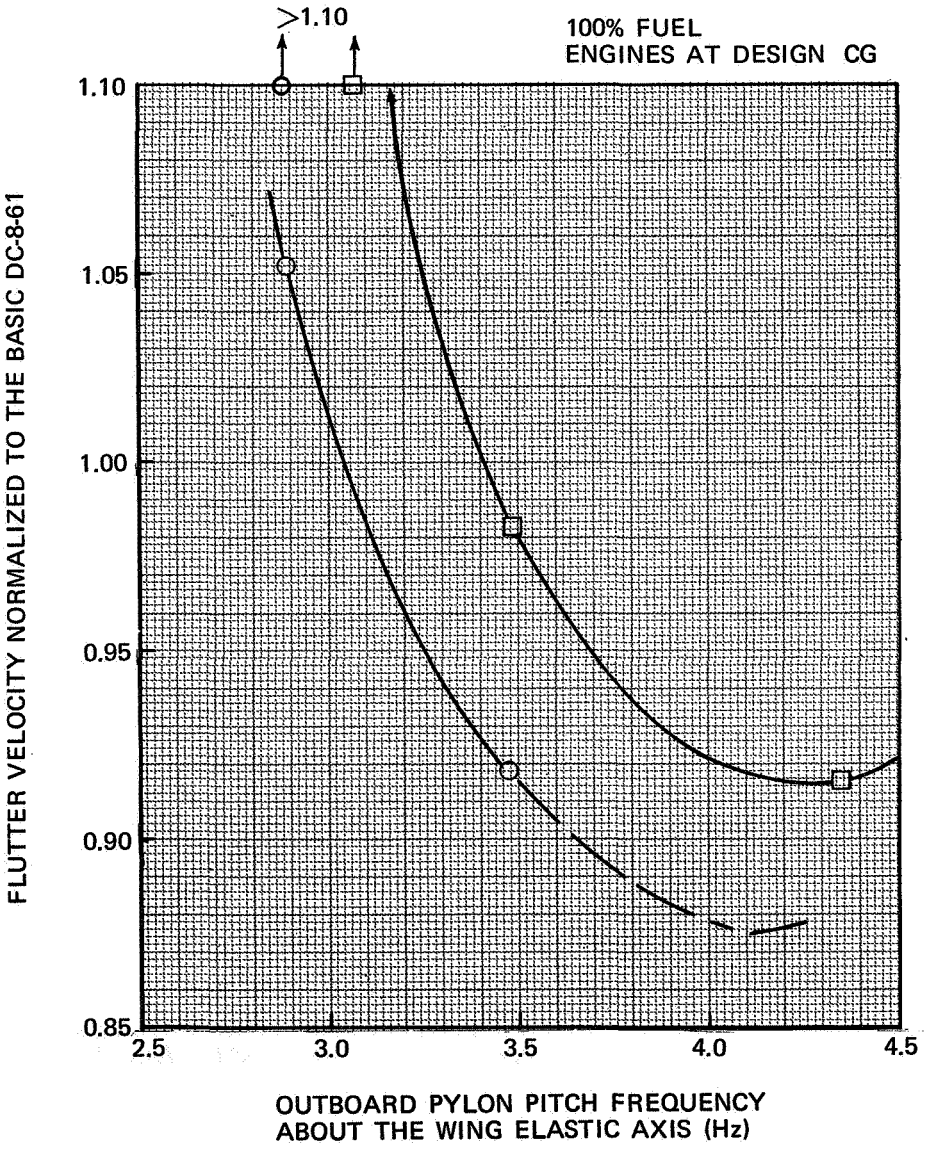

FIGURE VI-50. EFFECT OF ENGINE COWLINGS ON FLUTTER VELOCITY

Four fuel configurations were tested: 0 percent, 20 percent, 60 percent, and 100 percent fuel. A plot of flutter velocity versus fuel for the baseline DC-8-61 and for several quiet-engine configurations are shown in Figure VI-46. This plot establishes 100 percent fuel as the critical fuel configuration for both the quiet engine and the standard DC-8-61.

Four nacelle locations were tested: design, 16.25 inches (41.27 cm) aft of design, 32.5 inches (82.5 cm) aft of design, and 48.75 inches (123.82 cm) aft of design. A plot of flutter velocity as a function of nacelle location is shown in Figure VI-47 for the softest and for the stiffest pylons. The plot clearly shows the forward nacelle positions to be the most desirable for flutter prevention at 100 percent fuel.

Four outboard-pylon stiffnesses and three inboard-pylon stiffnesses were tested. Resulting cantilevered pitch and yaw frequencies are given in Table VI-XII. Two summary plots are shown. Figure VI-48 shows plots of flutter velocity versus inboard-pylon pitch frequency. The outboard-pylon stiffness was held constant for these tests. Figure VI-49 shows plots of flutter velocity as a function of outboard-pylon pitch frequency. These plots show that the softest pylons are desirable for flutter prevention.

The model was tested with and without engine cowlings. Figure VI-50 shows plots of flutter velocity as a function of outboard-pylon pitch frequency with and without the engine cowlings. These plots show that the engine cowlings are stabilizing.

Flutter Analysis

The results of the analyses are shown in Figures VI-51 and VI-52 These are plots of flutter velocity as a function of fuel quantity and outboard-engine pitch frequency. The purpose of the flutter analyses was to provide an independent check on the trends of the flutter-model tests. For this reason, fewer configurations were analyzed. Since good aerodynamic data were not available for the quiet-engine cowling and pylon, the analyses were performed without these data. Thus, comparison between the model and analysis should always be made with the stabilizing effect of the cowlings in mind.

Two fuel configurations were selected: 20 percent and 100 percent fuel. Flutter velocity as a function of percent fuel remaining is plotted in Figure VI-51 . This plot indicates that 100 percent fuel is the critical configuration for both the quiet engine and the standard DC-8-61.

Figure VI-52 shows a comparison between the flutter-model and the analysis data. Flutter velocity as a function of outboard-pylon pitch frequency is based upon both flutter-model and analysis data. Both curves show the effect of the retrofitted engine without engine-cowling aerodynamics.

DISCUSSION OF RESULTS

Vibration Data

The vibration data show that the flutter model and the vibration analyses agree to within 6 percent of the frequencies of primary modes of the standard DC-8-61. Overall, the data indicated that the flutter-model and the vibration analyses are in good agreement as to the structural simulation of the airplane.

Comparison of Test Results and Analyses

The flutter model was a low-speed model. Therefore, the results of the model were corrected to account for an increase in C_{ℓ_q} (slope of curve of lift as a function of angle-of-attack plot) with

increase in Mach number. The flutter analyses included the aerodynamic effects of Mach number. A comparison of the results is important, since the analyses indicate whether or not findings from the low-speed model test could be projected to higher Mach numbers.

Figure VI-50 shows that the engine cowlings added 7 percent to the flutter velocity. Since good aerodynamic data were not available for the nacelles and cowlings, the flutter analyses were made without cowling aerodynamics. Therefore, comparisons between the data should be made with this in mind.

Comparisons of the model and analyses show agreement in the following important areas:

1. Both show that 100 percent fuel is the critical fuel condition for the quiet engine.

2. Figure VI-52 shows that the model and the analysis predict similar behavior with respect to variations in pylon stiffness.

Because the flutter model predicted the forward nacelle position to be the most desirable, analyses were performed only for the forward positions. A second design parameter can be established by applying the 7-percent increase in flutter speed due to cowlings to the analysis results for the 3.2-Hz pylon. This increases the predicted flutter speed to 1.005 and thus establishes an upper bound on the permissible outboard-pylon pitch frequency.

The inboard-pylon pitch frequency can be established from Figure VI-48. This plot indicates that the most favorable frequency would be 3.5 Hz when the outboard pylon is at 3.47 Hz. For the softer outboard pylons, the flutter speed was in excess of test speeds. Therefore, 3.5 cps is at least a reasonable choice for the inboard-pylon stiffness.

The optimum pylon stiffness could be determined only by additional tests and analyses. However, on the basis of the results of this preliminary study, the design goals for the cantilevered-engine pitching frequency should be 3.0 to 3.5 Hz for the inboard engine and 3.0 to 3.2 Hz for the outboard engine. On the basis of previous DC-8 experience, it would seem that pylon stiffnesses that meet these goals can be realized with little, if any, weight penalty in relation to the strength requirements.

CONCLUSIONS

1. Both the flutter model and analysis showed 100 percent to be the critical fuel configuration.

2. The aerodynamic effects of the engine cowlings were stabilizing.

3. Increases in wing stiffness are not required with design pylon-pitch-frequency ranges as follows:

   a. Inboard Pylon: 3.0 to 3.5 Hz

   b. Outboard Pylon: 3.0 to 3.2 Hz

   It is reasonable to assume that these design frequencies could be realized with little or no weight penalty in relation to strength requirements.

4. The forward design engine locations are desirable.

FLUTTER ANALYSIS

LEGEND:

○ = ANALYSIS DC-8-61

□ = QUIET ENGINE, ANALYSIS
INBOARD ENGINE f_a = 4.5 Hz, OUTBOARD ENGINE f_a = 4.0 Hz

△ = QUIET ENGINE, ANALYSIS
INBOARD ENGINE f_a = 3.5 Hz, OUTBOARD ENGINE f_a = 3.2 Hz

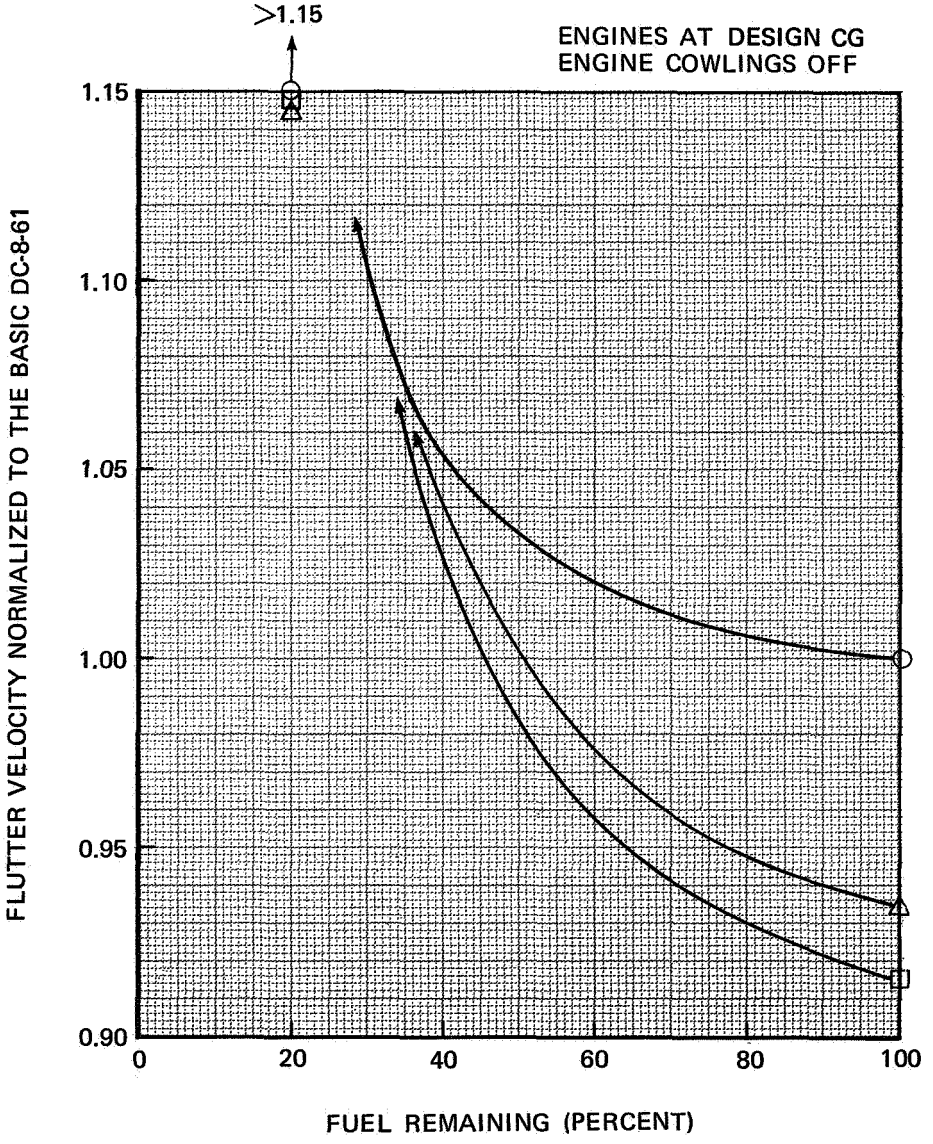

FIGURE VI-51. FLUTTER ANALYSIS

TEST DATA AND FLUTTER ANALYSIS COMPARISON

LEGEND:

○ = FLUTTER MODEL DATA, FULL FUEL
NO ENGINE COWLINGS

□ = ANALYSIS DATA, FULL FUEL
NO ENGINE COWLINGS

△ = ANALYSIS DATA, 20% FUEL
NO ENGINE COWLINGS

ENGINES AT DESIGN CG

ENGINE COWLINGS OFF

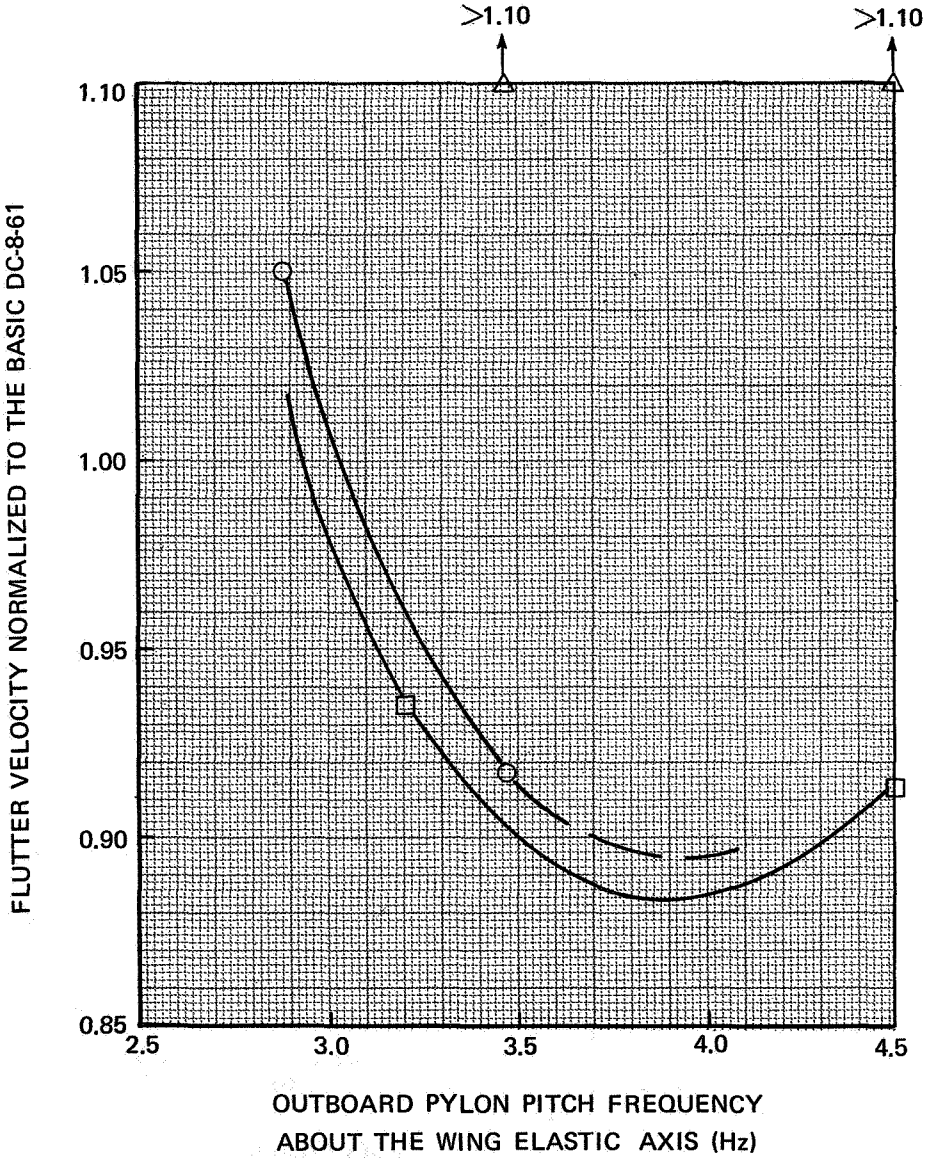

FIGURE VI-52. EFFECT OF OUTBOARD PYLON PITCH FREQUENCY ON FLUTTER VELOCITY

ECONOMIC ANALYSIS

RETROFIT COSTS

The retrofit costs, including downtime for the DC-8-61 based on the final costing study, are shown in Table VI-XVII. The table includes costs for three numbers of retrofitted airplanes, 100, 200, and 300, and for two years, 1969 and 1975.

There will be approximately 100 DC-8-61 airplanes in service in 1975. For this reason and also because it would not be economical to retrofit fewer than that, 100 were taken as the minimum number. The largest number, 300, is approximately the total number of DC-8's expected to be in United States service in 1975.

The 1969 retrofit costs include present labor and material costs. Completion of additional studies, legislation, development, and certification would take several years and probably would be paced by development of the engine. Consideration of these factors led to the assumption that the retrofit program would be carried out during the three-year period 1974 through 1976. The retrofit costs shown in the table are for 1975. A compounded inflation factor of four percent per year was used to escalate current prices to 1975 prices.

RETROFIT KIT PRICE

The final retrofit concept was significantly different from that considered and reported in Task I and Task II. New pylons and nacelles are still required, together with some wing rework and strengthening at the wing-pylon attach area for the outboard nacelle. Wing reskinning would not be necessary, but some control-system modifications would be required. The principal components of the final retrofit would therefore be as follows:

1. New engines
2. New nacelles
3. New pylons
4. Local wing rework at outboard pylon attach areas
5. Control-system modifications.

Furthermore, each of these components would require development, testing, tooling, production, and certification.

Final estimates of the retrofit-kit price were developed from the following:

1. Design-change work statement based on the design from Task IV.
2. Weight-change log.
3. Rate of inflation.
4. Engine price.

5. Program schedule.

6. Plans for laboratory tests, test-stand tests, wind-tunnel tests, ground tests, and flight tests.

7. Estimates of man-hours for necessary design engineering, laboratory work, flight test, and other support required for FAA certification of the nacelle-pylon modifications, wing work, and control-system modifications.

Retrofit-Kit Installation

It was estimated that installation of the retrofit kits would require 11,193 man-hours per airplane, whether 100 or 300 aircraft were modified.

Engine Price

The 1969 price of a quiet engine, $523,000, was defined in Task IV. The same price was assumed, regardless of quantity. A compounded rate of inflation of 4 percent was applied to obtain the 1975 cost.

Spares

The value of spare parts was obtained in accordance with ATA methods. Ten percent and forty percent spares were included for the airframe and the engines, respectively.

Downtime

Airplane downtime in 1969 was valued at $10,000 per day. A survey of DC-8 trunkline operators confirmed this as a reasonable value that is in general current use in evaluating airline operations. This cost was escalated to 1975 at the same rate as the other cost elements. The amount of downtime was estimated to be 25 days per aircraft, whether 100 or 300 airplanes were modified.

Assumed Program Schedule

The retrofit program schedule assumed for Task II was considered to be still valid. The schedule is shown in Table VI-XVIII. Basically, it covers a 45-month period from ATP to PFRT for the quiet engine. A design-to-certification cycle for the airframe integration part would take about the same time. Assuming an ATP date of October 1969 for the engine, the quiet engine would begin to enter airline service sometime in 1975.

The number of retrofitted aircraft and the date of completion of retrofit would be determined by equating these two time-dependent factors:

1. Cumulative number (growth with time) of quiet engines and nacelle kits.

2. Cumulative number (decrement with time) of total DC-8 fleet (according to the airlines' retirement schedules).

Estimates of production potentials for the quiet engine and associated airframe parts indicate that a DC-8 quiet engine retrofit program could be completed in early 1978.

TABLE VI-XVII
RETROFIT COST SUMMARY

PRODUCTION LEVEL OF AIRCRAFT KITS BUILT	CURRENT (1969) PRICES			ESTIMATED 1975 PRICES*		
	100	200	300	100	200	300
AIRCRAFT KIT PRICE	3,199,000	2,542,000	2,307,000	4,047,000	3,216,000	2,918,000
INSTALLATION COST	63,000	58,000	53,000	80,000	73,000	67,000
PRICE OF FOUR NEW QUIET ENGINES	2,092,000	2,092,000	2,092,000	2,646,000	2,646,000	2,646,000
SPARES:						
ENGINES 40%	837,000	837,000	837,000	1,059,000	1,059,000	1,059,000
AIRFRAMES 10%	320,000	254,000	231,000	405,000	321,000	292,000
COST INSTALLED PER AIRCRAFT	6,511,000	5,783,000	5,520,000	8,237,000	7,315,000	6,982,000
VALUE OF DOWNTIME FOR RETROFIT	265,000	260,000	255,000	335,000	329,000	323,000
TOTAL COST PER AIRCRAFT	6,776,000	6,043,000	5,775,000	8,572,000	7,644,000	7,305,000

*ESCALATED FROM 1969 BASE AT 4.0% PER YEAR

TABLE VI-XVIII
ASSUMED PROGRAM SCHEDULE

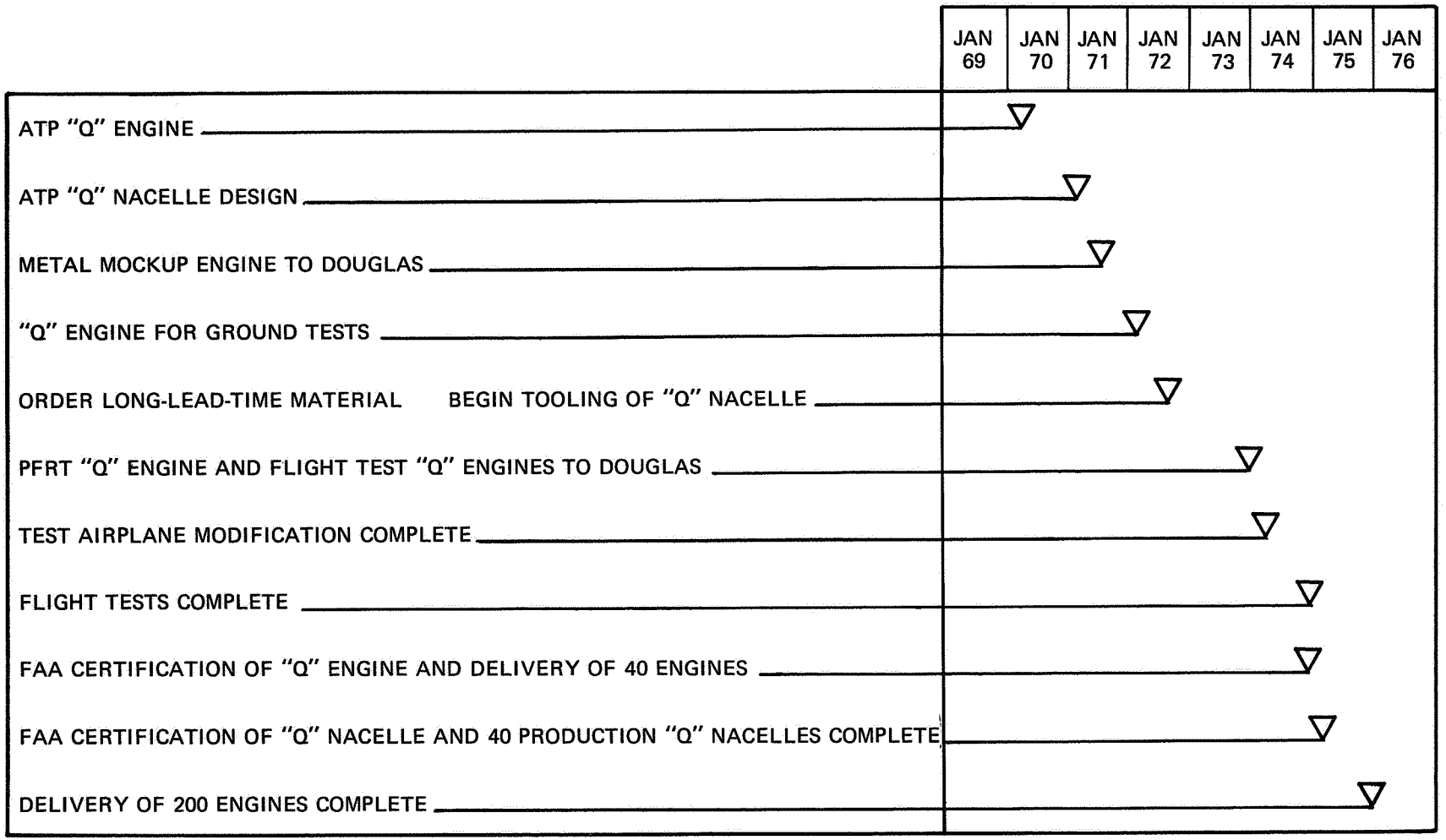

ECONOMIC FEASIBILITY OF RETROFIT

Figure VI-5 3 illustrates the analytic process used to assess the economic impact of airplane retrofit on the airline operator. A Douglas-developed digital computer program, designated PEL, was used for this purpose. The program uses two sets of inputs, traffic demand and aircraft capability. The economic impact of refitting the DC-8-61 with quiet engines was evaluated by means of the PEL program by comparing the economics of the present DC-8-61 with those of the retrofitted airplane, DC-8-61-Q2.

The capabilities of the PEL program permitted a parametric examination of the economic effects due to changes in DOC. The results are illustrated in a series of sensitivity curves. The dominant effect of the retrofit is to greatly increase the aircraft cost and hence its DOC. This effect is so predominant that other effects are almost insignificant by comparison and were therefore ignored in the economic analysis.

The parametric sensitivity approach should provide the analysis with useful versatility. It enables a quick determination of economic effects for any retrofit-kit price level. For instance, the effect of a change in the estimated price of the new quiet engine could be quickly evaluated without repeating the study.

ASSUMPTIONS AND DEFINITIONS

Tables VI-XIX and VI-XX describe the principal assumptions, definitions, and relationships that were used in the analysis.

TABLE VI – XIX

ASSUMPTIONS

1. The depreciation component of DOC is so dominant that the effects of changes in other costs are practically negligible.
2. The DC-8-61 retrofit costs and performance effects are fairly representative of all U.S.-operated conventional 4-engine jets (DC-8, 707, 720, 880).
3. Retrofit would be accomplished in a 3-year period (1974 through 1976).
4. The total 4-engine-jet fleet in operation during 1974, 1975, and 1976 would be retrofitted. Both the FAA and the McDonnell Douglas Corporation estimate that about 800 aircraft will be in operation.
5. No new aircraft of this type would be delivered during the period from 1974 to 1979.
6. The retrofit fleet would continue to serve the same traffic demand that it served before retrofit.
7. Investment is defined as the combined cost of the aircraft and retrofit.
8. There would be no fare increase above the present fare. If fares were free to respond competitively, they would be expected to increase as costs increase. Since fares are regulated, it is almost impossible to forecast any changes in fares.

TABLE VI-XX

DEFINITIONS
OF
PRINCIPAL EVALUATIVE RELATIONSHIPS

1.	OPERATING PROFIT	=	OPERATING REVENUE – OPERATING EXPENSES – TAXES ON EARNINGS
2.		OPERATING REVENUE	= Σ RPM x FARE PER PM
3.		OPERATING EXPENSES	= Σ INDIRECT OPERATING COSTS + DIRECT OPERATING COSTS
4.		INDIRECT OPERATING COSTS	= 0.42 x OPERATING REVENUE
5.		DIRECT OPERATING COST AS CALCULATED IN TASK V	
6.		TAXES ON EARNINGS	= 0.40 x GROSS EARNINGS
7.		GROSS EARNINGS	= OPERATING REVENUE – OPERATING EXPENSES
8.	OPERATING PROFIT DECREASES AS DIRECT OPERATING COST INCREASES (WHEN ALL OTHER ELEMENTS ARE UNCHANGED)		
9.	RETURN ON INVESTMENT	=	OPERATING PROFIT DIVIDED BY INVESTMENT
10.		INVESTMENT	= PRICE PER AIRCRAFT x NUMBER OF AIRCRAFT
11.	RETURN ON INVESTMENT DECREASES AS PROFIT DECREASES AND/OR AS INVESTMENT INCREASES (WHEN ALL OTHER ELEMENTS ARE UNCHANGED)		

PROJECTED AIRLINE SCENARIO AND ECONOMIC STATUS DURING 1975-1979

Table VI-XXI summarizes the PEL analysis of the basic case. Projected data for the 5-year period 1975-1979 were generated; then yearly averages were developed for operating profit, investment in aircraft, and ROI. The scenario and economic status attributable to the conventional 4-engine-jet fleets are shown in absolute projected quantities and also as the proportion they represent of the total projected U.S. domestic scheduled passenger operations. The forecasts of air traffic and aircraft inventory correlate very closely with the latest FAA forecasts.

SENSITIVITIES OF PROFIT TO INCREASES IN DOC

The DOC of the 4-engine jets was incremented by 10, 20, 40, and 80 percent, resulting in four sets of evaluation criteria. Since air-traffic demand and fares were not varied, operating revenue remained the same. The other criteria changed as shown in Table VI-XXII. Operating profit went from positive to negative (i.e., to a loss) between the 10- and 20-percent incremented DOC values and caused ROI to do likewise. Taxes were reduced to zero when earnings became negative. The subsequent losses on this phase of airlines operations would provide a carry-over tax credit against profitable portions of operations, but this could not be shown on the data for the 4-engine-jet fleet.

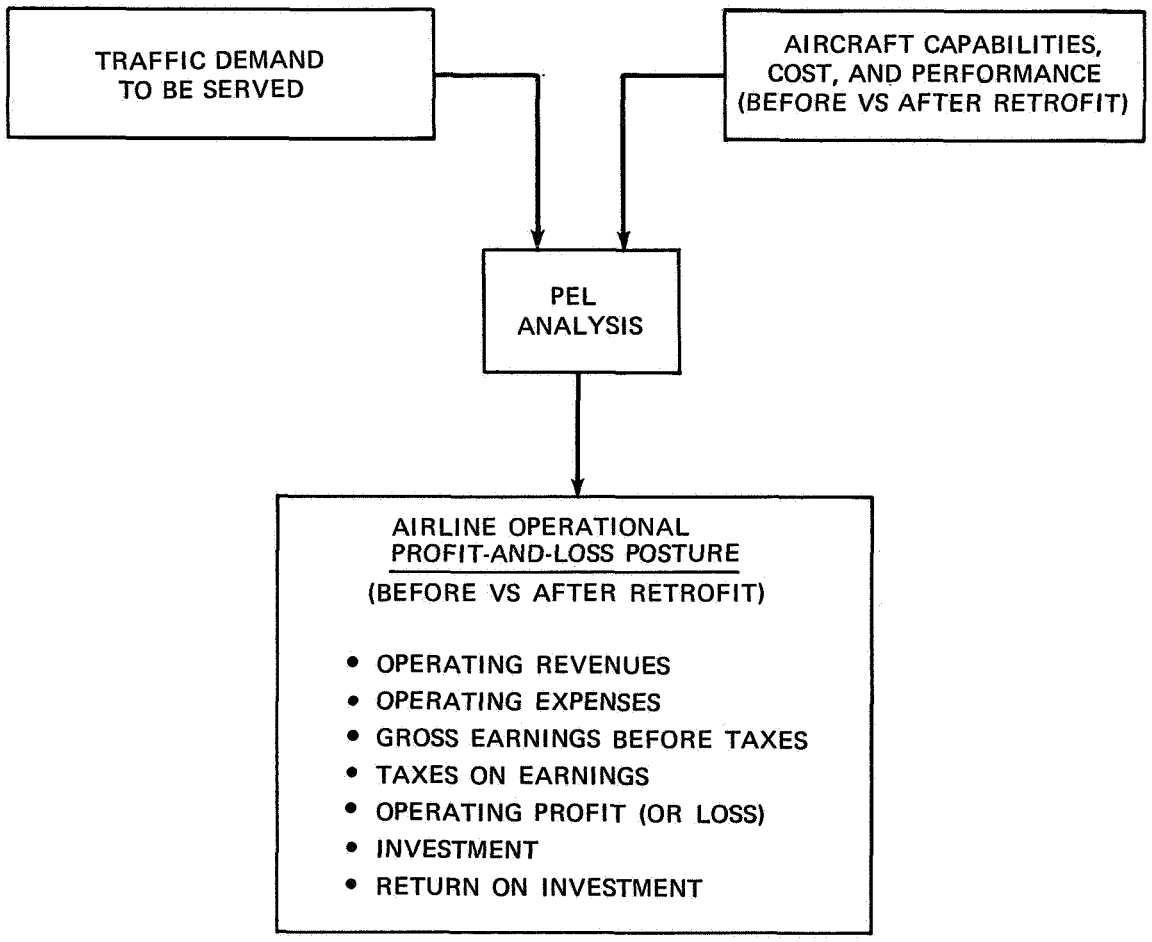

FIGURE VI-53. CRITERIA FOR ASSESSMENT OF ECONOMIC FEASIBILITY OF RETROFIT PROGRAM

TABLE VI-XXI

PROJECTED
AIRLINE SCENARIO AND PROFIT AND LOSS POSTURE
1975 – 1979
(ASSUMES NO RETROFIT)

	TOTAL U.S. DOMESTIC SCHEDULED PASSENGER OPERATIONS		CONVENTIONAL FOUR-ENGINE JET SUBSET OF TOTAL	
	VALUE	% OF TOTAL	VALUE	% OF TOTAL
SCENARIO, 1975 – 1979				
AIR TRAFFIC, 5-YEAR TOTAL (BILLIONS OF RPM)	1,145	100	255	22.3
AIRCRAFT INVENTORY PER YR AVG (UNITS)	2,837	100	800	29.2
INVESTMENT IN AIRCRAFT PER YR AVG ($ MILLIONS)	18,695	100	5,756	30.8
AIRLINE OPERATIONAL P&L POSTURE (5-YR TOTAL $ MILLIONS)				
OPERATING REVENUES	53,258	100	15,294	28.7
OPERATING EXPENSES	45,229	100	14,097	31.2
GROSS EARNINGS BEFORE TAXES	8,029	100	1,197	14.9
TAXES (AND ADJ) ON EARNINGS	3,212	100	478	14.9
OPERATING PROFIT (OR LOSS)	4,817	100	719	14.9
PER-YEAR AVERAGES ($ MILLIONS)				
OPERATING PROFIT (OR LOSS)	963	100	144	14.9
INVESTMENT IN AIRCRAFT	18,695	100	5,756	30.8
RETURN ON INVESTMENT (%)	5.2%	100	2.5%	49.0

TABLE VI-XXII
SENSITIVITIES OF PROFIT AND LOSS CRITERIA TO INCREASES IN DIRECT OPERATING COSTS

PROFIT AND LOSS CRITERIA 1975–1979	INCREASING LEVELS OF DIRECT OPERATING COST OF THE 4-ENGINE JETS									
	BASE (NO CHANGE) CASE		+10% DOC		+20% DOC		+40% DOC		+80% DOC	
	VALUE	% CHANGE	VALUE	% CHANGE	VALUE	% CHANGE	VALUE	% CHANGE	VALUE	% CHANGE
AIRLINE OPER P&L POSTURE (5 YR TOTAL, $ MILLIONS)										
OPER REVENUES	15,294	0	15,294	0	15,294	0	15,294	0	15,294	0
OPER EXPENSES	14,097	0	14,865	+5.4	15,633	+10.9	17,169	+21.8	20,241	+43.6
GROSS EARNINGS (LOSS) BEFORE TAXES	1,197	0	429	–64.2	(339)	–128.3	(1,875)	–256.6	(4,947)	–513.2
TAXES (AND ADJ) ON EARNINGS	478	0	172	–64.2	0	–100.0	0	–100.0	0	–100.0
OPER PROFIT (OR LOSS) ($ MIL)	719	0	257	–64.2	(339)	–150.0	(1,875)	–360.0	(4,947)	–780.0
PER YEAR AVERAGES ($ MIL)										
OPER PROFIT (OR LOSS) ($ MIL)	144	0	51	–64.2	(68)	–150.0	(375)	–360.0	(989)	–780.0
INVESTMENT IN A/C ($ MIL)	5,756	0	6,800	+15.4	7,850	+36.5	10,000	+77.6	14,000	+143.5
RETURN (LOSS) ON INVESTMENT (%)	2.5%	0	0.8%		(0.9%)		(3.7%)		(7.1%)	

Figures VI-54 and VI-55 are sensitivity curves that show the effects on DOC due to changes in depreciation interval and retrofit cost, respectively.

Figures VI-56 through VI-58 show the sensitivities of operating expenses, profits, and return on investment to DOC.

The arrows trace the effects of the kit price developed in this study. These effects are discussed in the following section.

ASSESSMENT OF THE DC-8-61 QUIET-ENGINE RETROFIT

The installed cost of the final DC-8-61 quiet-engine retrofit in 1975 would be $6,982,000 per aircraft for 300 aircraft. The cost would be $8,237,000 per aircraft for 100 aircraft. The value of downtime would add an additional $323,000 to the operator's expenses as a one-time cost, which could not be capitalized or amortized through DOC.

Figure VI-55 shows the sensitivity of DOC to retrofit cost. The $6,982,000 retrofit cost causes a 58 percent increase in DOC.

Figure VI-56 shows the sensitivity of operating expenses to DOC. The 58 percent increase in DOC would result in a 32 percent increase in total operating expenses.

Figure VI-57 shows the sensitivity of profits to DOC. It shows that the 58 percent increase in DOC causes a decrease in profits to far below zero. The decrease in profit would be considerably greater than 500 percent.

Figure VI-58 shows the sensitivity of ROI to DOC. A 58 percent increase in DOC causes a change in ROI from +2.5 percent to −5.5 percent. (The Civil Aeronautics Board's current guidelines suggest that 10.5 percent is a reasonable value of ROI. The operator's ROI during 1975, even before retrofitting quiet engines, is projected to be only 2.5 percent.)

The economic effects in 1975 dollars due to retrofitting the DC-8-61 with quiet engines are summarized below for the base case:

Downtime expense	$ 323,000
Amortizable costs	6,982,000
Total	$7,305,000
Δ DOC	+58.0%
Δ Operating Expense	+32.0%
Δ Profit	−585%
Resulting Value of ROI	−5.5%

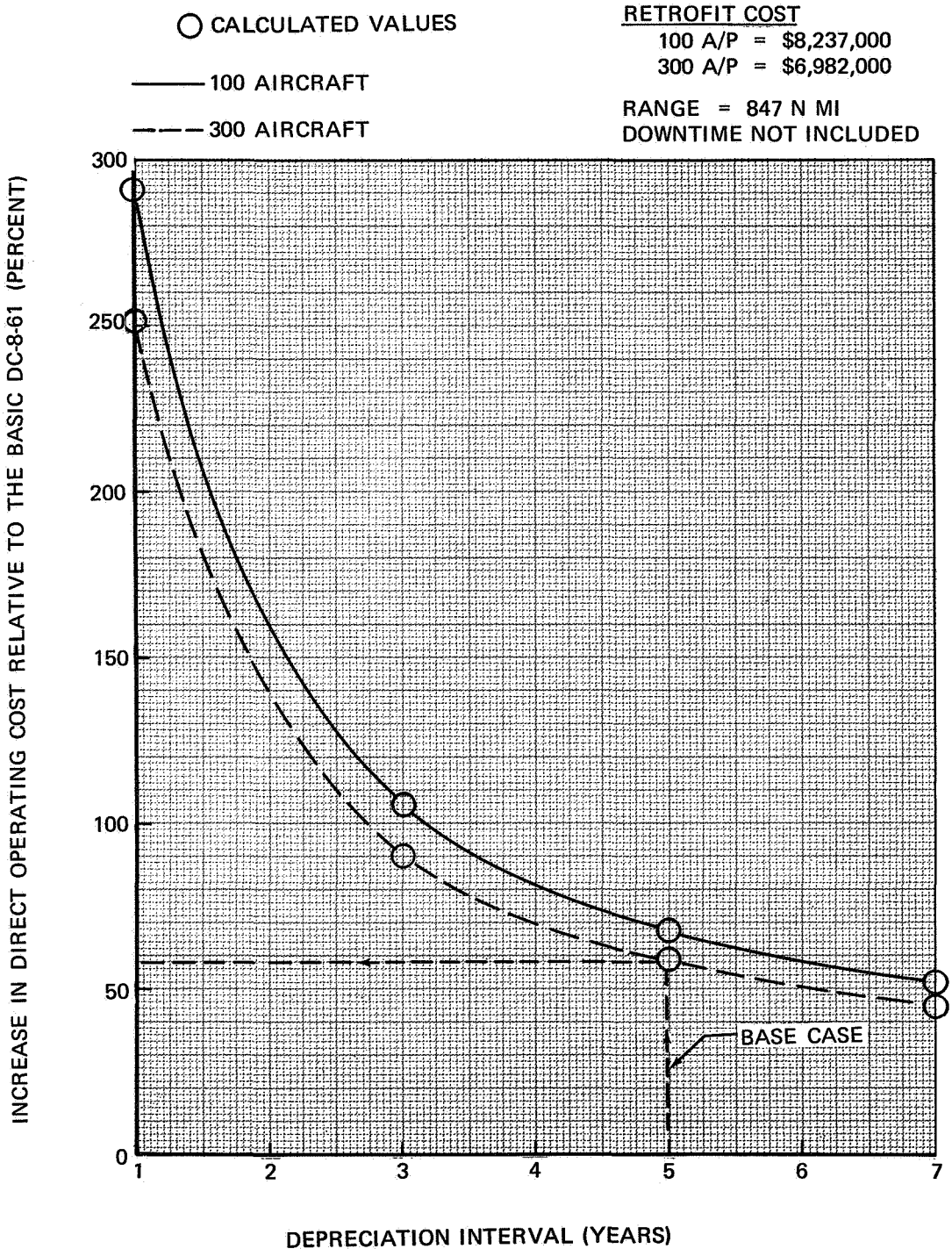

FIGURE VI-54. SENSITIVITY OF DIRECT OPERATING COSTS TO DEPRECIATION INTERVAL

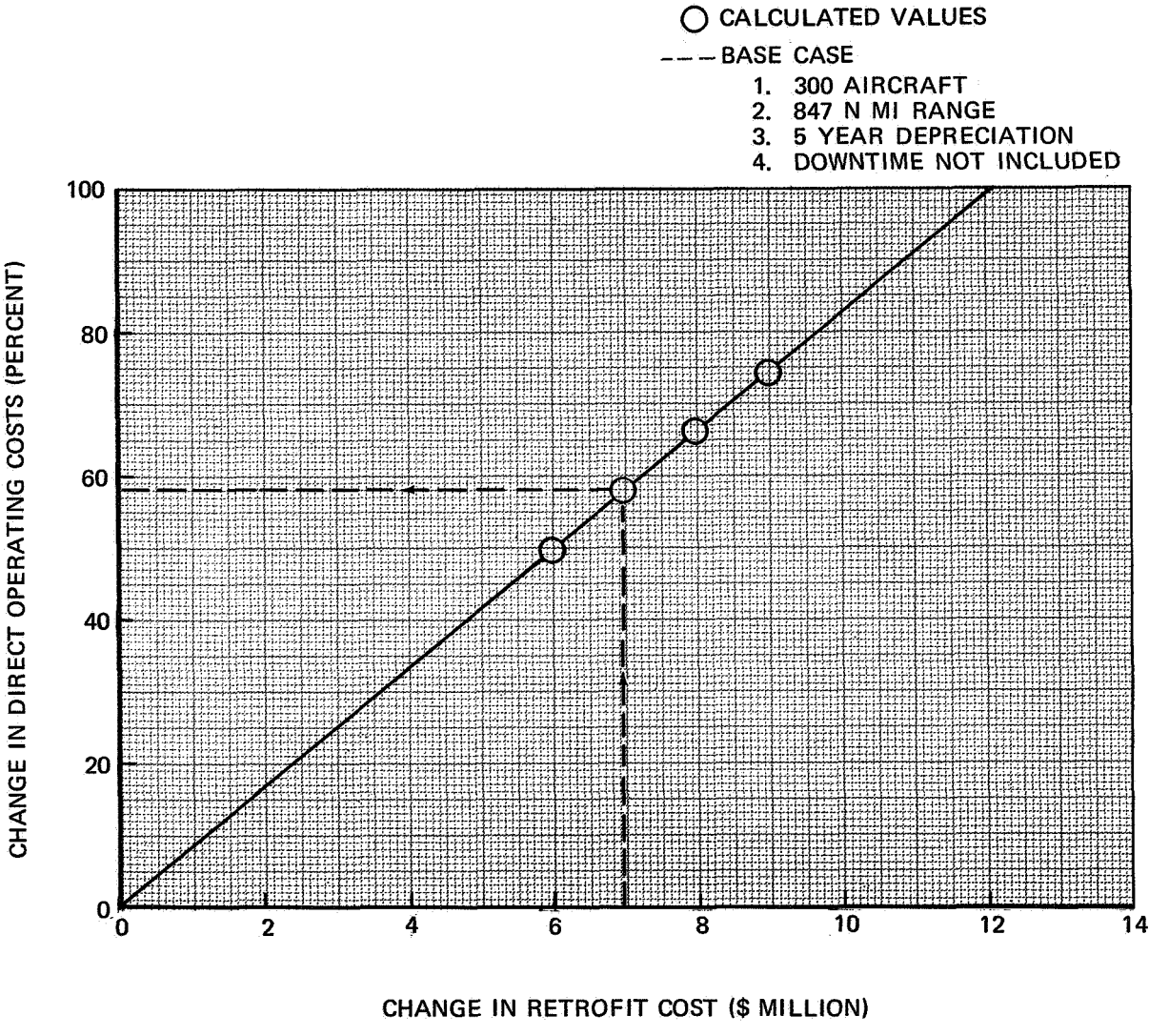

FIGURE VI-55. EFFECT OF RETROFIT COST ON DIRECT OPERATING COSTS

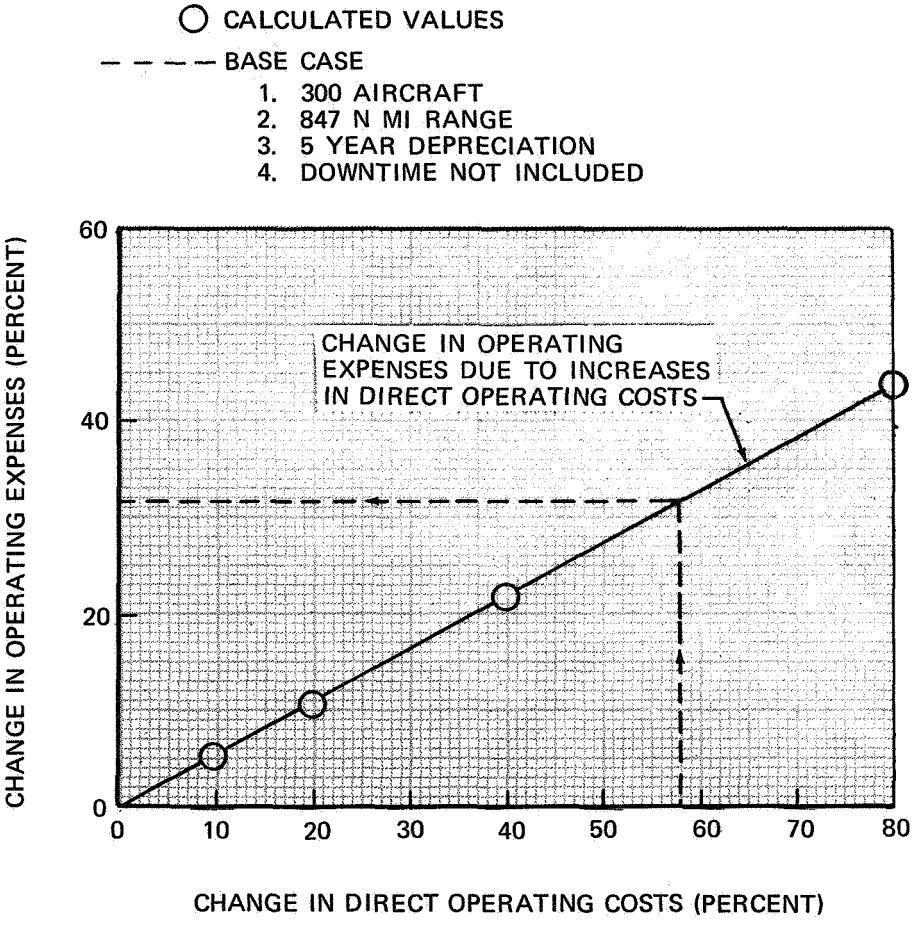

FIGURE VI-56. SENSITIVITY OF OPERATING EXPENSES TO DIRECT OPERATING COSTS (4-ENGINE JETS)

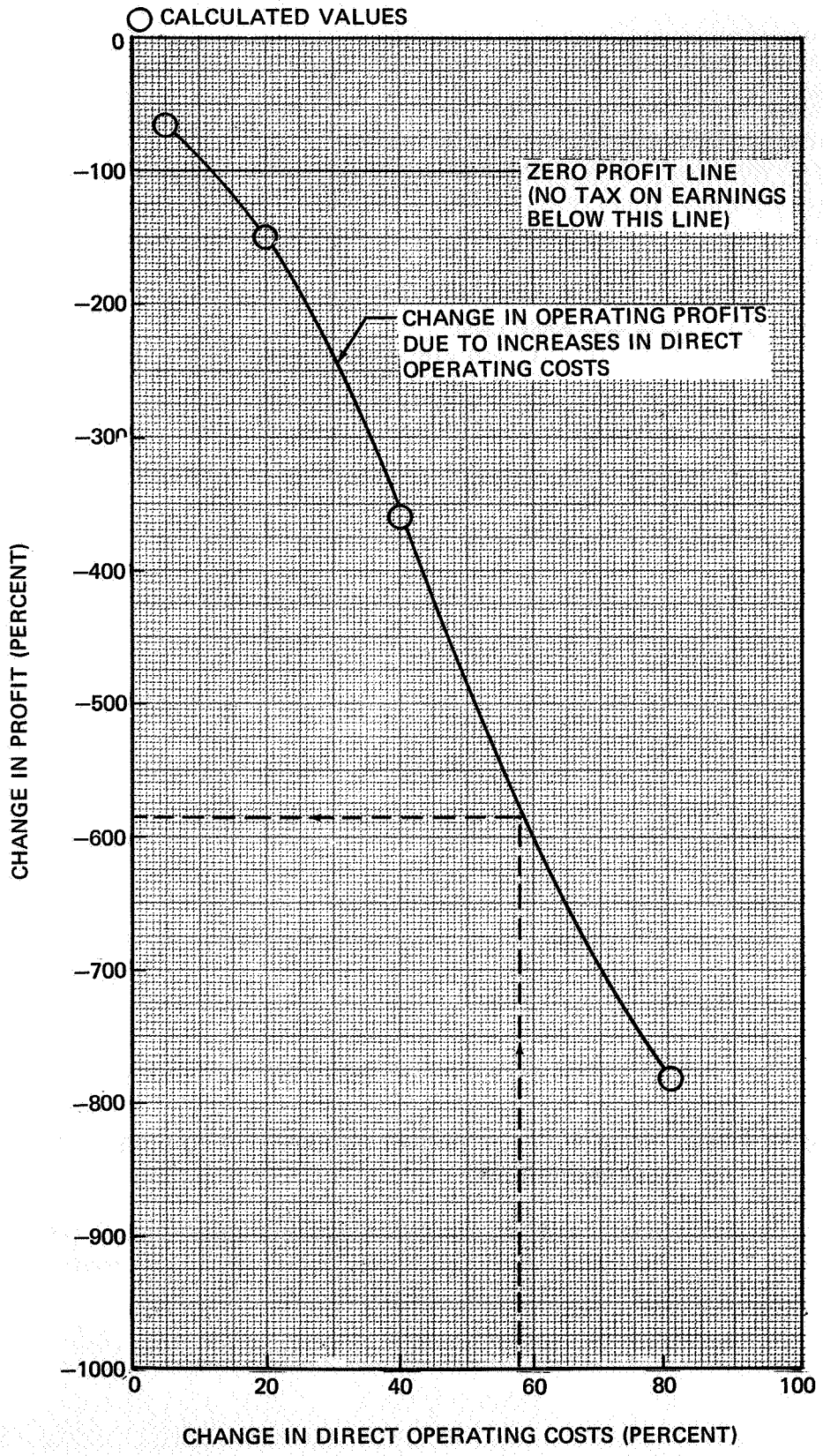

FIGURE VI-57. SENSITIVITY OF PROFITS TO DIRECT OPERATING COSTS (4-ENGINE JETS)

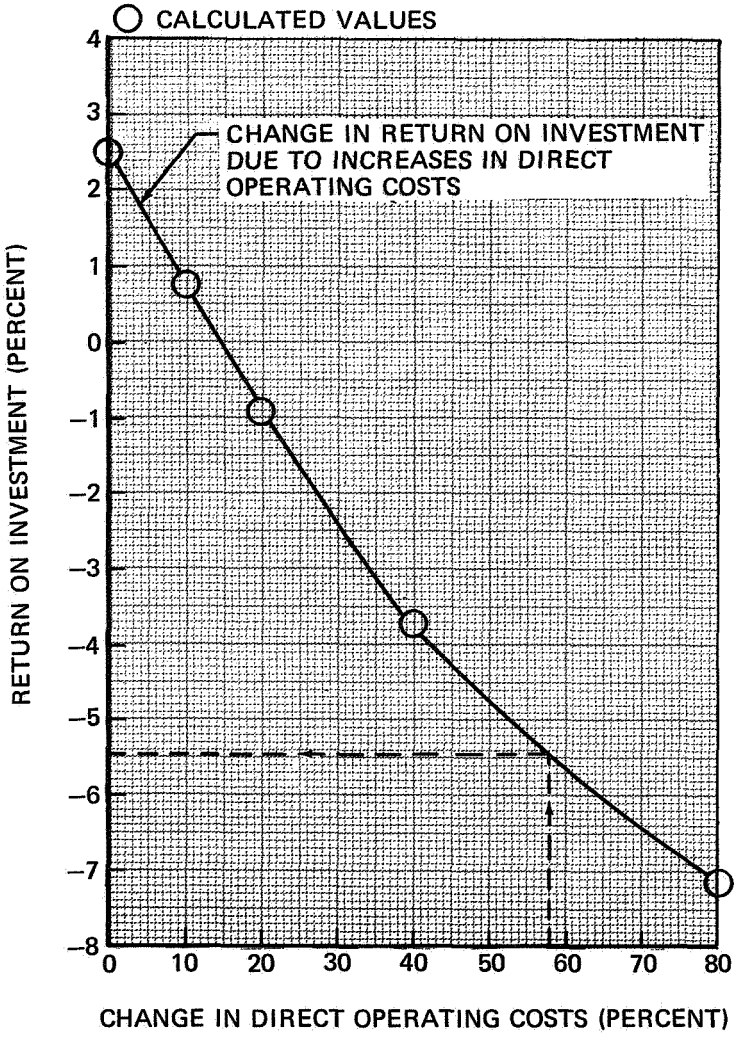

FIGURE VI-58. SENSITIVITY OF RETURN ON INVESTMENT TO DIRECT OPERATING COSTS (4-ENGINE JETS)

REFERENCES

VI-1 Douglas Report LB 32887, "DC-8-61 Airplane Ground Vibration Test Modes and Frequencies," dated June 1966.

VI-2 Douglas Report DAC-33734, "DC-8-61F Dynamic Analysis Basic Data," May 1967.

VI-3 Yates, E. Carson Jr., "Modified-Strip-Analysis Method for Predicting Wing Flutter at Subsonic to Hypersonic Speeds," Journal of Aircraft, 3 (1966), pp 25-29.

APPENDIX A

DEFINITION OF SYMBOLS

APPENDIX A

DEFINITION OF SYMBOLS

C_L	Lift coefficient
C_D	Drag coefficient
C_Y	Side-force coefficient
C_m	Pitching-moment coefficient
$C_{m_{AH}}$	Change in pitch coefficient with angle of attack of the horizontal tail
C_ℓ	Rolling-moment coefficient
C_n	Yawing-moment coefficient
C_p	Static-pressure coefficient
C_w	Wind chord, ft
g	Gravitational constant, ft/sec/sec
–HDV	Less horizontal, dorsal, and vertical
i_H	Incidence of horizontal stabilizer relative to the fuselage reference plane
$_n$	Longitudinal distance from inlet-highlight to center of gravity
M	Free-stream Mach number
q	Free-stream dynamic pressure, lb/sq ft
R_N	Free-stream Reynolds number
S_w	Reference wing area, sq ft
S_{61}	DC-8-61 fuselage model
V_e	Equivalent airspeed, kn
W_a	Engine inlet airflow, lb/sec
X_{ac}	Location of the aerodynamic center
α_F	Angle of attack relative to the fuselage reference plane, deg
β	Sideslip angle, deg

DEFINITION OF SYMBOLS (Continued)

δ_F	Flap deflection angle, deg
ϵ	Downwash angle, deg
$\frac{\partial \epsilon}{\partial \alpha}$	Downwash gradient
σ	Ratio of ambient density to sea-level standard-day density

Subscripts:

A	Tail on
NF	Normal force
N+P	Nacelle and pylon
T.O.	Tail off

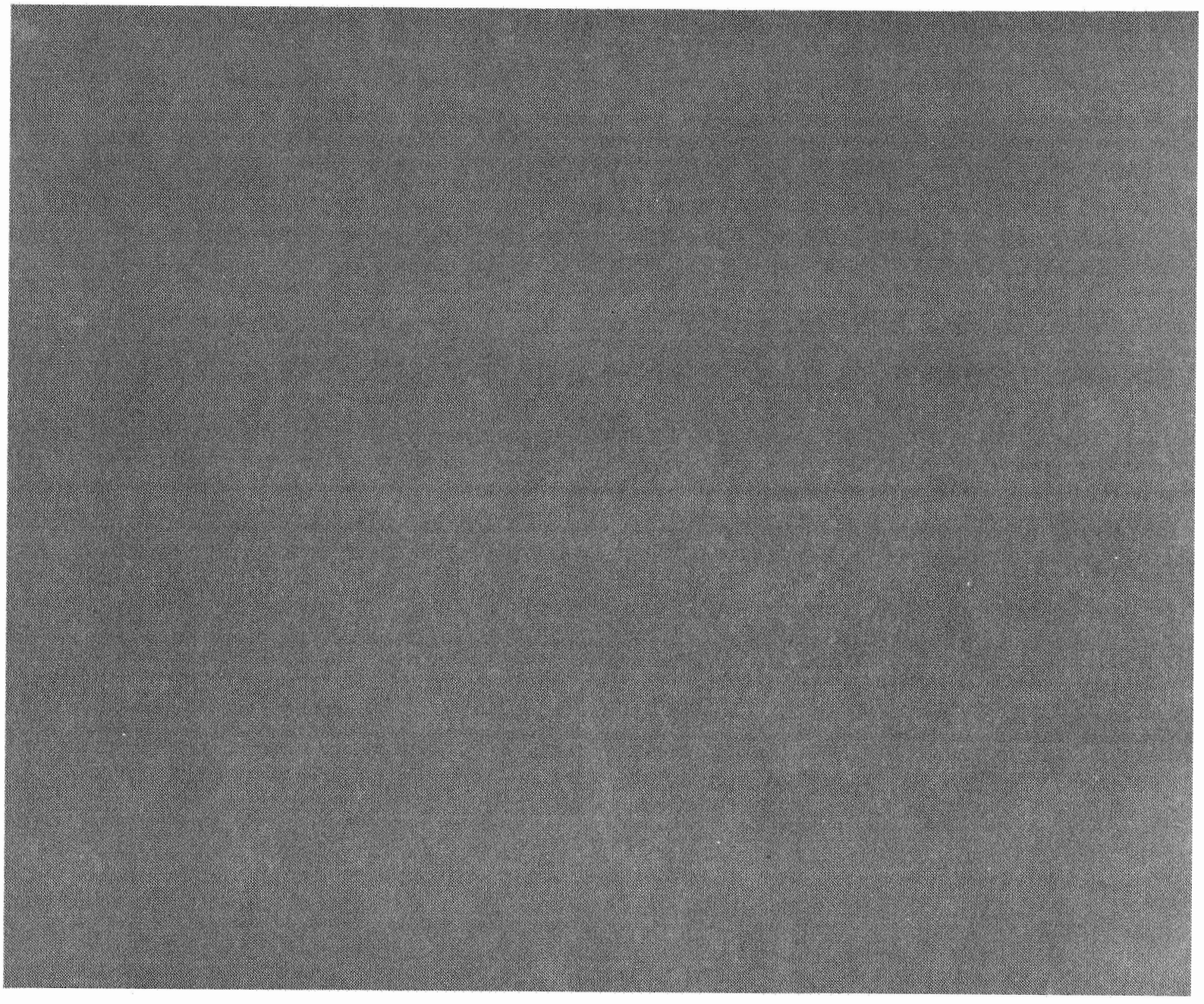

DOUGLAS AIRCRAFT COMPANY

3855 LAKEWOOD BLVD., LONG BEACH, CALIFORNIA 90801

MCDONNELL DOUGLAS